Tertiary limestones and sedimentary dykes on Chatham Islands, southwest Pacific Ocean, New Zealand

A thesis
submitted in partial fulfilment
of the requirements for the degree
of
Master of Science in Earth and Ocean Sciences
at the
University of Waikato

THE UNIVERSITY OF
WAIKATO
Te Whare Wānanga o Waikato

By
Jeremy Titjen

The University of Waikato
Hamilton, New Zealand
2007

“It seems to me that the natural world is the greatest source of excitement; the greatest source of visual beauty; the greatest source of intellectual interest. It is the greatest source of so much in life that makes life worth living.”
- David Attenborough

Limestone dyke at Red Bluff, Chatham Island
(Photo taken by Jeremy Titjen, January, 2006

ABSTRACT

The Chatham Islands are located in the SW Pacific Ocean, approximately 850 km to the east of the South Island of New Zealand. This small group of islands is situated near the eastern margin of the Chatham Rise, an elongated section of submerged continental crust that represents part of the Late Paleozoic-Mesozoic Gondwana accretionary margin. The location and much of the geology of the Chatham Islands are attributed to intra-plate basaltic volcanism, initiated during the Late Cretaceous, in association with development of a failed rifting system to the south of the Chatham Rise. Despite the volcanic nature of much of the geology, the majority of the Cenozoic sedimentary stratigraphic record on the islands comprises non-tropical skeletal carbonate deposits whose deposition was often coeval with submarine volcanics and volcaniclastic deposits. This has resulted in complex stratigraphic relationships, with the volcanic geology exerting a strong influence on the geometry and distribution of the carbonate deposits. These limestones, despite some general field descriptions, have been little studied and are especially poorly understood from a petrographic and diagenetic perspective.

The carbonate geology in detail comprises eleven discrete limestone units of Late Cretaceous through to Pleistocene age which were studied during two consecutive field expeditions over the summers of 2005 and 2006. These limestone occurrences are best exposed in scattered coastal outcrops where they form prominent rugged bluffs. While many of the younger (Oligocene to Pliocene) outcrops comprise of poorly exposed, thin and eroded limestone remnants (<5 m thick), older (Late Paleocene to Early Oligocene) exposures can be up to 100 m in thickness. The character of these limestones is highly variable. In outcrop they display a broad range of textures and skeletal compositions, often exhibit cross-bedding, display differing degrees of porosity occlusion by cementation, and may include rare silicified horizons and evidence of hardground formation.

Petrographically the limestones are skeletal grainstones and packstones with a typical compositional makeup of about 70% skeletal material, 10% siliciclasts, and 20% cement/matrix. Localised increases in siliciclastics occur where the carbonates are diluted by locally-derived volcaniclastics. The spectrum of skeletal assemblages identified within the Chatham Island limestones is diverse and appears in many cases to be comparable to the bryozoan dominant types common in mainland New Zealand and mid-latitude Australian cool-water carbonates in general. However, some key departures from the expected cool-water carbonate skeletal makeup have been identified in this study. The occurrence of stromatolitic algal mats in Late Cretaceous and Early Eocene carbonate deposits indicates not cool-temperate, but certainly warm-temperate paleoclimatic conditions. A change to cool-temperate conditions is recorded in the limestone flora/fauna from the mid-Late Miocene times following the development and later northward movement of the Subtropical Front. An uncharacteristic mix of shallow-shelf (bryozoans) and deeper water fauna (planktic foraminifera), together with their highly fragmented and abraded nature, is indicative of the likely remobilisation and redistribution of carbonate, primarily during episodic storm events.

The Chatham Islands limestones formed within the relative tectonic stability of an oceanic island setting, which was conducive to ongoing carbonate accumulation throughout much of the Cenozoic. This contrasts markedly with other mainland New Zealand shelf carbonates which formed over sporadic and short-lived geological periods, experiencing greater degrees of burial cementation controlled by a relatively more active tectonic setting. As a consequence of the tectonically stable setting, the Chatham Islands limestones have experienced little burial and exhibit a paucity of burial cementation effects. They remain commonly soft and friable. Detailed petrographic investigations have shown the limestones are variably cemented by rare uneven acicular spar fringes, poorly to well-developed syntaxial rim cements about echinoderm fragments, and equant/blocky microsparite. Staining of thin sections and cathodoluminescence petrography show these spar cement generations are non-ferroan and their very dull- to non-luminescent nature supports precipitation from Mn-poor oxygenated waters, likely of an either meteoric or combined marine/shallow burial origin. Micrite is the dominant intra- and inter-particle pore fill and occurs both as a microbioclastic matrix and as precipitated homogenous and/or micropeloidal cement. The rare fringing cements often seen in association with homogenous and/or micropeloidal micrite may be indicative of true early marine (seafloor) cement precipitation and localised hardground development.

An interesting feature of the geology of the Chatham Islands is the occurrence of carbonate material within sedimentary dykes. The locations of the dykes are in association with volcanic and volcaniclastic deposits. Similarities between dyke characteristics at Red Bluff on Chatham Island with mainland occurrences from East Coast and Canterbury Basins (North and South Islands, respectively) on mainland New Zealand have been recognised. They show complex structures including sidewall striations, internal flow structures as revealed by grain sorting, and extra-clast inclusions of previous fill lithologies which are characteristic of carbonate injection. This is in contrast to other dykes which are known to be of a passive fill origin. Multiple phases of carbonate sediment injection can be recognised by crosscutting relationships enabling the determination of a parasequence of events. Possible injection mechanisms are most likely associated with sediment overloading or hydrothermal pressurisation associated with emplacement of submarine volcanics.

The Chatham Islands provide an exciting example of a geologically unique and complex non-tropical carbonate depositional setting. The production of carbonates is controlled by volcanic and volcaniclastic sediment input with the types of carbonate deposits and water depth variations related to thermal uplift/subsidence in association with global eustatic sealevel and temperature changes associated with development of Southern Ocean water fronts from the Late Cretaceous-Cenozoic. Carbonate deposition on the Chatham Islands is considered to relate to a rather variable and small scale oceanic, high energy, cool-water carbonate ramp setting whose geometry was continually evolving/changing as a consequence of periodic volcanic episodes.

ACKNOWLEDGEMENTS

A huge thank you to my long suffering partner Deborah whose unconditional love and tremendous support over the years has made all this possible. Thank you to my Mum and Dad for all their encouragement and support and for always picking me up when I'm down. Thank you to my partner's mother Margaret for her support through the tough times. Thank you to my kids (Omar and Asher) and to their mother Philippa for putting up with my geology obsession.

Thank you to my supervisors Cam Nelson and Steve Hood who have changed my life in immeasurable ways. Also a big thank you to Peter Kamp for all his support and much appreciated financial assistance through funding from FRST to the University of Waikato Sedimentary and Petroleum Research Group via contract UOWX0301. Thanks to Adam Vonk and Kyle Bland for their advice and guidance throughout my studies. Big thanks to GNS Science, especially Hamish Campbell and John Begg for organising two fantastic field trips to the Chatham Islands and for all their valuable insights and advice on Chatham Island geology. Thank you to Noel James and Brian Jones for all their support in the field and a memorable experience. A big thank you to the technical staff in the Department of Earth and Ocean Sciences at the University of Waikato, especially Ganqing Xu and Renat Radosinsky for their assistance in thin section preparation. Thank you so much to Bill and Kay Carter, and Ian and Moana King for their warm hospitality on Chatham Island, and also James and Annett Moffit at the Bluff Homestead on Pitt Island. Thank you to fellow Chatham Islands research students Kat Holt and Chris Consoli for all their help and support in the field, and also to Vaughn, the Catlans fisherman. Big thanks to Robert Holmes for his help at The Horns and also Tiri and Donna Tuanui at Tioriori along with the Department of Conservation on Chatham Island. Big thanks to Steven Gannaway and Gary Davis for putting me up and putting up with me in Wellington. Thanks to John Simes at GNS Science and Helen Neil from NIWA for their help with samples. Thanks to Doug Lewis for his help in the South Island. Thanks to the following people also for their help and support: Roger Briggs, Sydney Wright, Anand Tripathi, Stephanie Nyman, Dolan Hewitt, Anna Griffin, Jessica Bell, Kate Pishief, Orla Hansen, Kate Jackson, Andre Caccioppoli, and last but not least the coffee lady for assisting with alertness levels.

TABLE OF CONTENTS

LIST OF FIGURES

LIST OF TABLES

CHAPTER 1

Introduction

1.1 Carbonate sedimentology

In general, shelf carbonates can occur in a continuum of depositional settings from the poles to the equator, in seawater temperatures ranging from -2º to 40°C. A number of divisions can be imposed across these environments based on skeletal assemblages and platform architecture in the modern context to help decipher the depositional settings of ancient carbonates in the rock record (Nelson, 1988; Pedley and Carannante, 2006). There are a number of parameters (controls) that can account for the distribution of modern tropical (warm-water) or non-tropical (cool-water) shelf carbonates, but primarily these are seawater temperature, nutrient availability and light (Pedley and Carannante, 2006).

Geographically, the modern distribution of tropical shelf carbonates is restricted roughly to equatorial latitudes between about 30°S to 30°N in water temperatures greater then 18ºC (the minimum isotherm for hermatypic coral growth). Non-tropical shelf carbonates form beyond these locations in both the northern and southern hemispheres (Nelson, 1988; Rao, 1996). Divisions of non-tropical carbonates based on seawater temperature can be extrapolated further into temperate carbonates forming in seawater temperatures of over 10ºC to 25ºC (30º-50°S and N) and polar carbonates forming in seawater temperatures of less then 10ºC having latitudes beyond 50ºS or N (Rao, 1996). Similarly tropical carbonates may be divided into true tropical carbonates with seawater temperatures over 22ºC (equatorial latitudes, inside 15ºS or N) and subtropical carbonates with seawater temperatures from 18 to 22ºC over latitudes 15-30ºS or N (James, 1997).

Latitudinal shifts in the modern distribution of shelf carbonates outside the above climatic zones can occur by as much as 5-10º, typically because of displacement of seawater temperatures due to oceanic currents delivering cold water or warm water into tropical or non-tropical regions, respectively (Lees, 1975; Nelson, 1988; Rao, 1996).

This study focuses on Tertiary shelf carbonates that formed in an isolated volcanic island situation at mid- or temperate-latitudes in the Southwest Pacific Ocean. Intuitively they are anticipated to show features aligned with the cool-water shelf carbonate system.

Table 1.1: Comparison of several attributes of warm- and cool-water shelf carbonate systems (adapted from Nelson, 1988 and James, 1997).

Environmental and facies parameters	WARM-WATER CARBONATES (>18°C) between 30°N and 30°S		COOL-WATER CARBONATES (<18°C) beyond 30°N and 30°S		
	Tropical	Subtropical	Temperate	Subpolar	Polar
Setting					
Latitude	0° to 30° S or N		30° to 50° N or S	Slope mounds, open shelves or ramps	>50° S or N
Depositional	Reefs, shallow rimmed shelves, open shelves, ramps			Stable to unstable	
Tectonic	Stable			Low to high	
Terrigenous supply	Low				
Water properties					
Mean temperature	>25°C	Above 23°C	>10°C to 25°C	Below 20°C	<10°C
Minimum temperature	>22°C	About 14°C	~10 to 18°C	Below 12°C	Cold <5°C
Bottom water temperature		~18 to 22°C		~5 to 10°C	
Salinity		Normal to hypersaline		Normal to reduced	
Carbonate saturation		Supersaturated to saturated		Saturated to undersaturated	
Circulation		Restricted to open		Open	
Structures					
Reefs	Abundant	Few reefs		Rare to absent	
Algal mats & stromatolites		Common		Absent or not preserved	
Bulk sediment properties					
Carbonate content		Very high (>90%)		Moderate to very high (50-100%)	
Texture		Mud,sand & gravel		Mainly sands and gravels	
Sedimentation rate		Relatively high (>10 cm/1000 y)		Relatively low (< 10 cm/1000 y)	
Non-skeletal carbonate components					
Ooids		Common		Absent	
Aggregates		Common		Absent	
Peloids		Common		Rare or absent	
Major skeletal carbonate components	*Photozoan*	*Heterozoan* + minor *Photozoan*	*Heterozoan*	*Heterozoan*	
Flora		Calcareous green algae		Calcareous red algae	
		Calcareous red algae		Coccolithophorids	
Fauna		Hermatypic corals		Bryozoans, bivalve molluscs	
		Benthic foraminifers		Benthic foraminifers, barnacles	
		Molluscs		Echinoderms, serpulids, brachiopods	
Skeletal attributes					
Shell thickness	Thick			Mainly thinner	
Rates of production	High			Low to high	
Diversity	High			Mainly lower	
Equitability	Low			Mainly higher	
Shell preservation	Generally good			Poor to good	
Non-carbonate components					
Terrigenous material	Rare			Rare to abundant	
Glauconite	Rare			Common	
Diagenesis					
Carbonate mud	Abundant carbonate mud	Minor carbonate mud	Minor, mainly skeletal abrasion, bioerosion,	Rare, locally common	
Origin of carbonate mud	Marine inorganic precipatation, micritization, bioerosion	Mainly floral disaggregation, bioerosion, ?cementation minor	maceration, boring, ?cementation minor		
Carbonate mineralogy	Aragonite + Mg calcite	Aragonite + calcite	Low- and/or high-Mg calcite dominant		No cementation

Cool-water carbonates characteristics

This study will predominantly deal with cool subtropical to temperate water carbonates that have affinities with the cool-water depositional realm. Distinctive attributes of tropical and non-tropical shelf carbonates, that can help their recognition in the rock record, are summarised in Table 1.1.

A number of specific depositional models have been devised for cool-water carbonates, but in general cool-water carbonates accumulate on open ocean shelves covered in skeletal material which are usually devoid or low in terrigenous or siliciclastic input (Table 1.1) (Nelson, 1988; James, 1997; Pedley and Carannante, 2006). Cool-water skeletal assemblages are devoid of hermatypic corals and calcareous green algae (the photozoan assemblage), and instead mainly reflect a dominance of animals that can live below the photic zone, referred to as the heterozoan association (Table 1.1) (Nelson, 1988; James, 1997; Pedley and Carannante, 2006). Modern cool-water carbonates are dominated by skeletal remains of bryozoans, bivalves, calcareous red algae and barnacles and are devoid of non-skeletal carbonates such as ooids and aggregates (Table 1.1). Mineralogy is predominantly low to high Mg calcite with ancient equivalents consisting entirely of low Mg calcite.

Classification of dominant skeletal assemblages in the heterozoan association in modern cool-water carbonates allows a degree of palaeoenvironmental interpretation from the rock record (e.g. Hayton et al., 1995). In general it has been shown that the deposition of cool-water carbonates increases (as would be expected) during periods of increased global ice cover and consequently the rock record shows an increase in cool-water carbonates during major glacial times, especially during the Ordovician (mini global icehouse) and Cenozoic (Nelson, 1988; Johnson, 2004).

Such periods associated with eustatic sea level change are relatively short and facilitate the importance of placing carbonate deposits in a sequence stratigraphic framework and thereby the development of depositional models. Work of this nature has been carried out on New Zealand and South Australian examples and has yielded important information on early diagenesis in non-tropical carbonates (James and Bone, 1989; Nelson and Smith, 1996; Pedley and Carannante, 2006).

Interpretation of cool-water carbonates from the rock record can further be complicated by deposits formed in epeiric seas (land locked water bodies such as the Mediterranean Sea) which have high biodiversity and clearly definable water depth facies zonations occurring at shallower depth than open ocean analogues (Pedley and Grasso, 2002; Pomar et al., 2004; Pedley and Carannante, 2006). Such environments lack the hydrodynamic controls that are typically important in carbonate deposits of epicontinental settings associated with macro-tidal regimes. The differences occur from the fair-weather reworking processes that operate in epicontinental settings which promote colonisation and preservation of sediment within the inner-ramp zone, although areas of actual carbonate production occupy deeper waters (mid-outer shelf), especially on storm dominated shelves, with wider shelves generally being sites of massive amounts of bioclastic reworking (James, 1997; Pedley and Carannante, 2006).

1.2 New Zealand carbonates

Modern New Zealand carbonates

Carbonate sedimentation on the continental shelves (< 250 m water depth) surrounding New Zealand is generally low (<10% by area) due to high terrigenous material inputs reflecting an active convergent tectonic setting (Nelson et al., 1988b). There are, however, two main areas where carbonate accumulation is significantly increased to cover >70% of shelf depths; namely the Three Kings platform situated to the northwest of the very top of the North Island and the Snares platform situated to the southeast of Stewart Island and the southern South Island. These carbonate rich platforms are associated with some terrigenous sediments, but new inputs of the latter are very low. Both areas also have firm rocky and shelly substrates that encourage the growth of epifaunal and infaunal organisms. Both are situated in oceanic settings that are energetic with continued renewal of high nutrient waters. The Three Kings platform is situated in an area where the Tasman Sea and Pacific Ocean waters meet, while the Snares platform lies across the current position of the Subtropical Front, delivering nutrient rich waters from the Antarctic (Nelson et al., 1988b).

Characteristically the carbonate deposits are extremely coarse grained and carbonate mud is relatively rare at shelf depths, likely bypassed into deeper waters. Mineralogically calcite is dominant over metastable aragonite with high-Mg calcite dominating in the Three Kings area but low-Mg calcite dominating the Snares platform. Dominant skeletal remains are bryozoans and bivalves with locally important foraminifers, barnacles, calcareous red algae and echinoderms. Bioerosion is an important process in skeletal fragmentation and degradation, especially of aragonite shells (Nelson et al., 1988b).

Ancient New Zealand carbonates

Limestones are widely distributed throughout the Cenozoic rock record in New Zealand and are particularly prevalent during the Oligocene due to widespread submergence in a passive tectonic setting (Nelson, 1978a, 1978b; Fleming, 1979; Kamp, 1986; Kamp et al., 1988; Nelson et al., 1988a). Much

like modern examples, sequences show an intimate relationship between carbonate and mixed carbonate-terrigenous deposits, and often include a significant terrigenous component and glauconite, particularly those limestones of Neogene age associated with development of the Pacific/Indo-Australian plate boundary through New Zealand (Ballance, 1976; Nelson and Hume, 1977; Nelson, 1978b; Kamp and Nelson, 1987; Kamp et al., 1988; Ballance, 1993). These limestones were formed on open marine shelves and ramp environments at paleo-latitudes ranging from 60º-35ºS (Hayton *et al.*, 1995).

In general, New Zealand shelf limestones tend to be calcarenites or calcirudites with inter- and intraparticle carbonate mud derived from abrasion and fragmentation of the abundant skeletal constituents (bryozoans, echinoderms, benthic foraminifera, barnacles, brachiopods, bivalves and coralline red algae). Packstones in general are far less common than grainstones (Nelson, 1978b). Calcilutites (or micrites) composed of planktic foraminifera and coccoliths mainly formed in bathyal environments (Nelson, 1978b). All New Zealand limestones are represented by cool-water carbonate facies with no tropical elements such as hermatypic coral reefs or non-skeletal grains like ooids and aggregates, and there is typically poor preservation of aragonitic fragments (Nelson, 1978b).

Diagenetically, any primary magnesium calcite is replaced by stable calcite while aragonite in many limestones has not been preserved or appears as skeletal moulds or is defined by micritic envelope structures. Dissolution of aragonite and replacement of magnesium calcite has been argued to occur within the marine environment at a very shallow depth of burial or directly on the sea floor (Nelson, 1978b). Such stabilisation reactions are encouraged by the inferred relatively low degree of carbonate saturation of sea water at temperate latitudes and the rather slow rates of sedimentation estimated to have been <5 cm/1000 years for at least the mid-Tertiary New Zealand limestones (Nelson, 1978b).

The major cementation process in the majority of New Zealand limestones has involved the precipitation of sparry, usually ferroan, calcite cement within pore spaces. Pre-Pliocene limestones are mainly well lithified while many younger Plio-Pleistocene limestones are softer with an open

porous fabric. Cementation fabrics include granular sparite, syntaxial rim sparite and sparite grain coatings. The carbonate for cement was derived from external sources, aragonite dissolution and/or either non-selective or selective dissolution of calcitic skeletal fragments (Nelson, 1978b). Of these sources the latter two dominate in many of the mid-Tertiary limestone occurrences (Nelson et al., 1988a).

1.3 Chatham Island carbonates - the focus of this study

Tertiary limestone occurrences on the Chatham Islands, 800 km east of South Island, are very limited in distribution but are diverse in age (Late Cretaceous to Pleistocene), fossil content, facies type and diagenetic history. Their stratigraphy and general field features have previously been reviewed by Wood et al. (1989) and Campbell et al. (1988, 1993). During February 2005, and again in 2006, detailed sedimentological field work was conducted on most of the main limestone sections cropping out on both Chatham and Pitt Islands. The purpose of this thesis study is to report through qualitative petrographic analysis the general depositional and diagenetic characteristics of the Chatham Island limestones. In particular the study documents the skeletal assemblages forming the limestones and their inter- and intraparticle matrix/cement types so as to determine broad depositional paleoenvironments and preliminary diagenetic histories. Petrographic analysis of carbonate dykes from the Chatham Islands has also been conducted and from this work and field observations possible mechanisms of dyke emplacement and the origins of the carbonate dyke fills are made.

There are several unique aspects about the limestones on the Chatham Islands. First, they are temperate latitude limestones developed upon isolated oceanic islands far from mainland New Zealand, not upon extensive shelves or platforms. Second, oceanographically the islands straddle the late Tertiary position of the Subtropical Front bounding cool subtropical water to the north from subantarctic water to the south, which should be reflected in the development of distinctive limestone facies. Third, the wide spread of ages of the limestones throughout the Tertiary affords an excellent opportunity to

compare biotic and facies changes over time. Fourth, stratigraphically these temperate limestones are intimately associated with coeval basaltic volcanic and volcaniclastic deposits that appear to have exerted a strong influence on their distribution and geometry, as well as on their facies associations and skeletal assemblages. Fifth, unlike many mainland New Zealand limestones, the carbonates have never been deeply buried, so that pressure-dissolution is unlikely to be a source of calcite cement. While many of the limestones are expectedly only weakly cemented, others are tightly cemented, implying either a marine or subaerial diagenetic origin rather than burial origin like many other New Zealand limestone occurrences. And sixth, limestone dykes are associated with several of the Chatham limestone sections, seemingly as both passive fills and forceful downward fissure injections and veins into volcaniclastic substrates. Multiple episodes of injection are sometimes evident. All these aspects will be addressed and interpreted.

Ongoing more detailed and site specific work associated with this study is being conducted by Canadian colleagues of Professor Nelson (UOW, NZ), namely Professor Noel James (Queen's University, Ontario) and Professor Brian Jones (University of Alberta, Edmonton). This thesis provides an underpinning overview of the Chatham Island's limestones upon which their detailed petrographic, diagenetic and geochemical studies will build.

CHAPTER 2
Regional Geology

The Chatham Rise represents a prominent morphological feature of the submerged continental crust of the New Zealand landmass (Zealandia), extending approximately 1400 km to the east of central South Island (Fig. 2.1). The Rise is truncated to the west by the Southern Alps and structurally underlies central Canterbury and Banks Peninsula (Fig. 2.2). The Rise is bounded to the northeast by the Hikurangi Trough and to the south by the Bounty Trough, with the Chatham Islands forming the only subaerially exposed area on the Rise, situated near its eastern end (Fig. 2.1). The eastern terminus of the Rise is generally considered to be at longitude 171°W, although little is known about this area. Water depths over the 100 km width of the crest of the Rise are less then 500 m, while the total area of the Rise is considered to be that bounded by the 1500 m isobath (Houtz et al., 1967; Davey, 1977; Campbell et al., 1988; Wood et al., 1989; Campbell et al., 1993).

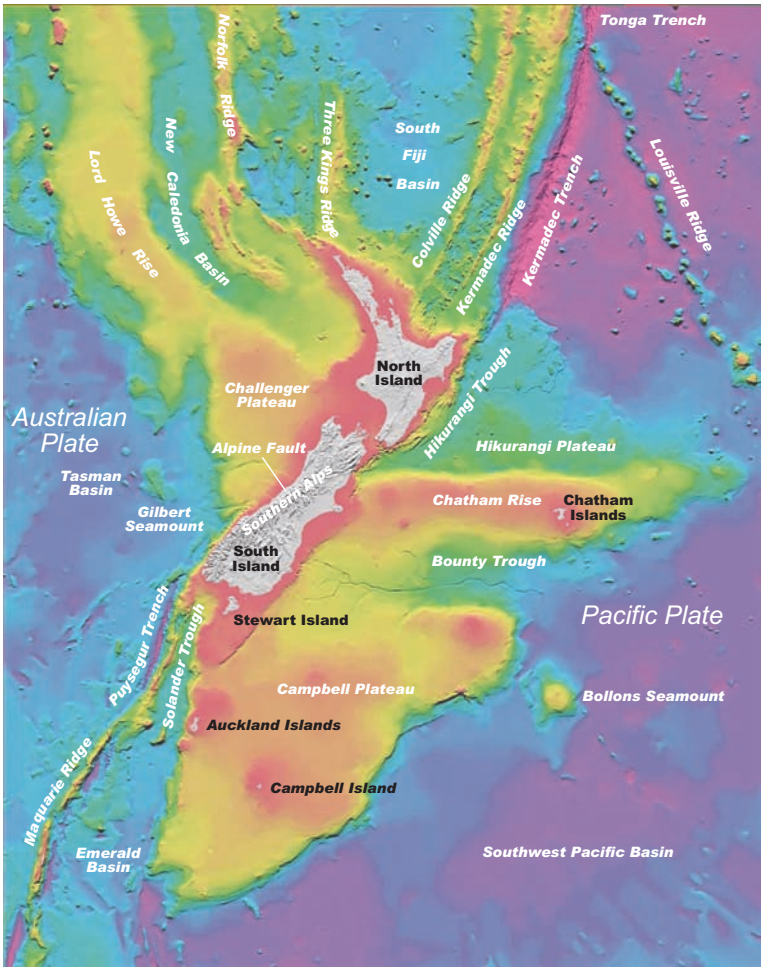

Figure 2.1: Significant bathymetric features of the New Zealand subcontinent showing the Chatham Rise extending to the east of the South Island with the Chatham Islands situated at its eastern end (image sourced from NIWA).

2.1 Structure and tectonic setting of Chatham Rise

Tectonically, the Chatham Rise may be regarded as a block of continental crust that formed in the proto-Pacific accretionary margin of Gondwana. With the break-up of the super-continent, the block including the Rise has been carried to its current position as part of the Pacific Plate (Fig. 2.1). Deformation has affected the Rise as a consequence of various processes of accretion, subduction, rifting and thermal expansion and contraction. It is likely that the Rise has probably always been proximal to the Pacific/Indo-Australian plate boundary since the development of the Alpine Fault in the Early Miocene (Fig 2.1) (Ballance, 1993; Campbell et al., 1993; King, 2000).

Interpretation of seismic data over the Chatham Rise has revealed numerous half-graben structures within the basement rock that are hinged to the south of the Rise and are controlled by well developed east to west normal faulting (Fig. 2.2). These conspicuous features probably developed from the mid-Cretaceous over a period from 110-75 Ma, with some reactivation of movement during the Cenozoic (Hay et al., 1970; Field et al., 1989; Wood et al., 1989; Sutherland, 1999).

The Chatham Rise lies to the north of another submerged continental block, the Campbell Plateau (Fig. 2.1). The Campbell Plateau is structurally similar to Chatham Rise and includes some prominent half-graben structures and is separated from the Rise in part by the Bounty Trough (Beggs, 1993). The Bounty Trough is a major depression (1000 km long, 350 km wide) that formed as a result of rifting and crustal thinning during the mid-Cretaceous (Fig. 2.1) (Davey, 1977; Wood et al., 1989; Campbell et al., 1993; Davey, 1993; Sutherland, 1999).

Structurally, the western end of Chatham Rise extends into central Canterbury with no evidence of any lateral offset of the two regions. These have been linked since the Late Cretaceous and the westernmost extent of this feature is now truncated by the Alpine Fault plate boundary (Fig. 2.2) (Grindley et al., 1977; Campbell et al., 1993).

Tectonic processes forming the northern flank of Chatham Rise are poorly understood. There has been speculation that the northern flank represents a pre-Late Cretaceous convergent margin, for which there is some seismic evidence (Campbell et al., 1993). This has led to a number of authors (Kingma, 1974; Katz and Wood, 1980) speculating on the existence of some pervious landmass in this area (Fig. 2.1). The Hikurangi Plateau is considered to represent thickened oceanic crust (~15 km, typical oceanic crust thicknesses about 10 km), that structurally underlies the southern North Island (Kingma, 1974; Haines, 1979; Katz and Wood, 1980; Bradshaw et al., 1981; Robinson, 1986; Campbell et al., 1993; Davey and Wood, 1994; Wallace and Beavan, 2004).

There are a number of bathymetric highs along the crest of Chatham Rise where water depths shallow significantly. These highs result from high-standing basement blocks associated with Cretaceous volcanics and include the Matheson Bank, Reserve Bank and Mernoo Bank, with the Veryan Bank known to be a guyot (Fig. 2.2) (Herzer and Wood, 1988; Herzer et al., 1989; Campbell et al., 1993).

The Chatham Islands sit astride the largest of these bathymetric highs, defined by the 200 m isobath around the Chatham Island forming a rhomboid shape (150 km in a NW-SE direction and 100 km in a SW-NE direction), known as the Chatham Islands shelf (Fig. 2.2). The origin of this high probably relates to a degree of thermal uplift (Cullen, 1967, 1969; Krause and Cullen, 1970; Campbell et al., 1993).

The eastern extent of Chatham Rise marks the boundary between continental crust and oceanic crust forming the Southwest Pacific Basin (Fig. 2.1) (Campbell et al., 1993).

2.2 Geology of Chatham Rise

The Chatham Rise has the thickest sedimentary successions (2-3 km) along its southern flank, while the crest of the Rise itself supports sequences only a few hundred metres thick. These sequences consist mainly of marine tuffs, limestones, and authigenic precipitates whose ages indicate that the Rise has been a prominent subcontinental structure since the Cretaceous (McDougall, 1982; Herzer and Wood, 1988; Wood et al., 1989; Kamp, 1992).

The Chatham Rise is underlain by continental crust, evidenced by seafloor outcrops of basement greywacke and the existence of schist on the Chatham Islands, which belong to the Permian to Early Cretaceous Torlesse terrane meta-sediments (Fig. 2.2) (Wood and Herzer, 1993; Sutherland, 1999). The thickness of the continental crust along the Chatham Rise (and Campbell Plateau) is about 20-25 km, considerably thinner than mainland New Zealand (30-40 km). This reflects crustal extension during the Middle to Late Cretaceous which probably increased the crustal surface area along the Rise by about 25 per cent (Kamp, 1992; Campbell et al., 1993).

Thick sedimentary sequences have built up in half-graben structures along the southern flank of the Rise (Fig. 2.2). The half-grabens have accumulated fluvial and marginal marine sediments, intermixed with rhyolitic and basaltic deposits as old as Late Cretaceous. At this time large areas of the Rise were likely subaerially exposed (Wood et al., 1989; Kamp, 1992; Campbell et al., 1993).

Deposition in the half-graben structures had ceased by the latest Cretaceous, although there were minor amounts of folding, peneplanation, thermal subsidence and episodes of voluminous alkaline basaltic volcanism during the Late Cretaceous of which the most significant formed a considerable area of the Chatham Islands (Fig. 2.3) (Campbell et al., 1993).

Along the western margin of the Rise during the Late Cretaceous there is a record of lagoonal and marginal marine deposits that are relatively widespread, indicating that an extensive area here must have been subaerial. In general, the geometry of sediments along the Rise indicates that it has been an arch since the Late Cretaceous (Campbell et al., 1993).

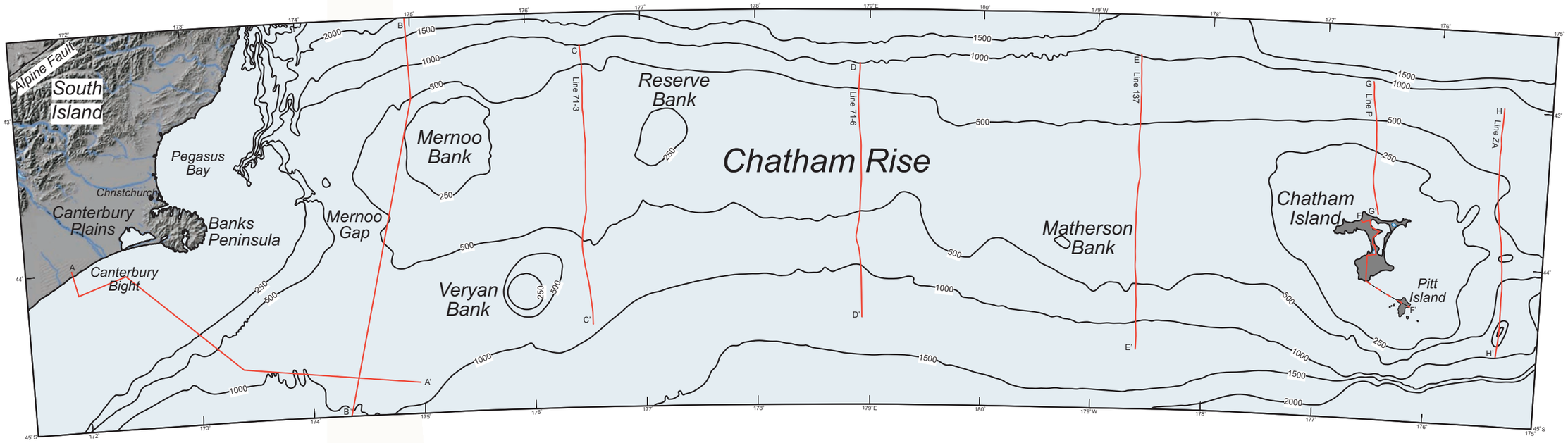

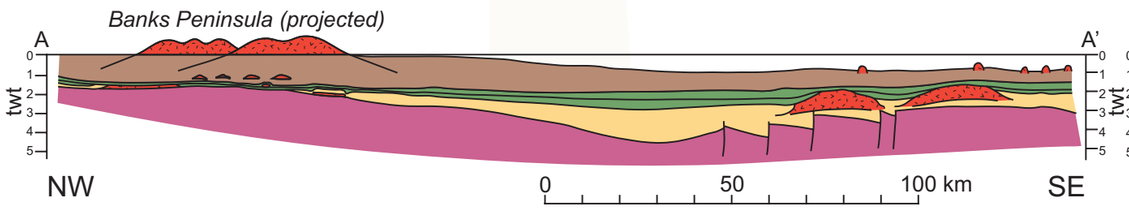

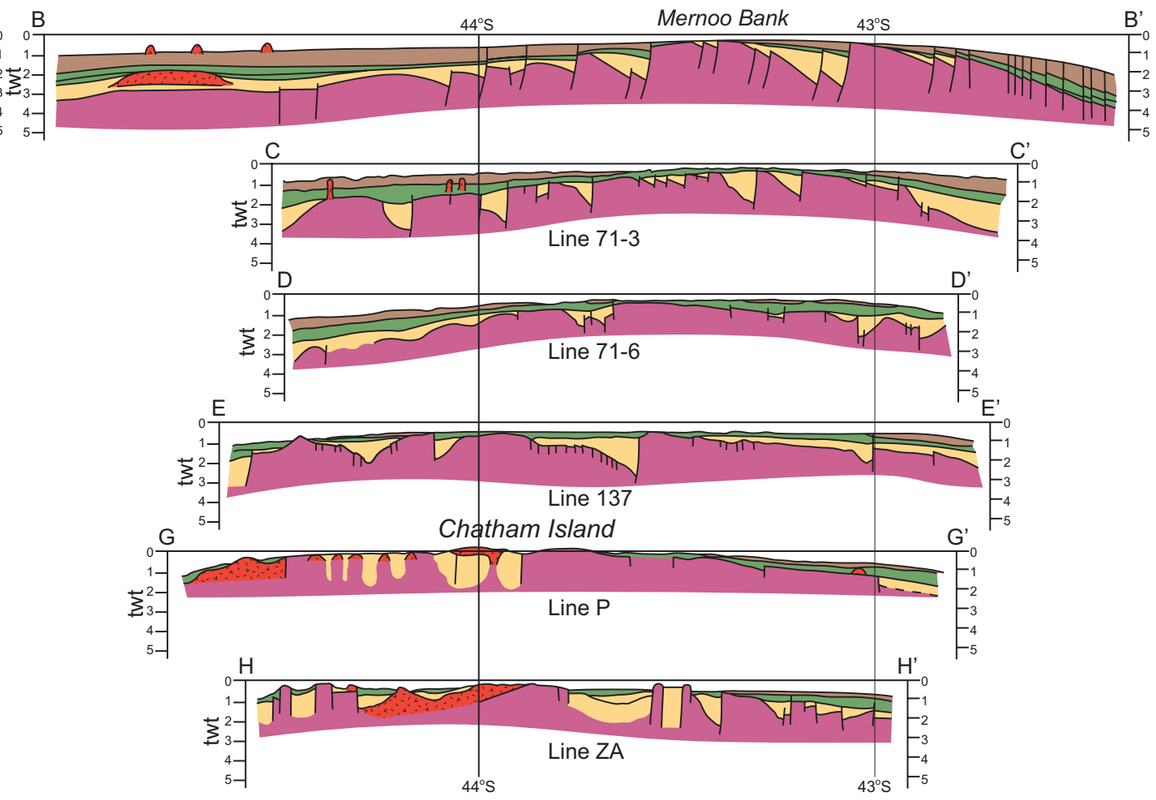

Cretaceous-Cenozoic Volcanics
Neogene Sediments
Paleogene Sediments
Cretaceous Sediments
Mesozoic Basement

Figure 2.2: Generalised bathymetric map (m) of the Chatham Rise (upper) with seismic profile lines shown in red and interpreted in cross sections below.
On lines A - A' and B - B' the lower Paleogene sediments are of Paleocene age, while the upper units are Eocene - Oligocene sequences. The seismic line F - F' through the Chatham Islands is shown in Fig. 2.3 (after Wood et al., 1989).

The accumulation of thin shallow marine deposits indicate that the Rise remained tectonically stable through the Paleocene, interrupted only by sporadic localised basaltic volcanism (Campbell et al., 1993).

During the Eocene, the Cretaceous east-west trending normal faults were reactivated by a period of mild widespread tectonism which is particularly evident at the western extent of the Rise with the deposition of clastic sediments. Much of the Rise at this time was at mid to outer shelf depths and accumulated carbonate deposits over the central and eastern areas (Campbell et al., 1993). The Oligocene was a period of erosion and non-deposition along the Rise, marked only by scarce phosphatised fragments, glauconitic sands, marls and foraminiferal oozes that formed nannofossil chalks which buried Early Oligocene erosional surfaces (Wood et al., 1989).

During the Neogene, the patchy distribution of biogenic and authigenic sediments along the Rise is indicative of tectonically relatively quiescent conditions. The major influences on sedimentation at this time were localised basaltic volcanism, minor faulting, ocean circulation patterns, water temperatures and sea level oscillations, with minor effects from distal volcanism and dropstone material (Campbell et al., 1993).

With the development of a convergent plate margin (the Alpine Fault) through the southern half of the New Zealand landmass in the Early Miocene, the western end of the Chatham Rise exhibits a different geological history from about the mid-Miocene. Significant uplift and dextral movement developed the proto-Southern Alps and an adjacent foreland basin which was infilled by clastic sediments shed from the rising alpine chain. These covered an area comprising the modern Canterbury Plains, Canterbury Shelf and the Mernoo Gap, and extended out onto the axis of the Rise (Fig. 2.2). A major volcanic centre developed on Banks Peninsula on the arched area of the basin from the Middle to Late Miocene (Campbell et al., 1993).

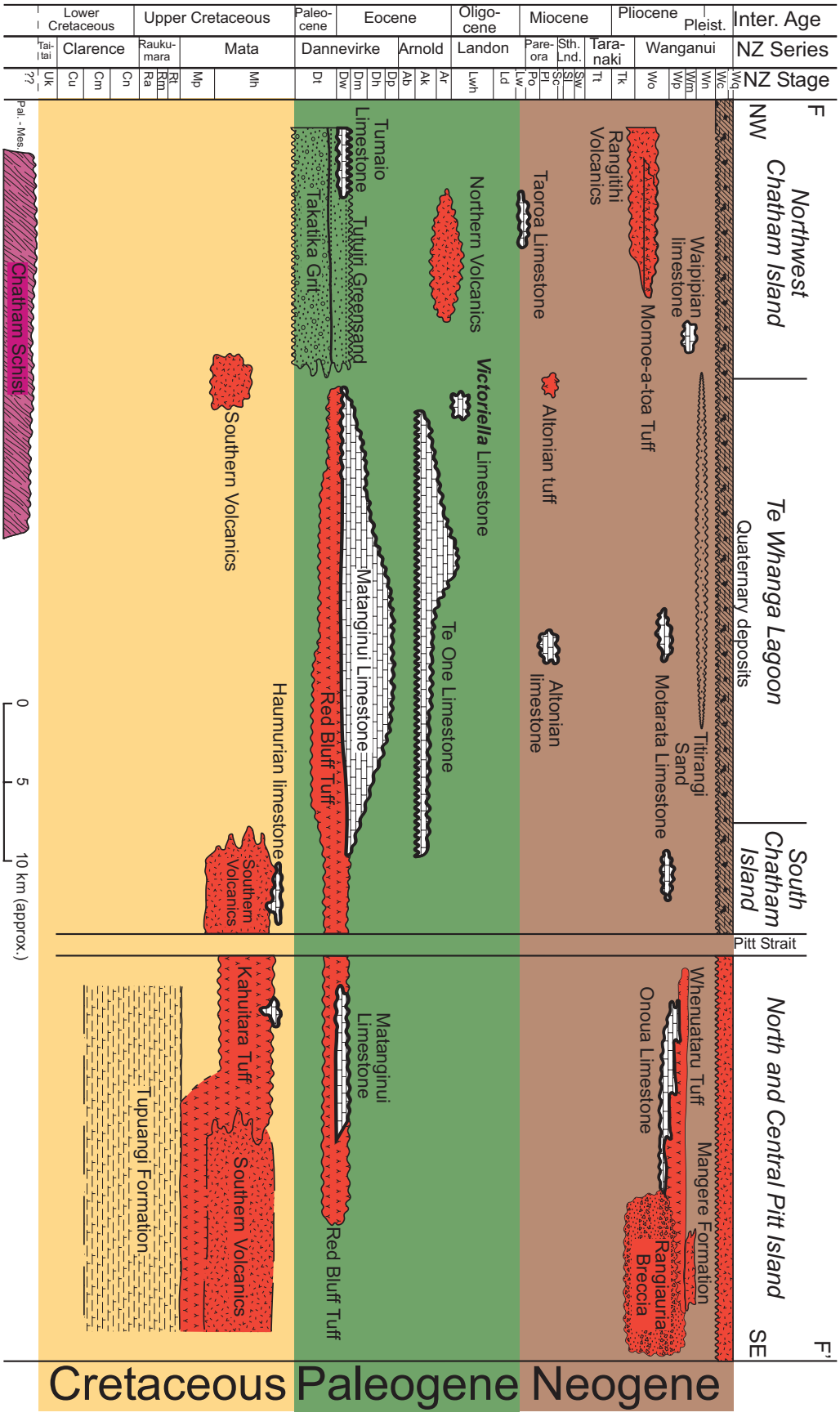

Figure 2.3: Interpretation of the seismic line F - F' through the Chatham Islands shown in Fig. 2.2. This figure encapsulates all the significant geological units of the Chatham Islands with the background coloured bands relating to the stratigraphic time divisions and volcanics shown in the cross-sections of the Chatham Rise in Fig. 2.2 (adapted from Campbell et al., 1993; Wood et al., 1989).

2.3 Structure, tectonics and geology of Chatham Islands

The Chatham Islands, with highest point c. 250 m above sealevel, sit upon a large block of basement and volcanic material and stand 150-350 m above the average water depth of the Rise itself (Fig. 2.4). There are a number of large volcanic centres along the Chatham Rise (e.g. Veryan Bank and Mernoo Bank; Fig. 2.2) but the volcanic centre associated with the thermal uplift of the Chatham Islands is the only centre that has any significant emergence at the present day (Wood et al., 1989; Campbell et al., 1993). Oceanographically the present position of the Chatham Islands sits astride a significant zone of water mass convergence, namely the Subtropical Convergence Zone or Subtropical Front, with subtropical (or temperate) waters to the north of the Rise and sub-Antarctic water to the south (Fig. 2.4B).

Structurally, the Chatham Islands are much like the Chatham Rise with east-west trending faults and half-graben subsurface structures within the basement rocks (Austin et al., 1973). Campbell et al. (1993) proposed that structurally the Chatham Islands may be considered in three domains consisting of:

1. an upthrown Chatham Schist basement (metamorphosed Torlesse Terrane metasediments) horst in the north of Chatham Island
2. with graben fill sediment exposed in central graben Chatham Island and another separate graben fill exposed on Pitt Island
3. and a stratovolcano forming the southern end of Chatham Island.

The stratovolcano responsible for creating the large highland southern end of Chatham Island is the most voluminous in a series of volcanic episodes that occurred during the Late Cretaceous. It is represented by the lava flows and pyroclastic deposits of the Southern Volcanics and to a lesser extent the pyroclastic deposits of the Kahuitara Tuff (Table 2.1 and Fig. 2.3). A large magnetic anomaly in Pitt Strait is thought to represent the volcanic centre of this Cretaceous edifice which is dissected at the southern end of Chatham

Island with high coastal cliffs having heights in excess of 200 m in some places (Austin et al., 1973; Campbell et al., 1993).

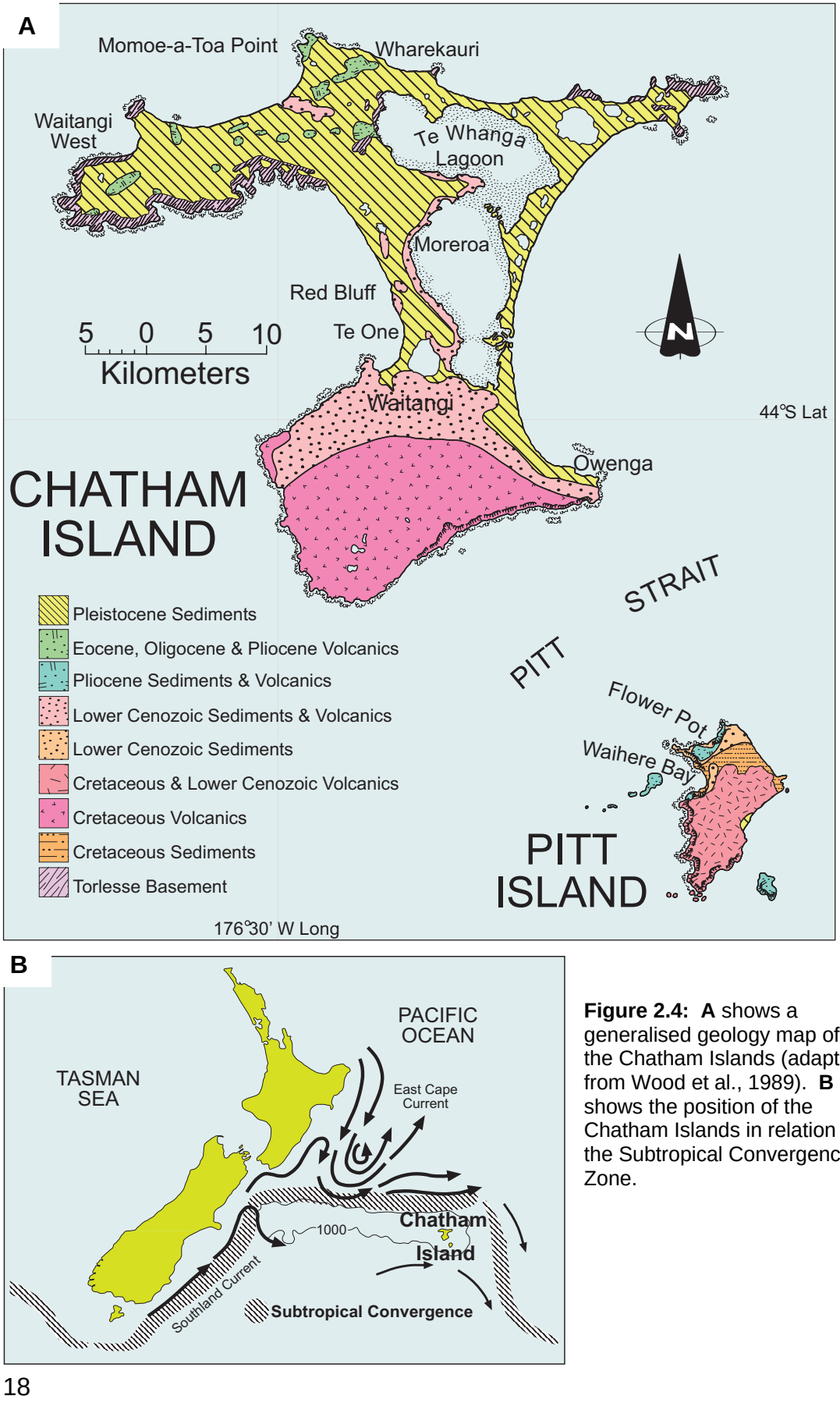

Figure 2.4: **A** shows a generalised geology map of the Chatham Islands (adapted from Wood et al., 1989). **B** shows the position of the Chatham Islands in relation to the Subtropical Convergence Zone.

This Late Cretaceous volcanism was associated with thermal uplift that enhanced the emergence of adjacent basement fault block structures and led to exposure of the basement horst in northern Chatham Island and the Forty Fours islands, and also resulted in the uplift of mid-Late Cretaceous graben fill deposits of the Tupuangi Formation on Pitt Island (Table 2.1 and Figs 2.3, 2.4A) (Campbell et al., 1993).

The overlying Paleocene to Eocene tuffs and limestones overlap these structures and are not affected by them. This suggests that the graben structures were likely related to Late Cretaceous rifting in the Chatham Rise and Bounty Trough area at about 100 Ma, predating the separation of New Zealand from Antarctica and Australia at 80 Ma (Campbell et al., 1993).

The Cenozoic stratigraphic succession of bioclastic and volcaniclastic deposits is interspersed with localised, predominantly shallow marine volcanism (Fig. 2.4A). The sedimentary sequences exposed on the Chatham Islands show that the islands have essentially remained tectonically stable since the Late Cretaceous with only minor faulting and folding (mostly on Pitt Island) associated with localised volcanism (Campbell et al., 1993).

Initial Paleocene deposits include the Tioriori Group with a lower lag deposit member of the Takatika Grit of recent fame for identification of theropod and marine reptile bones (Stilwell et al., 2006). Within the Tioriori Group, volcaniclastic deposits are evidence for widespread volcanism associated with the deposition of the Red Bluff Tuff that continued into the Eocene, to be eventually succeeded by widespread carbonate deposition of the Matanginui and Te One limestones through to the Early Oligocene (Table 2.1 and Figs 2.3, 2.4A) (Campbell et al., 1993).

Early Oligocene volcanics are marked by the conspicuous and highly weathered edifices of the Northern Volcanics, a prominent feature of the northern Chatham Island landscape (east-west), although little eruptive material is preserved in the stratigraphic record. The sedimentary record during the Oligocene and Miocene times is patchy with only three limestones (*Victoriella*, Taoroa and Altonian limestones, and xenoliths in the Rangiauria Breccia) and an Altonian aged tuff (Table 2.1 and Figs 2.3, 2.4A) (Campbell et al., 1993).

A resurgence of volcanism in the Late Miocene to Early Pliocene is marked by the Rangiauria Breccia on Pitt Island and the Rangitihi Volcanics in northern Chatham Island and The Sisters islands. Both of these eruptives are associated with fossiliferous volcaniclastic deposits of the Whenuataru and Momoe-a-toa tuffs (Table 2.1). Accumulation of limestone is patchy through the Pliocene, represented by occurrences of the Motarata and Waipipian limestones on Chatham Island and the Onoua Limestone on Pitt Island (Fig. 2.3) (Campbell et al., 1993).

There are a number of other volcanics that occurred during the Pliocene, represented on Southeast and Star Keys islands and The Pyramid (Table 2.1), causing reactivation of localised faulting on Pitt Island. More significant volcanics developed during the Late Pliocene on Mangere and Little Mangere islands, represented by the Mangere Formation (Table 2.1) (Campbell et al., 1993).

An uplift event is evidenced at the end of the Pliocene by a contact observed on Chatham Island where the Motarata Limestone is overlain disconformably by the Titirangi Sand. It is thought to possibly relate to changes in the motion of the Pacific Plate at this time. During the Pleistocene, changes in eustatic sealevel have probably substantially modified the landscape and there has been extensive accumulation of sands (notably the Wharekauri Sand) and development of extensive blanket peats that have preserved ash fall (Rekohu Ash) from the cal. 26.5 ka Oruanui eruption from Lake Taupo (Table 2.1 and Fig. 2.3) (Campbell et al., 1993).

In general, the Chatham Islands are representative of Late Cretaceous volcanic islands geochemically associated with intra-plate basaltic volcanism. During much of the Cenozoic, these islands have been submerged, accumulating thin marine deposits with interruptions in deposition by episodes of localised volcanism (Table 2.1 and Figs 2.3, 2.4A). A shift to terrigenous provenance sediments indicates that the islands have probably been emergent since the Late Pliocene (Campbell et al., 1993).

Table 2.1: Summary of the Chatham Island volcanic units (after Campbell et al., 1993)

Summary of Chatham Island Volcanics			
Volcanic units	**Age**	**Lithology/Description**	**Environment/Structure/Abundance & Distribution**
KAREWA GROUP			
Rekohu Ash Shower Member	late Haweran; (Late Pleistocene)	Oruanui eruption of Lake Taupo, North Island, New Zealand, 22 590 +/- 230 ^{14}C years B.P. (26.5 ka calander years)	distal air fall ash, source Taupo, North Island 800 km to the northwest Chatham Island, wide-spread horizon of Moorland Peat
MAIRANGI GROUP			
unnamed Pliocene volcanics	late Opoitian; (Early Pliocene)	lapilli & breccia tuff & basaltic dykes, with xenoliths of Southern Volcanics & Te Whanga Limestone	submarine?, forms Southeast Island & Star Keys islands, east of Pitt Island
Pyramid Phonolite	Mangapanian; (Late Pliocene)	fine-grained alkaline, sanidine phenocyrsts in trachytic groundmass (sanidine, aegirine, sodalite, minor nepheline, patches of zeolite)	subaerial?, phonolite plug-dome, The Pyramid islet c. 9 km south of Pitt Island
Whenuataru Tuff	late Opoitian-Waipipian; Mangapanian?; (Early-Late Pliocene)	fossiliferous, calcareous, well-bedded volcaniclastic sand-silt, coarse, blocks & bombs palagonitic (crystal, lithic), limburgitic basalt tuff	marine deposition in mid to inner shelf depths, northernmost Pitt Island and Mangere Island
Rangiauria Breccia	late Tongaporutuan-early Kapitean; (Late Miocene)	limburgitic basalt, pyroclastic breccia	submarine & subaerial, eruptive centres along west Pitt Island, Rangiauria Head, Waihere Head & south-west Mangere Island
Momoe-a-toa Tuff	early Opoitian; (Early Pliocene)	fossiliferous, hornblende-rich, limburgite basalt, fine-coarse volcaniclastic sandstone & tuff	submarine deposition in near shore, mid to inner shelf depths, source from Rangitihi Volcanics eruptive centres, northern Chatham Island
Rangitihi Volcanics	Kapitean?-early Opoitian; (Late Miocene?-Early Pliocene)	extrusive & intrusive agglomerate & scoriaceous limburgitic basalt (basic alkaline)	submarine & subaerial eruptive, Maunganui & Cape Young edifices, & The Sisters islands, northern Chatham Island
KEKERIONE GROUP			
unnamed Altonian tuff	early Altonian; (Early Miocene)	fossiliferous, calcareous, vesicular glassy or hypocrystalline basaltic tuff	marine deposition mid to outer shelf depths, Northern Volcanics source?, rare borehole sample, northern Chatham Island
Northern Volcanics	Runangan?-Whaingaroan?; (Late Eocene?-Oligocene?)	extrusive & intrusive? agglomerate & scoriaceous limburgitic basalt (basic alkaline)	subaerial, submarine?, strombolian cone volcanoes & diatreme volcanism, northern Chatham Island
Red Bluff Tuff	late Teurian-late Waipawan; (Late Paleocene-Early Eocene)	basaltic, calcareous, palagonitic tuff with beds of lapillistone & tuff-breccia	submarine mid-shelf to upper bathyal depths, localised volcanic mounds?, central & northern-south Chatham Island, northern Pitt Island
TIORIORI GROUP			
Takatika Grit	Haumurian-Teurian; (Late Cretaceous-Paleocene)	minor volcanogenic inclusions, (altered basic or intermediate), Red Bluff Tuff? or Kahuitara Tuff?	submarine, mid-outer shelf depths, Tioriori, northern Chatham Island
PITT ISLAND GROUP			
Southern Volcanics	Piripauan-Haumurian; (Late Cretaceous)	extrusive alkali olivine basalts (hawaiites), interbedded scoriaceous-tuffaceous sediments; minor intrusive trachyandesites & trachytes, basalt-trachybasalt-trachyte dykes & sills	subaerial stratovolcano with minor marine elements, forms most of southern Chatham and Pitt Islands
Kahuitara Tuff	Piripauan-Haumurian; (Late Cretaceous)	basaltic sandstone-grit, scoriaceous conglomerate & lapilli tuff; alkali basalt bombs & blocks interbedded with pillow breccia	inner shelf deposition, relatively common in north & central Pitt Island
WAIHERE BAY GROUP			
Tupuangi Formation	Motuan to Teratan; (mid to Late Cretaceous)	volcaniclastic marine sediments (uppermost beds, passes gradationally into Kahuitara Tuff)	fluvial, estuarine, abundant in northern Pitt Island

CHAPTER 3
Chatham Islands Limestone Stratigraphy

A number of workers have conducted detailed work on the geology and stratigraphy of the Chatham Islands, but notably Hay et al. (1970) and Campbell et al. (1988, 1993). It is intended that this chapter recalls the more important aspects of their work as it relates to limestone occurrences on the Chatham Islands, as well as contributing to the understanding of the limestones by including new field information made by me on trips to the Chatham Islands in 2005 and 2006. All grid references cited come from the NZMS 260, 1:50,000 Chatham Islands Sheet 1 (CH1) and Sheet 2 (CH2).

A useful time-space diagram summarising the distribution of lithological units on Chatham and Pitt Islands was prepared by Campbell et al. (1993) and has been adapted here to emphasis the occurrence of limestone on these islands (Fig. 3.0). In the following text I will introduce the geological characteristics of the main limestone occurrences on the Chatham Islands (i.e. Haumurian, Matanginui, Te One, Taoroa, Motarata and Onoua limestones), followed by brief mention of the other more minor occurrences.

Large panel diagrams showing the limestone stratigraphy at different localities on the Chatham Islands, and their lateral correlations, are included as Enclosures 1 and 2 in this thesis. For reader convenience, smaller versions of these are also reproduced at the end of this chapter (on pages 79 and 81) and can be folded out for viewing while reading the chapter. Additionally, Table 3.1 near the end of the chapter summarises aspects of the limestone stratigraphy.

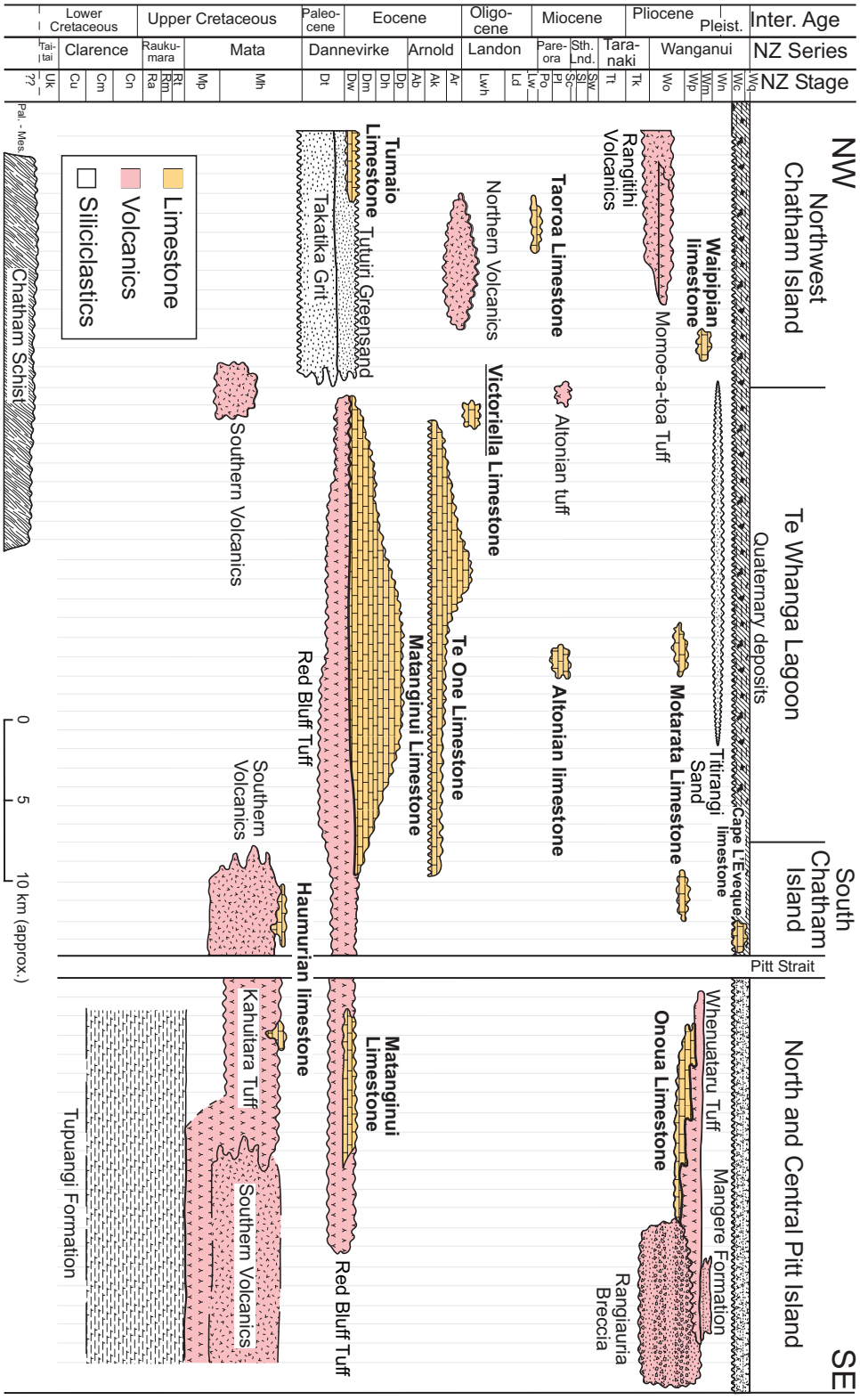

Figure 3.0: Distribution of limestones in the Chatham Island stratigraphy. Note the inclusion of the Pleistocene aged Cape L'Eveque limestone (adapted from Campbell et al., 1993; Wood et al., 1989).

3.1 Main limestone occurrences

3.1.1 Haumurian limestone

Name and definition

The Haumurian limestone here is the 'unnamed Haumurian limestone' of Wood et al. (1989) and Campbell et al. (1988, 1993), but with a simplification of the name by omission of 'unnamed'. The Haumurian limestone was not noted by Hay et al. (1970) or Grindley et al. (1977), but the limestone is the basis of a paleontological paper by Strong and Edwards (1979). The Haumurian limestone is recorded as a minor, non *in situ* constituent of the Kahuitara Tuff on Pitt Island (Figs 3.1, 3.2) and the Southern Volcanics on Chatham Island (Figs 3.5, 3.6) (Campbell et al., 1988, 1993).

Reference sections

The occurrences of Haumurian limestone on both islands are extremely localised, namely at Flowerpot Bay on Pitt Island (Fig. 3.1; CH2/708233) and Ngakuha Reef on Chatham Island (Fig. 3.5; CH1/433539). The limestone is not a mappable unit, so that no type section exists. Flowerpot Bay and Ngakuha Reef can be treated as reference sections for these localised limestone occurrences.

Distribution and thickness

On Pitt Island the Haumurian limestone appears in fissures that range in thickness from a cm or two up to 20 cm within an intertidal sea platform on the western side of the wharf at Flowerpot Bay (Figs 3.1, 3.2). On Chatham Island the Haumurian limestone is preserved as interstitial fills within alkaline olivine pillow basalts of the Southern Volcanics, which form the Ngakuha Reef promontory situated on the west coast, 2.5 km southwest of Waitangi (Figs 3.5, 3.6). There may also be an occurrence of the Haumurian limestone somewhere along the southern coast of Chatham Island near Cascade Gorge, where carbonate cobbles accumulate along the shoreline, although no *in situ* source has been found (Fig. 3.9). The cobbles are extremely hard and highly polished, with some being highly coloured and patterned, making them very collectable and apparently highly prized by the Moriori people (Fig. 3.9) (H.

Campbell, GNS Science, pers. comm., 2006). The cobbles are thought to either be the product of hydrothermal precipitation or alteration of biogenic limestone associated with the Late Cretaceous Southern Volcanics (Campbell et al., 1993).

Contacts

The fissure fills of Haumurian limestone on Pitt Island occur within the Late Cretaceous Kahuitara Tuff which forms a gently dipping coastal platform. Here the Kahuitara Tuff is considered to be part of a small fault block uplifted a few metres and bounded by northeast trending faults (Strong, 1979; Campbell et al., 1993). The character of the Kahuitara Tuff is somewhat different to its type at this locality, it comprising finer volcaniclastic material and being slightly calcareous due to the presence of foraminiferal microfossils indicative of shallow water (5-50 m) deposition. The Kahuitara Tuff is unconformably overlain by Early Paleogene Red Bluff Tuff (Strong and Edwards, 1979; Strong, 1979; Campbell et al., 1988, 1993), but is locally overlain also by the Matanginui Limestone at this locality, due to the up-throw of the Kahuitara Tuff, with the Matanginui Limestone infilling pockmarks and holes upon a possible ravinement surface on the Kahuitara Tuff (Fig. 3.4).

The Chatham Island occurrence at Ngakuha Reef (Pukekio-Waikaripi coastline) appears as fill material within early Haumurian (Grindley *et al.*, 1977) pillow basalts of the Southern Volcanics (Figs 3.5, 3.6, 3.7). These olivine pillow basalts sit in the upper stratigraphic levels of the Southern Volcanics which are unconformably overlain by Red Bluff Tuff (Strong and Edwards, 1979; Campbell et al., 1988, 1993).

Lithologies

There is a considerable difference in lithology between the Pitt and Chatham Island sites. The Pitt Island occurrence has previously being described as a homogenous, pale grey, hard, non-tuffaceous, saccharoidal limestone, while the Chatham Island example is described as being a more indurated micritic limestone with inclusions of subangular and subrounded pebbles and granules (Strong and Edwards, 1979; Campbell et al., 1988, 1993).

The Haumurian limestone filling fissures within the Kahuitara Tuff on Pitt Island is most commonly pale grey to brown (weathered) and fine grained, but also appears as a fine conglomerate of rounded pebble sized lithoclasts within a fine, white to pale grey limestone matrix. This second, less common conglomerate fissure fill from the Flowerpot Bay locality is very similar to the carbonate conglomerate material that is associated with pillow basalts of the Southern Volcanics at Ngakuha Reef on Chatham Island. At both Ngakuha Reef and Flowerpot Bay the lithic inclusions appear to be mixed sedimentary and igneous lithologies, and are rounded to subrounded, although at Ngakuha Reef the inclusions are more angular and include some much larger cobbles and boulders of basalt (Figs 3.3, 3.7).

Paleontology

The main fossil groups are foraminifera, calcareous nannofossils and bivalves. Micropaleontological work by Strong and Edwards (1979) identified a number of Upper Haumurian (late Maastrichtian) index foraminifera and nannofossils. Identification of microfossils was only possible on the Pitt Island samples as the Ngakuha Reef material from Chatham Island was too indurated to allow any fossil extraction. The occurrence of planktic and benthic foraminifera was, however, noted in thin section, along with other microfossil fragments, but there were no obvious nannofossils (Strong and Edwards, 1979; Campbell et al., 1988, 1993).

The Haumurian limestone at Flowerpot Bay on Pitt Island was noted to be associated with echinoderm fragments and spines, while sponge spicules, pectinids, bryozoans, echinoderms and serpulids are noted in outcrops at Ngakuha Reef (Fig. 3.8).

Age

Association with the Southern Volcanics and some key microfossils imply a latest Cretaceous age, in the Upper Haumurian based on the presence of foraminifera *Bolivina* cf. *incrassata*, *Bolivinoides draco dorreeni*, *Gaudryina healyi*, *Nuttallides* cf. *tholus*, *Patellina piripaua*, *Hedbergella monmouthensis*, *Globigerinelloides volutus* and *Rugoglobigerina rugosa*, and

the calcareous nannofossil *Nephrolithus frequens* (Strong and Edwards, 1979; Campbell et al., 1988, 1993).

Depositional environment

Identification of the benthic foraminifera *Anomalina*, *Colomia*, *Florilus*, *Gravelinella* and *Patellina*, coupled with the sparseness of slope faunal species, suggests an outer shelf (100-200 m) depositional environment for the carbonate source of the non *in situ* Haumurian limestone dykes. The high abundance of foraminifera relative to calcareous nannofossils may represent selective sorting by bottom currents within this allochthonous dyke limestone (Strong and Edwards, 1979). The overlying Red Bluff Tuff represents a mid-shelf depositional environment and Strong and Edwards (1979) suggest that a rapid uplift event was related to localised tectonics associated with volcanism in the latest Cretaceous to earliest Paleogene time (Campbell et al., 1988, 1993).

Figure 3.1: Locality of the Haumurian limestone on the eastern side of the wharf at Flowerpot Bay, Pitt Island (CH2/708233). The foreground platform is a localised uplifted block of Kahuitara Tuff which is criss-crossed with sinuous fissure fills of the Haumurian limestone. In the central left-hand corner of the picture Cam Nelson (white shirt) is crouched down inspecting the overlying contact with the Matanginui Limestone (Noel James mid-foreground with Jeremy Titjen frontmost). Beyond the wharf in the background (top right-hand corner of the image) is The Bluff of lower dipping beds of Red Bluff Tuff overlain by horizontal beds of Whenuataru Tuff.

Figure 3.2: The sea platform of Kahuitara Tuff on the eastern side of the wharf at Flowerpot Bay on Pitt Island with sinuous and bifurcating fissure fills of Haumurian limestone. Brian Jones pictured in the top right-hand corner for scale.

Figure 3.3: Two different fill types of the Haumurian limestone on Pitt Island. The top right photograph is the typical fine-grained pale grey to brown limestone, while the lower photo is the fine granular conglomeratic fill with inclusions of numerous gravel to pebble sized lithics of both sedimentary and igneous origin.

Figure 3.4: Matanginui Limestone infilling depressions within the Kahuitara Tuff at Flowerpot Bay, Pitt Island.

Figure 3.5: The Chatham Island location of the Haumurian limestone at Ngakuha Reef (CH1/432540) on the western shoreline, 2.5 km southwest of Waitangi. The Ngakuha Reef promontory is made up of pillow basalts of the Southern Volcanics which also stretch from this point along the southwestern coast toward Point Durham. The white colouration is not limestone but an algal weathering growth on the outer surface of the pillow basalts.

Figure 3.6: The Haumurian limestone at Ngakuha Reef has infilled the spaces between the individual pillows, cementing smaller brecciated boulders and cobbles of the basalt as well as fossiliferous material and more rounded lithic pebbles and cobbles.

Figure 3.7: Lithic inclusions within Haumurian limestone at Ngakuha Reef include angular boulders and cobbles of basalt as well as other angular to subangular, pebble to cobble sized lithics.

Figure 3.8: Fossil material observed in the Haumurian limestone at Ngakuha Reef, Chatham Island. **A** shows an unknown pectinid species; **B** serpulid tube; and **C** possible crinoid stem (Echinodermata).

Figure 3.9: Cascade Gorge (CH2/474384) on the central southern coastline of Chatham Island, where pebbles of possibly hydrothermally altered limestone that may correlate to the Haumurian limestone accumulated on the gravel strewn beach. Samples of the variably coloured and textured limestone collected by local resident Moana King.

3.1.2 Matanginui Limestone

Name and definition

Original definitions by Hay et al. (1970) and Austin et al. (1973) have the Matanginui Limestone along with the Te One Limestone grouped and collectively known as the Te Whanga Limestone. Subsequent work on the Te Whanga Limestone by Campbell et al. (1988) showed that there were two lithologically distinctive limestones within the Te Whanga Limestone, a lower named the Matanginui Limestone Member (packstone) which in places is overlain by the Te One Limestone Member (grainstone). The name Te Whanga Limestone was retained by Campbell et al. (1988) and used wherever differentiation between the two members was uncertain and as the name of the formation that contains the two members. The Te Whanga Limestone formation of Campbell et al. (1988) replaces the Matanginui, Te Whanga, Te One and Flowerpot limestones of Hay et al. (1970) (Campbell et al., 1993). For convenience in this thesis the use of the word member is omitted when referring to the Matanginui and Te One Limestones, and their undifferentiated equivalents are referred to as Te Whanga Limestone.

Campbell et al. (1988, 1993) describe the Matanginui Limestone as a soft, white, poorly bedded bryozoan-echinoid-foraminiferal-bivalve packstone, that is distinguished from the Te One Limestone by the presence of the large benthic foraminifera *Asterocyclina* (see Fig. 4.9C) and large echinoid spines of *Eucidaris strobilata* (Fig. 3.10). Grain size and other bioclastic types were also used by Campbell et al. (1988, 1993) to distinguish the two limestones, although the exact criteria are not mentioned.

The name Matanginui Limestone derives from limestone outcrops described by Hay et al. (1970) at the mouth of the Matanginui Stream on the western shore of Te Whanga Lagoon. Additionally, Campbell et al. (1988, 1993) included as Matanginui Limestone the Te Whanga and Flowerpot Limestones of Hay et al. (1970) from Pitt Island.

Type and reference sections

The type section for the Matanginui Limestone is situated on the northwestern coast of Te Whanga Lagoon, extending from the mouth of Waipapa Creek (CH1/451755) south towards the bluffs near the mouth of Blind Jims Creek (CH1/454745) (Campbell et al., 1988) (Fig. 3.11, Enclosures 1 & 2 - Column 4). The contact with the overlying Te One Limestone was observed at Moreroa on Chatham Island (CH1/481653) (Fig 3.12, Enclosures 1 & 2 – Column 6), while thick cyclic successions of Matanginui Limestone were observed at Rocky Side on Pitt Island (CH2/689224-2689224) (Fig. 3.16, Enclosures 1 & 2 – Column 11).

Distribution and thickness

On Chatham Island the Matanginui Limestone crops out discontinuously along the northwestern shoreline of Te Whanga Lagoon. The northernmost exposure is in a tributary of the Waitaha Creek with occurrences stretching south along the coast to Moreroa (Fig. 3.12). A single isolated outcrop occurs south of Moreroa at Whareama (Fig. 3.13). Average thicknesses on Chatham Island are about 25 m. Matanginui Limestone also occurs on the western oceanic coastline of Chatham Island at Red Bluff (also known as Te Whenuhau) where it interfingers with and overlies the Red Bluff Tuff, draping the volcanic mound of Red Bluff (Fig. 3.14). The Matanginui Limestone at Red Bluff becomes progressively thicker to the north and south (from 1 m up to 15 m), which is effectively down-slope of the Red Bluff volcanic mound, and also occurs as carbonate dykes within the Red Bluff Tuff which have been interpreted as fissure fills by Campbell et al. (1993) (Fig. 3.14).

On Pitt Island the Matanginui Limestone is associated with exposures of the Red Bluff Tuff and is most prevalent in the northwest corner of the island along the Tarawhenua Peninsula, with a maximum thickness of 35 m at Rocky Side and Smugglers Cove (Fig. 3.16, Enclosures 1 & 2 – Columns 11 & 13). Matanginui Limestone tends to thin to the east and west of Rocky Side, occurring as interfingering lenses within the Red Bluff Tuff (Fig. 3.15). Easternmost outcrops of Matanginui Limestone occur to the south of Lake Tupuangi (Campbell et al., 1993).

Contacts

On Pitt Island the Matanginui Limestone interfingers or conformably overlies the Red Bluff Tuff (Fig. 3.17), as it does on Chatham Island (Fig. 3.14), and is disconformably overlain by (Pliocene) Onoua Limestone with a sharp contact (Fig. 3.18) (Campbell et al., 1993).

On Chatham Island the Matanginui Limestone is disconformably overlain by the Te One Limestone at some of the outcrops along the north-western shore of Te Whanga Lagoon. The contact between these two units is conspicuously sharp at Moreroa and Blind Jims Creek (Figs 3.11, 3.12, Enclosures 1 & 2 – Columns 4 & 6), showing micro-relief, while the contact at Cattle Point is strongly eroded with infilling by Te One Limestone that has inclusions of quartz, schist and phosphatised limestone pebbles. At Waitaha Creek the Te One Limestone is absent and the Matanginui Limestone is locally disconformably overlain by the *Victoriella* Limestone of Early Oligocene age (Fig.3.37; Enclosure 1 & 2 – Column 2). Te One Limestone is also absent in southern exposures where the Matanginui Limestone is instead disconformably overlain by the Motarata Limestone across a sharp contact with minor relief (Campbell et al., 1993). The distribution of large indurated Matanginui Limestone blocks at Whareama morphologically suggests that this contact could have been a considerably irregular one from which the soft and friable Motarata Limestone has been subsequently eroded out (Fig. 3.13; Enclosure 1 & 2 – Column 9).

Lithologies

Campbell et al. (1988, 1993) describe the Matanginui Limestone on Chatham Island as typically a white or yellowish packstone with skeletal types (decreasing in abundance) of bryozoans, echinoids, foraminifera, brachiopods and bivalves. The lower 1-3 m of some sections are reported to contain inclusions of subrounded to rounded pebbles and cobbles of schist, quartz, tuff (maybe limonite encrusted), basalt (age correlatives indicate either the Red Bluff Tuff or the Northern Volcanics in part) and claystone. Very glauconitic sections are noted from Waimahana Creek and Moreroa on Chatham Island (Campbell et al., 1993). At Moreroa a prominent hardground has formed along the contact with overlying Te One Limestone preserving

conspicuous serpulids which are infilled with a glauconitic, medium sand sized bioclastic hash (Fig. 3.12).

Grain sizes coarsen near the stratigraphic top and bottom and show better sorting of bioclasts as the typical packstone grades into a grainstone. Within these upper and lower grainstone zones there is also usually a marked increase in the content of the benthic foraminifera *Asterocyclina* or of brachiopods, bryozoans and barnacles, and sometimes bivalves. These zones are bedded at dm-cm scale with some cm scale cross bedding. In general, however, the bulk of the Matanginui Limestone is massive, likely a result of extensive bioturbation as is clearly evident, for example, at the top of the unit at Moreroa (Fig. 3.12, Enclosures 1 & 2 – Column 6) (Campbell et al., 1993).

In contrast to the dominance of packstone on Chatham Island, Pitt Island exposures of Matanginui Limestone are more usually a moderately indurated and porous grainstone. Dominant skeletal components include bryozoans, echinoderms and benthic foraminifera, with oysters recorded from rubbly weathered horizons in some sections (Fig. 3.10, 3.16).

Paleontology

A variety of foraminifera, calcareous nannofossils, bryozoans, brachiopods, bivalves, gastropods, barnacles, echinoderms, vertebrate remains (teeth) and trace fossils are recorded from the Matanginui Limestone by Campbell et al. (1993).

The main skeletal fragments in the limestones include bryozoans, brachiopods, bivalves, barnacles and echinoderms. The echinoderm *Eucidaris strobilata* is the most abundant macrofossil within the Matanginui Limestone. Brachiopods and molluscs (*Spondylus*) are most prevalent near the base of outcrops, especially at Waipapa Creek on Chatham Island, and Flowerpot Bay and Rocky Side (Fig. 3.16, Enclosures 1 & 2 – Column 11) on Pitt Island (Campbell et al., 1993).

The large benthic foraminifera *Asterocyclina speighti* can be used to help differentiate the Matanginui Limestone from the overlying Te One Limestone (Fig. 4.9C) and is big enough to be readily identifiable with a hand

lens in the field. *Asterocyclina* is present in Matanginui Limestone on both Chatham Island and Pitt Island.

Age

Ages for the Matanginui Limestone based on foraminiferal assemblages described by Campbell et al. (1993) range from the Early to Middle Eocene (Waipawan to Bortonian). On Pitt Island the ages are similar to the enclosing Red Bluff Tuff and probably range from the Paleocene to Early Eocene (late Teurian to Mangaorapan). On Chatham Island the oldest ages are Waipawan from outcrops at the northernmost Waitaha Creek and southernmost Whareama exposures (Fig. 3.13), with the exposed Matanginui Limestone progressively becoming younger toward a central point south of Matanginui Creek, where a Mangaorapan age exits. The youngest Chatham Island age is Porangan at Waimahana Creek (Campbell et al., 1993).

Depositional environment

Campbell et al. (1993) suggested that the Matanginui Limestone probably formed in warm waters based on the occurrences of macrofossils such as the bivalve *Spondylus*, the brachiopods *Probolarina*, *Thecidellina* and *Lingula*, and also the large spined echinoid *Eucidaris*. The large benthic foraminifera *Asterocyclina* also suggests warm water (probably cool subtropical), but is also known to be restricted to the euphotic zone. This coupled with the occurrence of the deeper water mollusc *Acesta* may indicate that beds with *Asterocyclina* are representative of changes in water depth, from outer shelf to shallower (euphotic zone) mid shelf depths, respectively (50-200 m).

Figure 3.10: Close-up field shot of the Matanginui Limestone from Rocky Side (CH2/688225-689224), on the southwest coast of the Tarawhenua Peninsula, northwestern Pitt Island. Abundant echinoid spines and bryozoans.

Figure 3.11: Outcrops of Matanginui Limestone near Blind Jims Creek (CH1/454745), mid-way between Waipapa Creek (CH1/451755) mouth and Cattle Point on the northwestern shore of Te Whanga Lagoon, Chatham Island. Scattered scrappy outcrops occur along the north-western shoreline but become more 'bluff-like' toward Cattle Point. Here, the upper section is possibly the overlying Te One Limestone. Jeremy Titjen standing to the left of the blocks for scale,

Figure 3.12: Outcrop at Moreroa (CH1/481654) showing the prominent hardground contact (pointed to by Jeremy Titjen) between the Matanginui Limestone and the overlying Te One Limestone. The contact point is a highly burrowed and cemented hardground up to 20 cm thick.

Figure 3.13: Large remnant block of Matanginui Limestone at Whareama (CH1/512558) near Te Matarae, at the southern end of Te Whanga Lagoon. Here the Matanginui Limestone overlies Red Bluff Tuff and is overlain itself by the Motarata Limestone. The position of the remnant blocks of Matanginui Limestone (indurated) suggest that the Motarata Limestone (soft) possibly infilled embayments in the Matanginui Limestone. Jeremy Titjen for scale.

Figure 3.14: Matanginui Limestone draping and inter-fingering with the volcanic mound forming Red Bluff (CH1/465612), on the western coastline of Chatham Island. The dashed line indicates the local contact between Matanginui Limestone (above) and Red Bluff Tuff. The arrows indicate the position of a large carbonate dyke of Matanginui Limestone.

Figure 3.15: Matanginui Limestone lenses (upper section) within Red Bluff Tuff at Waihere Bay (CH2/710205) on the northwestern coast of Pitt Island.

Figure 3.16: Outcrop of Matanginui Limestone on the Tarawhenua Peninsula, northwest Pitt Island. Top photograph is Rocky Side (CH2/688225-689224) on the west coast while the lower outcrop is only 200 m to the north and known locally as Smugglers Cove (or Boat Harbour, CH2/692227) at a thin point near the end of the peninsula. In the upper Rocky Side photo Hamish Campbell appears three times for scale.

Figure 3.17: Rocky Side (CH2/688225-689224) on the Tarawhenua Peninsula, Pitt Island, looking southeast. Dipping beds of lower pale brown Kahuitara Tuff (below white dashed line) are unconformably overlain by thin truncated beds of Red Bluff Tuff which in turn are conformably overlain by the Matanginui Limestone (red arrowed.

Figure 3.18: Onoua Limestone sharply and disconformably overlies the Matanginui Limestone on the northwestern Pitt Island coastline at the beginning of the Tarawhenua Peninsula (CH2/700233). Jeremy Titjen is standing on the planar surface of the Matanginui Limestone in the centre right of the photograph.

3.1.3 Te One Limestone

Name and definition

The Te One Limestone was first described by Hay et al. (1970) and later redefined by Campbell et al. (1988, 1993) as a member of the Te Whanga Limestone. The Te One Limestone Member included most Chatham Island occurrences previously defined as the Te Whanga Limestone by Hay et al., (1970), with the exception of those where differentiation between Matanginui and Te One limestone members was not possible, in which case the Te Whanga Limestone designation remains.

Type section

The type section for the Te One Limestone occurs at Ohuru on the western shore of Te Whanga Lagoon (CH1/497618-495619) (Enclosures 1 & 2 – Column 8).

Distribution and thickness

Te One Limestone is only known to occur on Chatham Island where it extends from Waipapa Creek in the north, to Ohuru in the south and west to Big Bush (Fig. 3.19). Some occurrences of more lithified Te Whanga Limestone at the northern and southern end of Te Whanga Lagoon (Papapohatu Point and Te Matarae, respectively) are cited as being possible undifferentiated Te One Limestone equivalents (Campbell et al., 1993).

Thicknesses range from 14 m at the type section at Ohuru to 25 m at Big Bush Quarry (Fig. 3.19, Enclosure 1 & 2 – Column 7). From the thickest point in the vicinity of Big Bush Quarry and Moreroa (12-15 m, Fig. 3.12), the Te One Limestone thins toward its northern and southern extents where it is <5 m thick.

Contacts

Te One Limestone disconformably overlies either the Red Bluff Tuff or the Matanginui Limestone (Fig. 3.11, 3.12). The upper surface of the Te One limestone is exposed over the shore platform near the Inia William Tuuta Memorial Aerodrome, stretching from Karewa Point to Moutapu Point (Fig. 3.20). Here Te One Limestone is disconformably overlain by the Late Pliocene Titirangi Sand or by the Pliocene Motarata Limestone in some places at Moutapu Point alone (Fig. 3.29). However, prior to deposition of these young units, the surface registers a very complex depositional/diagenetic evolution involving, among other features, boring, encrustation (including by stromatolites) and iron-manganese impregnation. This highly condensed section appears to represent a history of multiple hardground development during the mid-Tertiary, a topic being addressed elsewhere by Noel James (pers. comm. 2005)

Lithologies

In outcrop the Te One Limestone is white to pale grey, but increasingly yellowish to orange where highly weathered. The limestone can be either soft (Fig 3.21) or consolidated (Fig. 3.20) in outcrop, although the latter may simply reflect a degree of case hardening during weathering. Lithologies are typically porous, massive and moderately well sorted. Some outcrops show development of crude 2-8 m scale bedding at upper stratigraphic levels, with some graded beds noted at Kaiparakau and prominent cross bedding in 0.2-0.8 m thick sets at Ohuru (Fig. 3.22), Papapohatu Point and Te Matarae. Dips on the internal stratification range from 20-35°, and local bi-directional orientations implicate dune migration under the influence of tidal currents (Fig. 3.22, Enclosures 1 & 2 – Column 7).

Te One Limestone is a fragmental bryozoan grainstone with subordinate bivalve and echinoid material (Fig. 3.23). Also noted at some localities is the occurrence of coarse bands of pebble sized bioclasts of oysters, barnacles and brachiopods, with glauconite and pebbles and cobbles of subangular quartz, schist, basalt, phosphatised tuff and grainstone (presumably limestone intra- or extra-clasts), along with shark teeth and fish bones recorded near the base of some sections (Campbell et al., 1993).

Paleontology

In general there is less macrofossil material in Te One Limestone than in the Matanginui Limestone, although the same assemblages are present in both limestones. The most notable difference in the Te One Limestone is the absence of the echinoderm *Eucidaris strobilata*. There is also less diversity amongst the brachiopod and molluscan species. Barnacles are noted to be locally very common at the Ohuru outcrop (Campbell et al., 1993).

Age

Key fauna give a Kaiatan to early Whaingaroan age (Late Eocene to Early Oligocene) (Campbell et al., 1993).

Depositional environment

The assessment of depositional environment is based mainly on benthic foraminiferal assemblages and abundances, which suggest mid to outer shelf depths on a shallow marine platform, despite the presence of quite common planktic foraminifera (Campbell et al., 1993).

Figure 3.19: Te One Limestone exposed at Big Bush Quarry (CH1/472629), central west Chatham Island. Noel James (circled) in the centre of the quarry floor for scale.

Figure 3.20: Top of the Te One Limestone exposed from Karewa Point (CH1/544712) to Moutapu Point (CH1/520698) along the western shoreline of Te Whanga Lagoon. The exposed surface is a hardground with conspicuous stromatolite encrustations and a condensed and complex depositional and diagenetic paragenesis. Jeremy Titjen for scale.

Figure 3.21: Te One Limestone at Big Bush Quarry has virtually no cementation and, once the case hardened surface has been broken, pours freely from Brian Jones hands.

Figure 3.22: Te One Limestone at Big Bush Quarry showing crude bedding (both foreground and background outcrops) with obvious cross-beds in the foreground outcrop. Hammer (circled) for scale.

Figure 3.23: Close-up of the Te One Limestone at the Big Bush Quarry showing a very porous coarse grainstone with abundant bryozoan and echinoid fragments.

3.1.4 Taoroa Limestone

Name and definition

The Taoroa Limestone was originally mapped and described by Hay et al. (1970) as the Te One Limestone. Later work by Grindley et al. (1977) on the faunal assemblages suggested that the Taoroa Limestone was comparable in age to, and a stratigraphic correlative of, the Momoe-a-toa Tuff. Further sampling and analysis by Campbell et al. (1988) showed that the sample examined by Grindley et al. (1977) was a considerably coarser, burrowed, foraminiferal packstone that formed a diffuse, gradational disconformity over the uppermost 0.5 m of the outcrop that was significantly younger then the underlying unit (Fig. 3.25). Because of the distinctiveness of this underlying unit, Campbell et al. (1988) gave the unit formal recognition as the Taoroa Limestone Lithofacies, the Taoroa name being derived from the area at the western end of Manganui Beach, northern Chatham Island. For the purpose of this thesis the use of the name 'lithofacies' is omitted from the formal name designated by Campbell et al. (1988), and the unit is simply referred to as the Taoroa Limestone.

Type section

The type section corresponds to its limited distribution at the western end of Manganui Beach, northwestern Chatham Island (CH1/283760) (Campbell et al., 1988, 1993) (Fig. 3.24, Enclosures 1 & 2 – Column 3).

Distribution and thickness

The Taoroa Limestone is restricted in distribution to outcrops in the coastal cliffs at the western end of Manganui Beach, northwestern Chatham Island (Fig. 3.24). Here the unit is no more then 4 m in thickness, with the upper 0.5 m of the unit being an unnamed limestone (Fig. 3.25) that is chronologically and stratigraphically a correlative to the Momoe-a-toa Tuff. Preservation of this small outcrop is due to burial by basaltic lava flows of the overlying Rangitihi Volcanics, now all exposed by coastal erosion (Fig. 3.24, Enclosures 1 & 2 – Column 3).

Contacts

The lower contact of the Taoroa Limestone is not exposed. The Taoroa Limestone is overlain disconformably by a thin bed of unnamed Pliocene limestone which in turn is overlain by basaltic lavas and pillow basalts of the Rangitihi Volcanics (Fig 3.24, 3.25, Enclosures 1 & 2 – Column 3). The upper contact with the unnamed Pliocene limestone is diffuse because of bioturbation (Fig. 3.25, Enclosures 1 & 2 – Column 3).

Lithologies

In general, the Taoroa Limestone is a white to yellowish, soft to consolidated, massive, slightly sandy and glauconitic, bryozoan-foraminiferal rich, fine grainstone and packstone (Campbell et al., 1993).

The Taoroa Limestone is at least 4 m thick at the type locality (Fig. 3.27, Enclosures 1 & 2 – Column 3). About 2 m below this upper exposure is a very white, chalky, micro-bioclastic limestone (Fig. 3.26). It is unclear whether these lower blocks are *in situ*, or are simply fall blocks from the upper exposure, but the former is most likely. This lower exposure resembles a brecciated block flow with apparent folded flow structures present and with vaguely bedded horizontal structures near the top of the exposure (Fig. 3.26).

The overlying 4 m type section is predominantly an abraded bryozoan-echinoderm fine grained packstone with a very fine grained micro-bioclastic matrix. Vague bedding is present throughout the lower 2 m of the section and appears to be very low angle, planar cross-bedding (Fig. 3.27). The overlying, upper 2 m appears more massive, although extremely vague cross-bedding remains. The uppermost 0.5 m is extremely burrowed, with the overlying unnamed Pliocene limestone infilling the burrowed upper surface of the Taoroa Limestone (Fig. 3.25, Enclosures 1 & 2 – Column 3). The unnamed Pliocene limestone is lithologically distinct from the Taoroa Limestone, being a glauconitic, coarse bioclastic packstone with conspicuous brachiopods, serpulids and volcanic clasts, and forms a sharp to diffuse contact with the Taoroa Limestone (Fig. 3.25).

Paleontology

The main skeletal types include foraminifera, calcareous nannofossils, bryozoans, echinoderms and trace fossils. A macrofossil previously collected from the Taoroa Limestone locality was the echinoid *Taimanawa* cf. *greyi* (Hutton, 1873 in Campbell et al., 1993) in a glauconitic zone 0.3 m from the upper contact with the unnamed Pliocene unit. On the recent 2006 excursion, an as yet unidentified pectinid was collected from a similar position near the upper contact.

Age

Key fauna indicate a Waitakian (Early Miocene) age (Campbell et al., 1988, 1993).

Depositional environment

Benthic foraminiferal assemblages indicate mid to outer shelf depositional depths with common planktic foraminifera indicating an open ocean setting (Campbell et al., 1993).

Figure 3.24: The Taoroa Limestone at the southwestern end of Manganui Beach (CH1/283760), north-west Chatham Island, is overlain by lava flows and pillow basalts (elsewhere) of the Rangitihi Volcanics along this coastline of the Manganui edifice. Jeremy Titjen for scale.

Figure 3.25: Uppermost 0.5 m section of the Taoroa Limestone outcrop showing the coarse, yellowish unnamed Pliocene limestone infilling burrows (circled) and the irregular surface upon the much finer, white Taoroa Limestone.

Figure 3.26: Outcrops of limestone below the main Taoroa Limestone section. Morphologically the outcrop resembles a brecciated block flow (lower 1.5 m) with some folded flow structures (insert). Upper parts show near horizontal lamination and vague bedding. These rocks are compositionally very fine grained micro-bioclastic limestone and distinctive from the overlying Taoroa Limestone.

Figure 3.27: The Taoroa Limestone is a fine grained packstone underlying a lava flow of the Rangitihi Volcanics. Low angle planar cross-stratification is present in the middle to the bottom part of the section.

3.1.5 Motarata Limestone

Name and definition

The name of the Motarata Limestone is derived from a local name for the area along the southwestern shore of Te Whanga Lagoon where the type section is situated (Fig. 3.28). The Motarata Limestone was first described by Campbell et al. (1988) as a lensoidal limestone that is similar in age to the Onoua Limestone but is considered lithologically different.

Type section

Motarata Limestone is only known from two small lensoidal occurrences on Chatham Island. The type section is at Whareama to the south of Te Matarae on the south-western shore of Te Whanga Lagoon (CH1/512558) (Fig. 3.28, Enclosure 1 & 2 – Column 9) (Campbell et al., 1988, 1993).

Distribution and thickness

Both occurrences of Motarata Limestone are known from the western shoreline of Te Whanga Lagoon. At the type section at Whareama (just 1 km south of Te Matarae) the Motarata Limestone is at least 5 m thick (Fig. 3.28). The only other known outcrop of Motarata Limestone is situated at Moutapu Point (CH1/520698) near the Inia William Tuuta Memorial Aerodrome, where it is 2.3 m thick (Fig. 3.29, Enclosures 1 & 2 – Column 5).

Contacts

The Motarata Limestone at Whareama (type section) disconformably overlies Red Bluff Tuff (Late Paleocene-Early Miocene), although this contact was not observed in 2005. The gradational contact between the Matanginui Limestone and Red Bluff Tuff was observed, however, near the shoreline at Whareama (Fig. 3.30, Enclosure 1 & 2 – Column 9) along with large isolated outcrops of Matanginui Limestone (Fig. 3.13). These outcrops morphologically suggest that the disconformable contact between the Matanginui Limestone and the Motarata Limestone is highly irregular with Motarata Limestone infilling a deeply eroded surface on the Matanginui Limestone. The contact between the Matanginui Limestone and the Motarata Limestone was not observed in 2005, but presumably has been observed by Campbell et al. (1988, 1993)

along the shoreline of Whareama, along with the direct disconformable contact between the Motarata Limestone and the underlying Red Bluff Tuff. This would further suggest that the Motarata Limestone was deposited onto a highly eroded surface, with possible erosional structures that dissect the entire thickness of the Matanginui Limestone, allowing direct deposition onto the Red Bluff Tuff. But the two different underlying contacts of the Motarata Limestone could also reflect interfingering of the Matanginui Limestone with the Red Bluff Tuff at this locality. At Moutapu Point the Motarata Limestone disconformably overlies the Te One Limestone and is itself disconformably overlain by the Titirangi Sand (Late Pliocene) (Fig. 3.29, Enclosure 1 & 2 – Column 5).

Lithologies

The Motarata Limestone is a pale yellow to brown, soft, porous, well sorted, glauconitic and sandy, fine grainstone with sparse bryozoan and echinoid fragments. The soft and fine grained nature of the Motarata Limestone is probably due to it being rich in planktic foraminifera (Fig. 3.28, 3.29). Phosphate pebbles and vertebrate remains are not well exposed at the Whareama locality, but are reported to litter the nearby lagoon shoreline and to be derived from the base of the Motarata Limestone (Campbell et al., 1993).

Paleontology

The main skeletal components of the Motarata Limestone are foraminifera, calcareous nannofossils, bryozoans, brachiopods (Fig. 3.28), bivalves, ostracods and echinoderms. Basal lag deposits in the outcrop at Whareama have yielded vertebrate teeth and bone. These vertebrate remains are considered by Campbell et al. (1993) to be considerably older then the Motarata Limestone itself and are thought to represent hiatal deposition over the entire Oligocene and Miocene time. Furthermore the phosphatic horizon from which these vertebrate remains are derived is reported by Campbell et al. (1993) to be correlative to a similar horizon known on the Chatham Rise (Cullen, 1980) and in Gippsland, Victoria, Australia (Carter, 1978).

Age

The age of the Motarata Limestone is Opoitian (Early Pliocene) based on foraminiferal assemblages (Campbell et al., 1993).

Depositional environment

The assemblage of benthic foraminifera and ostracods (large *Bradleya* species) indicate a mid to outer shelf depth setting that is fully oceanic based on the abundance of large planktic foraminifera (Campbell et al., 1993).

Figure 3.28: The Motarata Limestone within an old disused quarry (possibly Fahey's Quarry) at Whareama (CH1/512558), near the type section at Te Matarae on the southwestern shore of Te Whanga Lagoon, Chatham Island. Here the Motarata Limestone is up to 4 m thick over the whole area and the contact with the underlying Matanginui Limestone is probably very close to the quarry floor, marked by phosphatic clasts near the base of the section. George Davies for scale. The inset photo shows a discontinuous layer of brachiopods (arrowed) near the top of the section.

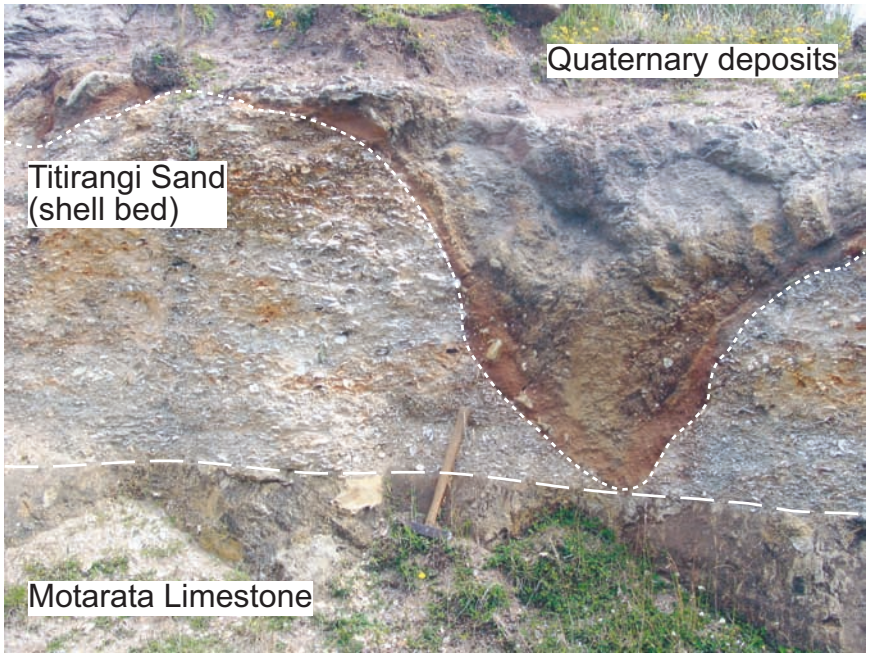

Figure 3.29: Motarata Limestone at the base of the outcrop (lowermost brown weathered unit, next to hammer head revealing yellow under weathered exterior) overlain disconformably by a shell bed of the Titirangi Sand which itself is cross-cut by a channel structure infilled with Quaternary deposits, Moutapu Point, Chatham Island.

Figure 3.30: Matanginui Limestone gradationally overlies Red Bluff Tuff at Whareama near Te Matarae, on the western shoreline of Te Whanga Lagoon, Chatham Island.

3.1.6 Onoua Limestone

Name and definition

The Onoua Limestone was first named and described by Hay et al. (1970) and its definition has remain unaltered since then. The derivation of the name is unknown.

A pale yellow, massive, soft, porous, well sorted, bryozoan grainstone (Campbell et al., 1988, 1993). The Onoua Limestone is similar to the Motarata Limestone on Chatham Island, but the Onoua Limestone has a slightly different lithology, is younger and is restricted to Pitt Island.

Type section

The type section for the Onoua Limestone is in the coastal cliffs at the northwestern end of Tarawhenua Peninsula, northwestern Pitt Island (Enclosure 1 & 2 – Column 12) (Campbell et al., 1988, 1993).

Distribution and thickness

The Onoua Limestone crops out extensively along both sides of the Tarawhenua Peninsula in northwestern Pitt Island, reaching thicknesses of 26 m at the type section, but probably greater elsewhere along the peninsula (Enclosures 1 & 2 – Column 12). The Onoua Limestone is 12 m thick in northern coastal cliffs (Fig. 3.18) and thins in an eastward direction until it is represented by lenticular deposits at Flowerpot Bay (Fig. 3.31, Enclosure 1 & 2 – Columns 13 & 14) and coastal cliffs north of The Bluff Homestead (Fig. 3.32) toward Motutapu Point, where it is 3 m thick. There are no known exposures of Onoua Limestone along the west coast of Pitt Island and the only known inland exposure is in a quarry northwest of the Pitt Island Primary School (Campbell et al., 1993).

Contacts

Onoua Limestone disconformably overlies either Matanginui Limestone (the end of Tarawhenua Peninsula) or Red Bluff Tuff (northwestern Pitt Island coast, east of the Tarawhenua Peninsula). The Onoua Limestone is conformably and gradationally overlain by Whenuataru Tuff, interfingering with the Whenuataru Tuff along the northwest coastal cliffs at Flowerpot Bay (Fig. 3.32, Enclosure 1 & 2 – Columns 13 & 14).

Lithologies

The Onoua Limestone is a relatively soft and porous bryozoan dominated grainstone that appears white to pale yellow, massive and well sorted. The bioclastic composition is almost exclusively calcitic and includes whole brachiopod shells throughout the unit (Fig. 3.33). Campbell et al. (1988, 1993) also noted that the Onoua Limestone becomes more tuffaceous (palagonitic) up-section (Fig. 3.32).

Paleontology

The Onoua Limestone is dominated by whole and fragmented bryozoans, foraminifera, brachiopods, bivalves and echinoderms (Fig. 3.33), as well as occasional solitary corals, barnacles and vertebrate teeth. Campbell et al. (1993) suggested that the occurrence of exclusively calcitic shell fragments in the Onoua Limestone may either be due to a depositional environment dominated by epifaunal taxa, or be a function of diagenetic removal of aragonite soon after deposition.

Age

Some of the foraminiferal assemblages indicate that deposition commenced in the earliest Late Opoitian (Early Pliocene), but in general a Waipipian to Mangapanian (Late Pliocene) age is registered for most samples of Onoua Limestone (Campbell et al., 1993).

Depositional environment

The abundance of planktic foraminifera near the top of the unit indicates an oceanic setting. The assemblages of benthic foraminifera are poor, but in consideration with the planktic foraminifera indicate mid to outer shelf water depths (Campbell et al., 1993).

Figure 3.31: Onoua Limestone at Flowerpot Bay (CH2/710233), northern Pitt Island. Inset shows Brian Jones standing in the old jail cell carved in the Onoua Limestone.

Figure: 3.32: Onoua Limestone in the coastal cliffs to the northeast of the Bluff Homestead (CH2/717243), northern Pitt Island. Here the lower unit of Onoua Limestone (just visible through the grass section below where Jeremy Titjen is standing) is disconformably overlying Red Bluff Tuff. The central orange unit on which Jeremy is standing grades up into another section of Onoua Limestone, which becomes more tuffaceous up-section.

Figure 3.33: Close-up of brachiopods and pectinid shells in the Onoua Limestone in coastal cliffs to the northwest of Flowerpot Bay, Pitt Island (CH2/702233).

3.2 Other limestone occurrences

These are limestone occurrences that were either not visited or not examined extensively in the field. This was because they had very restricted exposure and were often remote and difficult to access.

3.2.1 Tumaio Limestone

Name and definition

The Tumaio Limestone was originally described by Hay et al. (1970) as the Waikaripi Limestone. Campbell et al. (1988) considered that the Waikaripi Limestone did not constitute a viable unit at the type section, necessitating the need for a new name for this northern occurrence of Waikaripi Limestone. Moreover, the occurrence has a different lithology from the type section of the Waikaripi Limestone (now the Tumaio Limestone). Campbell et al. (1988) renamed this unit the Tumaio Limestone and considered it to be a sub-member unit of the Tutuiri Greensand. The Tumaio name itself is derived from the local name of Tumaio Beach, which extends from Lake Waikauia to Tioriori, at the northeastern end of the Manganui Beach coastline in northern Chatham Island.

Type section

The type section for the Tumaio Limestone is situated 700 m southwest from the Takapu Creek on Tumaio Beach (CH1/380786) at the northeastern end of Manganui Beach coastline in northern Chatham Island (Fig. 3.34, Enclosures 1 & 2 – Column 1) (Campbell et al., 1993).

Distribution and thickness

In situ outcrops of the Tumaio Limestone are restricted to the type section locality at Tumaio Beach, appearing in scattered outcrops over a 1 km distance southeast of Takapu Creek. An important aspect of these outcrops, and especially the type section, is the degree to which the exposures become buried by shifting coastal sand dunes (Fig. 3.34). The type section was well exposed in 1924 when visited by Marwick (Marwick, 1928; Allan, 1930 in Hay et al., 1970), but was then nearly entirely covered in 1957 when visited by

Hay et al. (1970). The type section was very well exposed again in 1977 when Campbell et al. (1988) visited the site, but only the upper 3 m were exposed when visited by me in the 2005 summer.

Campbell et al. (1988, 1993) describe the type section as the thickest exposure, with 8 m of outcrop, although the base of the unit has not been sighted (Enclosures 1 & 2 – Column 1). Blocks of Tumaio Limestone are also present along the beach at the head of the Whangamoe Inlet, on the northwestern edge of Petre Bay, Chatham Island (Marwick, 1928; Hay et al., 1970; Campbell et al., 1993). The *in situ* source of these blocks is not known but is thought to lie in the sand dunes backing the coastline (Campbell et al., 1993).

Contacts

The Tumaio Limestone is defined by Campbell et al. (1993) as a lateral subunit within the Tutuiri Greensand (Enclosures 1 & 2 – Column 1). The base of the exposure at the type section is not exposed, but is considered to conformably overlie and grade into the Tutuiri Greensand. However, it is noted that Marwick (1928) described a lower disconformable contact with 'green unfossiliferous tuffs'. The Tumaio Limestone is conformably overlain by a further 2 m of Tutuiri Greensand at the type section.

Lithologies

At the type section the Tumaio Limestone consists of 8 m of green to yellow and grey, poorly bedded, echinoid spine-bearing packstone (Fig. 3.35). The lower 5 m of the type section was noted by Campbell et al. (1993) to be very glauconitic, gritty and thoroughly burrowed, but free of terrigenous material.

Silicified nodular horizons are recorded in the Tumaio Limestone and include conspicuous sponge spicules (Fig. 3.36). Campbell et al. (1993) suggested that these horizons are a likely source for chert pebbles found in Pleistocene deposits on the island.

Paleontology

The main skeletal components in the Tumaio Limestone include foraminifera, calcareous nannofossils, sponges, brachiopods, bivalves, echinoderms, polychaete tubes and trace fossils. The most conspicuous macrofossils are echinoid spines of *Eucidaris strobilata*, along with bivalve shells of *Pycnodonte (Notostrea) tarda*, which occur as two separate horizons at 3.5 m (just visible at the exposed outcrop in 2005) and 7 m below the top of the type section outcrop. The presence of these two species is cited as evidence for the Tumaio Limestone being a lateral equivalent of the Tutuiri Greensand, with both species being common to both units (Campbell et al., 1993).

The Tumaio Limestone is significant in New Zealand geology as it yielded one of the first fossil collections made by Ernst Dieffenbach in 1840 (Dieffenbach, 1841 in Campbell et al., 1993).

Age

Key fossils indicate the Tumaio Limestone has an Early Waipawan (Early Eocene) age (Campbell et al., 1993).

Depositional environment

The abundance and diversity of benthic and planktic foraminifera suggest a relatively low energy oceanic setting that was probably at mid-shelf depths given the position of the Tumaio Limestone within the Tutuiri Greensand. Changes in bottom current activity presumably allowed for the removal of detrital material of the Tutuiri Greensand and deposition of carbonate banks forming the Tumaio Limestone (Campbell et al., 1993).

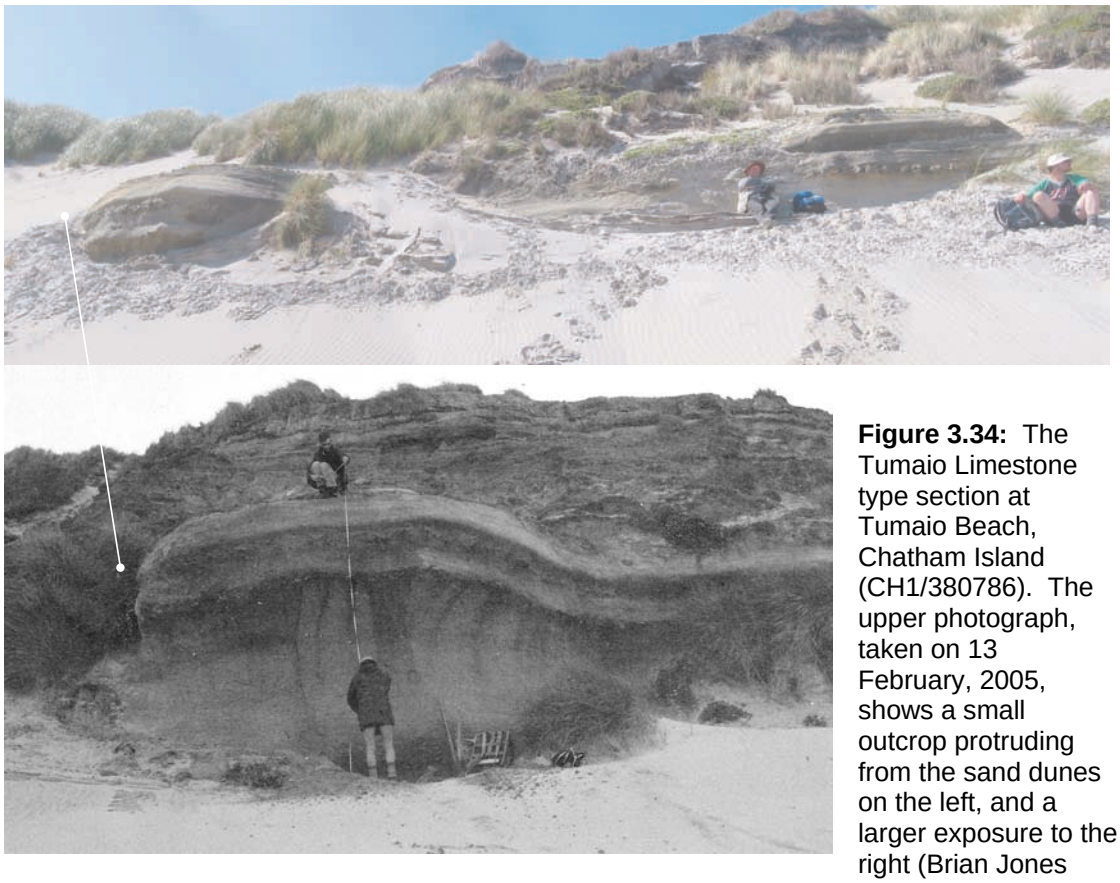

Figure 3.34: The Tumaio Limestone type section at Tumaio Beach, Chatham Island (CH1/380786). The upper photograph, taken on 13 February, 2005, shows a small outcrop protruding from the sand dunes on the left, and a larger exposure to the right (Brian Jones and Jeremy Titjen for scale). Only the upper 3 m of section was exposed in 2005 compared to the lower photograph from Campbell et al. (1993) taken in 1977 which shows an 8 m thickness (Tony Edwards at the top of the section and Alan Beu at the bottom). Clearly the section is prone to periodic burial by coastal sand dunes.

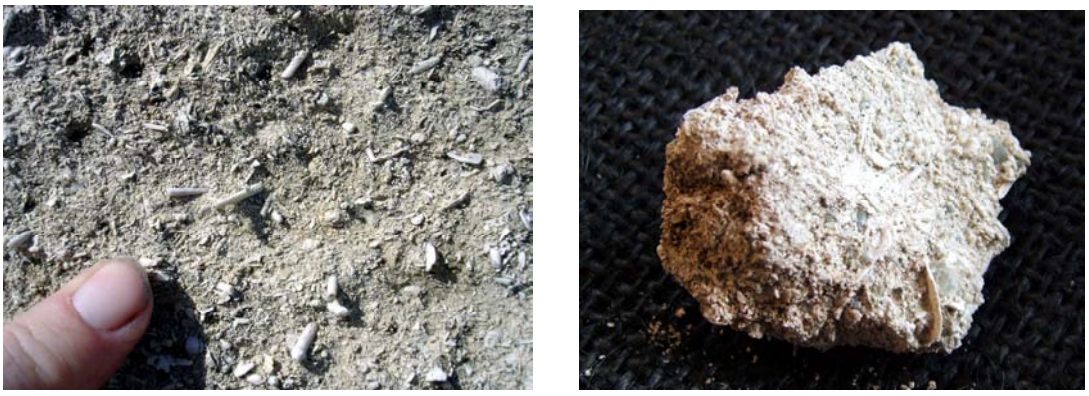

Figure 3.35: The Tumaio Limestone at the type section showing conspicuous echinoderm spines: left, 2005 near top of the section, and right, GNS sample (CH/f505, GS12459).

Figure 3.36: Upper silicified horizons (arrowed) of the Tumaio Limestone. The lower nodular horizons include conspicuous sponge spicules.

3.2.2 *Victoriella* Limestone

Name and definition

The *Victoriella* Limestone was first recognised and described by Campbell et al. (1988), who called it the *Victoriella* Limestone Lithofacies. The name is derived from the obvious presence of the large benthic foraminifera *Victoriella conoidea*, which are the dominant skeletal component in the limestone (Campbell et al., 1993). Here the word Lithofacies is omitted from the limestone name which is simply referred to as the *Victoriella* Limestone.

Type section

The *Victoriella* Limestone is extremely restricted in its distribution and is only known from sinkholes occurring within a small tributary of the Waitaha Creek, near the junction of the Wharekauri and North Roads on northern Chatham Island (CH1/454787) (Fig. 3.37). This is the type section for the limestone (Enclosures 1 & 2 – Column 2) (Campbell et al., 1993).

Distribution and thickness

The type section and only known occurrence of the *Victoriella* Limestone occurs in a tributary of the Waitaha Creek, which has cut peat tunnels and sink holes down through sequences of Mooreland Peat at the Wharekauri and North Road junction, northern Chatham Island (Fig 3.37). The limestone is about 2.8 m thick (Campbell et al., 1988, 1993).

Contacts

The *Victoriella* Limestone disconformably overlies the Matanginui Limestone and is in turn disconformably overlain by the Titirangi Sand.

Lithologies

The *Victoriella* Limestone is an unconsolidated, massive, well sorted medium grainstone (Campbell et al., 1988, 1993). It is either orange to brown (presumably peat staining) or grey (reduction coloured) in outcrop (Fig. 3.38). Campbell et al. (1988, 1993) noted that the basal section of the unit contains subangular to subrounded granular detrital material (Fig. 3.38).

Paleontology

The main skeletal components of the *Victoriella* Limestone are foraminifera, bryozoans and echinoderm fragments. Bryozoan species were not identified by Campbell et al. (1993), but the worn echinoderm fragments are *Eucidaris strobilata* spines and were probably reworked from the underlying Matanginui Limestone. The most obvious and abundant microfossil is *Victoriella conoidea*.

Age

Planktic foraminifera yield an early Whaingaroan (Early Oligocene), age. Campbell et al. (1993) suggested that there may be a considerable amount of mixing of Eocene (possibly from the Te One Limestone) and Oligocene zonal species, or it may be possible that the *Victoriella* Limestone accumulated over a considerably long period of time.

Depositional environment

The *Victoriella* Limestone is thought to have been slowly deposited over a lengthy period of time in a sheltered oceanic setting, considering the abundance of planktic foraminifera. The occurrence of the large benthic foraminifera *Victoriella conoidea* may indicate warm shallow conditions, probably inner shelf (Campbell et al., 1993).

Figure 3.37: Sampling the *Victoriella* Limestone in a tributary of the Waitaha Creek (CH1/454787), near the junction of Wharekauri and North Roads, northern Chatham Island. Access to the exposure is difficult with the best exposures occurring in small tunnels cut through the peat by the Waitaha Creek (Jeremy Titjen for scale).

Figure 3.38: Photograph of *Victoriella* Limestone samples. Note the peat staining (right sample) and grey colouration caused by reduction (left sample). Subrounded to subangular clasts are present in the left-hand sample that was retrieved from the creek bed, near the base of the unit.

3.2.3 Altonian limestone

Name and definition

An occurrence of Altonian limestone on Chatham Island was first described by Campbell et al. (1988), although barnacles from the limestone had previously been described by Buckeridge (1984). The occurrence is known from quarried blocks that were unearthed by a bulldozer during construction from 1979 – 1981 of the Inia William Tuuta Memorial Aerodrome, between Moutapu and Karewa points on Chatham Island. The Altonian limestone is significant in that its occurrence in the Miocene falls within a period in the Chatham Islands rock record that is sparsely represented. However, given the isolated and 'float-like' nature of the occurrence, the limestone is informally named only.

Type section

The exact stratigraphic and geographic location is unknown and consequently there is no type section or formal name given to the Altonian limestone (Campbell et al., 1988, 1993).

Distribution and thickness

The Altonian limestone is thought to be less then 5 m in thickness, presumably based on the dimensions of the unearthed blocks themselves (Campbell et al., 1988, 1993).

Contacts

On the basis of known stratigraphic relationships at Moutapu Point, Campbell et al. (1988, 1993) suggested that the Altonian limestone probably disconformably overlies the Te One Limestone and is in turn disconformably overlain by the Motarata Limestone (Fig. 3.20, 3.29, Enclosure 1 & 2 – Column 5). They also noted that the blocks include a phosphatic horizon that may correlate to a similar basal horizon in the Motarata Limestone.

Lithologies

The Altonian limestone is a glauconitic, pale yellow, bryozoan-foraminiferal-echinoderm packstone with variable grain sizes (Fig. 3.39). Lithological descriptions also indicate that the limestone blocks are associated with horizons that are glauconite rich, fossiliferous, and phosphatic with a rubbly appearance. The phosphatic horizon (possible correlative to the basal Motarata Limestone) is described as containing conspicuous black glistening phosphate nodules, with concentrated areas of glauconitic sand and patches of white to grey and red-brown limestone (Campbell et al., 1993).

Paleontology

Main fossil groups are foraminifera, calcareous nannofossils, bryozoans, brachiopods, bivalves, gastropods, barnacles, echinoderms, ostracods, vertebrate bones and teeth, and trace fossils (Fig. 3.39) (Campbell et al., 1993). The most conspicuous macrofossils are brachiopods and bivalves (Buckeridge, 1984; Campbell et al., 1993).

Age

An Altonian age (Early Miocene) based on planktic foraminiferal assemblages (Buckeridge, 1984; Campbell et al., 1993).

Depositional environment

Considered to be no shallower then outer shelf depths based on the lack of shallow water foraminiferal species (Campbell et al., 1993).

Figure 3.39: The Altonian limestone, GNS Science sample CH/f526, GS12998. A trace fossil is visible in the front corner of the sample. The sample shows a white to grey limestone with variable iron staining.

3.2.4 Waipipian limestone

Name and definition:

A single occurrence of a thin fossiliferous limestone of Waipipian age is known from a borehole drilled by Fletcher Challenge (Borehole No. CHA59) during 1985 as part of a peat survey near Tioriori Creek to the southeast of Motuariki Hill, northern Chatham Island (Richards, 1987 in Campbell et al, 1988 & 1993). The limestone was first formally described by Campbell et al. (1988) from the drill core submitted to the New Zealand Geological Survey (now GNS Science) by Fletcher Challenge. This occurrence is significant in that it represents an *in situ* correlative of the Onoua Limestone and Whenuataru Tuff on Pitt Island. Campbell et al. (1988, 1993) note that this limestone was previously known from hand-cut slab blocks discovered during field work in 1977 near Lake Waikauia, northern Chatham Island.

Type section

The Waipipian limestone is not formally named and consequently has no type section, being known only from a single borehole core and geographically displaced blocks near Lake Waikauia.

Distribution and thickness

The occurrence of Waipipian limestone from the borehole core (CHA59, 50 mm diameter and 78 cm in length) drilled near Tioriori Creek shows that the limestone occurs at a depth of 13.85 m to 14.63 m below the surface, which at this locality is 32 m above sea level. The probable thickness of the Waipipian limestone from the core is approximately 3 m (Richards, 1987; Campbell et al., 1988, 1993).

The occurrences of hand-cut slabs of limestone of the same lithology are known from bricks making up a fireplace within a derelict house near Lake Waikauia. Apparently the bricks (that measure 1m by 0.6 m by 0.15 m) are derived from a site along the nearby lake shoreline. On investigation Campbell et al. (1988, 1993) observed some 0.5 m long blocks along the shoreline, although their *in situ* source is not known.

Contacts

Evidently the borehole core did not penetrate the base of the Waipipian limestone. Based on the northern Chatham Island stratigraphy it is inferred to disconformably overlie the Tutuiri Greensand. The Waipipian limestone itself is probably overlain by the Titirangi Sand, although this cannot be definitely ascertained as there is a section of missing core above the limestone (Campbell et al., 1988, 1993).

Lithologies

The Waipipian limestone is described as a relatively soft, white to pale grey, fine bryozoan grainstone with minor inclusions of volcaniclastic sand (Fig. 3.40) (Campbell et al., 1988, 1993).

Paleontology

Skeletal components include foraminifera, nannofossils, bryozoans, bivalves and gastropods. Conspicuous macrofossils include gastropod moulds and pectinids, particularly *Sectipecten allani* (Fig. 3.40). No non-molluscan macrofossils are reported from the Waipipian limestone, with the general assemblage of taxa indicating a correlation to the Onoua Limestone, although it should be noted that no micropaleontogical study has been conducted on this deposit (Campbell et al., 1988, 1993).

Age

The presence of *Sectipecten allani* (Fig. 3.40) suggests an Opoitian or younger age. The Waipipian limestone is in general considered to be a better correlative to the Onoua Limestone then to the Motarata Limestone (based on appearance and macrofossil assemblage) and is therefore considered to be Opoitian-Waipipian (Early-Late Pliocene) in age (Campbell et al., 1988, 1993).

Depositional environment

The depositional environment of the Waipipian limestone was probably mid to outer shelf (Campbell et al., 1988, 1993).

Figure 3.40: The Waipipian limestone, GNS Science sample CH/f588, GS14155, recovered from a borehole drill core. Note the pectinid mould on the surface of the sample.

3.2.5 Cape L'Eveque limestone (new)

Name and Definition

The Cape L'Eveque limestone is an informal name used in this thesis to identify thin bedded exposures of limestone occurring within tuffaceous deposits near Cape L'Eveque, southern Chatham Island. An occurrence is mentioned in Campbell et al. (1993) as a southern occurrence of Te Whanga Limestone that was discovered by Robert Holmes on his property in 1975. A group from GNS Science first visited the site in 2005, and again in 2006 when the author of this thesis accompanied the group.

Type and reference sections

The Cape L'Eveque limestone occurs around an area known locally as Snake Gully. The outcrops in Snake Gully itself occur in a creek bed in the bottom of the gully as well as scattered patchy exposures within the eastern wall of the gully (Fig. 3.41, 3.42). To the east of Snake Gully (<0.5 km, CH2/418362) a high coastal southeast-facing exposure records a sequence of volcaniclastic deposits that appear to gradationally pass up into bioclastic limestone (Fig. 3.44, Enclosures 1 & 2 – Column 10). As this exposure to the east of Snake Gully shows the limestone in a stratigraphic context with the underlying volcaniclastic deposits it is suggested it be the type section locality.

Another occurrence of calcareous material occurs to the west of Snake Gully, immediately behind (and to the northeast of) Cape L'Eveque itself (CH2/396364) (Fig. 3.43), and can be used as a reference section.

Distribution and thickness

The type section outcrop has a total thickness of 4-5 m, although the fully calcareous limestone unit proper occurs only in the upper 1 m of this exposure (Fig 3.44, Enclosures 1 & 2 – Column 10). Exposure along the eastern side of Snake Gully suggests a thickness of up to 3 m, although it is unclear how much of this is actual limestone; much of it is essentially a calcareous matrix between volcanic cobbles and boulders (Fig. 3.41). Similar deposits occur immediately behind Cape L'Eveque where they are 3-4 m thick (Fig. 3.43).

Strata at the type locality are inferred to dip at 4-18° towards the

southeast, based on the dip of an overlying lava flow (Fig 3.44). However, this may not be a good indication of the orientation of the strata given that similar lithologies in Snake Gully appear to be dipping at about 4° towards the northwest (Fig. 3.31, 3.32).

Contacts

The Cape L'Eveque limestone is considered to be represented by the upper 1-1.5 m of the exposure at the type section, due to the inclusion of obvious shell material and strong effervescent reaction to hydrochloric acid (Fig. 3.44, Enclosures 1 & 2 – Column 10). The lowermost 2.5 m of outcrop at the type section is non-calcareous and is of a considerably different lithology and bedding direction to the overlying limestone (Fig. 3.44). It is therefore inferred that an angular unconformity probably exists between the lowermost 2.5 m of volcaniclastic material and the overlying bioclastic material (Fig. 3.44, Enclosure 1 & 2 – Column 10). The Cape L'Eveque limestone therefore probably constitutes designation as an individual lithofacies or possible member within a formation consisting of lower volcaniclastic deposits, bioclastic calcareous horizons and overlying lava flows (Campbell, GNS Science, per. comm., 2006).

Lithologies

At the type section of the Cape L'Eveque limestone the lowermost 2.5 m of the outcrop consists of a pale brown, non-calcareous volcaniclastic deposit, which appears to coarsen upwards from silt to fine sand, with inclusions of possible fine sparse shell material (Fig. 3.44, Enclosures 1 & 2 – Column 10). Also noticeable within this lower 1-2.5 m are large green subangular clasts interpreted at this stage as glauconite, but may constitute reworked olivine crystals derived from the overlying Plio-Pleistocene volcanics (recently recognised and Ar-Ar dated at 4.5 Ma) (Campbell, GNS Science, pers. comm., 2007). At 2.5 m there appears to be a change in facies to a calcareous volcaniclastic deposit with inclusions of large oyster shells and rounded pebble sized volcaniclastics. This lower section of the upper 1.5-2 m is coarser and more granular in appearance then the uppermost 1 m. Large volcanic clasts also grade from subangular pebble and cobble size up into

subrounded and rounded cobbles and boulders (Fig. 3.44).

Lithologies of the limestone on the east side of Snake Gully are inferred to be the same unit/facies as the uppermost 1 m at the suggested type section 0.5 km to the northeast (Fig. 3.41, 3.44). An occurrence within the base of the creek in Snake Gully is different in that the large volcanic clasts are absent but the limestone appears to have coarser bioclastic material, with oyster and pectinid shells being particularly conspicuous.

The lithology of the 'limestone' immediately behind Cape L'Eveque is similar to that of the uppermost section at the suggested type section locality, but is different in that the subrounded and rounded cobbles and boulders are considerably more abundant so that the limestone is essentially a 'matrix' or 'fill' around these clasts.

Paleontology

Oysters and pectinids (*Pecten novaezelandiae*) have been recorded (A. Beu & H. Campbell, GNS Science, pers. comm., 2006).

Age

An Opoitian-Castlecliffian (Early Pliocene-Early Pleistocene) age range is presently suggested. Castlecliffian (Pleistocene) age is based on the inclusion of the modern pectinid *Pecten novaezelandiae* (A. Beu & H. Campbell, GNS Science, pers. comm., 2006). However, more recently acquired ages on the Plio-Pleistocene volcanics present in the area indicate an Ar-Ar age of 4.5 Ma (Early Pliocene), and it is now thought that the inclusions of the modern pectinid *Pecten novaezelandiae* within the limestone may actually be a new genus of pectinid and possibly of mid Pliocene (2.5 Ma) age (H. Campbell, GNS Science, pers. comm., 2007).

Depositional environment

Numerous lag deposits occur along the top of the coastal cliff around the Cape L'Eveque area. Stratigraphically the Cape L'Eveque limestone occurs above these lag deposits. Based on observations made of the 'limestone' occurrence behind Cape L'Eveque, it is suggested the limestone fill associated with the cobble and boulder sized volcanic clasts represents a

deepening water environment (Fig. 3.43). The stratigraphically lower lag deposits of large boulder sized clasts with volcanic sand infills represent a shoreline deposit with infilling material derived from a terrigenous provenance. Increasing water depth has resulted in the reduction of terrigenous sediment input and allowed for formation of carbonates which have infilled 'stranded' lag deposits. It is unlikely that the carbonates formed on the lag deposits themselves but probably formed on rocky substrates of either Late Cretaceous or Plio-Pleistocene volcanics (H. Campbell, GNS Science, pers. comm., 2006) (if the lag deposits are Plio-Pleistocene in age) that occur at the southern end of Chatham Island and in Pitt Strait. The carbonates have subsequently been moved about by strong bottom currents along with reworked volcanic clasts to either infill the lag deposits or the large volcanic clasts have been deposited onto the carbonate material during storm events, as is probably the case with the Snake Gully exposures (Fig. 3.41, 3.43, 3.44). Tectonic uplift then has raised both the lag deposits and Cape L'Eveque limestone to their current position, about 150-175 m above sea level since the Plio-Pleistocene, probably by a thermal uplift mechanism.

Summary

The range of field characteristics of Chatham Island limestones is summarised in Table 3.1 and highlights their wide distribution of ages, thicknesses, compositions and fossil content.

Figure 3.41: Scattered outcrops of the Cape L'Eveque limestone along the eastern side of Snake Gully, southern Chatham Island (CH2418362). Alan Beu (closest) and Bob Carter (background) looking for fossil material in a more volcanic clast dense facies of the limestone.

Figure 3.42: The Cape L'Eveque limestone that crops out at the base of the creek in Snake Gully. There is a noticeable absence of large (cobble size) volcanic clasts and the deposit appears more fossiliferous with conspicuous pectinid and oyster shells.

Figure 3.43: Carbonate fill in a deposit of densely packed volcanic clasts behind Cape L'Eveque (CH2/396364) which is similar in lithology to outcrops in Snake Gully, although the outcrop is considerably thicker (>4 m) and more densely packed with volcanic clasts. Chris Consoli (left) and John Begg (right) in the left-hand photo for scale, with a close-up shot below.

Figure 3.44: The suggested type section locality of the Cape L'Eveque limestone, about 0.5 km northeast of Snake Gully (CH2/418362). The entire section is approximately 4 m in thickness with the lowermost 2.5 m (insets 1 to 2) being a predominantly non-calcareous tuffaceous deposit. Bioclastic material begins to appear at 2.5 m with a change to calcareous material and the gradual increase in conspicuous shell material (through insets 3 to 5) along with the inclusion of subrounded and rounded volcanic clasts (conspicuous in inset 5 at the top of the section).

Table 3.1: Summary of the Chatham Island limestone units (adapted from Campbell et al., 1993)

	Units	Age	Contacts	Distribution and Thickness	Composition and Fossil Content
	Cape L'Eveque limestone (new)	Opotian-Castlecliffian (Early Pliocene-Early Pleistocene)	Possibly overlain by Pliocene volcanics; overlies possibly Pliocene volcanics, Pliocene-Pleistocene lag deposits or Late Cretaceous Southern Volcanics	Restricted to scattered occurrences along coastal cliffs (150-200 m asl.) in the southwest comer of Chatham Island from Cape L'Eveque to Snake Gully, ~4 m thick	Volcaniclastic with fragmented bioclastic material, rounded volcanic cobble inclusions; oysters,pectinids (*Pecten novaezelandiae*)
	Onoua Limestone	Opoitian-Mangapanian (Early-Late Pliocene)	Conformably and gradationally overlain by Whenuatara Tuff; disconformably overlies Matanganui Limestone or Red Bluff Tuff	Tarawhenua Peninsula northeast to Motutapu Point, Pitt island, ~26 m thick	Fine bryozoan grainstone becomes tuffaceous up-section; foraminifera, corals, brachiopods, bivalves, echinoderms, barnacles and vertebrate remains
	Waipipian limestone	Opoitian-Waipipian (Early-Late Pliocene)	Disconformably overlain by Titirangi Sand; disconformably overlies Tutuiri Greensand	Borehole sample north of Tioriori Creek, southeast of Motuariki Hill, northern Chatham Island, ~3 m thick	Fine bryozoan grainstone with inclusions of volcaniclastic silt and sand; foraminifera, nannofossils, bivalves and gastropods
	Motarata Limestone	Opoitian (Pliocene)	Disconformably overlain by Titirangi Sand; disconformably overlies Red Bluff Tuff or Matanginui Limestone or Te One Limestone	Whareama, Te Matarae and Moutapu Point, western shore of Te Whanga Lagoon, Chatham Island, ~5 m thick	Fine foraminiferal grainstone and packstone, nannofossils, bryozoans, brachiopods, bivalves, ostracods, echinoderms and vertebrate remains
	Altonian limestone	Altonian (Early Miocene)	Disconformably overlain by Motarata Limestone; disconformably overlies Te Whanga Limestone	Precise geographic location unknown, Moutapu Point to Kawera Point area, western shore Te Whanga Lagoon, ~ 5 m thick	Bryozoan-foraminiferal-echinoderm packstone, calcareous nannofossils, brachiopods, bivalves, gastropods, barnacles, ostracods, vertebrate remains and trace fossils
	Taoroa Limestone	Waitakian (Early Miocene)	Disconformably overlain by 0.5 m of unnamed Pliocene limestone, inturn overlain by Rangitihi Volcanics; lower contact unknown	Taoroa, west end of Manganui Beach, northern Chatham Island, ~4 m thick	Foraminiferal-bryozoan grainstone and packstone, calcareous nannofossils, echinoderms and trace fossils
	***Victoriella* Limestone**	Lower Whaingaroan (Early Oligocene)	Disconformably overlain by Titirangi Sand; disconformably overlies the Matanginui Limestone	Restricted to peat sinkhole and tunnels in tributary of Waitaha Creek, near North and Wharekauri Roads junction, ~3 m	Medium grainstone, foraminifera, bryozoans and echinoderms
Te Whanga Limestone	**Te One Limestone**	Kaiatan-lower Whaingaroan (Late Eocene-Early Oligocene)	Disconformably overlain by Titirangi Sand or Motarata Limestone, disconformably overlies Matanginui Limestone or Red Bluff Tuff	Waipapa Creek south to Ohuru with undifferentiated equivalents at Papapohatu Point and Te Matarae and an inland exposure at Big Bush,along the western shore of Te Whanga Lagoon, Chatham Island, ~ 25 m thick	Bryozoan grainstone, foraminifera, calcareous nannofossils, brachiopods, bivalves, barnacles, echinoderms and vertebrate remains
Te Whanga Limestone	**Matanginui Limestone**	Waipawan-Bortonian (Early-Middle Eocene)	Disconformably overlain by Te One Limestone or *Victoriella* Limestone or Motarata Limestone on Chatham Island, and Onoua Limestone on Pitt Island; conformably overlies Red Bluff Tuff on both islands	Discontinuous exposure along the western shore of Te Whanga Lagoon and at Red Bluff on Chatham Island, exposures along the Tarawhenua Peninsula and Waihere Bay on Pitt Island	Bryozoan-echinoid-foraminiferal-bivalve packstone on Chatham Island with brachiopods and barnacles; more commonly a porous grainstone on Pitt Island
	Tumaio Limestone	Waipawan (Early Eocene)	Subunit within the Tutuiri Greensand	Scattered exposures over 1 km stretch of Tumaio Beach, north of Takapu Creek and non- in situ blocks at the head of the Whangamoe Inlet, north Chatham Island	Bryozoan grainstone and echinoderm packstone, foraminifera, calcareous nannofossils, sponges, brachiopods, bivalves, polychaete tubes and trace fossils
	Haumurian limestone	Haumurian (Late Cretaceous)	Fissure fills and dykes within pillow basalts of the Southern Volcanics on Chatham Island and within the Kahuitara Tuff on Pitt Island	Ngakuha Reef, 2.5 km south of Waitangi, Chatham Island; Flowerpot Bay, on western side of wharf, Pitt Island	Micritic limestone conglomerate on Chatham Island with foraminifera, calcareous nannofossils, bivalves, echinoids and serpulids; coarser limestone on Pitt island

Legend

- Tuffaceous deposit
- Fine bedded tuff
- Sandy tuff
- Lapillistone
- Tuffaceous conglomerate and claystone
- Tuffaceous conglomerate
- Tuffaceous breccia
- Basaltic lava flow
- Limestone
- Cross-bedded limestone
- Vaguely cross-bedded limestone
- Sandy limestone
- Limestone conglomerate
- Shell bed
- Quartzose sand
- Conglomerate
- Gravel lag
- Peat
- Schist
- Glauconitic
- Phosphatic
- Silicified or chert horizon
- Calcareous rubbly layer
- Karst surface
- Irregular or burrowed surface
- Burrowing/bioturbation
- Serpulids/worm tubes
- Unconformity
- Massive
- Cross-bedded
- Volcanic detritus
- Uncertain stratigraphy
- Fragmented shell material
- Foraminifera
- Planktic foraminifera
- Bryozoans
- Bryozoans - rigid sheet
- Bryozoans - rigid dendroid
- Echinoderms
- Bivalves
- Pectinids
- *Serripecten*
- Oysters
- Brachiopods
- Gastropods
- Barnacles

Time Scale

Inter. Age	NZ Series	NZ Stage
Pleist.	Castlecliffian	Haweran (Wq)
		Castlecliffian (Wc)
	Wanganui	Nukumaruan (Wn)
		Mangapanian (Wm)
		Waipipian (Wp)
Pliocene		Opoitian (Wo)
	Tara-naki	Kapitean (Tk)
Miocene		Tongaporutuan (Tt)
	Sth. Lnd.	Waiauan (Sw)
		Lillburnian (Sl)
	Pare-ora	Clifdenian (Sc)
		Altonian (Pl)
		Otaian (Po)
Oligo-cene	Landon	Waitakian (Lw)
		Duntroonian (Ld)
		Whaingaroan (Lwh)
Eocene	Arnold	Runangan (Ar)
		Kaiatan (Ak)
		Bortonian (Ab)
	Dannevirke	Porangan (Dp)
		Heretaungan (Dh)
		Mangaorapan (Dm)
Paleo-cene		Waipawan (Dw)
Upper Cretaceous	Mata	Teurian (Dt)
		Haumurian (Mh)
		Piripauan (Mp)
	Rauku-mara	Teratan (Rt)
		Mangaotanean (Rm)
		Arowhanan (Ra)
Lower Cretaceous	Clarence	Ngaterian (Cn)
		Motuan (Cm)
		Urutawan (Cu)
	Tai-Nai	Korangan (Uk)
		??

Stratigraphic columns constructed from characteristics observed in field work conducted in 2005 and 2006 by Jeremy Titjen for partial fulfilment of MSc degree in Earth & Ocean Sciences at the University of Waikato, with information also sourced from columns in Campbell *et al.* (1993). Grid references given are from NZMS 260 1:50,000 maps of the Chatham Islands, Sheet 1 (CH1) and Sheet 2 (CH2).

Enclosure 1
Stratigraphic Columns

Jeremy Q. Titjen
MSc Thesis
2007
Tertiary limestones and sedimentary dykes on Chatham Islands, southwest Pacific Ocean, New Zealand
Department of Earth & Ocean Sciences
The University of Waikato

1 Tumaio Beach (CH1/380786)

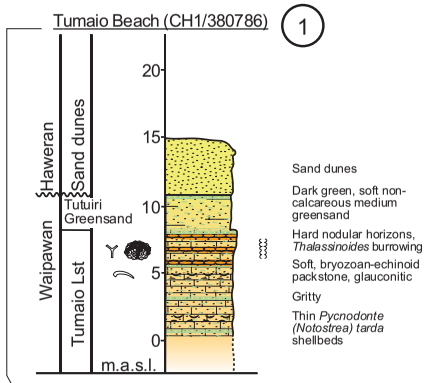

2 Waitaha Creek (CH1/454787)

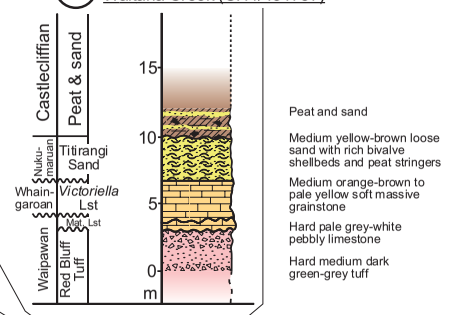

3 Maunganui (CH1/283760)

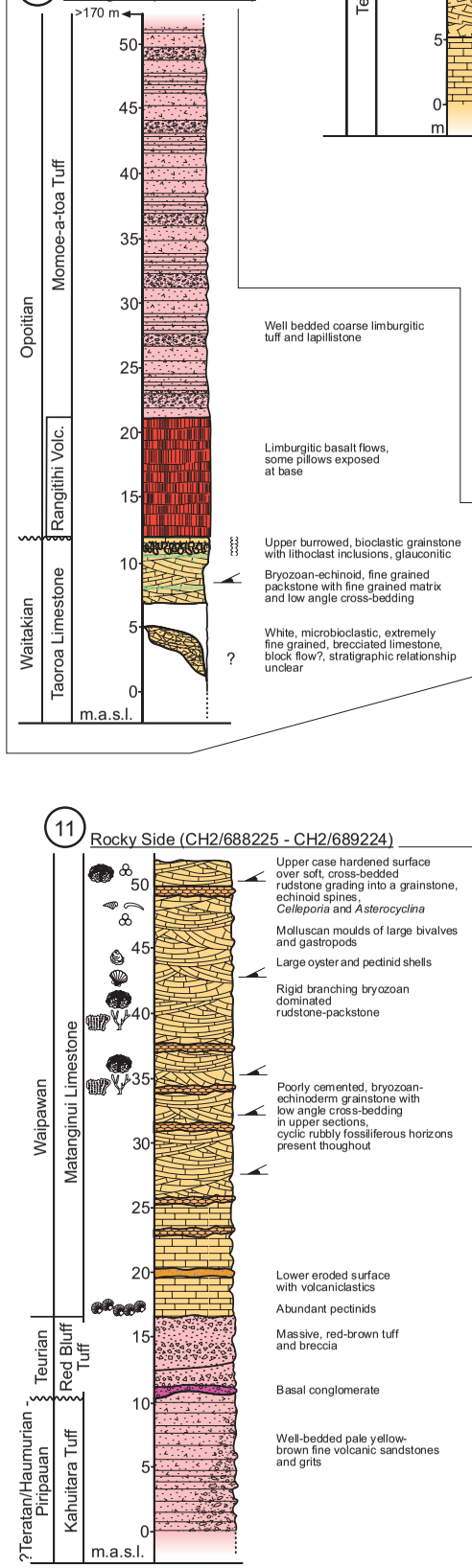

4 Waipapa Creek - Blind Jim's Creek (CH1/451755 - CH1/454745)

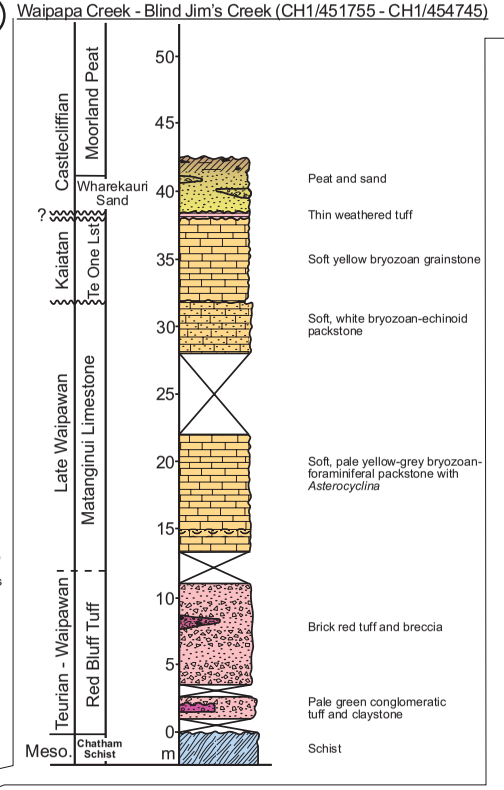

5 Moutapu Point (CH1/520698)

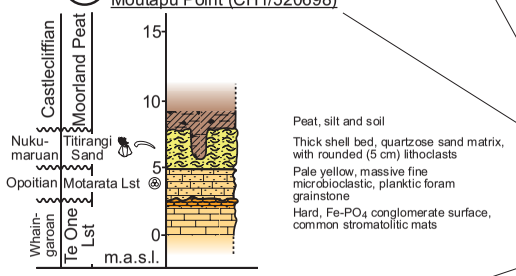

6 Moreroa (CH1/481653)

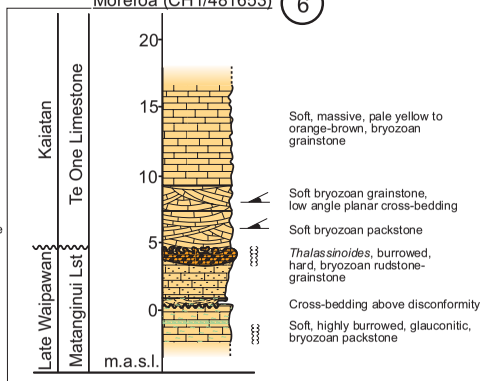

7 Big Bush Quarry (CH1/472629)

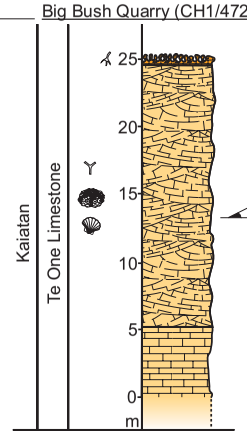

8 Ohuru Point (CH1/497618 - CH1/495619)

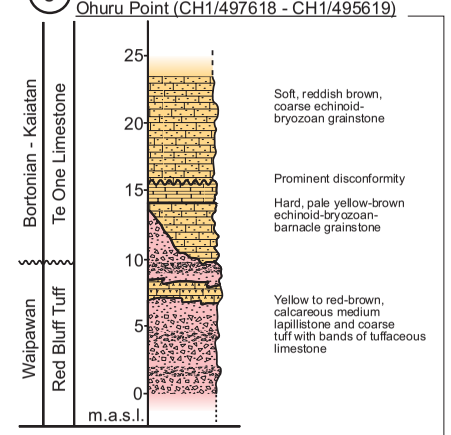

9 Whareama (CH1/512558)

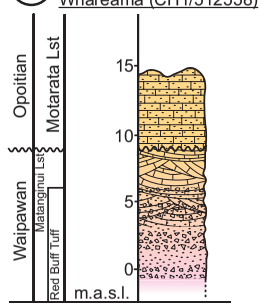

10 East of Cape L'Eveque, Snake Gully (CH2/418362)

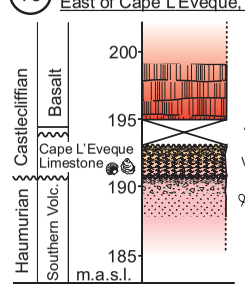

11 Rocky Side (CH2/688225 - CH2/689224)

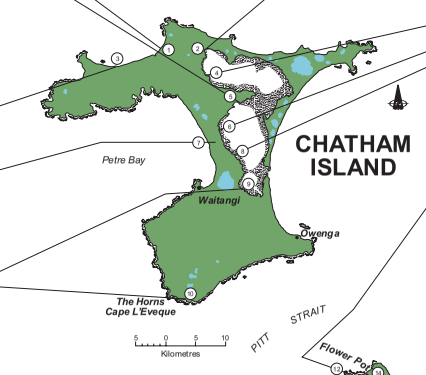

12 Tarawhenua Peninsula (CH2/679233)

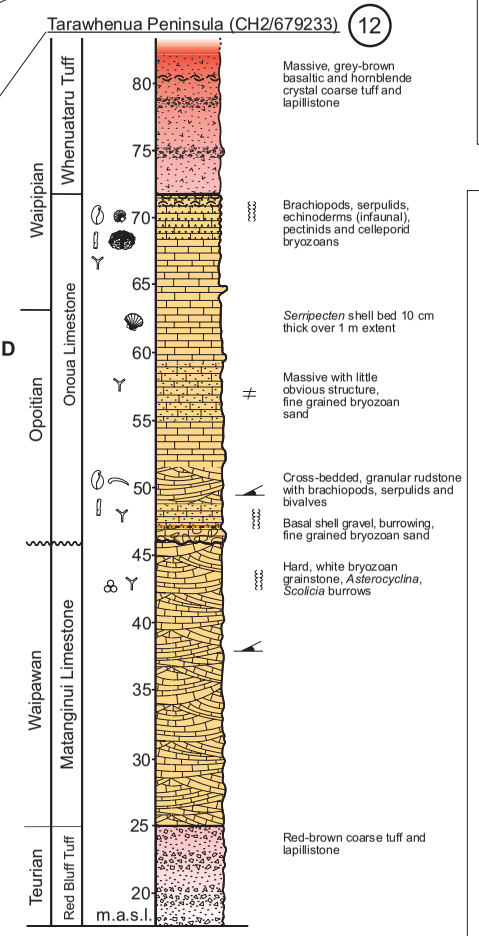

13 West of Flowerpot Bay (CH2/703232)

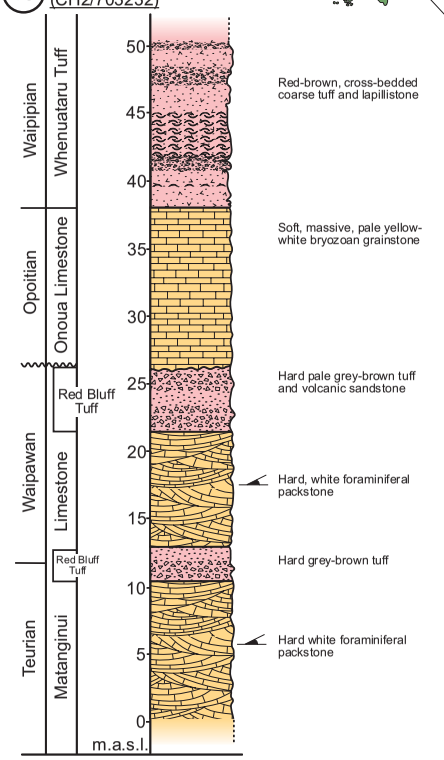

14 North of the Bluff (CH2/714236 - CH2/715235)

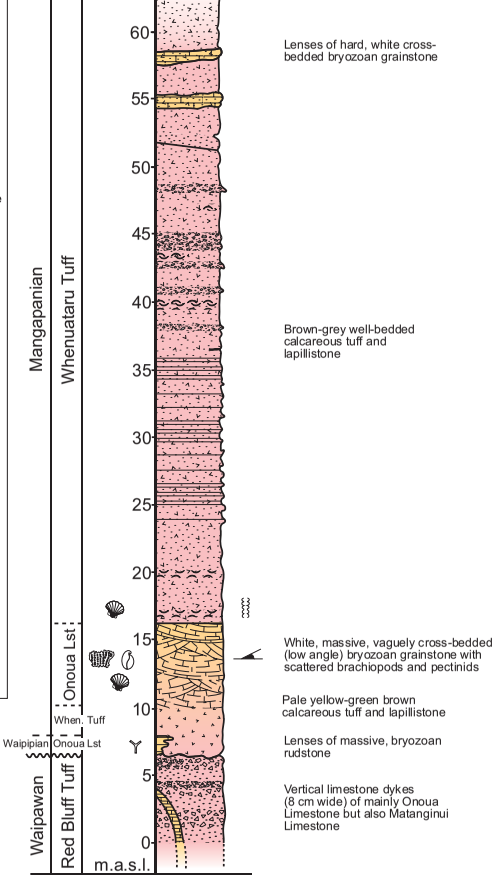

NORTH

SOUTH

Chatham Island

Pitt Strait

Pitt Island

Maunganui 3

Tumaio Beach 1

Waitaha Creek 2

Waipapa Creek - Blind Jim's Creek 4

Moutapu Point 5

Moreroa 6

Big Bush Quarry 7

Ohuru Point 8

Whareama 9

East of Cape L'Eveque, Snake Gully 10

Tarawhenua Peninsula 12

Rocky Side 11

West of Flowerpot Bay 13

North of the Bluff 14

Opoitian (Early Pliocene)

Waitakian (Early Miocene)

Momoe-a-toa Tuff

Rangitihi Volc.

Taoroa Limestone

>170 m

Holocene

Waipawan (Early Eocene)

Sand dunes

Tutuiri Greensand

Tumaio Lst

Castlecliffian

Peat & sand

Titirangi Sand

Nukumaruan

Whaingaroan

Victoriella Lst

Waipawan

Red Bluff Tuff

Haumurian

Castlecliffian

Basalt

Southern Volc.

Cape L'Eveque Limestone

Te One Limestone

Matanginui Limestone

Red Bluff Tuff

Chatham Schist (pre-middle Cretaceous)

Whenuataru Tuff

Onoua Limestone

?Teratan/Haumurian - Piripauan (Late Cretaceous)

Kahuitara Tuff

m.a.s.l.

Legend

- Quaternary Peat and Sands
- 1 Titirangi Sand (Late Pliocene)
- Whenuataru Tuff (Early-Late Pliocene)
- Onoua Limestone (Late Pliocene)
- 2 Motarata Limestone (Pliocene)
- Te One Limestone (Late Eocene-Early Oligocene)
- Matanginui Limestone (Early-Middle Eocene)
- Red Bluff Tuff (Late Paleocene-Early Eocene)

Stratigraphic columns constructed from characteristics observed in field work conducted in 2005 and 2006 by Jeremy Titjen for partial fulfilment of MSc degree in Earth & Ocean Sciences at the University of Waikato, with information also sourced from columns in Campbell *et al.* (1993). Grid references given are from NZMS 260 1:50,000 maps of the Chatham Islands, Sheet 1 (CH1) and Sheet 2 (CH2).

Enclosure 2

Stratigraphic Correlation

Jeremy Q. Titjen 2007

MSc Thesis

Tertiary limestones and sedimentary dykes on Chatham Islands, southwest Pacific Ocean, New Zealand

Department of Earth & Ocean Sciences

The University of Waikato

CHAPTER 4

Chatham Islands Limestone Petrography

Petrographic analysis has been undertaken on both the major and minor limestone occurrences on the Chatham Islands (Fig. 4.0). This involved the production and analysis of 118 thin sections over 94 samples (Appendix B). Whole rock, bioclastic, and siliciclastic compositions, along with cement types and diagenetic features have been determined under a petrographic microscope. Qualitative values were assigned to the abundance of individual components over multiple samples, with average compositional values and rock classifications being summarised from these values (Appendix B). Classification of limestone units is based on the Dunham (1962) scheme.

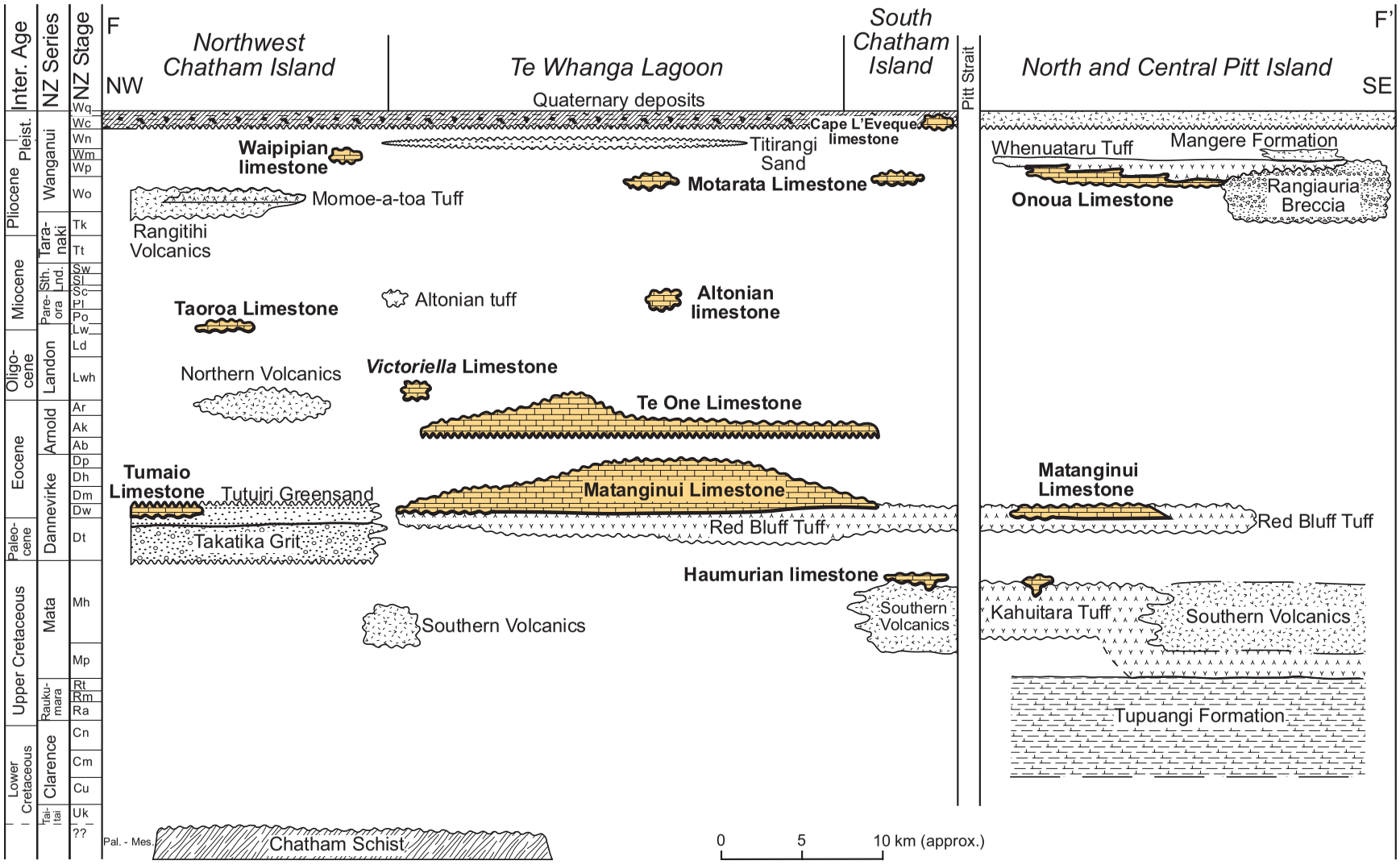

Figure 4.0: Time-space distribution diagram for the limestones on Chatham Islands (adapted from Campbell et al., 1993; Wood et al., 1989).

4.1 Main limestone occurrences

4.1.1 Haumurian limestone

Whole rock composition

The Haumurian limestone has a considerably significant siliciclastic component (Fig. 4.1). Although there appears to be a number of different fill lithologies present at Flowerpot Bay on Pitt Island, analysis is primarily based on the common conglomeratic fill type also seen at Ngakuha Reef on Chatham Island (Fig. 4.4C). Here the whole rock composition shows that carbonate material comprises at least 60% of the total rock, with 34% siliciclastics and porosity of 2% (Fig. 4.1).

Bioclastic composition

The high percentage of stromatolitic material within the Haumurian limestone is of localised importance only, being abundant at a specific section from Ngakuha Reef on Chatham Island (Figs 4.2, 4.4E & Appendix B Fig. B2). Consequently it is likely that bryozoans are generally the most abundant skeletal component in the Haumurian limestone, with common echinoderms and bivalves. The dominance of bryozoans, echinoderms and bivalves does not fit any of the triangle skeletal assemblage plots devised by Hayton et al. (1995), and is closest to the bryomol assemblage (James, 1997). Limestone intraclasts were noted to occur within some areas of the thin sections and are typically the same bioclastic assemblage as the surrounding limestone (Fig. 4.4A).

Siliciclastic composition

Siliciclastic material makes up a very similar proportion of the rock as do bioclasts (Fig. 4.1). The dominant siliciclastics are expectedly volcanic rock fragments and ash material, given the association with the Southern Volcanics at Ngakuha Reef on Chatham Island and the Kahuitara Tuff on Pitt Island (Fig. 4.3). Often the igneous material appears palagonitic in thin section while other rock fragments display trachytic textures (Fig. 4.4B). The occurrence of opaque minerals is locally significant at Flowerpot Bay on Pitt Island (Fig. 4.3)

and appears to be mainly manganese oxides precipitated along the fissure walls into which the Haumurian limestone has been deposited.

Interparticle material

In general the Haumurian limestone shows 2% porosity with approximately 20% of the whole rock consisting of matrix fill material or cement (Figs 4.1 & Appendix B Figs B6, B11, B12). Micrite is the dominant interparticle material and occurs as either microbioclastic mud or homogenous and possibly precipitated micrite (Fig. 4.4) (Reid et al., 1990; Nelson and James, 2000). Spar cements are less common (with a 2:1 ratio of micrite to spar) but spar cements occur in equal quantities at both localities. Cathodoluminescence shows that the spar cements are generally non-luminescent with a bight luminscencent zone toward the edge of some syntaxial overgrowths (Fig. 4.5).

Classification

Thin section analysis indicates relatively little grain to grain contact within many samples of the Haumurian limestone. This observation, coupled with the dominance of micrite in many samples, classifies them as either wackestones or mudstones, but also as packstones. More sparry lithologies are grainstones (Figs 4.4, 4.5).

Interpretation

The bioclastic content of the Haumurian limestone generally shows a bryomol assemblage with some inclusions of stromatolitic algae hinting at warm temperate water temperatures, at possibly inner to mid shelf depths (Fig. 4.2). However, it should be noted that this is a rather tentative assessment as there appears to be multiple lithologies present within the Flowerpot Bay limestone dyke occurrences and only one appears to show any real connection to the Haumurian limestone occurrence from Ngakuha Reef on Chatham Island, discussed later (Fig. 4.4). The high abundance of volcanic rock fragments and volcaniclastic sediment in the Haumurian limestone (Fig. 4.3) emphasises the close volcanic association with the up-thrust Kahuitara Tuff fault block on Pitt Island and pillow basalts of the

Southern Volcanics on Chatham Island (see Section 3.1.1). This volcanic association has exerted a strong influence on the lithology and geometry of the Haumurian limestone. Diagenetically, the occurrence of biomoulds, epitaxial spar cement rinds and syntaxial rim overgrowths about echinoderm fragments (Fig. 4.4), in conjunction with the cathodoluminescence showing multiple thin bright zoned signatures (Fig. 4.5), may indicate a shallow burial/meteoric diagenetic environment (Tucker and Wright, 1990; Hood and Nelson, 1996; Nelson and James, 2000).

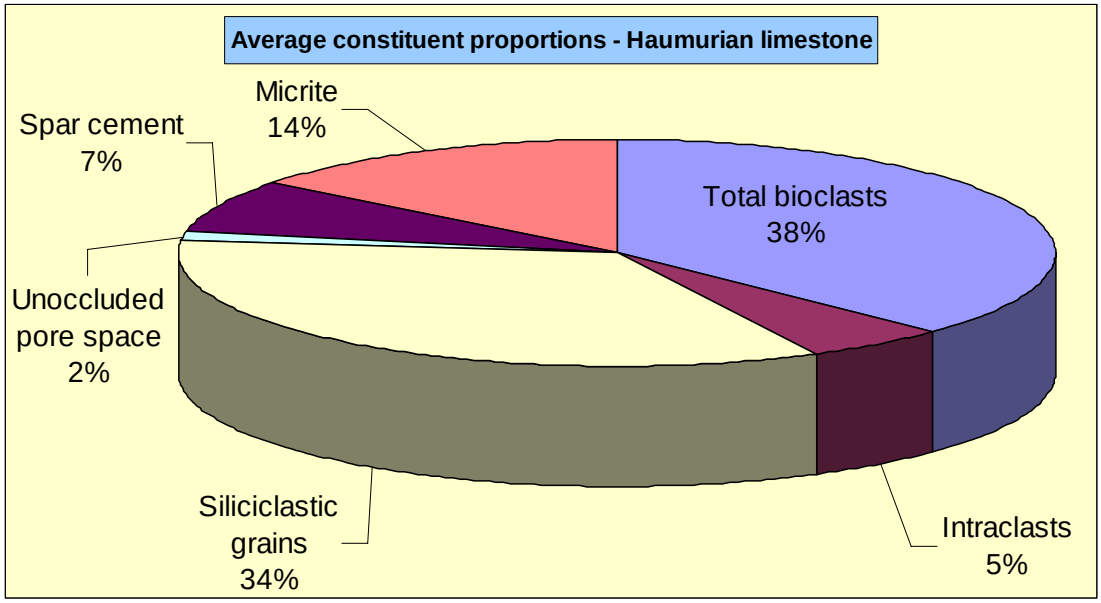

Figure 4.1: Whole rock composition of the Haumurian limestone, in which siliciclastics are an important component.

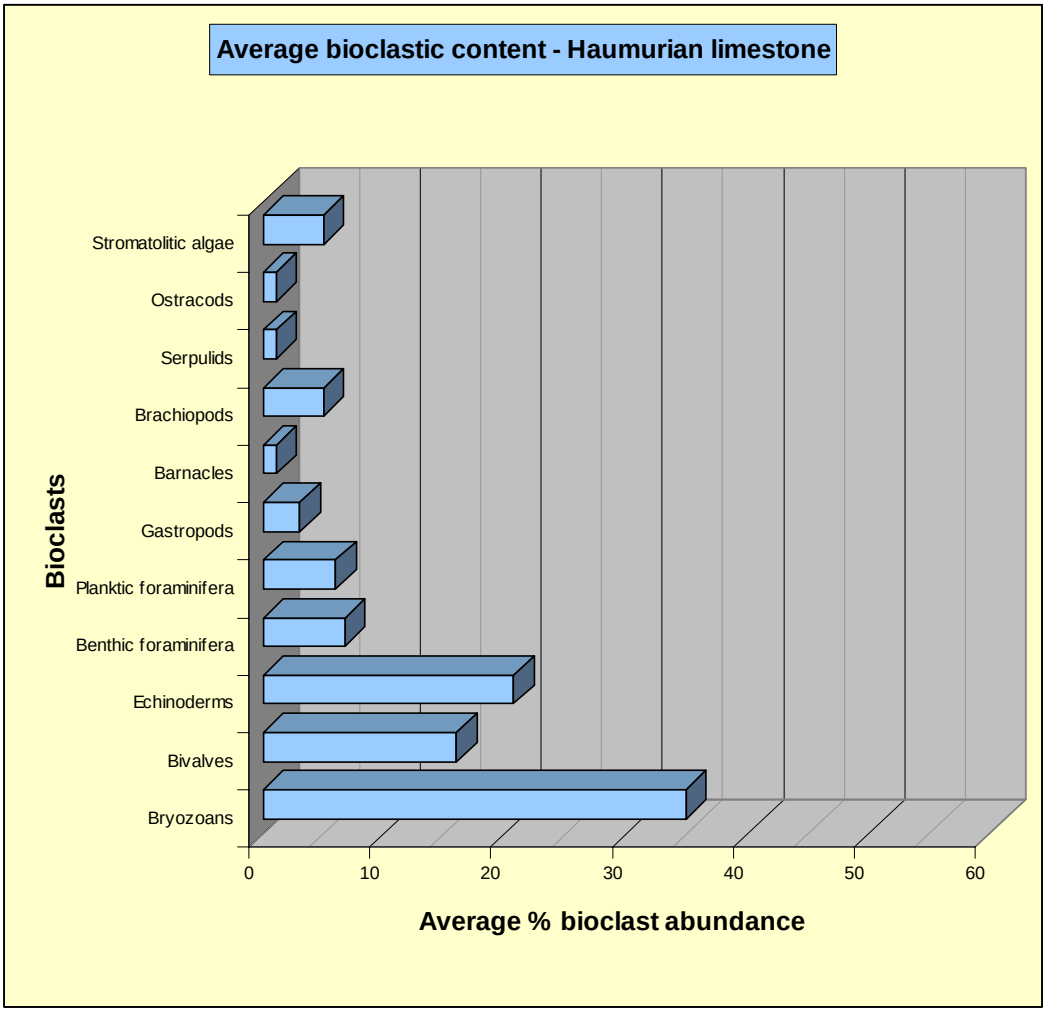

Figure 4.2: Skeletal components of the Haumurian limestone. The apparent abundance of stromatolitic material is of localised significance at the Flowerpot Bay locality on Pitt Island only.

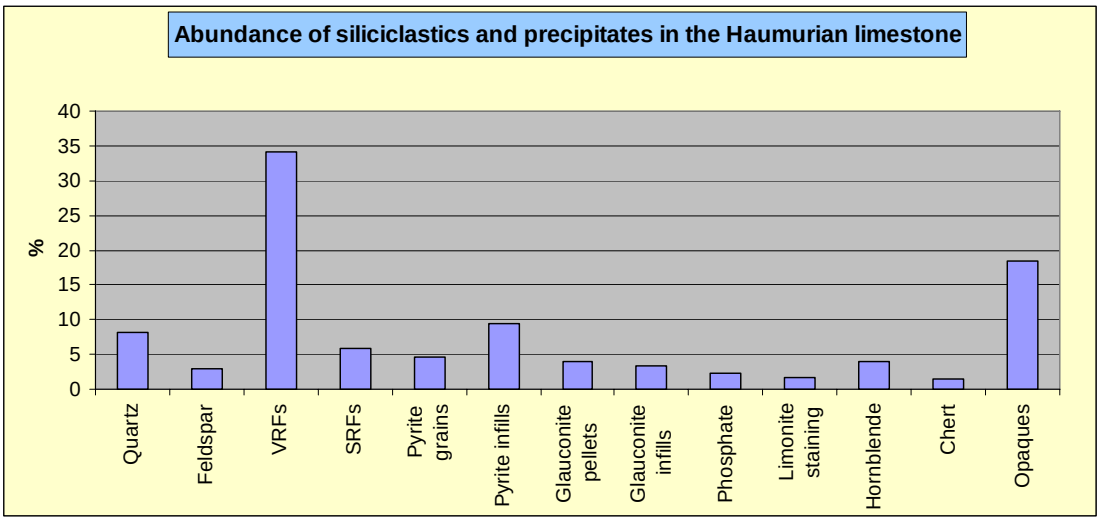

Figure 4.3: Siliciclastic and precipitate components in the Haumurian limestone. The close association of this unit with volcanic deposits has expectedly resulted in a dominance of igneous material. Opaque minerals are localised feature at Flowerpot Bay, Pitt Island.

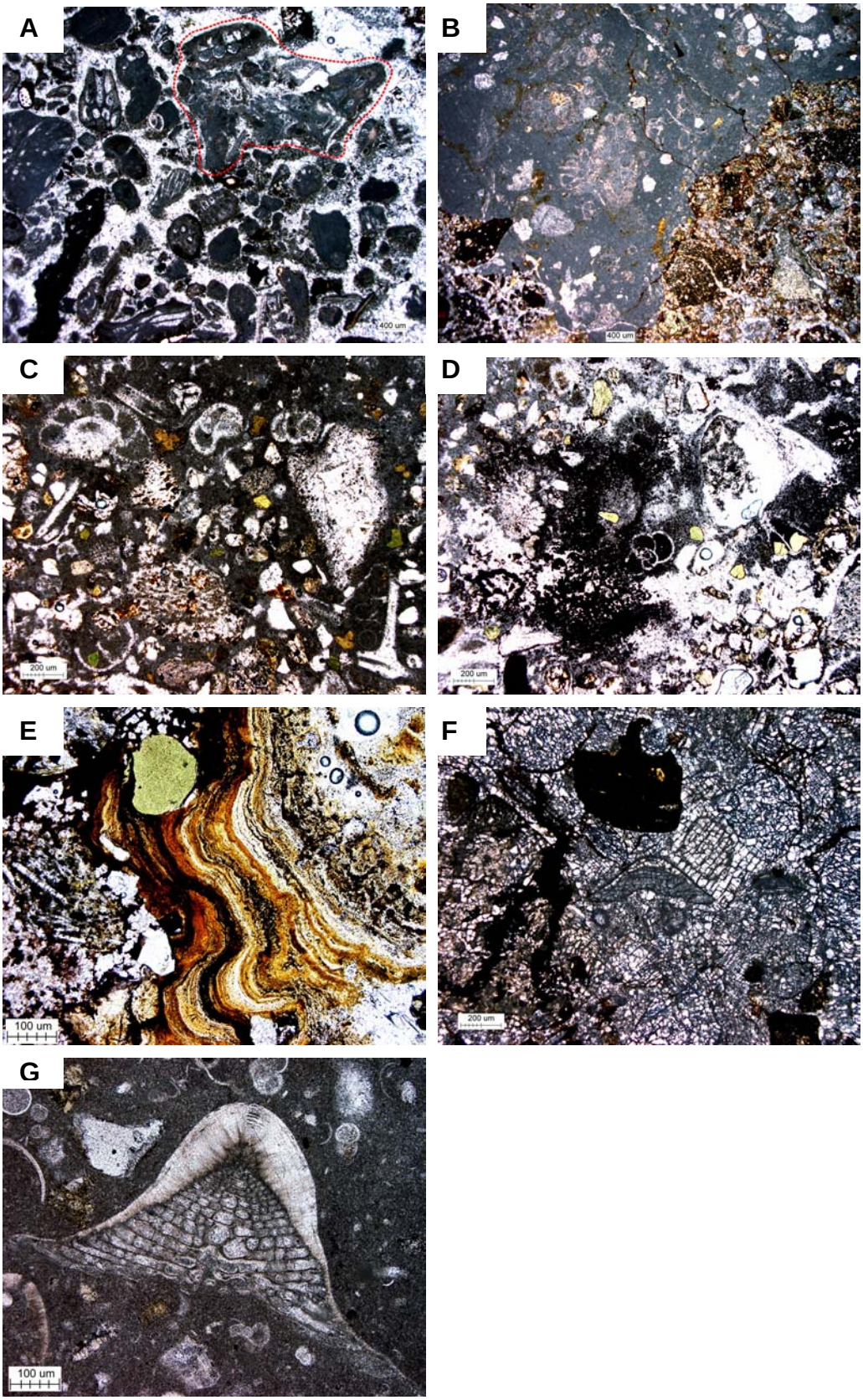
A
400 um
B
400 um
C
200 um
D
200 um
E
100 um
F
200 um
G
100 um

Figure 4.4: Photomicrographs of the Haumurian limestone from Ngakuha Reef on Chatham Island and Flowerpot Bay on Pitt Island. **A** Flowerpot Bay example (CH05-9.1 [sample], PPL [plain polarised light]) showing a bryozoan dominated limestone with coarse equant spar cement. A large intraclast containing bryozoan fragments can be seen towards the top of the image (circled with a red dashed line) Contrast this to **B** (CH05-9.3, PPL), also from Flowerpot Bay, but with large volcanic rock fragments and with seemingly homogenous micritic matrix cement. **C** (CH05-15.2, PPL) coarse conglomeratic lithofacies from Ngakuha Reef with mixed bioclasts, siliciclastics and precipitates. Also from Ngakuha Reef **D** (CH05-15.4, PPL) showing both inter- and intraparticle pyrite precipitation highlighting a planktic foraminifera in the centre of the micrograph. **E** (CH05-15.3, PPL) laminated growth rings typical of stromatolitic algae, here occurring within the conglomeratic lithofacies at Ngakuha Reef. The larger glauconite pellets near the top of the slide is lodged within a boring within the stromatolite rather then the stromatolite having grown around the pellet. **F** (CH05-9.1B, PPL) from Flowerpot Bay shows an equant spar cement that has an unusual fractured appearance which could be mistaken for silicification. Cathodoluminescence has shown that this is calcite. Also present within F are sparite envelopes and an unknown, possible benthic foraminifer (centre), the latter also seen in significant numbers within the Haumurian limestone at Ngakuha Reef, shown in **G** (CH05-15.1, PPL).

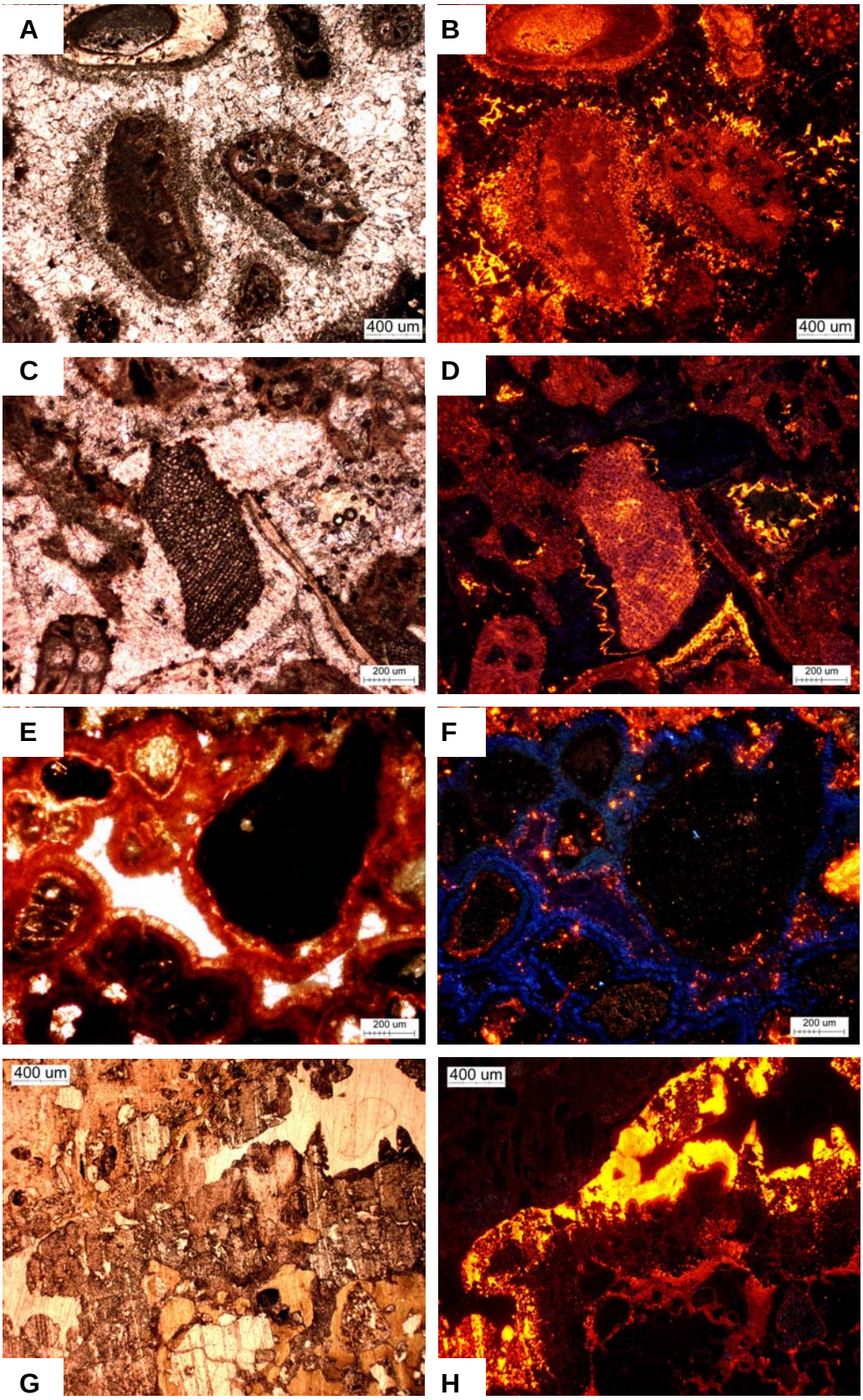
A
400 um
B
400 um
C
200 um
D
200 um
E
200 um
F
200 um
400 um
G
400 um
H

Figure 4.5: PPL and cathodoluminescence (CL) micrograph pairs of the Haumurian limestone. **A** and **B** (CH05-9.4, PPL and CL) from Flowerpot Bay show a micrite rind about bioclasts with equant spar cement and acicular 'spiky' rim cements (left-hand side of the central left bryozoan). Cathodoluminescence in B shows that equant spar cement is dull and non-luminscencent while the micrite rind is reasonably luminescent with some bright luminescent zones present around the edges of the acicular rim growths. **C** and **D** also from Flowerpot Bay (CH05-9.6, PPL and CL) shows an echinoderm with a large syntaxial rim (C) that in luminescence (D) shows an immediate dull zone followed by an outer edge bright zone. **E** and **F** (CH05-9.4, PPL and CL) show an interesting feature of the Haumurian limestone at Flowerpot Bay with rinds of silica crystals around volcaniclastics giving a blue luminescent signal (F). From Ngakuha Reef on Chatham Island in **G** and **H** (CH05-15.1, PPL and CL) the dirty equant spar cements show both dull and bright zones of luminescence. Note the tightly zoned area toward the outer edges with a large bright zone surrounding a pore space in the top right-hand corner of the image.

4.1.2 Matanginui Limestone

Whole rock composition

In general, the Matanginui Limestone contains 60% bioclastic material and 9% siliciclastic material set in 22% micrite plus calcite spar along with 6% pore space (Fig. 4.6). The Matanginui Limestone is reported to have carbonate contents ranging from 95% to 100%, with lower detrital rich zones showing ranges from 52% to 85% on Chatham Island and Pitt Island (Campbell et al., 1993).

Bioclastic composition

Average bioclastic abundances show a dominance of bryozoans, which are at least 50% more common than any other skeletal type (Fig. 4.7). Both planktic and benthic foraminifera are equally abundant at 10% each of the total bioclasts. Also common are echinoderms and to a lesser extent bivalves. Geographically, planktic foraminifera are only locally significant, with high values recorded for the exposure at Moreroa on the western shore of Te Whanga Lagoon (Appendix B Fig. B13). Benthic foraminifera are also locally significant to a lesser degree, particularly in exposures of the northern Red Bluff area. In general, bryozoans and bivalves (bryomol skeletal assemblage) are dominant at all locations, along with more localised occurrences of echinoderms. Most exposures have skeletal fragments that are abraded and poorly sorted, with modal grain sizes from 0.5-2.5 mm (Appendix B Figs B13, B15, B16). Intraclasts which accounted for an estimated 3% of the whole rock composition were generally the same lithology as the Matanginui Limestone and were often composed nearly entirely of micrite with some skeletal grain inclusions, typically planktic foraminifera (Fig. 4.9C). The micritic nature of the intraclasts made them sometimes difficult to detect, they being most obvious where spar cements occur.

Siliciclastic composition

Siliciclastics are represented by both quartz and feldspar minerals, the latter commonly being slightly more abundant (Fig. 4.8). Both volcanic and sedimentary rock fragments are ubiquitous, but the volcanic fragments are abundant only in deposits that are closely associated with pyroclastics, such

as those at Red Bluff and Flowerpot Bay (Appendix B Fig. B14). Glauconite pellets are relatively common with some precipitation of glauconite in skeletal fragments (Fig. 4.9C). Pyrite infills tend to be more common than glauconite, but still of generally low abundance (Appendix B Fig. B14). Phosphorite is present at all localities and limonite staining is prevalent at some exposures. Campbell et al. (1993) recorded sand sized inclusions as rare and consisting of quartz, volcanic rock fragments (tuff), metamorphic rock fragments, glauconite and phosphorite.

Siliciclastic grain sizes are mostly <1 mm although there are coarser grain sizes at the Whareama site, at the southern end of Te Whanga Lagoon. Grains are typically sub-rounded and moderately to moderately poorly sorted (Appendix B Figs B15, B17).

Interparticle material

Interparticle material averages about 22% of the whole rock composition, plus some 6-10% of open pore space (Fig. 4.6). Micrite dominates many samples, although spar cement is locally important, especially at Whareama (Appendix B Fig. B18). Micrite typically occurs as homogenous or clotted precipitated types, and there is also some micritization of bioclasts (Fig. 4.9) (Reid et al., 1990; Nelson and James, 2000). Spar cement fabrics range from acicular ‘spiky’ fringe rims to equant spars, the latter also occurring as neomorphic replacements of possible aragonitic bioclasts (Fig. 4.9) (Scholle and Ulmer-Scholle, 2003). Cathodoluminescence of these sparry samples shows that the acicular fringe cements and equant spar replacement crystals are mainly non-luminescent, although luminescent zones may occur along the outer edges of syntaxial overgrowth cement about echinoderm fragments (Fig. 4.10).

Campbell et al. (1993) reported that Pitt Island occurrences of the Matanginui Limestone contained radiating sparite fills within pore spaces and also some recrystallisation of sparry cement to ‘large single crystals’, presumably meaning large blocky spar cements.

Classification

Campbell et al. (1993) considered the Matanginui Limestone as being predominantly a moderately well sorted grainstone with up to 10% silt sized carbonate fragments trapped within the bryozoan skeletal frames. Petrographic analysis in this study demonstrates the importance of micrite as an interparticle fill, so that many of the Matanginui Limestone samples are packstones or wackestones rather than grainstones. However, there is a need to positively identify the origin(s) of micrite, whether detritus, a precipitate or a replacement product. This question is addressed later.

Interpretation

The Matanginui Limestone shows a bryomol skeletal assemblage (Fig. 4.7) with the presence of the large benthic foraminifera *Asterocyclina* possibly indicating warm temperate shallow water conditions in conjunction with the presence of calcareous algae (Fig. 4.9C). Facies without *Asterocyclina* present may indicate deposition at greater depths. The abundance of volcanic rock fragments and volcaniclastic sediment (Fig. 4.8) emphasises the close association with deposition of the Red Bluff Tuff (Figs 3.14, 3.15), which has exerted a strong influence on the lithology and geometry of the Matanginui Limestone, particularly at Red Bluff on Chatham Island with the formation of limestone dykes (discussed later). Elsewhere the formation of hardgrounds (Figs 3.12, 3.16) in conjunction with isopachous cement rinds (Figs 4.9A & E, 4.10G), syntaxial rim overgrowths about echinoderm fragments (Figs 4.9D, 4.10C), spar cement envelope structures (Fig. 4.9F) and biomoulds (Fig. 4.10E) may indicate seafloor cementation with later meteoric diagenesis. Cathodoluminescence signatures may indicate a degree of shallow burial diagenesis with only a single bright zone of luminescence present about the outer edges of syntaxial rim overgrowths (Fig. 4.10) (James and Bone, 1989, 1992; Hood and Nelson, 1996).

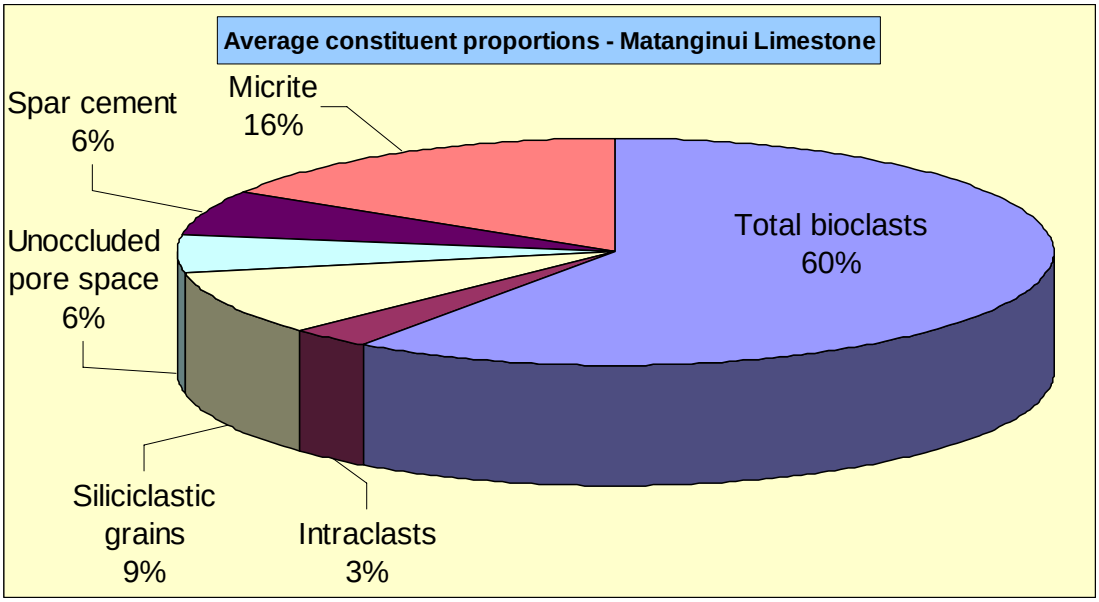

Figure 4.6: Whole rock composition of the Matanginui Limestone on the Chatham Islands showing micrite to be a significant component of the limestone composition.

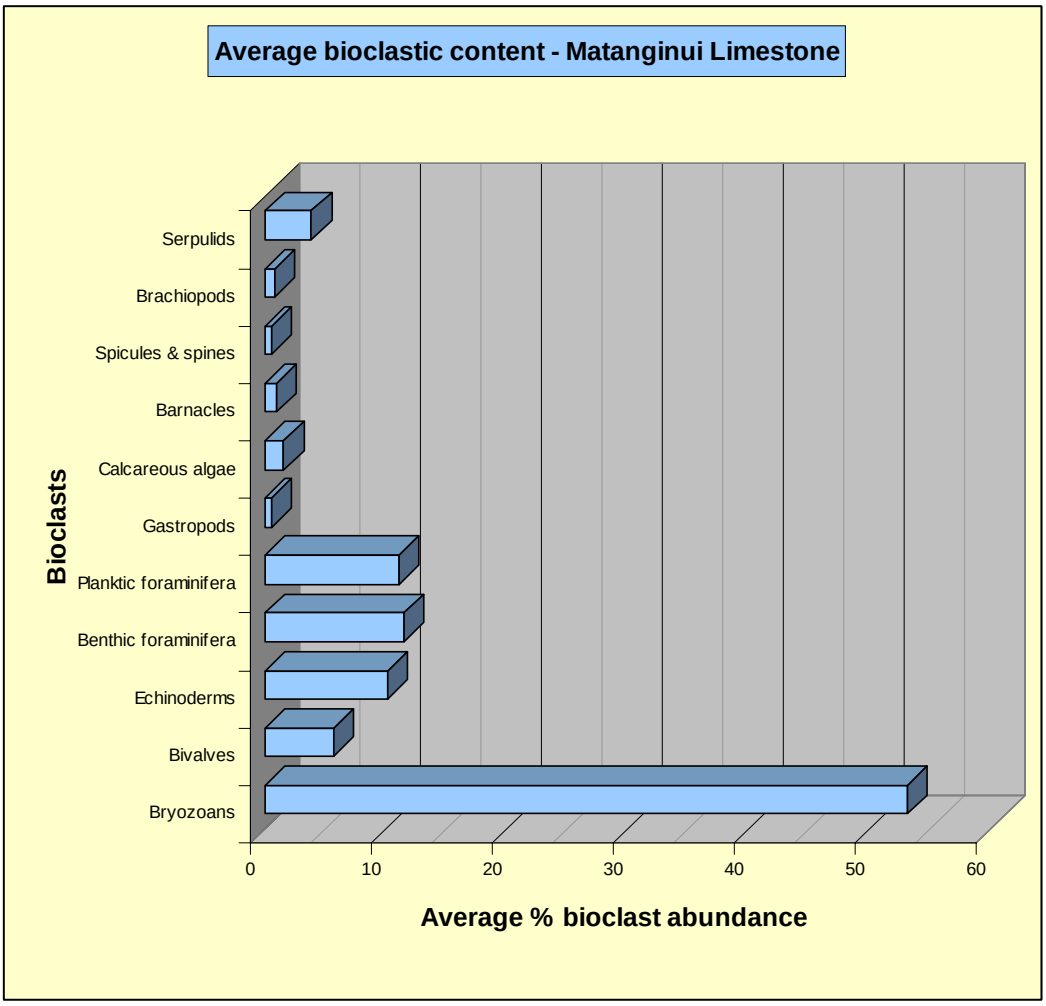

Figure 4.7: Bar graph of the skeletal types within the Matanginui Limestone on the Chatham Islands showing a dominance of bryozoans and a significant contribution also from foraminifera.

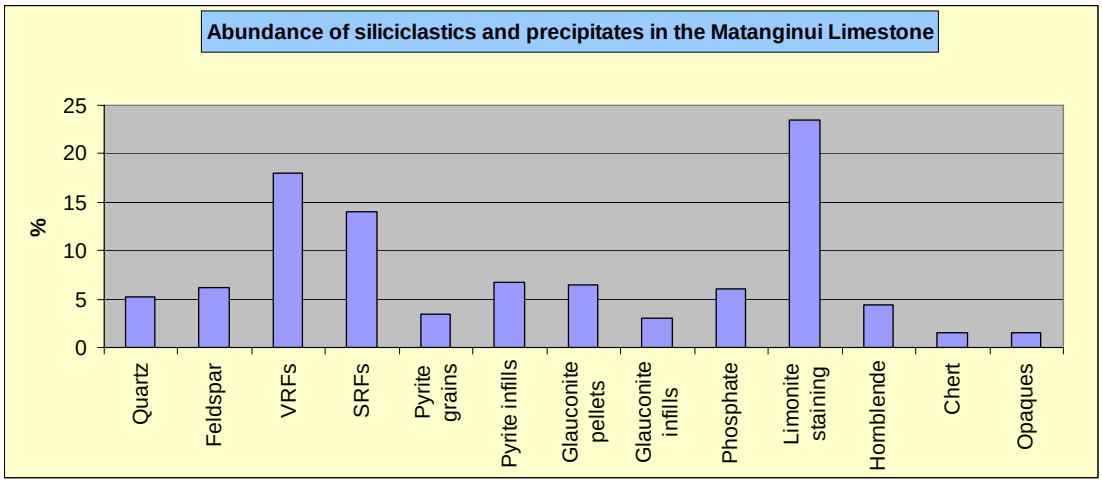

Figure 4.8: Bar graphs of the siliciclastic and precipitate components in the Matanginui Limestone. The spike in volcanic rock fragments (VRFs) indicates the close association of the limestone with the Red Bluff Tuff.

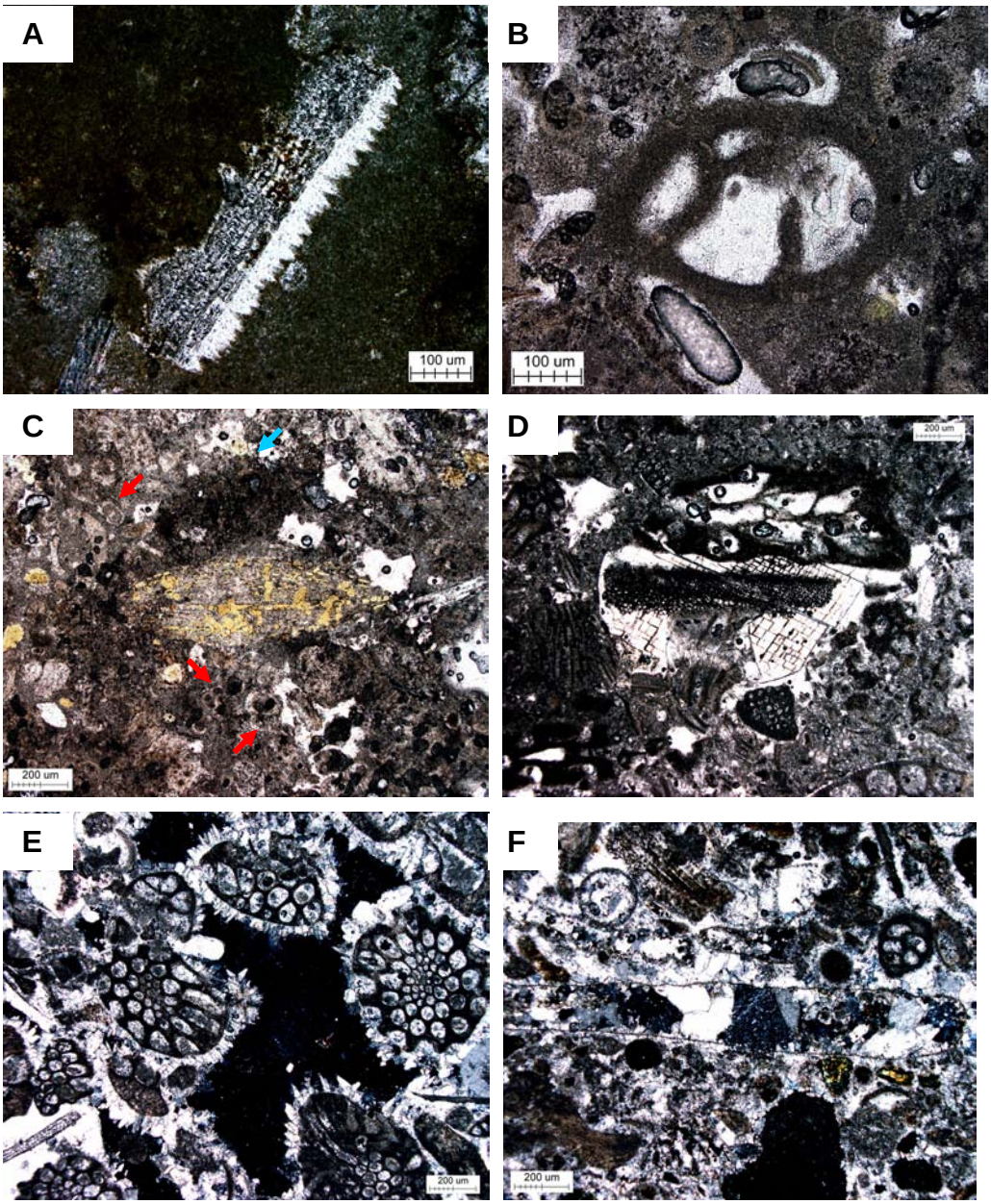

Figure 4.9: Petrographic characteristics of the Matanginui Limestone. **A** (CH05-6.10, XPL [cross polarised light]) echinoderm plate with a 'spiky' acicular rim cement within a homogenous micrite matrix/cement from Rocky Side, Pitt Island. Also from Rocky Side **B** (CH05-6.10, PPL) showing total micritization of benthic foraminifera. **C** (CH05-1.8, PPL) sample from Moreroa Point, Chatham Island showing glauconite infills within the large benthic foraminifera *Asterocyclina.* Note the planktic foraminifera within the micritic cement/matrix which can make their skeletal identification difficult (red arrowed) and also a micritic intraclast (blue arrowed). **D** (CH05-6.1, PPL) sample from Rocky Side shows a large syntaxial spar growth around an echinoderm plate with bryozoans in a micritic matrix/cement. **E** (CH05-14.2, XPL) acicular fibro-radiating cements surrounding bryozoan fragments from the southwest corner of Te Whanga Lagoon, Chatham Island (near the Motarata Limestone type section). Note here the syntaxial rim growth around an echinoderm plate in the bottom left-hand corner of the image and the open porous fabric of the limestone. **F** (CH05-14.3, XPL) also from the Motarata Limestone type section shows neomorphism by coarse calcite grains of a former ?aragonite bioclast across the centre of the image.

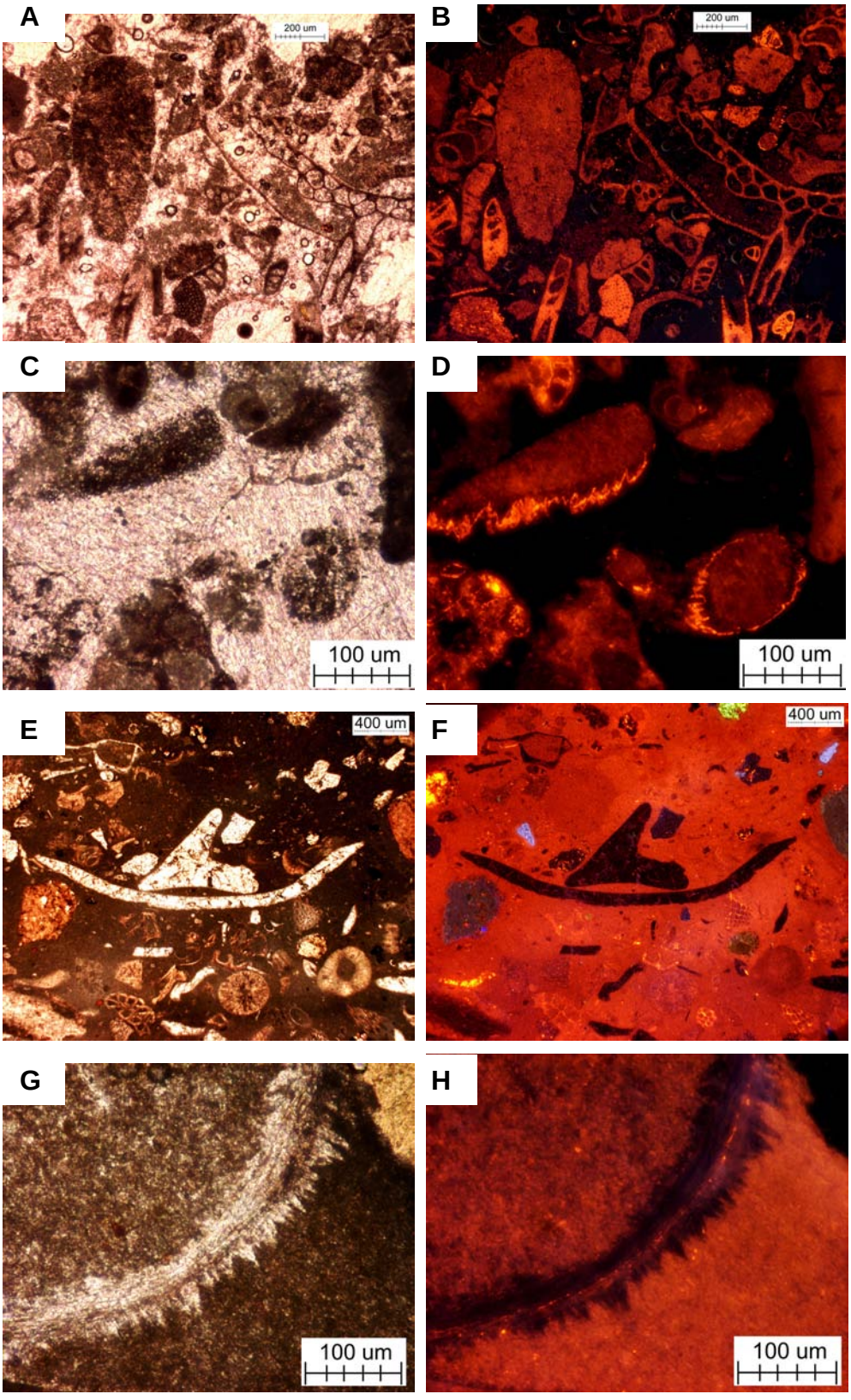
A
200 um
B
200 um
C
100 um
D
100 um
E
400 um
F
400 um
G
100 um
H
100 um

Figure 4.10: PPL and CL micrograph pairs of the Matanginui Limestone. **A** and **B** (CH05-16C1, PPL and CL) sampled north of Red Bluff, Chatham Island. These micrographs show the typical petrographic and luminscencent signature of the Matanginui Limestone with mixed micrite and spar matrix/cements that display dull to non-luminescent signatures. **C** and **D** (CH05-14.2, PPL and CL) from the Whareama, echinoderms within a dirty spar cement show an outer fringing luminescent zone, while the spar cement is completely non-luminescent. **E** and **F** (CH05-13A, PPL and CL) an isolated occurrence at Flowerpot Bay on Pitt Island showing biomoulds with neomorphic spar cement fills which display a non-luminescent signature in contrast to the surrounding micrite matrix. **G** and **H** (CH05-6.10A, PPL and CL) high magnification shot of the acicular fringe cements on a bivalve are non-luminescent, suggesting that early marine or meteoric cement types are present within the Matanginui Limestone.

4.1.3 Te One Limestone

Whole rock composition

The Te One Limestone averages 72% bioclasts, has a small (3%) siliciclastic component, and 17% interparticle material plus 5% porosity (Fig. 4.11). This porosity value is unexpectedly low considering the limestones poorly indurated and friable field characteristics. Carbonate contents range from about 96% to 99%, the terrigenous material being rare and consisting mainly of quartz and altered feldspars (Campbell et al., 1993).

Bioclastic composition

Bryozoans are by far the dominant bioclast within the Te One Limestone (Fig. 4.12). Echinoderms and planktic foraminifera are also significant along with noteworthy contributions from brachiopods and bivalves. However, planktic foraminifera are locally significant only at the Big Bush Quarry locality, and likewise brachiopods are important only at Moreroa Point (Appendix B Fig. B31). Campbell et al. (1993) noted that the abundance and diversity of both benthic and planktic foraminifera increased up section until they became as abundant as bryozoans in the uppermost stratigraphic levels of the Te One Limestone. Bioclastic fragments are mainly >2 mm in size, moderately abraded and display moderately poor sorting (Appendix B Figs B33, B34, B35). Intraclasts represent 3% of the whole rock component within the Te One Limestone and are generally present as micritic clasts of presumably the same lithology as the interparticle micrite in the limestone (Fig. 4.14B). The highly abraded and micritic nature of the Te One Limestone made their identification difficult. They were generally observed to have very vague (blurred) edges defining their presence from the surrounding limestone.

Siliciclastic composition

The Te One Limestone is one of the ‘cleaner’ limestones on the Chatham Islands, with only minor amounts of siliciclastic material. The main contribution is from precipitates, specifically glauconite pellets and glauconite infills, but also pyrite infills (Fig. 4.13). However, glauconite infills are absent at Moreroa Point, where instead the phosphatic content is highest (Appendix B Fig. B32). Quartz contents are maximum at Big Bush Quarry. Siliciclastic

and precipitate grain sizes are generally fine (<0.5 mm), with subrounded grains and moderate sorting (Appendix B Figs B33, B34, B35).

Intraparticle material

The intraparticle material within the Te One Limestone is predominantly micrite, usually a clotted variety but also sometimes homogenous (Figs 4.11, 4.14B & Appendix B Fig. B36). Spar cements are also present in minor amounts, usually as acicular fringing cements or as syntaxial overgrowths about echinoderm fragments (Fig. 4.14). Due to the extremely friable and poorly indurated properties of the Te One Limestone, preservation of the *in situ* original textures and fabrics was difficult to maintain during the thin section production process. Consequently, analysis of many of the samples was done by way of grain mounts. This also meant that preservation of spar cements was minimal and this, along with the dominance of micrite, made cathodoluminescent analysis difficult. However, a syntaxial overgrowth preserved within a grain mount showed the spar to be dull to non-luminescent with an extremely thin luminescent zone toward the outer edge of the overgrowth (Figs 4.14G & H).

Classification

Even though the Te One Limestone is generally soft and friable, behaving more like a sea floor grab sample than a 40 million year old limestone, the occurrence of micrite as an intra- and inter-particle cement/fill classifies the Te One Limestone as mainly a packstone, with grain-to-grain support of bioclasts.

Interpretation

The Te One Limestone has a similar bryomol skeletal assemblage to the underlying Matanginui Limestone, but the absence of the benthic foraminifera *Asterocyclina* offers one way of distinguishing it from the latter. The Te One Limestone probably represents a similar mid to inner shelf depth depositional setting, but would possibly appear to be more oceanic given the absence of calcareous algae (Fig. 4.12). In the field the Te One Limestone is extremely friable (Fig. 3.21) and this is suggested to be a reflection of its

diagenetic history involving minimal marine cementation evidenced by acicular fringe cement (Fig. 4.14C, D & E) and minor shallow burial cements derived from syntaxial rim overgrowths about echinoderm fragments (Fig. 4.14F & G). A degree of possible meteoric diagenesis is also observed in the development of rare neomorphic spar cement replacement (Fig. 4.14B). Cathodoluminescence signatures were poor and showed a dull luminescence with the faintest hint of an outer bright zone at the edge of syntaxial rim overgrowths, supportive of possibly marine/shallow burial diagenesis (Hood and Nelson, 1996).

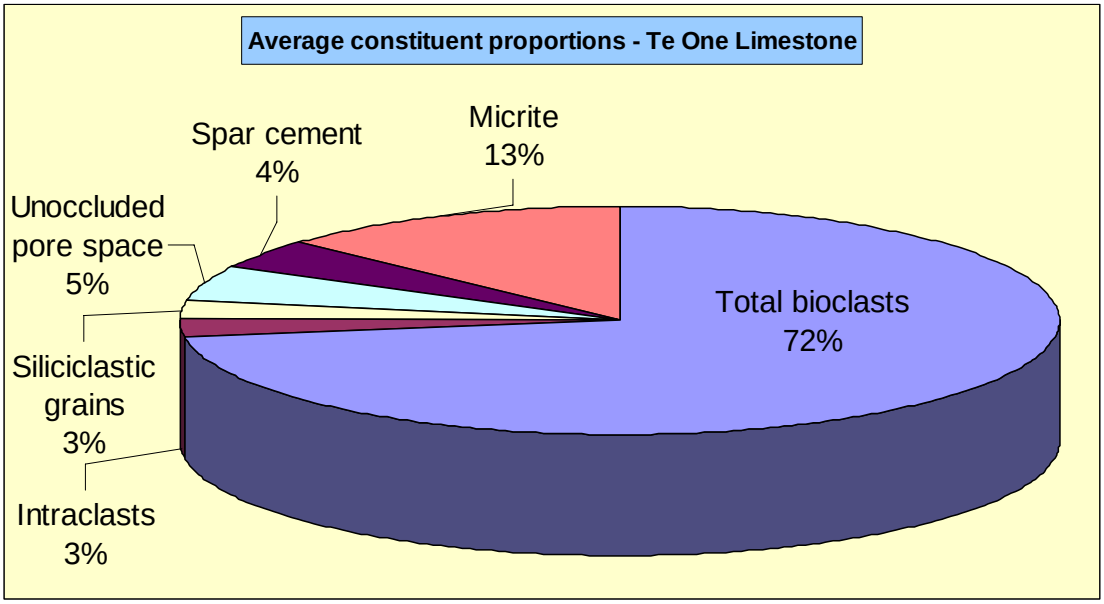

Figure 4.11: Whole rock composition of the Te One Limestone on the Chatham Islands. Note the significant micritic component, similar to the Matanginui Limestone.

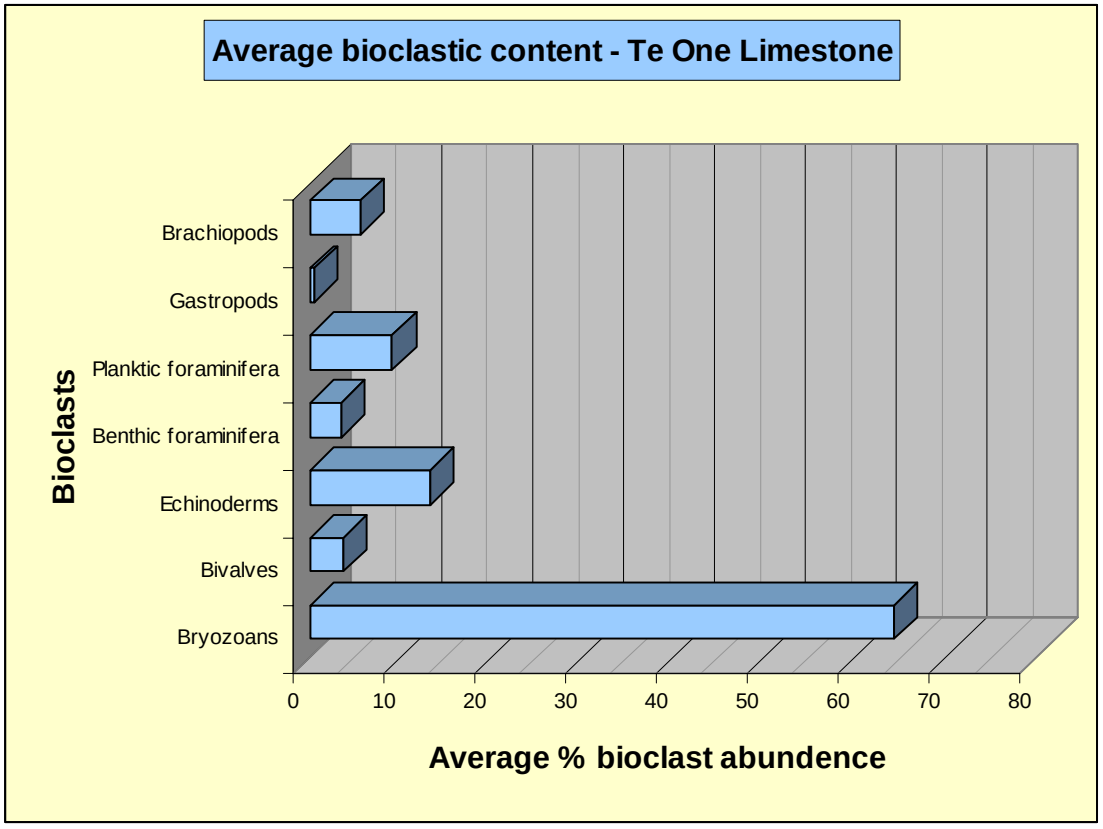

Figure 4.12: Bar graph showing the bioclastic percentages for the Te One Limestone indicate the dominance of bryozoans and significant contributions from planktic foraminifera and echinoderms.

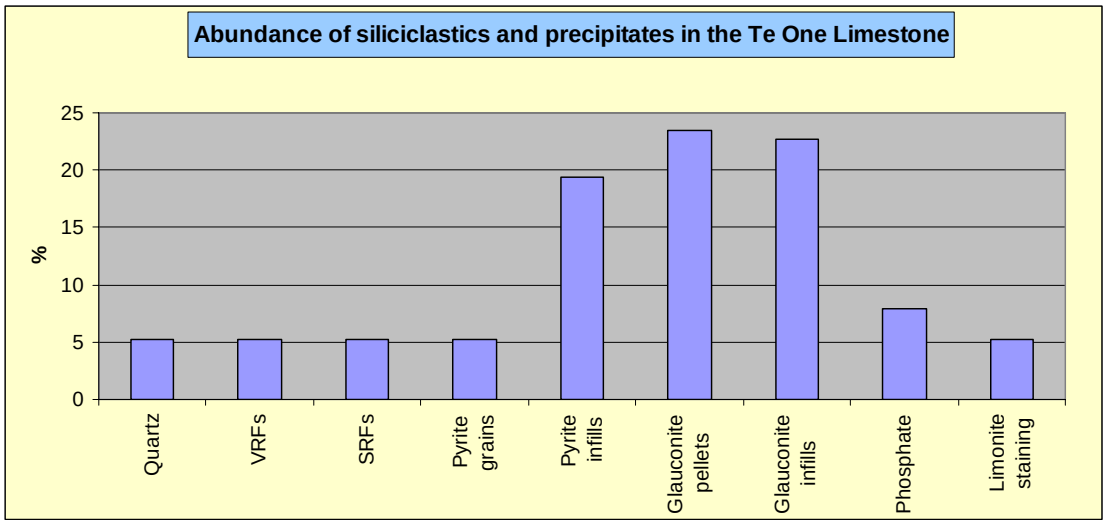

Figure 4.13: Siliciclastic and precipitate component percentages for the Te One Limestone on Chatham Islands. Note the significant contribution by glauconite.

Figure 4.14: Te One Limestone micrographs. Most of the micrographs (A–E) pictured here are from Moreroa Point, Chatham Island as these samples were made by epoxy impregnation of soft rock. The majority of thin sections for the Te One Limestone were analysed by making grain mounts. **A** (CH05-1.2, PPL) a stained thin section showing the pinkish stain colour which indicates a non-ferroan mineralogy seen in nearly all Chatham Island limestones. A shows a mixture of fragmented bryozoans, planktic foraminifera and glauconite. Thin section **B** (CH05-1.3, XPL) is similar to A with bryozoan fragments within clotted micrite/matrix cement. Pictured across the centre is neomorphic replacement of a bivalve fragment with equant spar calcite. Possible micritic intraclast of the same lithology as the intraparticle micrite of the Te One Limestone are indicated in this image (blue arrowed). **C** (CH05-1.4, XPL) micritization of benthic foraminifer with thin acicular spar cements at the edge of the bioclast. These acicular fringe cements can be seen clearly at the edges of other bioclasts, and in **D** (CH05-1.5, XPL) note the open porous fabric. **E** (CH05-1.5, XPL) is a higher magnification shot of D showing the detail of these acicular cements along the edge of a much abraded bivalve fragment. **F** (CH05-5.5, PPL) thin section made from one of the few intact samples from Big Bush Quarry, Chatham Island, showing syntaxial spar overgrowth about an echinoderm fragment. PPL and CL micrograph pair of the Te One Limestone, **G** and **H** (CH05-5.1, PPL and CL) grain mount of another Big Bush sample that includes an echinoderm fragment that shows a dull luminescence with a very thin luminescent zone near the edge of the overgrowth.

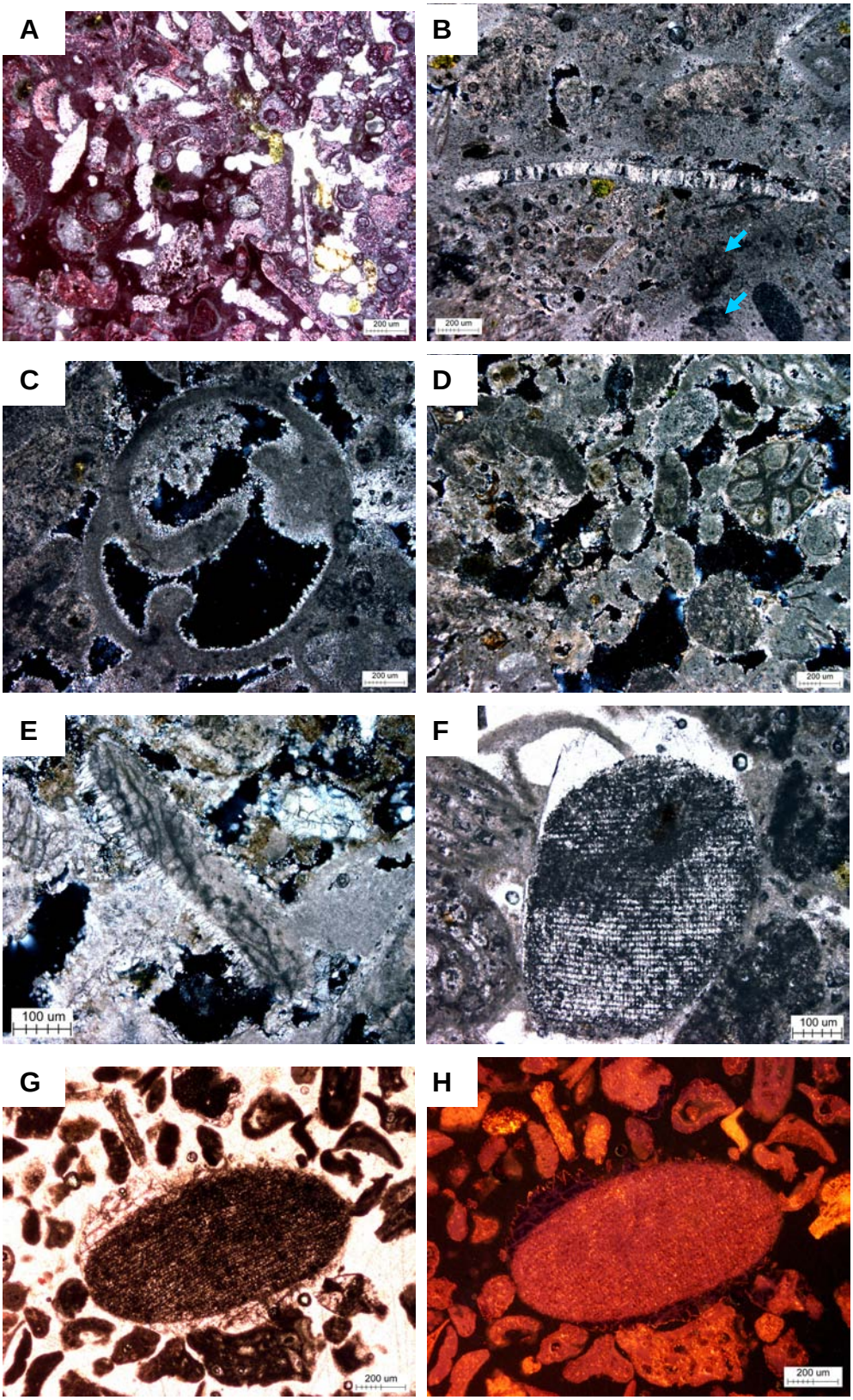
A
200 um
B
200 um
C
200 um
D
200 um
E
100 um
F
100 um
G
200 um
H
200 um

4.1.4 Taoroa Limestone

Whole rock composition

On average, the Taoroa Limestone is composed of 72% bioclasts, 11% siliciclastics and 14% interparticle material (Fig. 4.15). The Taoroa Limestone also includes about 2% porosity.

Bioclastic composition

Generally the Taoroa Limestone is a relatively fine grained deposit, and this is reflected in the dominance of planktic foraminifera in the skeletal assemblage (Fig. 4.16). Benthic foraminifera are also abundant along with bivalve and echinoderm fragments (~2 mm) and some noted inclusions of sponge spicules (Appendix B Fig. B45). Compared to the other Chatham Island limestones described so far there is a significant decline in the bryozoan content in the skeletal composition. Skeletal fragments are generally very abraded and assemblage sorting becomes progressively poorer up column, from moderately sorted to poorly sorted, with a general increase in bioclast size (Appendix B Figs B47, B49, B50).

Campbell et al. (1993) noted the mixing of Pliocene foraminifera from the upper unnamed Pliocene limestone contact with reworked elements of the Taoroa Limestone. Assemblages of benthic foraminifera were considered to indicate a mid to outer shelf setting, while the abundance of large planktic foraminifera supported an oceanic setting. Intraclasts are of minor significance representing about 1% of the whole rock composition (Fig. 4.15) and occur only in thin sections from upper stratigraphic levels of the Taoroa Limestone. Intraclasts are considered to be the same lithology as that of the Taoroa Limestone (Fig. 4.18B).

Siliciclastic composition

Quartz fragments (some polycrystalline) are the dominant siliciclastics along with a smaller percentage of feldspars (Fig. 4.17). Glauconite pellets comprise a significantly higher percentage, representing 40% of the siliciclastic materials (Figs 4.18G & H). Phosphorite inclusions are also another significant precipitate. Siliciclastic grain sizes are typically <1 mm, subrounded and, like the bioclastic fragments, become progressively finer

grained up column, although the siliciclastics remain moderately well sorted throughout the column (Appendix B Figs B45, B48, B49, B50).

Interparticle material

The Taoroa Limestone has a considerable amount of micrite between and within grains (Figs 4.15, 4.18 A, B, C & D, Appendix B Fig. B46). The micrite is possibly mainly a precipitate given its homogenous and clotted appearance. Spar cement is much less common, occurring as minor fringing rim cements that tend to occur inside skeletal chambers. Cathodoluminescent analysis was able to be conducted on rare echinoderm fragments that had syntaxial rim overgrowths (Figs 4.18 E, F, G & H). The results were surprising considering the high content of micrite, the luminescence showing that the Taoroa Limestone has a diverse diagenetic history with complex luminescent zones towards the outer edges of these overgrowth cements.

Classification

The Taoroa Limestone is a highly fragmented bioclastic limestone with a high degree of grain to grain contact, and this in combination with the presence of micrite classifies the Taoroa Limestone as a packstone.

Interpretation

The Taoroa Limestone represents a nannofor skeletal assemblage indicative of deepish oceanic mid to outer shelf water depths, based on the abundance of planktic foraminifera (Figs 4.16, 4.18A & B). The abundance of glauconite should not be used as an indication of deposition in such a setting as this is considered to be associated with deposition of an unnamed Pliocene limestone present at the very top of the Taoroa Limestone (Figs 3.25, 4.17, 4.18C & D). Cathodoluminescent analysis of the Taoroa Limestone suggests shallow burial/meteoric diagenesis with the presence of syntaxial rim overgrowths about echinoderm fragments, with multiple zones of luminescence present (Fig. 4.18E, F, G & H) (Hood and Nelson, 1996; Caron and Nelson, 2003).

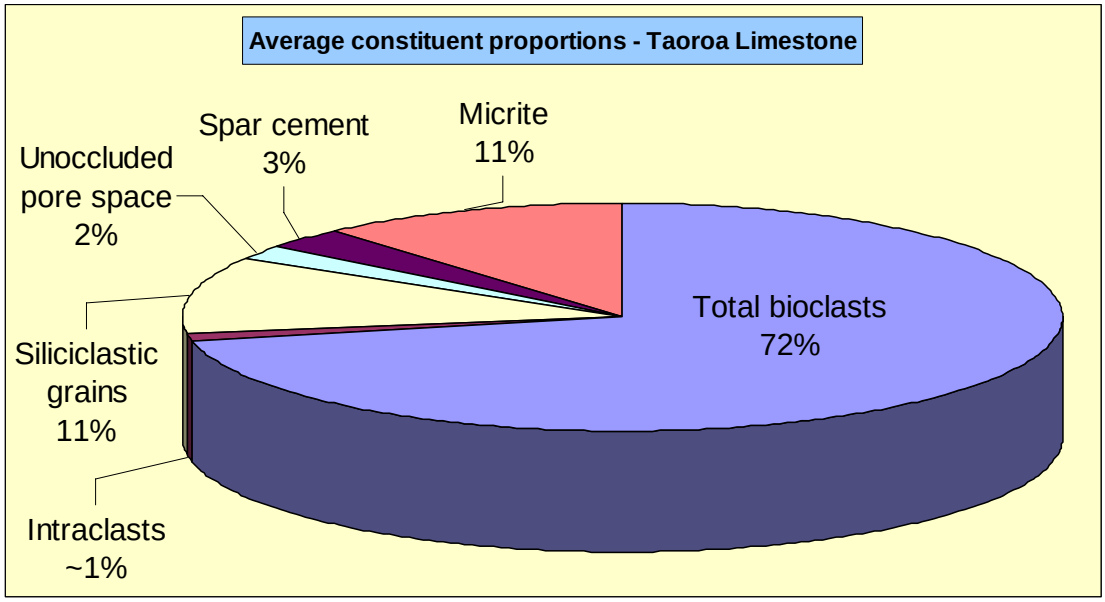

Figure 4.15: Whole rock composition of the Taoroa Limestone from the single occurrence at the northwest end of Manganui Beach, Chatham Island.

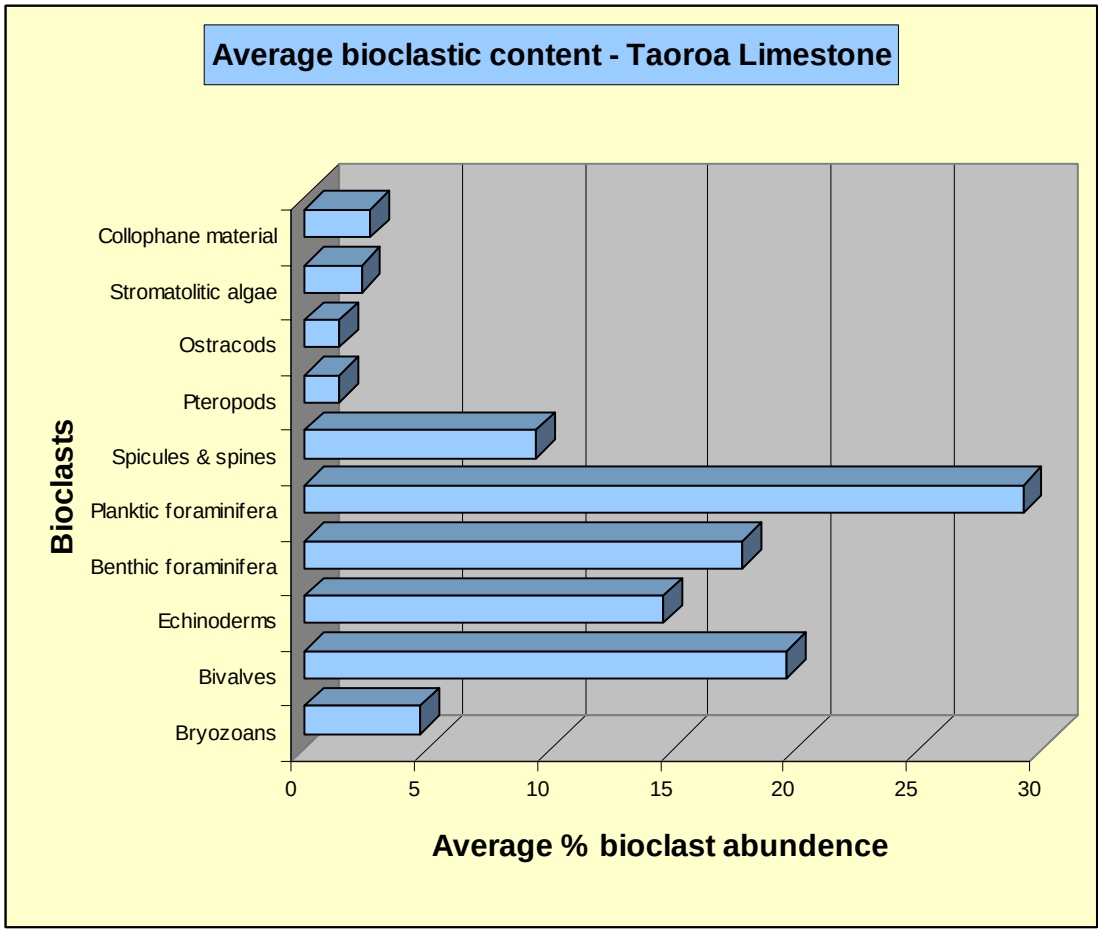

Figure 4.16: Skeletal type abundances in the Taoroa Limestone showing a diverse array of bioclasts with a dominance of planktic foraminifera.

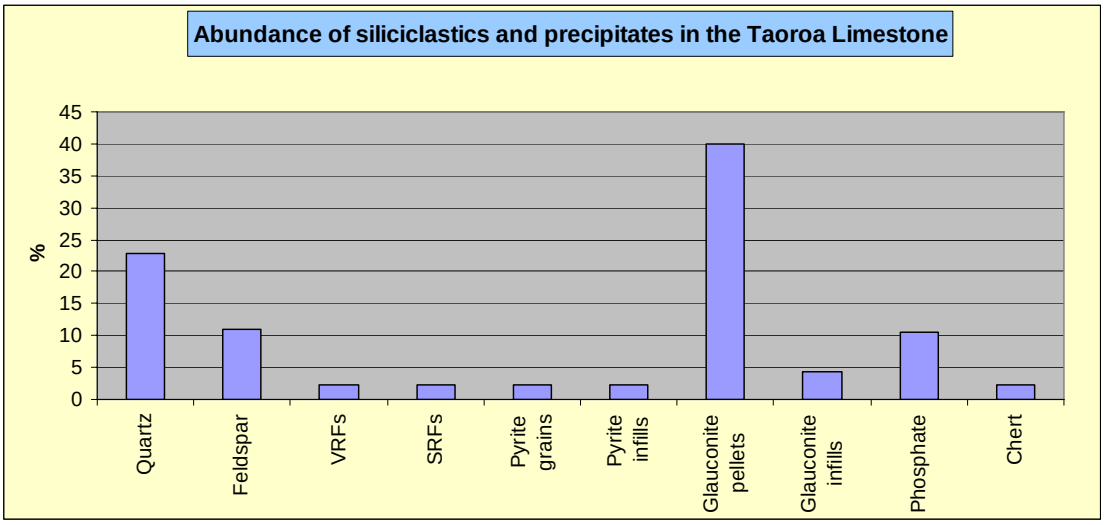

Figure 4.17: Siliciclastic and precipitate component percentages in the Taoroa Limestone, which shows a significant glauconitic component.

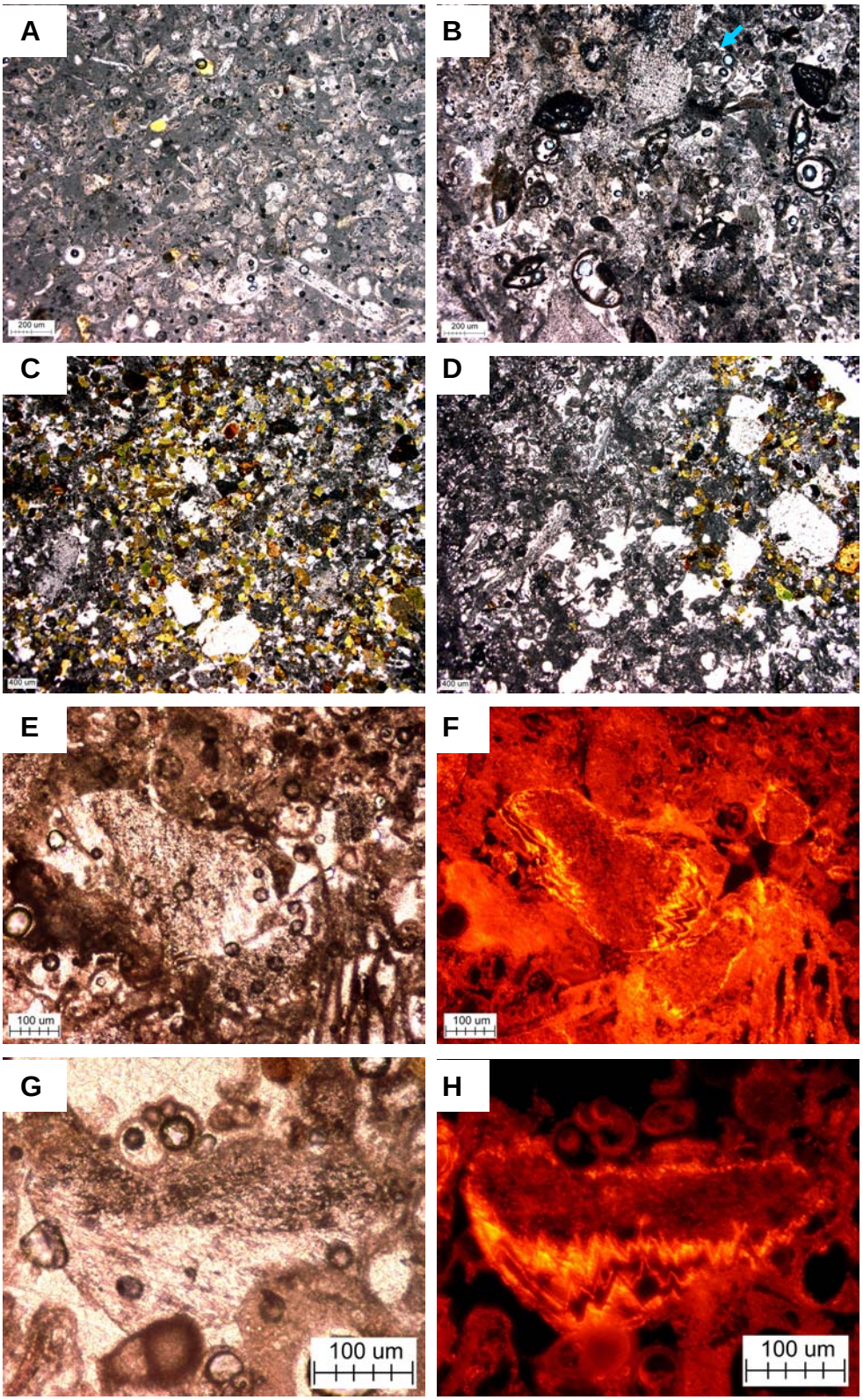
A
200 um
B
200 um
C
400 um
D
400 um
E
100 um
F
100 um
G
100 um
H
100 um

Figure 4.18: The Taoroa is a fine grained planktic foraminiferal limestone. **A** (CH05-21B, PPL) sample from the 2 m of the section at Maunganui Beach, Chatham Island. This part of the section is fine-grained then the rest of the section with planktic and benthic foraminifera, bryozoan, bivalve and echinoderm fragments. Homogenous micrite matrix/cement is prominent throughout the Taoroa Limestone section. **B** (CH05-21C, PPL) made from a mid-section sample of the Taoroa Limestone which is more porous and also shows development of microsparite cement with an increase in echinoderm material. Rare intraclasts are present in this mid-section area and are considered to be the same lithology as the surrounding Taoroa Limestone (blue arrowed). PPL and CL micrograph pairs, **C** (CH05-21D, PPL and CL) sample taken from upper 1.5 m in the position of the 'blended' unconformity with the overlying 'unnamed' Pliocene limestone, this highly glauconitic sample is considered to represent the uppermost extent of the Taoroa Limestone. **D** (CH05-21E, PPL and CL) another micrograph of the upper 'blended' unconformity with the upper glauconitic Taoroa Limestone on the rightside of the image and the overlying 'unnamed' Pliocene limestone on the leftside. **E** and **F** (CH05-21E, PPL and CL) cathodoluminescence signatures were only obtained from the upper 1.5 m of the section. Echinoderm syntaxial rims show multiple luminescent zones, evident in the high magnification shot in **G** and **H** (CH05-21E, PPL and CL).

4.1.5 Motarata Limestone

Whole rock composition

The Motarata Limestone has an average composition of 69% bioclasts, 7% siliciclastics and precipitates, and 4% of intraclasts (Fig. 4.19). Interparticle material comprises a total of 16%, with 12% of this being micrite and 4% spar cement. Porosity is estimated to account for approximately 4% of the total composition.

Bioclastic composition

The Motarata Limestone is reasonably fine grained and although bryozoans are the most abundant skeletal type, foraminifera account for a significant proportion of the skeletal assemblage (Figs 4.20, 4.22, Appendix B Fig. B54). Bivalve and echinoderm fragments are also important in the skeletal assemblage. Bioclasts have a modal size of about 2 mm and are typically very abraded (Appendix B Figs B56 & B57). Bioclastic grain sorting is significantly different between the two localities, being moderately well sorted at Moutapu Point but poorly sorted at Whareama (south of Te Matarae) near the Motarata Limestone type section (Appendix B Fig. B58). The difference in sorting likely reflects the stratigraphic position of sampling, with the exposure at Moutapu Point probably representing only the upper stratigraphic levels where grain sizes are finer (Appendix B Table B11, B12, Figs B58, B60, B63). The occurrence of fine grained microbioclastic micrite is considered to indicate intraclasts which occur in significant numbers (about 4%), particularly in lower sections of the Motarata Limestone (Fig. 4.19, 4.22C).

Siliciclastic composition

The Motarata Limestone has a significant phosphorite component along with glauconite pellets and infills (Figs 4.21, 4.22). Terrigenous material is uncommon, as are pyrite grains and infills. Grain sizes show similar trends to those seen for the bioclasts, with extremely fine grained material (<0.2 mm) present at Moutapu Point and coarser (~1.4 mm) siliciclastics at the type section (Appendix B Figs B56, B61). Siliciclastic grains are subrounded and show the same sorting trend displayed by the bioclasts (Appendix B Figs B62, B63).

Interparticle material

Micrite is the dominant interparticle fill material, present as either homogenous or sometimes clotted precipitated micrite (Figs 4.19, 4.22 B & E). Due to the soft and friable characteristics of the Motarata Limestone preservation of original textures and cement fabrics is limited and it is likely that microbioclastic micrite is also present given the high percentage of fine grain bioclasts such as foraminifera. Spar cement represents approximately 25% of the interparticle material, but its preservation is limited, occurring as minor fringing rim cements (Fig. 4.22B).

Classification

The Motarata Limestone is typically a packstone.

Interpretation

The Motarata Limestone is considered to represent a bryomol skeletal assemblage but also shows a considerable planktic foraminiferal component (Figs 4.20, 4.22). The abundance of phosphate and glauconite grains is probably derived from reworking of a hiatal deposit at the base of the Motarata Limestone identified by Campbell et al. (1993) (Figs 4.21, 4.22B & G). Diagenetically the Motarata Limestone shows characteristics of early marine cementation with some thin fibrous spar rinds (Fig. 4.22A), while a meteoric influence is suggested by the presence of rare interparticle equant spar cements precipitated from calcite saturated pore fluids (Fig. 4.22D).

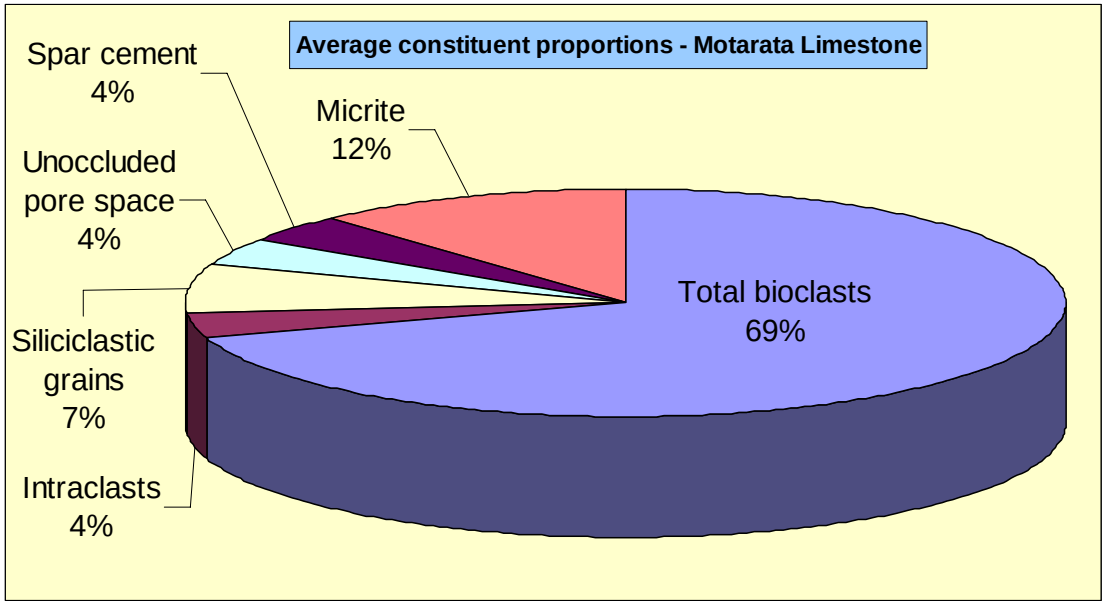

Figure 4.19: Whole rock composition of the Motarata Limestone, from samples at Moutapu Point and Te Matarae (type section), Chatham Island.

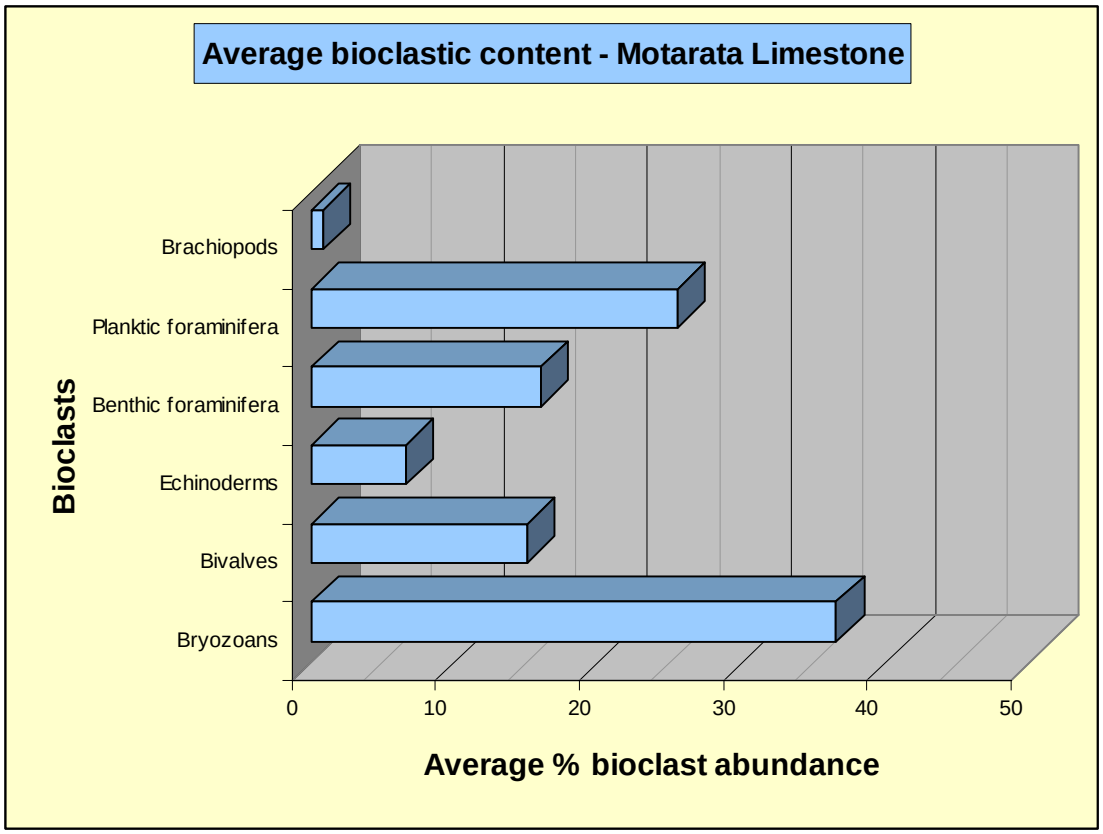

Figure 4.20: Bar graph of the skeletal assemblage percentages show a dominance of bryozoans but a significant contribution of planktic foraminifera.

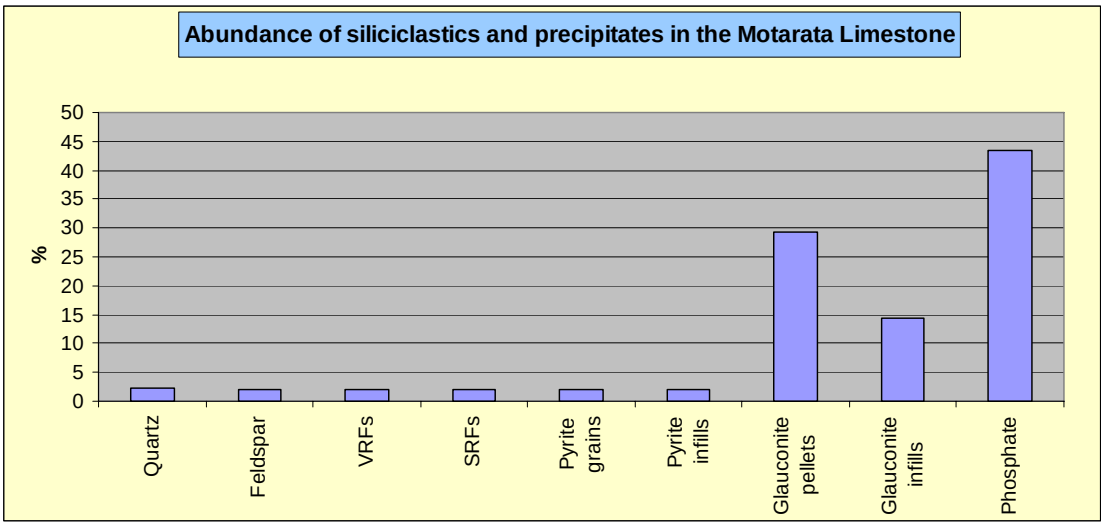

Figure 4.21: Siliciclastic and precipitate component percentages in the Motarata Limestone showing that phosphate and glauconite are significant components.

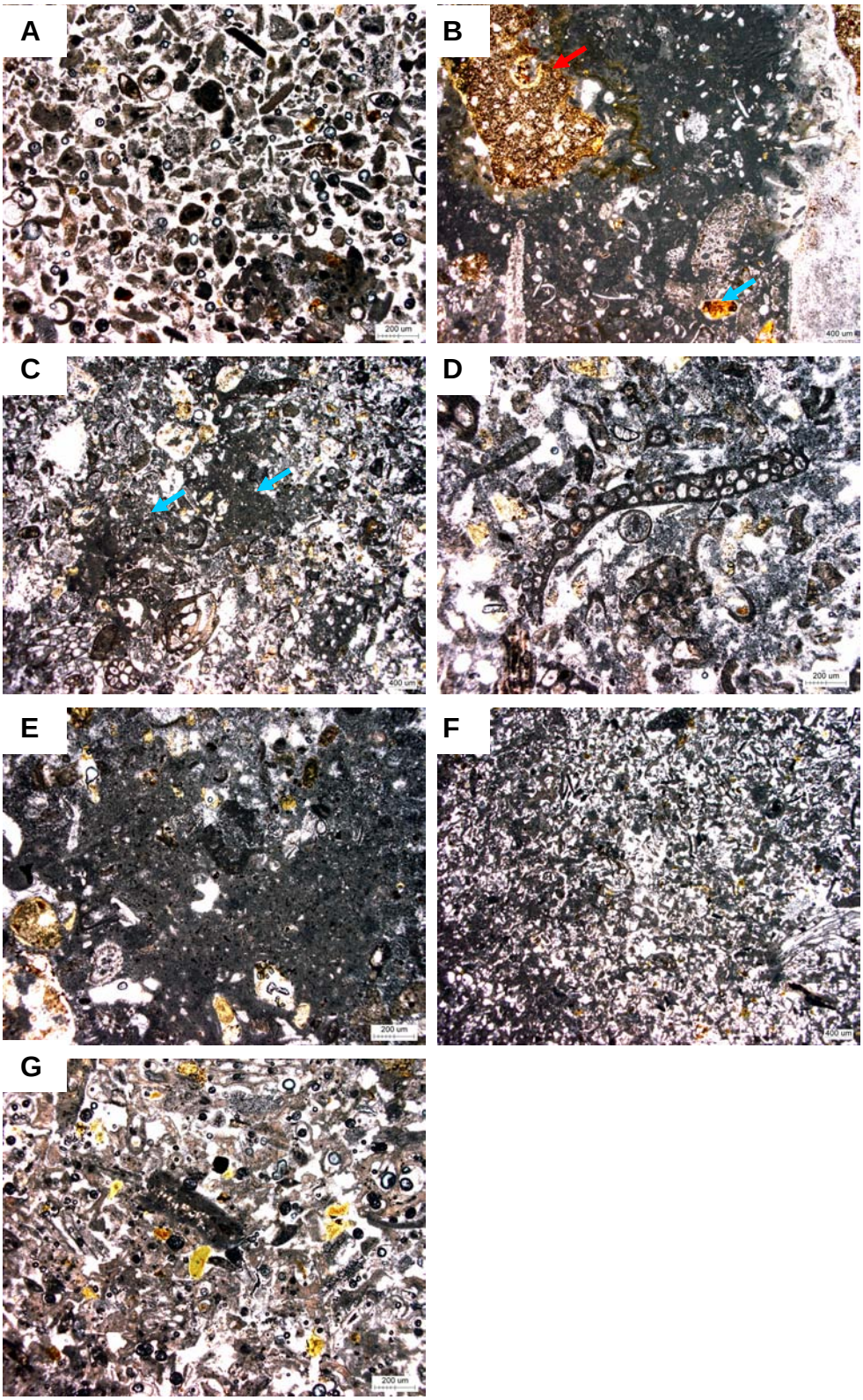
A
B
C
D
E
F
G

Figure 4.22: Photomicrographs showing the fine grained character of the Motarata Limestone with a paucity of any significant spar cement development, which precluded diagnostic cathodoluminescent analysis. **A** (CH05-3.2, PPL) sample from Moutapu Point, Chatham Island which is soft and friable with the thin section being made by way of a grain-mount. **B** (CH05-14.4E, PPL) sample from the lowermost contact with the Matanginui Limestone at Te Matarae, southwest corner of Te Whanga Lagoon, Chatham Island, marked by volcaniclastic inclusions (red arrowed) and phosphorite (blue arrowed). **C** (CH05-14.4, PPL) is again near the bottom of the section and shows the fragmented nature of the Motarata Limestone which here includes abundant foraminifera. The occurrence of fine grained microbioclastic 'patches' are considered to represent micritic intraclasts (blue arrowed). **D** (CH05-14.4, PPL) photomicrograph shows elongate bryozoans near the centre and some interparticle micrite. What appears as spar cements in these slides is predominately 'space' that is related to the soft nature of the limestone and thin section production rather than porosity. **E** (CH05-14.4, PPL) a more intact area of the slide reveals that the micrite has clotted to possibly microbioclastic textures. **F** (CH05-14.5, PPL) ~1 m above the lower Matanginui Limestone contact shows that there is little change in facies and that glauconite and phosphorite is present throughout. **G** (CH05-14.6, PPL) a sample from the middle of the section, at ~2 m above the lower contact, which again displays the uniform lithology of the Motarata Limestone.

4.1.6 Onoua Limestone

Whole rock composition

The Onoua Limestone averages 71% bioclasts, 6% siliciclastics, 1% intraclasts, and 15% interparticle material (Fig. 4.23). It has an estimated 7% porosity and the interparticle material averages 12% micrite and 3% spar cement.

Bioclastic composition

The bioclastic assemblage within the Onoua Limestone is diverse in comparison to many other Chatham Island limestones (Fig. 4.24). Bryozoans are by far the dominant bioclasts with an important contribution also from bivalve fragments. While the abundance of oysters is greater than that of echinoderms, oysters are only present at two of the localities while echinoderms are present at all three locations (Appendix B Fig. B68). Similarly, serpulids are of significance at two of the three sites. Overall the dominant bioclasts are typically bryozoans, bivalves and echinoderms, which does not conform readily to plotting on any of the skeletal assemblage triangles presented in Hayton et al. (1995). Based on the two most common skeletal groups the assemblage is a bryomol one (James, 1997). The Onoua Limestone is an extremely coarse limestone with the modal size of some grains being >4 mm (Appendix B Fig. B70). Bioclasts are generally very abraded and poorly sorted (Appendix B Figs B71 & B72). The occurrence of ‘patches’ of dark grey micrite with bioclastic fragment inclusions may be interpreted as intraclasts, although their occurrence is relatively minor accounting for about 1% of the whole rock composition (Figs 4.23, 4.26D).

Siliciclastic composition

The siliciclastic and precipitate composition of the Onoua Limestone is generally low with the terrigenous material comprising mainly quartz and volcanic and sedimentary rock fragments (Fig. 4.25). The Onoua Limestone also shows a significant amount of limonite staining, presumably derived from weathering of the volcanic components. Phosphorite is the dominant precipitate, with glauconite pellets and infills present as well as pyrite grains and infills. Siliciclastic and precipitate grain sizes are generally <1 mm,

subrounded and, like the bioclasts, are poorly sorted (Appendix B Figs B70, B71, B72).

Interparticle material

The porosity of the Onoua Limestone resides mainly within the open zooecia of the bryozoan fragments (Fig. 4.26A). Micrite is common and occurs as both inter- and intraparticle fills (Figs 4.23, 4.26, Appendix B Fig. B73). Intraparticle micrite may occur in conjunction with radiating spar cements forming geopetal structures, particularly within bryozoan skeletal lattices (Fig. 4.26B). Micrite occurs as microbioclastic and homogenous and clotted precipitate types (Fig. 4.26). Spar cements occur mainly as intraparticle fills, but also as syntaxial rim overgrowth cements around echinoderm fragments. Cathodoluminescence has revealed that many of the intraparticle spar cements exist as internal 'spiky' fringe cements and display at least two or three distinct luminescent zones: bright to non to an outer dull luminescence (Figs 4.26 F & G).

Classification

The Onoua Limestone is a packstone.

Interpretation

The Onoua Limestone represents a bryomol skeletal assemblage in a relatively low energy setting allowing for the preservation of abundant large bryozoans at probably mid to outer shelf depths (Figs 4.23, 4.26A). The occurrence of acicular fringing spar cement about bryozoan fragments may indicate some early marine cementation, while other intra- and interparticle spar cements possibly have a meteoric influence a indicated by a thin luminescent zone towards the edges of intraparticle 'spiky' spar cements (Fig. 4.26) (Hood and Nelson, 1996; Caron and Nelson, 2003; Ricketts et al., 2004).

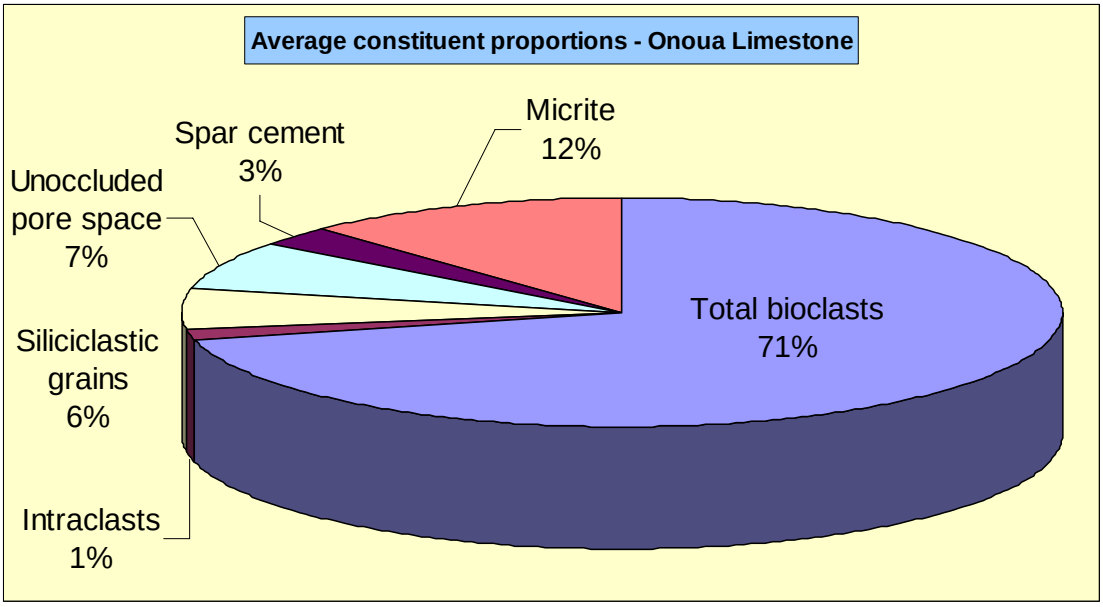

Figure 4.23: Whole rock composition of the Onoua Limestone from the Tarawhenua Peninsula and Flowerpot Bay, northern Pitt Island.

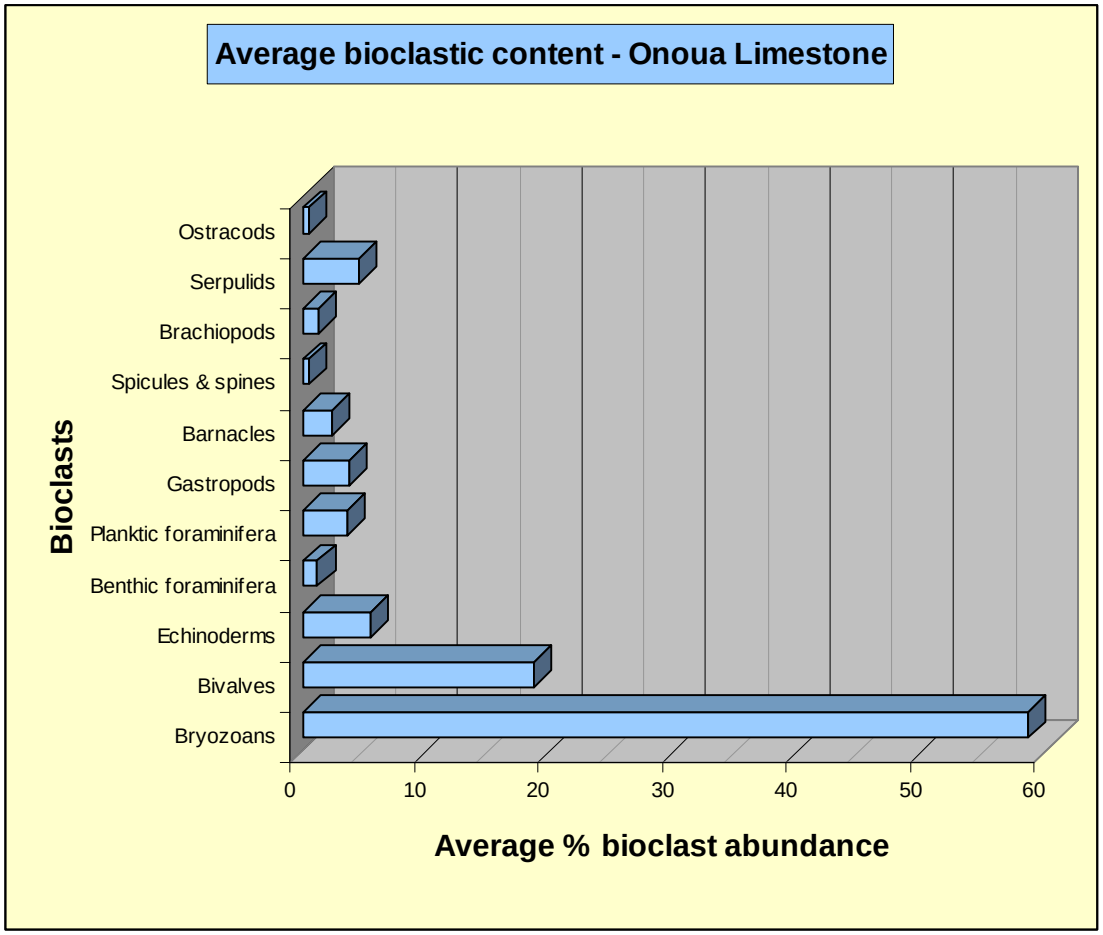

Figure 4.24: Skeletal assemblage percentages for the Onoua Limestone showing that this is a bryozoan dominated limestone.

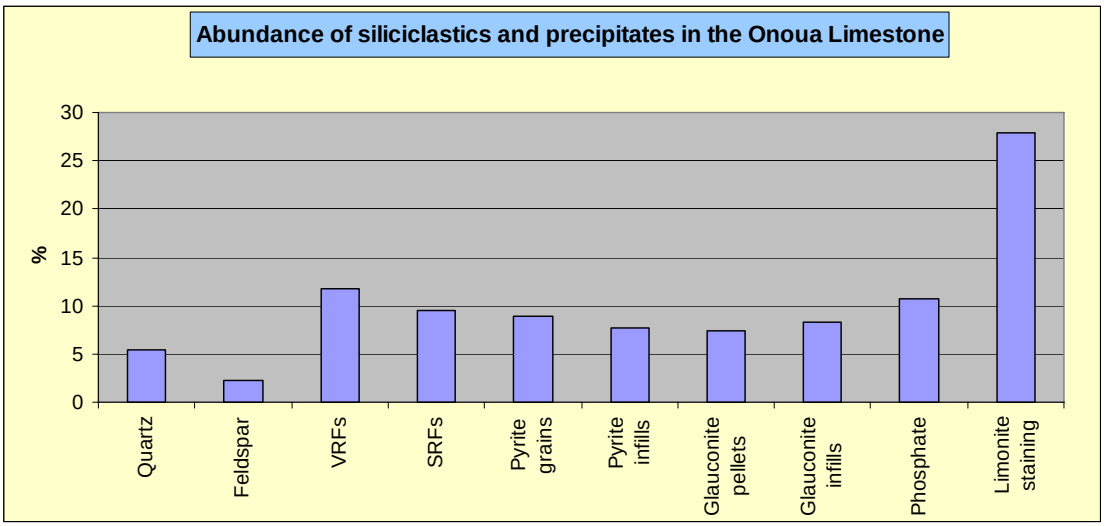

Figure 4.25: Siliciclastic and precipitate component percentages in the Onoua Limestone indicating a diverse array of inclusions.

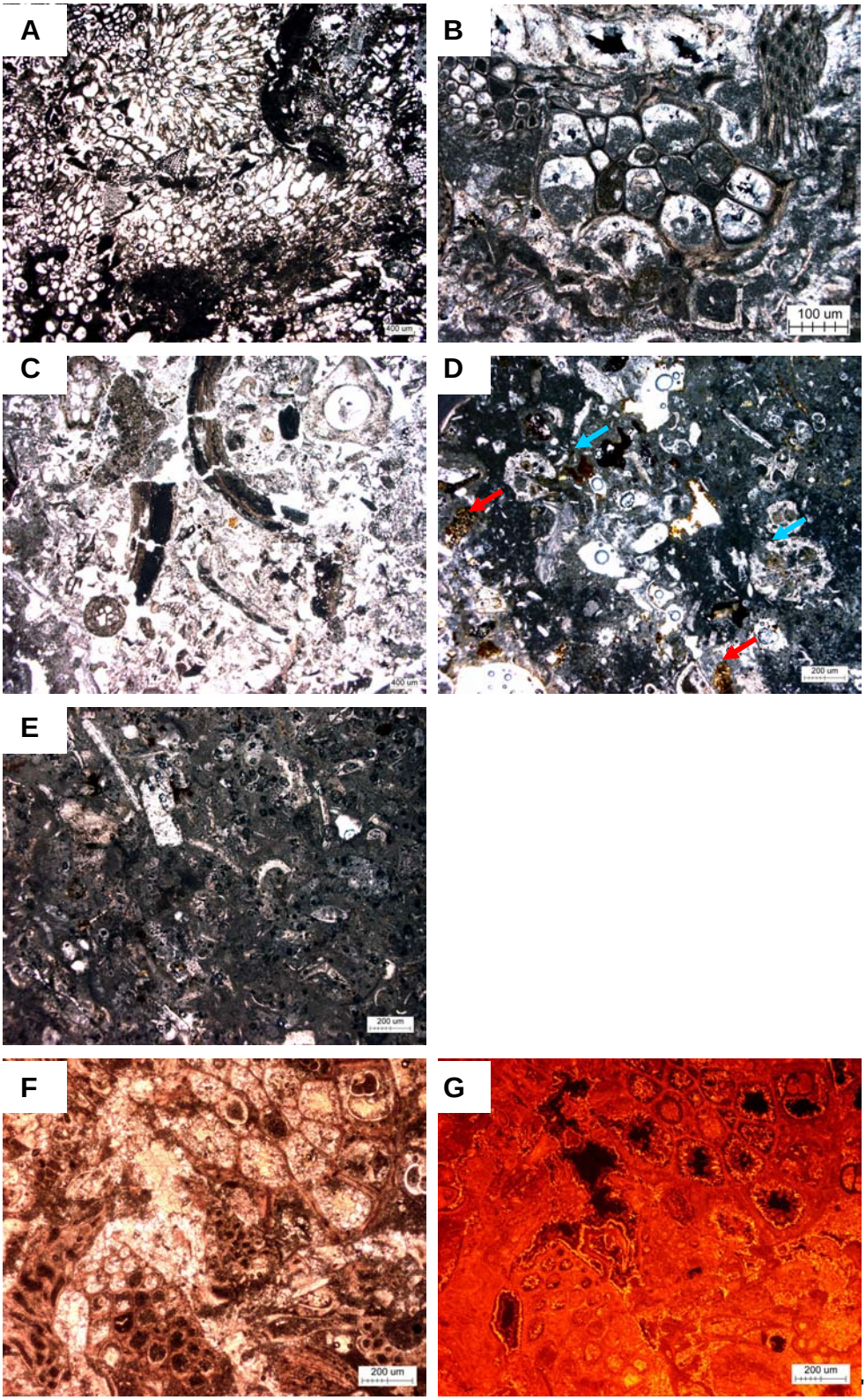
A
B
100 um
C
D
200 um
E
200 um
F
200 um
G
200 um

Figure 4.26: Photomicrographs of the Onoua Limestone from northern Pitt Island. **A** (CH05-8.4, PPL) sample from the Tarawhenua Peninsula illustrating the total dominance of bryozoans resulting in an extremely coarse and porous limestone. **B** (CH05-8.11, XPL) higher in the section on the Tarawhenua Peninsula showing the introduction of micrite in this high magnification shot of geopetal structures within a bryozoan and the development of radial spar cements. **C** (CH05-10.6, PPL) sample from the lower part of outcrop in Flowerpot Bay, Pitt Island showing an open and porous fabric with large bivalves near the centre of the image. **D** (CH05-10.2, PPL) another slide from the Flowerpot Bay location but from a rubbly horizon in the upper section showing a change in porosity and clotted and microbioclastic micrite filling the pore spaces. Note also volcaniclastic inclusions (red arrowed) and micritic intraclasts with bioclastic fragment inclusions (blue arrowed). **E** (CH05-11.1, PPL) this slide is from a sample from coastal cliffs to northwest of Flowerpot Bay near the Bluff Homestead. It again shows clotted micrite with fragmented bryozoans, bivalves and echinoderms. PPL and CL micrograph pair, **F** and **G** (CH05-8.11, PPL and CL) cathodoluminescence shows thin luminescent zones toward the edges of acicular spar cement fringes that are both inter- and intra-particle. The uniform luminescent layered zones indicate that the open pore spaces are probably actual porosity and not a function of thin section production.

4.2 Other limestone occurrences

4.2.1 Tumaio Limestone

Whole rock composition

The Tumaio Limestone is unusual in that it has an extremely high silica and siliciclastic content, with a combined total of up to 45% of the whole rock composition (Fig. 4.27). However, the total amount of carbonate mainly exceeds 50%: bioclasts (32%), micrite (17%), spar (2%) and intraclasts (2%). The deposit has about 2% porosity.

Bioclastic composition

The bioclastic content show a near equal abundance of bryozoans and bivalves, with a significant contribution from echinoderm fragments (Fig. 4.28). Again the dominance of these three skeletal fragments make the application of the Hayton et al. (1995) skeletal assemblage scheme difficult, but it is close to the bryomol assemblage (James, 1997). In upper stratigraphic horizons the percentage of silica as a cement or replacement material of some bioclasts often makes identification of the latter difficult (Fig. 4.30B, Appendix B Figs B89, B91). Bioclasts are generally <1.5 mm size with very abraded grains displaying poor sorting (Appendix B Figs B83, B85, B87, B88). The occurrence of circular micritic 'balls' is identified in the Tumaio Limestone and are tentatively interpreted as intraclasts (Figs 4.27, 4.30G). While these features were observed in the silicified horizons, they were initially considered to be altered bioclasts. Subsequent observations made in non-silicified areas revealed a homogenous micritic texture that was occasionally observed to contain glauconite inclusions.

Siliciclastic composition

Silica occurs as the predominant interparticle material, but there is also a high percentage of polycrystalline quartz fragments and volcanic rock fragments present (Figs 4.27, 4.29, 4.30, Appendix B Fig. B84). Glauconite pellets are common although their presence in silicified horizons is not evident. It is possible that the glauconite has either been replaced or obscured by the presence of silica, or that possibly the silica horizons

represent a depositional environment that was not conducive to glauconite precipitation. Glauconite also occurs less commonly as infills, not only within bioclasts but also within fractures in polycrystalline quartz grains. Siliciclastic and precipitate grain sizes are generally <1.2 mm and commonly <0.5 mm, and the grains are subrounded with moderate to poor sorting (Appendix B Figs B83, B86, B87, B88).

Interparticle material

Silica occurring as interparticle material would appear to comprise 30% of the Tumaio Limestone (Fig.4.27, Appendix B Fig. B84). However, approximately 15% of the silica is estimated to occur as replacement silica of original carbonate bioclasts. Within the silicified horizons silica cements have been identified as having chalcedony mineralogy and displaying radiating splay and zebraic cement textures, with confirmation of the mineralogy through cathodoluminescence analysis (Figs 4.30 C & D, 4.31) (Scholle and Ulmer-Scholle, 2003). Non-silicified areas of the Tumaio Limestone reveal that the unit has a significant content of micrite that is mainly of homogenous or clotted types (Figs. 4.27, 4.30F, Appendix B Fig. B84). Spar cements are a relatively minor feature, occurring as fibrous bioclastic fringe spar and commonly as extremely thin acicular fringe cements that are also common lining intraparticle pore spaces (Fig. 4.30 E & G) (Nelson and James, 2000). While echinoderm fragments are present in significant numbers, syntaxial rim overgrowths are not overly prevalent.

Classification

Non-silicified lithologies of the Tumaio Limestone are packstones, otherwise they are silicified packstones.

Interpretation

The Tumaio Limestone comprises a bryomol/bimol skeletal assemblage and may represent deposition of skeletal fragments sorted by bottom water currents in mid to outer shelf water depths (Fig. 4.28) (Campbell et al., 1993). Inclusions of glauconite are likely derived from Tutuiri Greensand with volcanic rock fragments and polycrystalline quartz grains possibly derived from erosion

of the underlying Takatika Grit (Figs 4.29, 4.30E, F & G). Spar cements are relatively rare within the Tumaio Limestone samples analysed in this study and there has been considerable alteration of the original carbonate cements fabrics by replacement with silica cements (Figs 4.30A, B, C & D; 4.31).

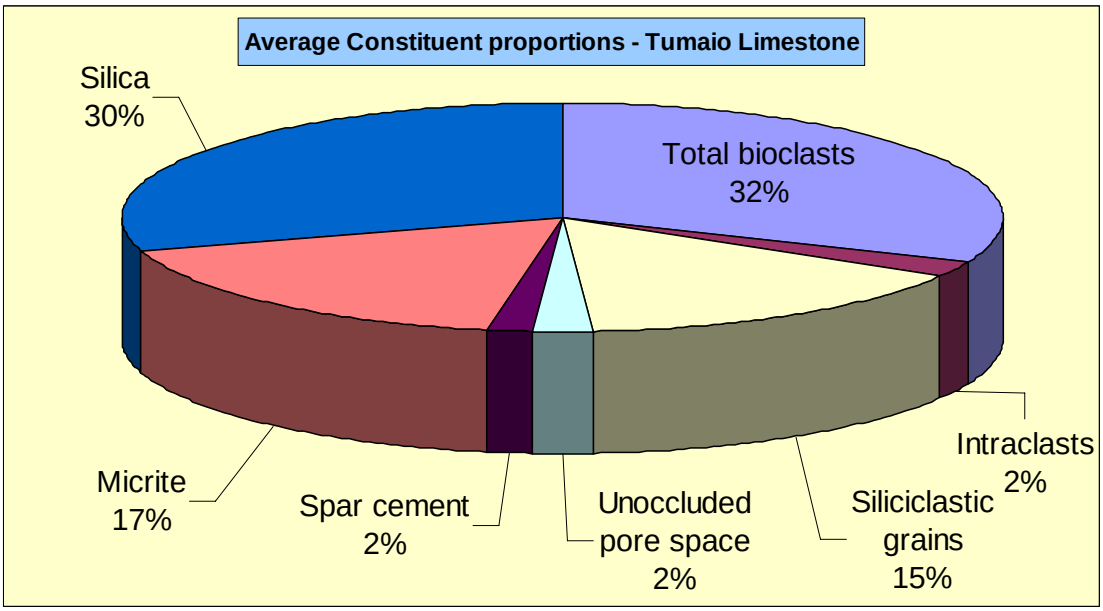

Figure 4.27: Whole rock composition of the Tumaio Limestone from the type section at Tioriori, northern Chatham Island, showing a significant silica component.

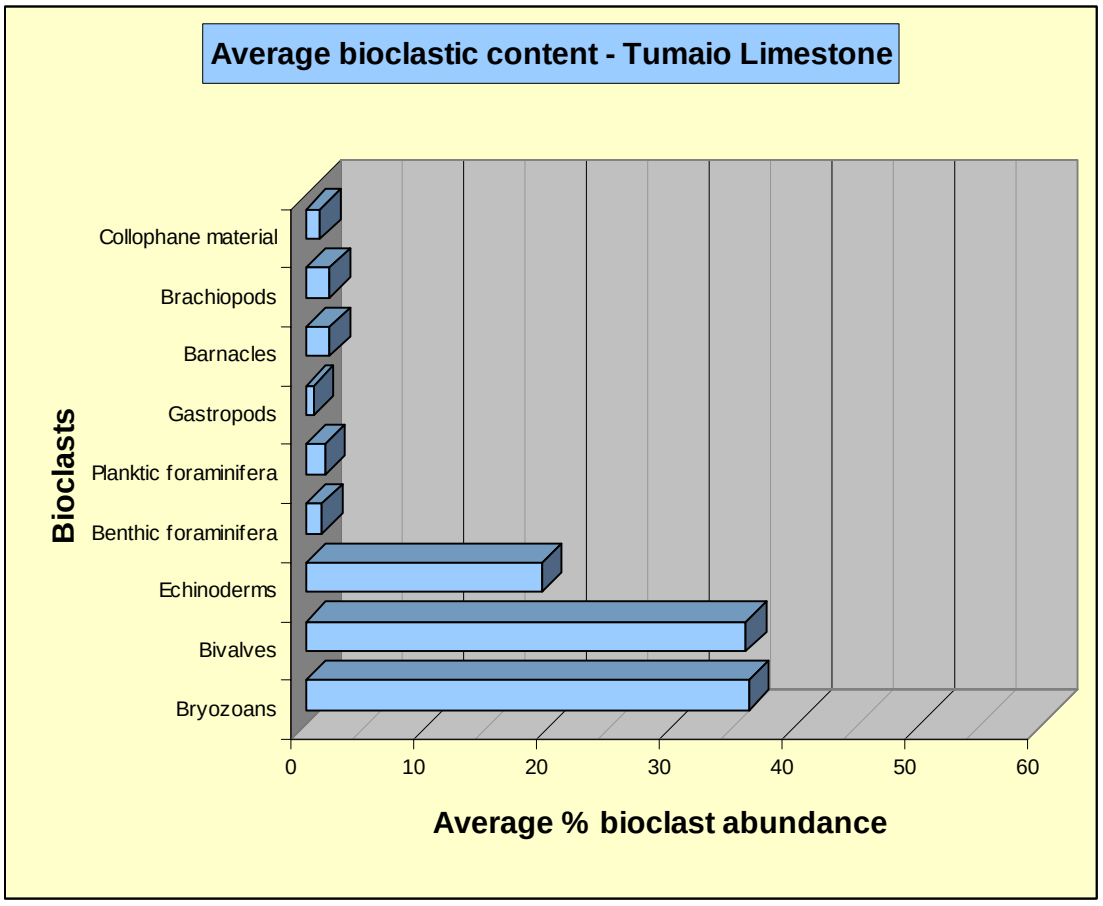

Figure 4.28: Skeletal assemblage percentages in the Tumaio Limestone show a near equal dominance of bivalves and bryozoans.

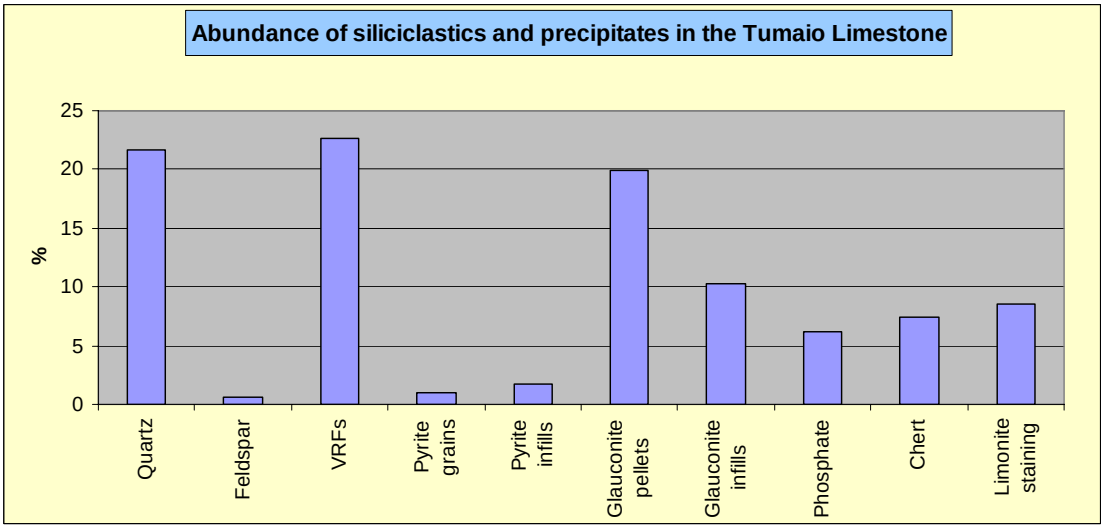

Figure 4.29: Siliciclastic and precipitate percentages in the Tumaio Limestone showing a significant quartz and volcanic rock fragment input, hinting at the probable source of silica.

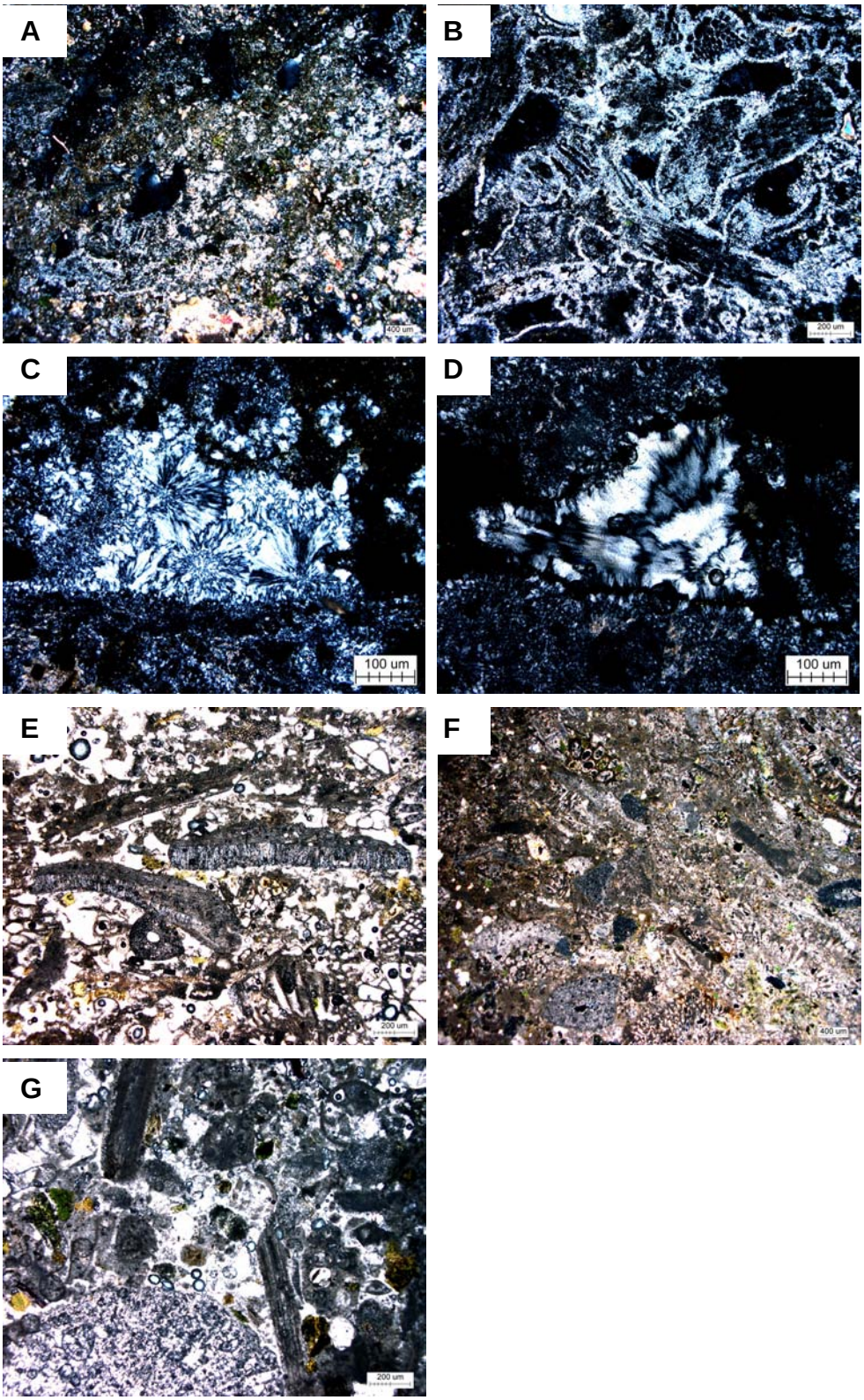
A
400 um
B
200 um
C
100 um
D
100 um
E
200 um
F
400 um
G
200 um

Figure 4.30: Photomicrographs of the Tumaio Limestone. **A** (CH05-18A, XPL) sample from the lowermost exposed section of the outcrop in 2005. The 'glassy' appearance is silicic cement with a large polycrystalline quartz grain or grains toward the bottom of the image. Grey areas toward the top of the image are micrite that have not been silicified, with light green glauconite pellets scattered throughout. **B** (CH05-18B3, XPL) sample from near the top of the section from one of the prominent rubbly silicified horizons evident in outcrop. The sample shows total silica replacement of bioclasts and any associated calcite cements. **C** (CH05-18B2, XPL) high magnification shot of a chalcedony fill showing black and white radiating splays from a lower silicified horizon and **D** from the same sample showing zebraic chalcedony within the pore space surrounded by fringing fibrous micro-quartz. **E** (CH05-18C1, PPL) sample of the Tumaio Limestone proper between the silicified horizons. The sample shows an open porous fabric with relatively intact bryozoans and large bivalves displaying equant spar neomorphic replacement. Also prominent in the Tumaio Limestone is the inclusion of glauconite pellets which are abundant in a lower non-silicified section **F** (CH05-18C2, XPL). F also shows a number of echinoderm grains within clotted micrite. **G** (E85-GS12459, PPL) thin section made from a GNS Science sample collected in 1977, comparable in lithology to 'F'. The inclusion of circular micritic 'balls' are tentively interpreted as intraclasts (blue arrowed).

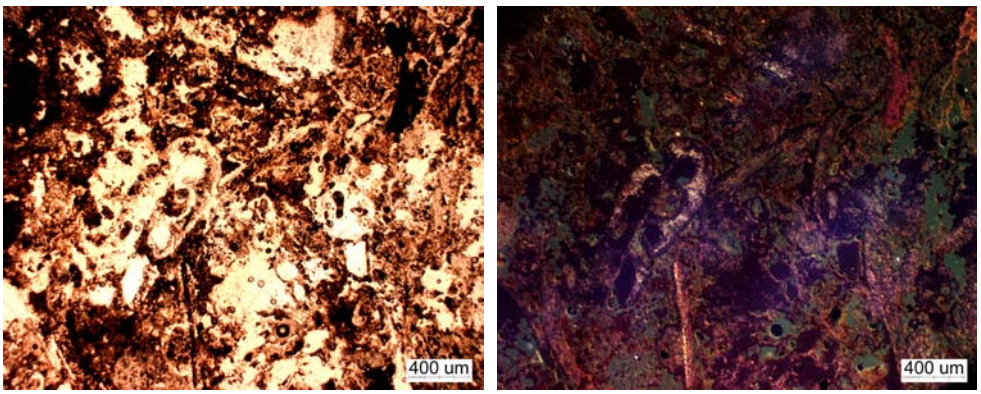

Figure 4.31: PPL and CL micrograph pair of sample CH05-18B2 from a mid-section silicified horizon showing dark blue and green luminescence of replacement and interparticle silica.

4.2.2 *Victoriella* Limestone

Whole rock composition

The *Victoriella* Limestone has a bioclastic content of 73% with siliciclastics comprising 7% of the whole rock composition and intraclasts a further 2% (Fig. 4.32). Matrix material represents ~16% of the whole rock composition with 8% micrite, 3% spar cement and 5% silica. Porosity is represented by 2% unoccluded pore space.

Bioclastic composition

Bryozoans are by far the dominant bioclast type in the Tumaio Limestone (Fig. 4.33). Echinoderms occur in significant numbers and to a lesser degree bivalves. This assemblage is best described as a bryomol assemblage although as with other Chatham Island limestones the *Victoriella* Limestone does not readily fit the assemblage classification scheme of Hayton et al. (1995). Bioclastic grain sizes are generally <2 mm, and the skeletons are abraded and poorly sorted (Appendix B Figs B92, B94, B96, B97). Minor micritic inclusions were observed in thin and are considered to be the same lithology as the surrounding *Victoriella* Limestone (Fig. 4.32).

Siliciclastic composition

The siliciclastic composition is dominated by volcanic rock fragments (with minor hornblende minerals) which is the probable source of the significant limonite staining and also the small ‘pockets’ of silicification (Figs 4.34, 4.35 B & F). Glauconite pellets and pyrite grains are the only precipitates present, with no noted infills (Fig. 4.35B). Siliciclastic and precipitate grains are generally <2.5 mm, abraded and poorly sorted (Appendix B Figs B92, B95, B96, B97).

Interparticle material

The *Victoriella* Limestone like the Tumaio Limestone, has a silica cement component (Fig. 4.32, Appendix B Figs B93, B98, B100). Unlike the Tumaio Limestone the silicification is relatively minor, occurring as small pockets with little alteration or as replacement of bioclasts. Micrite is the dominant matrix fill occurring as all of homogenous, clotted and microbioclastic

types (Figs 4.35 A, B, C, G). Spar cements occur to a lesser degree as mouldic cavity fills forming large blocky equant spar crystals or envelope structures (Fig. 4.35C & E). Spar cements are also present as unusual fringing cements and seem to be a partial replacement of bioclasts rather than any acicular growth cement. Cathodoluminescence of these cements shows a brighter luminescence than the surrounding intraparticle micrite (Figs 4.35 G & H).

Classification

The *Victoriella* Limestone is a packstone or sometimes wackestone, variably silicified.

Interpretation

The *Victoriella* Limestone is representative of a bryomol skeletal assemblage that probably formed in mid to outer shelf water depths (Figs 4.33, 4.35). The inclusion of planktic foraminifera may indicate an oceanic setting, possibly a sheltered platform or shoal given the preservation of delicate bryozoan forms (Fig. 4.35A & G). The included volcanic rock fragments are likely derived from erosion of the Northern Volcanics (Fig. 4.34). Spar cement envelopes and biomoulds indicate meteoric diagenesis with cathodoluminescence possibly indicating shallow burial (Fig. 4.35). There are no discernible features associated with early marine cementation, and some minor silicification is present.

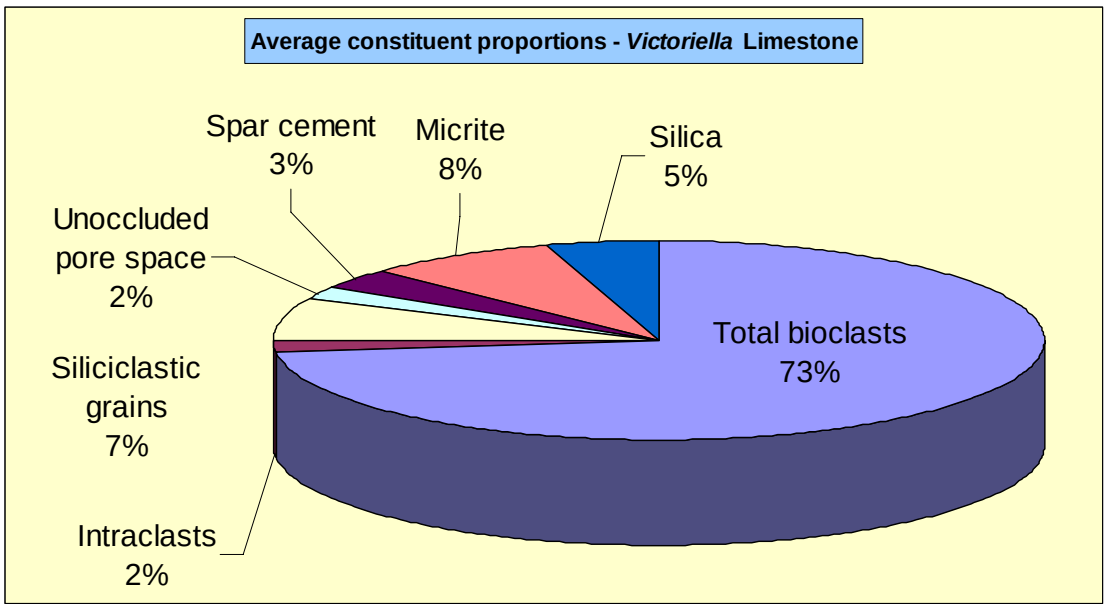

Figure 4.32: Whole rock composition of the *Victoriella* Limestone from isolated outcrops in streambeds in northern Chatham Island.

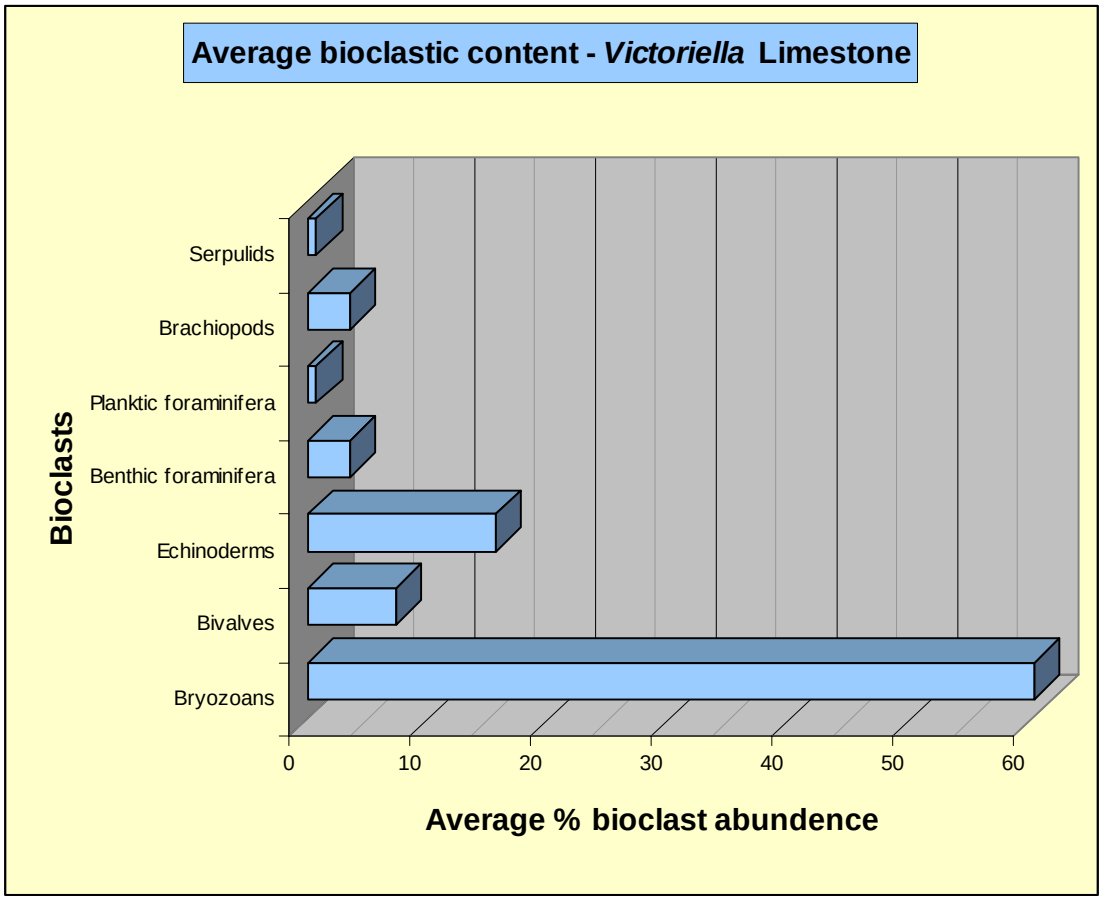

Figure 4.33: Skeletal assemblage percentages in the *Victoriella* Limestone showing bryozoans are by far the major bioclasts.

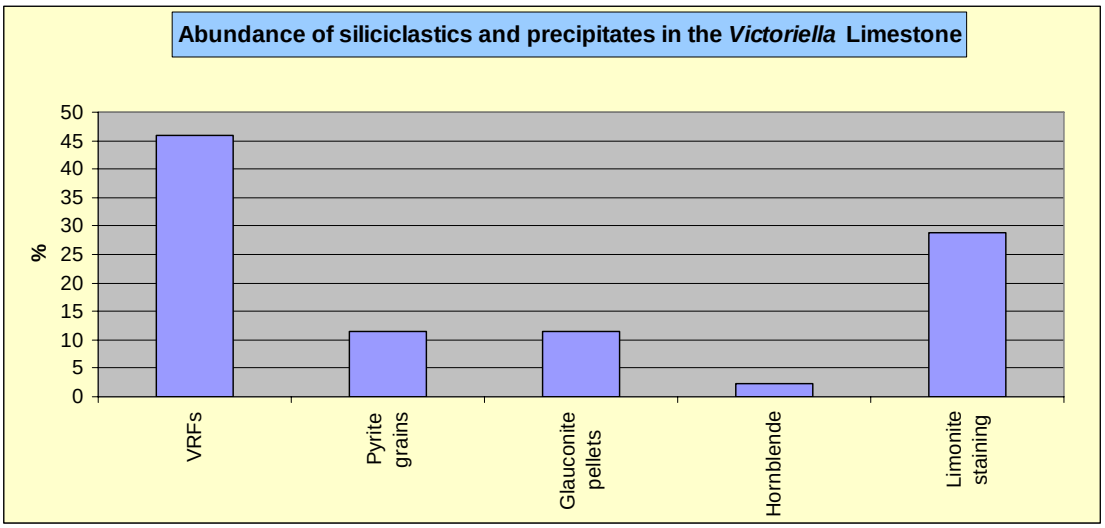

Figure 4.34: Siliciclastic and precipitates percentages for the *Victoriella* Limestone showing an abundance of volcanic rock fragments.

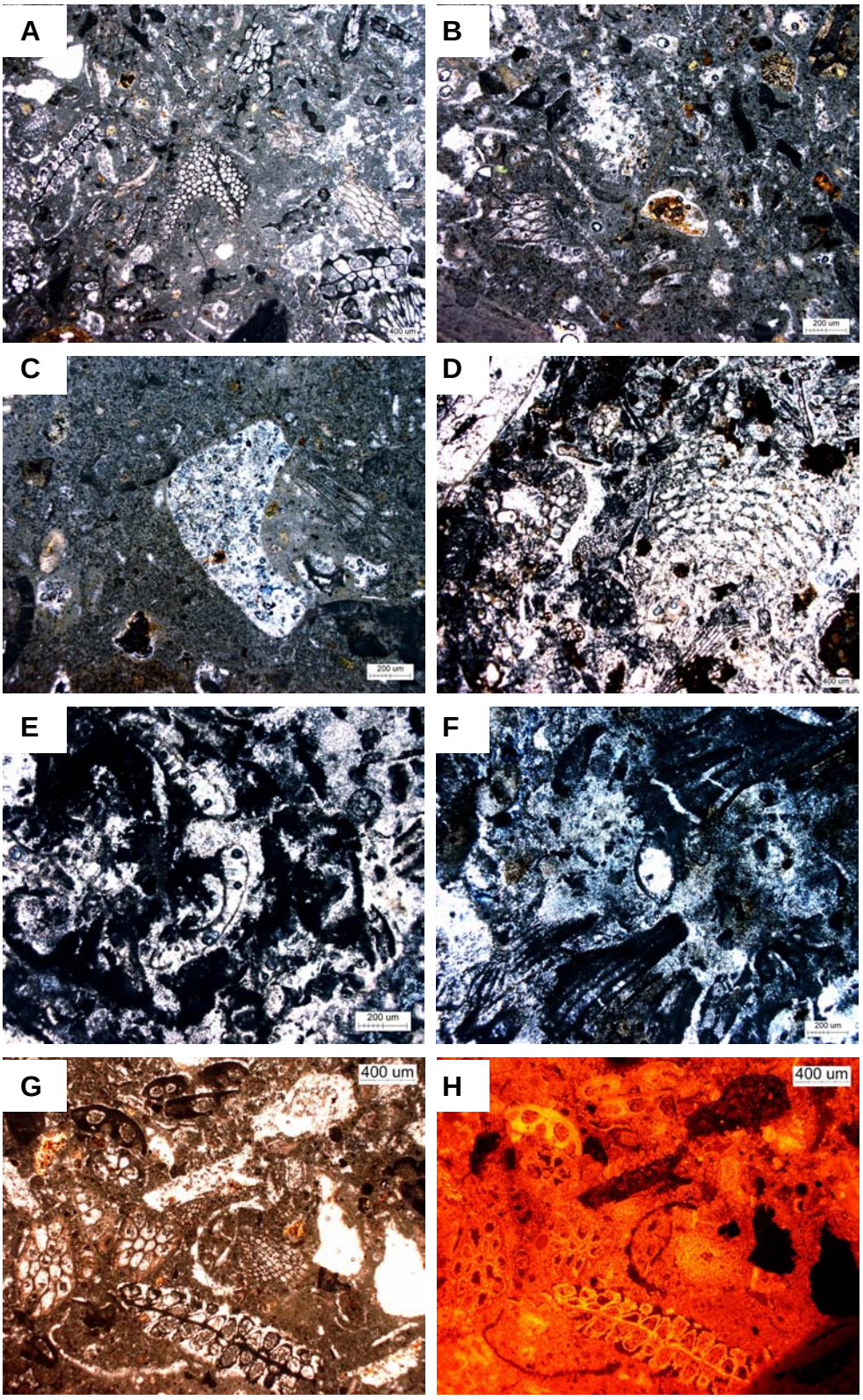
A
B
C
D
E
F
G
400 um
H
400 um

Figure 4.35: Petrographic characteristics of the *Victoriella* Limestone (CH05-30A), Chatham Island. **A** (PPL) is a general shot showing abundant bryozoans and smaller fragmented bioclasts within a homogeneous matrix/cement. **B** (PPL) shows volcanic rock fragment inclusions with some glauconite pellets and phosphorite. **C** (XPL) evidence of changes in porosity with the dissolution of probably aragonitic elements and infilling with spar cement of the mouldic porosity. **D** (XPL) a cross polarised shot showing a large bryozoan in the lower right half of the image and in the top left corner a spar calcite envelope structure. **E** (PPL) high magnification shot of two spar envelope structures under plain polarised light through centre of the image. Note the dark and glassy appearance of the matrix. This appears to indicate that silicification is a feature of the *Victoriella* Limestone, seen in **F** (XPL). PPL and CL micrograph pair, **G** and **H** (PPL and CL) calcitic areas of the slide reveal that there is an extremely thin bright luminescent signature toward the edge of some bioclasts.

4.2.3 Altonian limestone

Whole rock composition

The whole rock composition of the Altonian limestone reflects its brecciated mixed lithology, with 58% bioclasts, 18% siliciclastics and 9% extraclasts (Fig. 4.36). Interparticle material accounts for 13% of the whole rock composition with a further 2% porosity as unoccluded pore space.

Bioclastic composition

The bioclastic assemblage of the Altonian Limestone represents the combined assemblages of the brecciated extraclast inclusions within the sample obtained from GNS Science (Fig. 4.39). The sample is dominated by planktic foraminifera which are present in many brecciated extraclasts (Figs 4.37, 4.39 A, C, D, F). The presence of stromatolitic material is associated with one large inclusion which is limonite stained (Fig 4.39H). Apart from the unusual stromatolitic inclusions, bryozoans and bivalves are also present in equal quantities (Figs 4.39 B, E, and G). Other extraclast lithologies are noted to contain more minor occurrences of benthic foraminifera, brachiopods and echinoderms (Fig. 4.39E). Bioclasts across all lithologies generally have grain sizes <2 mm, and are moderately abraded and poorly sorted (Appendix B Figs B101, B103, B104).

Siliciclastic composition

The siliciclastic and precipitate component of the Altonian limestone is relatively high and is chiefly composed of volcanic rock fragments, pyrite grains and infills, and glauconite pellets (Fig. 4.38). The presence of abundant volcanic rock fragments is likely to be the source of the limonite staining (Fig. 4.39). Some sedimentary rock fragments are also present along with individual quartz grains and phosphorite clasts. Siliciclastic and precipitated grains are <2.5 mm size, abraded and poorly sorted (Appendix B Figs B101, B103, B104).

Interparticle material

Interparticle material in the Altonian limestone is predominately micritic with 9% of matrix material occurring as either precipitated homogenous or

clotted micrite (Figs 4.36, 4.39, Appendix B Fig. B102). Spar cements occur to a minor degree as internal bioclast fringing cements and rare mouldic equant replacement spar.

Classification

The Altonian limestone is a complex brecciated limestone containing multiple facies. All facies, however, display grain-to-grain contacts and contain micrite within the matrix. The Altonian limestone is therefore classified as a packstone.

Interpretation

The Altonian limestone generally represents a nannofor skeletal assemblage and is considered to represent an oceanic outer shelf deposit (Figs 4.37, 4.39A, B, C & D). However, at least two separate lithologies appear to be present: a planktic dominated facies and a bryozoan dominated facies (Fig. 4.39E & G). The bryozoan dominated facies may indicate a shallower depositional setting, particularly considering the presence of stromatolitic algae inclusions in the Altonian limestone (Figs 4.37, 4.39H). It is suggested that Altonian limestone may represent a brecciated mass emplacement deposit. The Altonian limestone has some characteristics associated with meteoric cementation, including the occurrence of biomoulds (Fig. 4.39B).

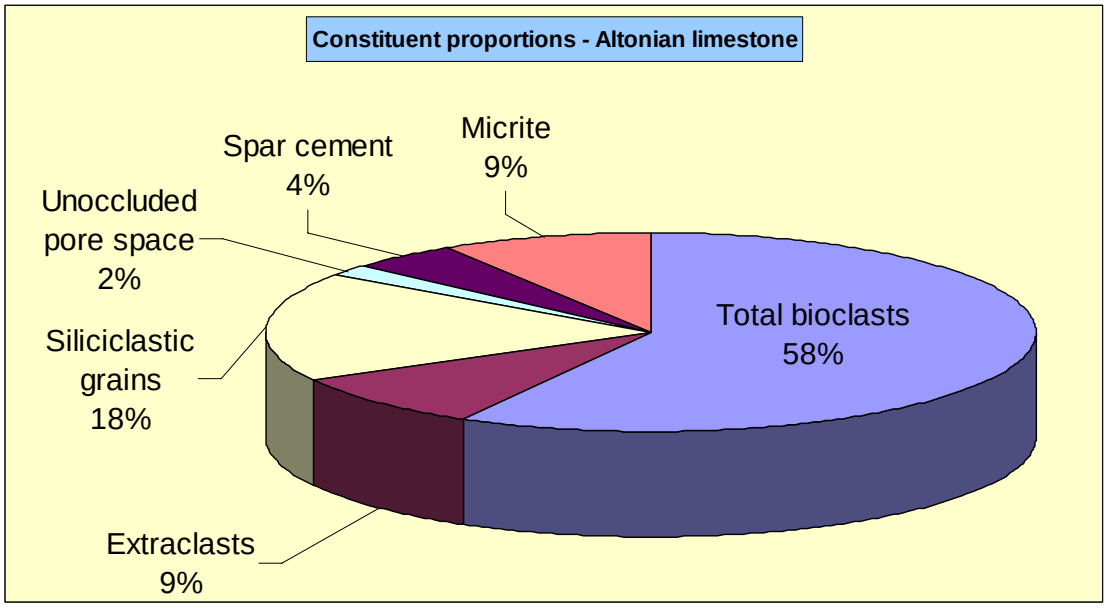

Figure 4.36: Whole rock composition of the Altonian limestone acquired from GNS Science.

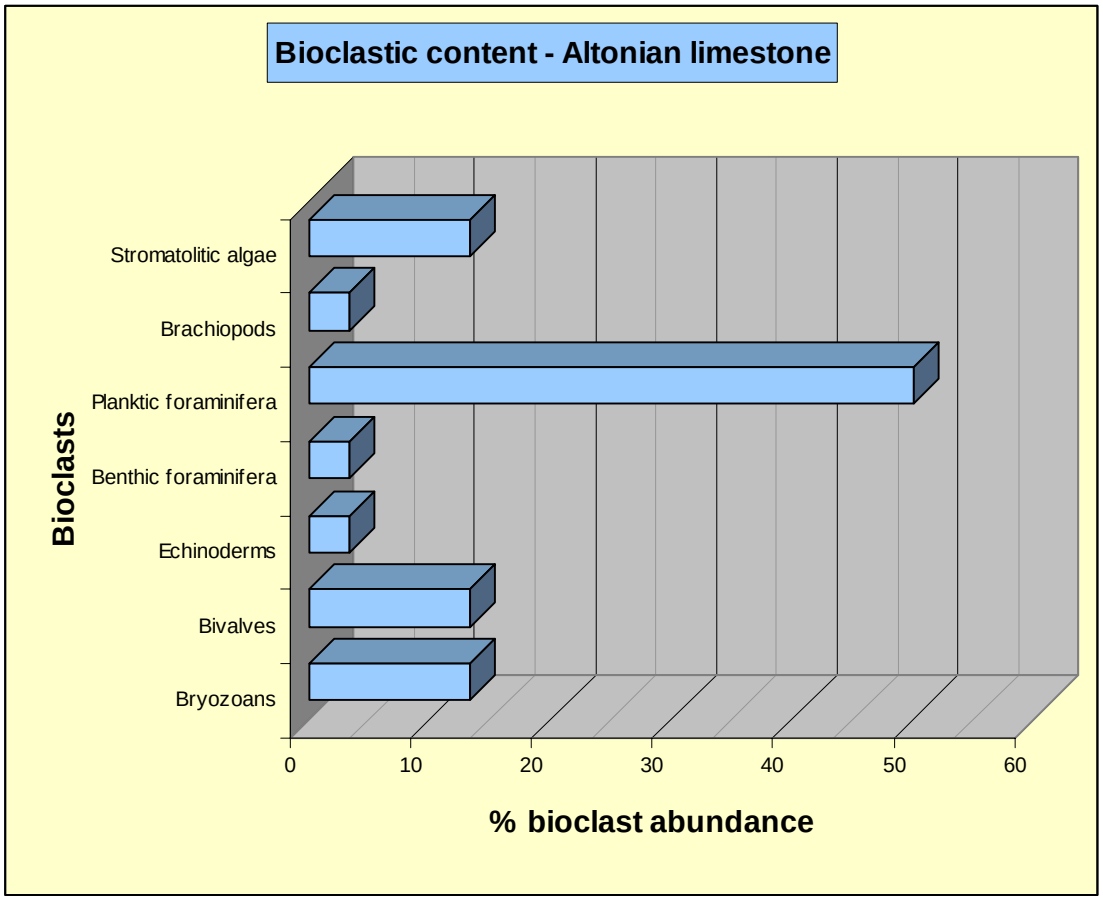

Figure 4.37: Skeletal assemblage percentages of the Altonian limestone showing a dominance of planktic foraminifera.

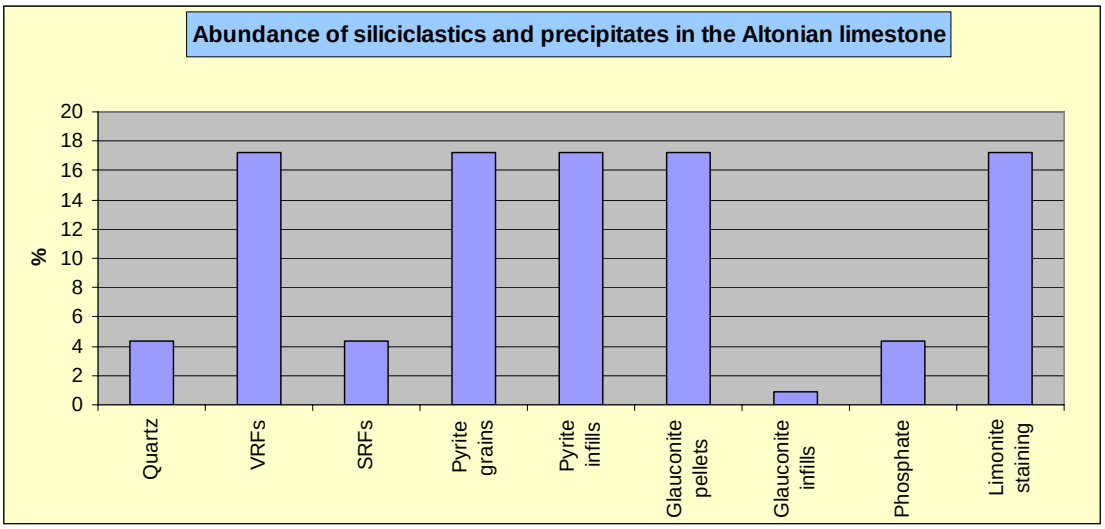

Figure 4.38: Siliciclastic and precipitate percentages in the Altonian limestone show an equal abundance of precipitates and volcanic rock fragments.

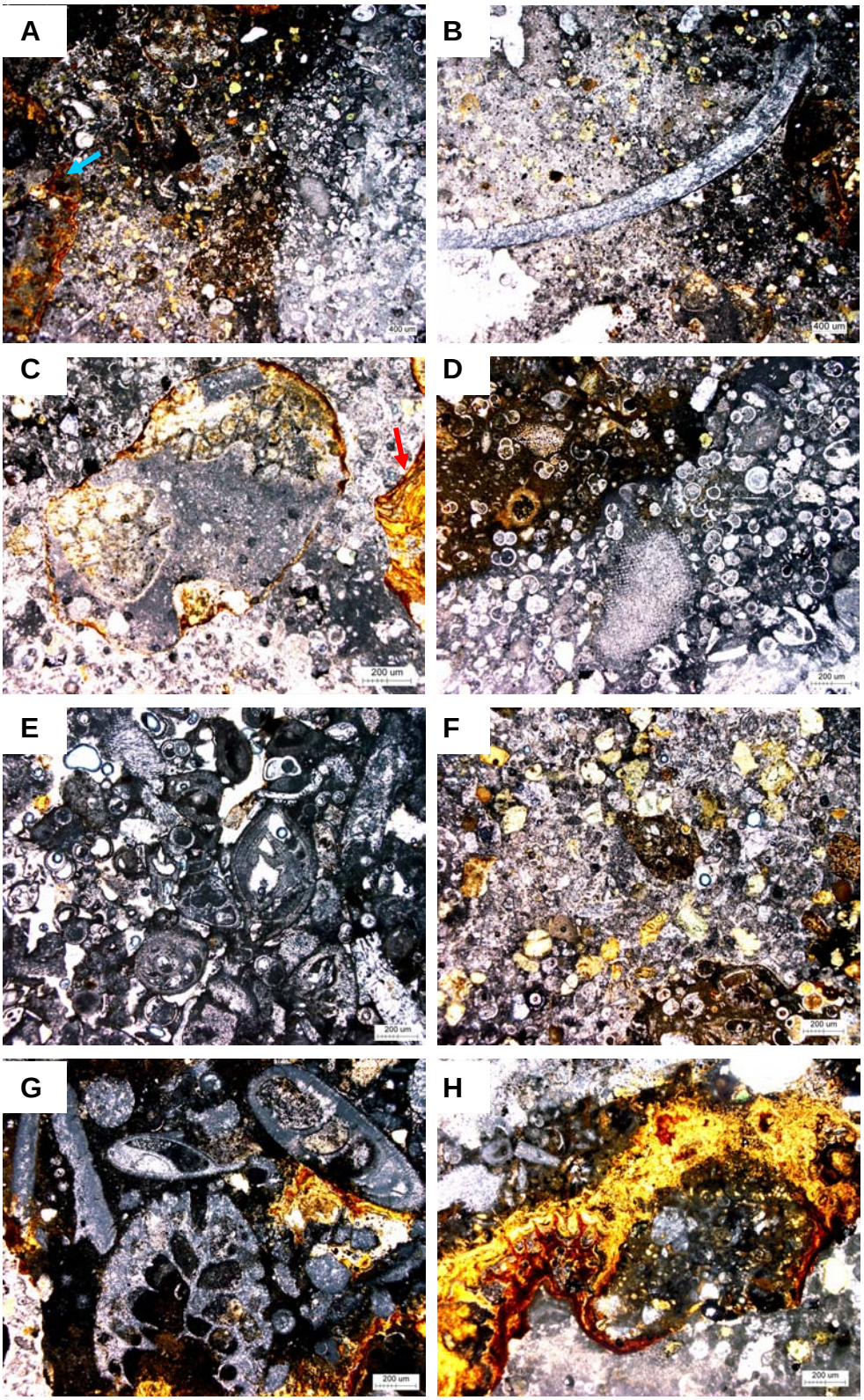
A
B
C
D
E
F
G
H
400 um
200 um

Figure 4.39: Photomicrographs of the Altonian limestone from GNS Science sample M363-GS12998. A and B (PPL), showing general shots of the Altonian limestone. **A** shows an abundance of planktic foraminifera and extraclast inclusions with large bryozoans (blue arrowed). **B** (PPL) shows a large bivalve with possible neomorphic spar cement replacement within a micritic matrix that has numerous glauconitic, phosphate, pyrite and volcanic fragments. **C** (PPL), a high magnification shot of a limestone extraclast with bryozoans in a homogenous micrite cement with limonite staining toward the outer edge of the clast. Note also a limonite stained stromatolite along the right-hand edge of the image (red arrowed). **D** (PPL) high magnification photo showing dense numbers of planktic foraminifera. Note the 'dirty' micrite intraclast in the top left corner and an echinoderm pictured centrally. **E** (PPL) another shot showing large benthic foraminifera in amongst planktics. **F** (PPL), photomicrograph to demonstrate the roundness of the siliciclastics and precipitates, while **G** (PPL) shows bryozoans and large benthic foraminifera surrounded by a dark coloured micritic matrix/cement and limonite stained stromatolitic algal growths. **H** (PPL) is a high magnification shot of a larger stromatolitic growth within a dark micrite facies in a different part of the rock.

4.2.4 Waipipian limestone

Whole rock composition

The Waipipian limestone is an extremely bioclastic limestone for the Chatham Islands, appearing considerably 'cleaner' in terms of non-carbonate inclusions. It is composed of 79% bioclasts, 5% siliciclastic grains and 2% intraclast inclusions (Fig. 4.40). The interparticle material represents 12% of the whole rock composition with a further 2% as unoccluded pore space.

Bioclastic composition

The Waipipian limestone is dominated by bryozoan fragments and also large whole intact bryozoans (Figs 4.41, 4.43 A, C). Bivalve and echinoderm fragments are the only other significant skeletal fragments observed in the Waipipian limestone, an assemblage which again fails to fit the assemblage models presented in Hayton et al. (1995), and the bryomol assemblage is substituted instead (bryozoan and bivalve abundance). Bioclast fragments are generally <2 mm, and they are moderately abraded and poorly sorted (Appendix B Figs B107, B109, B110). Some minor occurrences of intraclasts with the same lithology as the Waipipian limestone are considered to be present within the limestone (Fig. 4.40).

Siliciclastic composition

The Waipipian limestone is dominated by precipitates, with pyrite grains and infills being particularly abundant along with phosphorite (Fig. 4.42). Other precipitates such as glauconite pellets and infills were not as abundant, and neither are siliciclasts proper. Siliciclastic and precipitate grains are of fine size (<0.5 mm), subrounded and poorly sorted (Appendix B Figs B107, B109, B110).

Interparticle material

Interparticle material within the Waipipian limestone is predominantly micrite (Fig. 4.40). The micrite appears to be both homogenous and clotted types as well as microbioclastic micrite (Fig. 4.43). Spar cements are present as internal cavity radiating spar within bryozoans and to a limited extent as minor syntaxial rim overgrowths about echinoderm fragments.

Classification

For the most part bioclasts in the Waipipian limestone appear to 'float' within fine grained micrite (Fig. 4.43), so that the limestone is a wackestone.

Interpretation

The Waipipian limestone represents a bryomol skeletal assemblage likely deposited at mid to outer shelf water depths (Figs 4.41, 4.43). Intraparticle spar cements within bryozoan zooecia may indicate meteoric diagenesis by precipitation from calcite saturated fluids.

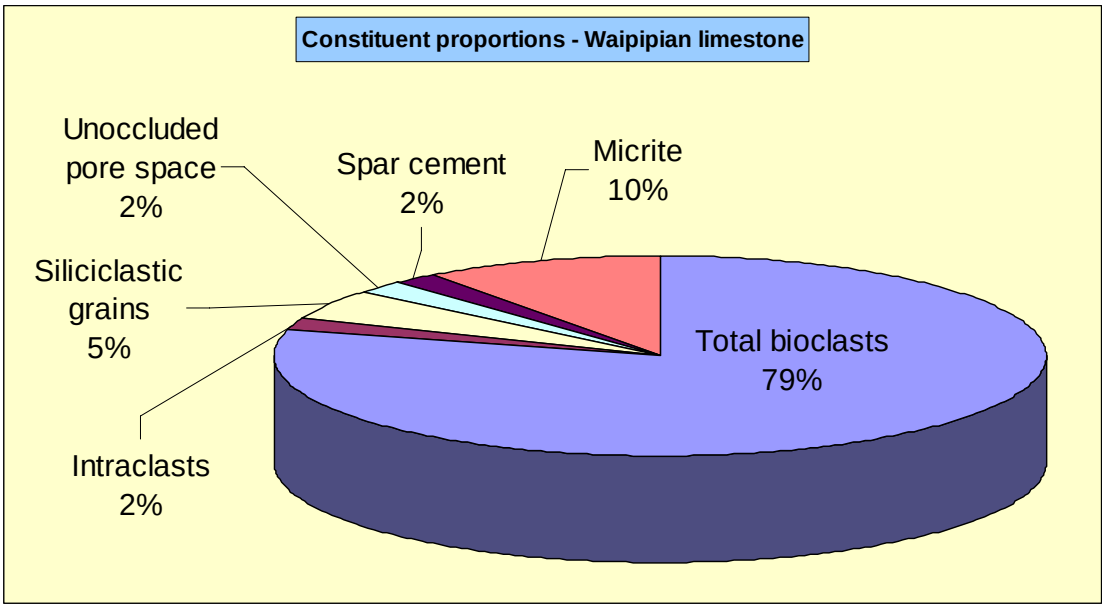

Figure 4.40: Whole rock composition of Waipipian limestone sample P-Q407-GS14155 from GNS Science.

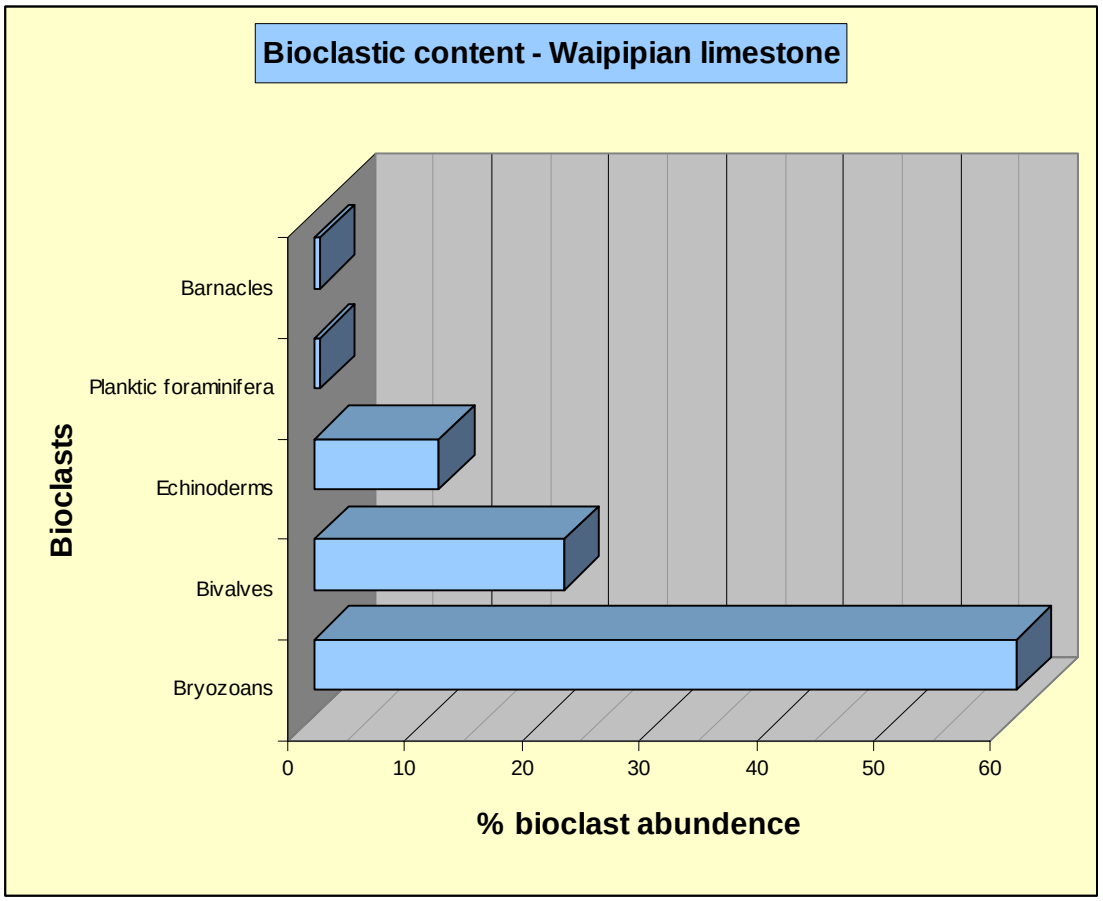

Figure 4.41: Skeletal percentages in the Waipipian limestone showing a dominance of bryozoans.

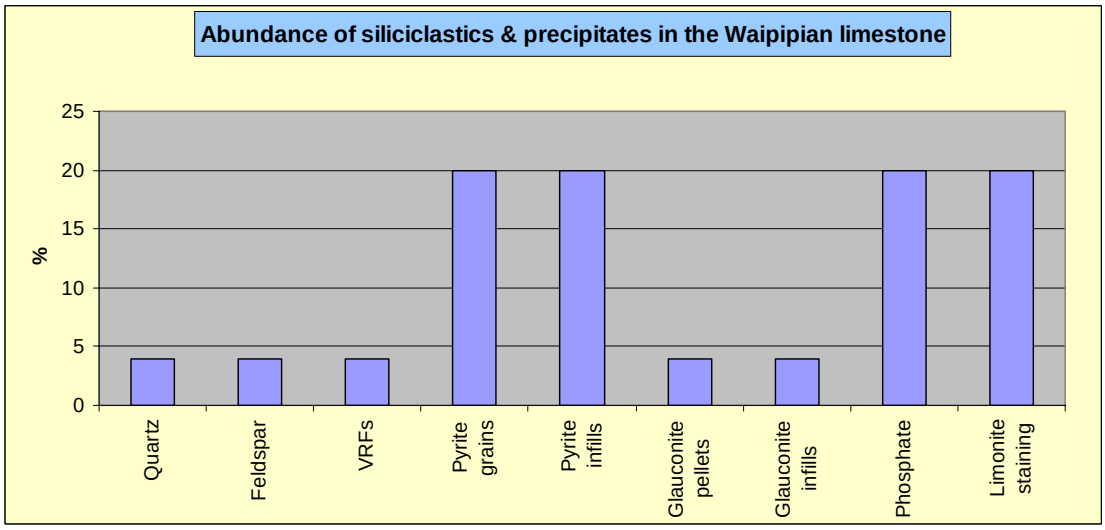

Figure 4.42: Siliciclastic and precipitate percentages in the Waipipian limestone.

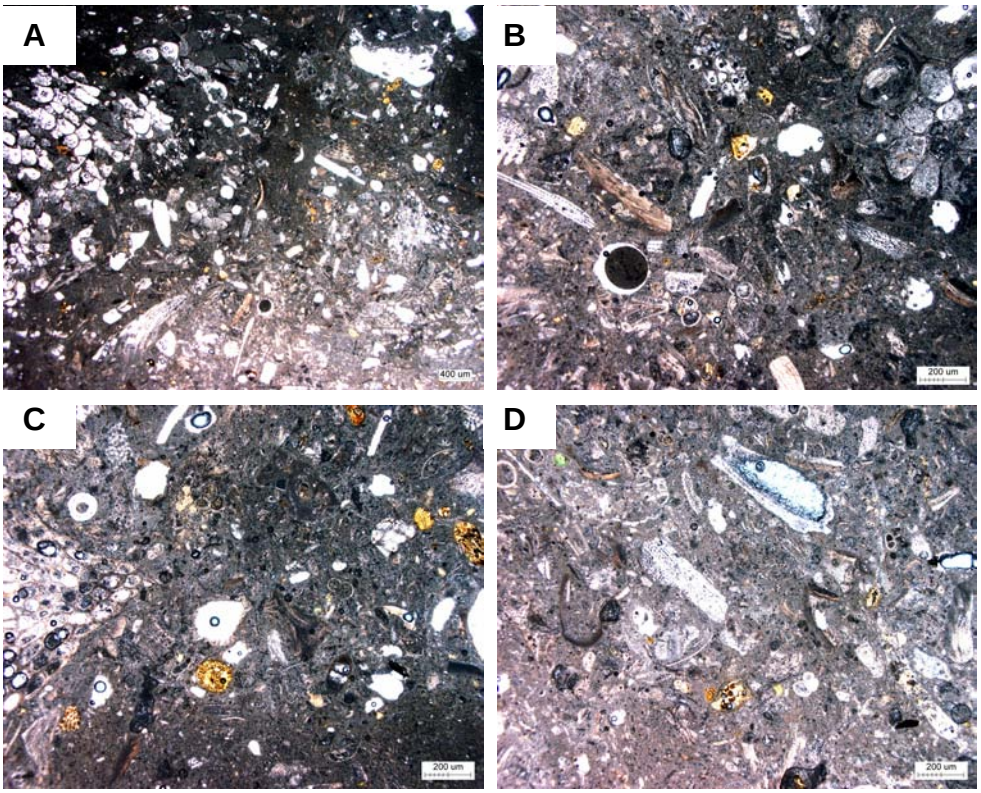

Figure 4.43: Photomicrographs of the Waipipian limestone sample P-Q407-GS14155. **A** (PPL), a large bryozoan dominates the image in the left-hand corner of the slide while fragmented bivalves and clotted micrite occurs in the foreground. **B** (PPL) shows bryozoan, bivalve and echinoderm fragments. **C** (PPL) in this image, planktic foraminifera can be seen in the centre. **D** (PPL) demonstrates the highly fragmented bioclastic nature and abundant intraparticle micrite within the Waipipian limestone.

4.2.5 Cape L'Eveque limestone

Whole rock composition

The average whole rock composition of the Cape L'Eveque limestone shows 71% bioclasts, 20% siliciclastics, 7% interparticle material and 2% porosity (Fig. 4.44).

Bioclastic composition

Bioclasts in the Cape L'Eveque limestone are dominated by bivalve fragments (Fig. 4.45). Calcareous red algae are also important, which is of particular note in that the Cape L'Eveque limestone, along with the Matanginui Limestone, are the only limestone units recording calcareous algae (Fig. 4.7). Bryozoans are equally abundant as calcareous algae and there are small amounts of echinoderms and foraminifera. Bioclast grain sizes are generally <1 mm, and grains are moderately abraded and poorly sorted (Appendix B Figs B113, B115, B116).

Siliciclastic composition

The Cape L'Eveque limestone contains a large number of volcanic rock fragments, some of which are considerably large (up to 10 mm) in thin section (cobble size in the field) (Fig. 4.46, Appendix B Fig. B113). The majority of volcanic material is, however, reasonably fined grained and similar in size to the bioclasts (Fig. 4.47). Minor precipitate inclusions of pyrite and glauconite pellets occur with all siliciclastics and "grainy" precipitates being subangular to subrounded and poorly sorted (Fig. 4.46, Appendix B Figs B115, B116).

Interparticle material

Micrite is the dominate carbonate matrix fill at 5% within the Cape L'Eveque limestone (Fig. 4.44, Appendix B Fig. B114). Spar cements are extremely limited, occurring only as minor stylolites and fracture fill cements within the fine volcanic clasts (Fig. 4.47).

Classification

The Cape L'Eveque limestone shows numerous grain-to-grain contacts between bioclasts and this, in conjunction with the occurrence of micrite, designates the Cape L'Eveque limestone as a packstone.

Interpretation

The Cape L'Eveque limestone is representative of a bimol skeletal assemblage and deposited in a nearshore depositional setting given the abundance of calcareous red algae (Figs 4.45, 4.47C & D). The abundance of volcanic rock fragments is considered to be derived from erosion of the Southern Volcanics or possible coeval deposition of Pliocene unnamed volcanics (Figs 4.46, 4.47) (H. Campbell, GNS Science, pers. comm., 2007). The occurrence of some interparticle spar cements may indicate meteoric diagenesis by precipitated from calcite saturated fluids.

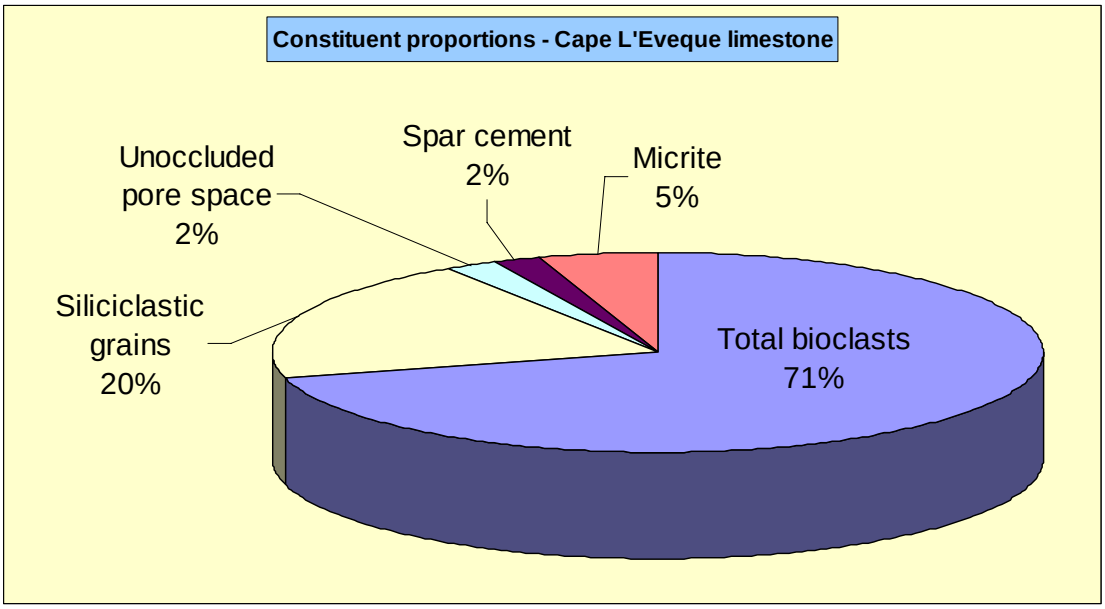

Figure 4.44: Whole rock composition of the previously un-described Cape L'Eveque limestone.

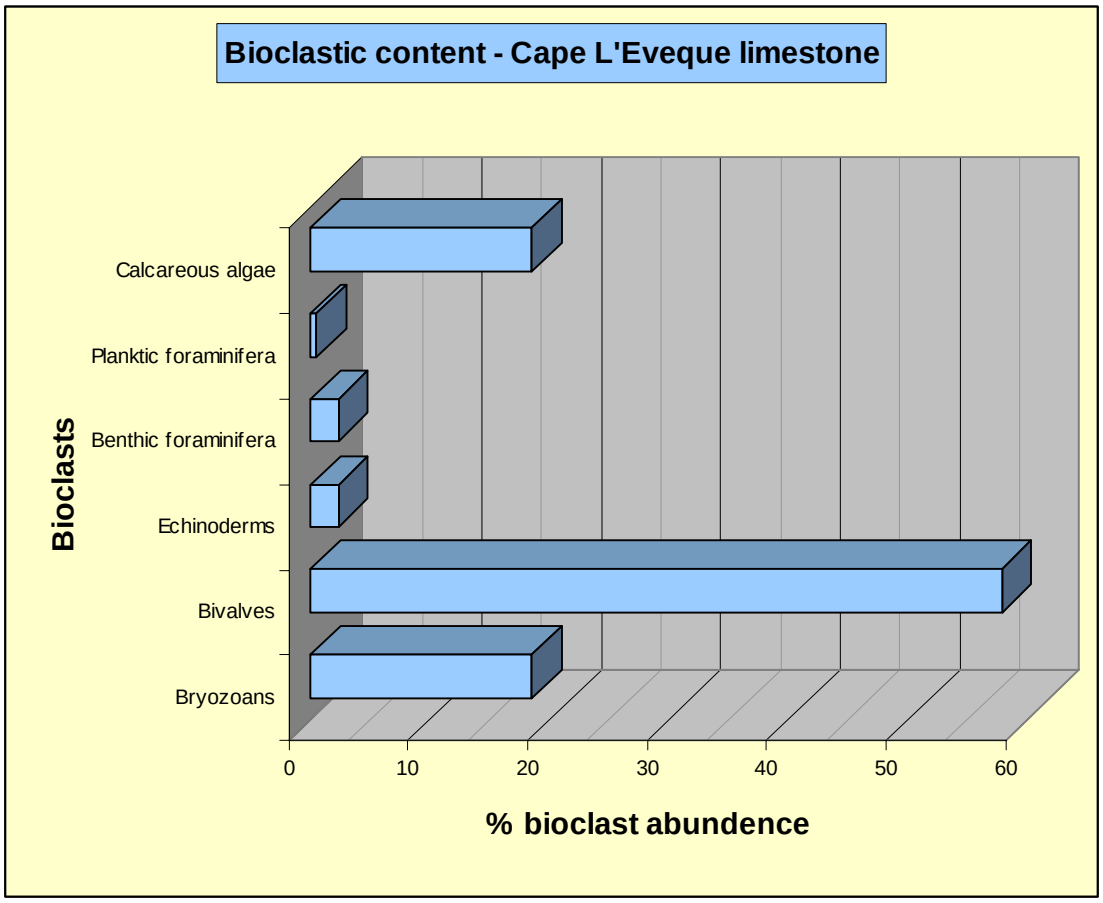

Figure 4.45: Bar graph of the skeletal content of the Cape L'Eveque limestone showing a dominance of bivalves and a significant contribution from calcareous algae.

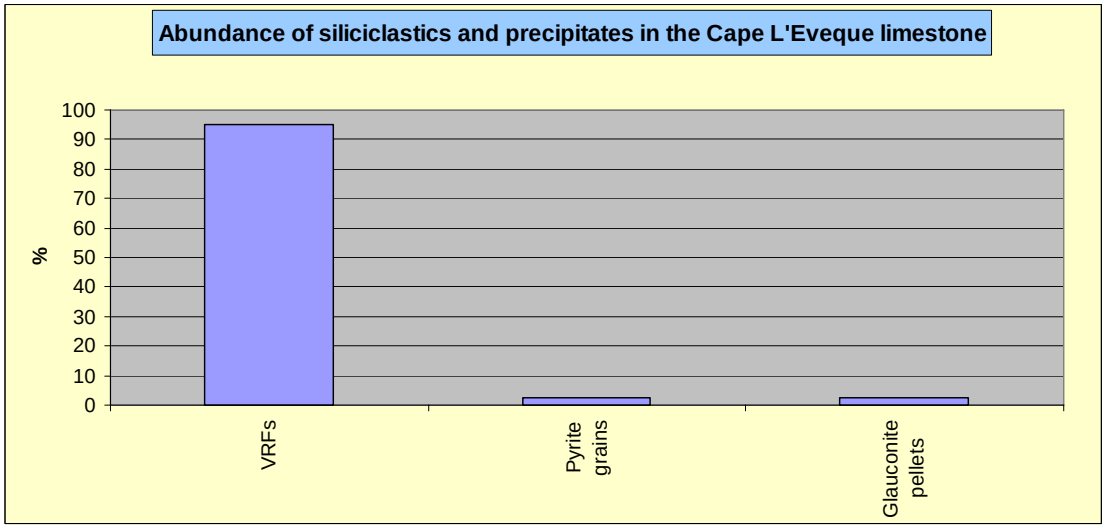

Figure 4.46: Siliciclastic and precipitate percentages in the Cape L'Eveque limestone demonstrating the limestones close association with volcanic deposits.

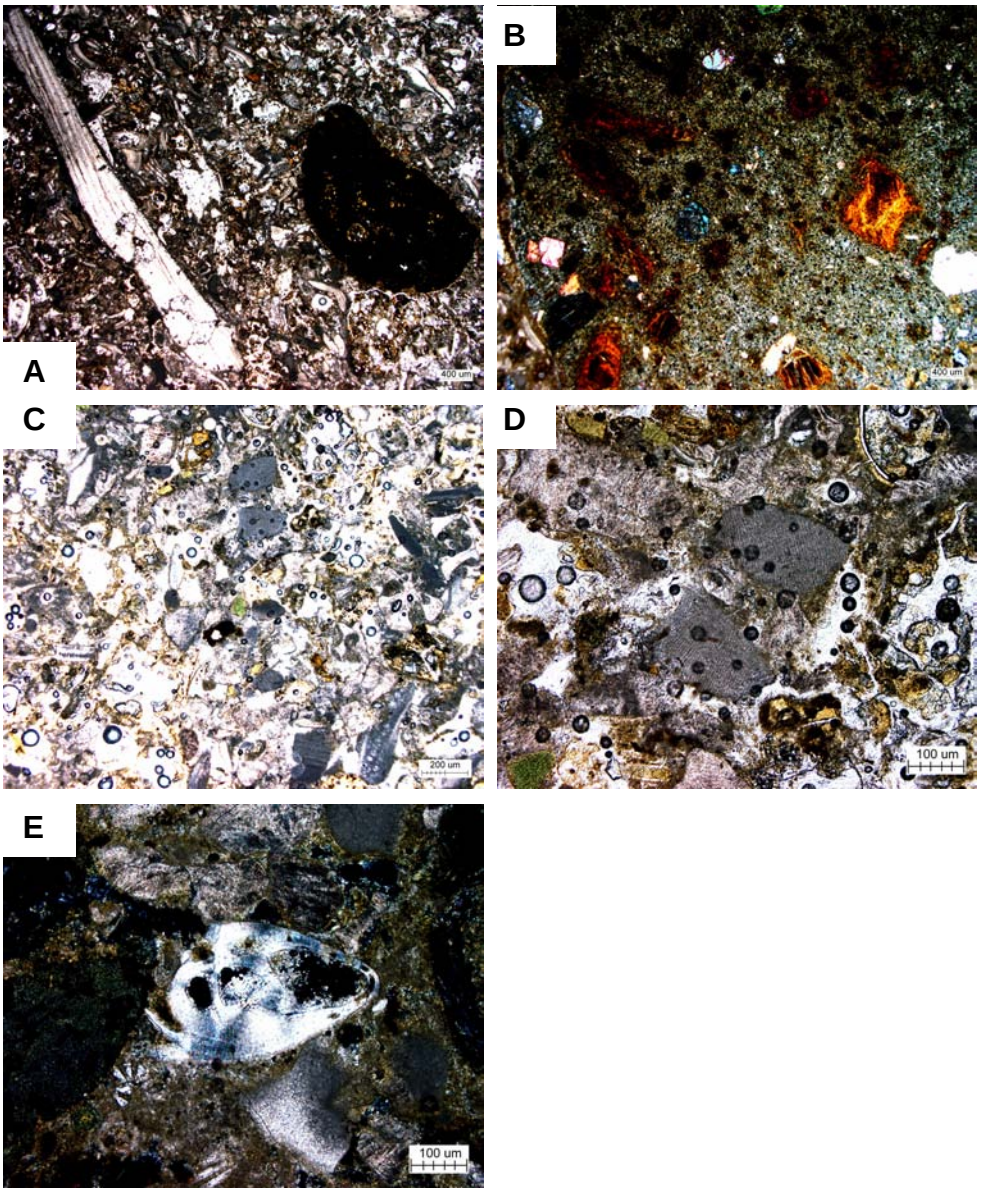

Figure 4.47: Photomicrographs of the Cape L'Eveque limestone sample CH06-TH02D, an isolated occurrence from the southwestern corner of Chatham Island. **A** (PPL) a general shot of the limestone showing the two most dominant elements, to the left a large bivalve (probably a pectinid or oyster shell) and to the right a large rounded volcanic clast. The surrounding matrix is composed of highly fragmented shell material and finer grained volcaniclastics. **B** (XPL) rounded volcanic clasts within the unit can be up to cobble size and is shown here at low magnification. **C** (PPL) higher magnification photo of the main facies showing an area with numerous calcareous algae (grey) and bivalve fragments. Note a single glauconite pellet in the centre of the slide and, where matrix material has been preserved through thin section production, that fine grained volcaniclastics are prevalent. **D** (PPL) high magnification shot of two calcareous algal grains showing the internal cellular structure. Also note that at higher magnification more subrounded glauconite pellets become apparent and the portions of the matrix are occupied by micrite and microspar cements. **E** (XPL) high magnification shot of a rare benthic foraminifera.

CHAPTER 5
Chatham Islands Limestone Dykes

An interesting feature related to the limestones on Chatham Islands is the occurrence of limestone dykes. These sedimentary dykes occur at four known locations, namely Red Bluff and Ngakuha Reef on Chatham Island, and at Flowerpot Bay and north of the Bluff Homestead on Pitt Island.

5.1 Introduction

The literature relating to sedimentary dykes is quite extensive. Sedimentary dykes are likely to be far more common then once thought. They are beginning to be considered as more then simply sedimentological curiosities and as potentially important features of the stratigraphic record. This is because sedimentary dykes can have a profound influence on aqueous and petroleum fluid flow dynamics in sedimentary basins (Jonk et al., 2005). An understanding of their formation and variable characteristics is of paramount importance for correct identification in the field and in petroleum exploration.

Sedimentary dykes are sediment bodies that are discordant with the surrounding strata; those concordant with the enclosing strata are sedimentary sills. Sedimentary dykes may be formed by passive infilling of younger sediment into fractures in older host deposits or by infilling of subaerially formed karst topography later exposed at the seafloor. Passive fills like this are referred to as ‘neptunian dykes’. Emplacement may also involve mechanisms of forceful injection of either plastic or liquefied sediment that is typically younger (but not always) than the host material, the injection exploiting planes of weakness such as fractures, faults and dewatering structures (Truswell, 1972; Archer, 1984; Larsen and Mangerud, 1992; Dreimanis and Rappol, 1997; Beacom et al., 1999; Jolly and Lonergan, 2002; Sano and Orchard, 2004; Jonk et al., 2005). Injected fills are referred to as ‘clastic dykes’.

The composition and rheology (consolidated or unconsolidated) of the host material exerts a strong influence on sedimentary dyke morphology. Sedimentary dykes are reported within a range of different lithologies, including various sedimentary facies, metamorphoric rocks associated with either syntectonically or post-tectonically developed regional cleavage structures, and plutonic and volcanic rocks that may themselves include igneous dykes and sills (Peterson, 1968; Truswell, 1972; Larsen and Mangerud, 1992; Sturkell and Ormo, 1997; Beacom et al., 1999; Phillips and Alsop, 2000; Jolly and Lonergan, 2002; Curtis and Riley, 2003; Tipper et al., 2003).

Clastic intrusions are most commonly cited as being associated with increases in hydrostatic pressure during normal burial of fluidised sediment, the injection occurring prior to lithification (Truswell, 1972). Clastic dykes are typical of tectonically active unstable environments, being particularly prevalent in deep marine sedimentary settings where they may record tectonic, post-sedimentary and sedimentary events that are often unseen in the stratigraphic record (Dreimanis and Rappol, 1997; Phillips and Alsop, 2000; Rowe et al., 2002; Sano and Orchard, 2004). Clastic dykes are commonly reported from deep subduction zone settings where seismicity may cause movement and deformation (slumping and folding) of sediment prior to lithification, providing a catalyst for forceful injection of sediment. However, similar processes can occur in fluvial, shallow marine, deltaic and shelf depositional environments (Truswell, 1972; Thorson et al., 1986; Phillips and Alsop, 2000; Pollock and Williams, 2000; Jolly and Lonergan, 2002; Rowe et al., 2002; Tipper et al., 2003; Le Heron and Etienne, 2005). Tectonically active areas may be closely associated with volcanic activity which can provide complex mechanisms for injection by way of associated hydrothermal dynamics that may operate within sediments deposited in such settings (Jolly and Lonergan, 2002; Curtis and Riley, 2003).

Other mechanism of intrusion of sediment into foreign bodies include those associated with meteorite impacts (Sturkell and Ormo, 1997; Shaw et al., 1999), and those formed sub-glacially involving massive or laminated till, diamictite and clay dykes injected into bedrock or frozen substrates (Larsen and Mangerud, 1992; Dreimanis and Rappol, 1997; Hyam et al., 1997; Le

Heron and Etienne, 2005). Clastic dykes are also reported in settings associated with sudden storm generated deposition of sediment, with turbidite sequences, with thrusting and with the upward flux of deep basin waters into shallow water sands (Truswell, 1972; Jolly and Lonergan, 2002; Le Heron and Etienne, 2005).

Seismic activity in tectonically active areas causing the propagation of faults systems can provide fissures and fractures in which neptunian passive filling may occur (Demoulin, 1996; Rey, 1997; Beavon, 1998; Beacom et al., 1999; Haas and Hámor, 2001). Neptunian dykes formed in this manner have been used to determine the timing of seismicity, to identify periods of volcanic activity and to estimate paleo-latitudes (Beacom et al., 1999; Lewandowski, 1999; Curtis and Riley, 2003; Speranza et al., 2003). Clastic dykes occurring in swarms that have common strikes and trends may be used as paleoslope indicators (Rowe et al., 2002).

Neptunian dykes consisting of bioclastic limestone are reported to occur within grainstones of the Capitan Reef in West Texas and New Mexico. Here they form vertical dykes that have been interpreted as passive infilling of fissures whose formation was associated with flexing of the carbonate platform (Wu and Chafetz, 2002; Boulvain et al., 2004; Staton and Pray, 2004). These neptunian carbonate dykes within the Capitan Reef are reported to be associated with at least three episodes of fissure flexing and re-opening of fissures, with subsequent infilling identified by layers of different carbonate facies that are typically repeated on either side of a central fill forming a symmetrical sequence of fills. Carbonate neptunian dykes are not always a simple infilling of platform carbonate sediment. For example, complex brecciated limestone dykes are known from the Cache Creek Complex in British Columbia within limestones capping an oceanic paleo-seamount (Sano and Orchard, 2004). Bioclastic dykes and sills are reported to occur as fluidised intrusion fills and brecciated lithologies associated with formation of the Ordovician Lockne meteorite impact crater in Central Sweden (Sturkell and Ormo, 1997).

Neptunian dykes and clastic dykes may contain micritic fill lithologies. The Gavilan Formation in southeast Spain is interpreted as a carbonate platform, with lower sections containing fracture fills of reddish to yellow

micrites with inclusions of rock from the Gavilan Formation itself which are interpreted as neptunian dykes infilling seismicity induced faults (Rey, 1997).

5.1.1 Sedimentary dyke features

The size of sedimentary dykes varies from infilling of polygonal shrinkage cracks and vein intrusions, to dykes that may be several metres wide and several kilometres in length, analogous to igneous dyke intrusions (Peterson, 1968; Beacom et al., 1999; Lewandowski, 1999). The emplacement of material maybe either gradual, as in neptunian fill dykes (generally from above) under the influence of gravity, or rapid by injection of pressurised water-charged sediment (Peterson, 1968; Dreimanis and Rappol, 1997). Neptunian passive fill dykes may occur as individual features while clastic injected dykes tend to occur as dyke swarms with a number of dykes localised in a specific area, typically exploiting planes of weakness within the host rock (Peterson, 1968).

Clastic injected dykes typically show a highly bifurcated (anastomosing) and complex pattern, often terminating in a taper which may indicate the direction of intrusion with the dyke tapering away from source material and thus its point of origin (Peterson, 1968; Archer, 1984; Larsen and Mangerud, 1992; Dreimanis and Rappol, 1997; Beacom et al., 1999; Pollock and Williams, 2000; Rowe et al., 2002; Le Heron and Etienne, 2005). Clastic dyke bifurcation may occur in a number of different directions away from a source dyke and may also intersect and join or cross-cut other dykes (Larsen and Mangerud, 1992; Le Heron and Etienne, 2005). The direction of intrusion may also be indicated by structures in the surrounding strata, particularly where the host rock was still ductile during intrusion, with beds often dipping or folding along the side of the intrusive body in the direction of injection (Waterhouse, 1955; Dreimanis and Rappol, 1997; Rowe et al., 2002). The source of injection of clastic dykes cannot readily be determined unless a direct origin can be seen or lithologies within a clastic dyke can be adequately matched to units occurring in either overlying or underlying strata (Peterson, 1968).

Where dyke side walls are exposed they may display striation marking, drag structures and slickenside features sometimes resembling ripple bedding

(Peterson, 1968; Demoulin, 1996; Phillips and Alsop, 2000). Side walls may also sometimes show 'blow out' intrusions which occur along planes of weakness in the dyke walls as secondary intrusions after the initial injection event (Demoulin, 1996). Concordant clastic sill injections have been observed to display scour and flute markings on previously injected and host material surfaces (Truswell, 1972; Archer, 1984). Discordant dykes (and sills) may also support these features but they are not as readily exposed in outcrop (Peterson, 1968; Archer, 1984).

Some clastic injection dykes are reported to contain large (>2 mm) clasts, at times sufficiently large and numerous enough to be classified as breccias, but these are more commonly referred to as brecciated dykes (Sturkell and Ormo, 1997; Beacom et al., 1999; Shaw et al., 1999; Sano and Orchard, 2004). Intruded clasts may be composed of failed material associated with the injected sediment (monomictic breccias, a single fill type) or of 'rip-up' clasts of the host material and/or previous injected dyke lithologies (polymicitic breccias, more than one fill type) (Sturkell and Ormo, 1997).

Both neptunian (passive fill) and clastic (injected) dykes can display lamination of internal units, but neptunian dykes tend to be massive or display crude horizontal bedding. Multiple fill units may also be observed in both neptunian and clastic dykes through repeated episodes of fracturing along the same dyke pathway (Thorson et al., 1986; Demoulin, 1996; Dreimanis and Rappol, 1997).

Within clastic dykes the evidence for injection can be found in the lamination, sorting and orientation of grains parallel to dyke walls. This is particularly evident for tabular grains and minerals associated with laminar viscous flow, while more central units are typically described as having massive textures. Neptunian dykes and clastic dykes that are intrusions of plastic material (by squeezing into the host material) are not reported to contain any kind of grain sorting (Peterson, 1968; Archer, 1984; Larsen and Mangerud, 1992; Dreimanis and Rappol, 1997; Hyam et al., 1997; Sturkell and Ormo, 1997; Beacom et al., 1999; Tipper et al., 2003; Jonk et al., 2005).

A distinction between the timing of emplacement of laminated units within sedimentary dykes may be appreciated by employing terminology used

by Lewis (1973) in his description of 'polyphase' dykes from Oamaru, New Zealand. His scheme involved the distinction between laminations that are of a similar lithology and display crude sorting of grains (grain stratification), referred to as pulses, and units which lay roughly parallel to the dyke walls but are distinctly different lithologies indicating probable emplacement at different times, referred to as phases (Lewis, 1973; Sturkell and Ormo, 1997; Phillips and Alsop, 2000).

5.1.2 Sedimentary dyke injection processes

Clastic dyke injection occurs in a general direction that is 'normal' to the least compressive stress direction, so that dykes are intruded vertically if the principle stress is also vertical. The strike of dykes is controlled by the difference between the intermediate and minimum horizontal stresses, resulting in clastic dykes with variable dip angles (Jolly and Lonergan, 2002; Le Heron and Etienne, 2005). Downward injection of clastic dykes with a hydraulic head applied from above is reportedly less common than injection from below an intruded strata (Dreimanis and Rappol, 1997; Pollock and Williams, 2000; Le Heron and Etienne, 2005).

When the host sediment becomes over-pressurised it can undergo hydraulic failure and allow for the formation of clastic dykes (Beacom et al., 1999; Jolly and Lonergan, 2002; Le Heron and Etienne, 2005). This results in the development of a pressure gradient between the fracture and the intruding sediment, mobilising the sediment inside the intruded void (Sturkell and Ormo, 1997; Pollock and Williams, 2000; Le Heron and Etienne, 2005). The morphology of the host material fracture and the resultant intrusion therefore reflect the state of the stress field present at the time of over-pressurisation, while the changes observed in dyke dip away from the source material are a reflection of the changes in the stress field orientation with increasing distance of intrusion (Beacom et al., 1999; Le Heron and Etienne, 2005). With increasing distance from the source material and point of injection, clastic dykes are observed to bifurcate and branch off from the main intrusive body. This has been interpreted as the result of a loss in hydraulic head and thereby a reduced pressure gradient which is required to fracture the host material with

anastomosing clastic dykes tapering out to nothing (Le Heron and Etienne, 2005). Upward injection of sediment has in some cases also been related to sediment dewatering processes which may convey saturated sediment into dewatering structures during the dewatering process, particularly when the underlying saturated sediment is also over-pressurised (Dreimanis and Rappol, 1997).

Fluidisation and intrusion of saturated shallow marine sediment has been associated with the emplacement of hot (c. 700°C) igneous material. Such intruded clastic dykes are reported to occur along the margins of igneous dykes and sills within the mid-Proterozoic Ritscherflya Supergroup from Dronning Maud Land, East Antarctica (Curtis and Riley, 2003). The clastic intrusions occur in cooling joints and fractures within the igneous intrusion as they rapidly cooled within wet sediment. The confining pressures within the sediment at shallow crustal levels are estimated at about 300 bars, which equates to a water boiling point of 400-450°C. Under these conditions the intrusion of hot igneous bodies would have resulted in a liquid to vapour phase change with the sediment developing a low (<6%) vapour flow component. The opening of these voids would have reduced the surrounding confining sediment pressure from about 300 bars to near zero, resulting in fluidisation of the sediment at temperatures near that of the igneous intrusions and allowing for sediment to be mobilised and flow along cooling joints and within the igneous intrusions with only thin zones of contact metamorphism (Curtis and Riley, 2003).

Table 5.1: Summary of the common characteristics and origins of neptunian and clastic sedimentary dykes gleaned from the literature reviewed in this study.

	Sedimentary dykes	
Characteristic	*Neptunian dykes*	*Clastic dykes*

Mechanism of formation	Passive infilling
	- Gravity (gradual)
	- Mass emplacement gravity flow (rapid)
		Forcible injection (~ instantaneous)
		- Head gradients associated with
		  - Normal burial, overburden loading (hydrostatic pressure)
		  - Volcanism (complex hydrothermal mechanism)

Infill structure	Infilling of
	- Fractures (platform flexing)
	- Regional cleavage
	- Eroded surfaces
	- Karst topography
		Injection exploiting
		- Planes of weakness
		  - Fractures
		  - Regional cleavage
		  - Faults
		  - Dewatering structures

Host material rheology	Typically consolidated	Consolidated or unconsolidated
Host material lithology	- Sedimentary facies - Metamorphic rocks - Plutonic rocks - Volcanic rocks	

Tectonic environment	Stable or unstable	Typically unstable associated with
		- Seismicity
		  - Slumping and folding (unconsolidated)
		  - Fractures and faults (consolidated)

Depositional environments	- Fluvial - Shallow marine - Deltaic - Continental shelves (storm events) - Deep marine (typically subduction zones, turbidites and fans) - Thrust belts - Zones of ocean upwelling - Sub-glacially - Volcanic structures - Meteoroid impacts	
Features	- Typically a single dykes (discordant with strata) - Single fill or multiple fill lithologies - May be stratified or massive - Geopetals	- Dykes (discordant) and sills (concordant with strata) - May occur as dyke swarms (polygonal), dyke cross-cutting - Single fill or multiple fill lithologies, cross-cutting of fills, that are closely timed (pulses) or separated by significant geological time (phases) - Vertical lamination or massive - Grain sorting - Bifurcated (anastomosing) - Taper away from source material - May include ‘rip-up’ clasts of host - Dyke wall striations
Fill lithologies	Clays, silts, sands, carbonate (bioclastic or precipated), breccias (monomictic or polymictic)	

5.2 Sedimentary dyke localities

5.2.1 Red Bluff, Chatham Island

Carbonate dykes are common within the Red Bluff Tuff along the coastal exposures at Red Bluff. The occurrence of some of these dykes was previously recorded in Campbell et al. (1993) where they were interpreted as near vertical fissure fills of Matanginui Limestone punctuating the Red Bluff Tuff. The Campbell *et al.* (1993) locality relates to a small, near vertical gully located at the northern end of the Red Bluff coastal exposure (CH1/464612) which has developed due to the preferential weathering of the softer tuff surrounding the more indurated limestone dyke (Fig. 5.1).

Dyke outcrops along the coastline at Red Bluff are exposed for just over 1 km distance from approximately CH1/465613 in the north to CH1/466605 in the south. Most of these dykes are probably best termed dykelets or, less formally, 'stringers' that are typically less then 20 mm thick and occur as either 'independent' dykelets or 'offshoot' dykelets from larger dyke intrusions. The lithology of these small dykelets is generally micritic with some bioclastic limestone, while some extremely small stringers <5 mm thick (type *1*) consist of large interlocking calcite crystals. These smaller stringer dykelets are extremely abundant, probably numbering in the thousands, and many may well be a diagenetic feature of the calcareous Red Bluff Tuff rather than sedimentary dykes *per se*.

Bigger dykes are far less common and have been divided into types *2* and *3*. Type *2* dykes are between 20 and 500 mm thick and have multiple fill lithologies including micrite, bioclastic limestone and volcaniclastic sediment. Dykes of this character are considered to number in the hundreds, but precise numbers are unknown given the inaccessibility of much of the Red Bluff coastline. Type *3* dykes are >0.5 m thick and include the occurrence mentioned by Campbell et al. (1993) seen in Fig. 5.1 and in the frontispiece of this thesis. The majority of these type *3* dykes contain mainly bioclastic limestone and bioclastic micrite, although some are noted to contain precipitated micrite units. Type *3* dykes probably number about a half a dozen, although several of these are observed only at a distance in high coastal cliffs at the southern end of Red Bluff area.

For the purpose of discussing observations made in the field on the dykes at Red Bluff the locality is divided into five discrete areas: *north Red Bluff*, *1 km north of the twin masts*, *big bluff*, *below the twin masts* and *south Red Bluff* (Table 5.2). The divisions are purely geographical and descriptions will follow in the north to south order as presented above. Dyke occurrences at Red Buff have been examined extensively and many of these are reviewed here along with the nature of all major fill lithologies. Each occurrence at each site has been assigned an alphabetic letter and will be discussed in terms of its field and petrographic characteristics in this chapter. Comment about the left- and right-hand sides of dykes is always given as if looking landward from an offshore position.

For reader convenience, individual limestone dyke occurrences in the *north Red Bluff* locality are shown in a photomontage in this chapter (on page 173, Fig. 5.2B) and can be folded out for viewing while reading this section.

Table 5.2: The Red Bluff locality divisions based on geographical location from north to south and the lettered names used for the dykes occurring in each designated locality.

Red Bluff dyke locality names	**Limestone dyke names**
- *north Red Bluff*	*A*, *B*, *C*, *D*, *E*, *F*, *G*, *H*, *I*, *J*, *K*, *L*, *M*, *N*, *O*, *P*, *Q*, *R* (complex),
- *1 km north of the twin masts*	*S* (collective of calcite veins)
- *big bluff*	*T*, *U* (brecciated)
- *below the twin masts*	*locality 27* dyke
- *south Red Bluff*	No designation
Division of localities is geographical from north to south along the Red Bluff coastline	

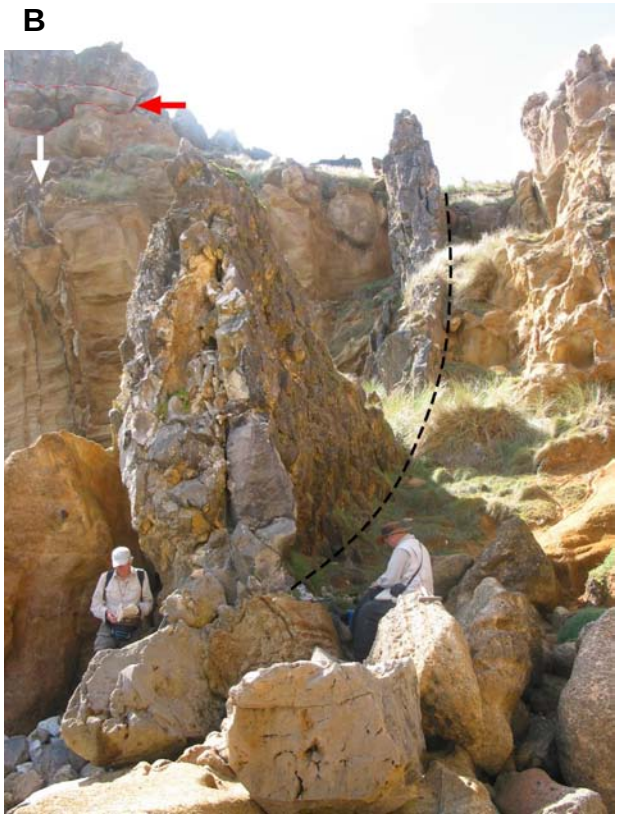

Figure 5.1: **A** shows of the Red Bluff 'volcanic mound' taken from the north looking south toward the main carbonate dyke occurrence at Red Bluff reported in Campbell et al. (1993). This dyke occurrence is pictured in the centre of the photo (white arrows) and runs the thickness of the tuff from sea level to the top of the Red Bluff Tuff, to nearly meet Matanginui Limestone that is 'draping' the northern side of the Red Bluff Tuff (indicated by the black dashed line). The red line in the top photo indicates the northern-most known carbonate dyke exposed at Red Bluff. **B** shows Noel James (left) and Brian Jones (right) at the base of the main carbonate dyke at Red Bluff (indicated by the black dashed line which sits on the right 'landward' side of the dyke). The white arrow the image indicates the position of a nearby sedimentary dyke complex named *Mad Dog* while the red arrow and dash outline indicate the 2005 position of a fall block that exposed an upper dyke/Matanginui Limestone contact in 2006.

North Red Bluff dykes

The area referred to as north Red Bluff relates to the general site of the dyke occurrences in Campbell et al. (1993). This is an area of many sedimentary dykes involving numerous stringers (type *1*), dykelets (type *2*) and large dykes (type *3*) (Fig. 5.2).

Dyke A (Lat 43.89661, Long 176.54295) is not the northernmost dyke occurrence at Red Bluff, but it is the first accessible dyke recorded on the 2006 Chatham Islands excursion. There are at least two observed occurrences to the north of dyke *A* (Fig. 5.2). In the field this dykelet was considered to contain up to four distinct fill lithologies across an average dykelet thickness of 25 mm. The fill sequence is 'asymmetrical' (an uneven distribution of fill lithologies) with the outer right side having a 5 mm thick sandy bioclastic fill, to the left of which is a 1-2 mm thick micrite fill, followed by a 5-10 mm thick limestone conglomeratic fill with volcaniclastics, and on the outermost left-hand side a 7 mm thick micrite fill. Stringer dykelets come off dykelet *A* at almost right angles higher in the section and tapered out over an average distance of about 1 m. The total outcrop height of dyke *A* is estimated to be 11 m, striking 024° with a sub-vertical dip.

Dyke B (Lat 43.89677, Long 176.54301) is a dykelet occurrence 5-10 m to the south of dyke *A* which bifurcates, is up to 10 cm thick, strikes 115° with a sub-vertical dip and has an observable height of 5-6 m (Fig. 5.2). This dyke contains a volcaniclastic sand fill of the Red Bluff Tuff that has intruded into the bioclastic limestone fill, showing a clear cross-cutting relationship with the limestone fill by meandering from the left- to right-hand walls of the dyke (Fig. 5.3).

Dyke C (Lat 43.89684, Long 176.54298) occurs approximately 3 m to the south of the previous dyke *B* and can be traced to an observable height of 7 m, striking 023° with a sub-vertical dip. The dyke bifurcates midway up the section to rejoin after a distance of 1 m (Fig. 5.2). This dykelet averages about 10 mm thick and comprises a micrite fill that is cross-cut by a porous bioclastic limestone fill which appears to repeatedly meander across the total thickness of the dyke (Fig. 5.4).

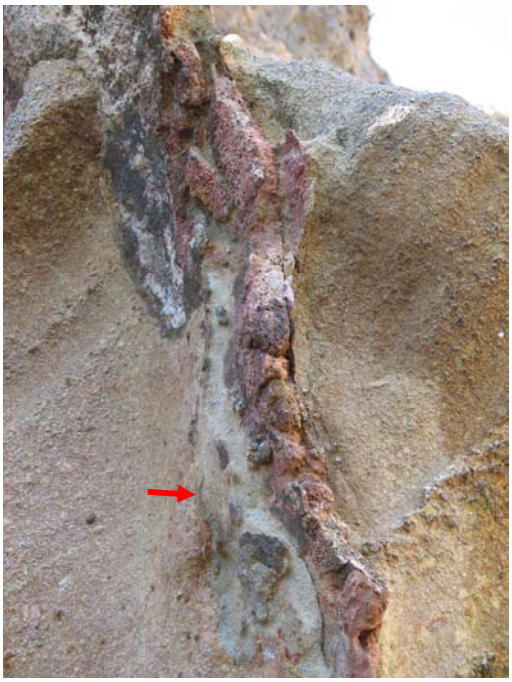

Figure 5.3: Upper section of dyke *B* shows the volcaniclastic intrusion along the right-hand side of the dyke that cross-cuts the limestone fill lithologies to 'skim' down the left-hand wall of the dyke (red arrowed). Refer to Fig. 5.2 for relative scale.

Figure 5.4: Close-up of a sample from dyke *C* showing an outer grey micrite fill on the lower right-hand, centre left and upper right-hand sides (blue arrowed). This micrite fill has been cross-cut by a porous bioclastic fill lithology which begins in the upper left-hand side and meanders across the centre right and down along the lower left-hand side.

Figure 5.5: Dyke *G* close-up of the outer right-hand side of the dyke showing the outermost 1-2 mm thick micrite fill with a crystalline outer surface (blue arrowed).

Dykes D, E, F and G represent a series of stringer dykelets that are typically 5-10 mm thick, but no more than 20 mm thick, extend vertically for 7-11 m in traceable outcrop extent and strike 118° with a sub-vertical dip. The first of these dykes, *D* is located 3 m to the south of dyke *C* and appears to be a straight precipitated micrite fill with no other lithologies present (Fig. 5.2). Dykelet *E* (1.5 m south of *D*) is of comparable size in thickness and height and also has a fully micrite fill (Fig. 5.2). Dykelet *F* (1 m south of *E*), although comparable in thickness and height to the previous two dykes, has a conglomeratic bioclastic limestone and volcaniclastic fill (Fig. 5.2). Dyke *G*, 2 m to the south of dyke *F*, is up to 20 mm thick at some points in the dyke. Dykes *G* and *F* join a cluster of dykes 2 m to the south, near an upper mid point in what is referred to as the '*mad dog*' dyke complex. Dyke *G* is also joined by an extremely thin (2 mm thick) micritic stringer whose outer edge is exposed along the right-hand wall of the dyke, but which in fact runs down both outer dyke walls (Fig. 5.5).

Dykes H and I are contained within what is named the '*mad dog*' dyke complex. They join the previous dykes *F* and *G* at the top of the lower dyke section (Fig. 5.2). There are two main dykes here, namely *H* and *I*. Dyke *H* is approximately 25 mm thick and thins towards the top of the lower section at about 7 m above sea level, where it become highly bifurcated over a 1-2 m section before condensing into a single dyke which is joined by dykes *F*, *G* and *I* (Figs 5.2, 5.6). Dyke *I* becomes thicker than *H* mid-section where it reaches 35-40 mm thick, and it also becomes bifurcated in the lower section (Fig. 5.7). Both dykes have multiple phase lithologies that include an outer micrite fill, a red micrite/bioclastic limestone fill, a coarse bioclastic fill and a volcaniclastic fill (Fig. 5.7).

Dykes J and K occur approximately 3 m to the south of the 'mad dog' complex and again are a complex of 2-3 dykelets that occur higher in the section and taper out before reaching the bottom of the section (Fig. 5.2). Because these two main dykes (*J* and *K*) occur high in the north Red Bluff section they are inaccessible and could not be sampled. The two dykes run parallel to each other throughout their distance with a 0.5 m gap between the two dykes near the bottom of the section, which widens to a 1 m gap at the top. Both dykes are approximately 10 mm thick, although dyke *K* appears to

increase in thickness to 20-30 mm at a mid-point in the dyke. Both dykes have a sub-vertical dip and strike 124°.

Dyke L is located roughly 2.5 m to the south of dykes *J* and *K* and is composed of a bioclastic fill with a dyke thickness of 5-10 mm and a sub-vertical dip and strike of 124° (Figs 5.2, 5.8).

Dyke M is the main dyke at the *north Red Bluff* location and relates to the occurrence mentioned in Campbell et al. (1993). This main dyke is 2-3 m thick and extends about 60 m in height to protrude some 12 m out of the top of the Red Bluff Tuff exposed at this coastal section (Figs 5.1, 5.2). Dyke *M*, however, does not at its upper end make an observable contact with the overlying Matanginui Limestone and at its lower end the dyke extends below sea level. Generally dyke *M* consists of an indurated bryozoan grainstone with conspicuous echinoderm spines and bivalve fragments, with macro-scale porosity (Fig. 5.9). Dyke *M* contains no evidence of horizontal bedding but does have near-vertical contacts that separate different fill lithologies (Fig. 5.1B). Near the lowermost reaches of dyke *M* there are cobble sized inclusions of volcaniclastics which appear to be calcified and stained lithologies of Red Bluff Tuff (Fig. 5.10).

Higher reaches of dyke *M* on the left-hand wall were observed to display striation markings where the dyke emerges from the Red Bluff Tuff (Fig. 5.11). The striations continue from the emergence point over a distance of 0.5 m, after which they become progressively weathered and untraceable. On close inspection of the side wall a thin veneer of micrite can be seen on the outermost wall. The interesting thing about this veneer is that it sits on the outside of the striations which occur within an inner bioclastic unit, although striations are also noted to occur on the inner side of the micrite veneer. The striations themselves trend horizontally in a general NW-SE direction (striking 124°, dipping 20°-40°), supporting a roughly horizontal shearing direction.

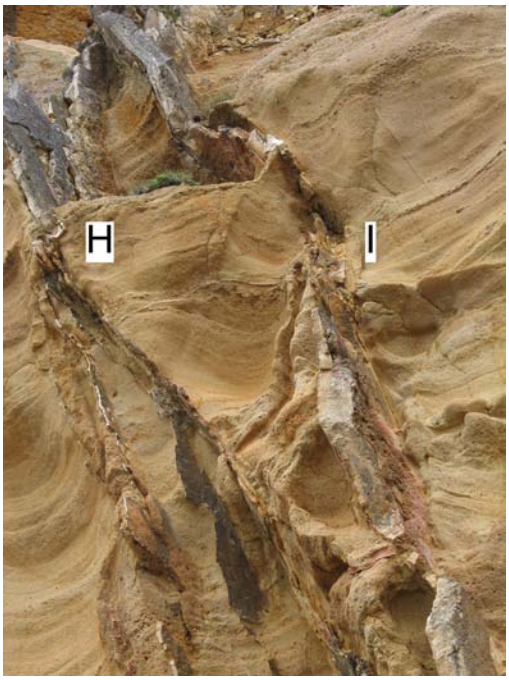

Figure 5.6: Photo of the top of the lower section of the 'mad dog' dyke complex showing dykes *H* (left) and *I* (right). The bifurcating nature of dyke *H* is evident, beginning at the letter *H* and continuing down out of sight of the photo. Dyke *I* is seen to be of considerable thickness through this mid-section and there appears to be a joining dyke between dykes *H* and *I*. Near the top of the photo the two dykes can be seen to join and condense into one dyke. Refer to Fig. 5.2 for relative scale.

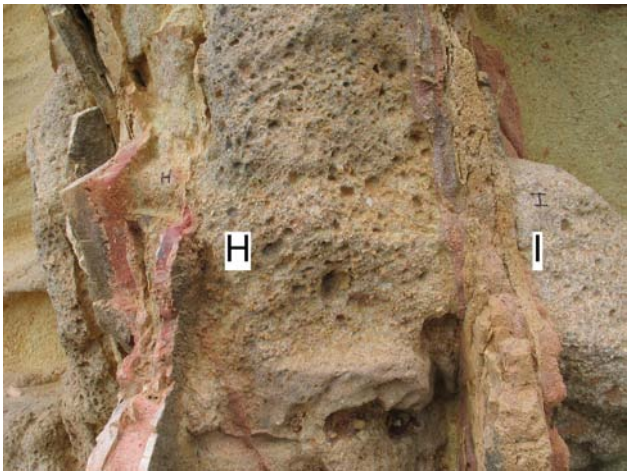

Figure 5.7: Dykes *H* and *I* showing the multiple fill lithologies present in both dykes with Red Bluff Tuff in between (on which the letter *H* is placed). Clear cross-cutting relationships can be seen in dyke *H* with a volcaniclastic fill splitting and dividing the red fill in two. Refer to Fig. 5.2 for relative scale.

Figure 5.8: Close-up shot of dyke *L* showing a thin bioclastic limestone fill.

Figure 5.9: Close-up shot of the typical bryozoan limestone fill within dyke *M* showing conspicuous echinoderm spines and bivalve (pectinid) remains.

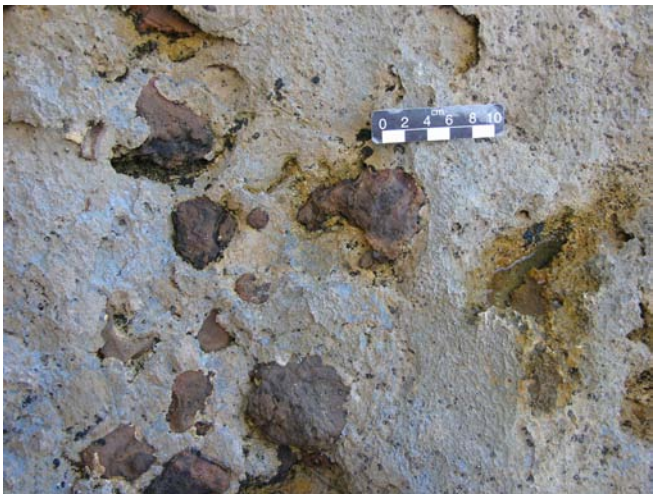

Figure 5.10: Near sea level within dyke *M* can be seen conspicuous rusty stained volcaniclastic cobble inclusions that appear to be calcified Red Bluff Tuff.

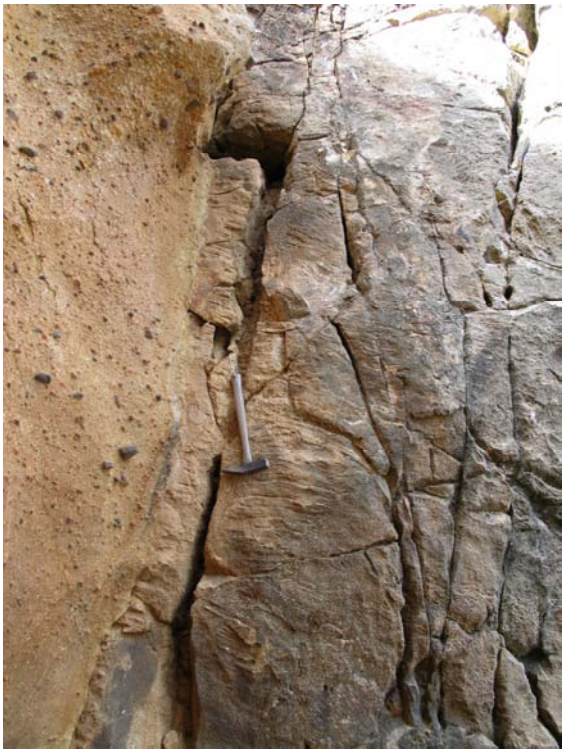

Figure 5.11: Higher in the dyke *M* section where the dyke emerges the Red Bluff Tuff, striation structures occur along the left-hand side of dyke. These striations are only observable near the eroded Red Bluff Tuff 'contact', being presumably weathered away along the remainder of the dyke.

Dykes N, O, P and Q, forms a dyke complex on the left-hand side at a distance of 0.5 m from the main dyke *M* (Fig. 5.2). The largest of the dykes (*P*) in this complex is an offshoot bifurcated dyke from the main dyke *M* and is 30-40 mm thick and appears to contain separate vertical units, revealed by weathering. These vertical units are considered to represent at least two separate phases; an initial phase that sits either side of a central later phase and an outermost micrite unit which is clearly traceable on the left-hand side of the dyke *P* (Fig. 5.12). On the right-hand side of dyke *P* the relationship with a similar outermost micritic unit is not so clear. The outermost micrite unit, along with the outer internal unit, splays off from dyke *P* and is separated from dyke *P* by pyroclastic material of the Red Bluff Tuff, which occurs between dyke *P* and the outer internal unit, and the outer internal unit and the outermost micrite unit (Fig. 5.13). These right-hand side splay dykelets are collectively referred to as dyke complex *Q*. Dyke *P* joins dyke *M* near the top of the lower cliff section and strikes 130° with a sub-vertical dip (Fig. 5.2).

Two other dykes occur along the left side of this main dyke *P* offshoot (Fig. 5.12). Both are thin, typically 10 mm thick, and consist fully of micrite fills. Dykelet *O* occurs about 30 cm north of dyke *P* and is best described as a scrappy intermittent occurrence. Dykelet *N* is the northernmost occurrence located some 40 cm to the north of dykelet *O* and thickens to 30 mm across up the dyke. Both dykelets join dyke *P* at 3.5 m above the lowermost exposure of the offshoot dyke *P* (Figs 5.2, 5.12).

Dyke complex R (Lat 43.54327, Long 176.54327) occurs to the right of (south of) the main dyke *M* within a mound of Red Bluff Tuff, being separated from it by a narrow 1.5 m wide gully that allows access to the *north Red Bluff* locality (Fig. 5.2). The mound is criss-crossed by 8-10 individual dykelets and stringers with thicknesses from 1-10 mm. The majority of these appear to be straight micritic fills, although there is one 10 mm thick dyke that has a notable bioclastic secondary phase fill in its centre (Fig. 5.14). Five metres south of the dyke *R* complex, near sea level, in the walls forming the southern end of the *north Red Bluff* locality, a number of extremely weathered dyke occurrences were also noted.

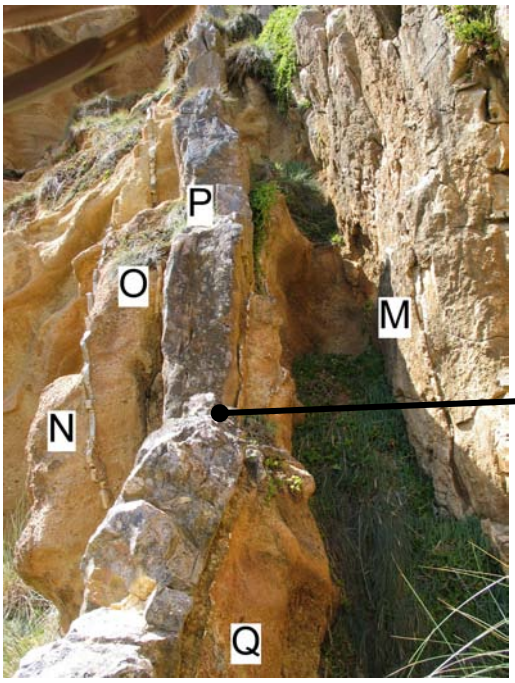

Figure 5.12: Photo (left) of the *N*, *O*, *P* and *Q* dyke complex with the main north Red Bluff dyke *M* to the right of the shot. Refer to Fig. 5.13 for relative scale.

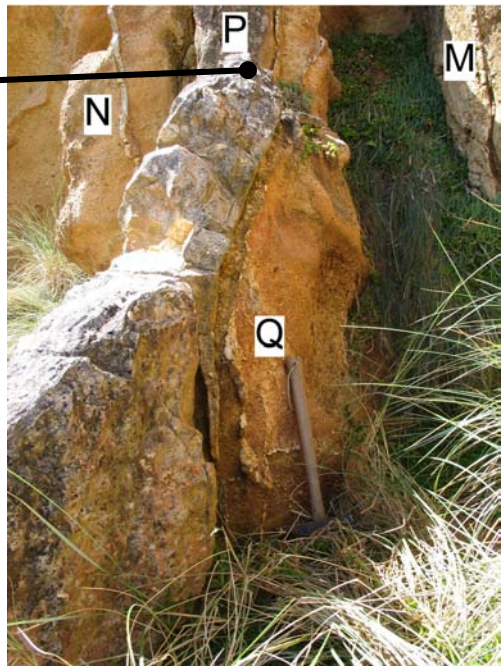

Figure 5.13: Close-up (right) of the right-hand side of dyke *P* showing the complex relationship of the two splayed units from dyke *P*, collectively referred to as dyke complex *Q*.

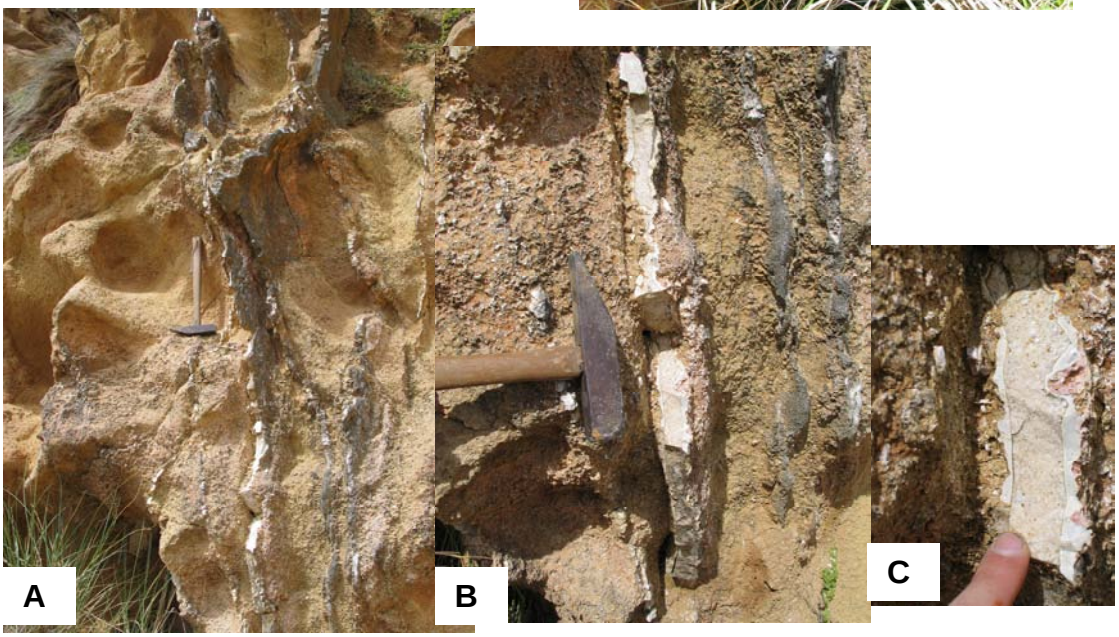

Figure 5.14: Shots of the bioclastic dyke in the *R* dyke complex. **A** showing the initial outer micrite fill in **C**. The bioclastic dyke is considerably thicker than the surrounding thin straight micrite stringer dykelets in **B**.

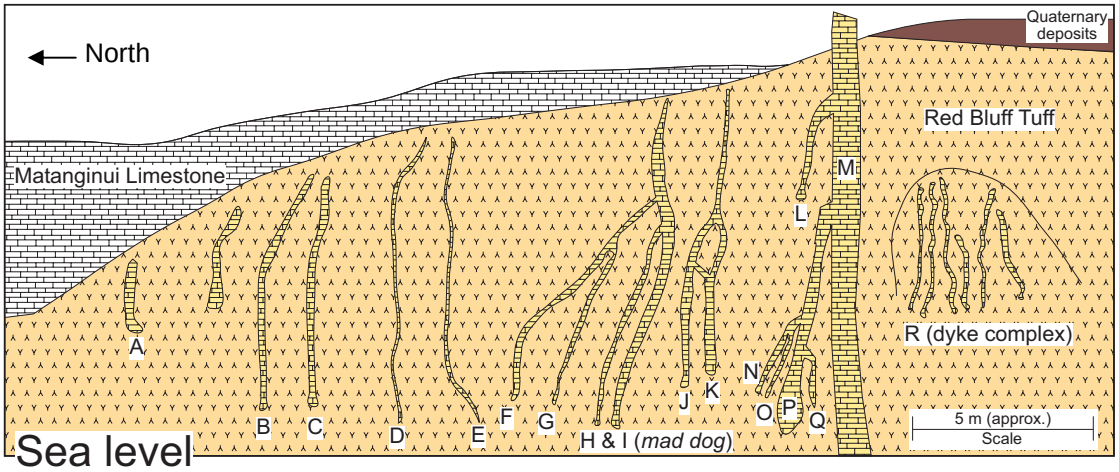

Figure: 5.2A: Schematic diagram of the north Red Bluff locality showing the relative position and relationships of limestone dyke occurrences recorded in photographs in Fig. 5.2B.

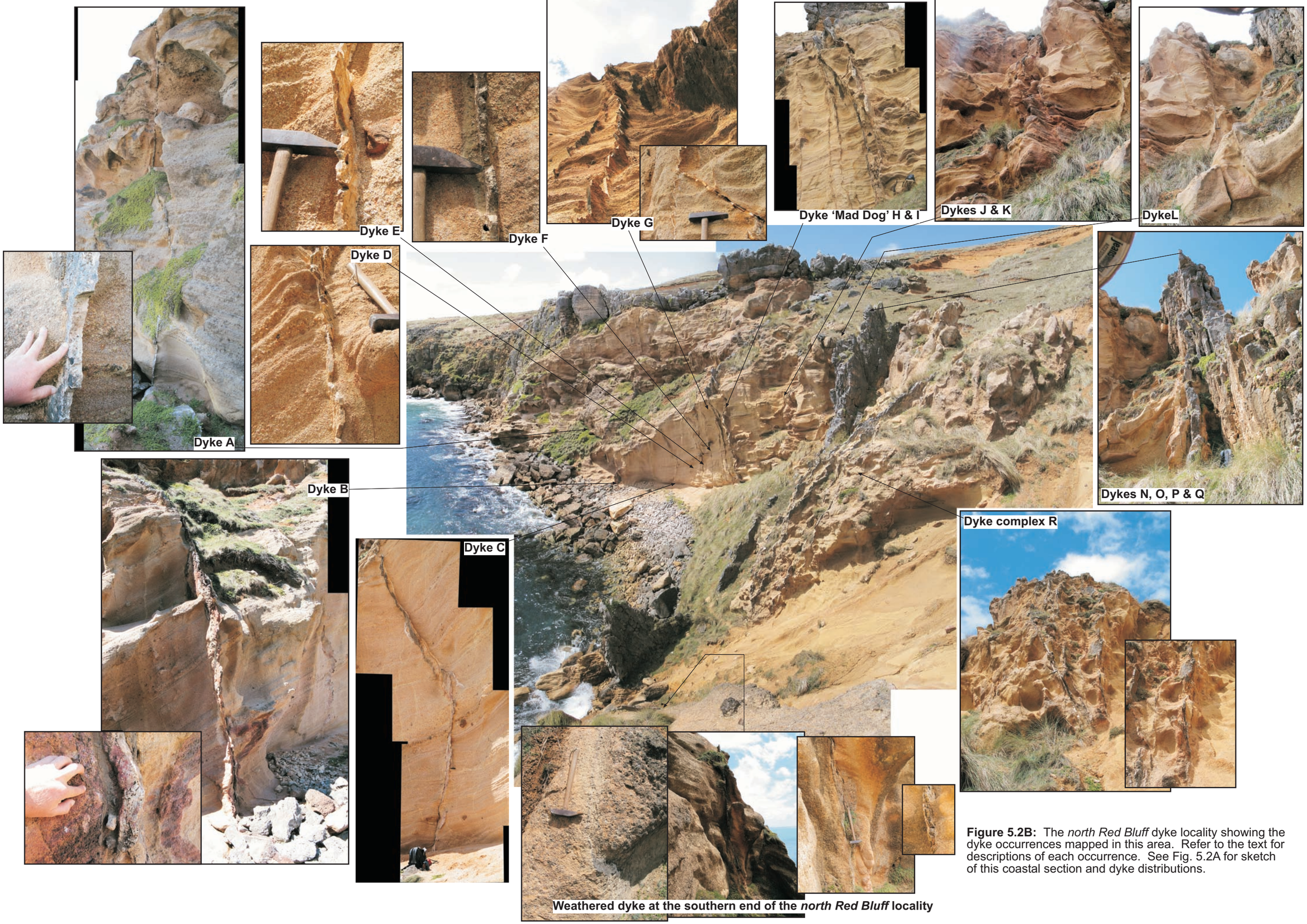

Figure 5.2B: The *north Red Bluff* dyke locality showing the dyke occurrences mapped in this area. Refer to the text for descriptions of each occurrence. See Fig. 5.2A for sketch of this coastal section and dyke distributions.

1 km north of the twin masts dykes

This is an intermediate area adjacent to, and to the south of, the *north Red Bluff* locality, that juts out of the coastline as a promontory. Numerous small thin type *1* dykelets and stringers are present in this area, each typically only a few millimetres thick (Fig. 5.15). These are not considered to be true dykes, but rather are calcite veins with 'dogtooth' interlocking crystals of calcite which often leave a central cavity within the calcite vein (Fig. 5.15). The calcite veins that occur along this stretch of the Red Bluff coastline are collectively referred to as dykes *S* and probably number hundreds to thousands. They are extremely common in the entire Red Bluff area but particularly prolific from this point south. These are considered to be diagenetic features of the Red Bluff Tuff and will not be considered or discussed any further here.

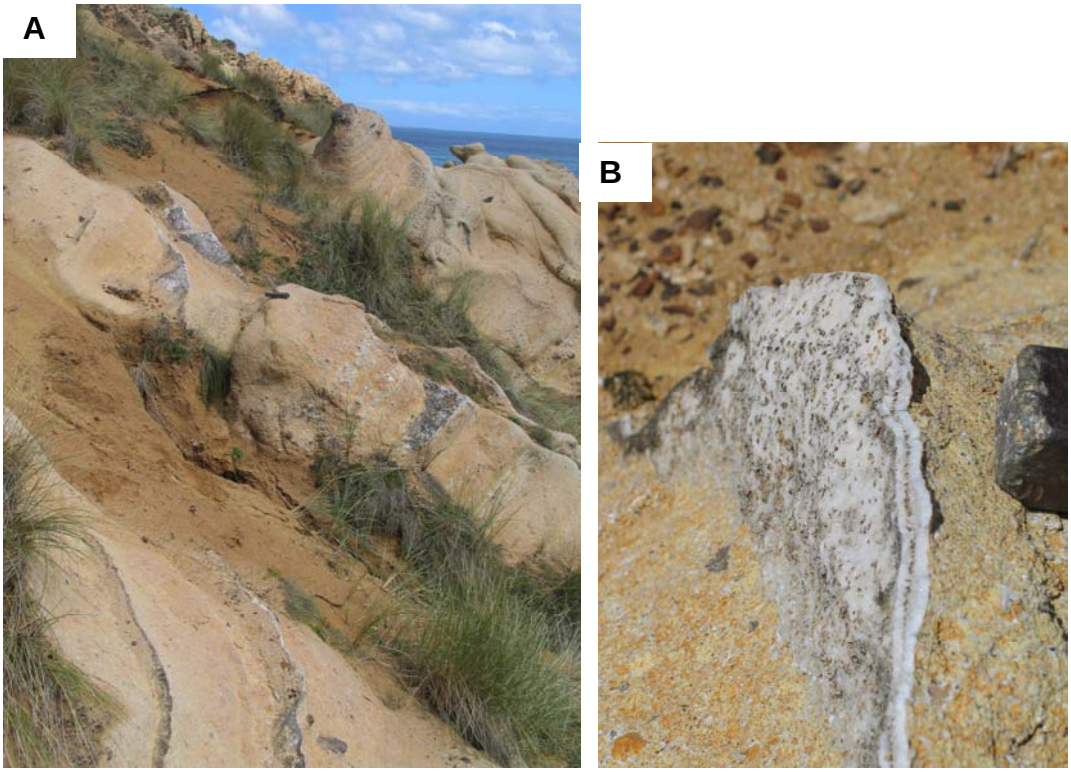

Figure 5.15: Calcite veins that occurs along a 200 m section of coastline forming a promontory that 'juts' out seaward from the adjacent *north Red Bluff* locality and the *big bluff* locality to the south. **A** shows how numerous these calcite veins are within the Red Bluff Tuff (hammer in the centre of the photo for scale). **B** shows a close up of the 'dogtooth' calcite growth from the walls of the veins leaving a central cavity (hammer head on the right of the photo for scale).

Big bluff dykes

Big bluff is an area that is directly adjacent to, and south of, the promontory containing the collective *S* dykes. The *big bluff* locality forms high (>40 m) coastal cliffs that are recessed back landward from the previous promontory (Fig. 5.16). Observations of large type *3* dykes were made at some considerable distance with at least four large sedimentary dykes being recognised in the high sea cliffs. Because of the extreme inaccessibility and hazardous nature of the locality only two of the four dykes were able to be sampled. Basaltic dykes having type *3* dimensions also occur along the *big bluff* locality and generally strike east-west like the carbonate dykes, although at least one basaltic dyke was noted to strike north-south (Fig. 5.16B). It is unfortunate that this north-south trending basaltic dyke was not exposed further toward the coastal cliff as this may have afforded the opportunity to examine the relationship between these basaltic dykes and the sedimentary dykes.

Two separate dykes were able to be accessed in this area. Both occur towards the southern end of the *big bluff* locality where the upper portion of the cliff formed a gentler slope. The first of these is dyke *T* (Lat 43.89862, Long 176.54456) of which only the top of the dyke was observed close-up and sampled (Fig. 5.16C). The top the dyke is about 0.5 m thick and consists of a highly indurated bioclastic limestone similar in lithology to the Matanginui Limestone.

To the south of the upper exposure of dyke *T* is the southernmost dyke occurrence in the sea cliffs of the *big bluff* locality. The occurrence forms a brecciated conglomeratic limestone and volcaniclastic dyke, referred to as dyke *U* (Lat 43.89864, Long 176.54495), striking 340° with a sub-vertical dip (Fig. 5.16D). This is a new facies of dyke in the Red Bluff area and while conglomeratic fills are present in other dykes and localities, this is the only brecciated dyke known to the author in the Chatham Islands. Dyke *U* is 0.6 m thick, with an exposed upper length here of 5-6 m. However, at the southern end of *big bluff* dyke *U* extends the full height of the cliff which is estimated to be 35 m high (Fig. 5.16).

The limestone forming dyke *U* is a mixture of indurated and softer micro-bioclastic and micritic facies. Some of the limestone was observed to

display fold type structures with apparent horizontal layering (Fig. 5.18B). Limestone was also observed to cross-cut volcanics blocks vertically becoming more brecciated where cross-cutting horizontally with right-angled changes in limestone intrusion direction (Fig. 5.18A). The limestone fragments, blocks and folded structures are far more prevalent at the top of the upper dyke section (Fig. 5.17) while the lower section is dominated by volcaniclastic material (fig. 5.18C). Volcaniclastics are primarily Red Bluff Tuff which itself appears not to have been brecciated but is considered to represent a fill material between the brecciated limestone fragments and blocks. Basaltic blocks are also noted within the dyke from the lowermost upper section and are cross-cut by calcite veins.

Figure 5.16: The *big bluff* dyke locality showing the dyke occurrences mapped in this area (indicated by the red dashed lines in **E**). Refer to the text for descriptions of each occurrence. The white dashed lines indicates the position of a north-south trending basaltic dyke. The *big bluff* itself (shown in **E**) represents the summit of the volcanic mound at Red Bluff with the thickest expanse of tuff, having an estimated height of about 40 m above sea level.

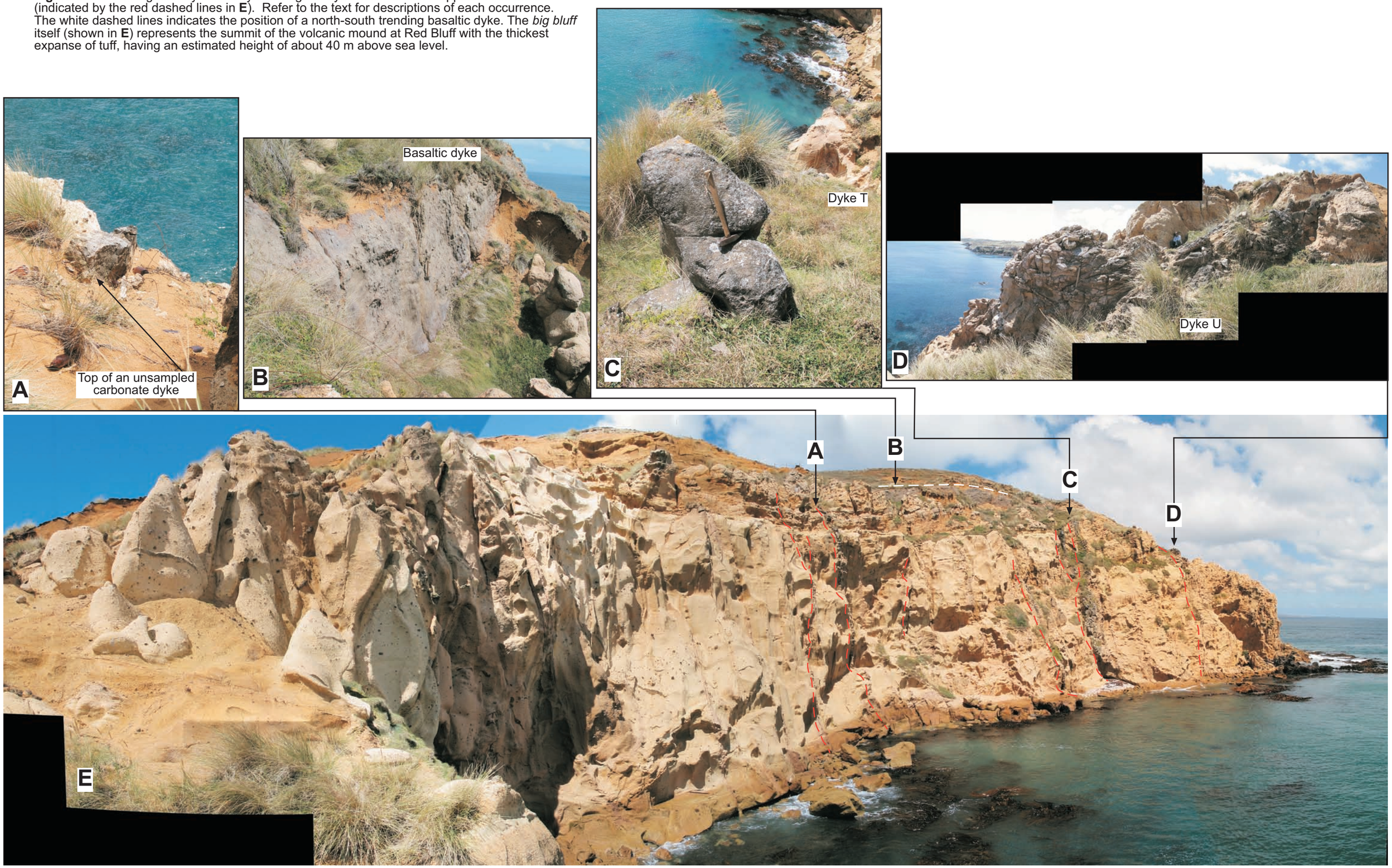

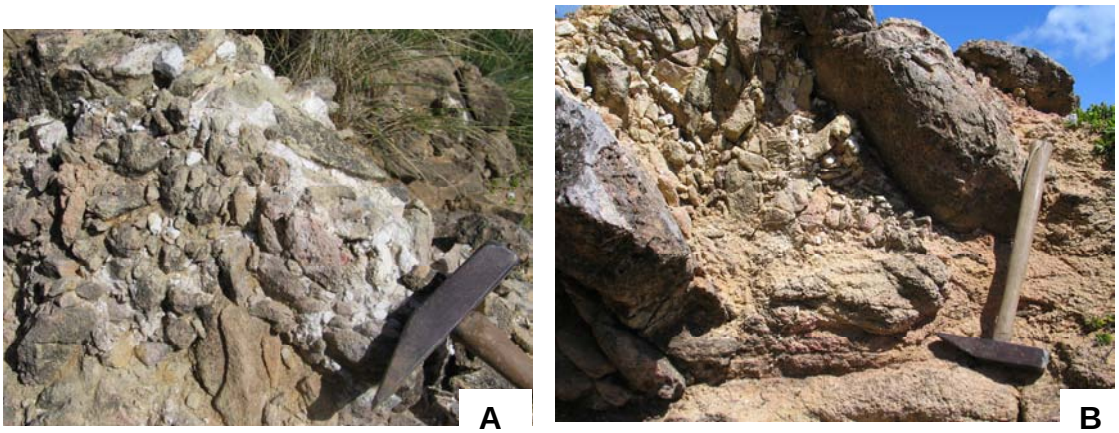

Figure 5.17: **A** shows the top brecciated limestone section of dyke *U*. **B** shows the uppermost section of the dyke, where the volcaniclastic material essentially appears to act as a fill between the limestone fragments and blocks which are both indurated and soft lithologies.

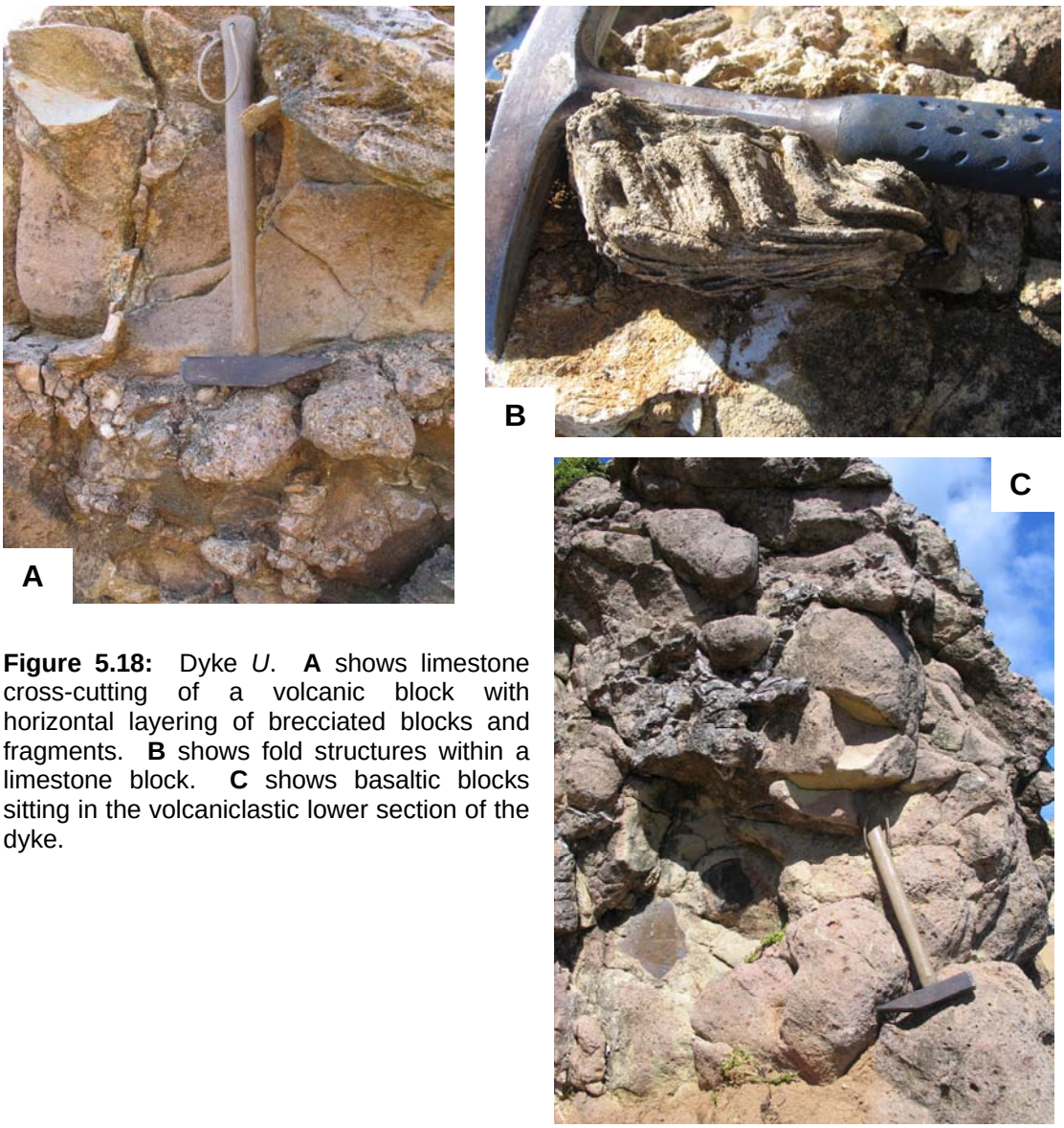

Figure 5.18: Dyke *U*. **A** shows limestone cross-cutting of a volcanic block with horizontal layering of brecciated blocks and fragments. **B** shows fold structures within a limestone block. **C** shows basaltic blocks sitting in the volcaniclastic lower section of the dyke.

Below the twin masts dykes

Ten metres to south of dyke *U* is the fourth locality in the Red Bluff area referred to as the *below the twin masts* locality; it is directly below the position of a radio relay tower. Here the coastline has receded to form a steep walled (>35 m) gut in the Red Bluff Tuff (Fig. 5.19). The gut is transected by numerous basaltic dykes that are primarily east-west trending although there is one north-south trending dyke that is most likely the same trending dyke from the adjacent *big bluff* locality. The carbonate dyke occurs on the northern edge of the gut and is exposed over a length of only 1 m. This occurrence was first observed in 2005 and was then referred to as *locality 27*. The carbonate dyke is 60 cm thick with an outer micrite laminated layer. The inner portion of the dyke appears to be a chemically precipated micrite and is extremely hard and smooth to the touch.

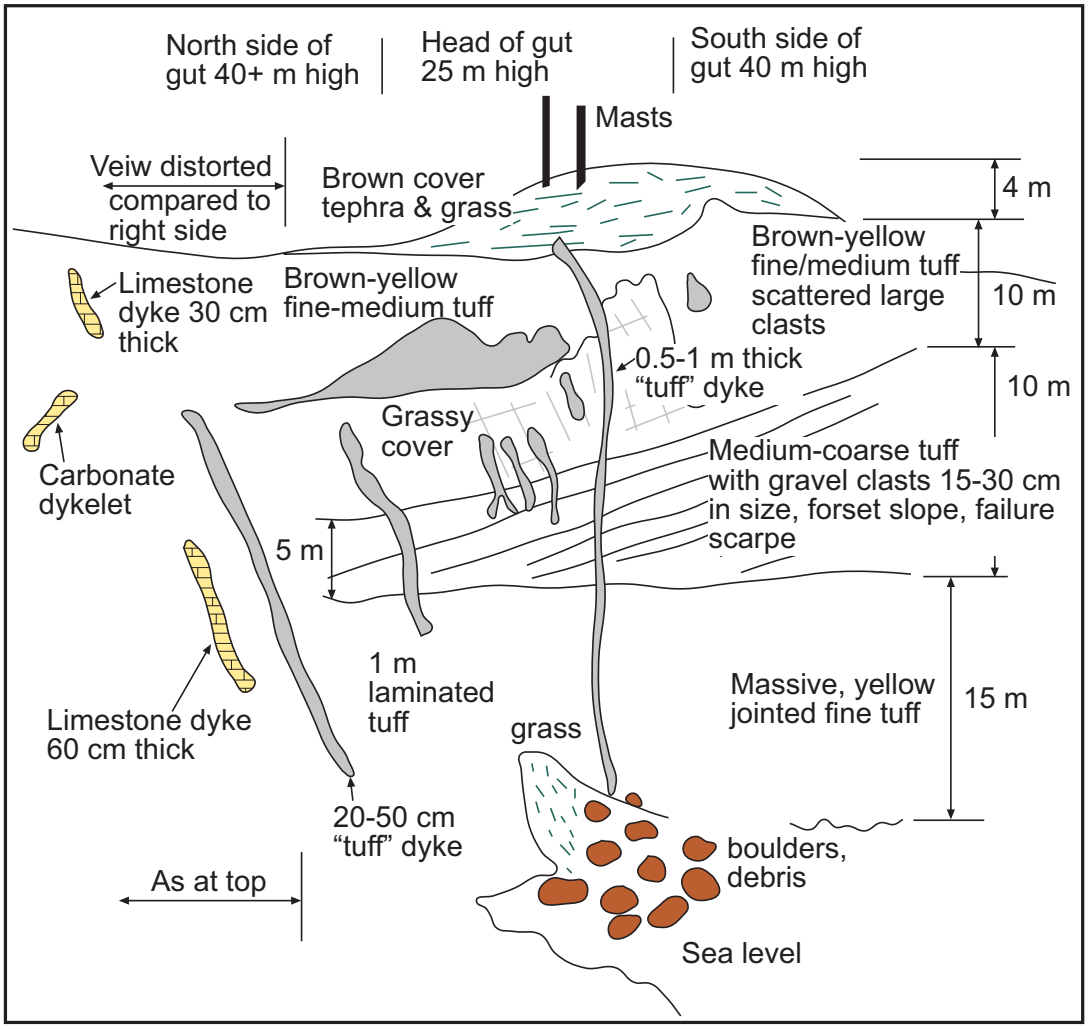

Figure 5.19A: Schematic diagram adapted from a field sketch of limestone and basaltic dykes at the *below the twin masts* locality.

Figure 5.19B: The *below the twin masts* dyke locality showing the numerous basaltic (indicated by the white dashed lines) dyke occurrences and the carbonate dyke (indicated by the red dashed line) in the foreground. Refer to the text for a description of the *locality 27* limestone dyke occurrence. The *below the twin masts* locality itself (**E**) is approximately 10 m south of limestone dyke occurrence *U* in the *big bluff locality*, representing the Red Bluff volcanic mound summit. The blue arrows on the southern wall are pointing out some of the larger *stringer* calcite veins present in vast numbers within the Red Bluff Tuff.

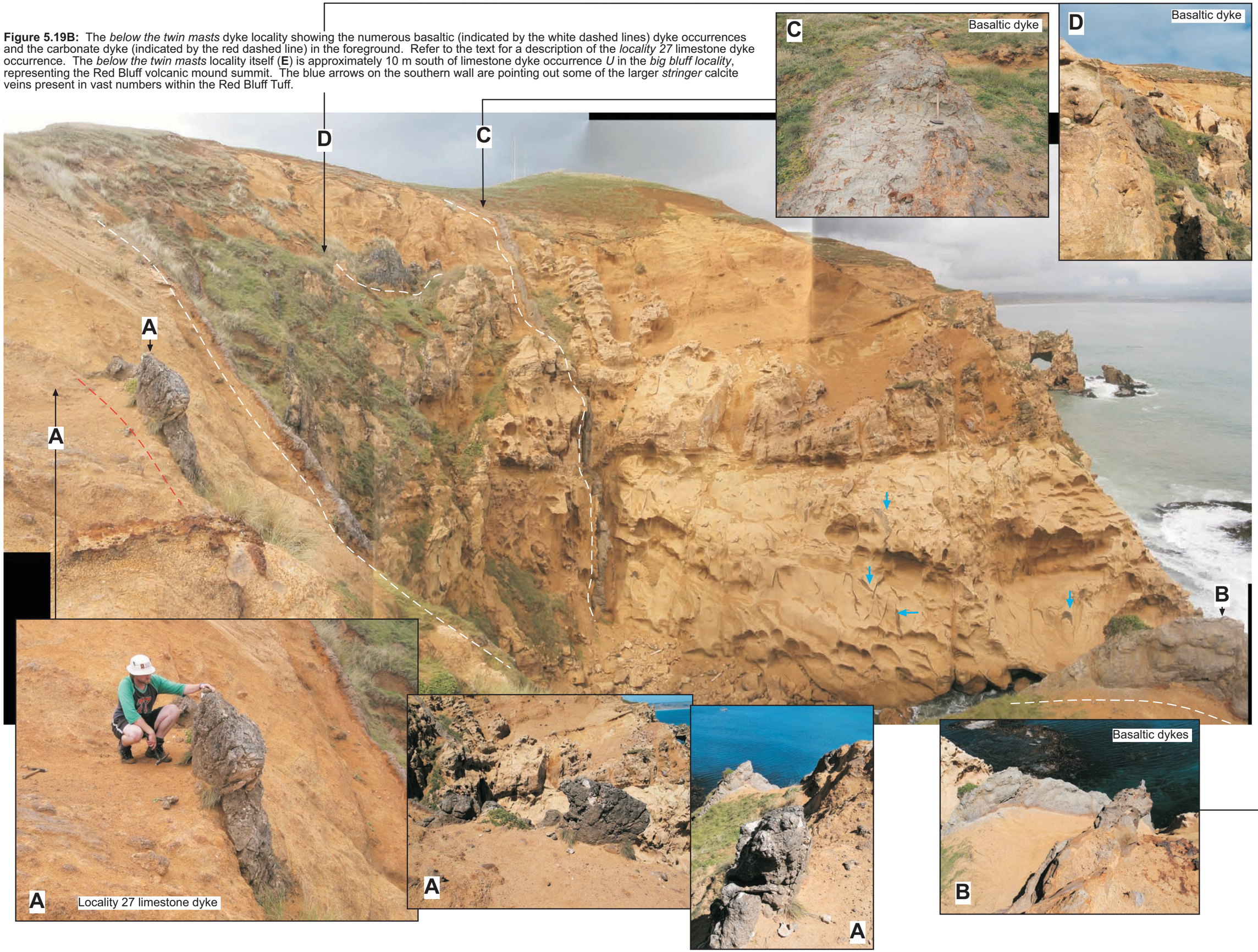

South Red Bluff dykes

The *south Red Bluff* locality describes the area south of the *below the twin masts* locality, as far as approximately by the southern end of Red Bluff coastal section. This area has not been covered in any detail here, but some general observations about dyke occurrences are made. Large type *3* (>0.5 m) dykes are not known to occur in this area although there are a number of type *2* (20 cm - 0.5 m) occurrences and countless numbers of carbonate stringers and calcite veins (Fig. 5.20).

Two type *2* dykes of particular interest were observed near the southern end of the Red Bluff area (Lat 43.90086, Long 176.54343) and demonstrate a relationship between what are interpreted as either intrusions or fills of tuff, with subsequent injection or filling of carbonate material (Fig. 5.21). It is unclear to the author whether these features that occur in much of the Red Bluff Tuff are water escape structures or represent forceful injection of volcaniclastic material. What is clear is that the volcanics display lamination and vague sorting within the features and carbonate deposition sometimes occurs within these features and is aligned centrally in the middle of the structure. The thickness of the carbonate material varies from 10-30 cm over a 3 m distance and is intermittent, being absent near the top of the structure, while tapering away to nothing at the bottom. The volcaniclastic structures in which the carbonate is located are 40-50 cm thick and generally taper into nothing some 1-3 m below the bottom of the carbonate material. These features are a distance of about 10 m apart, striking 158-178° with a sub-vertical dip of about 70°.

Another interesting observation made in the *south Red Bluff* area relates to the intrusion of basaltic dykes at the Red Bluff locality. The relationship between the basaltic dykes and sedimentary dykes could not be observed, however a small block of basalt noted towards the southern end of Red Bluff may give some indication (Fig. 5.22). This block of basalt is transected by a stringer of carbonate material. This may well be a unique and solitary occurrence, but it does hint that basalt was emplaced before the sedimentary stringer. Also, although much the basalt present in the Red Bluff area is now reasonably soft and highly weathered, it must have remained indurated and hard for a considerable amount of time following magma

intrusion and therefore must either have been fractured or forcibly intruded to allow emplacement of the carbonate material.

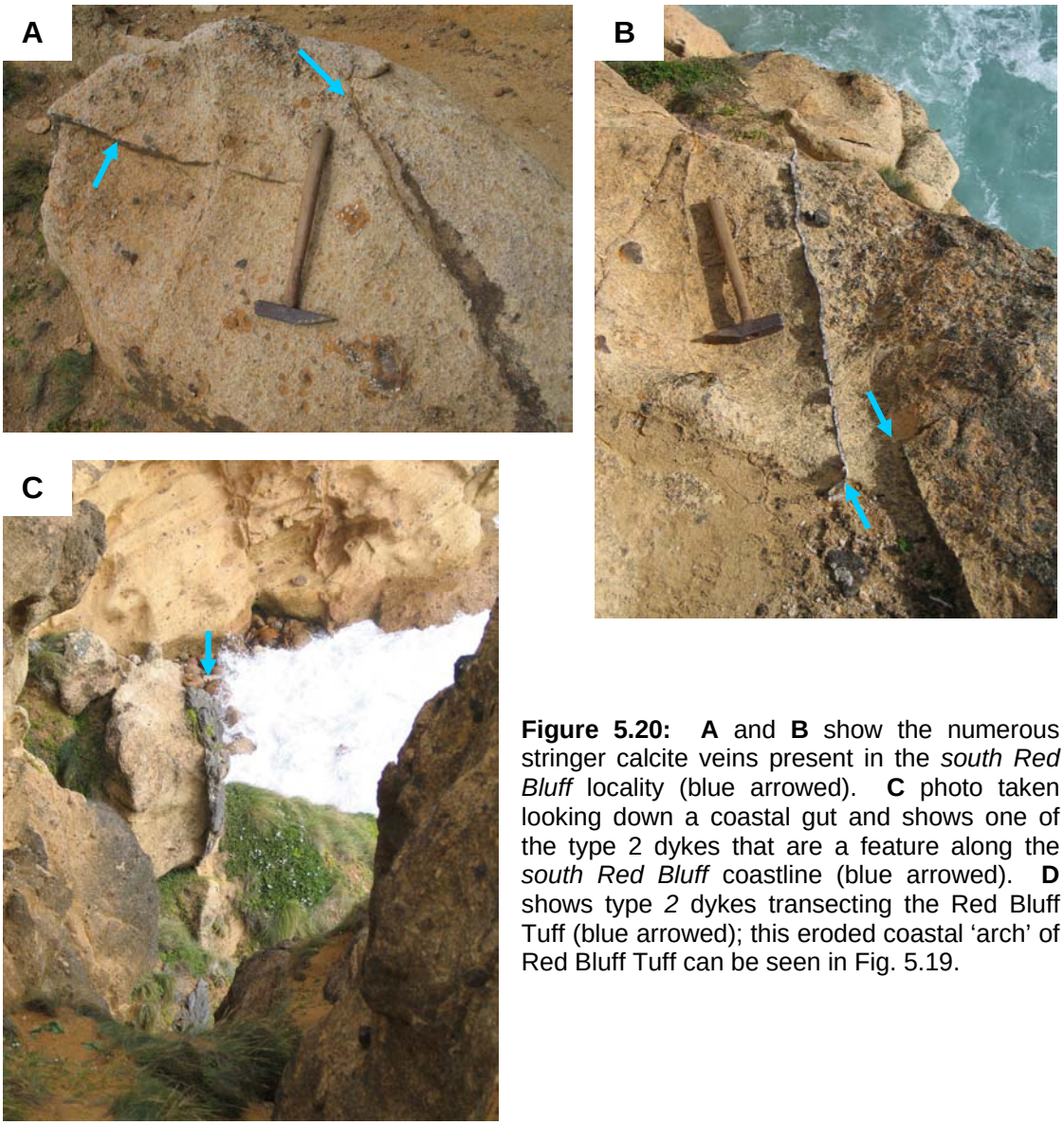

Figure 5.20: **A** and **B** show the numerous stringer calcite veins present in the *south Red Bluff* locality (blue arrowed). **C** photo taken looking down a coastal gut and shows one of the type 2 dykes that are a feature along the *south Red Bluff* coastline (blue arrowed). **D** shows type *2* dykes transecting the Red Bluff Tuff (blue arrowed); this eroded coastal 'arch' of Red Bluff Tuff can be seen in Fig. 5.19.

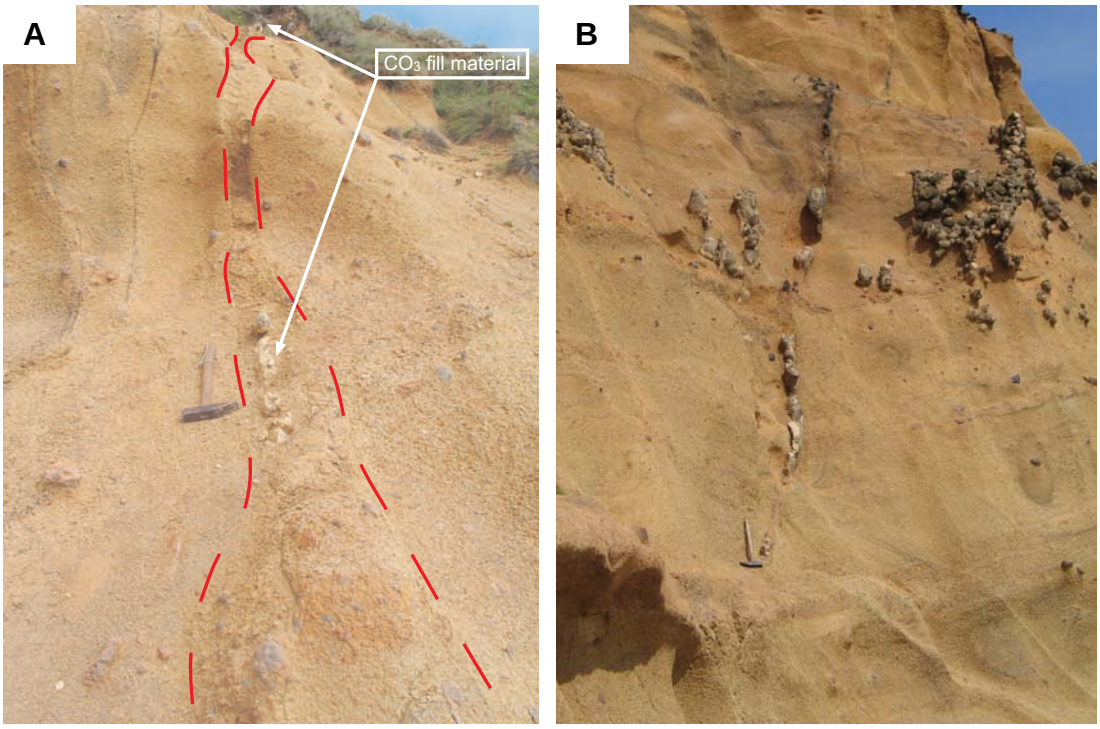

Figure 5.21: **A** and **B** show possible water escape structures within the Red Bluff Tuff that have been observed to also contain carbonate infills. These features are observed at other Red Bluff localities but were not as readily accessible.

Figure 5.22: A highly weathered block of basalt observed near the southern end of the *south Red Bluff* locality. Here the basalt has been transected by a stringer of carbonate material. The blocks occurrence raises an interesting hypothesis on the relationship between the basaltic and sedimentary dykes in the Red Bluff area, the latter possibly occurring after the former.

5.2.2 Red Bluff dyke petrography

Petrographic analysis of 24 dyke samples involving 67 thin sections and 46 petrographic descriptions has been conducted for sedimentary dykes in the Red Bluff area. The analysis is similar to that conducted on the limestone occurrences with both qualitative and semi-quantitive analysis of skeletal assemblages, siliciclastic content and interparticle material. However, the descriptions differ in that a single slide or slides that represent the width of a single dyke may contain multiple fill lithologies, which results in multiple descriptions for the slide(s). The purpose of thin section analysis is to define the common fill lithologies for the Red Bluff sedimentary dykes, determine the processes involved in the formation of the dykes, the source of filling material and any diagenetic features. Thin section analysis has been conducted on sedimentary dykes that are believed to represent adequately the processes of dyke formation and the range of dyke types present within the area. The analysis of these dykes has necessitated the use of fill type numbers or epithets which are of only specific relevance to the sedimentary dyke being discussed. Where the same fill number or epithet is used in a separate sedimentary dyke it is not intended to imply that these fills share a common lithology.

North Red Bluff dykes

Dyke A

Petrographic analysis has revealed at least three separate fill lithologies within dyke *A* (Fig. 5.23 & Appendix C Table C1, Figs C1, C2). It was observed that dyke *A* formed an asymmetrical fill sequence, with different lithologies occurring across the thickness of the dyke (Fig. 5.23A).

Within dyke *A*, fill type *1* which occurs along the left-hand edge of the dyke margin is noted as being similar in appearance and lithology to the basal left-hand side dyke fill from the main dyke *M* (CH05-28C) with a dominance of bryozoans (Fig. 5.30A & B & Appendix C Table C5, Fig. C18). The central micritic fill *2* shows strong vertical laminations and may be interpreted as resulting from grain sorting which would indicate motion of sediment and thereby an injection process of emplacement (Fig. 5.23A). Flow-like structures can also be observed on the right-hand side of the dyke in the breccia limestone fill *3*, where a laminated flow structure can be seen to have limestone lithoclast inclusions within a central micritic unit (Fig. 5.23C & D). These brecciated limestone inclusions can clearly be seen to contain the large benthic foraminifera *Asterocyclina* and are therefore probably clasts of Matanginui Limestone. The same foraminifera are also noted in other lithoclasts within fill type *3* of dyke *A* (Fig. 5.23E & F).

Figure 5.23: Photomicrographs of dyke *A* from the *north Red Bluff* locality. **A** (CH06-RB02A, PPL) general shot of the fill lithologies present in dyke *A*. The left-hand side of the image show fill type *1*, a bioclastic limestone fill which is one of the common fill facies in the Red Bluff area. In the centre of the image is a laminated micrite fill (fill type *2*), and to the right-hand side a brecciated limestone fill with volcaniclastic inclusions and interparticle micrite. **B** (CH06-RB02A, PPL) close-up of fill type *1* showing a bryozoan dominated limestone fill with benthic foraminifera (upper right-hand side) and echinoderm (upper left-hand side) grains and inter- and intraparticle micrite and spar. **C** (CH06-RB02A, PPL) limestone brecciated fill (type *3*) with large lithoclasts of limestone with palagonitic volcaniclastic inclusion in the lower half of the image, and a central image brecciated flow structure with laminated micrite walls. A large palagonitic volcanic clast in the upper left-hand corner sits within the homogenous micrite interparticle material. **D** (CH06-RB02A, PPL) close-up of the central brecciated flow structure from the previous slide in C showing broken fragments of the large benthic foraminifera *Asterocyclina* that are inclusions within limestone lithoclasts. **E** (CH06-RB02A, PPL) fill type *3* from the right-hand side of the dyke showing two whole *Asterocyclina* within homogenous micrite interparticle material surrounded by limestone lithoclasts and palagonitic volcaniclastics. **F** (CH06-RB02A, PPL) close-up of the *Asterocyclina* in the previous shot E showing they are likely part of a limestone lithoclast that is presumably Matanginui Limestone based on the presence of these benthic foraminifera.

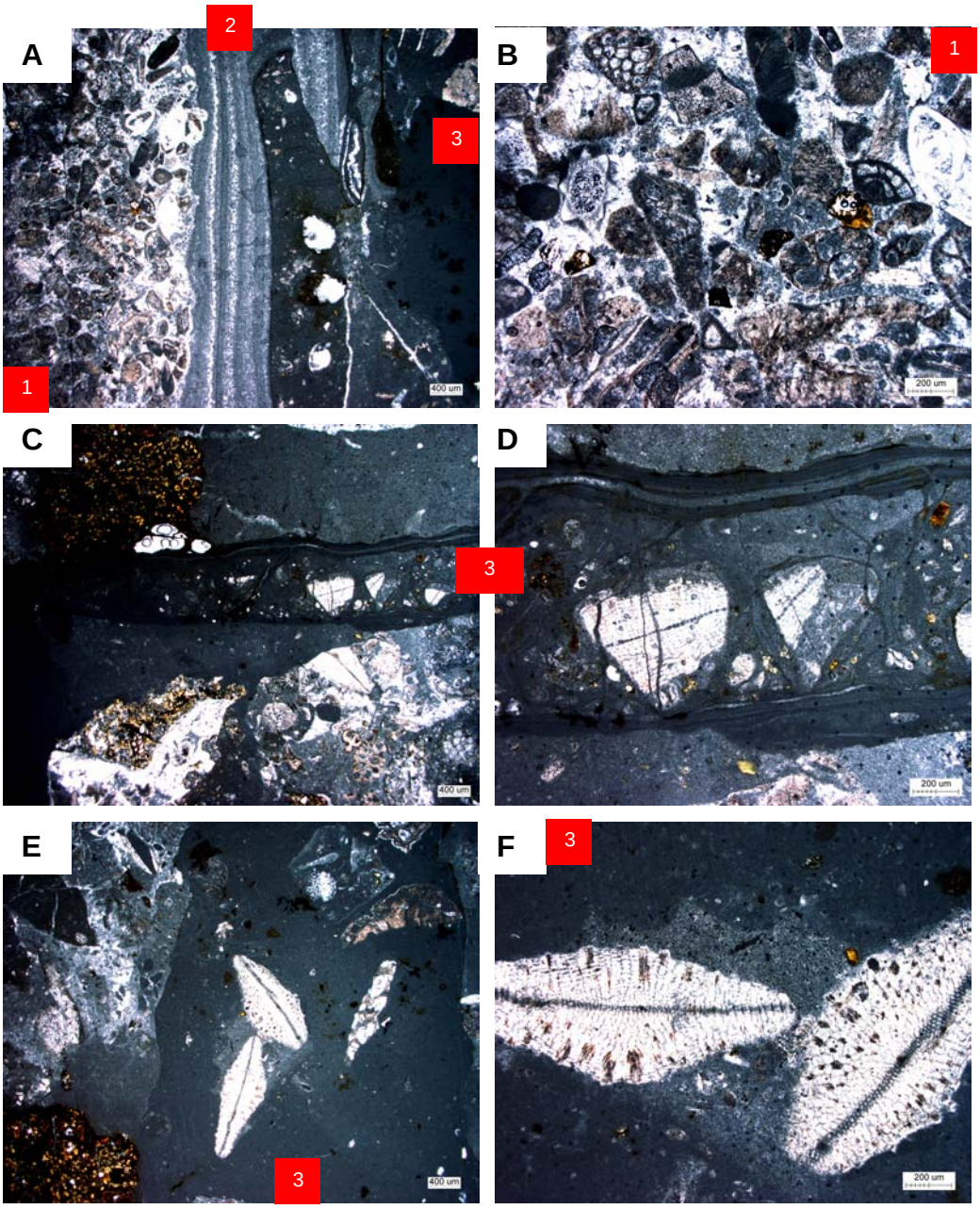
A
2
3
1
400 um
B
1
200 um
C
3
400 um
D
200 um
E
3
400 um
F
3
200 um

Dyke B

Dyke *B* is another asymmetrical fill sequence dyke from the northernmost *north Red Bluff locality*. Petrographic analysis shows that two distinct fill types are present, a limestone fill ('lst fill') on the left-hand side of the dyke and a tentatively named volcanic fill ('volc fill') on the right-hand side of the dyke (Fig. 5.24 & Appendix C Table C1, Figs C3 & C4).

The limestone has an abundance of bryozoan skeletal fragments and volcanic clasts within an interparticle microbioclastic micrite with noted inclusions of the large benthic foraminifera *Asterocyclina* indicating a possible Matanginui Limestone source origin (Fig. 5.24A, B, E & F). The tentatively named volcanic fill is so described because on first observation the fill appears to be related to possible igneous processes with volcanic clast inclusions and red iron colouration, with brecciated inclusions of its own lithology also displaying this staining. However, on closer analysis it is believed that this fill is probably a heavily iron stained micrite, as apart from the difference in colouration the material does resemble micrite. The 'volc fill' material also shows laminations of volcaniclastic inclusions parallel to the orientation of the dyke, indicating a momentum of sediment, and it also displays some stylolitic development (Fig. 5.24 C & D). The typical grey colouration of the micrite can be seen along a thin seam adjacent to a pyrite fracture infill which runs parallel to the irregular contact surface between the 'lst' and 'volc' fills (Fig. 5.24C).

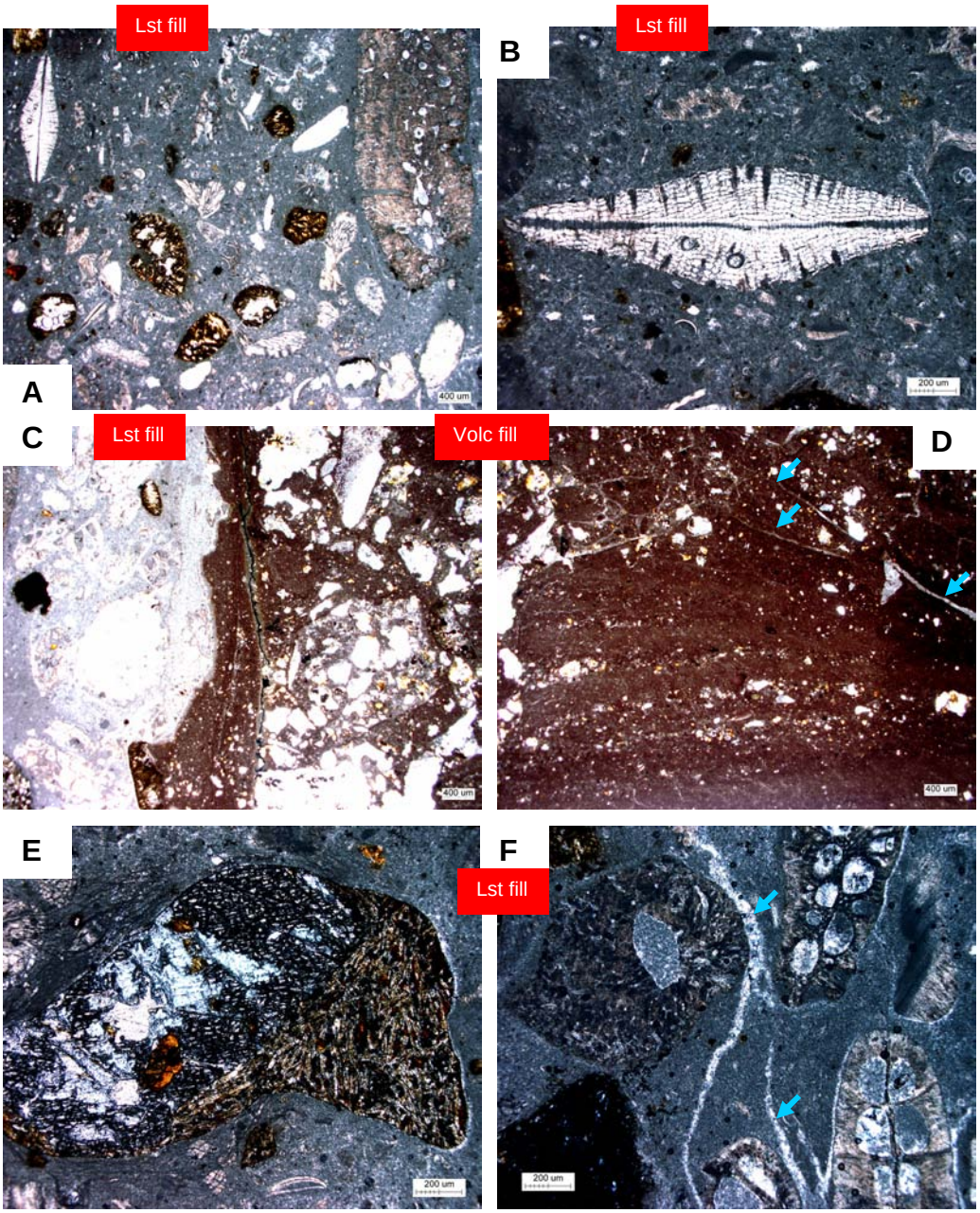

Figure 5.24: Photomicrographs of dyke *B* from the *north Red Bluff* locality. **A** (CH06-RB02B, PPL) a general shot of the limestone fill ('lst fill') within dyke *B* showing abundant bryozoan fragments. Note the large bryozoan along the upper right-hand side, scattered volcanic fragments and the large benthic foraminifera *Asterocyclina* in the upper left-hand corner. **B** (CH06-RB02B, PPL) close-up shot of the large benthic foraminifera *Asterocyclina* displaying surface micro-borings infilled with the surrounding bioclastic micrite. **C** (CH06-RB02B, PPL) contrast between the limestone fill and volcanic fill ('volc fill'). The contact between the two fills is very sharp. **D** (CH06-RB02B, PPL) shot of the 'volcanic fill' showing parallel sorting of volcaniclastic fragments aligned horizontally across the lower half of the image and stylolite formation in the upper half of the image (blue arrowed). **E** (CH06-RB02B, PPL) close-up of an unusual volcanic clast within the limestone fill, in which the left-hand side of the clast comprises a polycrystalline textured mineral with palagonitic clast inclusions, and the right-hand side displays a trachytic texture. **F** (CH06-RB02B, PPL) close-up of the limestone fill bryozoans with intraparticle micrite fills and some development of radiating spar cements on the left-hand side of the image. Stylolite formation occurs through the centre of the image (blue arrowed).

Dyke H

Petrographic analysis of dyke *H* revealed four distinct bioclastic fill lithologies that formed an asymmetrical sequence across the thickness of the dyke (Fig. 5.25 & Appendix C Table C2, Figs C5, C6, C7 & C8).

On the left-hand side of dyke *H*, fill type *1* for this dyke shows a dominance of bryozoan bioclasts with significant amounts of echinoderm and benthic foraminiferal material (Fig. 5.25A & D). To the right of fill type *1*, fill type *2* appears to be of a very similar lithology, although analysis indicates that bryozoans are the only significant bioclast and that interparticle material is predominantly micrite rather than spar cement as in fill type *1* (Fig. 5.25A, D & E, & Appendix C Figs C5 & C6).

A central fill unit between fill type *2* on the left-hand side of the dyke and fill type *3* on the right-hand side of the dyke may represent an original primary fill (Fig. 5.25B). Although bioclastic and volcaniclastic fragments are present within this central fill there is obvious vertical micrite laminations along its left margin (Fig. 5.25E). These laminations can clearly be seen to be truncated by fill type *2* indicating that this central fill was present before emplacement of fill type *2* and that the central fill emplacement may have involved an injection process.

On the right-hand side of the dyke adjacent to the central fill can be seen the red stained fill type *3* which is very similar in bioclastic content to fill type *1* from this dyke, namely a predominance of bryozoan, echinoderm and benthic foraminiferal grains (Fig. 5.25B, C & F). There are also notable inclusions of palagonitic volcanic fragments and limestone lithoclast inclusions. The inclusion of the large benthic foraminifera *Asterocyclina* again hints at a Matanginui Limestone source. The red staining seems to occur primarily around the edges of bioclasts and volcaniclastics, as well as affecting the intraparticle fill (Fig. 5.25F).

The far right-hand side of the dyke shows a predominantly micritic fill, fill type *4* with some bryozoan and benthic foraminiferal bioclasts but also lithoclast inclusions and some stylolite development, with pyrite inside fill fractures (Fig. 5.25C & G).

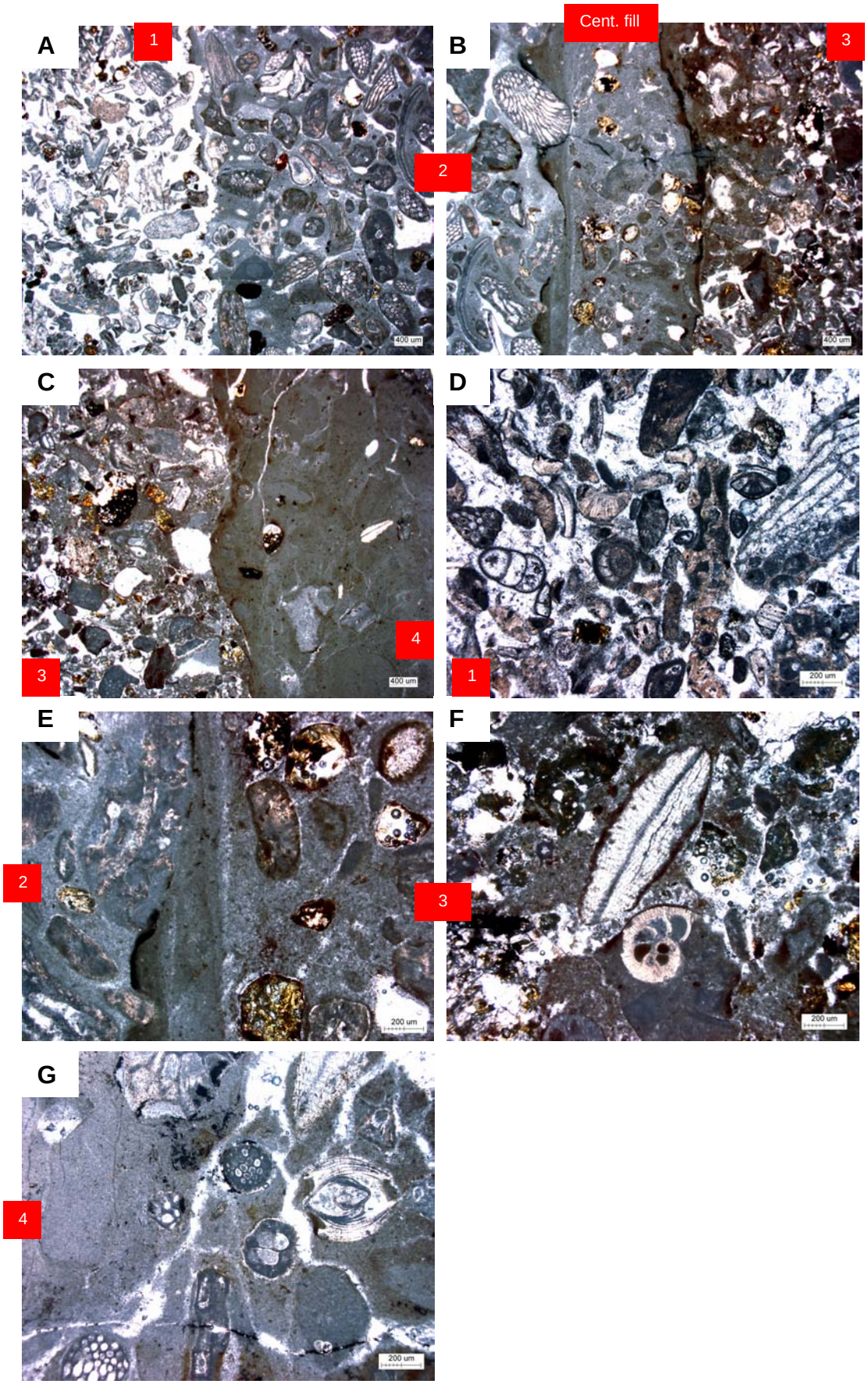
A
1
2
400 um
B
Cent. fill
3
400 um
C
4
3
400 um
D
1
200 um
E
2
200 um
F
3
200 um
G
4
200 um

Figure 5.25: Photomicrographs of dyke *H* from the *north Red Bluff* locality. **A** (CH06-RB02H, PPL) left-hand side of dyke *H* showing fill type *1* on the left-hand side of the image and fill type *2* on the right-hand side of the image. **B** (CH06-RB02H, PPL) a shot towards the centre of dyke *H* showing fill type *2* on the left-hand side of the image with an adjacent central fill displaying a laminated left-hand edge running through the centre of the image with fill type *3* on the right-hand side of the image. **C** (CH06-RB02H, PPL) a shot from the right-hand side of the dyke showing fill type *3* on the left-hand side of the image and fill type *4* on the right-hand side of the image. **D** (CH06-RB02H, PPL) close-up shot of fill type *1*, a bioclastic limestone with interparticle spar cement showing a dominance of bryozoans with some intraparticle micrite. **E** (CH06-RB02H, PPL) close-up of the secondary type *2* fill showing that the laminated micrite edge is in fact truncated by bioclasts within the main type *2* fill on the left-hand side of the image. This may indicate that the main bryozoan dominated type *2* fill is in fact a secondary fill. Note also the dominance of interparticle micrite within this fill and the precipitated pyrite growth along the laminated edge. The central secondary fill showing a mix of bioclastic and palagonitic volcaniclastics with red staining around clast rims, with interparticle micrite showing some stylolite development. **F** (CH06-RB02H, PPL) close-up shot of fill type *3*, a mixed bioclastic and palagonitic volcaniclastic lithology, with some interparticle micrite and micritic lithoclasts containing the large benthic foraminifera, *Asterocyclina*. **G** (CH06-RB02H, PPL) close-up shot of the right-hand dyke side fill *4* showing an abundance of interparticle micrite with some stylolite development and some infills of precipitated pyrite, which also occurs around bryozoan bioclasts. Note the benthic foraminifera to the central right of the image.

Dyke I

Dyke *I* is very close to dyke *H* and petrographic analysis reveals both common and contrasting fill lithologies, with four bioclastic fills and two micrite fills identified from this asymmetrical sequenced dyke (Fig. 5.26 & Appendix C Table C3, Figs C9, C10, C11 & C12).

From the far left-hand side of the dyke, fill type *5* shows a mixed bryozoan and volcaniclastic dominated fill with interparticle spar cement (Fig. 5.26A & C). This fill type was not seen in dyke *H* and is unusual in that both bioclasts and volcanic fragments appear to have micrite fringes with intraparticle micrite present within the bryozoan zoaria and little grain to grain contact. This may possibly indicate that these fragments are more likely lithoclasts, suggesting a possible catastrophic emplacement mechanism.

Adjacent to fill type *5* on the left-hand side of the dyke is a micritic fill *6*, with vertically oriented stylolite development (Fig. 5.26A). This micrite fill separates fill type *5* from fill type *7* to the right. Fill type *7* shows a dominance of bryozoan and volcanic fragments, similar in lithology to fill *5* but with interparticle micrite as well as spar cement (Fig. 5.26A & D). This fill would appear to be similar also to fill *3* from dyke *H* with red stained micrite fringing bioclasts and volcanic fragments (Fig. 5.25F).

On the right-hand side of dyke *I*, to the right of fill type *7*, is bioclastic fill *8*, with the two fills again being separated by a thin micrite fill of the same lithology as micrite fill *6* from this dyke. The bioclastic fill type *8* shows a dominance of bryozoan skeletal fragments with a significant amount of benthic foraminifera and bivalves (Fig. 5.26B & E). Interparticle material within fill type *8* is predominantly micrite although the micrite appears fractured in places and here the resultant space is infilled with spar cement. The fill type *8* in dyke *I* resembles the fill within dyke *P* (Fig. 5.27B), fill sample CH05-28D from the right-hand side of dyke *M* (Fig. 5.30H) and the sample CH06-RB02U2 from the top of the brecciated dyke from the *big bluff* locality (Fig. 5.33B).

From the far right-hand side of dyke *I* is another bioclastic fill *9* with interparticle micrite and a dominance of bryozoans with significant numbers of the benthic foraminifera *Asterocyclina,* again indicating that Matanginui Limestone is the probable source material for some of the dyke fill lithologies. This fill type *9* closely resembles the *Asterocyclina* limestone fill in dyke *B*, but

all other *Asterocyclina* inclusion fills are considered to be sufficiently lithologically dissimilar to be able to draw any relationship conclusions (Fig. 5.24A & B).

Figure 5.26: Photomicrographs taken from two separate thin sections covering the width of dyke *I* from the *north Red Bluff* locality. **A** (CH06-RB02I, PPL) a shot from the thin section covering the left-hand side of the dyke showing the outer left-hand dyke fill *5* on the left-hand side of the image, with the micrite fill type *6* to the right of it and fill type *7* on the right-hand side of the image. **B** (CH06-RB02I, PPL) a shot from the thin section covering the right-hand side of the dyke showing the fill type *8* on the left-hand side of the image and fill type *9* on the right-hand side of the image. **C** (CH06-RB02I, PPL) close-up shot of fill type *5* showing highly abraded skeletal fragments and rounded palagonitic volcanic clasts with interparticle spar cement. Note the echinoderm bioclast in the upper right-hand corner of the image. **D** (CH06-RB02I, PPL) is a close up of fill type *7*, which is similar in composition to *5* but shows interparticle micrite as well as spar cement, with both bioclastic and siliciclastic fragments rimmed with the red stained material seen in other dykes. **E** (CH06-RB02I, PPL) close-up of fill type *8* from the right-hand side of the dyke showing inter- and intraparticle micrite surrounding and within bryozoan fragments. Spar cements can be seen to be filling fractures and pore spaces within the micrite. **F** (CH06-RB02I, PPL) close-up of the far right dyke fill *9* showing limestone lithoclasts with interparticle clotted micrite. Lithoclasts within this fill type have bryozoan and benthic foraminifera (*Asterocyclina*) inclusions with some palagonitic volcaniclasts, indicating a possible Matanginui Limestone origin.

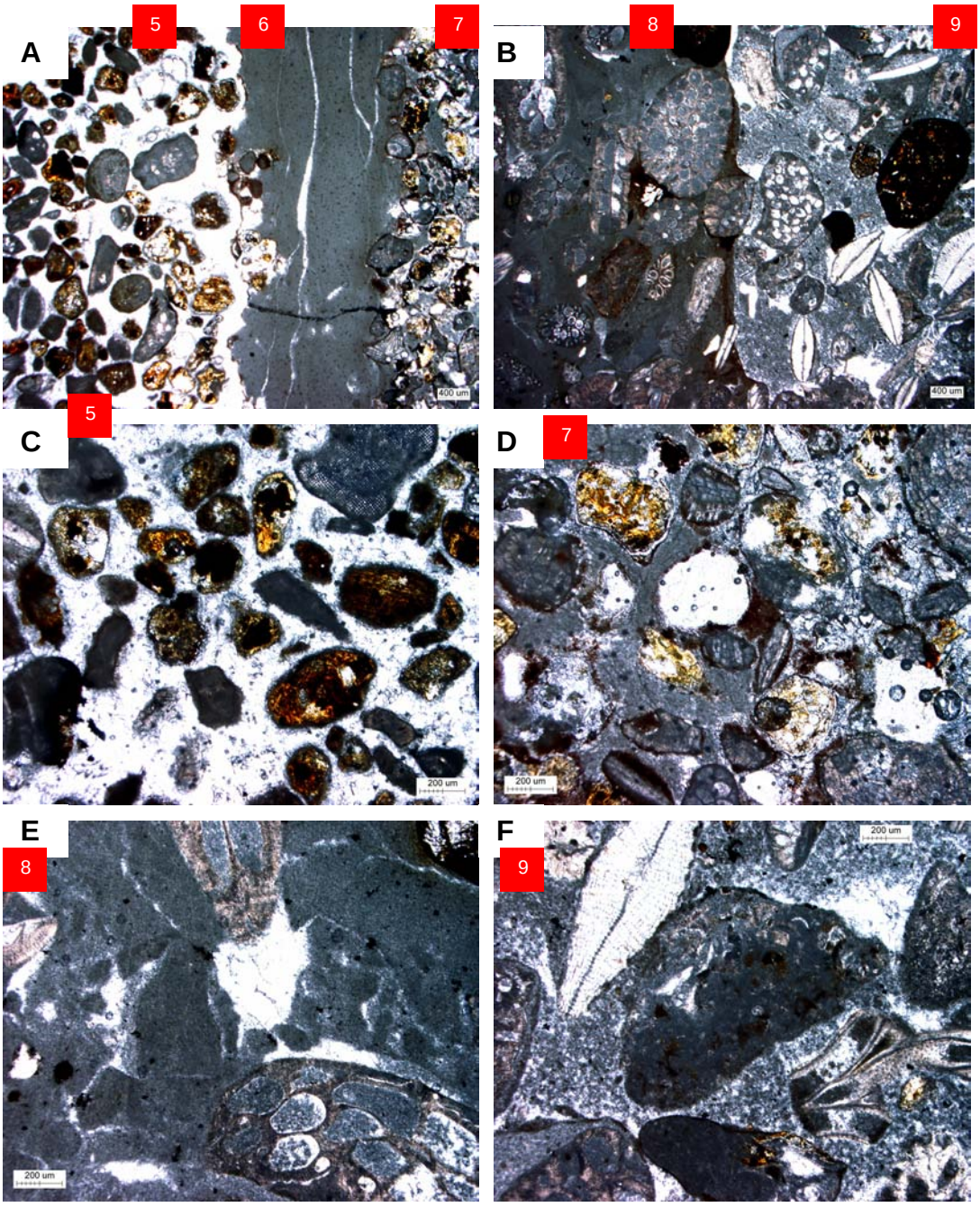
A
5
6
7
400 um
B
8
9
400 um
C
5
200 um
D
7
200 um
E
8
200 um
F
9
200 um

Dyke N and P

Dykes *N* and *P* are a dykelet and offshoot dyke (respectively) from the main dyke *M*. Petrographic analysis shows that dykelet *N* is a microbioclastic micrite with obvious planktic foraminiferal inclusions, with some micritic lithoclast inclusions and stylolite development (Fig. 5.27A & Appendix C Table C4, Fig. C13).

Dyke *P* shows abundant bryozoans which appear to be inclusions of micritic lithoclasts that have very little grain to grain contact (Fig. 5.27B & Appendix C Table C4, Fig. C14). The interparticle material is predominantly micrite and shows fracturing which has been infilled by spar cements.

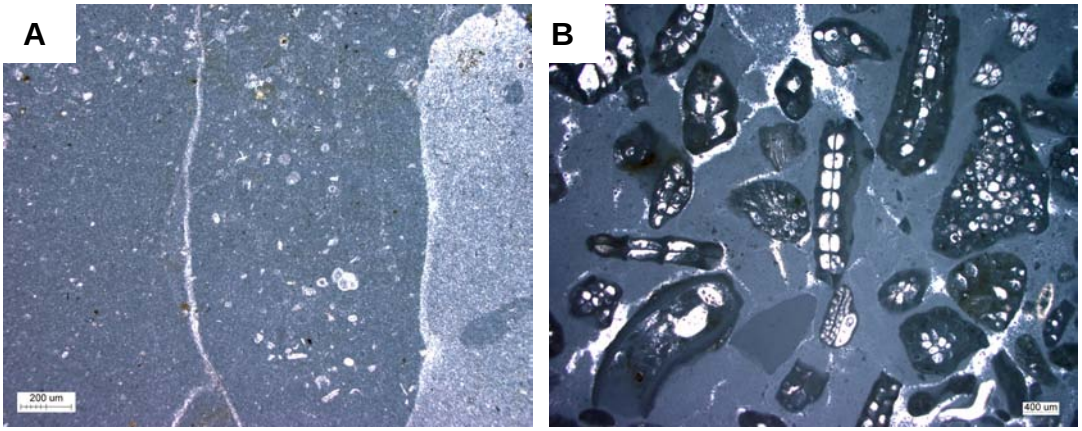

Figure 5.27: Photomicrographs of dykelet *N* (photo A) and offshoot dyke *P* (photo B) from the main dyke *M* at the *north Red Bluff* locality. **A** (CH05-28L, PPL) shows the fine grained micritic dykelet with inclusions of some planktic foraminifera and a brecciated micrite lithoclast (along the right-hand side of the image). Some stylolite development present. **B** (CH05-28K, PPL) shot from the offshoot dyke *P* with abundant bryozoan fragments, some of which are part of micritic lithoclasts. The interparticle micrite appears homogenous and stylolite development is possibly within fractures in the micrite.

Dyke M

Petrographic analysis of dyke *M* has identified at least eight fill types, although it is uncertain whether this represents all the fills present within this large dyke (Appendix C Table C5). It is therefore inconclusive if this dyke displays any symmetry within the sequences observed. Dyke *M* has also been analysed vertically, with sampling from a mid-section height of the dyke and at its exposed base (Fig. 5.28).

From the left-hand side of the mid-section the outermost type fill *1* shows a bioclastic fill dominated by planktic foraminifera with significant inclusions of bivalves, echinoderms and glauconite pellets in interparticle spar cement (Fig. 5.28A & B & Appendix C15). To the right of this outer fill from the dyke *M* mid-section is a contrasting bioclastic fill *2*, dominated by large bryozoan fragments supporting acicular fringing spar cements within interparticle micrite (Fig. 5.29A & C & Appendix C Fig. C16). Micrite also occurs in fill type *2* as an intraparticle fill. There is also a noticeable difference in interparticle micrite with darker micrite to the left of the dyke that has planktic foraminiferal bioclasts and fine palagonitic volcanic clasts, while interparticle micrite towards the right side of the dyke appears lighter and more homogenous, like precipitated micrite (Fig. 5.29C). Fill type *2* can also be seen in a mid-section sample collected in 2005 (Fig. 5.29D & Appendix C Fig. C17). Here this left-hand fill type *2* is separated from a central fill by a micritic flow structure showing orientation of fine skeletal fragments parallel to dyke walls, with alignment of grains along their long edges. The central fill here appears to be the same lithology as that from the basal section on the right-hand side (Figs 5.29D & 5.30H, Appendix C Figs C17 & C23 respectively).

The basal, left-hand side section shows an outermost fill with abraded bioclastics comprising abundant bryozoan fragments and some thin shelled bivalves and planktic foraminifera (Figs 5.28, 5.30A, B & C, & Appendix C Fig. C18). Micrite is the dominant interparticle material, with some development of spar cements. Intraparticle micrite is also present and radiating spar cement occurs within some bryozoan fragments. The fill from the left-hand centre of this basal section also shows a bryozoan dominated lithology with interparticle micrite which shows a gradual change from a coarser bioclastic micrite to a finer grained micrite fill towards the centre of the dyke (Figs 5.28, 5.30C & D, &

Appendix C Fig. C20). This gradual change (specifically of skeletal fragments) may indicate grain sorting on a larger scale than would be able to be identified in thin section.

The outer basal right-hand section fill *2* shows bryozoan and bivalve fragments with fringing micrite cements and interparticle spar cement (Figs 5.28, 5.30E & F, & Appendix C Fig. C22). The adjacent fill *1* towards the right of the dyke shows a marked contrast with interparticle micrite (Fig. 5.30E & G, & Appendix C Fig. C21). The outermost right-hand fill shows a bryozoan dominated lithology with interparticle micrite (Fig. 5.30H, & Appendix C Fig. C23). This fill is considered to be the same as the mid-section left-hand side fill (Fig. 5.29D & Appendix C Fig. C17) and also the same fill lithology as basal float blocks containing volcaniclastic cobbles (Fig. 5.30I & Appendix C Fig. C24 & C26). This basal float block is also interesting in that the volcanic clast inclusions contain lithoclasts of limestone (Appendix C Fig. C25), indicating a reworking of the volcanic material within the dyke.

Cathodoluminescence analysis was conducted on this dyke to emphasise any special diagenetic features. In general the fills within this dyke have dull or non-luminescent signatures, however luminescent signatures were observed in the central fill (Fig. 5.30J & K). Thin luminescent zones were observed around the edges of spar cements which appear to be infilling possible pore space or replacement features.

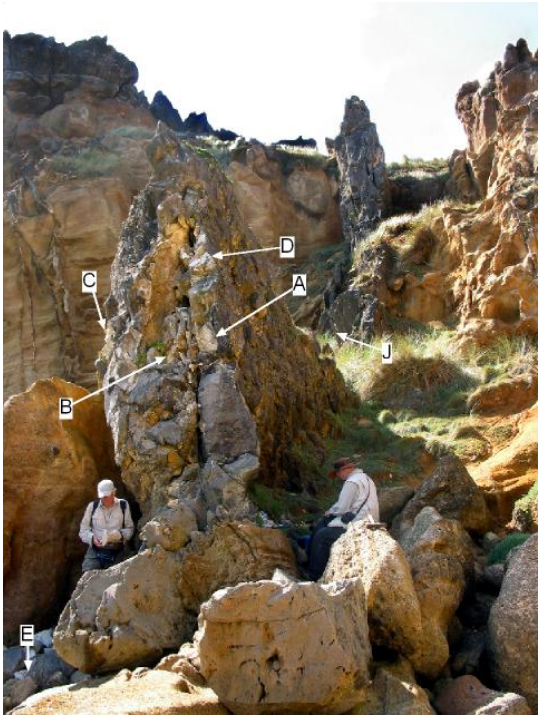

Figure 5.28: Left, the main dyke (*M*) occurrence at the *north Red Bluff* locality showing the position of samples collected in 2005 (CH05-28) with Noel James standing on the left-hand side of the dyke and Brian Jones to the right for scale. The letters denote the suffix letter used at the end of the sample number.

Figure 5.29: Photomicrographs of samples from the upper mid-section of dyke *M* from the *north Red Bluff* locality. **A** (CH06-RB02M, PPL) a shot from the far left-hand side of dyke *M* showing the outer fill type *1* on the left-hand side of the image and fill type *2* on the right-hand side of the image. **B** (CH06-RB02M, PPL) close-up shot of fill type *1* showing the abundance planktic foraminifera and glauconite pellets, and some larger benthic foraminifera and interparticle spar cement. **C** (CH06-RB02M, PPL) showing the fill type *2* with abundant large bryozoan fragments and inter- and intraparticle micrite. This fill type may constitute two separate fills with the interparticle micrite on the left-hand side of the image being darker with inclusions of planktic foraminifera and fine volcaniclastics, while the right-hand interparticle micrite appears lighter in colour and more homogenous. **D** (CH05-28J, PPL) thin section from a sample collected in 2005 near the same mid-section position in the dyke. In this image the fill type *2* runs horizontal across the top of the image and is separated from an inner fill (across the bottom half of the image) by a fine grained micritic flow structure.

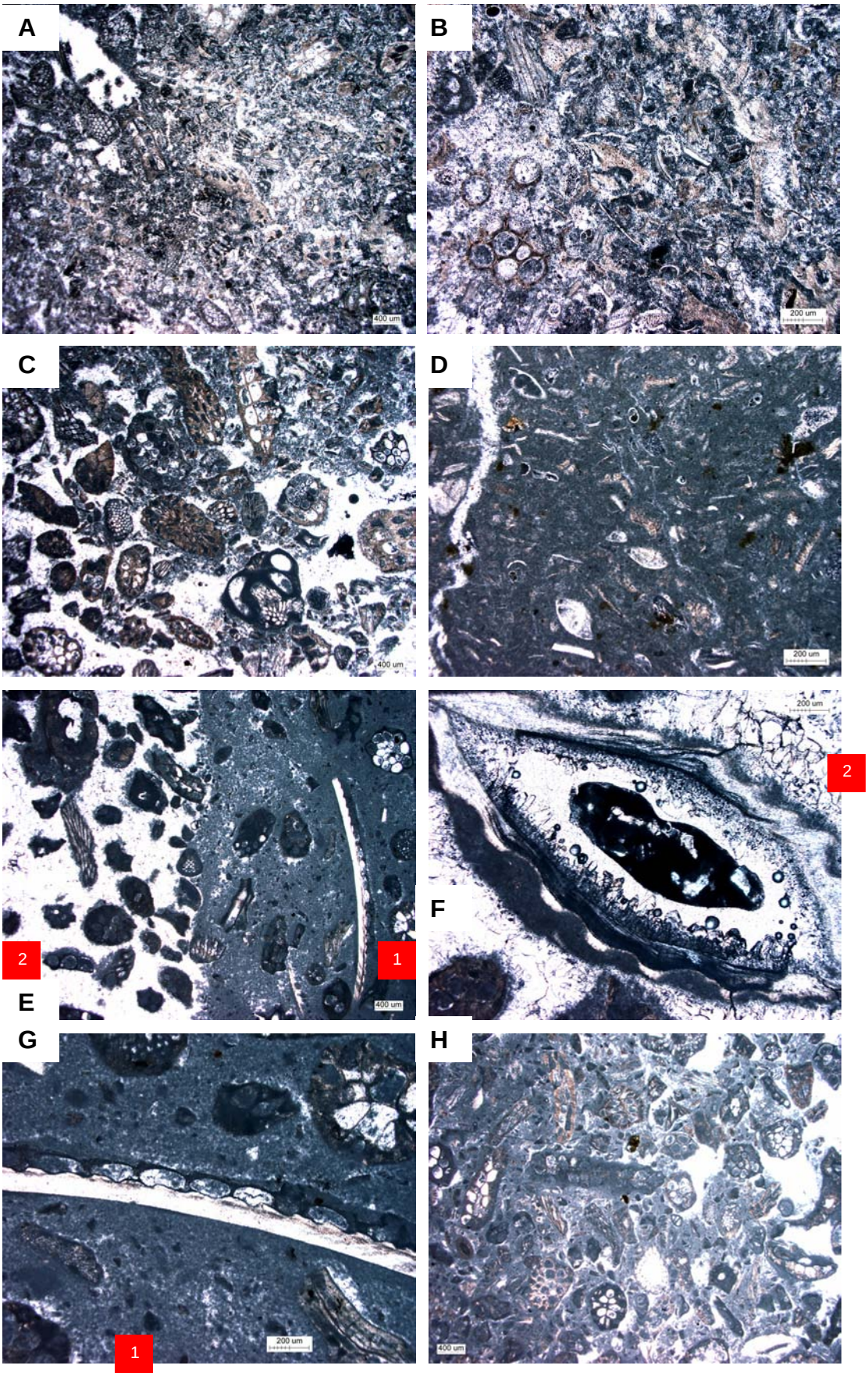
A
400 um
B
200 um
C
400 um
D
200 um
2
1
E
400 um
200 um
2
F
G
200 um
1
H
400 um

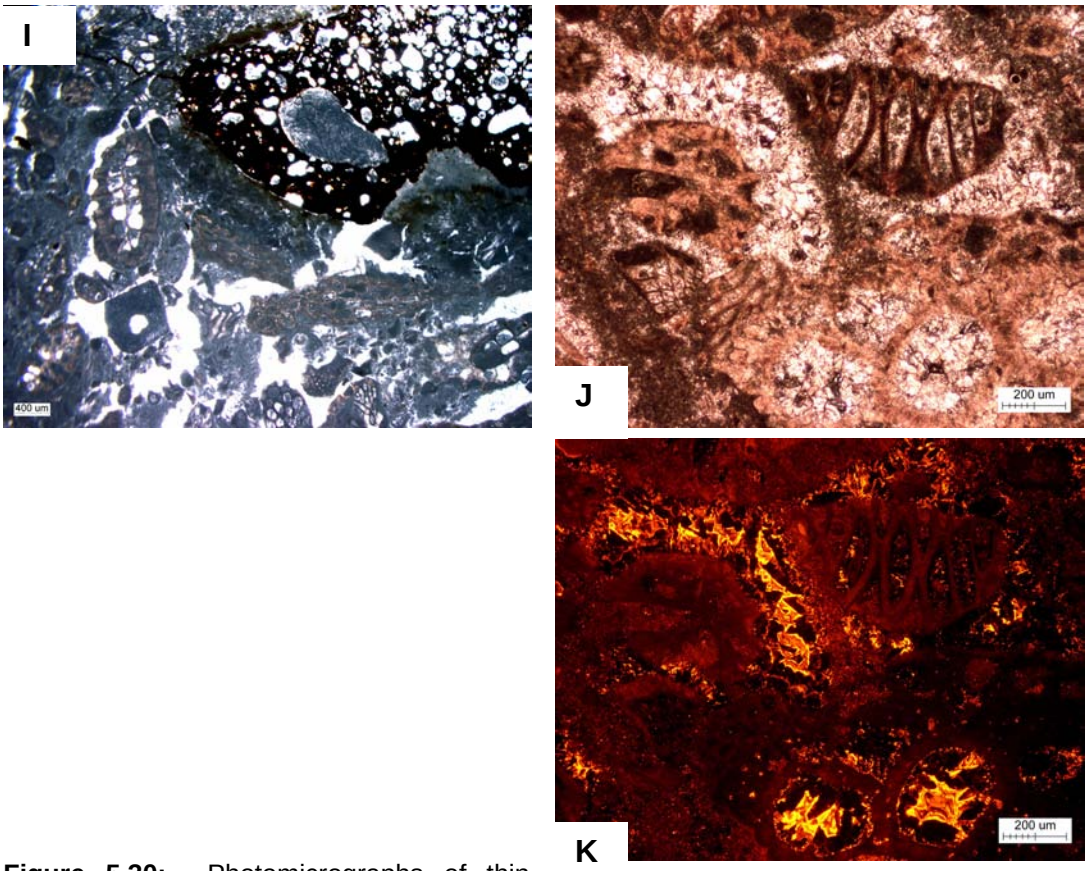

Figure 5.30: Photomicrographs of thin sections from samples collected in 2005 from the exposed base (at sea level) of dyke *M* at the *north Red Bluff* locality (refer Fig. 5.28 for sample positions). **A** (CH05-28C, PPL) a shot of the outer left-hand side of the dyke near the base of the dyke showing a highly abraded and fragmented bioclastic lithology. **B** (CH05-28C, PPL) close-up of the previous image showing skeletal fragments of bryozoans, thin shelled bivalves and rare planktic foraminifera with both inter- and intraparticle micrite present and development of some spar cement. **C** (CH05-28B, PPL) thin section from the centre of dyke *M* with the image orientated such that the bottom is toward the left-hand side of the dyke and the top toward the right. This shows the dominance of bryozoans within the central fill lithology, with interparticle spar cement being replaced by micrite from the left of the central section (bottom half of the image) towards the right central section (top of the image). **D** (CH05-28B, PPL) close-up of the central interparticle micrite fill (to the right of the previous sample) with fine grained bioclastic fragments and some planktic and benthic foraminifera. Note the stylolite or vein across the left-hand side of the image. **E** (CH05-28A, PPL) shot of thin section from the right-hand side of the dyke showing the contrast between the central fill *2* (left-hand side of the image) and an outer micritic fill *1* (right-hand side of the image). **F** (CH05-28A, PPL) close-up of the central spar fill *2* showing a whole small bivalve surrounded by a micrite rind, with intraparticle acicular spar development followed by granular spar cement. The central black object is a hole in the thin section with some broken spar fragments. **G** (CH05-28A, PPL) close-up of the outer micrite fill *1* on the right-hand side of the dyke showing scattered fragments of bryozoans with a bivalve (across the centre of the image) that has an encrusted bryozoan on its outer surface. **H** (CH05-28D, PPL) thin section shot from the far right-hand side of the dyke showing a similar lithology to the inner left-hand side (Fig. 5.28D) with abundant bryozoan fragments with interparticle micrite giving way to the spar cements toward the outer edge of the dyke on the right-hand side of the image. **I** (CH05-28E, PPL) thin section of a float block from the lower most right-hand side of the dyke that has large cobble sized volcaniclastic inclusions. The bioclastic fill is a similar lithology to the fills seen in this dyke (photomicrograph H). Interestingly the volcaniclastic cobbles show inclusions of limestone clasts indicating they formed from reworked volcaniclastic sediment. **J** and **K** (CH05-28B, PPL and CL) PPL and CL micrograph pair showing a thin zone of bright luminescence around the edge of some interparticle equant spar cements.

Dyke complex R

The dyke complex *R* shows that dykelets within the volcanic mound contain a central fill that is dominated by bryozoan skeletal fragments with also some bivalve and echinoderm material (Fig. 5.31A, B & C, & Appendix C Table C6, Fig. C27). Interparticle material comprises large equant spar cements and there is also some micrite present in the form of micritic envelope structures that are infilled with spar cement (Fig. 5.31C & D). This likely indicates dissolution of aragonitic skeletal fragments has occurred leaving porosity that was subsequently infilled with spar cement. These dykelets are symmetrical in that the outer left- and right-hand side show a homogenous micrite fill (Fig. 5.31A & B). These outer micrite fills show that there may be up to three episodes of micrite precipitation, with vertical laminations observed along the contact with the inner central bioclastic fill (Fig. 5.31A & B). The outer micrite fill is considered to represent the original dykelet fill material.

Cathodoluminescence has been conducted on this sample because the central fill has such large spar cement crystals. The analysis revealed that the majority of interparticle spar cements are dull or non-luminescent, although some thin zones of luminescence were observed on the edges of equant spar cements infilling some of the envelope structures (Fig. 5.31D & E).

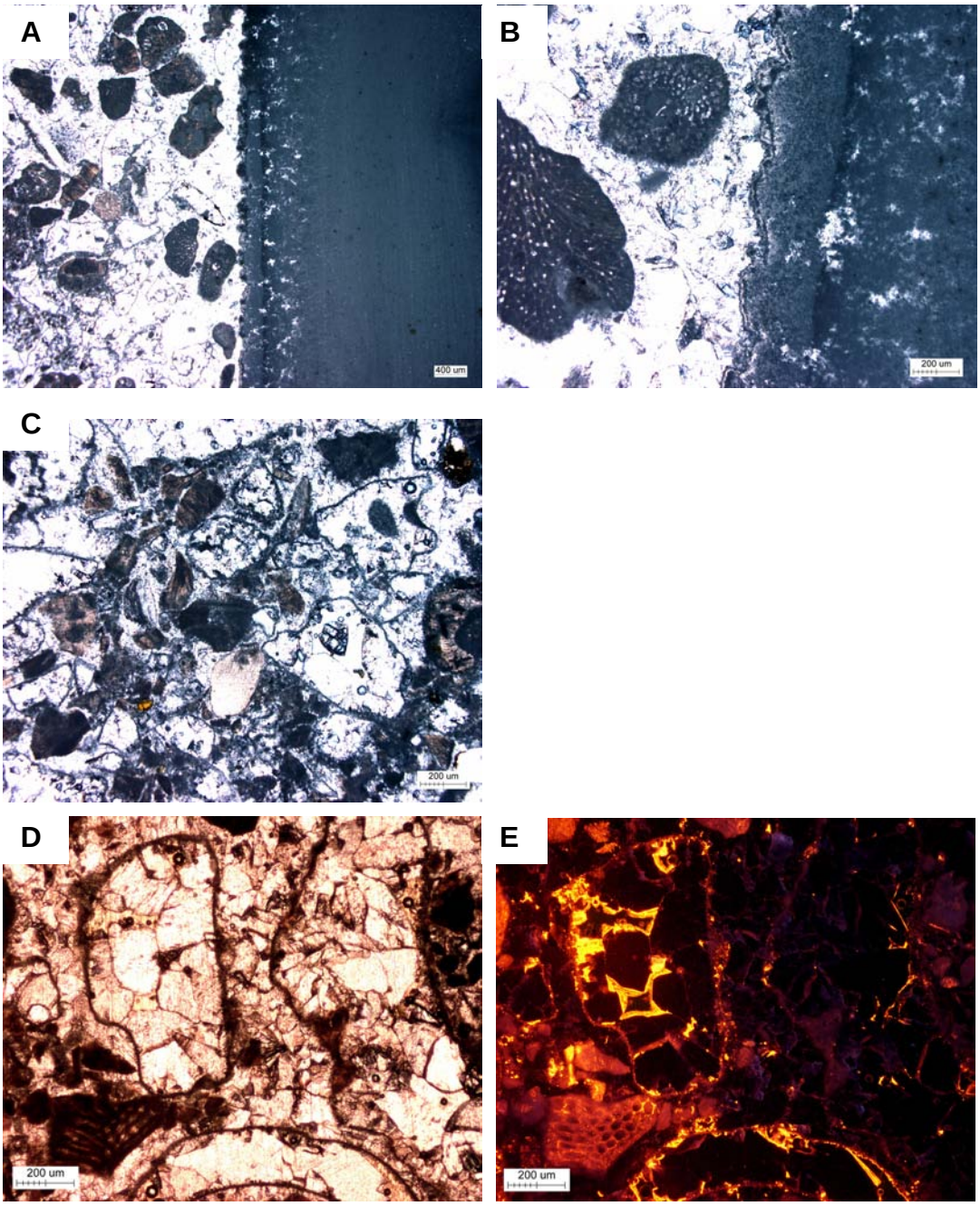

Figure 5.31: Photomicrographs of a dykelet typical of those seen in the dyke complex *R* at the *north Red Bluff* locality. **A** (CH05-28G, PPL) showing the left-hand side of the dykelet with a central bioclastic fill (fill type 'centre') fringed by an outer micrite fill (fill type 'edge') that is present along both dyke edges. **B** (CH05-28G, PPL) close-up of the contact between the two fills showing that the micrite displays a vague lamination with the outer thickest laminae appearing as a clotted micrite while the inner micrite laminae appears more homogenous and has a very thin sparry rind along the bioclastic contact edge. **C** (CH05-28G, PPL) close up of the 'centre' fill showing highly abraded skeletal fragments surrounded by equant spar cement with some patches of interparticle micrite and envelope structures with micrite rinds, indicating possible replacement of aragonitic elements. **D** and **E** (CH05-28G, PPL and CL) PPL and CL micrographs pair, showing that while the majority of inter- and intra-particle equant spar returned a dull luminescent signal, the equant spar thought to represent replacement of aragonitic fragments displays a thin zone of luminescence around their outer edges.

Big bluff dykes

Dyke T

Petrographic analysis of dyke *T* from the *big bluff* locality revealed another bryozoan dominated fill with interparticle spar cement (Fig. 5.32 & Appendix C Table C7 Fig. C28). This fill within dyke *T* is considered to be similar to the fill type seen in the main dyke *M* from the *north Red Bluff* locality (CH05-28A) with micrite rinds surrounding bioclasts (Fig. 5.30E & F). The fill within dyke *T* however shows a considerable amount of intraparticle micrite, which in many cases can be seen to be microbioclastic, as well as radiating spar cements, and there are also lithoclasts with inclusions of planktic foraminifera (Fig. 5.32B, C & D).

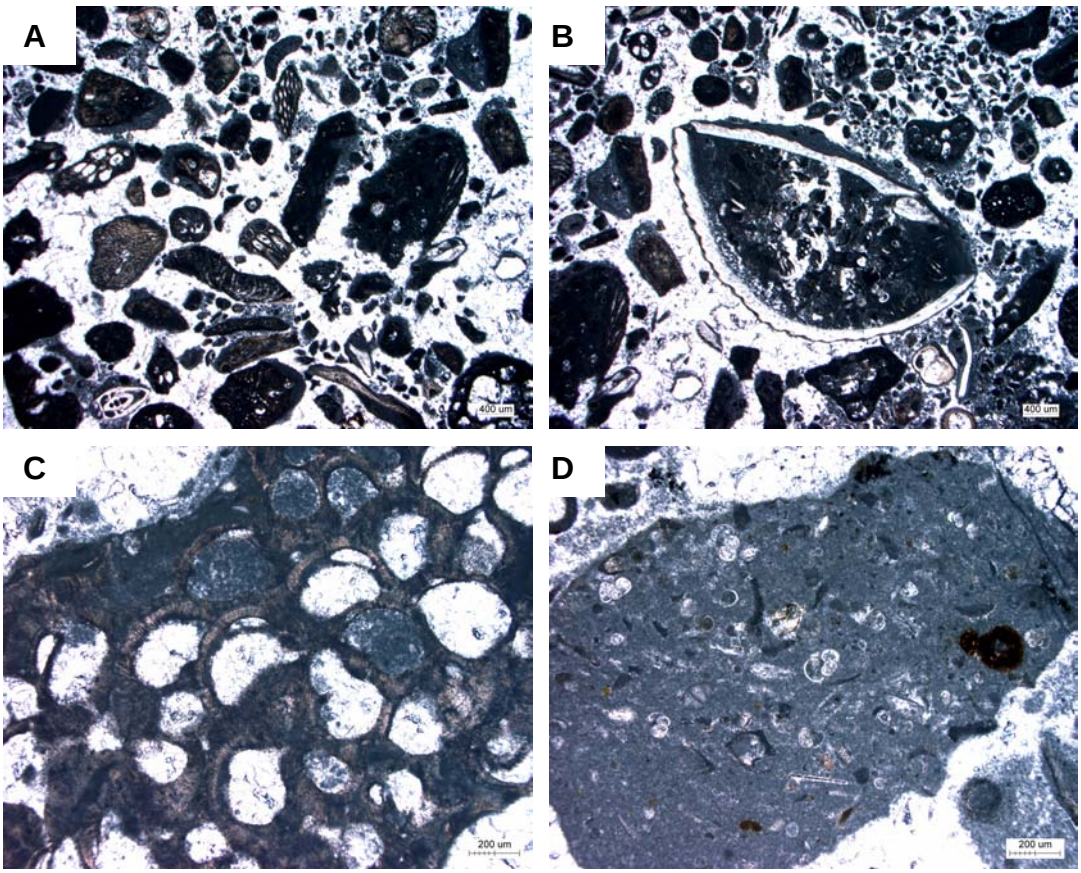

Figure 5.32: Photomicrographs of dyke *T* from the *big bluff* locality. **A** (CH06-RB02T, PPL) showing abundant bryozoan fragments with some bivalves and benthic foraminifera which appear mostly to be inclusions within micritic lithoclasts. **B** (CH06-RB02T, PPL) shows that the interparticle material consists of equant spar cements with some areas of micrite. The small bivalve in the centre of the image can be seen to contain fine bioclastic fragments and micrite. **C** (CH06-RB02T, PPL) close-up of a bryozoan showing intraparticle micrite and radiating spar cements within the skeletal lattice structure. **D** (CH06-RB02T, PPL) close-up shot of a micritic lithoclast showing inclusions of planktic foraminifera and small palagonitic volcaniclastics.

Dyke U

The brecciated dyke *U* from the *big bluff* locality shows at least three distinct fill types from the upper extent sampled (Fig. 5.33 & Appendix C Table C7 Figs C29, C30 & C31). Analysis from a brecciated section at the uppermost level of the dyke revealed a bryozoan dominated fill where the skeletal fragments were either surrounded by micrite or are inclusions within micritic lithoclasts (Fig. 5.33A & B, & Appendix C Fig. C29). Interparticle material is predominantly spar cement which also infills apparent fractures within the micritic lithoclasts. This micrite fracturing with spar cement development within fractures has also been observed in the offshoot dyke *P* in the *north Red Bluff* locality and may constitute a similar source or origin (Fig. 5.27B).

A structure interpreted to be a possible fold structure in the field was observed to contain abundant planktic foraminifera in thin section (Fig. 5.33C & D, & Appendix C Fig. C30). What appeared to be fold structures in the field were observed to represent laminations resulting from grain sorting of skeletal fragments in thin section (Fig 5.33D). The observed folding seen in the field is now considered to more likely be the result of preferential weathering of the sorted bioclastics, similar to the process of weathering of flaggy limestones where the coarser well cemented limestone flags protrude and the thin softer interflag sediment (seams) become recessed (Nelson, 1978a). In relation to dyke formation such a feature indicates momentum of sediment and therefore a possible injection process of formation.

Analysis of a soft brecciated block of limestone from lower in the upper dyke *U* extent also revealed the same planktic foraminiferal lithology, but did not display any observable grain sorting laminations (Fig. 5.33E & F, & Appendix C Fig. C31). The volcaniclastic fill seen in the field between limestone brecciated blocks is interpreted to be Red Bluff Tuff.

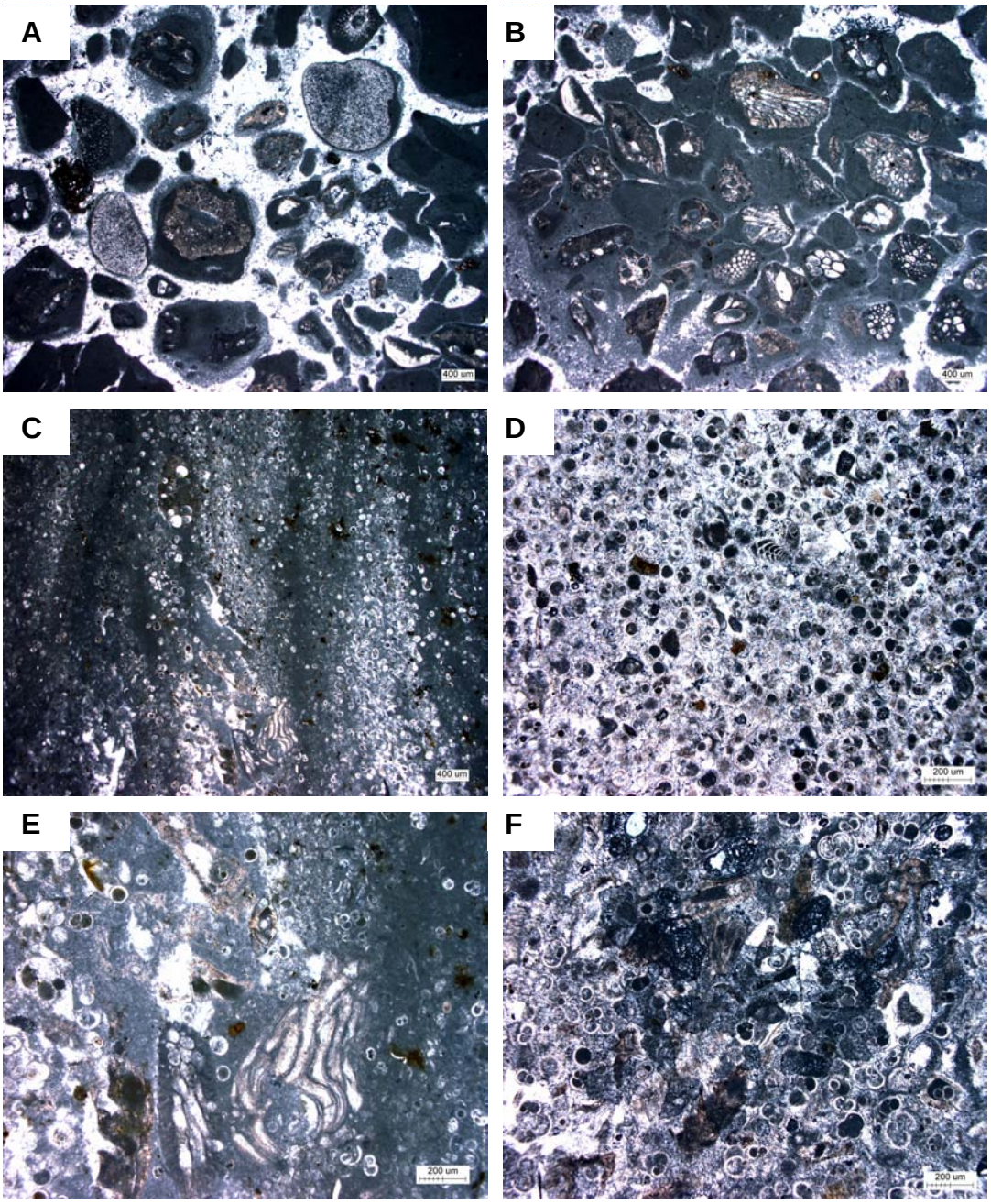

Figure 5.33: Photomicrographs of dyke *U* from the *big bluff* locality. **A** (CH06-RB02U2, PPL) thin section of a sample from the top of the brecciated limestone dyke showing fragments of bryozoans and echinoderms that appear either to have micritic fringe cements or be part of micritic lithoclasts. Note the interparticle equant spar cements. **B** (CH06-RB02U2, PPL) also from the same sample as the previous image (A) showing a number of bryozoan fragments separated by interparticle micrite which appears fractured with infilling of spar cements within these fractures. **C** (CH06-RB02U3, PPL) thin section of a section of micrite that appeared in the field to show fold structures. These apparent fold structures appear to be due to sorting of the abundant planktic foraminifera present in thin section. **D** (CH06-RB02U3, PPL) close-up shot of the folded sample showing that some benthic foraminifera and fine grained volcaniclastics are also present and that both micrite and spar make up equal quantities of the interparticle material. **E** (CH06-RB02U3, PPL) shows a more micrite dominated section of the folded sample with rare larger bryozoan fragments present. **F** (CH06-RB02U5) thin section of a sample of the soft fine grained brecciated limestone seen lower in the dyke section showing a dominance of planktic foraminifera, with intra- and interparticle micrite.

Below the twin masts dykes

Dyke locality 27

The dyke referred to as *locality 27* (collected in 2005) from the *below the twin masts* locality was observed to contain up to four distinct fill lithologies and is considered to form a symmetrical sequence of fills (Fig. 5.34 & Appendix C Table C8 Figs C32, C33, C34, C35, C36, C37, C38, C39 & C40).

The outermost right-hand side dyke fill *P4* shows a chaotic micrite fill with some coarse bioclastic bryozoan fragments as well as finer grained planktic and benthic foraminiferal fragments (Fig. 5.34E, G & H, & Appendix C Figs C37 & C40). The *P4* fill also contains laminated micrite intra/lithoclasts which appear to be a similar lithology as the fill itself, although somewhat finer grained (Fig. 5.34H). The *P4* fill was only observed from the right-hand side of the dyke and it is unknown if this fill type is present on the left-hand side of the dyke. The adjacent inner micrite fill *P3* was, however, observed on both sides of the *locality 27* dyke and displays lamination of planktic foraminiferal inclusions (Fig. 5.34A, B, E & F, & Appendix C Figs C4, C36 & C39). The *P3* fill is far less chaotic then the *P4* fill but appears to involve multiple pulses of sediment infill (Fig. 3.34E & F). Such pulses are thought to be present within the *P4* micrite fill but the diffuse contact boundaries between individual pulses makes interpretation difficult. If pulses are present, their existence represents multiple injection episodes occurring from a common source sediment, either simultaneously or as closely timed injection events.

The central fill sequence is also considered to show symmetry, with the outer central bioclastic fill *P2* showing dominance of bryozoan fragments with some planktic and benthic foraminiferal grains (Fig. 5.34A, B & D, & Appendix C Figs C33, C35 & C38). Some areas of the *P2* fill were also noted to have lithoclast inclusions with interparticle material being predominantly spar cement, although some interparticle micrite is present and is particularly common as an intraparticle fill. The central fill *P1* appears similar to the outer central *P2* fill but can be distinguished by the general (but not complete) absence of planktic foraminifera and the presence of micrite fringes around bioclast edges (Fig. 5.34A & C, & Appendix C Fig. C2). These fringing micrites have been observed in dyke *T* (Fig. 5.32A & B) and at the *north Red*

Bluff locality in the main dyke *M* from the central right-hand dyke fill *2* (Fig. 5.30E & F), which may therefore constitute a common fill in the Red Bluff area.

Cathodoluminescence analysis of the *locality 27* dyke generally showed spar cements to have dull to non-luminescent signatures (Fig. 5.35A & B). Some thin zones of bright luminescence were observed around the edges of acicular fringe spar cements in the outermost chaotic micrite fill *P4*. Considering the chaotic nature of this fill it is highly probable that the luminescent signatures are inherited.

Figure 5.34: Photomicrographs of samples from the dyke occurrence referred to as *locality 27* in the *below the twin masts* locality. **A** (CH05-27A, PPL) a shot from the left-hand side of the dyke (aligned along the bottom of the image) showing three of the four phase fills present. Across the bottom of the image is the micrite fill *P3* which is present on both sides of the dyke. Adjacent to this is a bioclastic fill *P2*, also present on both sides and can be seen again across the top of the image. The central fill *P1* can be distinguished running through the centre of the image by the presence of darker coloured interparticle micrite. **B** (CH05-27B, PPL) a shot showing the right–hand side of the dyke (aligned across the top of the image) with the inner outermost micrite fill *P3* in the upper half of the image and the bioclastic fill type *P2* across the bottom of the image. **C** (CH05-27A, PPL) the central bioclastic fill *P1* showing skeletal fragments of bryozoans, bivalves and echinoderms, with fringe micrite and interparticle spar cement. **D** (CH05-27C, PPL) close-up shot of fill type *P2* which would at first glance appears to be the same lithology as the central fill *P1* but is distinct in that the fill contains planktic foraminifera and the bioclasts do not have any micrite fringes. **E** (CH05-27C, PPL) showing the outermost right-hand side coarse micrite fill *P4* (on the left-hand side of the image) that appears laminated with possible lithoclast inclusions. Adjacent to this on the right hand-side of the image is the microbioclastic fill *P3* (the inner right-hand side of the dyke) with pyrite infills of fractures. Note the stylolite across the centre of the image which cuts only the outermost right-hand *P4* fill. **F** (CH05-27A, PPL) also from the right-hand side of the dyke (orientated across the top of the image) showing lamination with possibly three pulses of microbioclastic fill *P3*. Planktic foraminifera can be seen in the pulse fill across the top of the image (towards the outside right of the dyke) while possible volcaniclastic inclusions are present in the lower micrite pulse. **G** (CH05-27B, PPL) a shot of the outermost *P4* fill (right-hand side of the dyke), showing some large bryozoan fragments and large laminated micrite lithoclast inclusions. **H** (CH05-27B, PPL), a close-up shot of the laminated micrite lithoclasts seen in the lower right-hand corner of the previous image, G, showing a finer grained but similar lithology is present within the lithoclast.

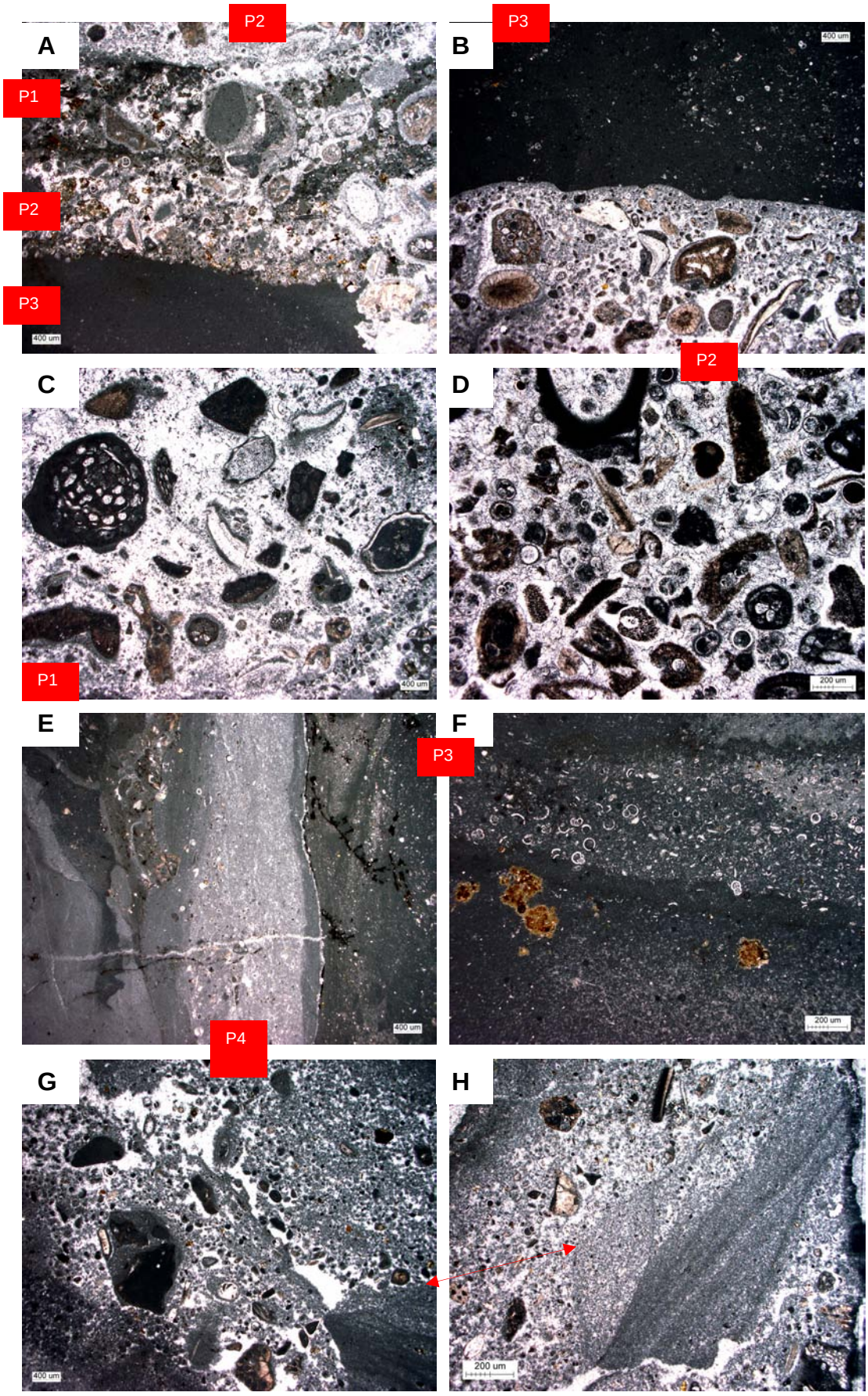
A
P2
P1
P2
P3
400 um
B
P3
400 um
C
P1
400 um
D
P2
200 um
E
400 um
F
P3
200 um
G
P4
400 um
H
200 um

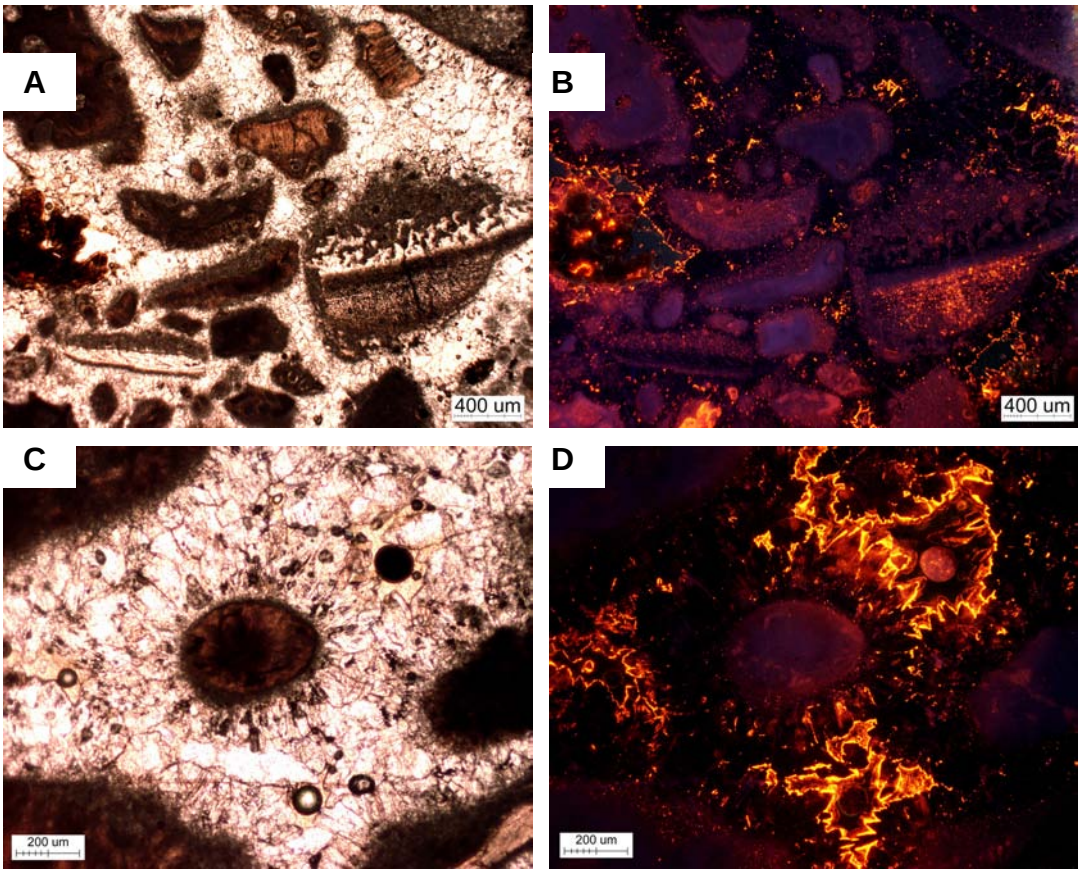

Figure 5.35: PPL and CL micrograph pairs **A** and **B**, **C** and **D** (CH05-27B, PPL and CL), from the central fill type *P1* from the dyke *locality 27* in the *below the twin masts* area at Red Bluff. Generally the interparticle spar cement shows a non-luminescent signature (B) although thin zones of luminescence can occur at the edges of acicular fringing cements.

5.2.3 Ngakuha Reef, Chatham Island

Dyke occurrences at Ngakuha Reef have previously been reported as interstitial fills of Haumurian limestone within pillow basalts of the Southern Volcanics (Strong and Edwards, 1979; Campbell et al., 1993). The pillow basalts of the Southern Volcanics have formed a peninsula at Ngakuha Reef on the western coastline of Chatham Island, approximately 2.5 km southwest of Waitangi (Figs 3.5, 5.36). In the field the interstitial limestone fill between these basalts contains angular and subangular to subrounded basaltic clast inclusions (Figs 3.7, 3.8, 5.37). Where angular clasts are exposed in the limestone surface they are likely to be the exposed and weathered surface of the *in situ* pillows into which the limestone has filled (Fig. 5.37). Subangular to subrounded clasts however must have undergone some degree of transport in order to blunted their angular corners, and so they are therefore considered to be part of the fill material that was derived from the pillows (Fig. 5.37).

It was also observed in the field that some of the Haumurian limestone fills appear to have been squeezed up into the spaces between the pillows (Figs 3.6, 5.38). This invokes a paragenesis situation where it is envisioned that basalt is being directly extruded onto a seafloor which is rich in carbonate material, and that the weight and/or associated pressures caused as a result of the extrusion results in carbonate material being forced up in between the pillow basalts. While this theory might appear feasible, the lack of any contact metamorphism within the interstitial limestone and also the lack of any observable sorting of clast inclusions which might be expected to be seen in a sediment in motion, makes this situation unlikely, although this kind of squeezing process is reported to result in fills that do not show any observable sorting (Peterson, 1968; Archer, 1984; Larsen and Mangerud, 1992; Dreimanis and Rappol, 1997; Hyam et al., 1997; Sturkell and Ormo, 1997; Beacom et al., 1999; Tipper et al., 2003; Jonk et al., 2005).

Petrographic analysis of the Haumurian limestone (refer Chapter 4) at Ngakuha Reef did not reveal any features to support the hypothesis of any forceful injection. While the observation of possible paragenetic squeeze features was made in the field, the petrographic analysis coupled with the lack

of any other forceful injection field features strongly support passive sediment filling.

Figure 5.36: The Ngakuha Reef locality on the western shoreline 2.5 km southwest of Waitangi. The photo is taken looking south with Ngakuha Reef in the foreground and two other basaltic peninsulas to the south.

Figure 5.37: Close-up shots of the interstitial Haumurian limestone showing angular and subangular to subrounded basalt clast inclusions.

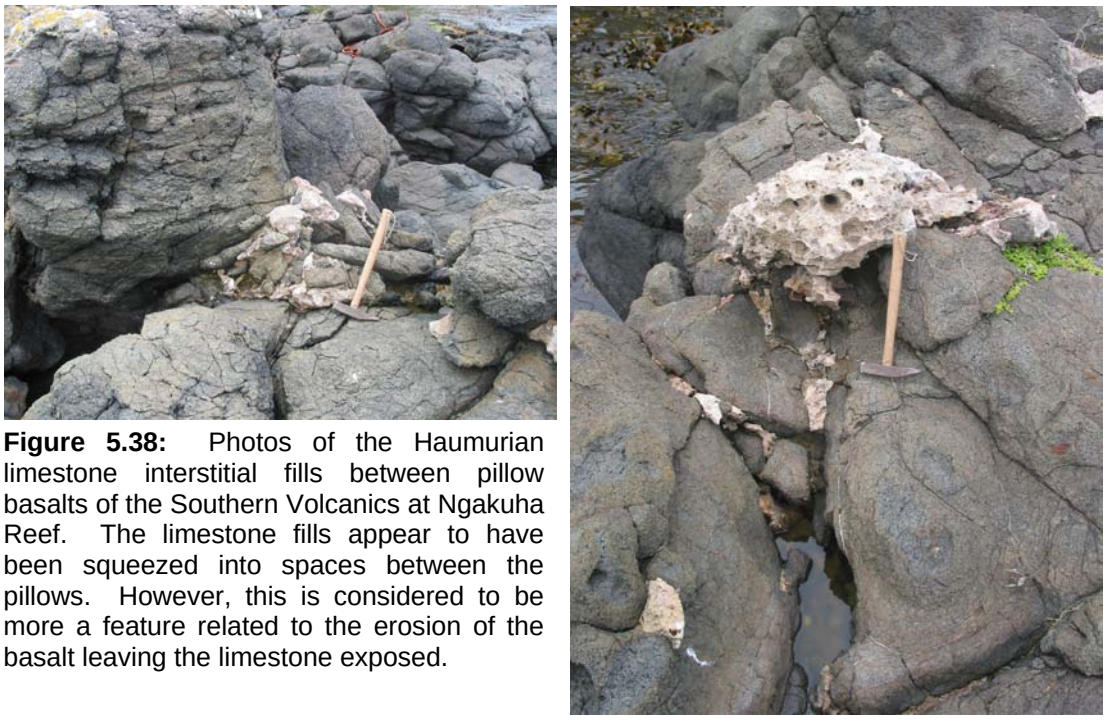

Figure 5.38: Photos of the Haumurian limestone interstitial fills between pillow basalts of the Southern Volcanics at Ngakuha Reef. The limestone fills appear to have been squeezed into spaces between the pillows. However, this is considered to be more a feature related to the erosion of the basalt leaving the limestone exposed.

5.2.4 Flowerpot Bay, Pitt Island

Haumurian limestone fills also occur in sea platforms of Kahuitara Tuff at Flowerpot Bay on Pitt Island, occurring as fissure fills within the tuff. These have previously been described by Campbell et al. (1993) in terms of a limestone occurrence (refer Chapter 3). The fissure fills at Flowerpot Bay were observed in the field to form sinuous and bifurcating sedimentary dykes across the Kahuitara Tuff platform (Figs 3.2, 5.39). The dykes at this locality involve two main lithologies: a pale brown fine grained carbonate fill and a conglomeratic fill with a pale grey interparticle carbonate (Figs 3.3, 5.40). It is not entirely clear how these fills relate to the Haumurian limestone from Flowerpot Bay described by Campbell et al. (1993) but it is likely that the "homogenous, pale grey, hard, non-tuffaceous saccharoidal limestone" represents the pale brown, fine grained fill, while the conglomeratic fill better fits the description of Haumurian limestone from Ngakuha Reef, namely "indurated, pale grey, micritic limestone containing numerous subangular to subrounded basalt pebbles and granules". This conglomeratic fill certainly is present at Ngakuha Reef, but it is conspicuous at Flowerpot Bay.

This area at Flowerpot Bay represents a faulted block of Kahuitara Tuff and is overlain by Matanginui Limestone towards sea level. The Matanginui Limestone was observed to fill fissure depressions within the tuff and, in a single known occurrence, to form a dykelet penetrating into the Kahuitara Tuff (Figs 3.4, 5.41).

Petrographic analysis of the dykes at Flowerpot Bay has partially also been presented in Chapter 4 in association with analysis of the Haumurian limestone. During analysis it soon became evident that the Haumurian fill lithologies were many and that the sequences of fills were extremely complex. The initial fills were probably manganese oxide precipitates and/or volcaniclastic sediment that had previously been variably reworked in a marine environment (Figs 4.4B, 4.5 E & F, 5.42, 5.43A, B, C & F, Appendix B Table B1, B7). Either both or one of these fills is always present on the outermost contact with the Kahuitara Tuff in each of the samples analysed.

Adjacent to either the precipitated manganese oxides or volcaniclastic sediment forming the next inner fill is the pale brown micritic fill which, if

correct in identification, is considered by other workers (Strong, 1979; Campbell et al., 1993) to be a lithofacies of the Haumurian limestone (Fig. 5.43A, B, E & Appendix B Table B1). This pale brown micritic fill is also considered to show some possible sorting of grains, represented by flow structures and laminations (Fig. 5.43A & E). This pale brown fill is sometimes adjacent to an inner bioclastic fill of the Haumurian limestone which contains an unidentified Cretaceous benthic foraminifera and abundant volcanic clasts (Figs 4.4F, 5.43B, C & Appendix B Table B1). This fill is probably representative of the conglomeratic fill observed in the field and is similar to the conglomeratic fill occurring at Ngakuha Reef on Chatham Island (Fig. 4.4C, D & G).

The innermost fills observed in some of the dykes at Flowerpot Bay are similar in their bioclastic components, with a dominance of bryozoans and significant echinoderm fragments, as well as some volcanic clast inclusions (Figs 4.4A, B, 5.43D, F, G & Appendix B Table B7). The distinction between these two fills is made on the presence of either spar cement (fill type *1*) or interparticle micrite (fill type *2*). Both fill types display similarities to the lithologies of the Matanginui Limestone (Figs 4.10D & E, 5.43D, G). This conclusion that fills *1* and *2* possibly represent infills of Matanginui Limestone is also based on the limestone's presence in the field as a possible fill material, but also that the known lithology of the Haumurian limestone is quite dissimilar.

The above sequence of fills represents a generalised order to the fills observed at Flowerpot Bay. By examining the field photos (Figs 5.39, 5.40, 5.41 & 5.42) and micrographs (Fig. 5.43) it is evident that the sequence is not always as given. This is due to cross-cutting relationships between fills and to the fact that there must have been repeated fracturing and refilling of fissures at different times. Laminations and grain sorting provide some evidence for injection within the pale brown fill of the Haumurian limestone.

Figure 5.39: (Left) Haumurian limestone fissure fills within the Kahuitara Tuff at Flowerpot Bay, Pitt Island showing the sinuous and bifurcating nature of these sedimentary dykes.

Figure 5.40: (Right) the Haumurian limestone fissure fills from Flowerpot Bay, Pitt Island showing the two main fill lithologies present at this locality: a conglomeratic carbonate fill (running vertically through the image) and a pale brown fine grained fill which can be observed in offshoot dykelets extending from the centre of the conglomerate fill towards the bottom left and right of the image.

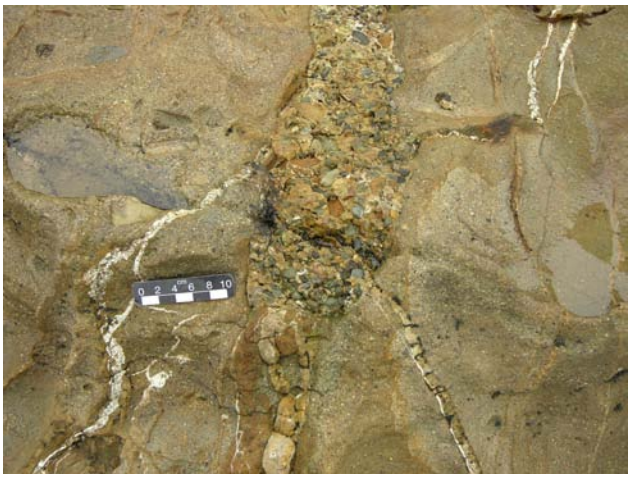

Figure 5.41: (Left) Matanginui Limestone overlying the Kahuitara Tuff near sea level at Flowerpot Bay, Pitt Island showing a thin dykelet extending from the Matanginui, near the position just to the left of the scale bar, down into the Kahuitara Tuff.

Figure 5.42: (Left) Manganese precipitate occurs along the walls and within a number of the small dykes at Flowerpot Bay, Pitt Island.

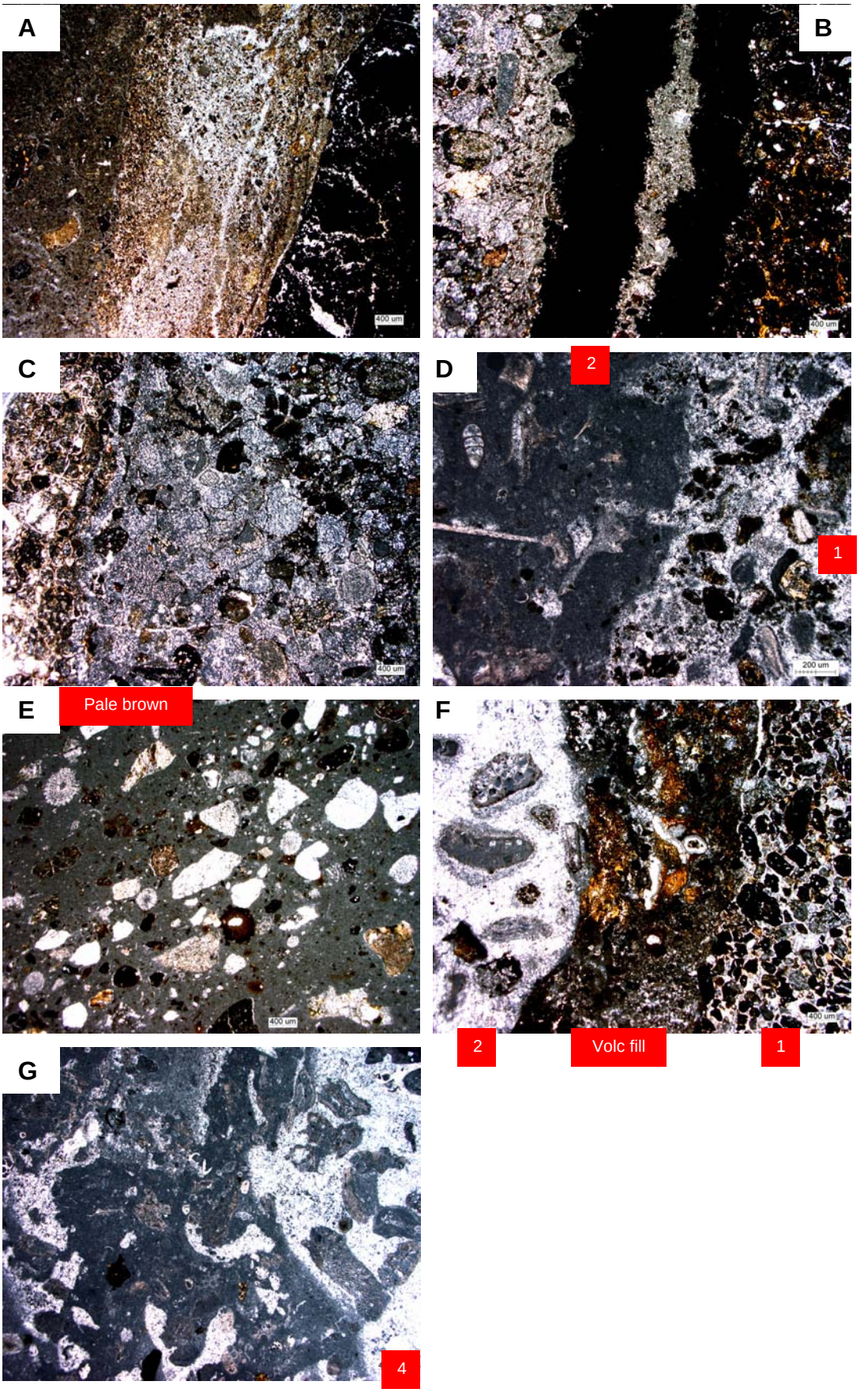
A
B
C
D
2
1
E
Pale brown
F
2
Volc fill
1
G
4

Figure 5.43: Photomicrographs of dyke associated features of the Haumurian limestone at Flowerpot Bay on Pitt Island. **A** (CH05-9.1) showing an outer pale brown fill with numerous fine grained volcaniclastic inclusions. The dark area along the right-hand side of the image represents what is probably precipitated manganese oxides. The contact with these wall oxides appears to display some wavy lamination. **B** (CH05-9.1A) showing the Kahuitara Tuff host material along the right-hand side of the image with dyke wall manganese oxides that have been divided by a lighter grey pale brown fill. This grey micritic fill can be seen on the inside of the inner manganese oxide fill and along the left-hand side of the image forms a contact with the bioclastic Haumurian limestone. **C** (CH05-9.1A) another section of the same sample as the previous image in B, showing the bioclastic Haumurian limestone in direct contact with the Kahuitara Tuff along the left-hand side of the image. **D** (CH05-9.2A) a shot showing two lithofacies fills: on the left-hand side of the image a bryozoan dominated fill (*2*) with significant bivalve and echinoderm fragments and interparticle micrite. The right-hand side of the image shows a bryozoan and echinoderm dominated fill (*1*) with significant volcanic clast inclusions and interparticle spar cement. **E** (CH05-9.2B) showing a different lithofacies of the pale brown fill. This dykelet fill *2* has coarse angular volcaniclastic fragments that appear to show some crude sorting of grains which was also apparent in hand specimen. **F** (CH05-9.4) showing an inner bryozoan dominated fill (*3*) along the right-hand side of the image, considered to be an infilling of Matanginui Limestone. To the left of this a volcanic fill (*2*) thought to represent the host Kahuitara Tuff, while the third fill (*1*) along the right-hand side of the image is possibly reworked volcaniclastic sediment of the Kahuitara Tuff. **G** (CH05-9.4) also from the same sample as the previous image F, a fourth fill (*4*) also possibly related to infilling of Matanginui Limestone. This fill also shows a dominance of bryozoans with apparent infilling of possible dissolution porosity by equant spar cements.

CHAPTER 6
Interpretive Synthesis of Carbonate Deposits and Dykes on Chatham Islands

6.1 Introduction

The wide range in ages of the limestones on Chatham Islands, from Late Cretaceous to Quaternary, affords the opportunity to compare regional depositional trends though time Some previous comparisons have been made by Campbell et al. (1993), but it is appropriate that a synthesis be conducted from a carbonate sedimentological perspective that takes into account the petrographic skeletal assemblages and diagenetic properties of the limestones. Such an approach may enhance understanding of the depositional and diagenetic evolution of the carbonates on Chatham Islands.

A short review of the conclusions of Campbell et al. (1993) is first given here so as to avoid subsequent repetition of information and for the purpose of comparing and enhancing aspect of the carbonate depositional history.

Campbell et al. (1993) suggested that the deposits on Chatham Islands reflect a prolonged history of relative tectonic stability, with the Chatham Island itself representing remnants of a Late Cretaceous stratovolcano which accumulated biogenic and volcanogenic deposits throughout the Cenozoic, interrupted by periodic minor episodes of volcanism. Comparisons to global sea level and onlap/offlap curves of Haq et al. (1987) were found to have little correspondence to the depositional history evident on Chatham Island. Regardless of this, some major depositional trends within the Chatham Islands have been identified with quartzofeldspathic inclusions in many of the Late Cretaceous to Eocene deposits (Tupuangi Formation, Tioriori Group) while Eocene to Pliocene Chatham Island deposits are predominantly non-quartzofeldspathic, with another major change observed in the Quaternary deposits which are again largely quartzofeldspathic. These quartzofeldspathic deposits and inclusions are considered to be derived from the basement Chatham Schist, but it remains unclear whether this deposition

relates to sea level fall or tectonic uplift, although Campbell et al. (1993) considered that the Chatham Islands have probably been subaerially exposed since the Pliocene and remained submerged though much of the Late Cretaceous and Cenozoic.

A review of the eleven known limestone occurrences on Chatham Islands (see Fig. 4.0) will now be given in relation to more recent available literature describing some regional depositional trends in New Zealnd. These observations include New Zealand limestone skeletal assemblages through the Cenozoic made by Hayton et al. (1995), and the broad New Zealand depositional trends of King et al. (1999) that encompass the 1st order 100 Ma 'megasequence' since the mid-Cretaceous and seven 2nd order cycles through this time period. Comparison will also be made with the development of oceanic fronts (Subtropical Front [STF], Subantarctic Front [SAF] and Antarctic Polar Front [AAPF]) through the Cenozoic in the New Zealand sector of the Southern Ocean (NZSSO) developed from analysis of sediment facies, microfossil assemblages, stable isotope records and onland sequences by Nelson and Cooke (2001), and with a New Zealand paleoclimatic curve developed by Hornibrook (1992), both of these examples depicting relative surface water temperatures. Consideration will also be given to paleoenvironments of deposition in relation to some current carbonate depositional models and limestone diagenesis scenarios.

6.2 Haumurian limestone (Late Cretaceous)

The Haumurian limestone lies with prominent localised unconformity on the Southern Volcanics on Chatham Island and the Kahuitara Tuff on Pitt Island. This Haumurian aged limestone has no primary deposit on the Chatham Islands and is only preserved as dyke fills within these Late Cretaceous volcanics.

The Haumurian limestone contains a bryomol skeletal assemblage, that is one dominated by bryozoan fragments and in this case common bivalves and also echinoderms (Fig. 6.1), an assemblage not directly plottable on the Hayton et al. (1995) triangular classification diagram. It is unclear how the

bryomol Haumurian limestones might relate to mainland New Zealand counterparts during this time, which typically are nannofossil-planktic foraminifera (or nannofor) micrites (e.g. Nelson, 1978a). Campbell et al. (1993) suggested correlation with the Amuri Limestone and Mead Hill Flint in NE South Island based on the inclusion of chert clasts in many of the overlying Chatham Island deposits, particularly those of Quaternary age. The chert inclusions were thought to possibly be remnants of the Haumurian limestone which formerly may have been considerably thicker and more widespread. Certainly the foraminifera and radiolarians extracted from the chert inclusions yield a Late Cretaceous age (C.J. Hollis and C.P. Strong in Campbell et al., 1993).

It is interesting to note that the only macrofossil identified by Campbell et al. (1993) from the Haumurian limestone is the bivalve *Acesta* from Ngakuha Reef on Chatham Island, while this study has shown that there are abundant fragmented bryozoans, echinoderms and bivalves at Ngakuha Reef on Chatham Island and at Flowerpot Bay on Pitt Island (refer Chapters 3,4 & 5). The presence of *Acesta* apparently suggests an upper bathyal depth of deposition while the benthic foraminifera *Anomalina*, *Colomia*, *Florilus*, *Gavelinella* and *Patellina* imply outer shelf water depths of 100-200 m (Appendix D Table D1). The presence of the calcareous nannofossil *Nephrolithus frequens* and the general planktic foraminiferal assemblage supports a highish latitude setting with temperate surface waters which is in keeping with the paleolatitude of 63°S derived from paleomagnetic measurements on the Southern Volcanics (Grindley et al., 1977; Campbell et al., 1993). Given the Late Cretaceous ages and the observed occurrence of stromatolitic algae in the limestone, warm temperate to marginally subtropical surface waters are the preferred marine conditions (Fig. 6.1).

While the benthic foraminiferal assemblage on Pitt Island is considered to represent outer shelf depths (100-200 m), Strong and Edwards (1979) have suggested an initial depositional setting for both the Chatham and Pitt Island localities that involves emplacement of shallow marine volcanics. At Flowerpot Bay the dyke host material, the Kahuitara Tuff, indicates a depositional depth of 5-50 m (inner shelf) based on foraminiferal assemblages (Strong, 1979), while the pillow basalts of the Southern Volcanics at Ngakuha

Reef are inferred to be shallow depth deposits based on their proximity to the volcanic edifice which is known to be subaerially exposed at the time of emplacement (Hay et al., 1970; Strong and Edwards, 1979). Subsequent deepening of water depth saw deposition of the Haumurian limestone which infilled fissures within the Kahuitara Tuff and cavities between pillows of the Southern Volcanics. The overlying Red Bluff Tuff at both localities is considered to once again indicate a shallowing depositional environment during the ensuing Late Paleocene-Early Eocene (Strong and Edwards, 1979).

This trend of 'shallow to deep to shallow' was considered by Strong and Edwards (1979) to show little correlation to global eustatic sea level or to depositional trends in New Zealand (Wellman, 1953; Wilson, 1956; Fleming, 1975; Cooper, 1977) and that Chatham Island "behaved as a structurally independent unit" at this time. More recent interpretations of wider New Zealand depositional trends by King et al. (1999) show a deepening water trend through the Late Cretaceous, while the global sea level curve of Haq et al. (1987) is also consistent with fluctuating water depths of up to 100 m which support the depositional scenario of Strong and Edwards (1979) (Fig. 6.1).

The departure of the regional and global trends from the shallow emplacement of the Southern Volcanics can be explained by localised thermal uplift associated with Late Cretaceous volcanism on the Chathams. Recent K-Ar dates obtained for the major volcanic episodes on Chatham Island by Panter et al. (2006) show a more constrained age range for the Southern Volcanics, from 85-82 Ma, with initiation of volcanism near the time suggested by Grindley et al. (1977) at 81 Ma, but it's cessation significantly earlier than Grindley's 71 Ma estimate (Fig. 6.1). Strong and Edwards (1979) considered that subsidence following the cessation of volcanism forming the Southern Volcanics resulted in the rapidly deepening depositional environment into which the Haumurian limestone formed. This interpretation, on the basis of the new age range (85-82 Ma) for the Southern Volcanics and the more recent regional depositional and global sea level trends, is considered here to be unnecessary, although it is quite feasible that localised subsidence may have occurred following cessation of this period of Late Cretaceous volcanism.

6.2.1 Dyke formation

While the interstitial fills in the pillows at Ngakuha Reef on Chatham Island show no evidence of injection of carbonate sediment (Fig. 5.37, 5.38) it is likely that the dykes within the Kahuitara Tuff on Pitt Island are far more complex then previously thought (Figs 5.41, 5.43). Petrographic analysis has demonstrated that multiple limestone and volcaniclastic fill lithologies are present within the dykes at Flowerpot Bay, Pitt Island. Volcaniclastic sediment fills at Flowerpot Bay are considered to be evidence of either forcible injection of sediment or water escape mechanisms. What is more intriguing is the occurrence of bryozoan-dominated fill, which is both genetically and diagenetically unrelated to the Haumurian limestone described by Strong and Edwards (1979) (refer Section 5.2.4). These bryozoan-dominated fills are inferred to originate from shallow marine (middle shelf depth, 50-100 m) skeletal assemblages/deposits and bear striking similarities to the dyke fills occurring at Red Bluff on Chatham Island (refer Section 5.2.2). Many of the fills at Red Bluff are thought to have been derived from Matanginui Limestone, which also has been observed to overlie (within Red Bluff Tuff) and penetrate the Kahuitara Tuff fault block at Flowerpot Bay on Pitt Island. It is here proposed that this bryozoan-dominated fill may represent infilling of Matanginui Limestone by re-opening of fissures previously filled by volcaniclastic sediment and Haumurian limestone. This re-opening is likely associated with seismic activity associated with the onset of localised Red Bluff volcanism during the late Teurian-late Waipawan, as was initial fracturing of the Kahuitara Tuff and infilling of Haumurian limestone during the Piripauan-Haumurian.

6.2.2 Diagenetic interpretation

The diagenetic history of the Haumurian limestone and associated fills is made somewhat complex by the number of different fill lithologies. However, overall the Haumurian limestone (this includes all related fills) has diagenetic features attributed to shallow burial (tens of metres) along with evidence of a meteoric influence. The meteoric influence is reflected in the

infilling of mouldic porosity by spar cement (removal and replacement of aragonitic elements) and in the generally dull cathodoluminescent signatures with multiple thin bright zones toward the edges of interparticle spar cements (Figs 4.4, 4.5, 5.43) (Hood and Nelson, 1996). The content of observed biomoulds probably accounts for much of the cementation through dissolution of aragonite and likely must have occurred within the phreatic zone, possibly near the freshwater phreatic and marine phreatic interface where aragonite is most readily dissolved (Land, 1970; Tucker and Wright, 1990).

Shallow burial cementation features are observed in the central fills at Flowerpot Bay (Pitt Island, Fig. 5.43F & G), attributed in this study to infills of Matanginui Limestone, and the Haumurian limestone at Ngakuha Reef (Fig. 4.5G & H). These fills show interparticle spar cement or bioclastic micrite, epitaxial spar rinds, and syntaxial rim overgrowth cement on echinoderm fragments which are characteristic of cool water shallow burial and meteoric influenced diagenesis (Figs. 4.4, 4.5, 5.43) (James and Bone, 1989; Dodd and Nelson, 1998; Nelson and James, 2000).

Given the absence of any pressure dissolution features between skeletal grains it seems unlikely that the burial depths in the preserved fill limestones could have ever exceeded more than a few 100 m, and there appears to be no evidence for any early seafloor cementation.

Comparative Skeletal Assemblage Diagram for Limestone Occurrences on the Chatham Islands

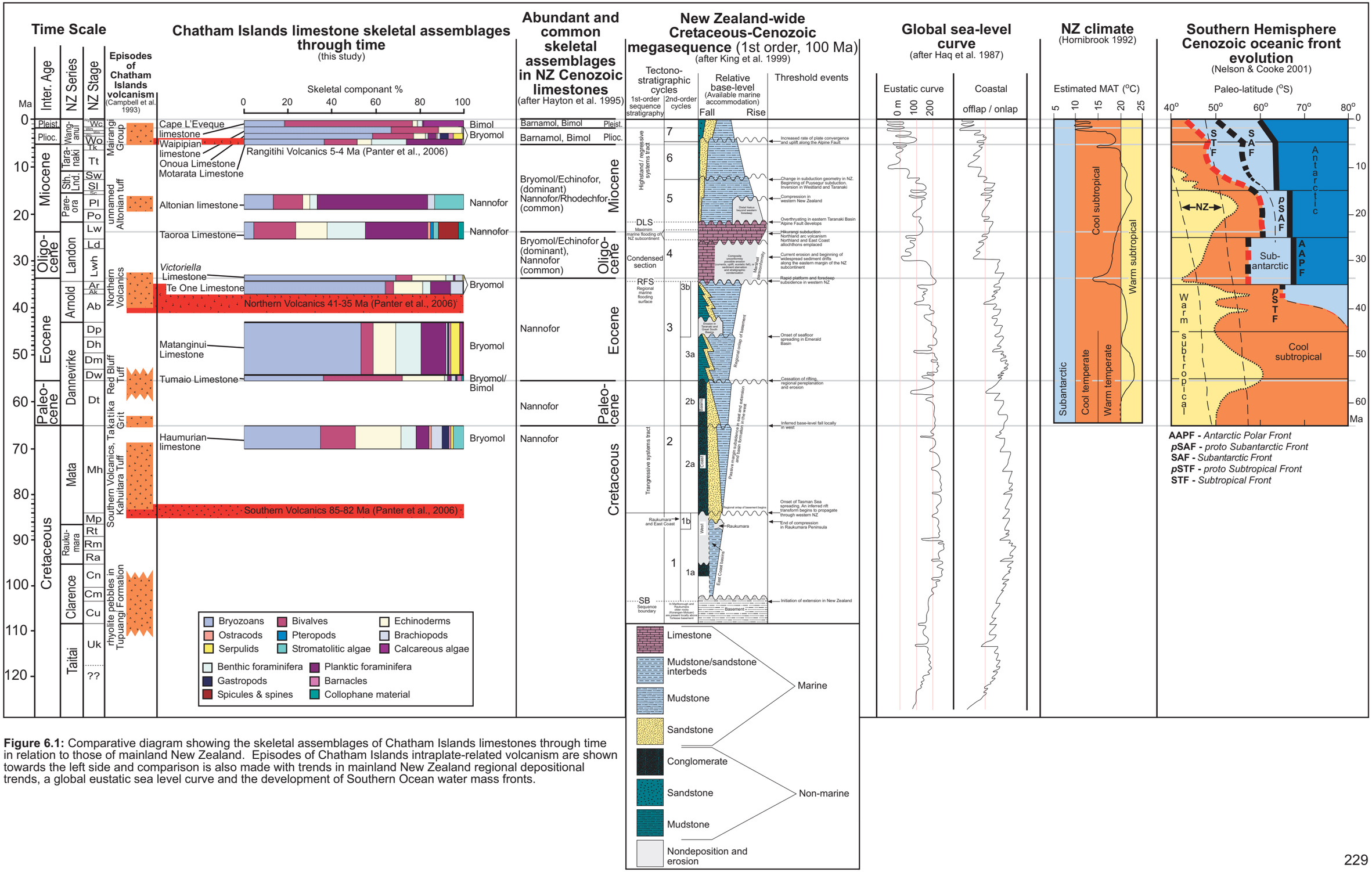

Figure 6.1: Comparative diagram showing the skeletal assemblages of Chatham Islands limestones through time in relation to those of mainland New Zealand. Episodes of Chatham Islands intraplate-related volcanism are shown towards the left side and comparison is also made with trends in mainland New Zealand regional depositional trends, a global eustatic sea level curve and the development of Southern Ocean water mass fronts.

6.3 Tumaio Limestone (Late Paleocene-Early Eocene)

The Tumaio Limestone has a bryomol/bimol skeletal assemblage based on a near equal abundance of bryozoan and bivalve fragments (Fig. 6.1). The abundance of these skeletal fragments, along with conspicuous echinoderm grains, again does not plot directly into the assemblage classification scheme of Hayton et al. (1995). The Tumaio Limestone is considered to be a shelly lateral equivalent of the Tutuiri Greensand shellbeds of *Pycnodonte (Notostrea) tarda* present at lower stratigraphic levels but not observed in this study (Appendix D Table D2) (Campbell et al., 1993). The Tumaio Limestone also shows an abundance of polycrystalline quartz grains, volcanic rock fragments and glauconite pellets (Figs 4.30A, 6.2)

The assemblage of planktic and benthic foraminifera within the Tumaio Limestone suggests a sheltered oceanic setting at water depths of mid to outer shelf (50-200 m) where sorting of sediment within the Tutuiri Greensand by bottom currents formed carbonate banks of Tumaio Limestone during the Waipawan (earliest Eocene) (Appendix D Table D3) (Campbell et al., 1993). The bryomol/bimol skeletal assemblages contrast markedly with common mainland New Zealand nannofor assemblages during the Paleocene and Eocene (Hayton et al., 1995), otherwise associated with the regional and global deepening of sea water (Fig. 6.1) (Haq et al., 1987; King et al., 1999). The shallower mid-shelf depths on the Chatham Island are likely a result of localised thermal uplift associated with volcanism and emplacement of the Red Bluff Tuff, as hypothesised by Strong and Edwards (1979), and the Red Bluff Tuff itself is thought to have been erupted in mid-shelf water depths (50-100 m) (Campbell et al., 1993). Surface water temperatures at this time are considered to be cool subtropical under the influence of a large South Pacific warm gyre, there being no ice cover on Antarctica or any frontal water mass development in the Southern Ocean in the Paleocene-Early Eocene (Fig. 6.1) (Hornibrook, 1992; Nelson and Cooke, 2001).

6.3.1 Silica cements

The presence of silicified nodular horizons in the upper stratigraphic levels of the Tumaio Limestone has been attributed to the inclusion of sponge spicules (Campbell et al., 1993). Petrographic analysis has not revealed any sponge spicules in the analysed samples (see Section 4.2.1), but given the ephemeral nature of outcrops on the open sandy coastline in NW Chatham Island it is unclear whether the silicified horizons observed and sampled relate to those of Campbell et al. (1993) (Figs 3.34, 3.36). Regardless of this, sponge spicules were not observed in the field or in thin section. Silicification within the lower Tioriori Group Takatika Grit member is considered to be derived by percolation of biogenic and volcanogenic silica through the entire column down to the stratigraphic level of the Takatika Grit (e.g. Knauth, 1979) or the flow of mixed meteoric-marine waters along the contact of the underlying Chatham Schist (Campbell et al., 1993). Such a mechanism is stratigraphically untenable for the silicification within the Tumaio Limestone.

In the absence of any observable sponge spicules within these horizons it is suggested that a similar percolation process of hypersaline/marginal marine water may have derived the silica from the large polycrystalline quartz grains present within these horizons, simultaneously dissolving the calcite skeletal fragments and replacing them with silica precipitated from the percolating pore waters (Knauth, 1979; Maliva and Siever, 1988; Hesse, 1989; McBride et al., 1999) (Fig. 6.2). The polycrystalline quartz grains probably represent periods of time when sediments of the laterally equivalent Tutuiri Greensand were delivered to the carbonate bank sites, being eroded originally from the underlying Takatika Grit. Silicification may also conceivably have taken place during early carbonate diagenesis within a submarine environment and be related to the formation of the nodular silica observed in outcrop, although the occurrence of zebraic chalcedony as evident in thin section (Fig. 4.30D) has been associated with silica replacement (Knauth, 1979; Hesse, 1989; Martin Penela and Barragan, 1995) and replacement of carbonate skeletal material has been clearly observed in thin section (Fig. 4.30B).

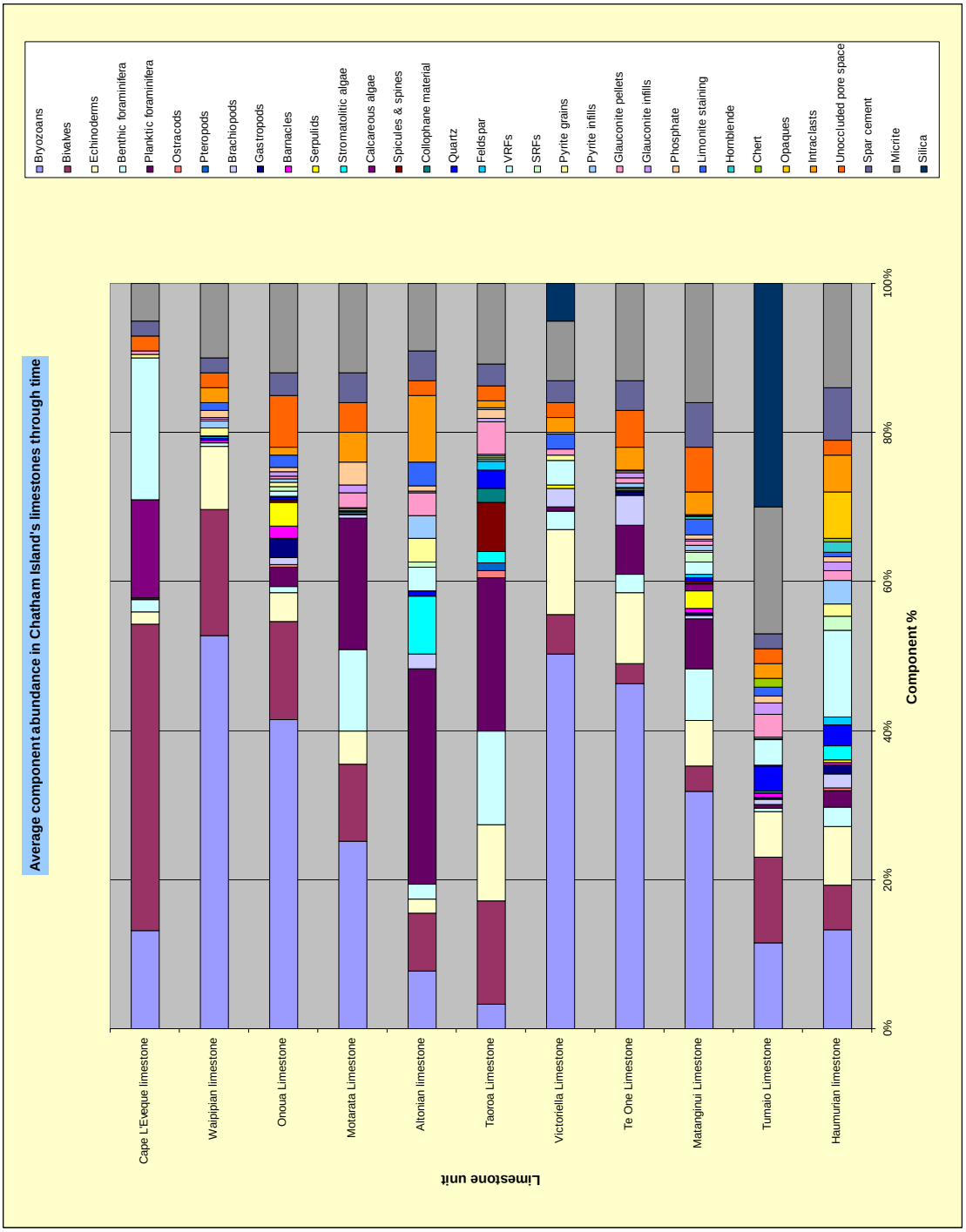

Figure 6.2: Whole rock composition of the eleven limestones on the Chatham Islands depicted here to show upward comparisons in the trends of bioclastic assemblages (also Fig. 6.1), siliciclastic material and interparticle micrite/cements.

6.4 Matanginui, Te One and *Victoriella* Limestones (Early Eocene-Early Oligocene)

6.4.1 Matanginui Limestone (Early Eocene)

Carbonate deposition from the Early Eocene through to the Early Oligocene on the Chatham Island is dominated by bryomol assemblage limestones (Fig. 6.1). This skeletal assemblage contrasts markedly with widespread nannofor assemblage limestones on mainland New Zealand through much of this time associated with relatively deep water regional depositional trends and relatively high global eustatic sea levels (Fig. 6.1) (Haq et al., 1987; King et al., 1999).

Surface water temperatures remain subtropical throughout the Early Eocene and continue conditions from the Paleocene, with no ice caps yet on Antarctica and warm subtropical water being delivered to the New Zealand region by the South Pacific gyre (Hornibrook, 1992; Nelson and Cooke, 2001). During most of this Early Eocene period deposition of the Matanginui Limestone was taking place and is preserved as the most widespread carbonate deposit on the Chatham Islands, present on both Chatham and Pitt Island. Coeval volcanism associated with the Red Bluff Tuff was occurring during the early deposition of Matanginui Limestone which interfingers with the Red Bluff Tuff at many sites (Figs 314, 3.15). Field observations clearly show that deposition of the Matanginui Limestone occurred on the slopes of Red Bluff Tuff volcanic mounds and that the two deposits, namely the Tumaio and Matanginui Limestones, shared an intimate relationship during early deposition of the limestone and the cessation of Red Bluff Tuff volcanism (Fig. 6.1).

The disparity between mainland New Zealand regional skeletal assemblages and depositional trends may be attributed to localised thermal uplift associated with the Red Bluff Tuff volcanism, as previously proposed by other workers (Strong, 1979; Campbell et al., 1993).

The general bryomol assemblage within the Matanginui Limestone indicates a relatively shallow depth of deposition, probably <35 m in subtropical waters. Evidence for this comes from the presence of the bivalve

Spondylus, the brachiopods *Probolarina*, *Thecidellina* and *Lingula*, and the echinoderm *Eucidaris*, all warm water genera, as well as the large benthic foraminifera *Asterocyclina speighti* which lived within the euphotic zone (Appendix D Tables D4 & D5) (Campbell et al., 1993). Such warm water conditions presumably existed on the shallower flanks of the volcanic mounds of Red Bluff Tuff and between individual tuff mounds with deepening environments on the flanks of outer oceanic mounds. Locally deeper water environments are indicated at some stratigraphic levels within the Matanginui Limestone by the presence of the deeper water mollusc *Acesta* (Appendix D Table D4) (Campbell et al., 1993).

6.4.2 Red Bluff sedimentary dykes

The intimate relationship between the Matanginui Limestone and the Red Bluff Tuff is also evident from the occurrence of sedimentary (predominantly carbonate) dykes at Red Bluff on Chatham Island (see Section 5.2.1). While at least some of the fill lithologies present within the dykes can be directly attributed to derivation from Matanginui Limestone, notably those containing the large benthic foraminifer *Asterocyclina* (Figs 5.23C, D, E & F ; 5.24A & B; 5.25F; 5.26B & F), the majority of the fills are distinctly different (Figs 5.23A & B; 5.24C, D, E, & F; 5.25; 5.26, 5.27; 5.29-5.35). These distinctive lithologies mainly occur towards the outer margins of the sedimentary dykes and are considered here to represent a variety of initial depositional settings prior to deposition of the Matanginui Limestone proper. Supporting evidence includes the high proportion of volcaniclastic inclusions in these fills, and their position toward outer dyke margins indicating they represent initial dyke fill lithologies. To strengthen this observation it would be good to have ages for the initial fills, unfortunately outside the time frame scope of this study. However, these sediment fills are certainly distinctive, and there presence may be considered to preserve a record of deposition during the Early Eocene (and possibly Late Paleocene given the known ages of Red Bluff Tuff) that has been removed elsewhere from the Chatham Islands rock record.

The observation by Campbell et al.(1993) that the sedimentary dykes within the Red Bluff Tuff are (passive) fissure fills of Matanginui Limestone is certainly supported in this study. However, there is also evidence of other fill lithologies and for emplacement by sediment injection processes at Red Bluff (Figs 5.23A, C & D; 5.24D, 5.25B & D; 5.29D; 5.33C; 5.34E & F). Dyke formation within the Red Bluff Tuff is considered to be directly associated with Red Bluff Tuff volcanism which allowed for fracturing within the Red Bluff mounds by associated seismic activity and passive fissure filling of the draping volcaniclastic and carbonate sediment. This associated seismic activity is also considered to have resulted in the development of hydraulic head gradients that allowed for the forceful injection of unlithified sediment draping the slopes of the Red Bluff Tuff mounds, exploiting fracture planes within the partially lithified (welded) tuff mounds. Both passive and forcible injection processes formed multiple episodes of filling, typically by reopening and filling of previously exploited fracture planes. Such processes are considered to have continued throughout the duration of volcanism associated with the Red Bluff Tuff, but are only known to have been of common occurrence at the Red Bluff locality.

6.4.3 Te One and *Victoriella* Limestones (Late Eocene-Early Oligocene)

Chatham Island skeletal assemblages through this period continue to be bryomol dominated, with deposition of the Te One Limestone during the Late Eocene-earliest Oligocene (Kaiatan-lower Whaingaroan) and the *Victoriella* Limestone during the Early Oligocene (lower Whaingaroan). These Late Eocene and Early Oligocene limestones on the Chatham Island again contrast with common occurrences of nannofor limestone on mainland New Zealand through this time associated with continued regional transgression and the onset of maximum regional flooding during the Oligocene with widespread submergence of the New Zealand subcontinent (Fig. 6.1) (Hayton et al., 1995; King et al., 1999). On the other hand, bryomol carbonates of this age certainly do occur in the mainland record, for example in the Oamaru district (Nelson, 1978a).

The Te One Limestone, given the absence of *Acesta* and the presence of the barnacle species *Calantica (Scillaelepas)* cf. *studeri* and *Pachylasma*

distortum, possibly formed at inner to mid shelf depths (0-100 m), although the presence of the barnacle *Chionelasmus darwini* may be an indication of water depths up to 400 m (Appendix D Table D6). The absence of foraminifera from the Lagenidae and Elphidiidae families, but the presence of Pleurostomellidae benthics, is considered to indicate mid to outer shelf water depths of 50-200 m (Appendix D Table D7) (Campbell et al., 1993). The *Victoriella* Limestone probably formed in a shoal or platform setting that was relatively oceanic given the inclusion of planktic foraminifera, at mid to outer shelf depths (Appendix D Table D8) (Campbell et al., 1993). In general, both deposits represent relatively shallow <200 m shelfal water depths.

More recently acquired dates for the timing of the eruptives of the Northern Volcanics by Panter et al. (2006) indicate that volcanism occurred from 41-35 Ma with eruptive centres active throughout the deposition of the Te One Limestone (Kaiatan-lower Whaingaroan) and the *Victoriella* Limestone (lower Whaingaroan) (Fig. 6.1). Recent field observations suggest that at least some of the associated cones and volcanic structures (maars) of the Northern Volcanics were subaerially exposed during this time (H. Campbell, GNS Science, pers. comm., 2006) (although it should be noted that the association of these structures with the Northern Volcanics is not entirely conclusive). On this basis, localised thermal uplift allowing for deposition of the shallow marine assemblages forming these limestones is anticipated (Campbell et al., 1993).

Surface water temperatures through the early Late Eocene remained similar to those in the preceding Early Eocene and Paleocene, with a probable West Antarctica warm surface water clockwise gyre system in operation. Changes in oceanographic conditions occurred towards the end of the Late Eocene, with shallowing global eustatic water depths and, in the Southern Ocean, with development of ice sheets in East Antarctica (Fig. 6.1) (Haq et al., 1987; Nelson and Cooke, 2001). This, in conjunction with development of initial circum-Antarctic polar currents as the Tasman Seaway began to leak and open, resulted in the development of separate warmer and cooler water masses separated by a proto-Subtropical Front in the latest Eocene at high latitudes (Nelson and Cooke, 2001). Water temperatures within the New Zealand region during the Late Eocene probably cooled to cool subtropical

with a significant 'spike' in cooling in the latest Eocene (Fig. 6.1) (Hornibrook, 1992; Nelson and Cooke, 2001). This may have had some effect on the skeletal assemblages ultimately developed on the Chatham Islands with the inclusion of the mollusc *Spondylus* within the Te One Limestone indicating cooler water temperatures than those associated with the older Matanginui Limestone (Appendix D Table D6) (Campbell et al., 1993). While the abundance of planktic foraminifera within the *Victoriella* Limestone was not directly observed in this study, their presence described by Campbell et al. (1993) could also support an increasing global eustatic sea level (Haq et al., 1987) and a regional rise in relative sea level (through the latest Eocene and Oligocene) (Fig. 6.1) (King et al., 1999).

6.4.4 Diagenetic interpretation

The diagenetic characteristics of the Matanginui Limestone are considered to indicate early seafloor and shallow burial/meteoric cementation (see Section 4.1.2). The evidence for early seafloor cementation is readily observed in the field by local hardground development (Figs 3.12, 3.16) and is characterised in thin section by isopachous rinds of dusty to clear fibrous (acicular) or bladed spar cement (Fig. 4.9A & E) (Hood and Nelson, 1996). Otherwise shallow burial/meteoric diagenetic features characterise the Matanginui Limestone in the form of syntaxial rim overgrowths about echinoderm fragments and envelope structures (spar biomoulds) with neomorphism of aragonite elements (Fig. 4.9D & F). Evidence for shallow burial also comes from the cathodoluminescent signatures of the spar cement which show a single bright band of luminescence towards the outer edges of syntaxial rim overgrowths while the acicular shallow marine rind cement has a dull luminescence (Fig. 4.10) (James and Bone, 1989, 1992; Hood and Nelson, 1996).

A similar shallow/meteoric burial diagenetic environment is suggested for the *Victoriella* Limestone where the occurrence of biomoulds indicates that dissolution of aragonite is the likely source of cement (Fig. 4.35C). However, in this case there appears to be little evidence for any early marine cementation (Fig. 4.35) and the depth of burial is considered to be shallower than for the Matanginui Limestone in the absence of luminescent zonations in the spar

cement (Fig. 4.35G & H) (Hood and Nelson, 1996; Dodd and Nelson, 1998; Nelson and James, 2000).

The Te One Limestone shows similar diagenetic features to those developed under a shallow burial/meteoric influence in the South Australian non-tropical carbonates described by James and Bone (1989, 1992) and likely correspond to their soft-friable paragenetic diagenetic stages, although the Te One Limestone overall lacks any pressure dissolution features (Fig. 6.3). Early marine cementation in the Te One Limestone, however, appears not to have generally resulted in the formation of widespread hardgrounds as occurred in the James and Bone (1992) Australian examples and in the Matanginui Limestone. The rarity of biomoulds and neomorphism indicates that few aragonitic species were associated with deposition of the Te One Limestone, leaving the limestone virtually unlithified under shallow burial (Fig. 4.14B). Minor lithification is due to acicular spar rinds and the development of syntaxial rim cement around echinoderm fragments associated with shallow burial (Fig. 4.14) (cf. James and Bone, 1989, 1992).

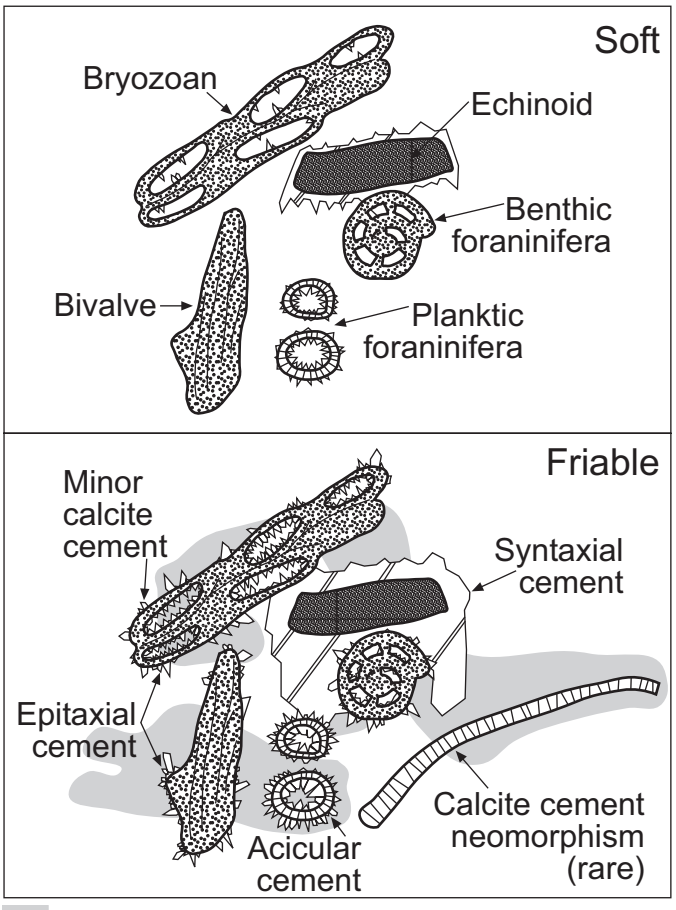

Figure 6.3: Common petrographic attributes of the Te One Limestone, Chatham Island. The Te One Limestone shares some similar characteristics to South Australian limestones (James and Bone, 1989, 1992) that are considered to have been cemented within a marine environment (marine cementation) with later subaerial exposure contributing little to the development of cements associated with meteoric diagenesis. The Te One Limestone does differ from the Australian examples in that there is no pressure dissolution present in the Te One Limestone and it also contains considerably more micrite (Fig. 4.14) (adapted from James and Bone, 1989).

6.5 Taoroa and Altonian limestones (Oligocene-Late Miocene)

The carbonate record for the Chatham Islands is extremely patchy through this time with only two known limestone occurrences, namely the Taoroa Limestone (Waitakian) straddling the Oligocene/Miocene boundary and the Altonian limestone (late Early Miocene-earliest Middle Miocene). Both occurrences are extremely restricted in distribution and show a nannofor skeletal assemblage, comparable to several of the similarly aged mainland New Zealand limestones, but not to the widespread development of bryomol and echinofor assemblages in associated limestones on the mainland (Fig. 6.1) (Hayton et al., 1995). The nannofor assemblage of these Chatham Island limestones indicates deposition in a deepish marine setting with abundant planktic foraminifera, previously interpreted to have been at oceanic mid to outer shelf depths (50-200 m) (Campbell et al., 1993). An outer shelf depth (100-200 m) is preferred here given the abundance of planktic foraminifera in the Chatham Island limestone (Figs 4.16, 4.18 & Appendix D Tables D9, D10 & D11).

During the Oligocene initial deepening may be attributed to global eustatic sea level change and regional maximum marine flooding of the New Zealand subcontinent (Fig. 6.1) (Haq et al., 1987; King et al., 1999). Despite the minor occurrences of Oligocene-Late Miocene limestone on the Chatham Islands, their nannofor composition could also relate to general subsidence of the islands following the Late Eocene. Fluctuating and general falling global eustatic sea level from the Middle Miocene to Pliocene probably removed other more widespread deposits from this time period (Fig. 6.1) (Haq et al., 1987). The divergence in regional depositional trends from those on the Chatham Islands near the Oligocene/Miocene boundary can be directly attributed to uplift of the New Zealand subcontinent associated with the development of active convergence at the Australian-Pacific plate boundary through New Zealand at this time (Fig. 6.1) (King et al., 1999).

Major ice sheets developed on Antarctica during the Oligocene, instigating a general decline in global climate temperatures and subsequent changes in biota through the Oligocene. Intensification of the Antarctic

circum-polar current resulted in development of an Antarctic Polar Front close to the Antarctic continent (60-65°S), 'forcing' the proto-Subtropical Front somewhat further north to 55°S (Nelson and Cooke, 2001). This northward migration of the identified oceanic fronts through the Oligocene, along with the bryozoan dominant nature of the widespread mainland New Zealand limestones, suggests that cool subtropical to warm temperate waters bathed the region at this time (Fig. 6.1) (Nelson, 1978a; Hornibrook, 1992; Hayton et al., 1995; Nelson and Cooke, 2001).

By the Early-Middle Miocene the Southern Ocean was beginning to establish the circum-polar frontal water mass divisions recognised today, with the Antarctic Polar Front positioned at paleolatitudes from 55-65°S (Nelson and Cooke, 2001). The Oligocene/Miocene is not marked by any significant biotic changes (Jenkins, 1993) although the increased flow of circum-polar currents created a major hiatus within the Oligocene, named the Marshall Paraconformity in New Zealand depositional sequences, and this may account for some of the omission of deposits on the Chatham Islands during this time (King et al., 1999; Nelson and Cooke, 2001). A hiatal deposit at the base of the Motarata Limestone (Pliocene; Opoitian) is considered to cover all of Oligocene and Miocene time and may represent a local correlative of the Marshall Paraconformity on the Chatham Islands (Campbell et al., 1993). The division of cold, cool and warm surface water masses resulted in clearly definable circum-polar belts and a slight southward shift in the proto-Subtropical Front to ~50-60°S (position probably defined around New Zealand by the southern continental margin) resulting in warmer subtropical waters around New Zealand during the Early Miocene-Middle Miocene (Hornibrook, 1992; Nelson and Cooke, 2001).

The warming during the Early Miocene continued until 16 Ma, and marked the Neogene climate optimum in the Middle Miocene. From this time on and through the remainder of the Cenozoic climatic conditions cooled and took on the more familiar glacial/interglacial patterns heralded by permanent ice sheet formation in East Antarctica during the later Middle Miocene and then ice sheet formation in West Antarctica during the Late Miocene. With the formation of widespread Antarctic ice sheets and ongoing widening of the Southern Ocean circum-polar flows intensified (Nelson and Cooke, 2001).

Evidence indicates that by this time the proto-Subtropical Front became a fully fledged Subtropical Front as is recognised today, passing across the Campbell Plateau and extending along the Chatham Rise (50°S paleolatitude) influenced by its bathymetric relief. A subdivision of Antarctic water is also evident where development of the Sub-Antarctic Front contoured the continental margin of the southern Campbell Plateau at paleolatitude 58°S while the Antarctic Front lay at a paleolatitude of about 62°S (Nelson and Cooke, 2001). The wider New Zealand region is characterised by deep marine facies through the Middle to Late Miocene with a decline in foraminiferal diversity considered to indicate cooling climatic conditions, although some warm climatic excursions are observed during the Middle Miocene in the north of New Zealand (Hornibrook, 1992).

6.5.1 Diagenetic interpretation

The deep marine limestones from the Late Oligocene-Early Miocene (Taoroa Limestone) and late Early Miocene (Altonian limestone) are considered to have a diagenetic history involving shallow burial and meteoric cementation. Evidence for their diagenetic features is sparse, particularly for the Altonian limestone, but the presence of syntaxial spar rims on rare echinoderm fragments and rare stylolite development in the Taoroa Limestone suggests cement was derived from shallow depths (tens of metres) of burial (Fig. 6.4) (Hood and Nelson, 1996). Meteoric influenced cementation is indicated in the Taoroa Limestone by multiple zones of luminescence towards the edges of the rare syntaxial rim cements (Fig. 4.18E, F, G & H) and possible biomould spar replacement within the Altonian limestone (Fig. 4.39B) (Hood and Nelson, 1996; Caron and Nelson, 2003).

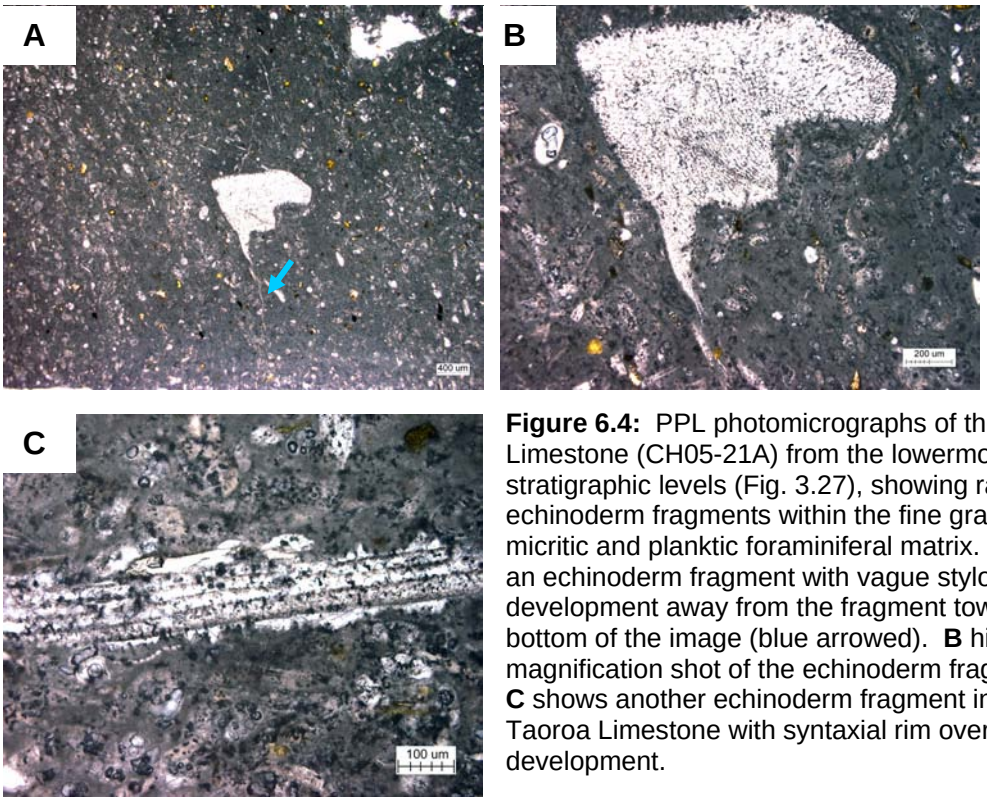

Figure 6.4: PPL photomicrographs of the Taoroa Limestone (CH05-21A) from the lowermost stratigraphic levels (Fig. 3.27), showing rare echinoderm fragments within the fine grained micritic and planktic foraminiferal matrix. **A** shows an echinoderm fragment with vague stylolite development away from the fragment towards the bottom of the image (blue arrowed). **B** higher magnification shot of the echinoderm fragment in A. **C** shows another echinoderm fragment in the Taoroa Limestone with syntaxial rim overgrowth development.

6.6 Motarata, Onoua, Waipipian and Cape L'Eveque limestones (Pliocene-Pleistocene)

The Chatham Islands limestones of Pliocene age have bryomol skeletal assemblages, namely the Motarata Limestone (Opoitian), Onoua Limestone (Waipipian-Mangapanian) and Waipipian limestone (Opoitian-Waipipian). The newly described Cape L'Eveque limestone of likely (Castlecliffian) age contains a bimol assemblage.

The Motarata Limestone, otherwise dominated by bryozoans, also has a significant foraminiferal component (particularly planktics) and is considered to represent deposition at an oceanic mid to outer shelf depth (50-200 m) based on the assemblage of benthic foraminifera and large *Bradleya* spp. ostracods (Appendix D Table D12) (Campbell et al., 1993).

The Onoua Limestone was probably deposited in a relatively low energy environment with a lack of terrigenous input, based on the inclusion of thin shelled mollusca like *Cirsotrema* and large well preserved bryozoans (Appendix D Table D13) (Campbell et al., 1993). The presence of the

barnacles *Pachylasma distortum* and *Austromegabalanus (Notomegabalanus) miodecorus* suggests possible upper shelf depths, while the Chatham Islands endemic species of *Fosterella chathamensis* suggests cooler water temperatures (Campbell et al., 1993). Microfossil assemblages of benthic foraminifera with common *Elphidium*, along with planktic foraminifera and the ostracod *Bradleya*, are compatible with oceanic mid to outer shelf depths (50-200 m) (Appendix D Table D14) (Campbell et al., 1993).

The extremely restricted exposure of Waipipian limestone is considered to represent shallow marine, possibly mid to outer shelf carbonate (indicated by the bivalves *Purpurocardia*, *Dosinia* and *Tawera*) (Appendix D Table D15) (Campbell et al., 1993).

The Pleistocene aged Cape L'Eveque limestone is considered to be a shallow inner to mid shelf carbonate given the abundance of bryozoan, bivalve and calcareous algal (euphotic zone) fragments, in association with abundant volcaniclastic material (Fig. 4.47). This deposit probably represents a nearshore environment and is envisaged to have formed upon a wave planed shelf cut into the Southern Volcanics.

The bryomol assemblage through the Pliocene indicates that water depths were relatively shallow through this time (mid to outer shelf, 50-200 m) but probably mainly deeper than many mainland New Zealand limestones of this age which have a conspicuous barnamol/bimol composition during a regional depositional trend associated with an overall relative fall in sea level (Fig. 6.1) (Hayton et al., 1995; King et al., 1999). New age ranges on the Rangitihi Volcanics (5-4 Ma) during the earliest Early Pliocene indicate some subaerial exposure (basaltic lava flows and pillow basalts) in the north of Chatham Island which may be directly attributed to lowered global eustatic sea levels (Fig. 6.1) (Haq et al., 1987; Panter et al., 2006). A sharp rise in eustatic sea level (max. 100 m) post earliest Early Pliocene could conceivably be represented by the Motarata, Onoua and Waipipian limestones. Another sharp fall in eustatic sea level observed at the beginning of the Late Pliocene (Waipipian-late Nukumaruan) could have conceivably terminated carbonate deposition as none of these limestones is reported as being older than Mangapanian (earliest Late Pliocene) (Fig. 6.1) (Haq et al., 1987; Campbell et al., 1993).

The occurrence of the siliciclastic Titirangi Sand (Late Pliocene; Nukumaruan) above a prominent unconformity upon the underlying Motarata Limestone at Moutapu Point on the western shore of Te Whanga Lagoon has previously been interpreted as indicating uplift of the Chatham Islands into its present subaerial situation (Figs 3.29, 4.0) (Campbell et al., 1993). Fluctuating eustatic sea levels through the Pleistocene along with continued uplift of the New Zealand subcontinent make comparisons difficult (Fig. 6.1), but these fluctuations are marked on the Chatham Islands by several siliciclastic (near shore/beach) and terrestrial (sands and peat) deposits (Fig. 4.0) (Campbell et al., 1993). Many of these deposits are Late Pleistocene (Haweran) in age and their preservation can only be attributed to subaerial exposure of the islands (Campbell et al., 1993).

The comment is made here that the perceived initiation of uplift associated with the deposition of Titirangi Sand may also conceivably be a function of a fall in global eustatic sea level in the latest Late Pliocene (Nukumaruan) as the position of this unconformity is near present sea level which is similar to that in the latest Late Pliocene (Fig. 6.1) (Haq et al., 1987; Pillans et al., 1998). Another indicator of uplift (at least in the southern Chatham Islands) may be the occurrence of the recently described shallow marine Cape L'Eveque limestone, which possibly supports uplift since the Plio-Pleistocene. The limestone currently sits at ~178 m elevation above sea level and, presuming the Castlecliffian age (based on the pectinid *Pecten novaezelandiae*) is correct, than a rate of southern uplift would be about 0.1 mm/year since the Early Pleistocene. However, recent Ar-Ar dates obtained on the surrounding volcanics may have implications for the correct identification of the pectinid (placing it as a possible new Pliocene aged genus) which would significantly alter this rate of uplift (H. Campbell, GNS Science, pers. comm., 2007).

The Southern Ocean fronts situation is envisaged to have been much the same as modern conditions, particularly during interglacial periods with the Sub-Antarctic Front contouring the margin of the southern Campbell Plateau (~50-55°S) and the Subtropical Front 'sweeping' around the shelfal depth of the lower South Island (~48°) and north to the Chatham Rise (44°S), following its extent to the east (Nelson and Cooke, 2001). However, during glacial

periods there was northward migration of both the Antarctic Polar and Sub-Antarctic Fronts by 5-10°, but it is unclear whether the Sub-Antarctic Front extended across the Campbell Plateau or whether there was any associated northward migration of the Subtropical Front (Nelson and Cooke, 2001). The position of the Pliocene/Pleistocene Subtropical Front must result in upwelling of nutrient rich deep ocean cool temperate waters associated presently with the Southland Current (Chatham-Islands-Conservation-Board, 1996). This may in some respects account for the differences in Chatham Island skeletal assemblages though the Pliocene from those in mainland New Zealand limestones.

6.6 1 Diagenetic interpretation

The Motarata Limestone is an extremely soft foraminiferal limestone that is not considered to have undergone any significant degree of burial from which cements could be derived. Some early marine cementation appears to be present as most skeletal fragments do support extremely thin fibrous spar rinds (Fig. 4.22) (Hood and Nelson, 1996). Equant interparticle spar present in some thin sections may be associated meteoric cementation by calcite laden pore water fluids (Fig. 4.22D) (James and Bone, 1992; Hood and Nelson, 1996). Similarly the Onoua Limestone also appears to contain some early marine cements, more easily recognisable around large bryozoan fragments where it is generally more acicular in nature (Fig. 4.26). Meteoric diagenesis is also evidenced by intraparticle spar fills and interparticle spar with some neomorphism of bivalve fragments (Hood and Nelson, 1996; Caron and Nelson, 2003; Ricketts et al., 2004).

The diagenetic history of the Waipipian limestone is problematic as there is virtually no spar cements present with any distinctive diagenetic characteristics, only some inter- and intraparticle micrite (Fig. 6.2). Spar cements occurring as intraparticle fringes may be interpreted as being any of early marine, shallow burial or meteoric origin (Fig. 4.43). Similarly the Cape L'Eveque limestone does not appear to have any characteristics associated with early marine cementation and is probably better considered to have lithified by meteoric diagenetic processes with some interparticle spar cement

present and an absence of any characteristics associated with deep burial (Fig. 4.47).

6.7 Depositional and diagenetic summary

The skeletal assemblages in limestones on the Chatham Islands record a history of deposition extending from the Late Cretaceous to Pleistocene times. Carbonate deposition during the Late Cretaceous took place in cool (possibly warm) subtropical outer shelf water depths (100-200 m) with formation of bryomol limestones that were closely associated with the Southern Volcanics and Kahuitara Tuff. This volcanic association exerted a strong influence on the depositional water depths and the morphology of the Haumurian limestone.

Carbonate deposition on Chatham Island in the Late Paleocene-Early Eocene records deposition of carbonate by preferential sorting by bottom water currents to form carbonate shoals and banks of bryomol/bimol assemblage in protected and quite mid to outer shelf (50-200 m) water depths. These carbonate shoals and banks of Tumaio Limestone represent a lateral equivalent of the siliciclastic Tutuiri Greensand, accumulating in cool subtropical waters.

Carbonate deposition on the Chatham Islands during the Eocene is well represented with widespread deposition of the Matanginui Limestone and the overlying thick carbonate deposits of the Te One Limestone, along with a minor occurrence of the *Victoriella* Limestone at the Eocene/Oligocene boundary. Carbonate deposition during this time is marked by bryomol assemblages and water temperatures are considered to have warmed from the Paleocene to warm subtropical throughout the Eocene. Initial Early Eocene Matanginui Limestone deposition indicates shallow inner shelf (0-50m) water depths which deepened through the Late Eocene to mid shelf (50-100 m) water depths during deposition of the Te One Limestone and to outer shelf (100-200 m) depths by the close of the Eocene with deposition of the *Victoriella* Limestone. This succession possibly reflects localised thermal uplift associated with emplacement of the Red Bluff Tuff during the Early

Eocene followed by gradual subsidence towards the Oligocene. The volcanism associated with emplacement of the Red Bluff Tuff exerted a strong depositional and morphological influence on carbonate deposition through the Eocene, but was most pronounced in the Early Eocene during deposition of the Matanginui Limestone.

The Oligocene-Late Miocene carbonate record is sparsely represented on the Chatham Islands with only two nannofor limestone occurrences reflecting deepish marine, outer shelf water depths (100-200 m) of deposition through this time. The nannofor assemblage may relate to high eustatic sea levels and hiatal regional depositional trends at this time, and continued subsidence of the Chatham Islands with only minor volcanism recorded. The formation of major ice sheets on Antarctica resulted in a decline in water temperatures to cool subtropical during the Oligocene. Water temperatures warmed (warm subtropical) during the Early Miocene with southward migration of the proto-Subtropical Front (established in the mid Eocene) and then cooled (cool subtropical) during the Late Miocene with full establishment of the Southern Ocean frontal system that occurs today.

The Pliocene carbonate succession (marked by the Motarata, Onoua and Waipipian limestones) shows a dominant bryomol skeletal assemblage deposited in waters of mid to outer shelf (50-200 m) depth, probably during an overall rise in eustatic sea level during the Early Pliocene. The occurrence of a nearshore (inner shelf, 0-50 m) volcaniclastic Cape L'Eveque limestone during the mid Pleistocene is considered to be related to uplift of the Chatham Islands which resulted in their current subaerial exposure. Water temperatures through the Pliocene and Pleistocene probably fluctuated from cool subtropical to subantarctic with respective rises and falls in eustatic sea level associated with Northern Hemisphere glaciations. The Chatham Rise has probably been the site of subtropical water mass convergence throughout this time, as it is today, forced in part by its bathymetric relief.

As a whole, carbonate diagenesis in Chatham Islands limestones occurred at relatively shallow burial depths in the absence of features characterising any great degree of burial, such as pressure dissolution structures. Minor compaction related features are rarely observed and it is therefore concluded that in their absence, and the relatively limited evidence

for widespread early marine cementation, that meteoric cementation processes are a major contributor to the lithification of limestones on the Chatham Islands (Fig. 6.5). Meteoric cementation is considered to have occurred within the phreatic and marine phreatic environment with dissolution of aragonite (probably at the marine/freshwater interface) providing a source of cements. Any vadose cemented units have subsequently been removed from the Chathams rock record.

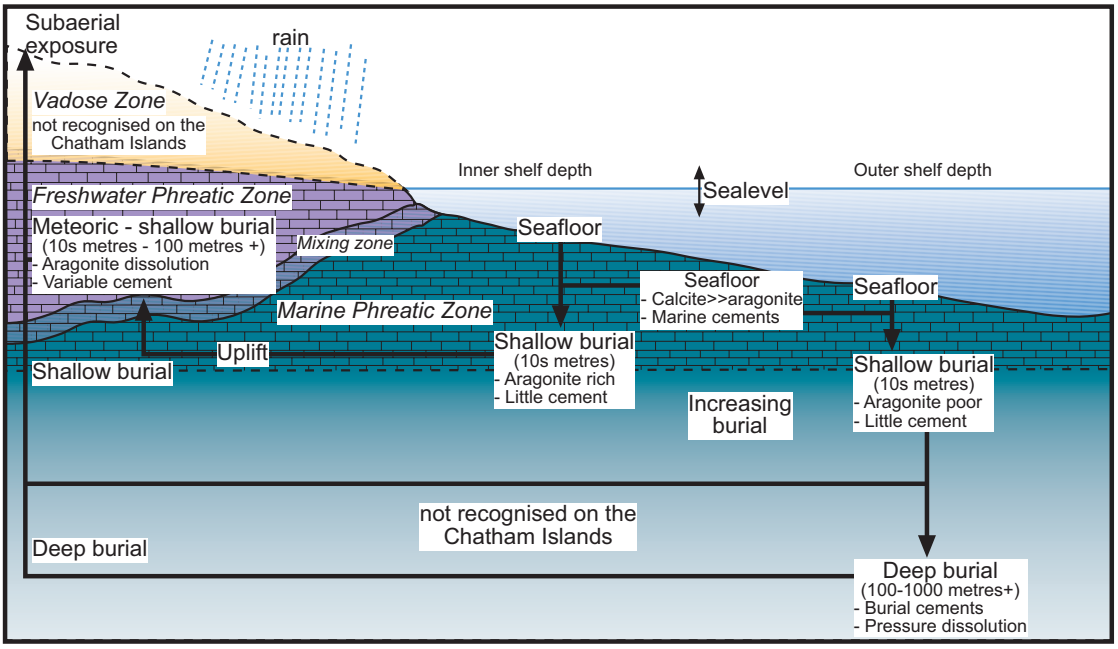

Figure 6.5: Diagenetic model for the Chatham Island carbonates. Faded and non-textured areas represent diagenetic environments not recognised for the Chatham Island limestones. Marine and meteoric diagenetic environments are considered to represent the main zones of cementation, with no great depth of burial (less then a few tens of metres). Any vadose zone cementation is considered to have been removed from the rock record (adapted from Hood and Nelson, 1996).

6.7.1 Origin of micrite

Micrite is widespread as both an intra- and interparticle fill within Chatham Islands limestones, it occurring within all the samples analysed in this study. Predominantly the intra- and interparticle micrite observed is considered to be of precipitated origin, either clotted (micropeloidal) or homogeneous (Reid et al., 1990; Nelson and James, 2000). These types of micrite are considered to be precipated within marine phreatic environments,

typically those associated with high energy depositional systems (Reid et al., 1990).

Microbioclastic micrite is also observed in some samples, identified by the inclusion of fine fragmented skeletal material. The extremely fine sizes of this micrite type could mean that it has been underestimated in this study. However, the occurrence of microbioclastic micrite does present a problem in that it is generally considered to be associated with deposition in relatively low energy settings (Reid et al., 1990). While it is conceivable that the carbonate environments on the Chatham Islands during the Cenozoic experienced relatively lowered energy conditions at times of deepening water depths associated with subsidence or rising sea levels, it is generally considered they occupied oceanic high energy depositional settings (Fig. 6.6). It has been suggested that reworked or *in situ* deposits of microbioclastic micrite may be washed into pore spaces of shallow marine limestones in relatively high energy environments during periods of lowered sea level, producing bryozoan dominated packstones (Nelson and James, 2000).

6.8 Depositional model

A depositional model has been developed for carbonate formation on the Chatham Islands based on the characteristics of the limestone occurrences (Fig. 6.6). The Chatham Islands are considered to represent an oceanic island high energy depositional environment.

A major control on carbonate production is considered to have been the input of volcanically derived material during periods of active intra-plate volcanism. The types of carbonate deposits are considered to be a function of the associated thermal uplift and subsequent subsidence, global eustatic sea level change and the development and position of Southern Ocean fronts within the New Zealand region.

The depth of deposition controlled by uplift/subsidence in conjunction with sea level change and energy conditions control grain size and skeletal assemblages and dictate the types of intra- and interparticle material. The bathymetric relief of the Chatham Rise is considered to have probably always

been a site of nutrient upwelling and water mass convergence of warmer northern and cooler southern waters. Upwelling of cooler nutrient rich bottom waters fosters cool-water carbonate production in the absence of any volcaniclastic sedimentation.

Development and position of ocean fronts within the New Zealand region of the Southern Ocean has resulted in periodic shifts from warm to cool subtropical water masses during the Late Cretaceous to Middle Miocene and from warm to cool (present) temperate water masses from the Late Miocene to the present.

The Chatham Islands are considered to represent a carbonate ramp, although deeper slope conditions exist along the southern continental margin and distally to the north and east. Carbonate deposition in association with volcanics controls the geometry and emplacement mechanisms of some carbonate deposits.

THE CHATHAM ISLANDS: A COOL-WATER, HIGH ENERGY, OCEANIC CARBONATE DEPOSITIONAL ENVIRONMENT

Chatham Islands depostional model for steepened ‘shelf-like’ southern region and distal northern edge of the Chatham Rise

calcite dominated ← SKELETAL MINERALOGY → *calcite & aragonite dominated*

APHOTIC CARBONATE PRODUCTION

PHOTIC PRODUCTION

Oceanic, high energy

kelp forests

Zone of wave abrasion

Thermocline

Swell wave base

Storm wave base

Upwelling

Resedimentation

azooxanthellate coral mounds

bryozoan/sponge mounds

SLOPE
- bryozoans
- azooxanthellate corals
- bivalves
- gastropods
- planktic foraminifera
- ostracods

OUTER SHELF
- bryozoans
- serpulids
- barnicles
- sponges
- bivalves
- echinoderms
- benthic & planktic foraminifera

MIDDLE SHELF
- kelp
- molluscs
- benthic forams
- coralline algae
- bryozoans
- sponges
- echinoderms

INNER SHELF
- kelp
- molluscs
- calcarious algae
- bryozoans
- echinoderms

Thermal uplift and subsidence

Deep seated thermal convection and associated intra-plate volcanism

Chatham Island depostional model for shallower ‘ramp’ western region and much of eastern region before terminus of the Chatham Rise

Rising eustatic sea-level / Falling eustatic sea-level

Periodic topographically forced water mass convergence, warm/cool subtropical (Late Creatceous-Mid Miocene), warm/cool temperate Late Miocene-present)

Red Bluff Tuff mounds

Oceanic, high energy

Southern Volcanics (Kahuitara Tuff)

INNER RAMP

MIDDLE RAMP

OUTER RAMP

Upwelling

Resedimentation (minor)

‘SLOPE’ DEPTH

Chatham Schist (basement)

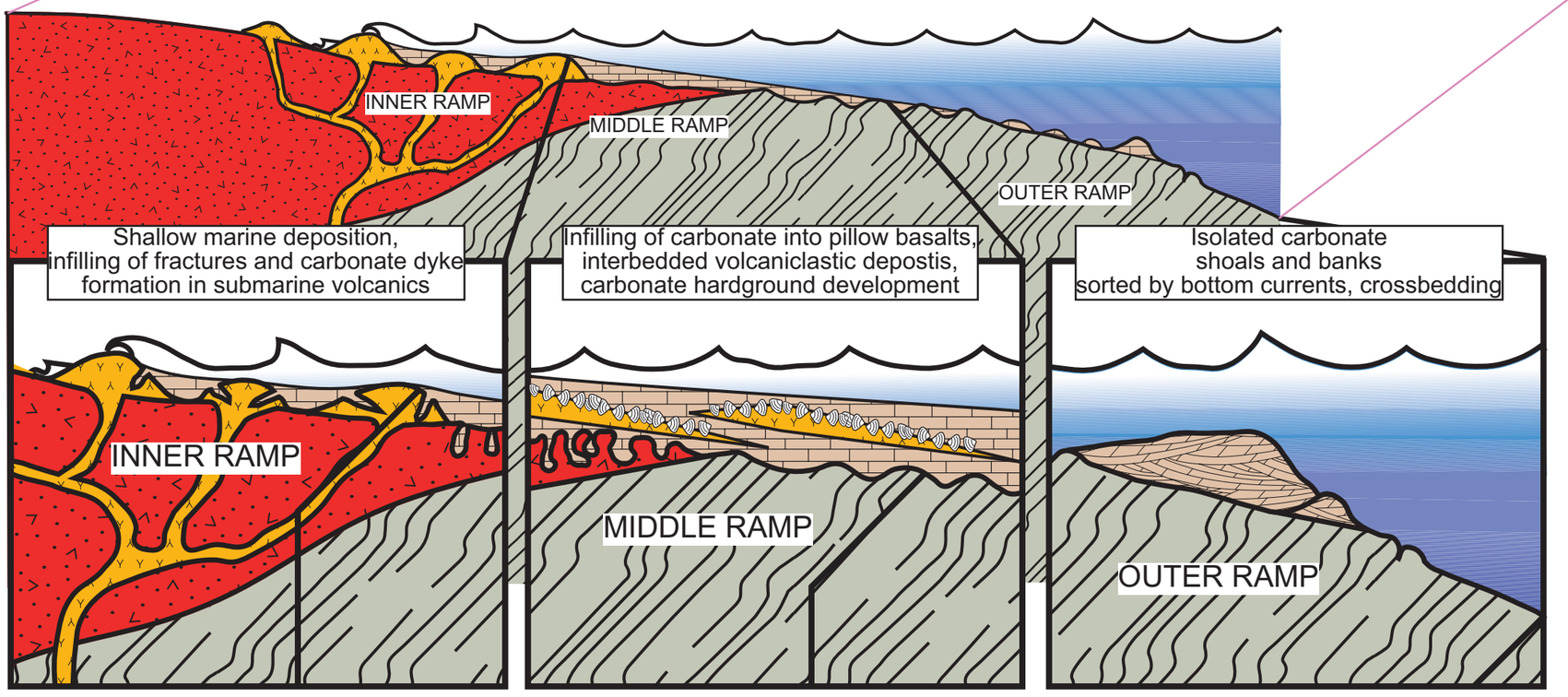

- Fossiliferous Beds
- Tertiary Limestone
- Tertiary Volcanics
- Late Cretaceous Volcanics
- Mesozoic Basement

Figure 6.6: Depositional model for Chatham Island carbonates. The main control on carbonate production is considered to be the input of volcaniclastic sediment with the type of carbonate deposit controlled by associated thermal uplift and subsidence, global eustatic sealevel change and fluctuating water temperatures associated with the development and position of Southern Ocean fronts through the Cenozoic. The upwelling of nutrient rich water is likely to have occurred for as long as the Chatham Rise has been a prominent bathymetric feature. The oceanic setting of the Chatham Islands means that this is a high energy, predominantly carbonate ramp depositional system, with steepening slope conditions to the south of the islands and distally to the north (diagram concept from James, 1997).

CHAPTER 7
Conclusion: Some Comments on the Chatham Islands Limestones as Temperate Carbonate Facies

The Chatham Islands are unique as a temperate latitude carbonate depocentre in that the accumulation of carbonate sediment has taken place on the flanks of an isolated cluster of intra-plate volcanoes and associated volcanic structures within a fully oceanic setting (Table 7.1). The uniqueness derives from the fact that the production of carbonate was strongly controlled and influenced by the distribution and degree of active volcanism. The volcanic structures at times grew to create shallow shelfal depth environments in which carbonate deposition could take place. Such settings were inevitably relatively restricted in distribution compared to the expansive cool water carbonate continental shelf margins occurring, for example, off southern Australia (James & Bone, 1989, 1992), and to the north and south of mainland New Zealand (Nelson et al., 1988b). The limited distribution of limestone units seen today on Chatham Islands may well partly reflect a limited extent of the original carbonate factory areas about the volcanic edifices.

The majority of the skeletal assemblages in the limestones on the Chatham Islands are those typical of temperate carbonate facies, and especially the predominance of bryomol carbonates which are widespread in cool- to warm-temperate depositional environments worldwide (Nelson, 1988; James 1997). Fully tropical carbonate facies, characterised by coral reef development, carbonate mud derived from calcareous green algae, and inorganically precipitated grains like ooids, are absent from the Chatham Islands record (Table 7.1).

The Chatham Islands have been positioned at temperate latitudes (40-55°S) throughout the Cenozoic (Fig. 6.1). However, temperate latitude sea water can vary in temperature as a function of the global ice budget. Fig. 6.1 demonstrates that in a greenhouse, essentially ice-free world, as in the early

Tertiary, warmish temperatures expand to high latitudes. Following ice build up on Antarctica since about the Late Eocene and the onset of icehouse conditions the world oceans have cooled at mid to high latitudes with evolution of latitudinal zones of contrasting surface water masses separated by major oceanic fronts. The effect has been to generally cool oceanic temperatures at mid latitudes (Fig. 6.1).

To an extent the temperate limestones on the Chatham Islands reflect these long term temperature contrasts. Prior to about mid-Tertiary times the sporadic occurrence of stromatolite development and preservation, and of hardgrounds, and the local importance of marine cements, large benthic foraminifera (e.g. *Asterocyclina*) and certain other taxa (e.g. the bivalve *Spondylus*, the brachiopods *Probolarina*, *Thecidellina* and *Lingula*, and the echinoderm *Eucidaris*), are indicative of marine temperatures towards the warm to very warm end of the spectrum of temperate carbonates (i.e. warm temperate or cool subtropical conditions). However, since the Oligocene the Chatham Islands limestones tend to reflect overall cooler temperatures, typically cool temperate to rarely even subantarctic (Table 7.1).

The above discussion highlights the problem of using terms like “warm-water carbonates” and “cool-water carbonates” as globally contrasting limestone facies without adequately defining the marine climatic regime more specifically. In a nutshell, cool-water limestones can form in warm waters but not so warm as to develop all those sedimentological and biological attributes characteristic of so-called tropical carbonates (Nelson, 1988; James, 1997).

The Chatham Islands have remained relatively tectonically stable in relation to mainland New Zealand, allowing for on-going, if sporadic, carbonate deposition throughout the Cenozoic. This is primarily a function of the large distance (>800 km) from the actively convergent plate boundary through New Zealand (Fig. 2.1). However, the Chatham Islands limestones have been variably shaped and influenced by coeval episodic volcanism, reflected by the common occurrence of included volcaniclastic material in many of the limestones. In the field some limestones interfinger with volcaniclastics, like the Matanginui Limestone within the Red Bluff Tuff (Figs 3.14 & 3.15) and the Onoua Limestone within the Whenuataru Tuff (Fig. 3.32), while the former in particular shows a close association exists between some

periods of volcanic activity, stress field fracturing and limestone dyke formation as passive fills or through forceful injection (Fig. 5.2b). In the case of the Late Cretaceous Haumurian limestone the only evidence of what was once likely a rather more widespread deposit is the local occurrence of the carbonates preserved in dykelets in basaltic volcanics at Flowerpot Bay on Pitt Island and Ngakuha Reef on Chatham Island. While the Chatham Islands have remained submerged throughout much of the Cenozoic with consequently little or no terrigenous input to interfere with carbonate production, the deposition and geometry of the Chatham Islands limestones have been strongly influenced at times by coeval volcanic activity (Table 7.1).

The oceanic position of the Chatham Islands means that it has been overall a predominantly high energy depositional setting. This has resulted in a situation whereby deeper water bioclastic micrite may be reworked and washed into interparticle pore spaces in many of the Chatham Island limestone occurrences. The occurrence of precipated interparticle micrite types (both homogenous and clotted micrite) is indicative of at times at least sporadic early marine cementation, which is also evidenced by the occurrence of acicular fringing cements about many bioclasts in thin section and also in the field by the formation of hardgrounds in some units (Table 7.1). Oceanic current upwelling may have played an important role here, enhanced by the upstanding topography of the Chatham Rise itself and by the volcanic edifices underpinning the Chatham Islands. This same upwelling would have provided and replenished nutrients in support of the biotic communities.

The relative tectonic stability of the Chatham Islands has meant the Cenozoic sedimentary record has experienced relatively little burial. Consequently many of the limestone units are soft or friable, virtually unlithified, as is particularly evident for the Te One Limestone and the foraminiferal Motarata Limestone. However, there is widespread evidence for at least patchy meteoric diagenesis in the presence of scattered biomoulds, syntaxial and epitaxial rim cements, and cathodoluminescent signatures which often display multiple bright zones of luminescence towards the edges of spar cements. The occurrence of micritic and bioclastic intraclasts in many of the Chatham Islands limestones suggests that some aggregation (incipient cementation) of carbonate material has taken place within the carbonate

depositional setting (Table 7.1). If this is indeed the case then the observation contrasts with most documented cool-water carbonate systems.

This study is the first detailed petrographic study of Chatham Islands limestones in regards to their skeletal assemblages and diagenetic characteristics. It has shown that several aspects about the deposition of carbonate facies on the Chatham Islands diverge in small to moderate ways from those given for typical cool water depositional models. This relates especially to the unique setting of the Chatham Islands which is best regarded as a fully oceanic intra-plate volcanic island group, which has been submerged throughout much of the Cenozoic accumulating carbonate deposits at mainly shelfal depths on the flanks of volcanic edifices, and often in conjunction with the coeval eruption and deposition of volcanic deposits. The Chatham Islands limestones afford a unique set of features that represent deposition across the cool temperate, warm temperate and cool subtropical oceanic realms.

While this study has covered many new aspects about the limestones on the Chatham Islands it is relavent to mention that other more detailed petrographic-diagenetic-geochemical work is also currently underway by Canadian professors Noel James (Queens University) and Brian Jones (University of Alberta). These studies should provide a better paragenetic sequence of depositional and diagenetic events for the limestones. When this is available, a closer comparison is deserved between the Chatham Islands limestones and those of comparable ages on mainland New Zealand (e.g. Nelson, 1978b). Also the limestone dykes on the Chathams deserve further study as to their age and origins, especially the Late Cretaceous Haumurian occurrences. Again a comparison with sedimentary dykes in the mainland New Zealand record (e.g. in coastal Wairarapa, North Canterbury and Oamaru districts) would be a worthwhile study, delineating more fully the distribution, origin and significance of these enigmatic geologic structures.

Table 7.1: Comparison of several attributes of warm- and cool-water shelf carbonate systems with the characteristics of Chatham Islands observed in this study (adapted from Nelson, 1988 and James, 1997).

Environmental and facies parameters	WARM-WATER CARBONATES (>18°C) Tropical-Subtropical	CHATHAM ISLANDS LIMESTONES Subtropical - Temperate	COOL-WATER CARBONATES (<18°C) Temperate-Subpolar
Setting			
Latitude	0° to 30° S or N	50° to 43° S	30° to 50° N or S
Depositional	Reefs, shallow rimmed shelves, open shelves, ramps	Open narrow ramps on volcanic flanks	Slope mounds, open shelves or ramps
Tectonic	Stable	Relatively stable, intraplate volcanism	Stable to unstable
Terrigenous supply	Low	Low	Low to high
Water properties			
Mean temperature	Above 23°C	Late Cretaceous - Miocene = warm temperate Miocene - present = cool temperate	>10°C to 25°C
Minimum temperature	About 14°C		
Bottom water temperature	~18 to 22°C		~10 to 18°C
Salinity	Normal to hypersaline		Normal to reduced
Carbonate saturation	Supersaturated to saturated		Saturated to undersaturated
Circulation	Restricted to open		Open
Structures			
Reefs	Few reefs	Absent	Rare to absent
Algal mats & stromatolites	Common	Some	Absent or not preserved
Bulk sediment properties			
Carbonate content	Very high (>90%)	High (70%)	Moderate to very high (50-100%)
Texture	Muds, sands and gravels	Muds, sands and gravels	Mainly sands and gravels
Sedimentation rate	Relatively high (>10 cm/1000 y)		Relatively low (< 10 cm/1000 y)
Non-skeletal carbonate components			
Ooids	Common	Absent	Absent
Aggregates	Common	Some	Absent
Peloids	Common	Absent	Rare or absent
Major skeletal carbonate components	*Heterozoan* + minor *Photozoan*	*Heterozoan* + minor *Photozoan*	*Heterozoan*
Flora	Calcareous green algae Calcareous red algae	Calcareous red algae	Calcareous red algae Coccolithophorids
Fauna	Hermatypic corals Benthic foraminifers Molluscs	Bryozoans, bivalve molluscs Benthic & planktic foraminifers, barnacles Echinoderms, serpulids, brachiopods	Bryozoans, bivalve molluscs Benthic foraminifers, barnacles Echinoderms, serpulids, brachiopods
Skeletal attributes			
Shell thickness	Thick		Mainly thinner
Rates of production	High		Low to high
Diversity	High		Mainly lower
Equitability	Low		Mainly higher
Shell preservation	Generally good		Poor to good
Non-carbonate components			
Terrigenous material	Rare	Abundant, volcanic clasts	Rare to abundant
Glauconite	Rare	Common	Common
Diagenesis			
Carbonate mud	Minor carbonate mud	Common	Rare, locally common
Origin of carbonate mud	Mainly floral disaggregation, bioerosion, ?cementation minor	Skeletal abrasion, bioerosion, maceration, boring, patchy cementation	Minor, mainly skeletal abrasion, bioerosion, maceration, boring, ?cementation minor
Carbonate mineralogy	Aragonite + calcite		Low- and/or high-Mg calcite dominant

References

Allan, R.S., 1930: Chatham Islands - the physical features and structure. *Transactions of the New Zealand Institute*, *59*:824-839.

Archer, J., 1984: Clastic intrusions in deep-sea fan deposits of the Rosroe Formation, lower Ordovician, western Ireland. *Journal of Sedimentary Petrology*, *54*:1197-1205.

Austin, P.M., Sprigg, R.C. and Braithwaite, J.C., 1973: Structure and petroleum potential of eastern Chatham Rise, New Zealand. *American Association of Petroleum Geologists Bulletin*, *57*:477-497.

Ballance, P.F., 1976: Evolution of the Upper Cenozoic magmatic arc and plate boundary in northern New Zealand. *Earth and Planetary Science Letters*, *28*:356-370.

Ballance, P.F., 1993: The New Zealand Neogene forearc basins. *In*: Ballance, P.F. *ed*. Sedimentary Basins of the World - South Pacific Sedimentary Basins. 2. Amsterdam, Elsevier. Pp. 177-191.

Beacom, L.E., Anderson, T.B. and Holdsworth, R.E., 1999: Using basement-hosted clastic dykes as syn-rifting palaeostress indicators: an example from the basal Stoer Group, northwest Scotland. *Geological Magazine*, *136*:301-310.

Beavon, R.V., 1998: Archean neptunian fissures and early history of the Destor-Porcupine fault zone, Timmins, Ontario, Canada. *Canadian Journal of Earth Sciences*, *35*:1402-1408.

Beggs, J.M., 1993: Depositional and tectonic history of the Great South Basin 2. *In*: Ballance, P.F. *ed*. Sedimentary Basins of the World - South Pacific Sedimentary Basins. Amsterdam, Elsevier. Pp. 365–373.

Boulvain, F., Cornet, P., da Silva, A.C., Delaite, G., Demany, B., Humblet, M., Renard, M. and Coen-Aubert, M., 2004: Reconstructing atoll-like mounds from the Frasnian of Belgium. *Facies*, *50*:313-326.

Bradshaw, J.D., Andrews, P.B. and Adams, C.J.D., 1981: Carboniferous to Cretaceous on the Pacific margin of Gondwana: the Rangitata phase of New Zealand. Fifth International Gondwana Symposium. Wellington, New Zealand. Pp. 217-221.

Buckeridge, J.S., 1984: Two new Tertiary scalpellid barnacles (Cirripedia: Thoracica) from the Chatham Islands, New Zealand. *Journal of the Royal Society of New Zealand*, *14*:319-326.

Campbell, H.J., Andrews, P.B., Beu, A.G., Edwards, A.R., Hornibrook, N. de B., Laird, M.G., Maxwell, P.A. and Walters, W.A., 1988: Cretaceous-Cenozoic lithostratigraphy of the Chatham Islands. *Journal of the Royal Society of New Zealand*, *18*:285-308.

Campbell, H.J., Andrews, P.B., Beu, A.G., Maxwell, P.A., Edwards, A.R., Laird, M.G., Hornibrook, N. de B., Mildenhall, D.C., Watters, W.A., Buckeridge, J.S., Lee, D.E., Strong, C.P., Wilson, G.J. and Hayward, B.W., 1993: Cretaceous-Cenozoic geology and biostratigraphy of the Chatham Islands, New Zealand. *Institute of Geological & Nuclear Sciences monograph 2*:269.

Caron, V. and Nelson, C.S., 2003: Developing concepts of high-resolution diagenetic stratigraphy for Pliocene cool-water limestones in New Zealand, and their sequence stratigraphy. *Carbonates and Evaporites*, *18*:63-85.

Carter, A.N., 1978: Phosphatic nodule beds in Victoria and the late Miocene-Pliocene eustatic event. *Nature*, *276*:258-259.

Chatham-Islands-Conservation-Board, 1996: The Chatham Islands - heritage and conservation. Christchurch, Canterbury University Press in association with the Department of Conservation. 136 p.

Cooper, M.R., 1977: Eustacy during the Cretaceous: its implications and Importance. *Palaeogeography, Palaeoclimatology, Palaeoecology*, *22*:1-60.

Cullen, D.J., 1967: Chatham Islands, provisional bathymetry, New Zealand Oceanographic Institute chart, island series 1:200,000. Wellington, Department of Scientific and Industrial Research.

Cullen, D.J., 1969: Chatham bathymetry, New Zealand Oceanographic Institute chart, oceanic series, 1:1,000,000. Wellington, Department of Scientific and Industrial Research.

Cullen, D.J., 1980: Distribution, composition and age of submarine phosphorites on Chatham Rise, east of New Zealand. *SEPM Special Publication*, *29*:139-148.

Curtis, M.L. and Riley, T.R., 2003: Mobilization of fluidized sediment during sill emplacement, western Dronning Maud Land, East Antarctica. *Antarctic Science*, *15*:393-398.

Davey, B. and Wood, R., 1994: Gravity and magnetic modelling of the Hikurangi Plateau. *Marine Geology*, *118*:139-151.

Davey, B.W., 1993: The Bounty Trough — basement structure influences on sedimentary basin evolution. *In*: Ballance, P.F. *ed*. Sedimentary Basins of the World - South Pacific Sedimentary Basins 2. Amsterdam, Elsevier. Pp. 69-92.

Davey, F.J., 1977: Marine seismic measurements in the New Zealand region. *New Zealand Journal of Geology & Geophysics*, *20*:719-777.

Demoulin, A., 1996: Clastic dykes in east Belgium: Evidence for upper Pleistocene strong earthquakes west of the Lower Rhine rift segment. *Journal of the Geological Society*, *153*:803.

Dickson, J.A.D., 1965: A modified staining technique for carbonates in thin section. *Nature*, *205*:587.

Dieffenbach, E., 1841: An account of the Chatham Islands. *Journal of the Royal Geographical Society of London*, *11*:195-215.

Dodd, J.R. and Nelson, C.S., 1998: Diagenetic comparisons between non-tropical Cenozoic limestones of New Zealand and tropical Mississippian limestones from Indiana, USA: Is the non-tropical model better than the tropical model? *Sedimentary Geology*, *121*:1.

Dreimanis, A. and Rappol, M., 1997: Late Wisconsinan sub-glacial clastic intrusive sheets along Lake Erie bluffs, at Bradtville, Ontario, Canada. *Sedimentary Geology*, *111*:225-248.

Dunham, R.J., 1962: Classification of carbonate rocks according to depositional texture. *Classification of carbonate rocks: American Association of Petroleum Geologists Memoir*, *1*:108-121.

Field, B.D., Browne, G.H., Davy, B., Herzer, R.H., Hoskins, R.H., Raine, J.I., Wilson, G.J., Sewell, R.J., Smale, D. and Watters, W.A., 1989: Cretaceous and Cenozoic sedimentary basins and geological evolution of the Canterbury Region, South Island, New Zealand. New Zealand Geological Survey basin studies 2. Lower Hutt, N.Z., New Zealand Geological Survey. 94 p.

Fleming, C.A., 1975: The geological history of New Zealand and its biota. *In*: Kuschel, G. *ed*. Biogeography and ecology in New Zealand. Hague, W. Junk B.V. Publishers. Pp. 1-86.

Fleming, C.A., 1979: The geological history of New Zealand and its life. Auckland, Oxford University Press. 141 p.

Flugel, E., 1982: Microfacies analysis of limestones. Berlin, Springer-Verlag. 633 p.

Grindley, G.W., Adams, C.J.D., Lumb, J.T. and Watters, W.A., 1977: Paleomagnetism, K-Ar dating and tectonic interpretation of Upper Cretaceous and Cenozoic volcanic rocks of the Chatham Islands, New Zealand. *New Zealand Journal of Geology & Geophysics*, *20*:425-467.

Haas, J. and Hámor, G., 2001: Geological garden in the neighbourhood of Budapest, Hungary. *Episodes*, *24*:257-261.

Haines, A.J., 1979: Seismic wave velocities in the uppermost mantle beneath New Zealand. *New Zealand Journal of Geology & Geophysics*, *22*:245-257.

Haq, B.U., Hardenbol, J. and Vail, P.R., 1987: Chronology of fluctuating sea levels since the Triassic. *Science*, *235*:1156-1167.

Hay, R.F., Mutch, A.R. and Watters, W.A., 1970: Geology of the Chatham Islands. New Zealand Geological Survey bulletin, 83.

Hayton, S., Nelson, C.S. and Hood, S.D., 1995: A skeletal assemblage classification system for non-tropical carbonate deposits based on New Zealand Cenozoic limestones. *Sedimentary Geology*, *100*:123.

Herzer, R.H. and Wood, R.A., 1988: The geology and structure of Mernoo Bank and surrounding area, western Chatham Rise. *New Zealand Geological Survey record*, *29*:1-22.

Herzer, R.H., Challis, G.A., Christie, R.H.K., Scott, G.H. and Watters, W.A., 1989: The Urry Knolls, late Neogene alkaline basalt extrusives, southwestern Chatham Rise. *Journal of the Royal Society of New Zealand*, *19*:181-192.

Hesse, R., 1989: Silica diagenesis: origin of inorganic and replacement cherts. *Earth-Science Reviews*, *26*:253-284.

Hood, S.D., 1993: Skeletal and diagenetic petrofacies of temperate-latitude limestones, North Island, New Zealand, Hamilton, University of Waikato.

Hood, S.D. and Nelson, C.S., 1996: Cementation scenarios for New Zealand Cenozoic nontropical limestones. *New Zealand Journal of Geology and Geophysics*, *39*:109-122.

Hornibrook, N. de B., 1992: New Zealand Cenozoic marine paleoclimates: a review based on the distribution of some shallow water and terrestrial biota. *In*: Tsuchi, T., Ingle, J.C.J. *eds*. Pacific Neogene environment, evolution, and events. Tokyo, University of Tokyo Press. Pp. 83-106.

Houtz, R., Ewing, J., Ewing, M. and Leonardi, A.G., 1967: Seismic reflection profiles of the New Zealand plateau. *Journal of Geophysical Research*, *72*:4713-4729.

Hutton, F.W., 1873: Catalogue of the Tertiary Mollusca and Echinodermata of New Zealand, in the collection of the Colonial Museum. Wellington, Government Printer. 48 p.

Hyam, D.M., Marshall, J.E.A. and Sanderson, D.J., 1997: Carboniferous diamictite dykes in the Falkland Islands. *Journal of African Earth Sciences*, *25*:505-517.

James, N.P. and Bone, Y., 1989: Petrogenesis of Cenozoic, temperate water calcarenites, South Australia: a model for meteoric/shallow burial diagenesis of shallow water calcite sediments. *Journal of Sedimentary Petrology*, *59*:191-203.

James, N.P. and Bone, Y., 1992: Synsedimentary cemented calcarenite layers in Oligo-Miocene cool-water shelf limestones, Eucla Platform, Southern Australia. *Journal of Sedimentary Petrology*, *62*:860-872.

James, N.P., 1997: The cool-water carbonate depositional realm. *In*: James, N.P., Clarke, J.A.D. *eds*. Cool-water carbonates. Special Publication No. 56. Tulsa, Society for Sedimentary Geology. Pp. 1-22.

Jenkins, D.G., 1993: The evolution of the Cenozoic southern high- and mid-latitude planktonic foraminiferal faunas. *In*: Kennett, J.P., Warnke, D.A. *eds*. The Antarctic paleoenvironment a perspective on global change, Part 2. 60. American Geophysical Union, Antarctic Research Series. Pp. 175-194.

Johnson, D.P., 2004: The geology of Australia. Cambridge, Cambridge University Press. 276 p.

Jolly, R.J.H. and Lonergan, L., 2002: Mechanisms and controls on the formation of sand intrusions. *Journal of the Geological Society*, *159*:605-617.

Jonk, R., Parnell, J. and Hurst, A., 2005: Aqueous and petroleum fluid flow associated with sand injectites. *Basin Research*, *17*:241-257.

Kamp, P.J.J., 1986: The mid-Cenozoic Challenger Rift System of western New Zealand and its implications for the age of the Alpine Fault inception. *Geological Society of America Bulletin*, *97*:255-281.

Kamp, P.J.J. and Nelson, C.S., 1987: Tectonic and sea-level controls on non-tropical Neogene limestones in New Zealand. *Geology*, *15*:610-613.

Kamp, P.J.J., Harmsen, F.J., Nelson, C.S. and Boyle, S.F., 1988: Barnacle-dominated limestone with giant cross-beds in a non-tropical, tide-swept, Pliocene forearc seaway, Hawke's Bay, New Zealand. *Sedimentary Geology*, *60*:173.

Kamp, P.J.J., 1992: Tectonic architecture of New Zealand. *In*: Soons, J.M., Selby, M.J. *eds*. Landforms of New Zealand - second edition. Auckland, Longman Paul Limited. Pp. 1-30.

Katz, H.R. and Wood, R.A., 1980: Submerged margin east of New Zealand and its petroleum potential. *CCOP/SOPAC Technical Bulletin*, *3*:221-235.

King, P.R., Naish, T.R., Browne, G.H. and Field, B.D., 1999: Cretaceous to Recent sedimentary patterns in New Zealand. Institute of Geological & Nuclear Sciences folio series,1. Lower Hutt, N.Z., Institute of Geological & Nuclear Sciences. 43 p.

King, P.R., 2000: Tectonic reconstructions of New Zealand: 40 Ma to the Present. *New Zealand Journal of Geology & Geophysics*, *43*:611-638.

Kingma, J.T., 1974: The geological structure of New Zealand. New York, Wiley.

Knauth, L.P., 1979: A model for the origin of chert in limestone. *Geology*, *7*:274-277.

Krause, D.C. and Cullen, D.J., 1970: Bounty bathymetry, New Zealand Oceanographic Institute chart, oceanic series, 1:1,000,000. Wellington, Department of Scientific and Industrial Research.

Land, L.S., 1970: Phreatic versus vadose meteoric diagenesis of limestones: evidence from a fossil water table. *Sedimentology*, *14*:175-185.

Larsen, E. and Mangerud, J., 1992: Subglacially formed clastic dikes. *Sueriges Geologisha Undersdhning*, *81*:163-170.

Le Heron, D.P. and Etienne, J.L., 2005: A complex subglacial clastic dyke swarm, Solheimajokull, southern Iceland. *Sedimentary Geology*, *181*:25.

Lees, A., 1975: Possible influences of salinity and temperature on modern shelf carbonate sedimentation. *Marine Geology*, *19*:159-198.

Lewandowski, M., 1999: A palaeomagnetic study of fracture fills in the Holy Cross Mountains of Central Poland and its application in dating tectonic processes. *Geophysical Journal International*, *137*:783-792.

Lewis, D.W., 1973: Polyphase limestone dikes in the Oamaru region, New Zealand. *Journal of Sedimentary Petrology*, *43*:1031-1045.

Maliva, R.G. and Siever, R., 1988: Mechanism and controls of silicification of fossils in limestone. *Journal of Geology*, *96*:387-398.

Marshall, D.J., 1988: Cathodoluminescence of geological materials: an introduction. Boston, Allen & Unwin.

Martin Penela, A.J. and Barragan, G., 1995: Silicification of carbonate clasts in a marine environment (Upper Miocene, Vera Basin, SE Spain). *Sedimentary Geology*, *97*:21-32.

Marwick, J., 1928: The Tertiary Mollusca of the Chatham Islands including a generic revision of the New Zealand Pectinidae. *Transactions of the New Zealand Institute*, *58*:432-506.

McBride, E.F., Abdel-Wahab, A. and El-Younsy, A.R.M., 1999: Origin of spheroidal chert nodules, Drunka Formation (Lower Eocene), Egypt. *Sedimentology*, *46*:733-755.

McDougall, J.C., 1982: Bounty sediments, New Zealand Oceanographic Institute chart, oceanic series 1:1,000,000. Wellington, Department of Scientific and Industrial Research.

Nelson, C.S. and Hume, T.M., 1977: The relative intensity of tectonic events revealed by Tertiary sedimentary record in the North Wanganui Basin and adjacent areas. *New Zealand Journal of Geology & Geophysics*, *20*:369-392.

Nelson, C.S., 1978a: Stratigraphy and paleontology of the Oligocene Te Kuiti Group, Waitomo County, South Auckland, New Zealand. *New Zealand Journal of Geology & Geophysics*, *21*:553-594.

Nelson, C.S., 1978b: Temperate shelf carbonate sediments in the Cenozoic of New Zealand. *Sedimentology*, *25*:737-771.

Nelson, C.S., 1988: An introductory perspective on non-tropical shelf carbonates. *In:* Nelson, C.S. *ed*. Special Issue: Non-tropical shelf carbonates - modern and ancient. *Sedimentary Geology*, *60*:3-12.

Nelson, C.S., Harris, G.J. and Young, H.R., 1988a: Burial-dominated cementation in non-tropical carbonates of the Oligocene Te Kuiti Group, New Zealand. *Sedimentary Geology*, *60*:233.

Nelson, C.S., Keane, S.L. and Head, P.S., 1988b: Non-tropical carbonate deposits on the modern New Zealand shelf. *Sedimentary Geology*, *60*:71.

Nelson, C.S. and Smith, A.M., 1996: Stable oxygen and carbon isotope compositional fields for skeletal and diagenetic components in New Zealand Cenozoic non-tropical carbonate sediments and limestones: a synthesis and review. *New Zealand Journal of Geology and Geophysics*, *39*:93-107.

Nelson, C.S. and James, N.P., 2000: Marine cements in mid-Tertiary cool-water shelf limestones of New Zealand and southern Australia. *Sedimentology*, *47*:609-629.

Nelson, C.S. and Cooke, P.J., 2001: History of oceanic front development in the New Zealand sector of the Southern Ocean during the Cenozoic - a synthesis. *New Zealand Journal of Geology and Geophysics*, *44*:535-553.

Panter, K.S., Blusztajn, J., Hart, S.R., Kyle, P.R., Esser, R. and McIntosh, W.C., 2006: The origin of HIMU in the SW Pacific: evidence from intraplate volcanism in southern New Zealand and subantarctic islands. *Journal of petrology*, *47*:1673-1704.

Pedley, H.M. and Grasso, M., 2002: Lithofacies modelling and sequence stratigraphy in microtidal cool-water carbonates: a case study from the Pleistocene of Sicily, Italy. *Sedimentology*, *49*:533-553.

Pedley, H.M. and Carannante, G., 2006: Cool-water carbonate ramps: a review. *In*: Pedley, H.M., Carannante, G. *eds*. Cool-water carbonates: depositional systems and palaeoenvironmental controls. Special Publication 255. London, Geological Society. Pp. 1-9.

Peterson, G.L., 1968: Flow structures in sandstone dikes. *Sedimentary Geology*, *2*:177.

Phillips, C.A. and Alsop, G.I., 2000: Post-tectonic clastic dykes in the Dalradian of Scotland and Ireland: implications for delayed lithification and deformation of sediments. *Geological Journal*, *35*:99-110.

Pillans, B., Chappell, J. and Naish, T.R., 1998: A review of the Milankovitch climatic beat: template for Plio–Pleistocene sea-level changes and sequence stratigraphy. *Sedimentary Geology*, *122*:5-21.

Pollock, J.C. and Williams, H., 2000: Clastic dykes in the Dunnage Melange, Halfmoon Bay, northeast Newfoundland, Newfoundland Department of Mines and Energy Geological Survey. 231-239 p.

Pomar, L., Brandano, M. and Westphal, H., 2004: Environmental factors influencing skeletal grain sediment associations: a critical review of Miocene examples from the western Mediterranean. *Sedimentology*, *51*:627-651.

Rao, C.P., 1996: Modern carbonates tropical temperate polar: introduction to sedimentology and geochemistry. Howrah, Tasmania, Carbonates. 206 p.

Reid, R.P., Macintye, I.G. and James, N.P., 1990: Internal precipitation of microcrystalline carbonate: a fundamental problem for sedimentologists. *Sedimentary Geology*, *68*:163-170.

Rey, J., 1997: A Liassic isolated platform controlled by tectonics: South Iberian Margin, southeast Spain. *Geological Magazine*, *134*:235-247.

Richards, G.W., 1987: Chatham Island peat deposit coal prospecting licence areas 35193, 35202, 35205, 35260. Preliminary geological report, Enim Developments Ltd. unpublished report, New Business Division, Fletcher Challenge Ltd. 2 Volumes.

Ricketts, B.D., Caron, V. and Nelson, C.S., 2004: A fluid flow perspective on the diagenesis of Te Aute limestones. *New Zealand Journal of Geology & Geophysics*, *47*:823–838.

Robinson, R., 1986: Seismicity, structure and tectonics of the Wellington region, New Zealand. *Geophysical Journal of the Royal Astronomical Society*, *87*:379-409.

Rowe, C.A., Mustard, P.S., Mahoney, J.B. and Katnick, D.C., 2002: Oriented Clastic Dike Swarms as Indicators of Paleoslope? An Example from the Upper Cretaceous Nanaimo Group, Canada. *Journal of Sedimentary Research*, *72*:192-200.

Sano, H. and Orchard, M.J., 2004: Necoslie breccia: mixed conodont fauna-bearing neptunian dyke in Carboniferous-Permian seamount-capping oceanic buildup (Pope succession, Cache Creek Complex, central British Columbia). *Facies*, *50*:133-145.

Scholle, P.A. and Ulmer-Scholle, D.S., 2003: A color guide to the petrography of carbonate rocks: grains, textures, porosity, diagenesis. AAPG Memoir, 77. Oklahoma, The American Association of Petroleum Geologists. 474 p.

Scoffin, T.P., 1987: An introduction to carbonate sediments and rocks. London, Blackie & Son Ltd.

Shaw, C.S.J., Young, G.M. and Fedo, C.M., 1999: Sudbury-type breccias in the Huronian Gowganda Formation near Whitefish Falls, Ontario: Products of diabase intrusion into incompletely consolidated sediments? *Canadian Journal of Earth Sciences*, *36*:1435-1449.

Speranza, F., Adamoli, L., Maniscalco, R. and Florindo, F., 2003: Genesis and evolution of a curved mountain front: paleomagnetic and geological evidence from the Gran Sasso range (central Apennines, Italy). *Tectonophysics*, *362*:183-197.

Staton, R.J. and Pray, L.C., 2004: Skeletal-carbonate neptunian dikes of the Captain Reef: Permian, Guadalupe Mountains, Texas, U.S.A. *Journal of Sedimentary Research*, *74*:805-816.

Stilwell, J.D., Consoli, C.P., Sutherland, R., Salisbury, S., Rich, T.H., Vickers-Rich, P.A., Currie, P.J. and Wilson, G.J., 2006: Dinosaur sanctuary on the Chatham Islands, Southwest Pacific: first record of theropods from the K-T boundary Takatika Grit. *Palaeogeography, Palaeoclimatology, Palaeoecology*, *230*:243-250.

Strong, C.P., 1979: Late Cretaceous foraminifera from Kahuitara Tuff, Pitt Island, New Zealand. *New Zealand Journal of Geology & Geophysics*, *22*:593-611.

Strong, C.P. and Edwards, A.R., 1979: Late Haumurian (Maastrichtian) microfossils from Chatham Islands, New Zealand. *New Zealand Journal of Geology & Geophysics*, *22*:613-619.

Sturkell, E. and Ormo, J., 1997: Impact related clastic injections in the marine Ordovician Lockne impact structure, Central Sweden. *Sedimentology*, *44*:793-804.

Sutherland, R., 1999: Basement geology and tectonic development of the greater New Zealand region: an interpretation from regional magnetic data. *Tectonophysics*, *308*:341-362.

Thorson, R., Clayton, W. and Seeber, L., 1986: Geologic evidence for a large prehistoric earthquake in eastern Connecticut. *Geology*, *14*:463-467.

Tipper, J.C., Sach, V.J. and Heizmann, E.P.J., 2003: Loading fractures and Liesegang laminae: new sedimentary structures found in the north-western North Alpine Foreland Basin (Oligocene-Miocene, south-west Germany). *Sedimentology*, *50*:791-813.

Truswell, J., 1972: Sandstone sheets and related intrusions from Coffee Bay, Transkei, South Africa. *Journal of Sedimentary Petrology*, *42*:578-583.

Tucker, M.E. and Wright, V.P., 1990: Carbonate sedimentology. London, Blackwell Scientific Publications. 482 p.

Wallace, L.M. and Beavan, J., 2004: Subduction zone coupling and tectonic block rotations in the North Island, New Zealand. *Journal of Geophysical Research*, *109*:1-21.

Waterhouse, J.B., 1955: Geology of the White Rock - Tora area, south-east Wairarapa. Unpublished M.Sc Thesis, Wellington, Victoria University. 321 p.

Wellman, H.W., 1953: The geology of the Geraldine Subdivision. *New Zealand Geological Survey bulletin*, *50*:1-72.

Wilson, D.D., 1956: The Late Cretaceous and Early Tertiary transgression in South Island, New Zealand. *New Zealand Journal of Science and Technology*, *37*:610-622.

Wood, R.A., Andrews, P.B., Herzer, R.H., Cook, R.A., Hornibrook, N. de B., Hoskins, R.H., Beu, A.G., Maxwell, P.A., Keyes, I.W., Raine, J.I., Mildenhall, D.C., Wilson, G.J., Smale, D., Soong, R. and Watters, W.A., 1989: Cretaceous and Cenozoic geology of the Chatham Rise region, South Island, New Zealand. New Zealand Geological Survey basin studies 3. Lower Hutt, N.Z., New Zealand Geological Survey. 76 p.

Wood, R.A. and Herzer, R.H., 1993: The Chatham Rise, New Zealand. *In*: Ballance, P.F. *ed*. Sedimentary Basins of the World - South Pacific Sedimentary Basins. 2. Amsterdam, Elsevier. Pp. 329-349.

Wu, Y. and Chafetz, H.S., 2002: 13C-Enriched Carbonate in Mississippian Mud Mounds: Alamogordo Member, Lake Valley Formation, Sacramento Mountains, New Mexico, U.S.A. *Journal of Sedimentary Research*, *72*:138-145.

APPENDIX B
Limestone Petrographic Data

Methodology

Thin section preparation and analysis

Preparation of Chatham Island samples collected in the field was achieved using standard methods with rock material cut using an 'Alegro-Super Cut' diamond saw. Many of the samples are extremely friable and soft and required whole block impregnation with 'Araldite' epoxy resin to maintain original fabrics, textures and porosity. In a few cases the samples were too friable to allow preservation and grain mounts were prepared by suspension of sediment within a block of epoxy resin.

Blocks were adhered to glass slides using 'Hillquest' slide glue. Blocks were cut from the glass slides and ground down to 0.03 mm on a 'Disco-planer' using quartz minerals and bioclasts as indicators of thickness. Finishing of thin sections was completed on a 'Buehler Metaserv' grinder-polisher using wet and dry sandpaper involving progressively finer grits from 600-800 grade. The use of carborundum powder was avoided because of the need to perform cathodoluminescence analysis on the thin sections. No cover slips were applied to any of the thin sections so that not only could cathodoluminescence be conducted but also the section could be stained for identification of carbonate cement mineralogy (Table B0).

Petrographic analysis was conducted using a standard petrographic microscope with bioclast identifications made by comparisons with several sources of information, including Hayton et al. (1995), Hood (1993), Scholle and Ulmer-Scholle (2003) and Scoffin (1987). All petrographic data were recorded using a system formulated by Hood (1993) which implements the use of designated letter codes to indicate the abundance of specific limestone components, including bioclasts, siliciclastics, precipitate minerals and matrix-cement. These percentages are then entered into tabular sheets (presented in the Appendix) which Hood (1993) based on tables by Flugel (1982).

Thin sections of the main limestone occurrences on Chatham Islands (Sections 3.1 & 4.1) were stained to help ascertain carbonate cement mineralogy using the procedure described in Dickson (1965) (Table B0).

Table B0: Summary of the technique and procedures for staining carbonate thin sections (A.R.S. = alizarin red S, P.F. = potassium ferricyanide) (after Dickson, 1965; Hood, 1993).

Stage	Procedure	Time	Carbonate	Result
STAGE 1	**Etching**	10-15 sec	Calcite Ferroan calcite	Considerable etch
			Dolomite Ferroan dolomite	Negligible etch
STAGE 2	**Staining** 0.2 g A.R.S. per 100 mls 1.5% HCL 2.0 g P.F. per 100 mls 1.5% HCL Mixed in ratio A.R.S.:P.F. = 3:2	30-40 sec	Calcite	Very pale pink-red depending on optical orientation
			Ferroan calcite	Very pale pink-red Pale blue-dark blue
			Dolomite	No colour
			Ferroan dolomite	Pale-deep turquoise depending on ferrous content
STAGE 3	**Staining** 0.2 g A.R.S. per 100 mls 1.5% HCL	10-15 sec	Calcite Ferroan calcite	Very pale pink-red
			Dolomite Ferroan dolomite	No colour

Cathodoluminescence (CL) analysis was also conducted on limestone and limestone dyke thin sections. Thin sections were prepared by polishing with 1200 grit metallographic grinding paper. The thin sections were analysed using a CL8200 Mk5-1 Optical Cathodoluminescence System with gun voltage 15-17 kV and a gun current of 500 micro-amps. Initial interpretations were made through reference to Marshall (1988).

Digital images during both petrographic and cathodoluminescence analysis were captured using a Nikon DXM1200 Digital Still Camera and processed through ACT-1 digital imaging software using a standard desktop PC.

Key to petrographic data tables in the Appendix
(adapted from Hood, 1993)

Abundance (as % of whole rock composition)

R = rare	<1%
S = some	1-5%
M = many	5-15%
C = common	15-25%
VC = very common	25-50%
A = abundant	50-75%
VA = very abundant	>75%

Shape

Calciclasts

SA = slightly abraded
MA = moderately abraded
A = abraded
VA = very abraded

Siliciclasts

A = angular
SA = subangular
SR = subrounded
R = rounded

Sorting (in relation to visible grain sizes)

P = poorly sorted
PM = poorly to moderately sorted
M = moderately sorted
MW = moderately to well sorted
W = well sorted
VW = very well sorted

Chatham Island main limestone petrographic data

Main limestone occurrences

Haumurian Limestone

Table B1: Component data for the Haumurian limestone, Flowerpot Bay, Pitt Island (continued over page).

Haumurian limestone		Flowerpot Bay, Pitt Island			
Stratigraphic column number		–	–	–	–
Sample running number		CH05-9.1A	CH05-9.1B	CH05-9.2A (1)	CH05-9.2A (2)
	Total bioclast %	0	5	60	70
	Bryozoans			C	VC
	Bivalves		R	R	M
	Echinoderms		S	C	M
C	Benthic foraminifera		S	R	S
a	Planktic foraminifera		R	R	S
l	Gastropods				
c	Calcareous algae				
i	Barnacles				R
c	Spicules & spines				
l	**Other**				
a	Brachiopods				
s	Serpulids			R	
t	Ostracods				
s	Stromatolitic algae				
	Modal size 1 (mm)		0.80	0.45	0.05
	Modal size 2 (mm)			2.00	2.25
	Shape/abrasion		VA	MA	A
	Sorting		P	P	P
	Extraclast %	0	0	10	0
	Siliciclastic grain %	50	80	2	2
	Quartz	R	VC	R	S
S	Feldspar		R		R
i	VRFs	A	VA	S	R
l	SRFs		M		
i	Micas				
c	Pyrite grains		M		
i	Pyrite infills		C		
c	Glauconite pellets			R	R
l	Glauconite infills			R	S
a	**Other**				
s	Phosphate	M	S	R	R
t	Limonite staining				R
s	Hornblende				
	Chert		R		
	Opaque		C		
	Modal size 1 (mm)	0.02	0.17	0.13	0.30
	Modal size 2 (mm)	3.50	3.50		
	Shape/abrasion	SR	SA-SR	SR	SR
	Sorting	P	P	P	PM
	Interparticle material %	50	15	40	30
	Spar cement %	10	10	30	5
	Micrite %	40	5	10	25
Unoccluded pore space %		2	2	2	2

Haumurian limestone		Flowerpot Bay, Pitt Island		
Stratigraphic column number		–	–	–
Sample running number		CH05-9.2B (1)	CH05-9.2B (2)	CH05-9.3
	Total bioclast %	0	5	35
	Bryozoans			
	Bivalves		S	VC
	Echinoderms		M	C
C	Benthic foraminifera		R	R
a	Planktic foraminifera			S
l	Gastropods			
c	Calcareous algae			
i	Barnacles			
c	Spicules & spines			
l	**Other**			
a	Brachiopods			
s	Serpulids		R	R
t	Ostracods			
s	Stromatolitic algae			
	Modal size 1 (mm)		0.50	0.25
	Modal size 2 (mm)			2.00
	Shape/abrasion		VA	A
	Sorting		PM	P
	Extraclast %	0	0	0
	Siliciclastic grain %	90	60	50
	Quartz	S	C	S
S	Feldspar			
i	VRFs	VA	VC	C
l	SRFs	S	S	C
i	Micas			
c	Pyrite grains			R
i	Pyrite infills			R
c	Glauconite pellets		R	R
l	Glauconite infills			
a	**Other**			
s	Phosphate		S	
t	Limonite staining		S	S
s	Hornblende			
	Chert			
	Opaque			
	Modal size 1 (mm)	0.05	0.05	0.25
	Modal size 2 (mm)	2.75	2.75	7.50
	Shape/abrasion	SR	SR	SA
	Sorting	P	P	P
	Interparticle material %	10	40	15
	Spar cement %	2	5	2
	Micrite %	8	35	13
Unoccluded pore space %		2	2	2

Table B2: Component data for the Haumurian limestone, Ngakuha Reef, Chatham Island.

Haumurian limestone		Ngakuha Reef, Chatham Island			
Stratigraphic column number		–	–	–	–
Sample running number		CH05-15.1	CH05-15.2	CH05-15.3	CH05-15.4
	Total bioclast %	75	35	80	25
	Bryozoans		M		S
	Bivalves		S		S
	Echinoderms	R	M		M
C	Benthic foraminifera	M	M		R
a	Planktic foraminifera	M	S		S
l	Gastropods	R	S		
c	Calcareous algae				
i	Barnacles				
c	Spicules & spines				
l	**Other**				
a	Brachiopods	S			
s	Serpulids				
t	Ostracods		R		
s	Stromatolitic algae			VA	S
	Modal size 1 (mm)	0.10	0.50		0.62
	Modal size 2 (mm)			2.50	2.80
	Shape/abrasion	VA	VA		VA
	Sorting	PM	PM		PM
	Extraclast %	0	0	2	0
	Siliciclastic grain %	10	35	8	50
	Quartz	M	M	M	S
S	Feldspar	S	S	M	
i	VRFs	M	VC	M	C
l	SRFs	S	R		M
i	Micas				
c	Pyrite grains	S	S		M
i	Pyrite infills				M
c	Glauconite pellets	M	M	S	M
l	Glauconite infills	M	S		S
a	**Other**				
s	Phosphate	R	R		S
t	Limonite staining				
s	Hornblende	R	M		S
	Chert	S	R		S
	Opaque				
	Modal size 1 (mm)	0.30	0.50	0.13	0.25
	Modal size 2 (mm)	3.75	3.25	2.00	5.75
	Shape/abrasion	SA-SR	SA-SR	SA-SR	SA-SR
	Sorting	P	P	P	P
	Interparticle material %	15	30	10	25
	Spar cement %	5	15	1	10
	Micrite %	10	15	9	15
Unoccluded pore space %		1	1	2	2

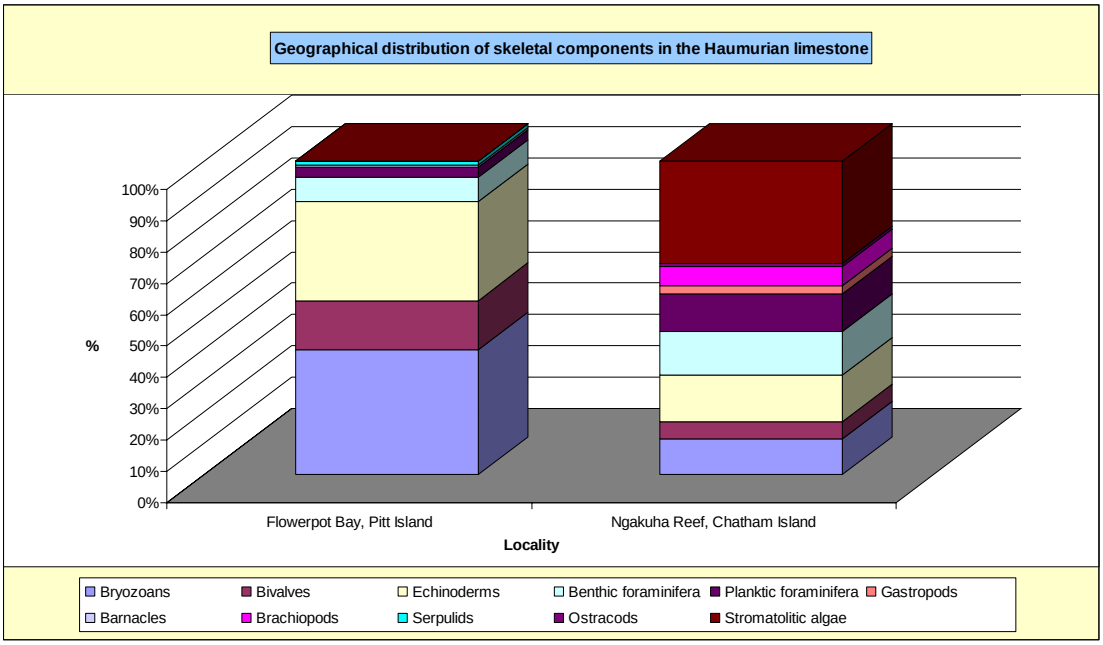

Figure B1: Geographical distribution of skeletal components in the Haumurian limestone on the Chatham Islands.

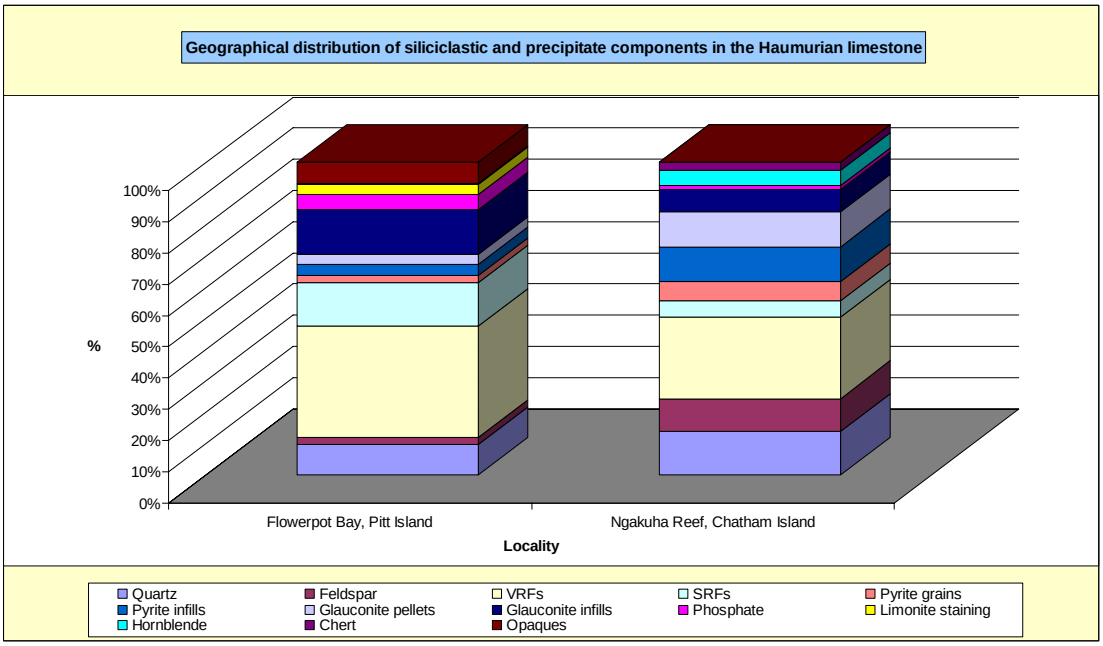

Figure B2: Geographical distribution of siliciclastic and precipitate components in the Haumurian limestone, Chatham Islands.

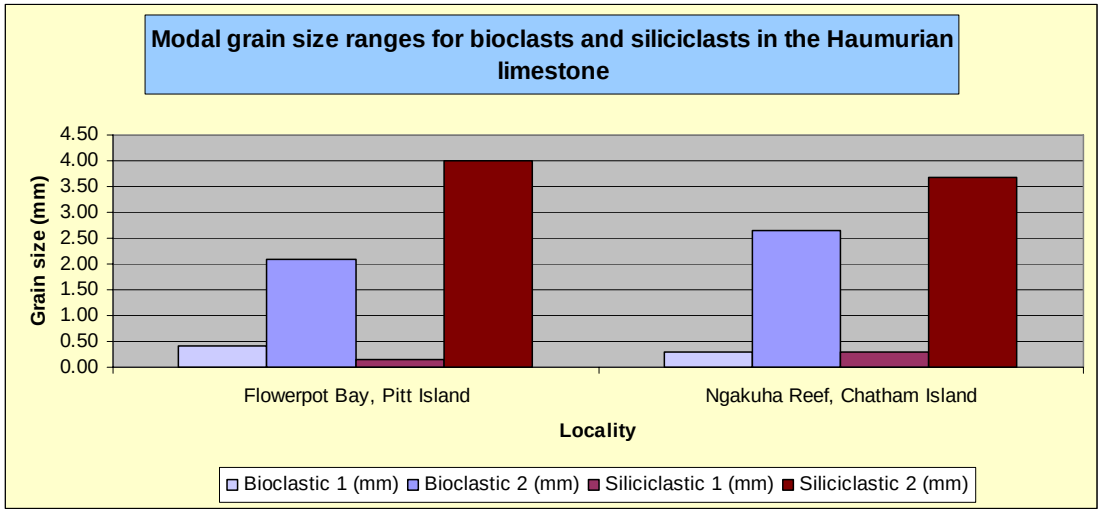

Figure B3: Geographical distribution of modal skeletal and siliciclastic/precipitate grain sizes in the Haumurian limestone, Chatham Islands.

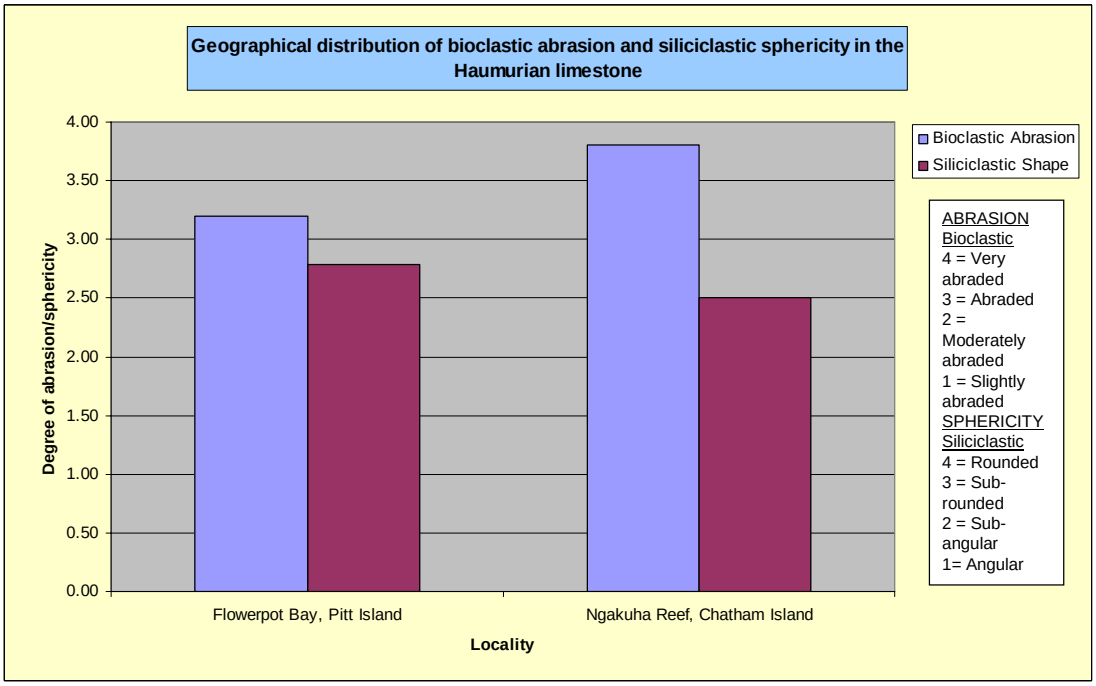

Figure B4: Geographical distribution of bioclastic abrasion and siliciclastic/precipitate grain sphericity in the Haumurian limestone, Chatham Islands.

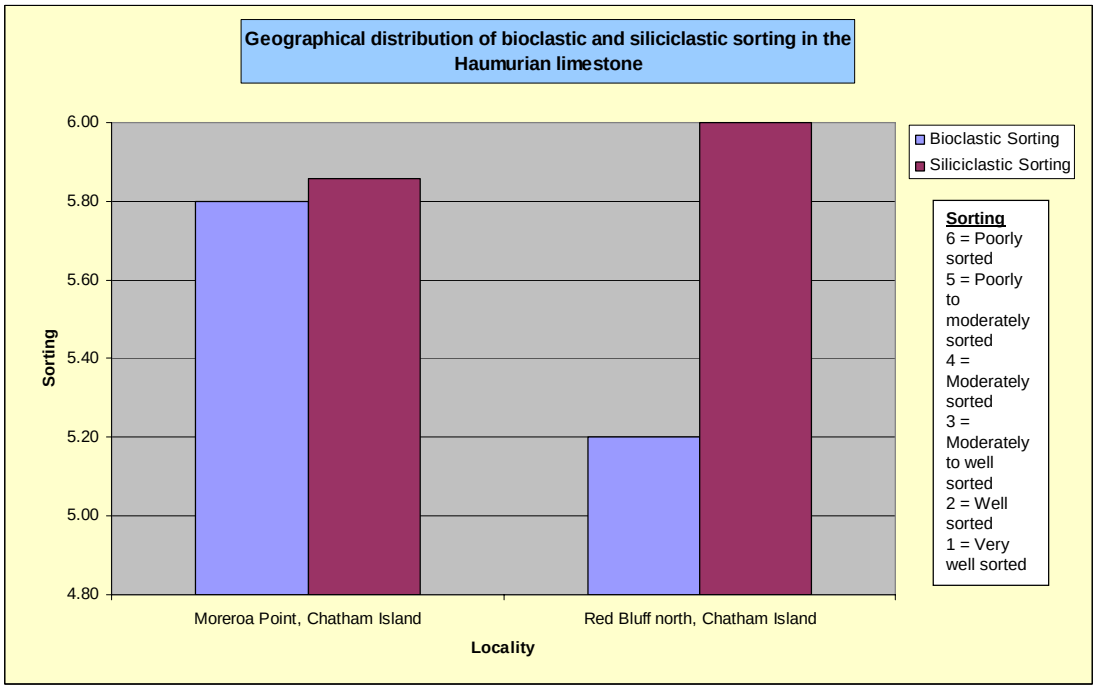

Figure B5: Geographical distribution of bioclast and siliciclastic/precipitate grain sorting in the Haumurian limestone, Chatham Islands.

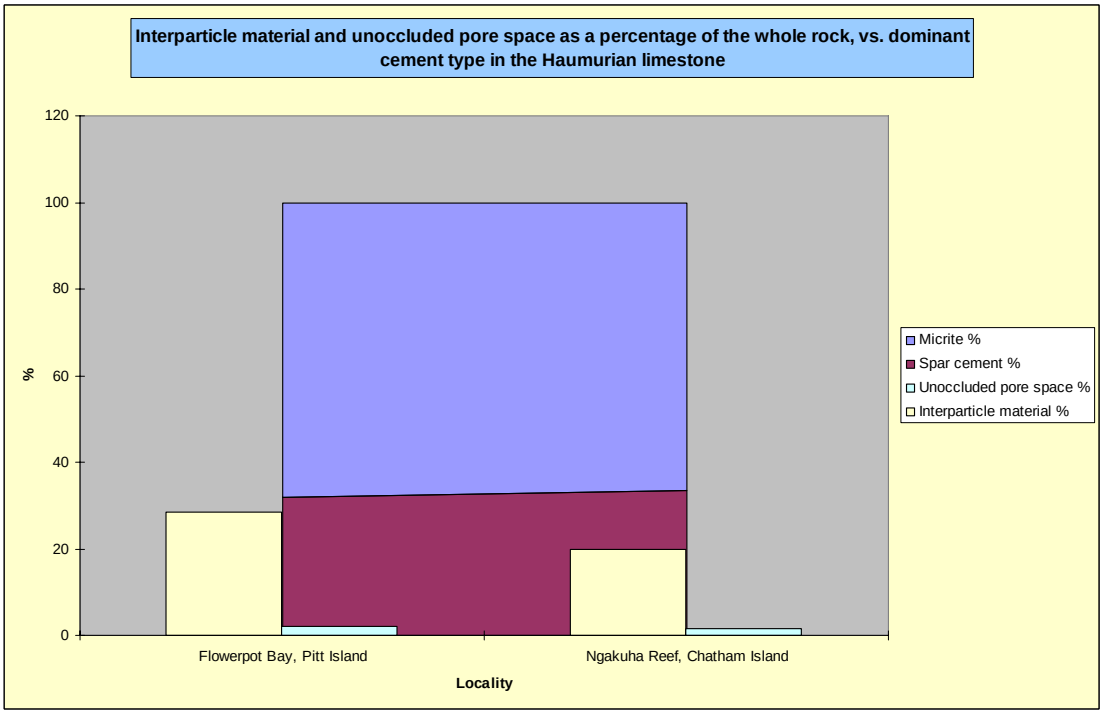

Figure B6: Geographical distribution of interparticle material and unoccluded pore space (foreground), and the amount of micrite and spar present in the Haumurian limestone, Chatham Islands.

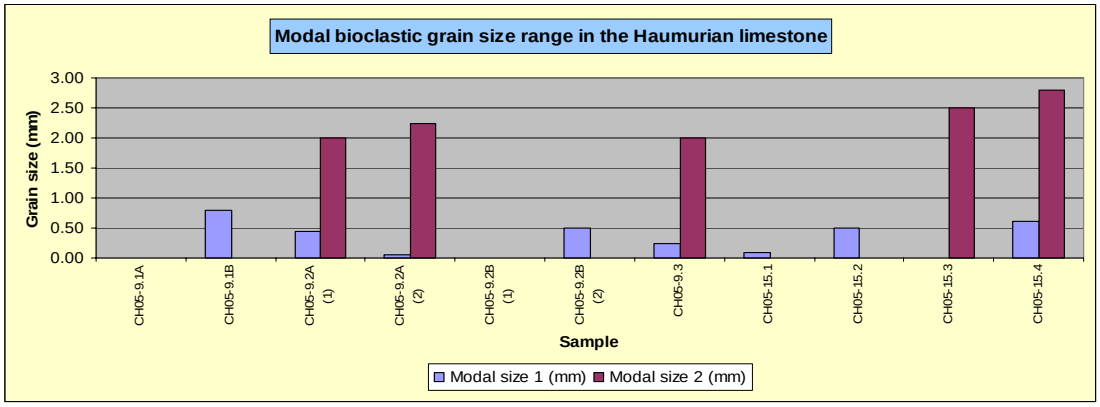

Figure B7: Modal bioclast grain sizes in the Haumurian limestone, Chatham Islands.

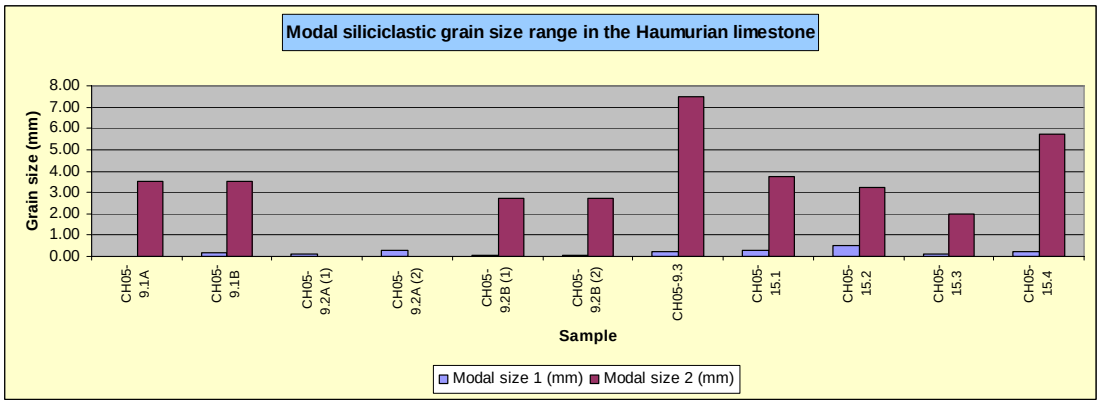

Figure B8: Modal siliciclastic grain sizes in the Haumurian limestone, Chatham Islands.

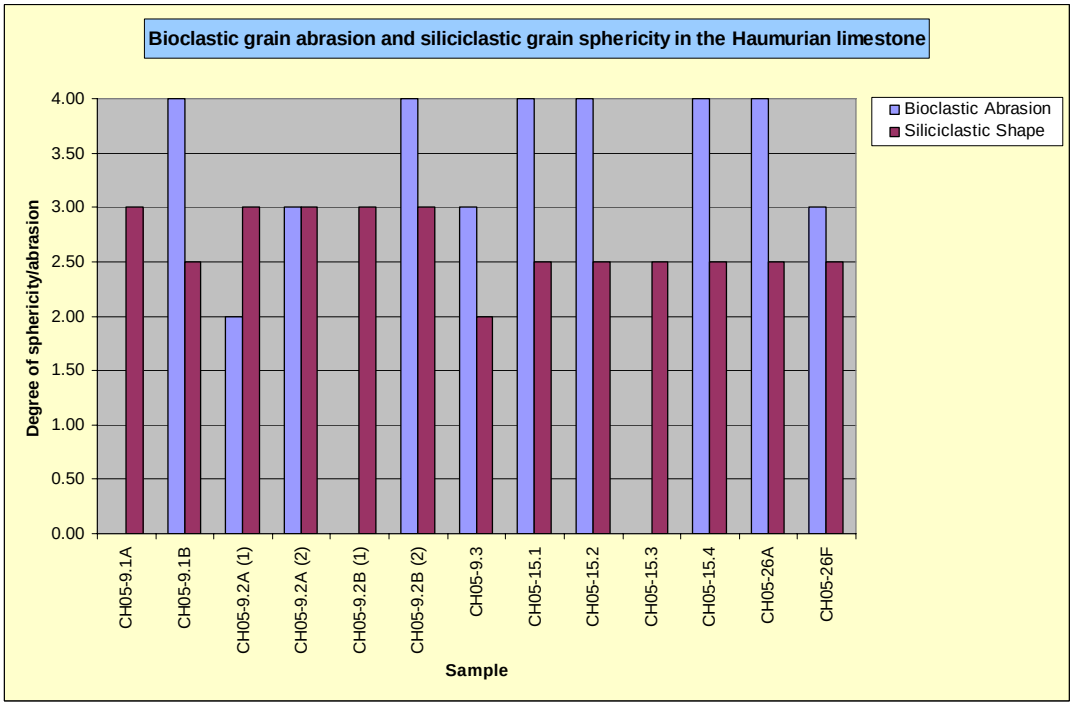

Figure B9: Bioclast abrasion and siliciclastic/precipitate sphericity in the Haumurian limestone, Chatham Islands.

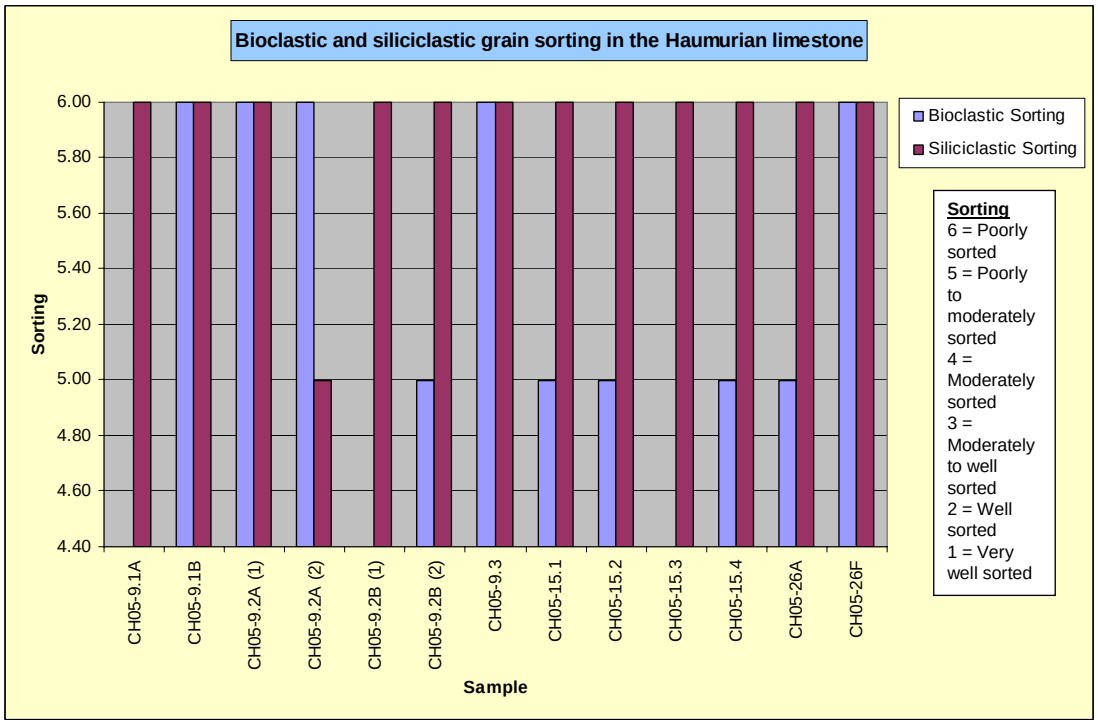

Figure B10: Bioclast and siliciclastic/precipitate grain sorting in the Haumurian limestone, Chatham Islands.

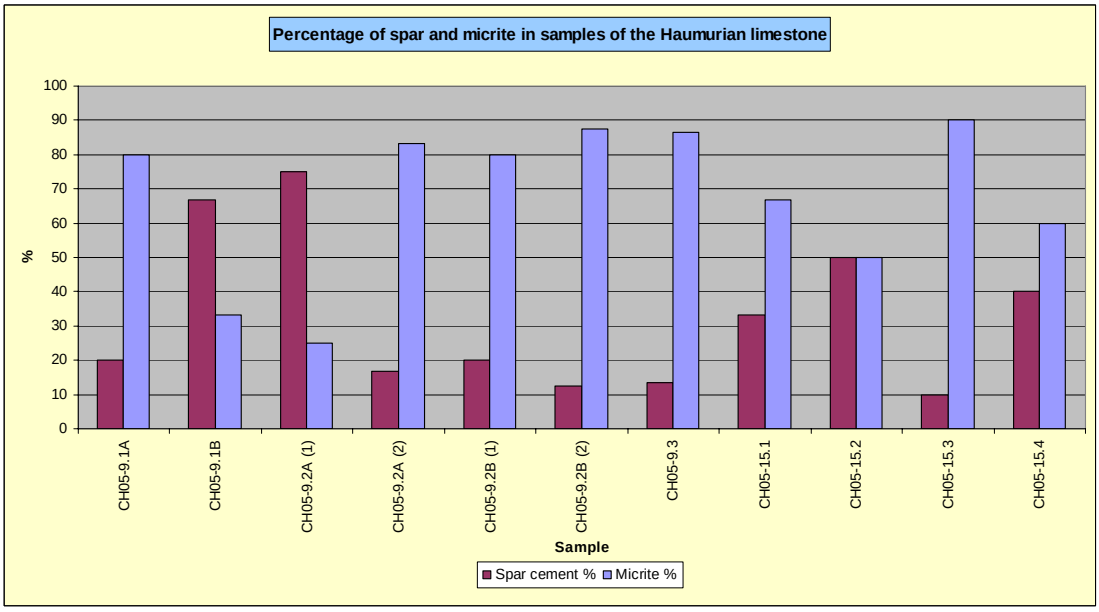

Figure B11: Percentage of spar versus micrite in samples of the Haumurian limestone, Chatham Islands.

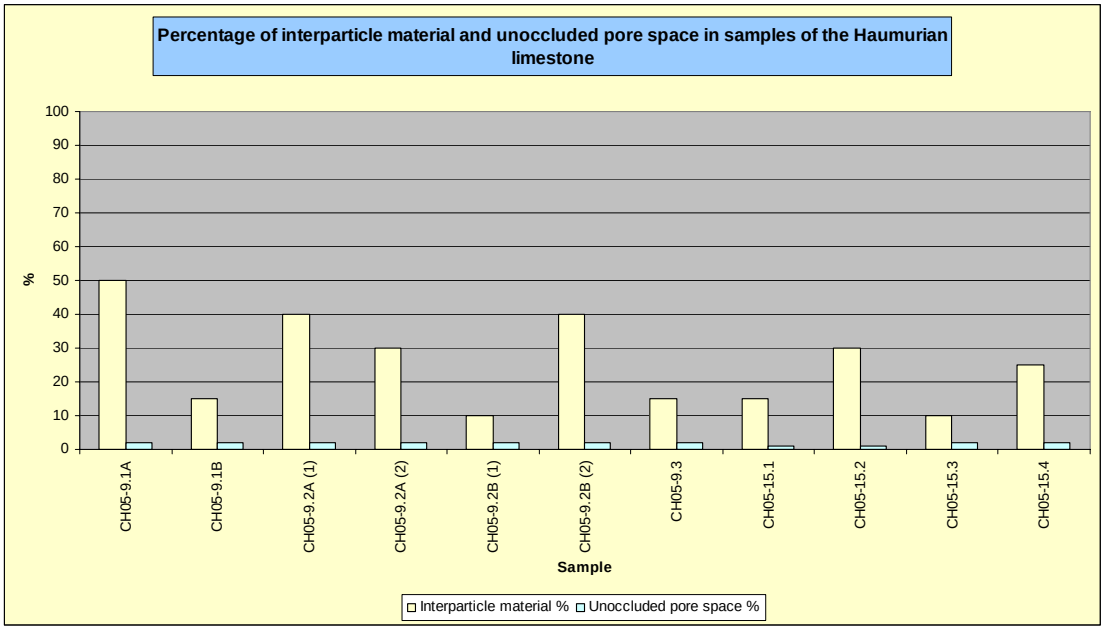

Figure B12: Percentage of interparticle material versus unoccluded pore space in samples of the Haumurian limestone, Chatham Islands.

Matanginui Limestone

Table B3: Component data for the Matanginui Limestone, Moreroa Point, Chatham Island (continued over page).

Matanginui Limestone		Moreroa Point, Chatham Island			
Stratigraphic column number		6	6	6	6
Sample running number		CH05-1.1A	CH05-1.1B	CH05-1.2	CH05-1.3
	Total bioclast %	65	60	60	70
	Bryozoans	VC	VC	VC	C
	Bivalves	M	S	S	S
	Echinoderms	S	S	S	S
C	Benthic foraminifera	S	S	S	R
a	Planktic foraminifera	M	M	M	S
l	Gastropods				
c	Calcareous algae				
i	Barnacles				
c	Spicules & spines				
l	**Other**				
a	Brachiopods				
s	Serpulids				
t	Modal size 1 (mm)	0.18	0.18	0.37	0.23
s	Modal size 2 (mm)	2.13	2.00	2.00	1.75
	Shape/abrasion	A	A	A	VA
	Sorting	P	P	P	PM
	Intraclast %	0	2	2	0
	Siliciclastic grain %	5	5	15	5
	Quartz	R	R	S	S
S	Feldspar				
i	VRFs			S	
l	SRFs		R	M	
i	Micas				
c	Pyrite grains				
i	Pyrite infills			S	
c	Glauconite pellets	S	S	M	S
l	Glauconite infills	R	R	R	
a	**Other**				
s	Phosphate	R	R	R	R
t	Limonite staining				
s	Hornblende				
	Chert				
	Opaque				
	Modal size 1 (mm)	0.18	0.25	0.25	0.30
	Modal size 2 (mm)			5.00	
	Shape/abrasion	SR	SR	SA-SR	SA-SR
	Sorting	PM	PM	P	PM
	Interparticle material %	30	30	22	20
	Spar cement %	2	5	2	5
	Micrite %	28	25	20	15
Unoccluded pore space %		5	2	2	10

Matanginui Limestone		Moreroa Point, Chatham Island			
Stratigraphic column number		6	6	6	6
Sample running number		CH05-1.4	CH05-1.5	CH05-1.6	CH05-1.8
	Total bioclast %	70	65	60	55
	Bryozoans	VC	C	VA	VC
	Bivalves	S	S	S	M
	Echinoderms	S	S	M	C
C	Benthic foraminifera	S	R	C	C
a	Planktic foraminifera	M	M	A	VC
l	Gastropods				
c	Calcareous algae				
i	Barnacles				
c	Spicules & spines		R		R
l	**Other**				
a	Brachiopods				
s	Serpulids				
t	Modal size 1 (mm)	0.20	0.20	0.25	0.30
s	Modal size 2 (mm)	2.38	2.13	1.75	1.00
	Shape/abrasion	A	A	MA	A
	Sorting	P	P	PM	P
	Intraclast %	0	0	10	5
	Siliciclastic grain %	5	5	5	10
	Quartz	R	R	S	S
S	Feldspar		R	R	
i	VRFs				
l	SRFs				
i	Micas				
c	Pyrite grains				S
i	Pyrite infills				
c	Glauconite pellets	S	S	C	S
l	Glauconite infills		R	R	S
a	**Other**				
s	Phosphate	R	R		
t	Limonite staining		R		
s	Hornblende				
	Chert				
	Opaque				
	Modal size 1 (mm)	0.25	0.15	0.15	0.30
	Modal size 2 (mm)				
	Shape/abrasion	SA-SR	SA-SR	SA	SA
	Sorting	PM	PM	M	PM
	Interparticle material %	20	20	20	30
	Spar cement %	5	5	3	2
	Micrite %	15	15	17	28
Unoccluded pore space %		5	10	15	10

Table B4: Component data for the Matanginui Limestone, Red Bluff, Chatham Island (continued over page).

Matanginui Limestone		Red Bluff north, Chatham Island			
Stratigraphic column number		–	–	–	–
Sample running number		CH05-16B1	CH05-16B2	CH05-16C1	CH05-16D1
	Total bioclast %	40	80	70	50
	Bryozoans	VC	A	A	VC
	Bivalves	M	R	M	S
	Echinoderms	S	M	M	S
Calciclasts	Benthic foraminifera	VC		C	C
	Planktic foraminifera			R	R
	Gastropods				
	Calcareous algae			R	
	Barnacles			S	R
	Spicules & spines			R	
	Other				
	Brachiopods		R		R
	Serpulids				
	Modal size 1 (mm)	0.27	0.25	0.25	0.37
	Modal size 2 (mm)	1.07	2.30	1.00	1.37
	Shape/abrasion	A	A	MA	A
	Sorting	P	P	PM	P
	Intraclast %	0	0	2	0
	Siliciclastic grain %	5	2	5	2
	Quartz	R	R		R
Siliciclasts	Feldspar				R
	VRFs				
	SRFs	R			
	Micas				
	Pyrite grains				R
	Pyrite infills				
	Glauconite pellets	R	R	S	R
	Glauconite infills	R	R	S	
	Other				
	Phosphate		S	R	R
	Limonite staining			S	R
	Hornblende		R		
	Chert				
	Opaque				
	Modal size 1 (mm)	0.20	0.13	0.10	0.10
	Modal size 2 (mm)				
	Shape/abrasion	SR	SA-SR	SR	SR
	Sorting	P	PM	M	M
	Interparticle material %	40	10	20	50
	Spar cement %	10	5	10	5
	Micrite %	30	5	10	40
Unoccluded pore space %		10	10	5	5

Matanginui Limestone				RedBluff S of 'twin radio masts'
Stratigraphic column number		–	–	(20m N of CH05-23)
Sample running number		CH05-16D2	CH05-16E	CH05-24A
	Total bioclast %	50	60	80
	Bryozoans	VC	VC	VA
	Bivalves	S	M	M
	Echinoderms	C	S	C
C	Benthic foraminifera	S	C	M
a	Planktic foraminifera	R	R	R
l	Gastropods			
c	Calcareous algae			
i	Barnacles		R	R
c	Spicules & spines			
l	**Other**			
a	Brachiopods			
s	Serpulids			
t	Modal size 1 (mm)	0.17	0.92	0.20
s	Modal size 2 (mm)	2.25	2.50	2.22
	Shape/abrasion	A	A	A
	Sorting	P	P	P
	Intraclast %	0	0	2
	Siliciclastic grain %	20	5	2
	Quartz	M	R	R
S	Feldspar	M		
i	VRFs		R	
l	SRFs			
i	Micas			
c	Pyrite grains	R	R	R
i	Pyrite infills			R
c	Glauconite pellets	S	R	R
l	Glauconite infills	S	R	R
a	**Other**			
s	Phosphate	S	R	R
t	Limonite staining	S	R	
s	Hornblende			
	Chert			
	Opaque			
	Modal size 1 (mm)	0.17	0.50	0.13
	Modal size 2 (mm)			
	Shape/abrasion	SA-SR	SR	SR
	Sorting	M	P	M
	Interparticle material %	15	30	10
	Spar cement %	7	10	5
	Micrite %	7	20	5
Unoccluded pore space %		15	10	10

Table B5: Component data for the Matanginui Limestone, Te Whanga Lagoon, Chatham Island.

Matanginui Limestone		Te Whanga Lagoon, Chatham Island		
Stratigraphic column number		9	9	9
Sample running number		CH05-14.1	CH05-14.2	CH05-14.3
	Total bioclast %	80	75	60
	Bryozoans	VC	A	VC
	Bivalves	M	S	M
	Echinoderms	C	VC	S
C	Benthic foraminifera	S	S	S
a	Planktic foraminifera	R		R
l	Gastropods			
c	Calcareous algae			
i	Barnacles			
c	Spicules & spines			
l	**Other**			
a	Brachiopods		R	
s	Serpulids			
t	Modal size 1 (mm)	0.15	0.13	0.13
s	Modal size 2 (mm)	2.38	1.75	2.60
	Shape/abrasion	A	A	A
	Sorting	M	P	M
	Intraclast %	0	2	0
	Siliciclastic grain %	5	2	20
	Quartz	R		R
S	Feldspar			
i	VRFs			R
l	SRFs		R	
i	Micas			
c	Pyrite grains			R
i	Pyrite infills			
c	Glauconite pellets	R	R	S
l	Glauconite infills	R	R	
a	**Other**			
s	Phosphate	R	R	C
t	Limonite staining			
s	Hornblende			
	Chert			
	Opaque			
	Modal size 1 (mm)	0.25	0.15	0.25
	Modal size 2 (mm)			2.50
	Shape/abrasion	SR	SR	SR
	Sorting	PM	M	P
	Interparticle material %	20	20	20
	Spar cement %	15	15	15
	Micrite %	5	5	5
Unoccluded pore space %		2	5	5

Table B6: Component data for the Matanginui Limestone, Tarawhenua Peninsula, Pitt Island (continued over the next 2 pages).

Matanginui Limestone		Tarawhenua Point, Rocky Side, Pitt Island				
Stratigraphic column number		11	11	11	11	11
Sample running number		CH05-6.1	CH05-6.4	CH05-6.5A	CH05-6.5B	CH05-6.6A
	Total bioclast %	70	85	60	80	60
	Bryozoans	VA	VA	A	C	C
	Bivalves	S		M	S	R
	Echinoderms	C	C	S	S	R
C	Benthic foraminifera			S	A	A
a	Planktic foraminifera			R	A	M
l	Gastropods			R		
c	Calcareous algae					
i	Barnacles					
c	Spicules & spines					
l	**Other**					
a	Brachiopods					
s	Serpulids					
t	Modal size 1 (mm)	0.20	0.15	0.25	0.03	0.12
s	Modal size 2 (mm)	2.25	2.30	1.75	3.00	2.50
	Shape/abrasion	VA	VA	VA	MA	A
	Sorting	P	P	M	P	M
	Intraclast %	0	0	0	0	0
	Siliciclastic grain %	2	2	2	2	5
	Quartz	R	R	R	R	R
S	Feldspar					
i	VRFs					
l	SRFs					
i	Micas					
c	Pyrite grains	R	S			R
i	Pyrite infills		S	S		
c	Glauconite pellets	R	S	R	S	R
l	Glauconite infills		S		S	
a	**Other**					
s	Phosphate	S	S	R	R	S
t	Limonite staining			R	R	R
s	Hornblende					
	Chert					
	Opaque					
	Modal size 1 (mm)	0.07	0.18	0.25	0.13	0.12
	Modal size 2 (mm)					1.10
	Shape/abrasion	SR	SR	SA-SR	R	SR
	Sorting	W	PM	P	M	P
	Interparticle material %	20	10	40	17	30
	Spar cement %	5	5	2	2	5
	Micrite %	15	5	40	15	30
Unoccluded pore space %		10	5	5	5	2

Matanginui Limestone		Tarawhenua Point, Rocky Side, Pitt Island			
Stratigraphic column number		11	11	11	11
Sample running number		CH05-6.10	CH05-7.4	CH05-7.5	CH05-7.5B
	Total bioclast %	65	60	55	70
	Bryozoans	VA	VC	VC	VC
	Bivalves	M	M	R	R
	Echinoderms	S	S	S	S
C	Benthic foraminifera	S	R	R	R
a	Planktic foraminifera	S	R		R
l	Gastropods				R
c	Calcareous algae	S			
i	Barnacles				
c	Spicules & spines				
l	**Other**				
a	Brachiopods	S			
s	Serpulids	R			
t	Modal size 1 (mm)	0.50	0.08	0.18	0.80
s	Modal size 2 (mm)	2.25	2.13	1.25	
	Shape/abrasion	A	A	VA	A
	Sorting	P	P	P	P
	Intraclast %	0	0	0	0
	Siliciclastic grain %	5	5	5	2
	Quartz	S	R	R	R
S	Feldspar				
i	VRFs				
l	SRFs				
i	Micas				
c	Pyrite grains	S	R		
i	Pyrite infills	S	R		S
c	Glauconite pellets	R	R	R	S
l	Glauconite infills		R		
a	**Other**				
s	Phosphate	S	R	R	S
t	Limonite staining	A	S	R	S
s	Hornblende				
	Chert				
	Opaque				
	Modal size 1 (mm)	0.25	0.20	0.10	0.13
	Modal size 2 (mm)				
	Shape/abrasion	SA	SR	SR	SA-SR
	Sorting	P	P	P	P
	Interparticle material %	30	30	40	15
	Spar cement %	10	5	5	5
	Micrite %	20	25	35	10
Unoccluded pore space %		5	2	5	5

Matanginui Limestone		Tarawhenua Point, Smugglers Cove, Pitt Island		
Stratigraphic column number		11	11	11
Sample running number		CH05-7.1	CH05-7.2	CH05-7.3
	Total bioclast %	70	60	80
	Bryozoans	A	A	VA
	Bivalves	S	M	R
	Echinoderms	M	C	M
C	Benthic foraminifera	R	S	
a	Planktic foraminifera			
l	Gastropods			
c	Calcareous algae			
i	Barnacles			
c	Spicules & spines			
l	**Other**			
a	Brachiopods			
s	Serpulids			
t	Modal size 1 (mm)	0.45	0.15	0.38
s	Modal size 2 (mm)	2.87	2.25	3.75
	Shape/abrasion	A	VA	VA
	Sorting	P	P	P
	Intraclast %	0	2	0
	Siliciclastic grain %	2	5	2
	Quartz		R	R
S	Feldspar	R	R	
i	VRFs			R
l	SRFs	R		
i	Micas			
c	Pyrite grains	R		
i	Pyrite infills			
c	Glauconite pellets	R	R	
l	Glauconite infills	R		
a	**Other**			
s	Phosphate	R	R	
t	Limonite staining	S	R	
s	Hornblende			S
	Chert			
	Opaque			
	Modal size 1 (mm)	0.15	0.45	0.30
	Modal size 2 (mm)			
	Shape/abrasion	SA-SR	SR	SR
	Sorting	P	M	M
	Interparticle material %	20	30	10
	Spar cement %	5	5	5
	Micrite %	15	25	5
Unoccluded pore space %		10	5	10

Table B7: Component data for the Matanginui Limestone, Flowerpot Bay, Pitt Island (continued over page).

Matanginui Limestone		Flowerpot Bay, Pitt Island		
Stratigraphic column number		–	–	–
Unit		Kahuitara Tuff	Kahuitara Tuff	Matanginui Lst
Sample running number (fill number)		CH05-9.4 (1)	CH05-9.4 (2)	CH05-9.4 (3)
	Total bioclast %	0	0	55
	Bryozoans			VC
	Bivalves			S
	Echinoderms			C
C	Benthic foraminifera			R
a	Planktic foraminifera			R
l	Gastropods			
c	Calcareous algae			
i	Barnacles			R
c	Spicules & spines			
l	**Other**			
a	Brachiopods			
s	Serpulids			S
t	Modal size 1 (mm)			0.63
s	Modal size 2 (mm)			2.25
	Shape/abrasion			A
	Sorting			P
	Intraclast %	0	0	0
	Siliciclastic grain %	90	80	20
	Quartz	M		
S	Feldspar			
i	VRFs	C	C	M
l	SRFs	C		M
i	Micas			
c	Pyrite grains	S	R	S
i	Pyrite infills	M	R	
c	Glauconite pellets			
l	Glauconite infills			
a	**Other**			
s	Phosphate		M	S
t	Limonite staining	M	M	
s	Hornblende			
	Chert			R
	Opaque			
	Modal size 1 (mm)	0.50	0.60	0.13
	Modal size 2 (mm)			2.50
	Shape/abrasion	SR	SR	SR
	Sorting	P	P	P
	Interparticle material %	10	30	25
	Spar cement %	10	20	15
	Micrite %	0	0	10
Unoccluded pore space %		1	1	2

Matanginui Limestone		Flowerpot Bay, Pitt Island		
Stratigraphic column number		–	–	–
Unit		Matanginui Lst	Matanginui Lst	Matanginui Lst
Sample running number (fill number)		CH05-9.4 (4)	CH05-13A	CH05-13B
	Total bioclast %	75	60	75
	Bryozoans	VC	A	VC
	Bivalves	S		M
	Echinoderms	C	M	M
C	Benthic foraminifera	M	S	M
a	Planktic foraminifera	S	S	R
l	Gastropods			
c	Calcareous algae			
i	Barnacles			
c	Spicules & spines			
l	**Other**			
a	Brachiopods	R	R	
s	Serpulids		R	M
t	Modal size 1 (mm)	0.60	0.15	0.50
s	Modal size 2 (mm)	2.00	1.5	2
	Shape/abrasion	MA	A	A
	Sorting	P	P	P
	Intraclast %	0	2	0
	Siliciclastic grain %	5	7	2
	Quartz	R	M	
S	Feldspar			
i	VRFs	S	S	S
l	SRFs	R	R	
i	Micas			
c	Pyrite grains			
i	Pyrite infills	R	S	R
c	Glauconite pellets	R	S	R
l	Glauconite infills			R
a	**Other**			
s	Phosphate		S	R
t	Limonite staining		M	M
s	Hornblende			
	Chert			
	Opaque	R		
	Modal size 1 (mm)	0.30	0.6	0.25
	Modal size 2 (mm)			
	Shape/abrasion	SA-SR	SR	SA
	Sorting	M	P	PM
	Interparticle material %	25	30	17
	Spar cement %	10	5	6
	Micrite %	15	25	12
Unoccluded pore space %		2	3	6

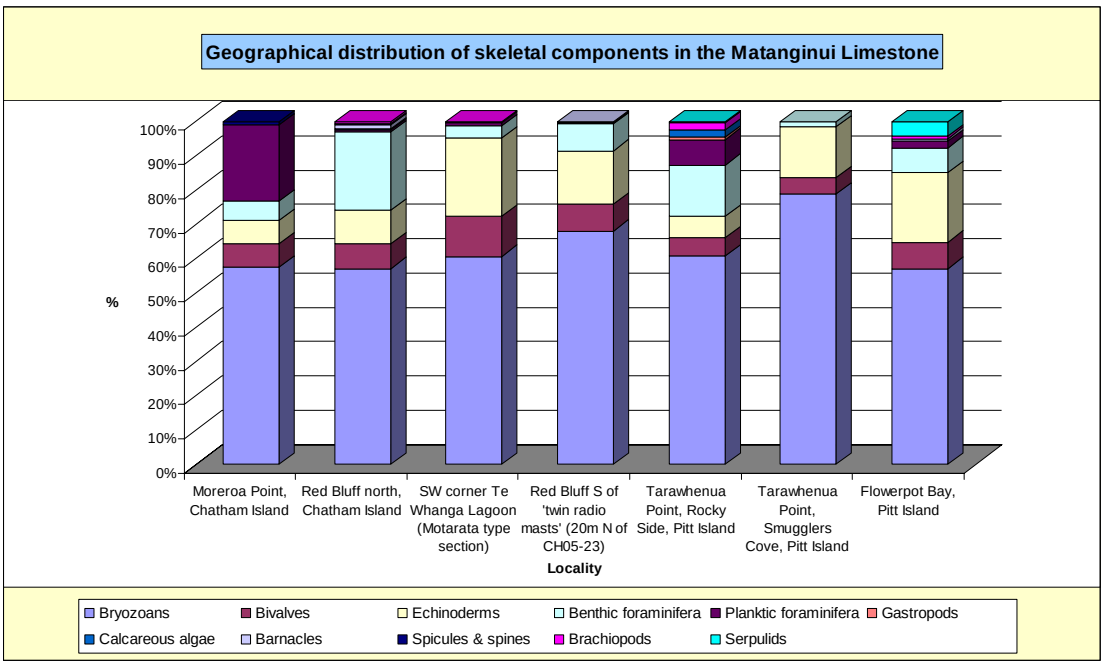

Figure B13: Geographical distribution of skeletal components in the Matanginui Limestone on the Chatham Islands.

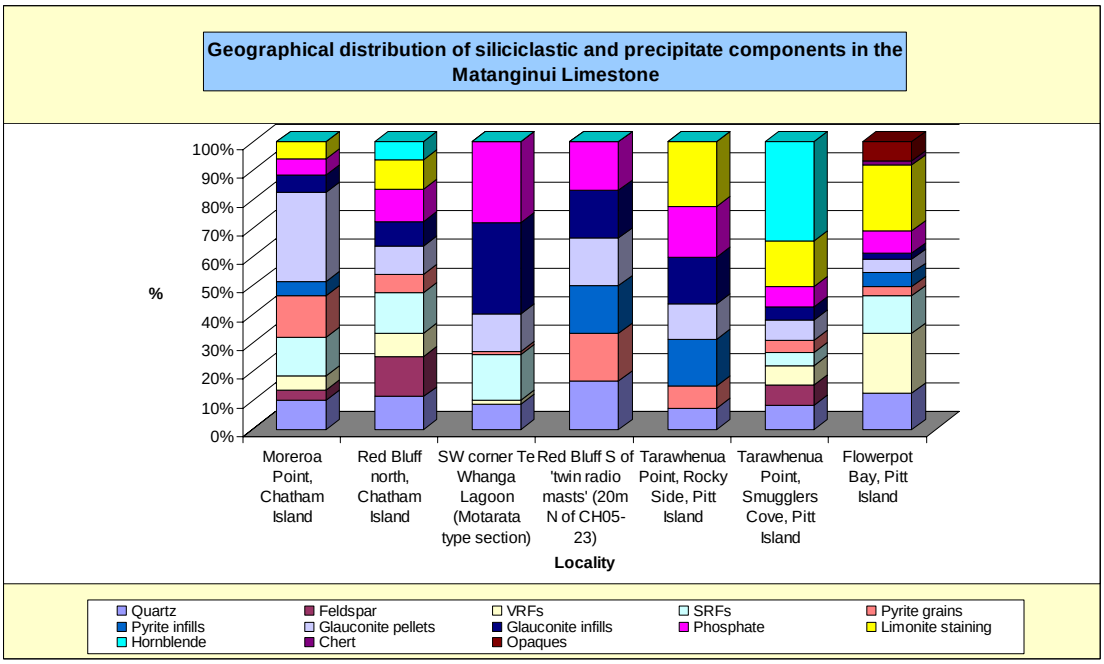

Figure B14: Geographical distribution of siliciclastic and precipitate components in the Matanginui Limestone, Chatham Islands.

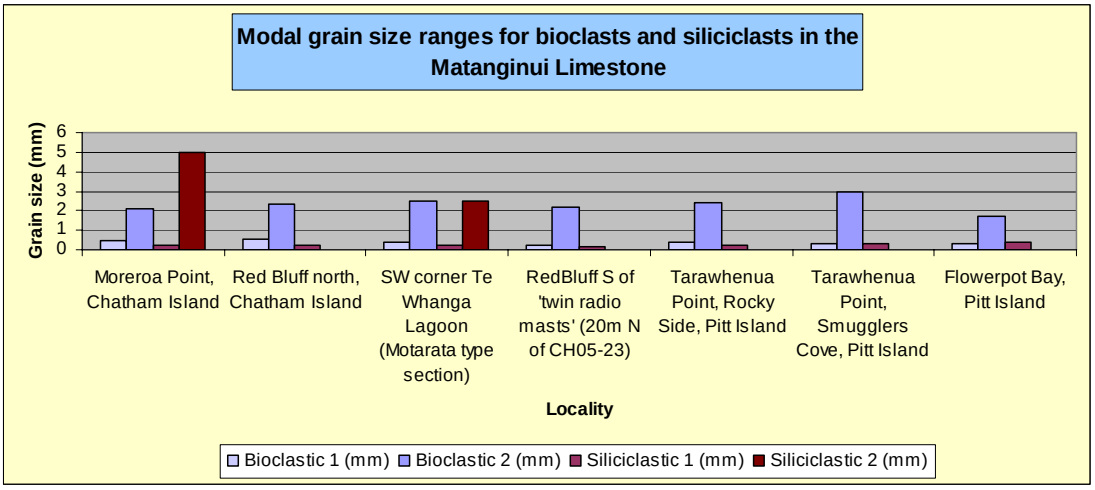

Figure B15: Geographical distribution of modal skeletal and siliciclastic/precipitate grain sizes in the Matanginui Limestone, Chatham Islands.

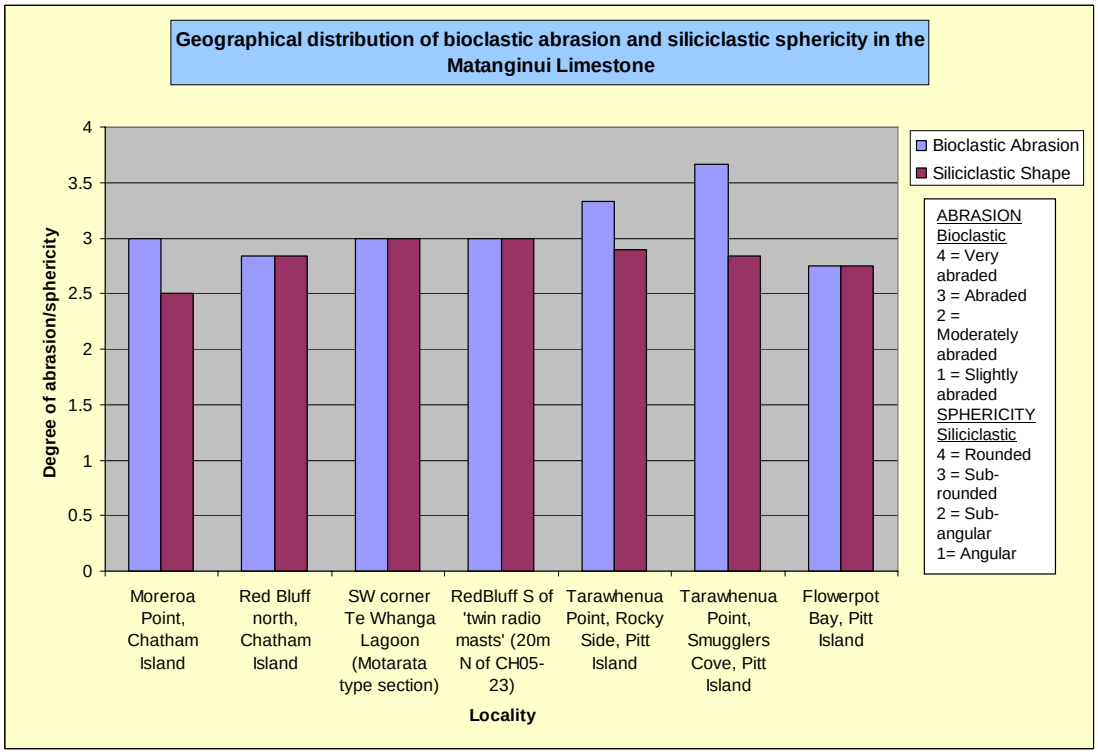

Figure B16: Geographical distribution of bioclastic abrasion and siliciclastic/precipitate grain sphericity in the Matanginui Limestone, Chatham Islands.

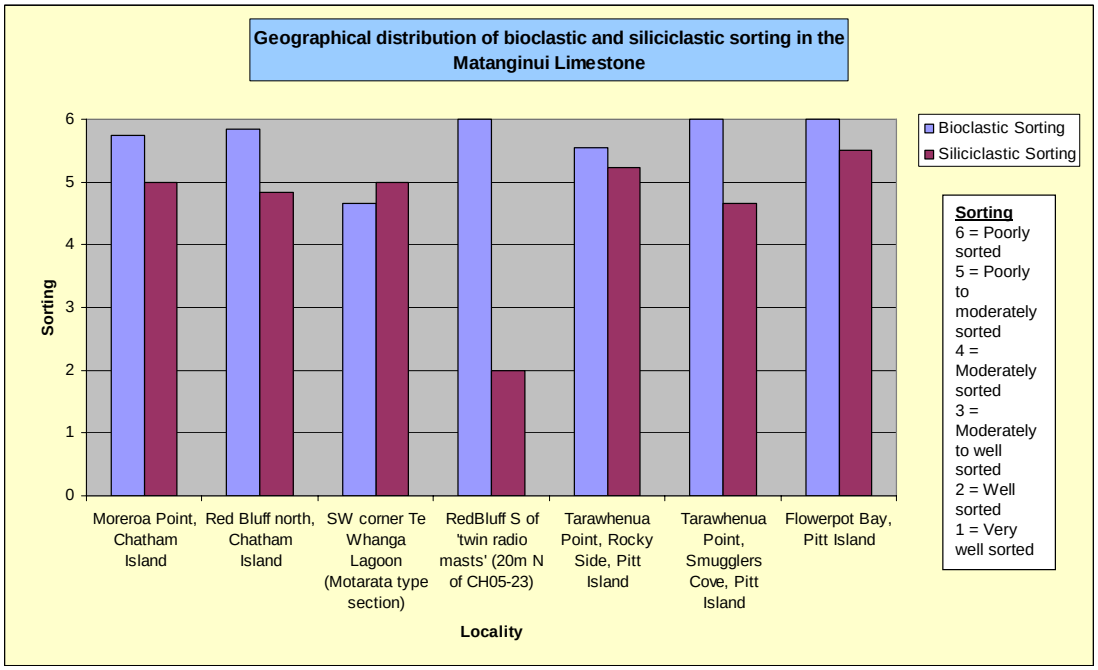

Figure B17: Geographical distribution of bioclast and siliciclastic/precipitate grain sorting in the Matanginui Limestone, Chatham Islands.

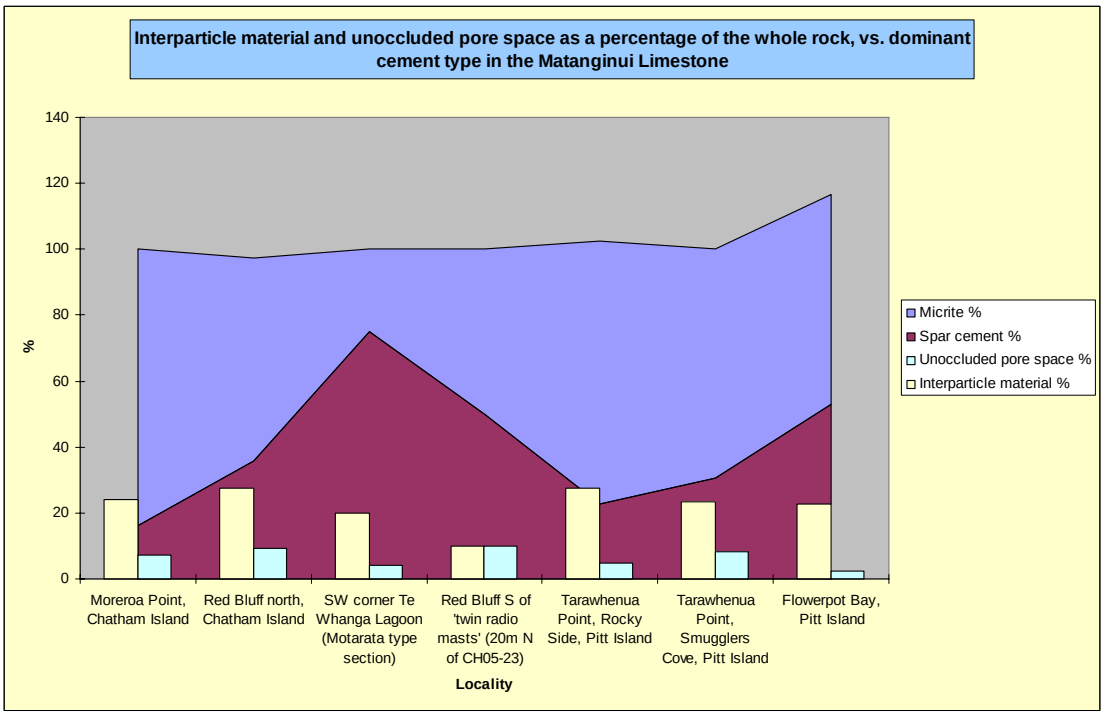

Figure B18: Geographical distribution of interparticle material and unoccluded pore space (foreground), and the amount of micrite and spar present (background) in the Matanginui Limestone, Chatham Islands.

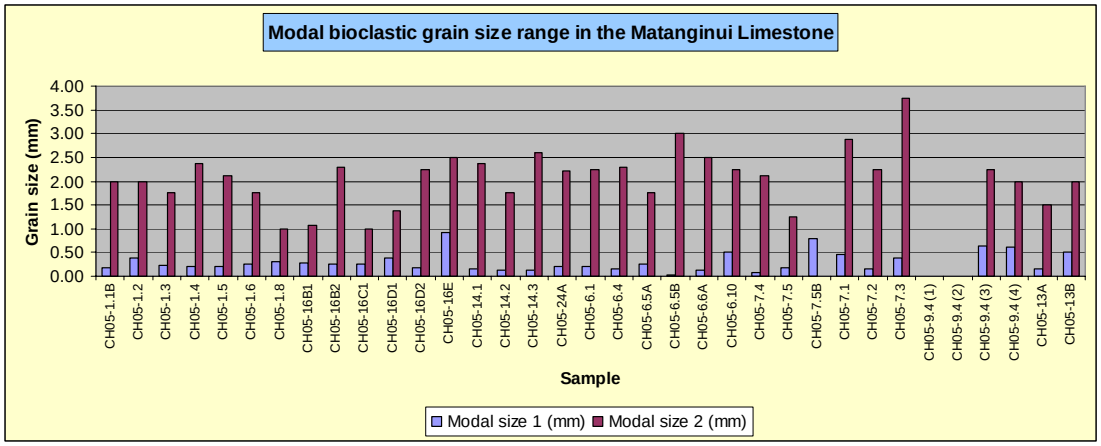

Figure B19: Modal bioclast grain sizes in the Matanginui Limestone, Chatham Islands.

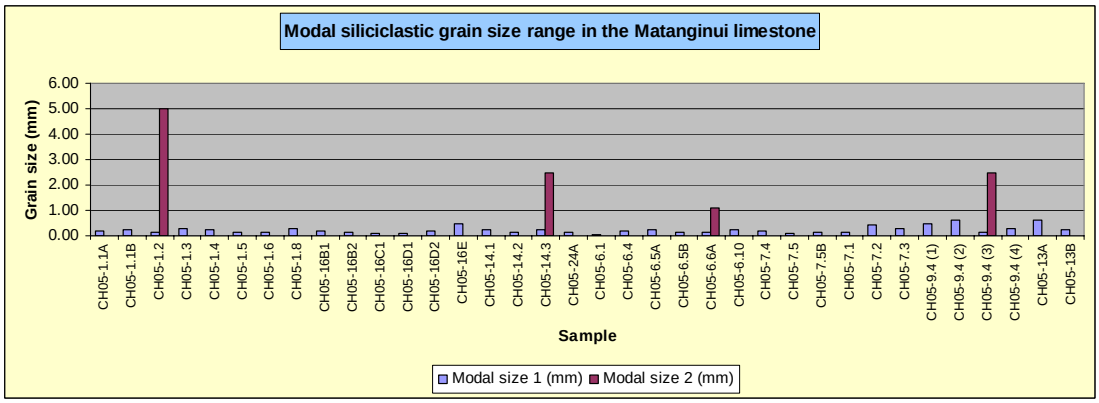

Figure B20: Modal siliciclastic grain sizes in the Matanginui Limestone, Chatham Islands.

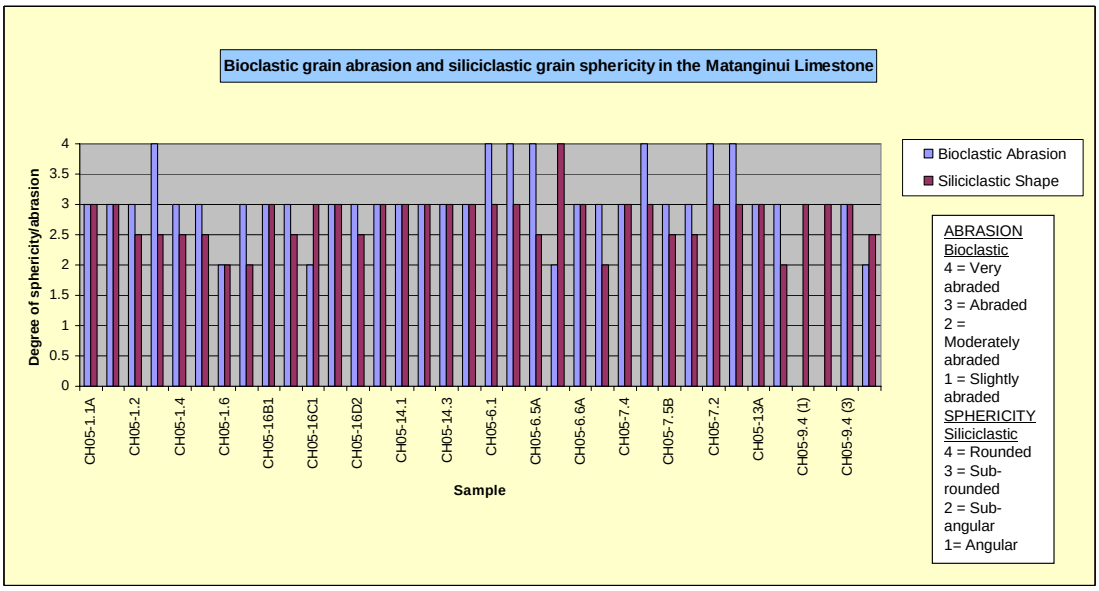

Figure B21: Bioclast abrasion and siliciclastic/precipitate sphericity in the Matanginui Limestone, Chatham Islands.

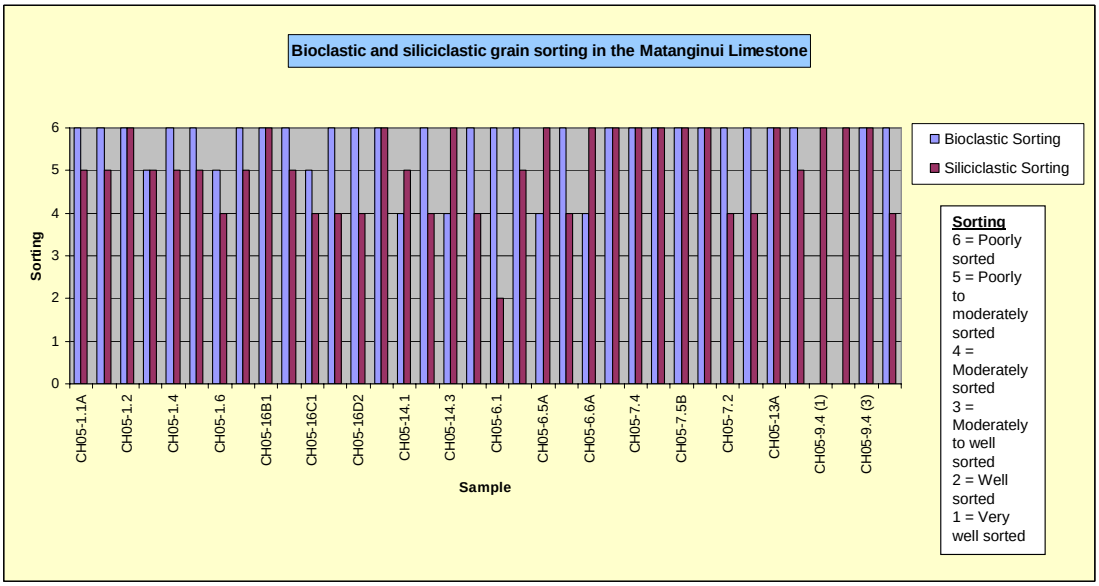

Figure B22: Bioclast and siliciclastic/precipitate grain sorting in the Matanginui Limestone, Chatham Islands.

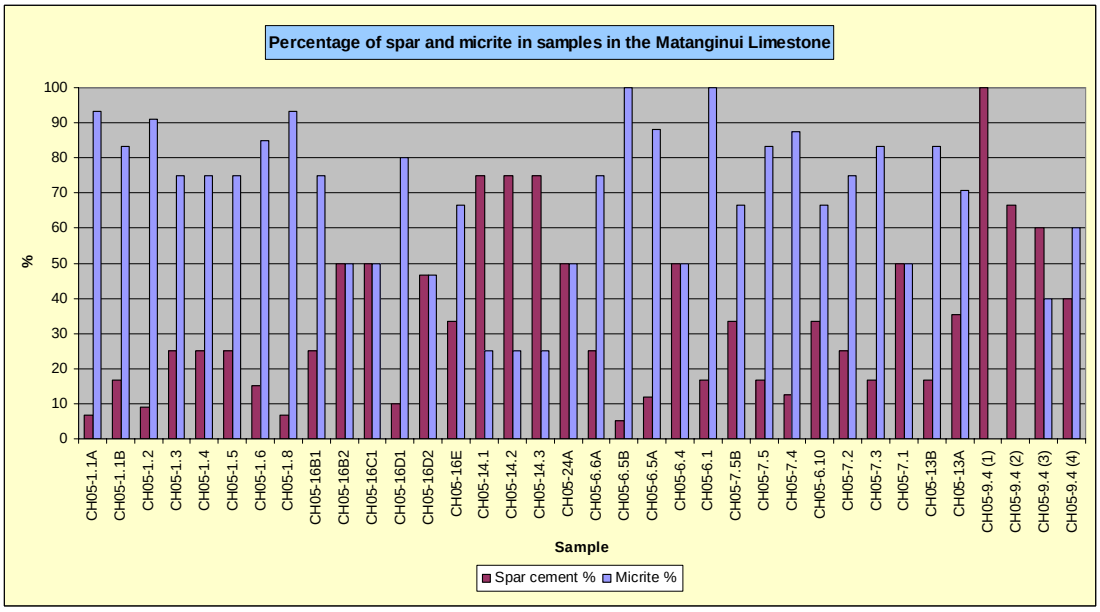

Figure B23: Percentage of spar versus micrite in samples of the Matanginui Limestone, Chatham Islands.

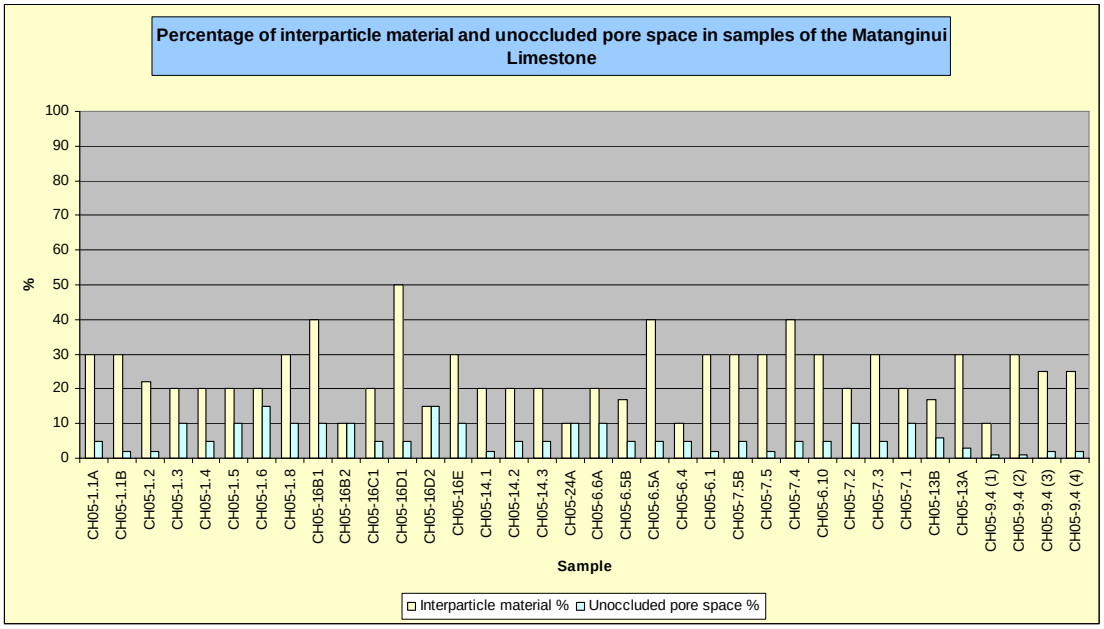

Figure B24: Percentage of interparticle material versus unoccluded pore space in samples of the Matanginui Limestone, Chatham Islands.

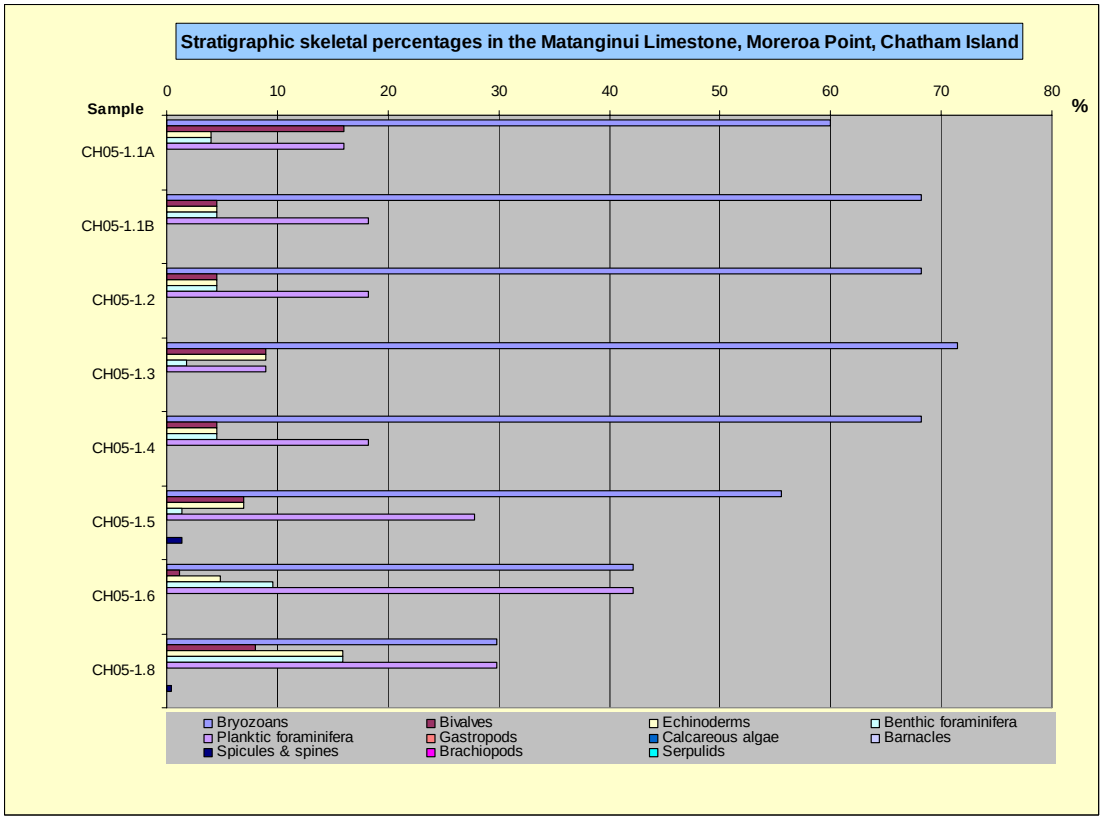

Figure B25: Stratigraphic skeletal percentages (up column) in the Matanginui Limestone at Moreroa Point, Chatham Island.

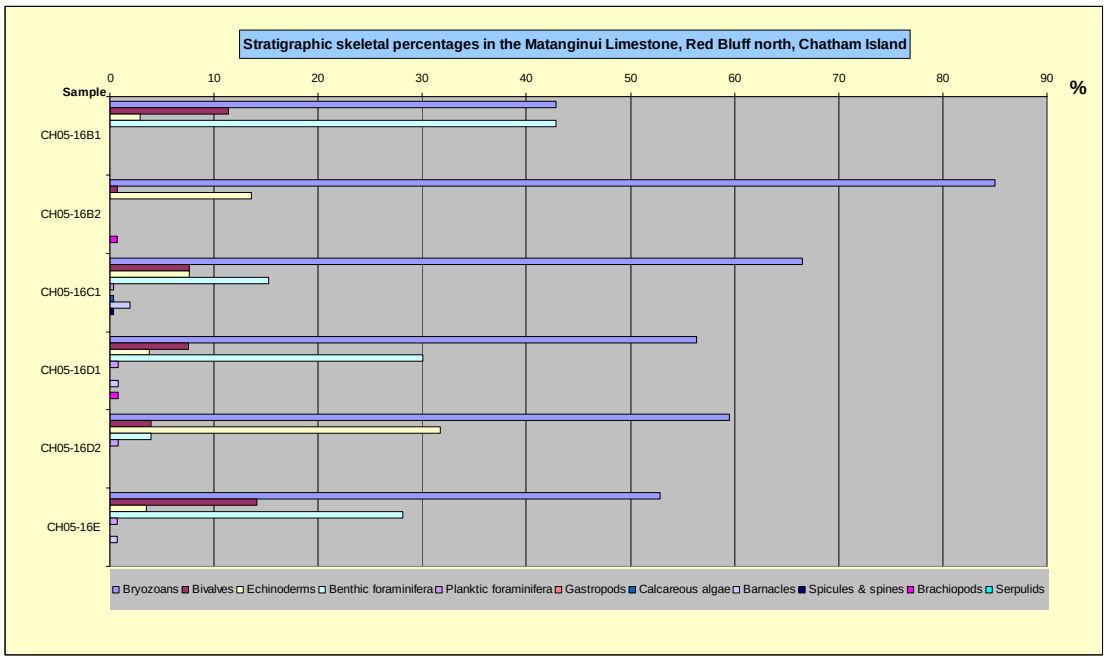

Figure B26: Stratigraphic skeletal percentages (up column) in the Matanginui Limestone at Red Bluff north, Chatham Island.

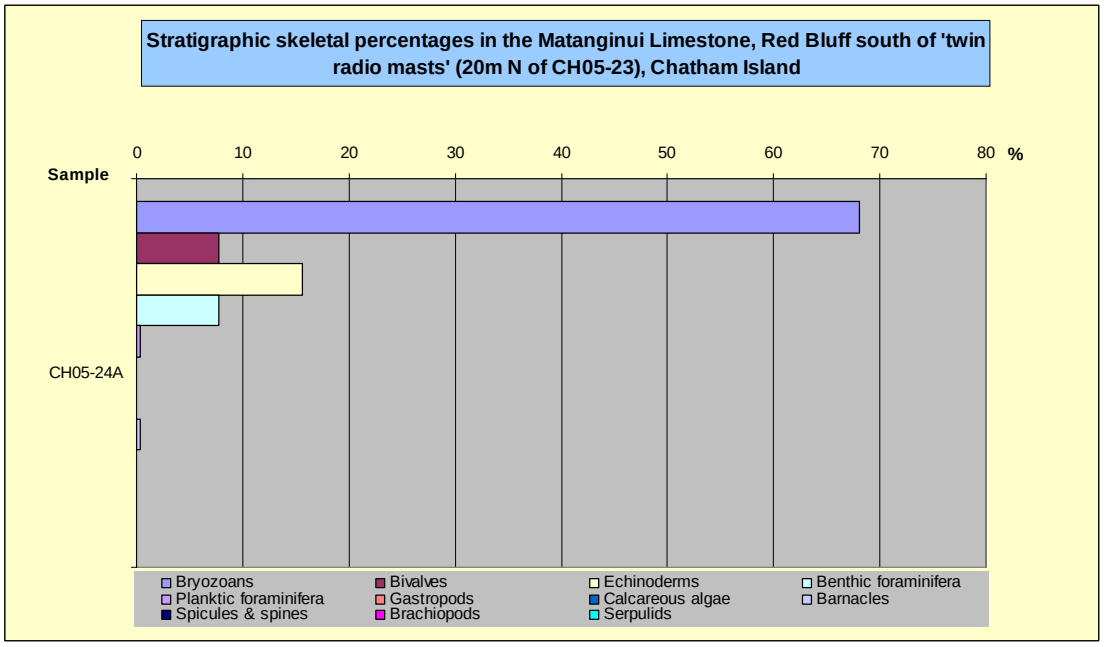

Figure B27: Stratigraphic skeletal percentages (up column) in the Matanginui Limestone at Red Bluff south, Chatham Island.

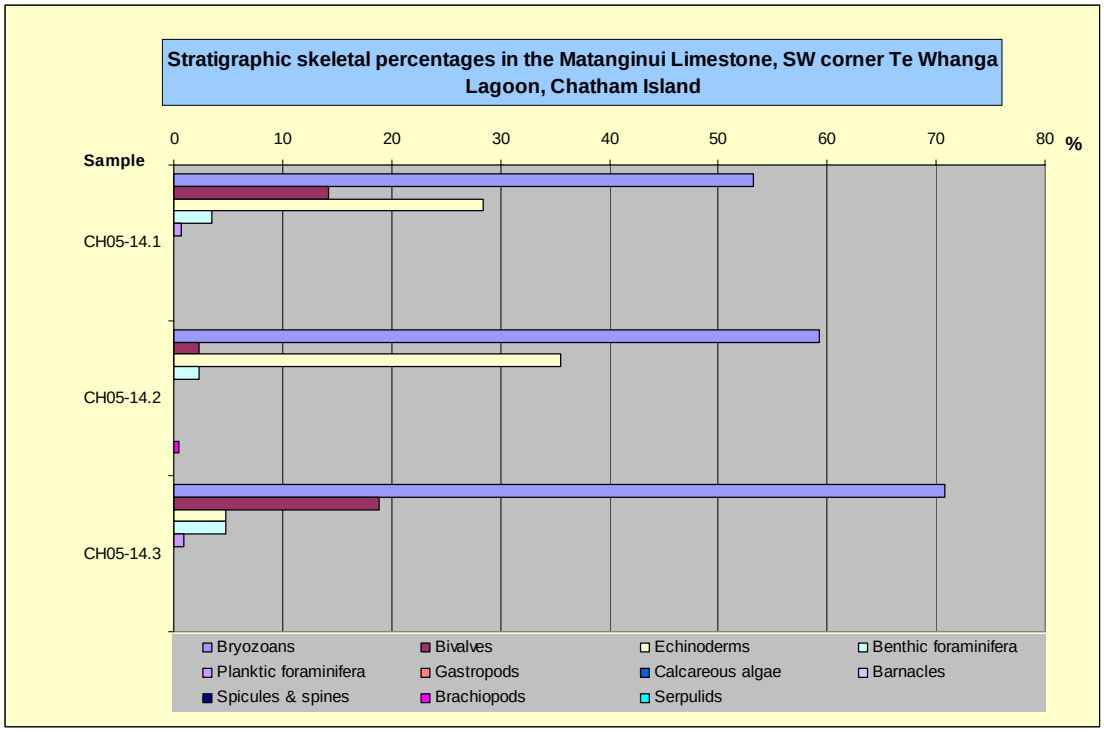

Figure B28: Stratigraphic skeletal percentages (up column) in the Matanginui Limestone at the south west corner of Te Whanga Lagoon, Chatham Island.

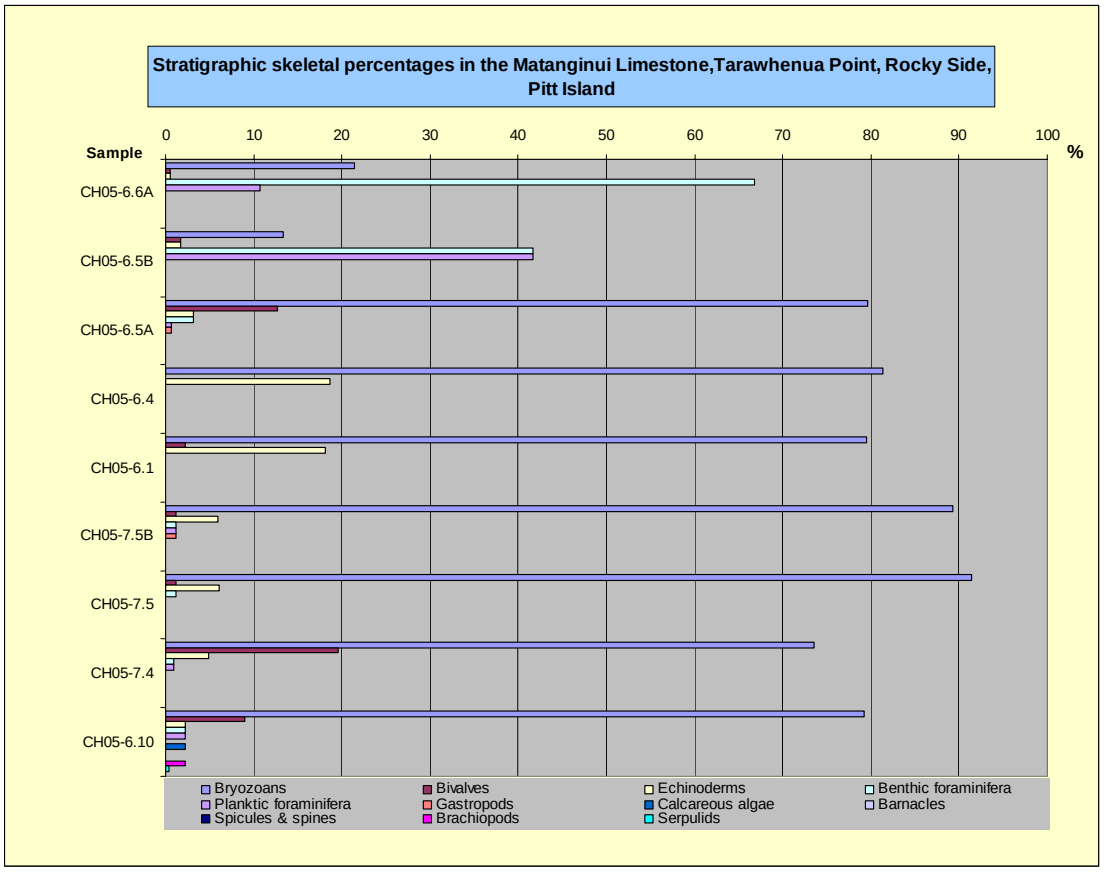

Figure B29: Stratigraphic skeletal percentages (up column) in the Matanginui Limestone at Rocky Side, Pitt Island.

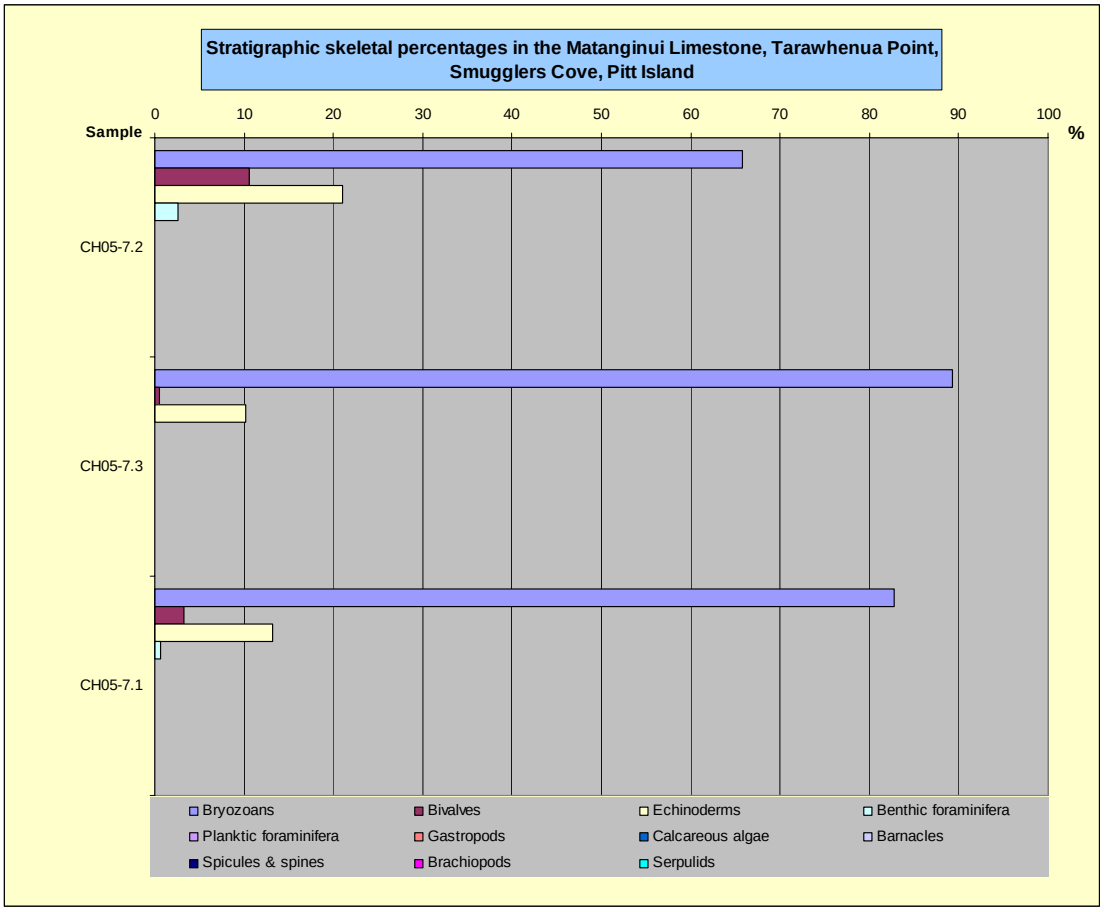

Figure B30: Stratigraphic skeletal percentages (up column) in the Matanginui Limestone at Smugglers Cove, Pitt Island.

Te One Limestone

Table B8: Component data for the Te One Limestone, Big Bush Quarry, Chatham Island.

Te One Limestone		Big Bush Quarry						
Stratigraphic column number		7	7	7	7	7	7	7
Sample running number		CH05-4.1	CH05-4.2	CH05-5.1	CH05-5.2	CH05-5.3	CH05-5.4	CH05-5.5
	Total bioclast %	70	85	90	75	75	80	70
	Bryozoans	VC	A	A	A	A	A	VC
	Bivalves	S	S	S	M	S	R	R
C	Echinoderms	S	S	C	S	S	C	C
a	Benthic foraminifera	R	R	M	R	M	S	R
l	Planktic foraminifera	R	M	C	C	M	M	S
c	Gastropods							R
i	Calcareous algae							
c	Barnacles							
l	Spicules & spines							
a	**Other**							
s	Brachiopods	R						
t	Modal size 1 (mm)	0.18	0.45	1.05	0.38	0.38	0.25	0.18
s	Modal size 2 (mm)	2.43	3.25		3.25	2.75	2.75	3.38
	Shape/abrasion	A	VA	VA	A	VA	A	A
	Sorting	P	PM	M	P	P	P	P
	Intraclast %	5	0	0	2	2	0	2
	Siliciclastic grain %	2	2	2	2	2	2	5
S	Quartz	R		R	R	R		R
i	Feldspar							
l	VRFs	R						
i	SRFs	R						
c	Micas							
i	Pyrite grains	R						
c	Pyrite infills	R						
l	Glauconite pellets	R	M	S	S	R	R	S
a	Glauconite infills	R	M	S	R	R	R	R
s	**Other**							
t	Phosphate	R	R	R	R	R	R	R
s	Limonite staining	R						
	Hornblende							
	Modal size 1 (mm)	0.18	0.23	0.13	0.13	0.10	0.10	0.28
	Modal size 2 (mm)							
	Shape/abrasion	SR	R	SR	SA-SR	SR	R	SA-SR
	Sorting	M	M	M	PM	PM	M	PM
	Interparticle material %	25	10	5	20	20	15	20
	Spar cement %	5	5	3	5	10	5	5
	Micrite %	20	5	2	15	10	10	15
Unoccluded pore space %		5	5	5	5	5	5	5

Table B9: Component data for the Te One Limestone, Moreroa Point, Chatham Island.

Te One Limestone		Moreroa Point, Chatham Island	
Stratigraphic column number		6	6
Sample running number		CH05-1.7	CH05-1.9
	Total bioclast %	80	70
	Bryozoans	A	VA
	Bivalves	M	R
C	Echinoderms	C	C
a	Benthic foraminifera	S	S
l	Planktic foraminifera	R	S
c	Gastropods		R
i	Calcareous algae		
c	Barnacles		
l	Spicules & spines		
a	**Other**		
s	Brachiopods		M
t	Modal size 1 (mm)	0.5	0.25
s	Modal size 2 (mm)	3	1.05
	Shape/abrasion	A	MA
	Sorting	PM	M
	Intraclast %	0	0
	Siliciclastic grain %	2	5
S	Quartz	R	R
i	Feldspar		
l	VRFs		
i	SRFs		R
c	Micas		
i	Pyrite grains		
c	Pyrite infills		
l	Glauconite pellets	S	S
a	Glauconite infills	R	R
s	**Other**		
t	Phosphate	S	
s	Limonite staining		R
	Hornblende		
	Modal size 1 (mm)	0.1	0.7
	Modal size 2 (mm)		
	Shape/abrasion	R	SA
	Sorting	M	M
	Interparticle material %	15	20
	Spar cement %	2	2
	Micrite %	13	18
Unoccluded pore space %		5	10

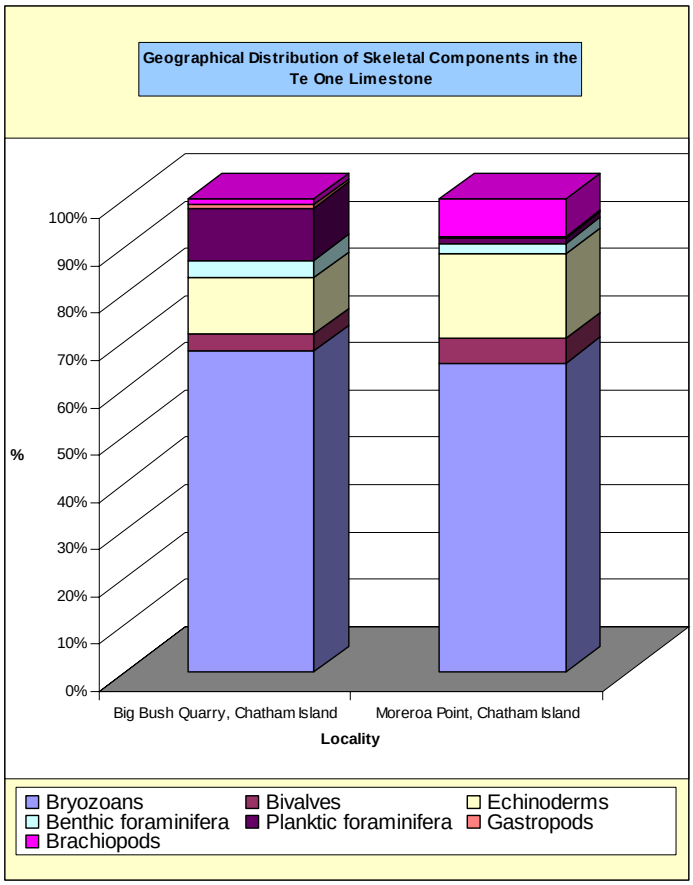

Figure B31: Geographical distribution of skeletal components in the Te One Limestone on the Chatham Islands.

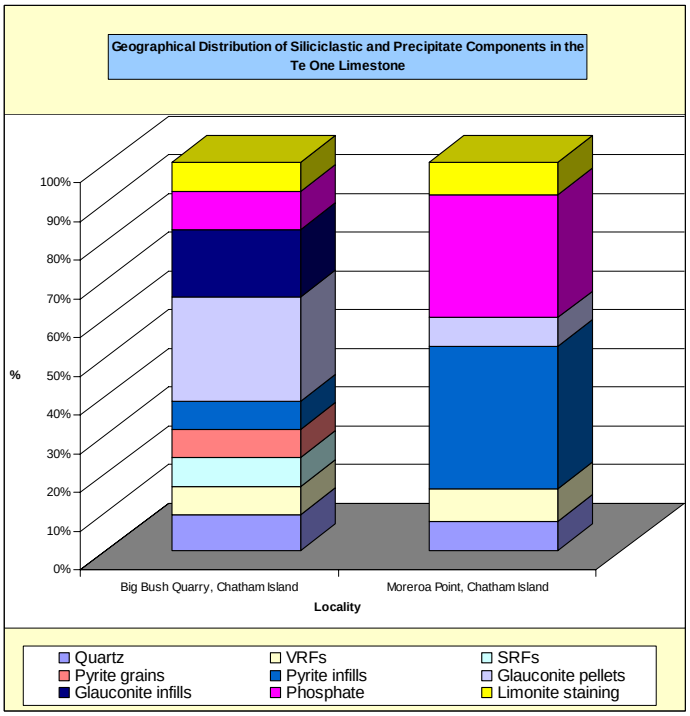

Figure B32: Geographical distribution of siliciclastic and precipitate components in the Te One Limestone, Chatham Islands.

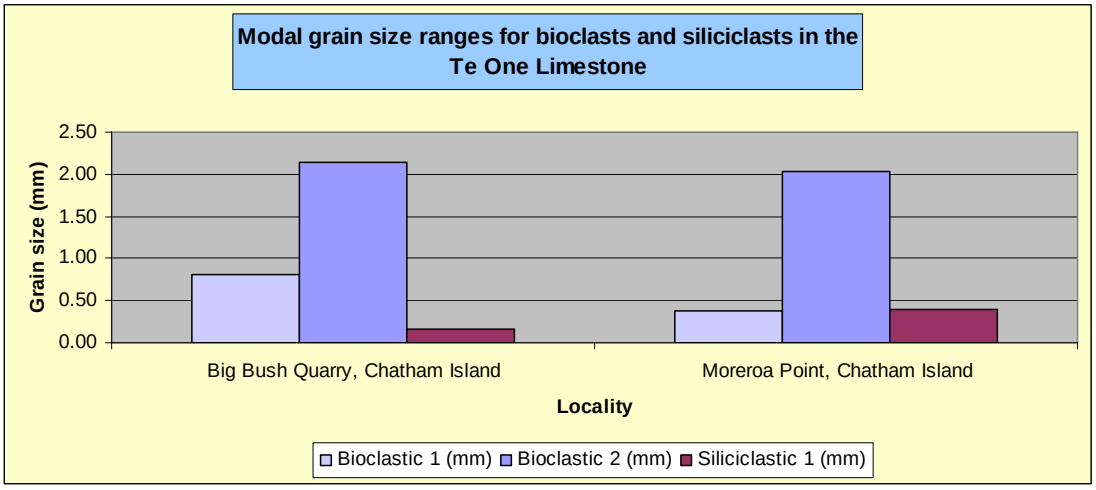

Figure B33: Geographical distribution of modal skeletal and siliciclastic/precipitate grain sizes in the Te One Limestone, Chatham Islands.

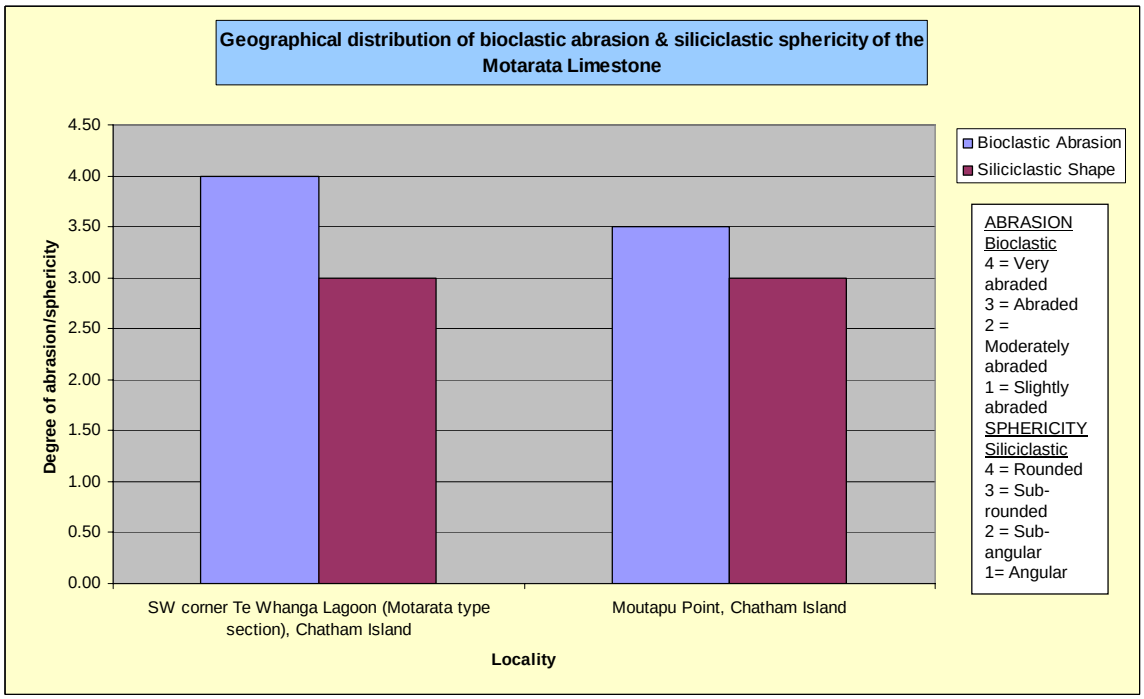

Figure B34: Geographical distribution of bioclastic abrasion and siliciclastic/precipitate grain sphericity in the Te One Limestone, Chatham Islands.

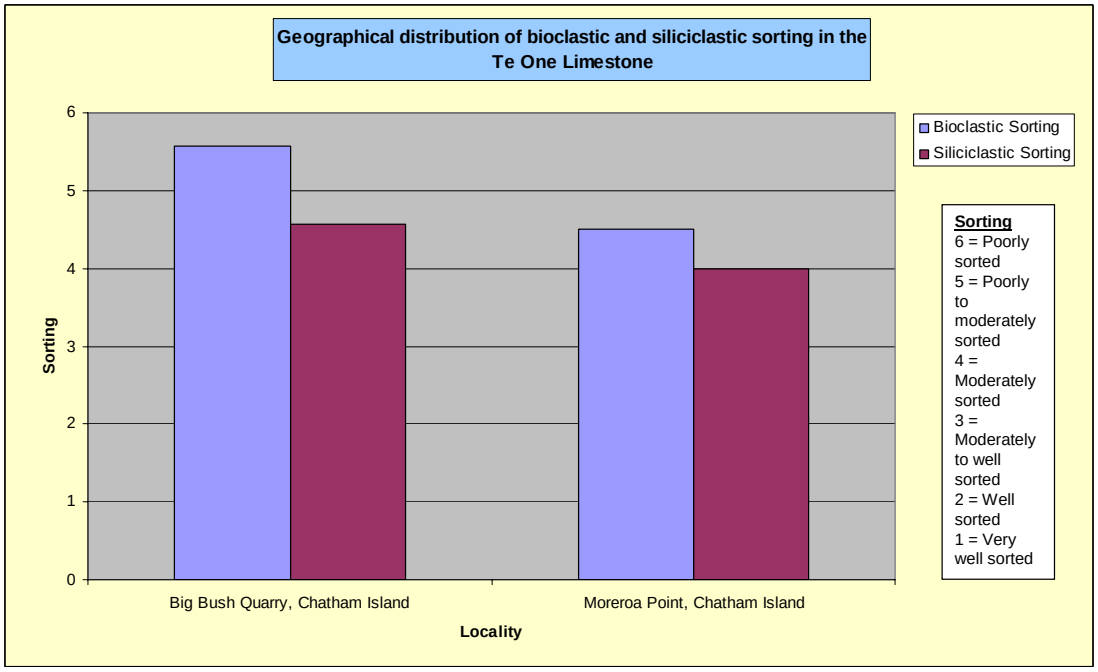

Figure B35: Geographical distribution of bioclast and siliciclastic/precipitate grain sorting in the Te One Limestone, Chatham Islands.

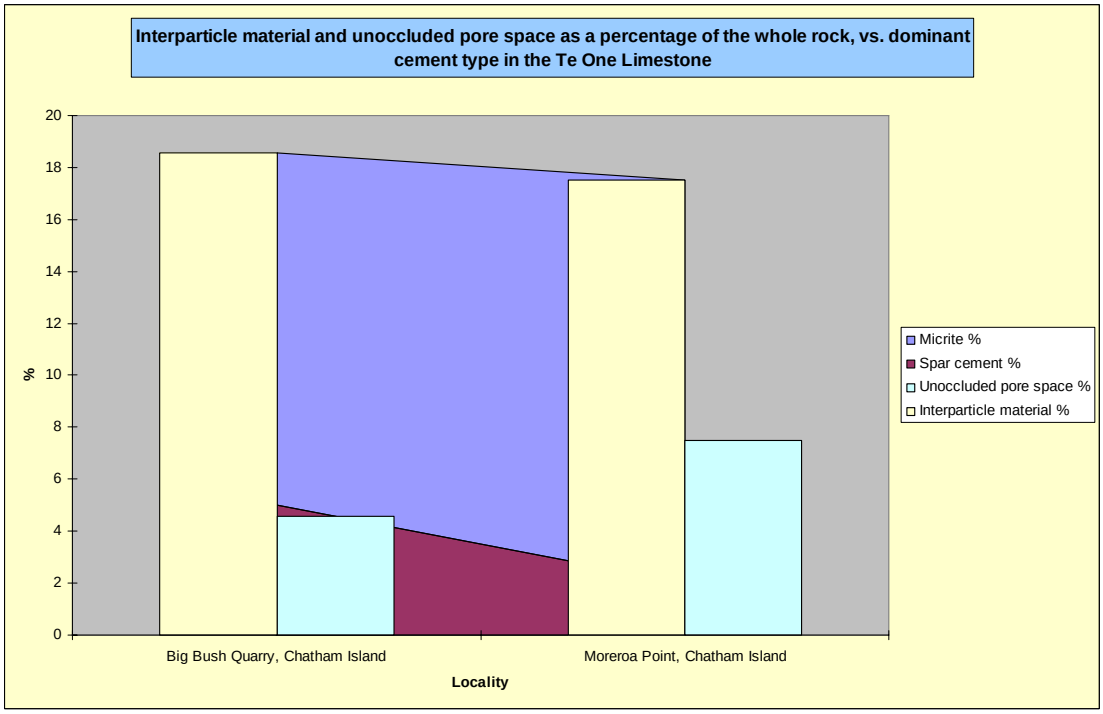

Figure B36: Geographical distribution of interparticle material and unoccluded pore space (foreground), and the amount of micrite and spar (background) present in the Te One Limestone, Chatham Islands.

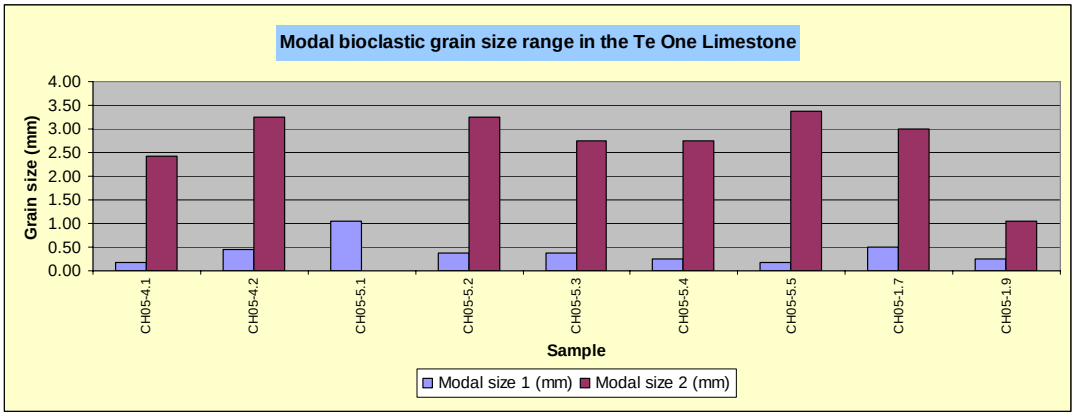

Figure B37: Modal bioclast grain sizes in the Te One Limestone, Chatham Islands.

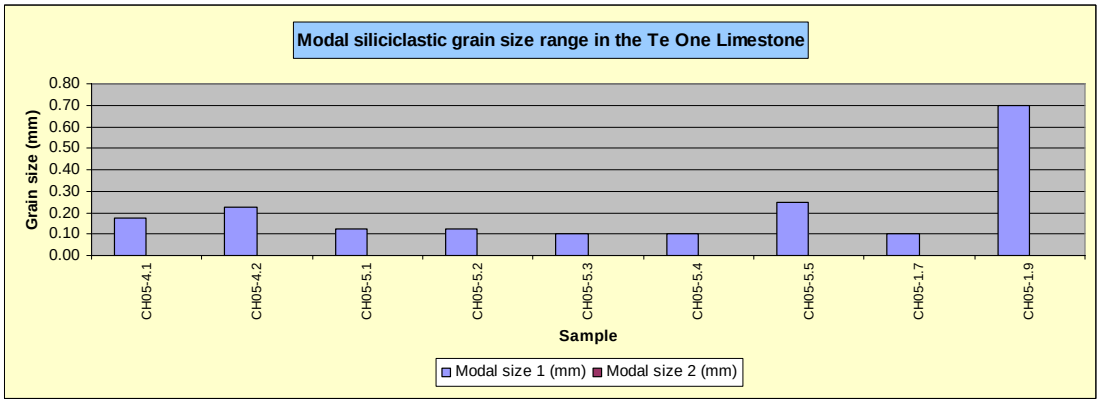

Figure B38: Modal siliciclastic grain sizes in the Te One Limestone, Chatham Islands.

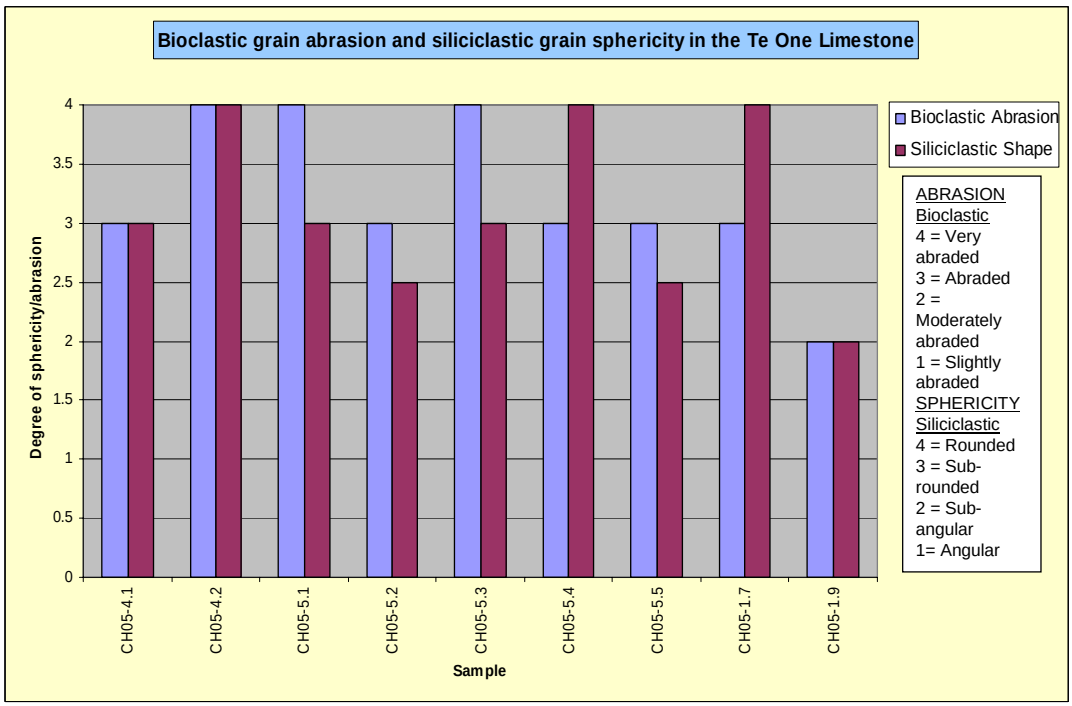

Figure B39: Bioclast abrasion and siliciclastic/precipitate sphericity for the Te One Limestone, Chatham Islands.

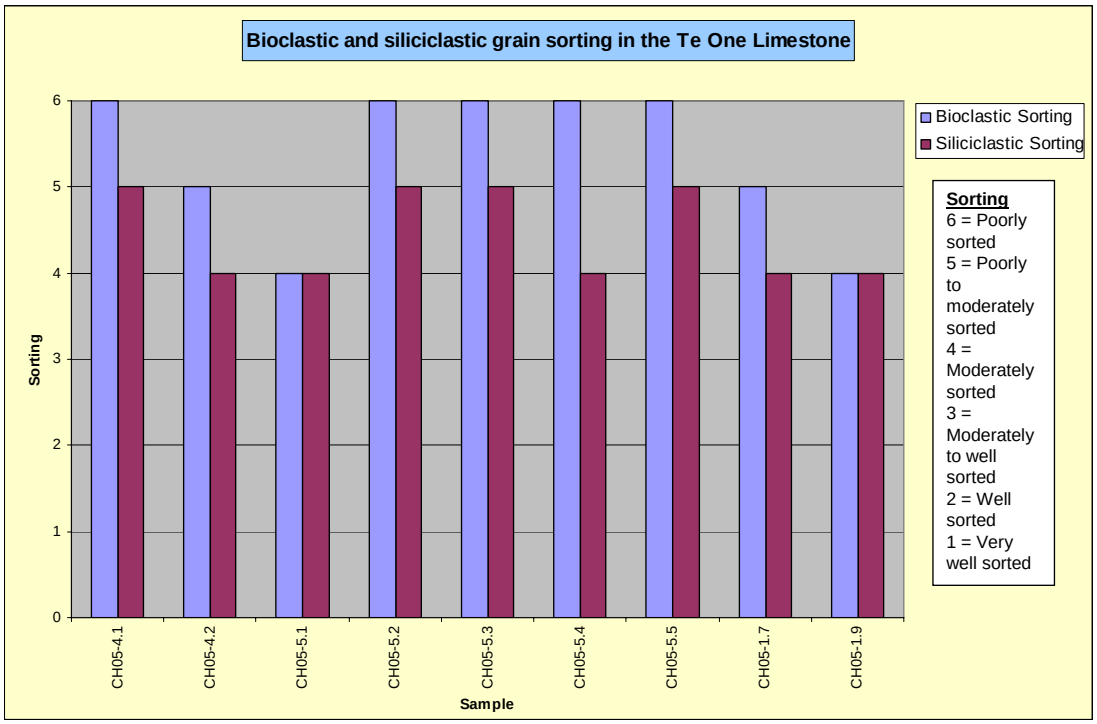

Figure B40: Bioclast and siliciclastic/precipitate grain sorting in the Te One Limestone, Chatham Islands.

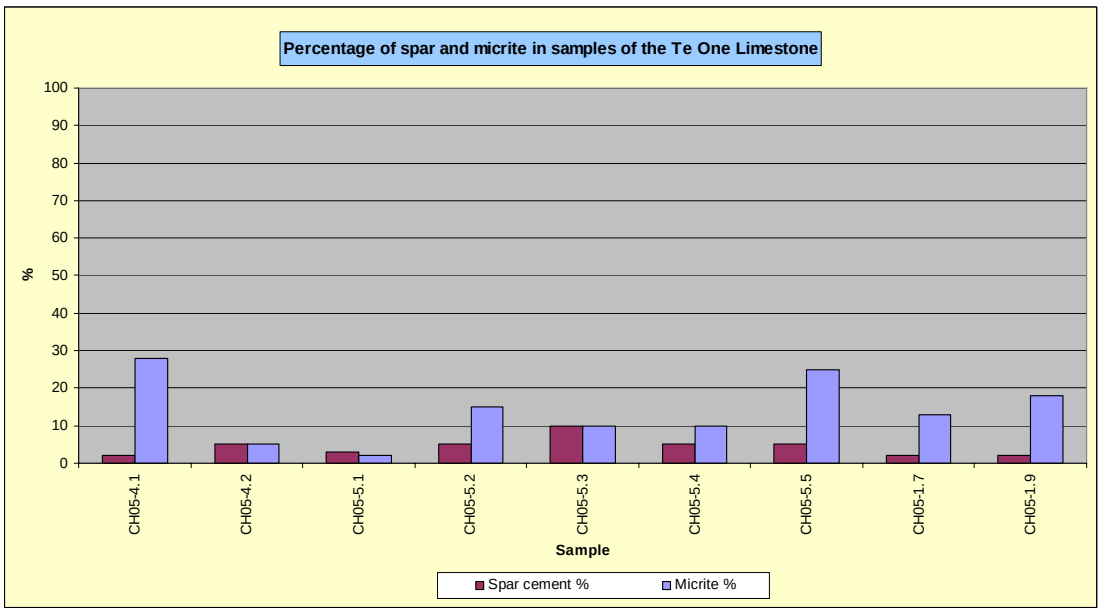

Figure B41: Percentage of spar versus micrite in samples of the Te One Limestone, Chatham Islands.

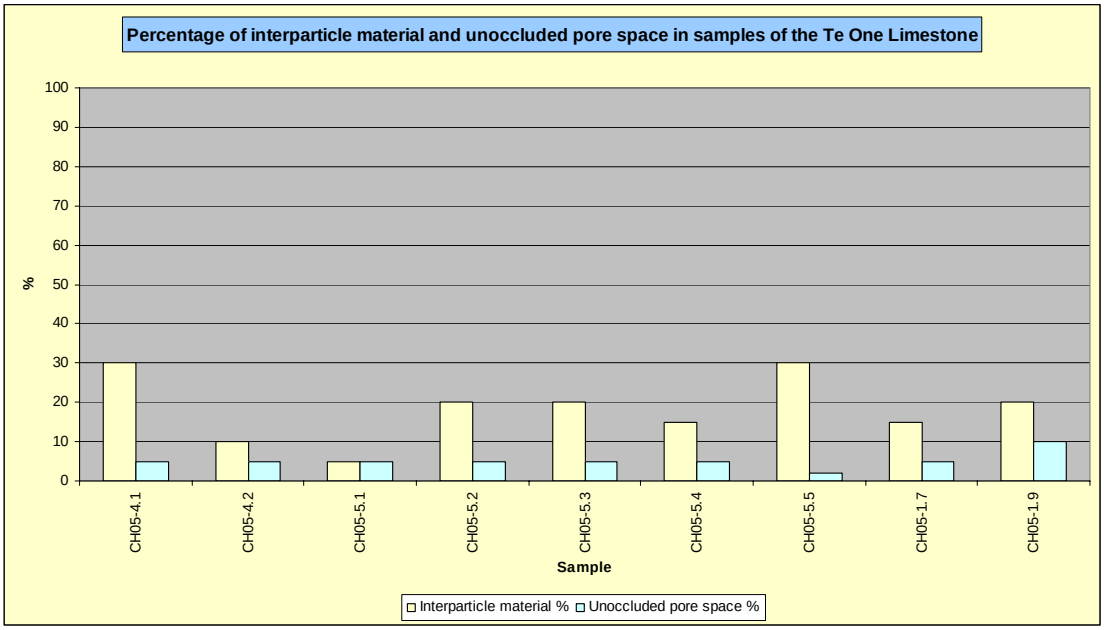

Figure B42: Percentage of interparticle material versus unoccluded pore space in samples of the Te One Limestone, Chatham Islands.

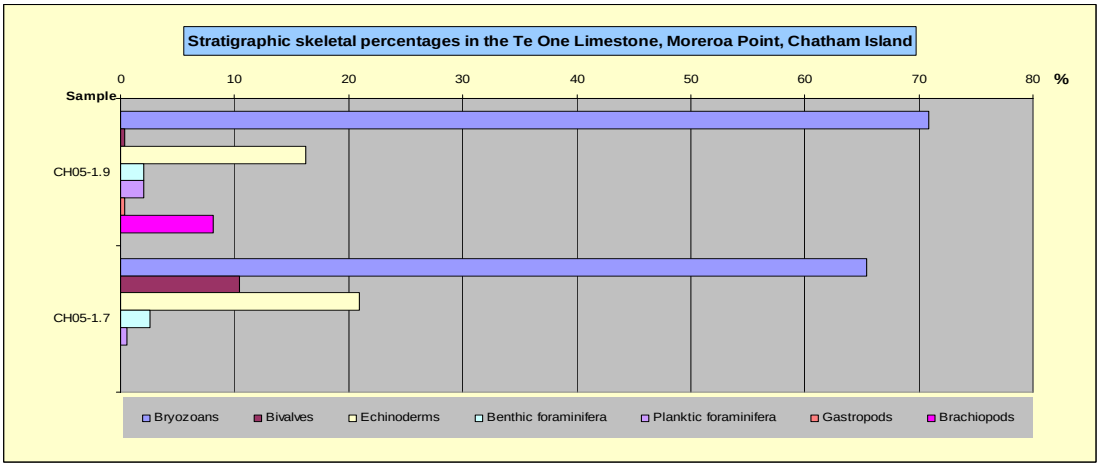

Figure B43: Stratigraphic skeletal percentages (up column) in the Te One Limestone at Moreroa Point, Chatham Island.

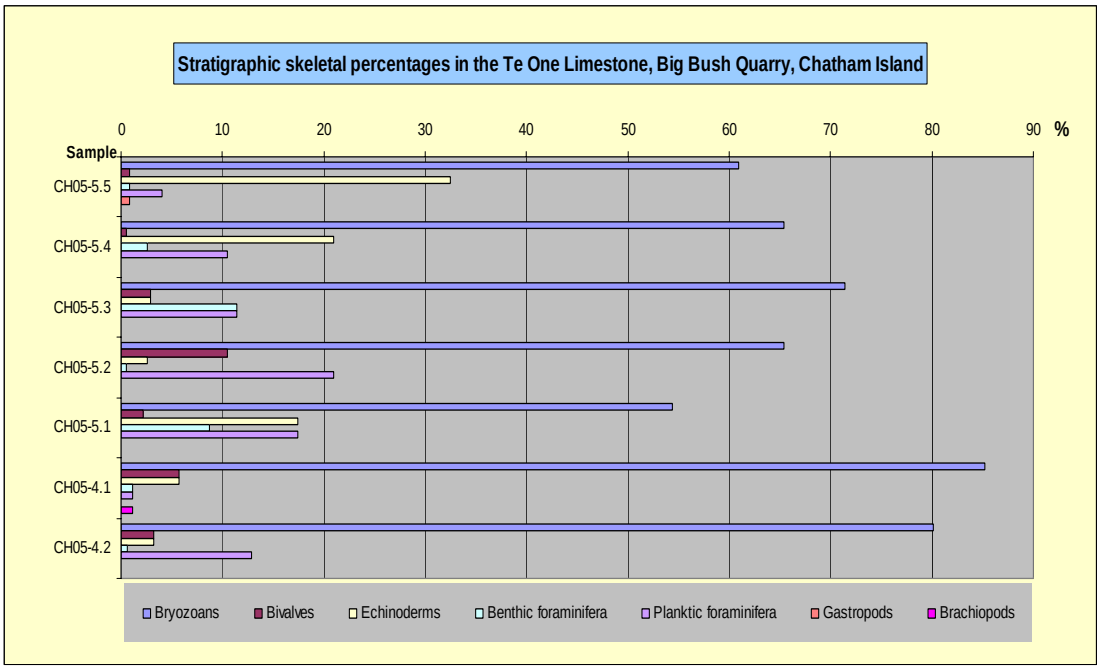

Figure B44: Stratigraphic skeletal percentages (up column) in the Te One Limestone at Big Bush Quarry, Chatham Island.

Taoroa Limestone

Table B10: Component data for the Taoroa Limestone, Cape Pattisson, Chatham Island.

Taoroa Limestone		Cape Pattisson, Chatham Island				
Stratigraphic column number		3	3	3	3	3
Sample running number		CH05-21A	CH05-21B	CH05-21C	CH05-21D	CH05-21E
	Total bioclast %	87	79	73	40	90
	Bryozoans	S	R	M	S	M
	Bivalves	VC	A	S	S	S
	Echinoderms	S	M	VC	M	C
C	Benthic foraminifera	M	C	C	M	VC
a	Planktic foraminifera	VC	VC	M	VC	VC
l	Gastropods					
c	Calcareous algae					
i	Barnacles					
c	Spicules & spines	R	C			
l	**Other**					
a	Pteropods	R			S	
s	Ostracods	M	R		R	R
t	Stromatolitic algae				R	
s	Collophane material	S	S		S	
	Modal size 1 (mm)	0.25	0.08	0.38	0.15	0.13
	Modal size 2 (mm)	2.25	2.40	2.50	1.63	1.30
	Shape/abrasion	VA	VA	VA	VA	A
	Sorting	M	M	PM	P	P
	Intraclast %	5	0	0	0	0
	Siliciclastic grain %	5	7	2	40	2
	Quartz	S	S	R	C	R
S	Feldspar				S	
i	VRFs				R	
l	SRFs				R	
i	Micas					
c	Pyrite grains	R	R		R	R
i	Pyrite infills	R	R		R	
c	Glauconite pellets	S	S	S	VC	R
l	Glauconite infills	R	R	R	S	
a	**Other**					
s	Phosphate	R	R	R	M	R
t	Chert				R	
s	Modal size 1 (mm)	0.15	0.13	0.15	0.88	0.10
	Modal size 2 (mm)				1.625	
	Shape/abrasion	SR	SR	SA-SR	SR-R	SR
	Sorting	M	W	M	PM	M
	Interparticle material %	7	13	25	20	11
	Spar cement %	1	3	5	2	4
	Micrite %	6	10	20	16	7
Unoccluded pore space %		1	1	5	2	1

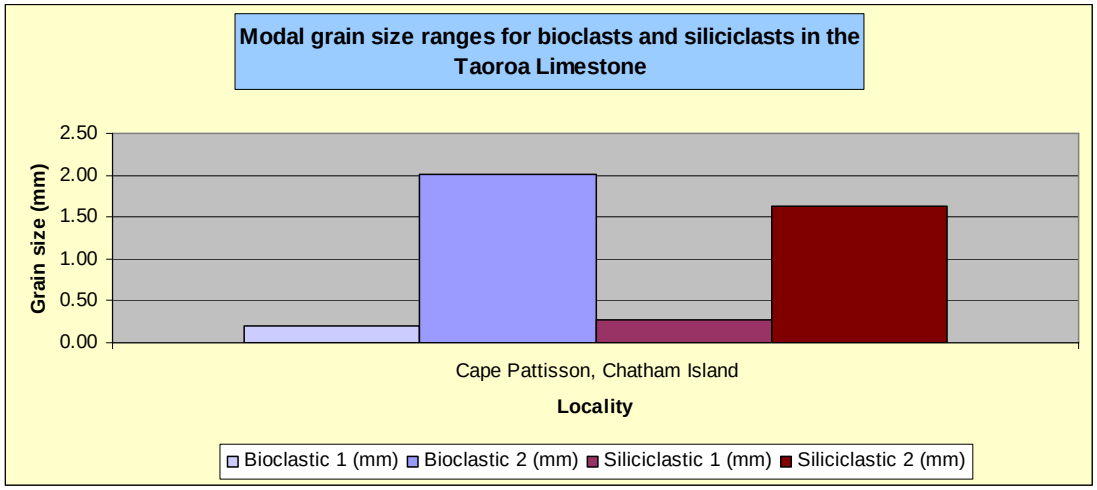

Figure B45: Modal skeletal and siliciclastic/precipitate grain sizes in the Taoroa Limestone, Chatham Islands.

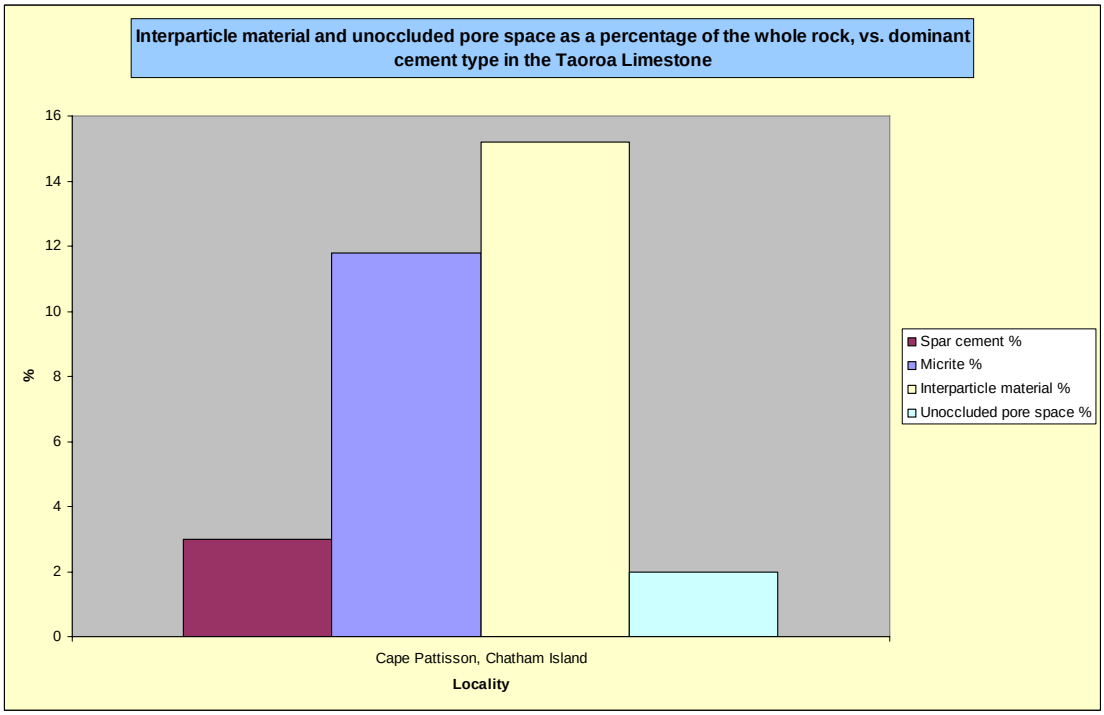

Figure B46: Percentages of interparticle material, unoccluded pore space, micrite and spar present in the Taoroa Limestone, Chatham Islands.

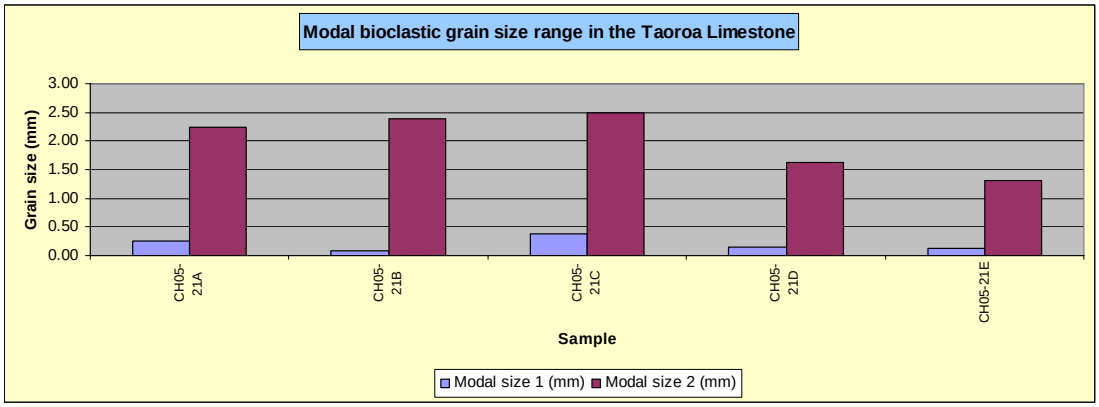

Figure B47: Modal bioclast grain sizes in the Taoroa Limestone, Chatham Islands.

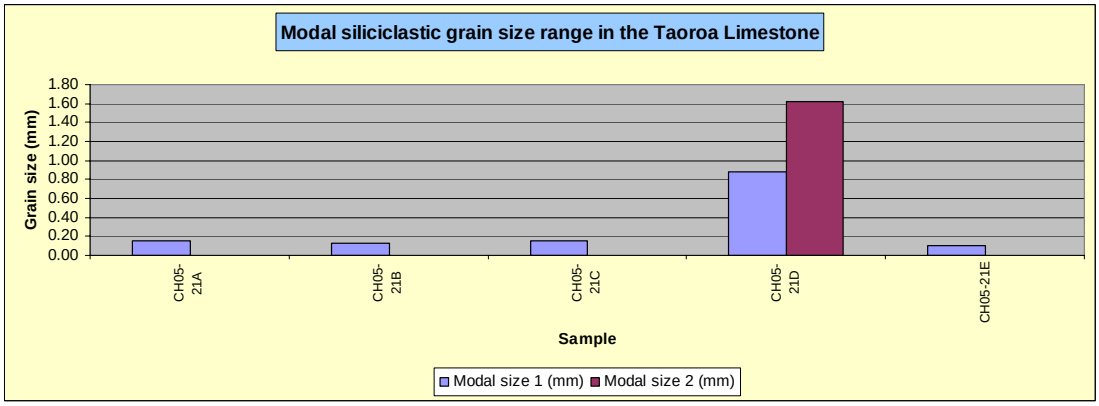

Figure B48: Modal siliciclastic grain sizes in the Taoroa Limestone, Chatham Islands.

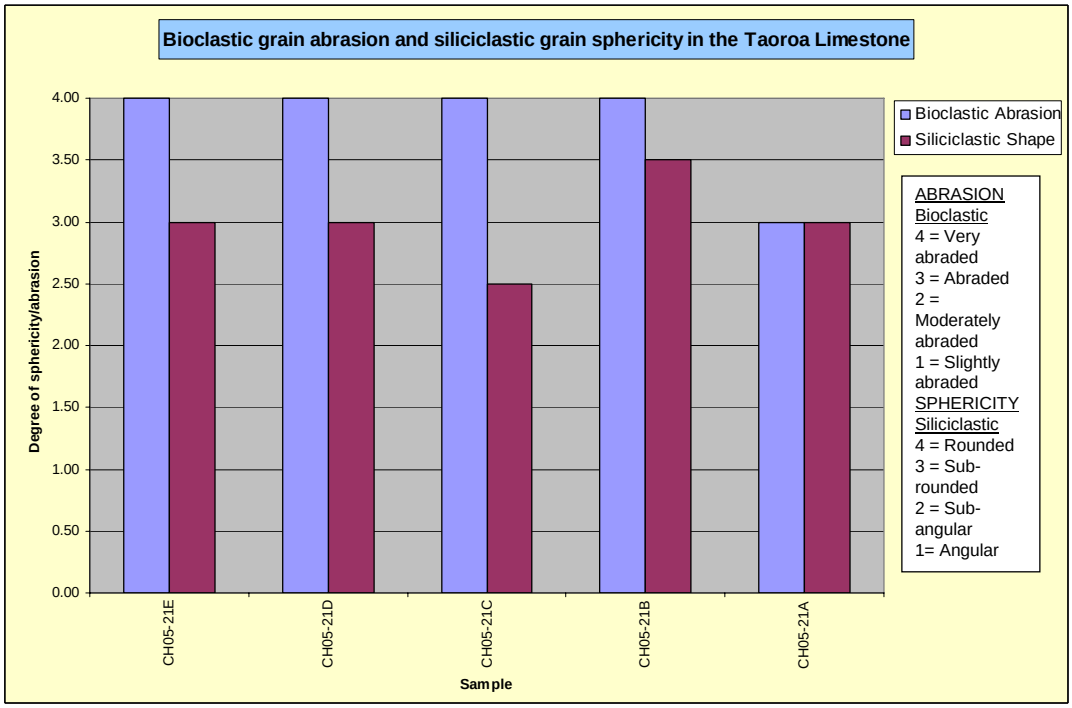

Figure B49: Bioclast abrasion and siliciclastic/precipitate sphericity in the Taoroa Limestone, Chatham Islands.

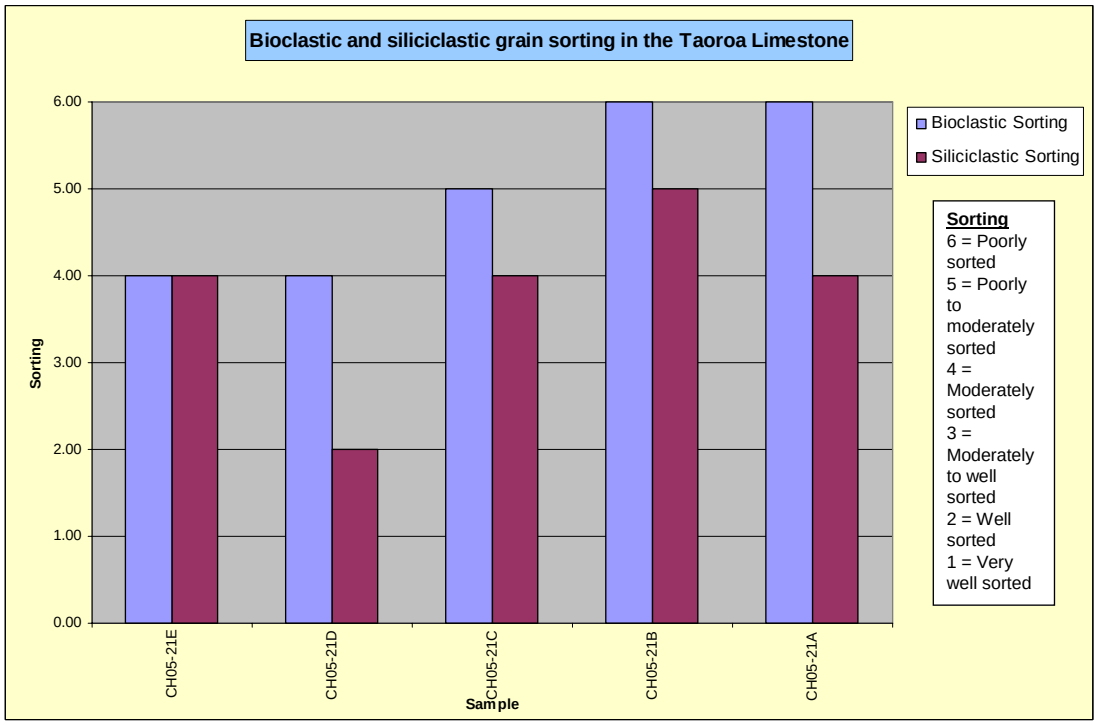

Figure B50: Bioclast and siliciclastic/precipitate grain sorting in the Taoroa Limestone, Chatham Islands.

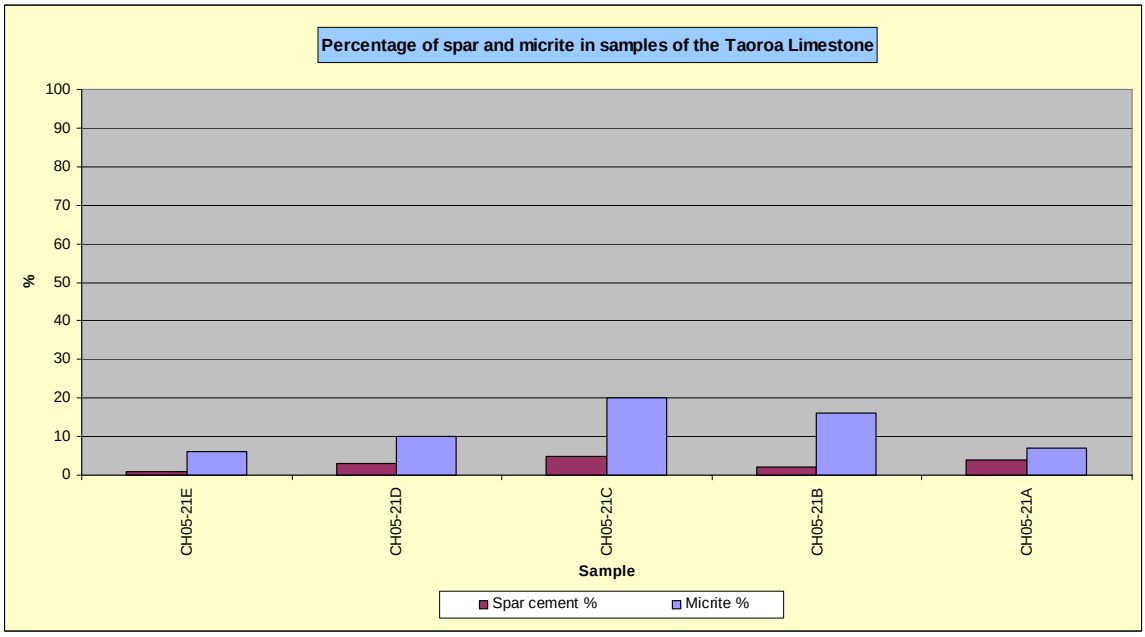

Figure B51: Percentage of spar versus micrite in samples of the Taoroa Limestone, Chatham Islands.

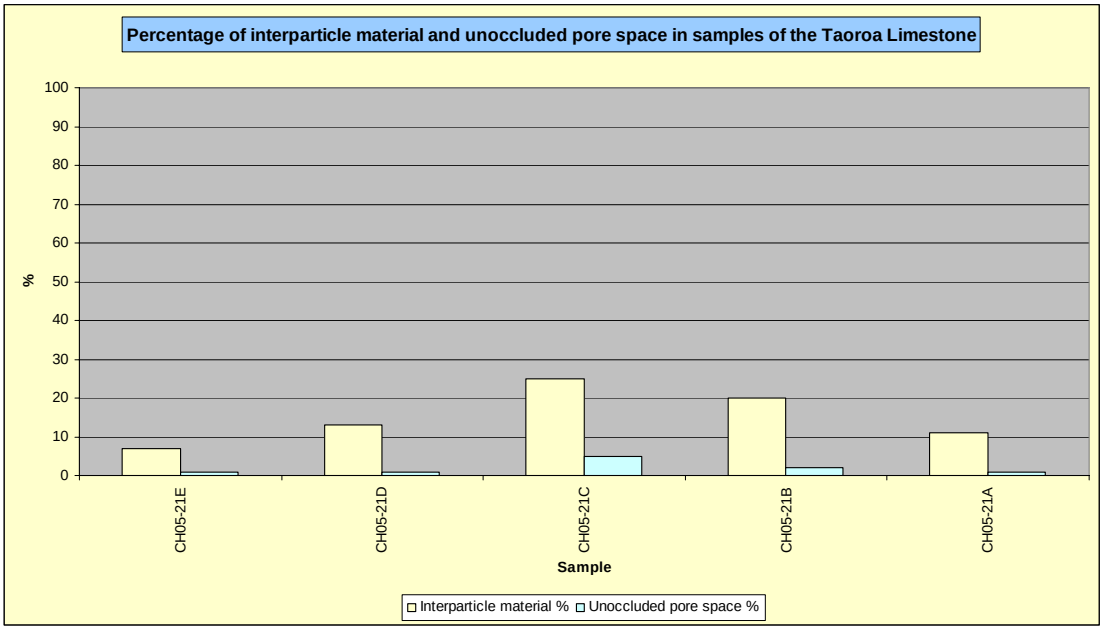

Figure B52: Percentage of interparticle material versus unoccluded pore space in samples of the Taoroa Limestone, Chatham Islands.

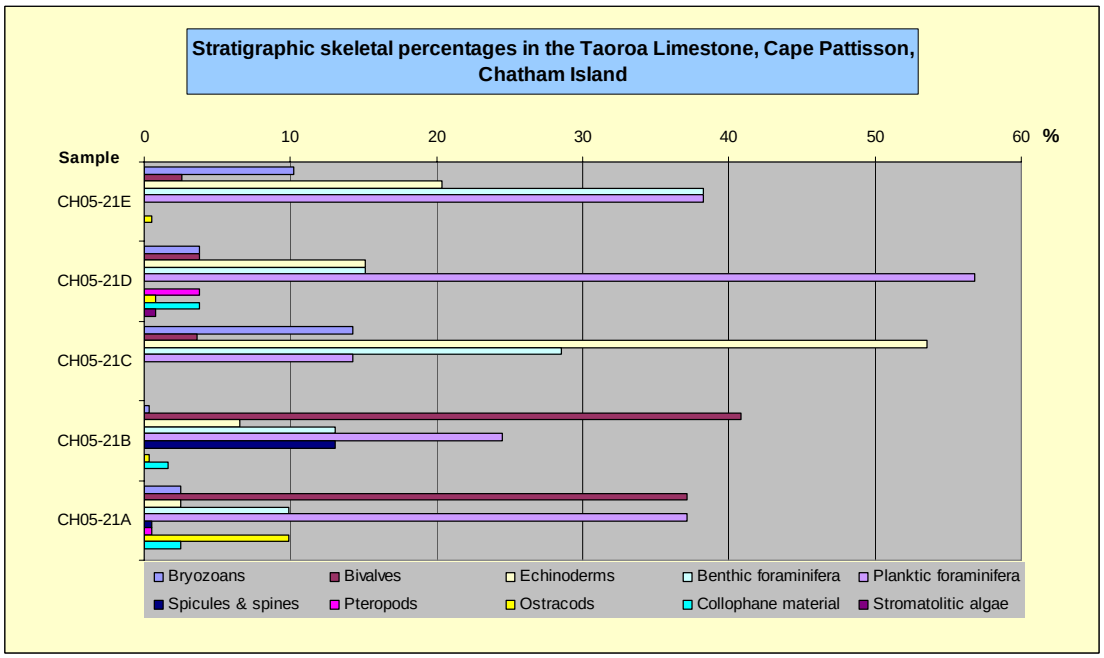

Figure B53: Stratigraphic skeletal percentages (up column) in the Taoroa Limestone at Cape Pattisson, Chatham Island.

Motarata Limestone

Table B11: Component data for the Motarata Limestone, Te Whanga Lagoon, Chatham Island.

Motarata Limestone		Te Whanga Lagoon, Chatham Island	
Stratigraphic column number		9	9
Sample running number		CH05-14.4	CH05-14.5
	Total bioclast %	60	80
	Bryozoans	VC	C
	Bivalves	M	M
	Echinoderms	S	S
C	Benthic foraminifera	S	C
a	Planktic foraminifera	R	VC
l	Gastropods		
c	Calcareous algae		
i	Barnacles		
c	Spicules & spines		
l	**Other**		
a	Brachiopods	R	R
s	Modal size 1 (mm)	0.18	0.13
t	Modal size 2 (mm)	2.33	2.22
s	Shape/abrasion	VA	VA
	Sorting	P	PM
	Intraclast %	2	0
	Siliciclastic grain %	15	3
	Quartz	R	R
S	Feldspar	R	R
i	VRFs	R	
l	SRFs	R	
i	Micas		
c	Pyrite grains	R	R
i	Pyrite infills		R
c	Glauconite pellets	C	S
l	Glauconite infills	M	R
a	**Other**		
s	Phosphate	M	R
t	Modal size 1 (mm)	0.15	0.10
s	Modal size 2 (mm)	1.4	
	Shape/abrasion	SR	SR
	Sorting	P	PM
	Interparticle material %	23	12
	Spar cement %	6	4
	Micrite %	16	8
Unoccluded pore space %		2	5

Table B12: Component data for the Motarata Limestone, Moutapu Point, Chatham Island.

Motarata Limestone		Moutapu Point, Chatham Island	
Stratigraphic column number		5	5
Sample running number		CH05-3.2	CH05-3.3
	Total bioclast %	80	70
	Bryozoans	C	C
	Bivalves	M	M
	Echinoderms	M	S
C	Benthic foraminifera	M	M
a	Planktic foraminifera	M	C
l	Gastropods		
c	Calcareous algae		
i	Barnacles		
c	Spicules & spines		
l	**Other**		
a	Brachiopods		
s	Modal size 1 (mm)	0.2	0.5
t	Modal size 2 (mm)		
s	Shape/abrasion	VA	A
	Sorting	MW	M
	Intraclast %	5	5
	Siliciclastic grain %	5	5
	Quartz	R	R
S	Feldspar		
i	VRFs		
l	SRFs		
i	Micas		
c	Pyrite grains		
i	Pyrite infills		
c	Glauconite pellets	S	S
l	Glauconite infills	R	S
a	**Other**		
s	Phosphate	M	C
t	Modal size 1 (mm)	0.125	0.15
s	Modal size 2 (mm)		
	Shape/abrasion	SR	SR
	Sorting	M	M
	Interparticle material %	10	20
	Spar cement %	4	2
	Micrite %	6	18
Unoccluded pore space %		5	5

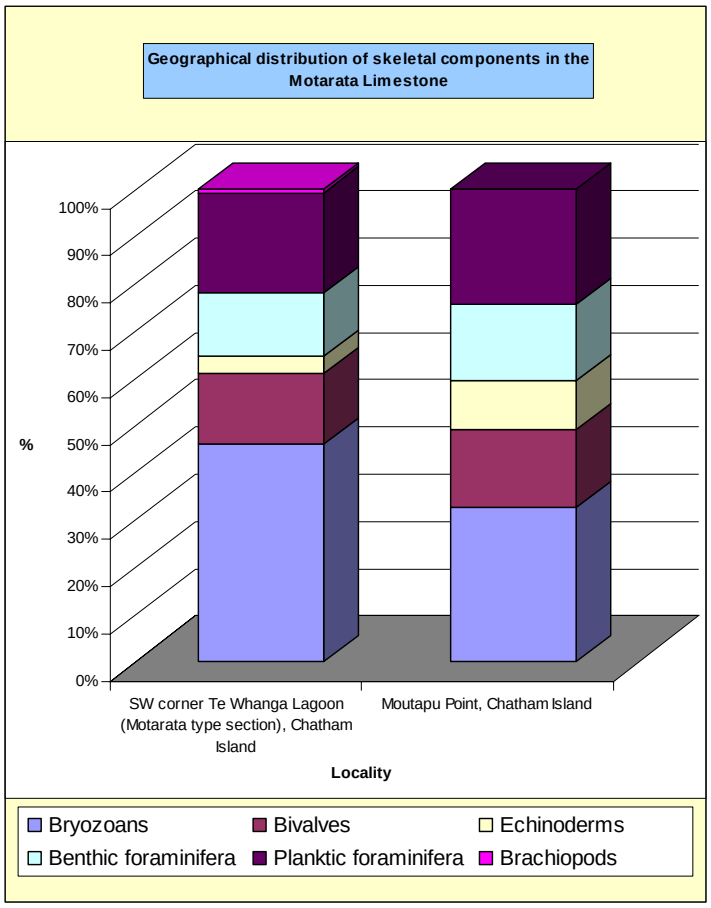

Figure B54: Geographical distribution of skeletal components in the Motarata Limestone of the Chatham Islands.

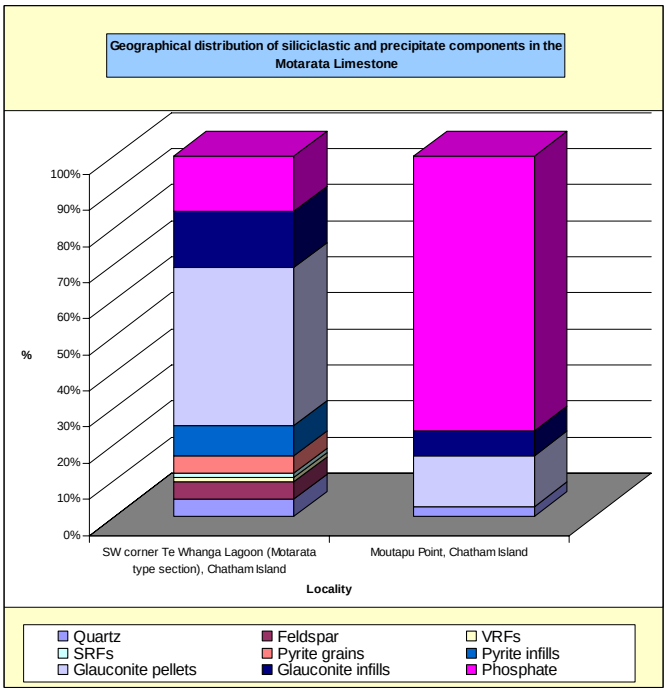

Figure B55: Geographical distribution of siliciclastic and precipitate components in the Motarata Limestone, Chatham Islands.

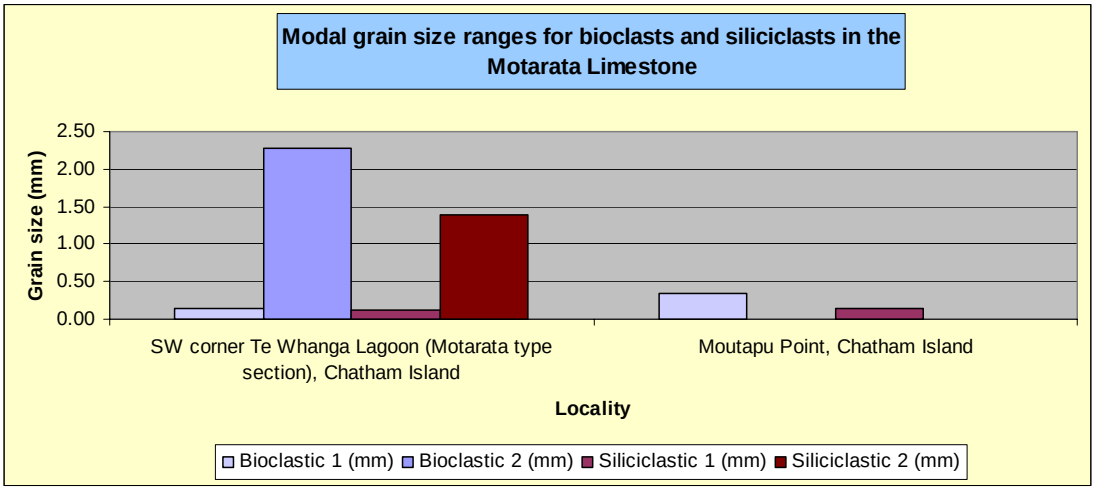

Figure B56: Geographical distribution of modal skeletal and siliciclastic/precipitate grain sizes in the Motarata Limestone, Chatham Islands.

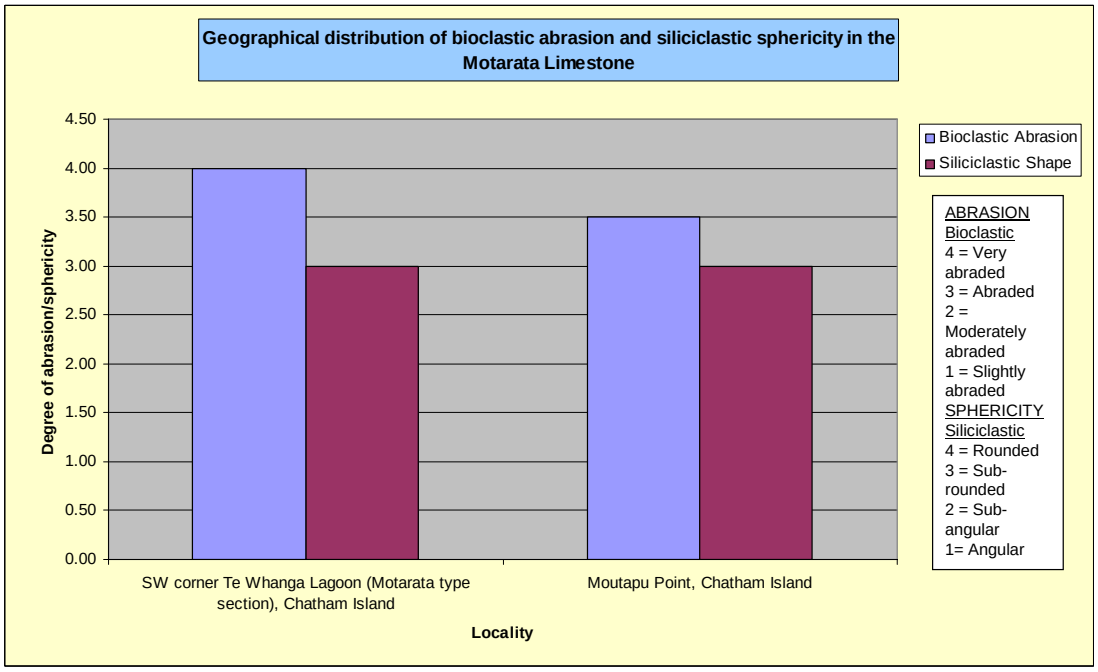

Figure B57: Geographical distribution of bioclastic abrasion and siliciclastic/precipitate grain sphericity in the Motarata Limestone, Chatham Islands.

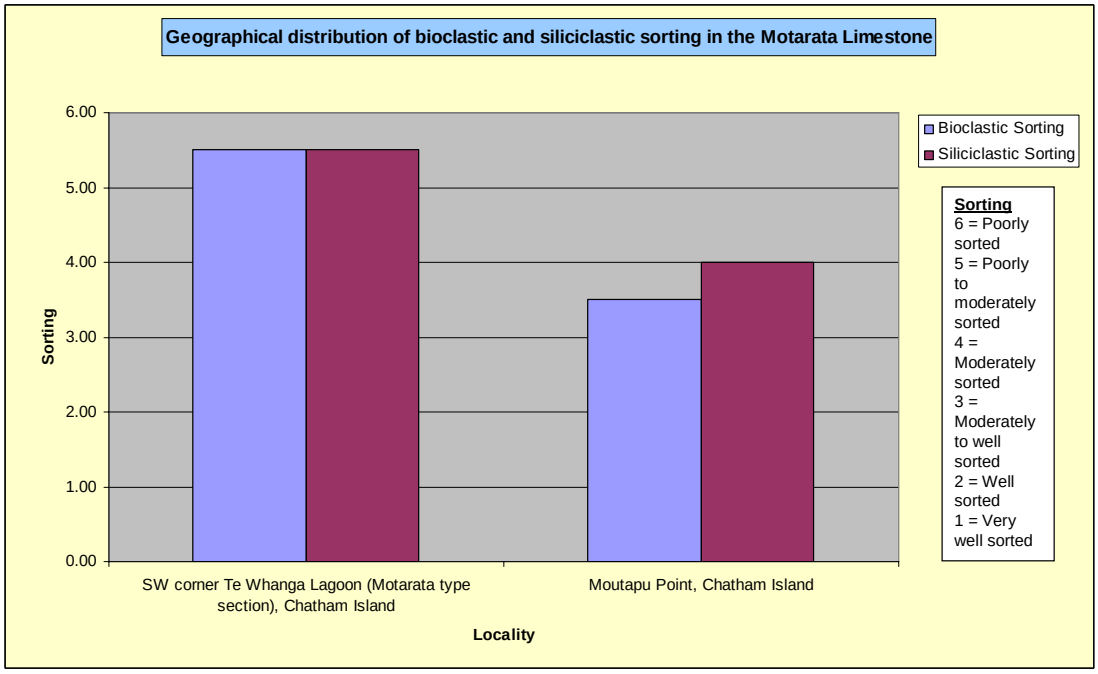

Figure B58: Geographical distribution of bioclast and siliciclastic/precipitate grain sorting in the Motarata Limestone, Chatham Islands.

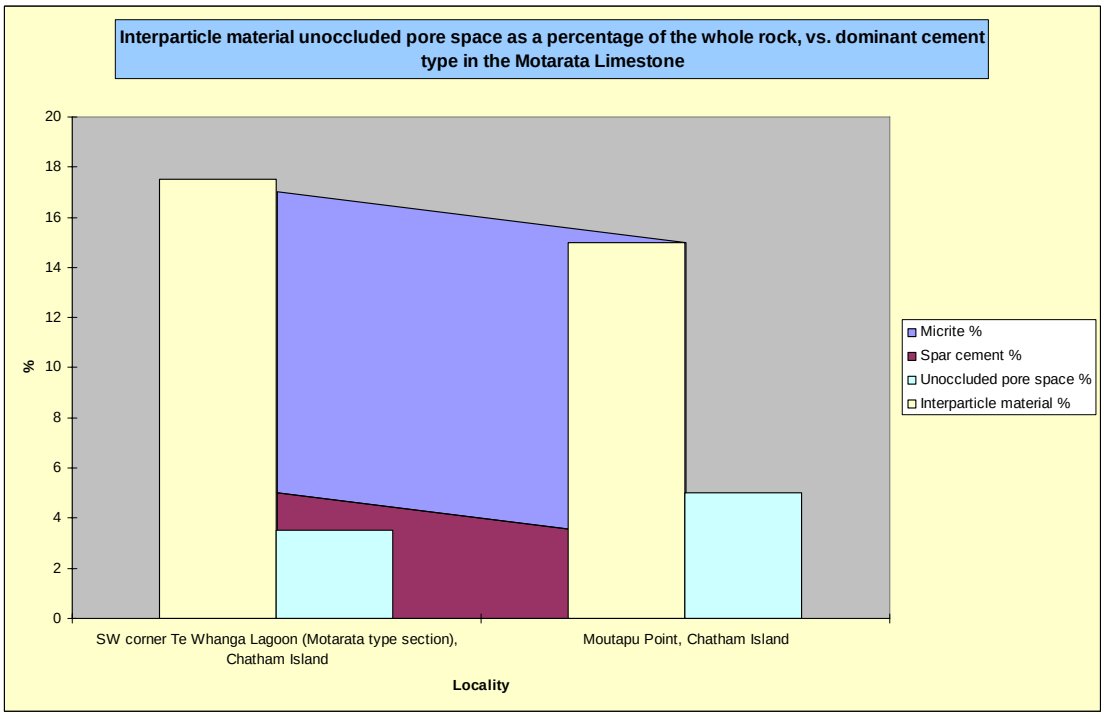

Figure B59: Geographical distribution of interparticle material and unoccluded pore space (foreground), and the amount of micrite and spar (background) present in the Motarata Limestone, Chatham Islands.

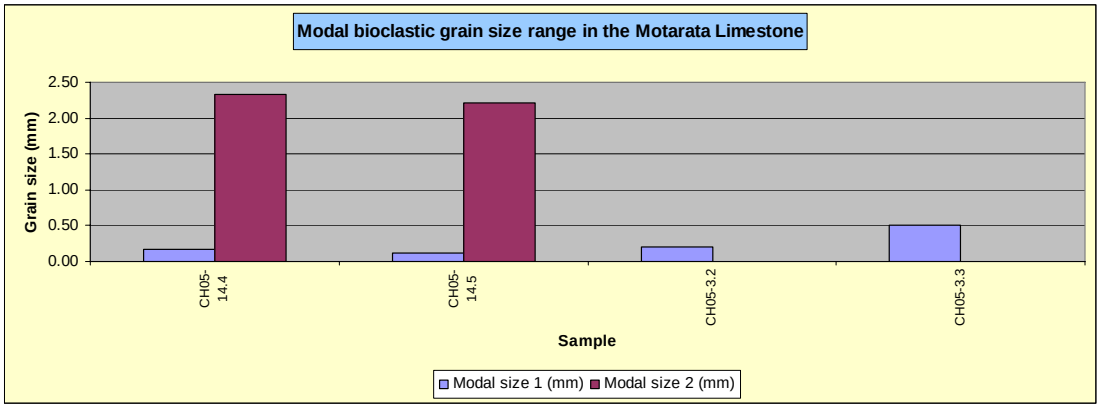

Figure B60: Modal bioclast grain sizes in the Motarata Limestone, Chatham Islands.

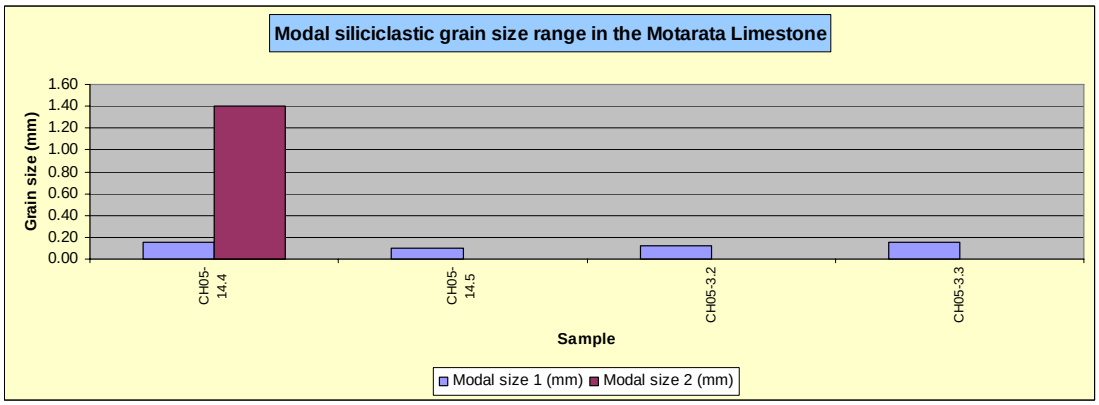

Figure B61: Modal siliciclastic grain sizes for the Motarata Limestone, Chatham Islands.

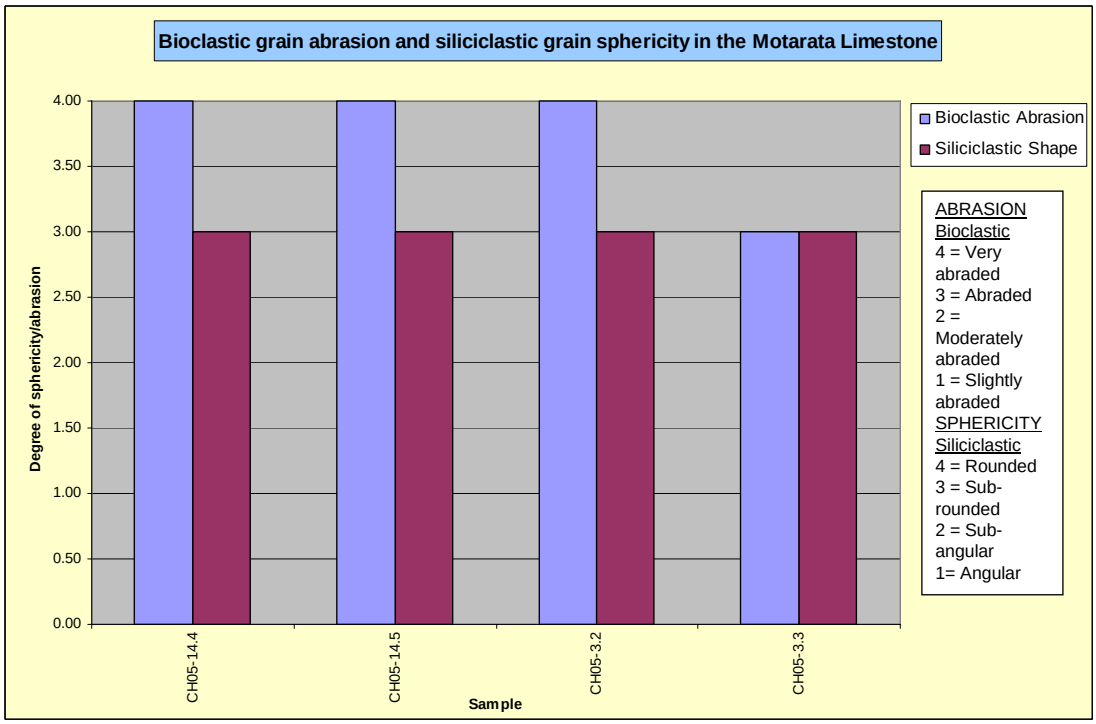

Figure B62: Bioclast abrasion and siliciclastic/precipitate sphericity in the Motarata Limestone, Chatham Islands.

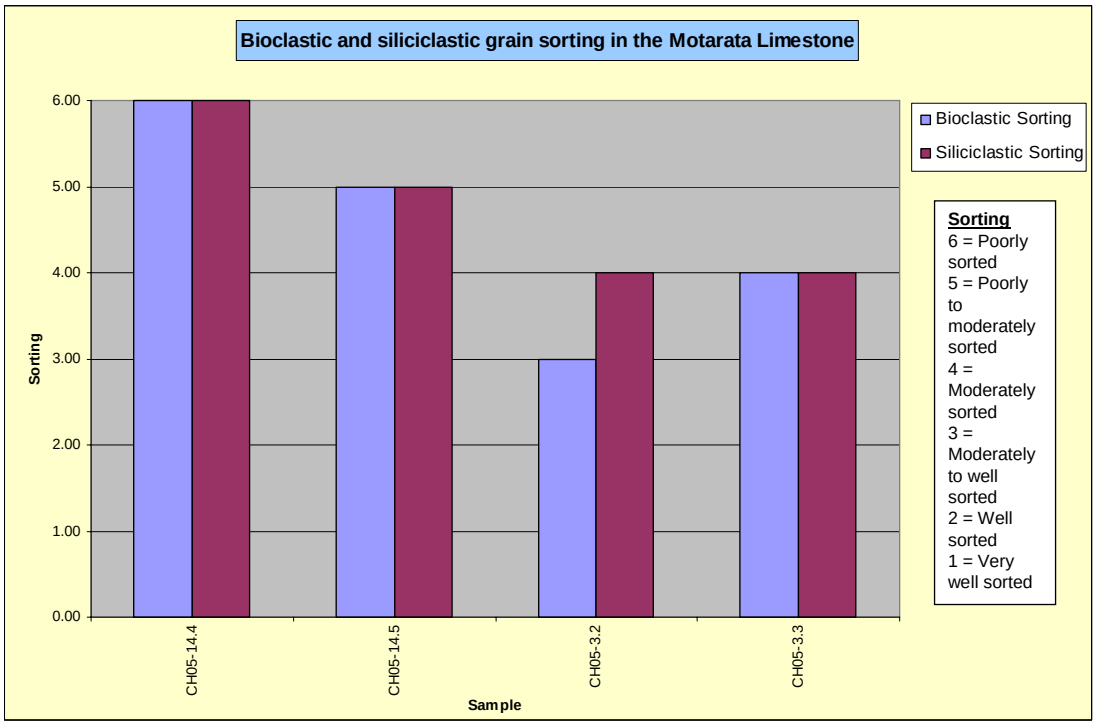

Figure B63: Bioclast and siliciclastic/precipitate grain sorting in the Motarata Limestone, Chatham Islands.

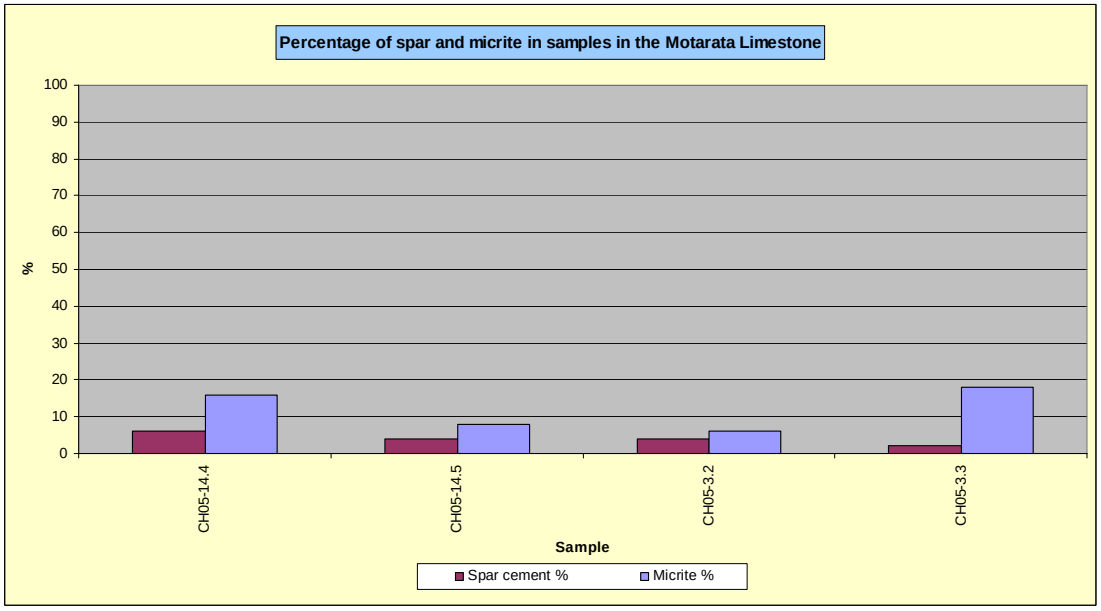

Figure B64: Percentage of spar versus micrite in samples of the Motarata Limestone, Chatham Islands.

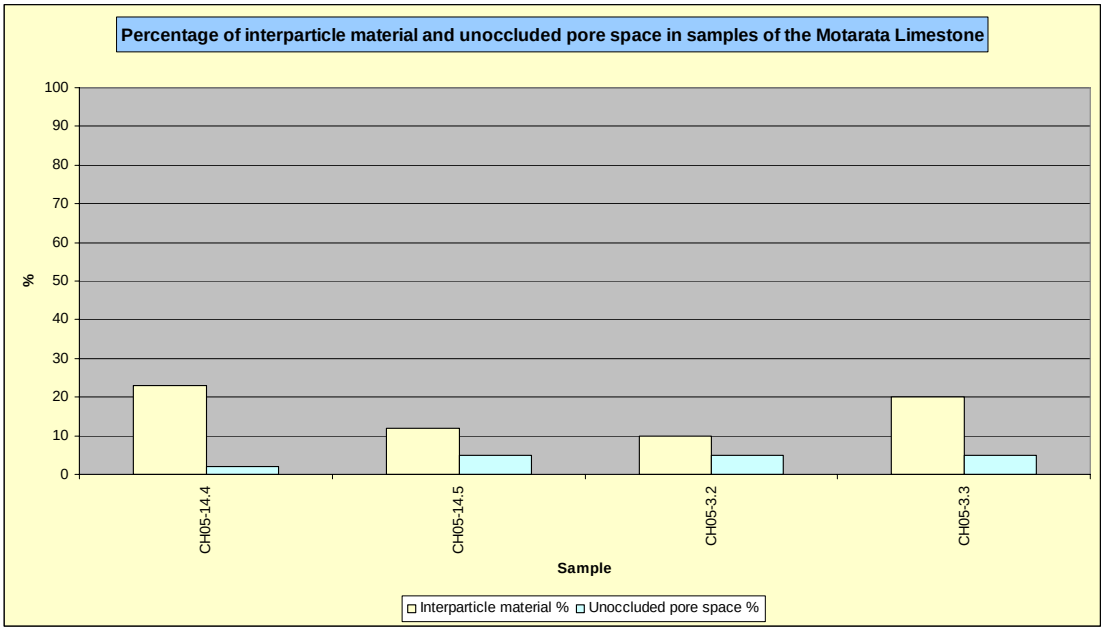

Figure B65: Percentage of interparticle material versus unoccluded pore space in samples of the Motarata Limestone, Chatham Islands.

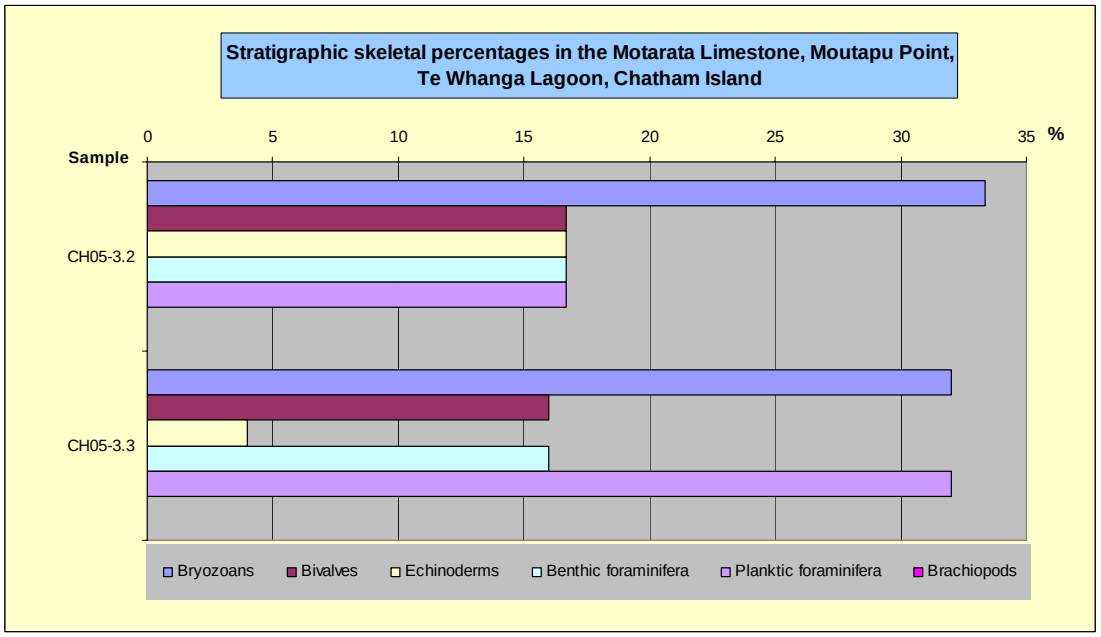

Figure B66: Stratigraphic skeletal percentages (up column) in the Motarata Limestone at Moutapu Point, Chatham Island.

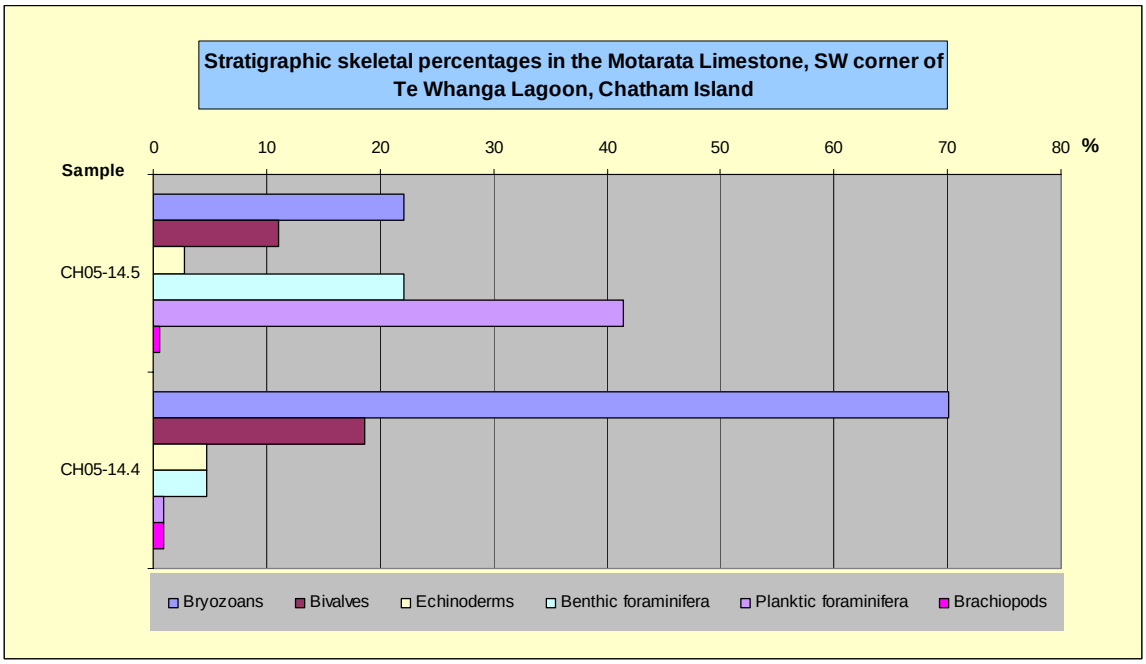

Figure B67: Stratigraphic skeletal percentages (up column) in the Motarata Limestone at the type section near Te Matarae, south-west corner of Te Whanga Lagoon, Chatham Island.

Onoua Limestone

Table B13: Component data for the Onoua Limestone, Tarawhenua Peninsula, Pitt Island.

Onoua Limestone		Tarawhenua Peninsula, Pitt Island			
Stratigraphic column number		13	13	13	13
Sample running number		CH05-8.3	CH05-8.4	CH05-8.5	CH05-8.11
	Total bioclast %	75	80	85	86
	Bryozoans	A	VA	VA	A
	Bivalves	C	S	M	C
	Echinoderms	S	M	M	S
C	Benthic foraminifera	S	R	R	S
a	Planktic foraminifera	S	R	R	S
l	Gastropods				
c	Calcareous algae				
i	Barnacles				S
c	Spicules & spines				
l	**Other**				
a	Brachiopods				
s	Serpulids				S
t	Ostracods				R
s	Modal size 1 (mm)	0.25	0.87	0.80	0.18
	Modal size 2 (mm)	2.00	3.50	3.75	2.63
	Shape/abrasion	VA	A	A	VA
	Sorting	P	PM	PM	P
	Intraclast %	2	0	0	0
	Siliciclastic grain %	5	3	1	2
	Quartz	S	R	R	R
S	Feldspar	S	R		R
i	VRFs	S		R	R
l	SRFs	R	R		R
i	Micas				
c	Pyrite grains	R		R	R
i	Pyrite infills	R		R	R
c	Glauconite pellets	S	R	R	R
l	Glauconite infills	R	R	R	R
a	**Other**				
s	Phosphate	S	R	R	R
t	Limonite staining	S			
s	Modal size 1 (mm)	0.30	0.25	0.20	0.10
	Modal size 2 (mm)		1.13		
	Shape/abrasion	SA	SR	SR	SR
	Sorting	P	P	PM	PM
	Interparticle material %	20	7	10	10
	Spar cement %	5	5	2	5
	Micrite %	15	2	8	5
Unoccluded pore space %		5	10	5	4

Table B14: Component data for the Onoua Limestone, Flowerpot Bay, Pitt Island (continued over page).

Onoua Limestone		Flowerpot Bay, Pitt Island				
Stratigraphic column number		–	–	–	–	–
Sample running number		CH05-10.1A	CH05-10.1B	CH05-10.2	CH05-10.3	CH05-10.3A
	Total bioclast %	73	70	70	60	67
	Bryozoans	VA	A	A	C	A
	Bivalves	C	M	C	S	C
	Echinoderms	M	R	M	M	M
Calcicl asts	Benthic foraminifera		R	S	R	S
	Planktic foraminifera		S	S	S	S
	Gastropods			M		
	Calcareous algae					
	Barnacles		R	S		
	Spicules & spines					
	Other					
	Brachiopods			R		
	Serpulids			S		S
	Ostracods					
	Modal size 1 (mm)	0.60	0.50	0.63	0.88	0.28
	Modal size 2 (mm)	4.75	6.00	5.25	7.25	0.93
	Shape/abrasion	A	VA	A	A	VA
	Sorting	P	P	P	P	PM
	Intraclast %	0	2	0	0	5
	Siliciclastic grain %	7	10	5	5	1
	Quartz	M	R	R	R	R
Siliciclasts	Feldspar		R	R	R	
	VRFs		S	S	R	
	SRFs		S	S	R	
	Micas					
	Pyrite grains	M	M	S	R	
	Pyrite infills	M	M	S	S	R
	Glauconite pellets	R	C	R	R	R
	Glauconite infills	S	M	R	R	
	Other					
	Phosphate	S	M	S	S	R
	Limonite staining					
	Modal size 1 (mm)	0.60	0.05	0.08	0.08	0.45
	Modal size 2 (mm)	3.75	1.13	1.13	1.05	
	Shape/abrasion	SA-SR	SR-R	SR-R	SR-R	R
	Sorting	P	P	P	P	M
	Interparticle material %	12	18	20	30	8
	Spar cement %	2	2	2	2	1
	Micrite %	10	16	18	28	7
Unoccluded pore space %		7	5	5	5	25

Onoua Limestone		Flowerpot Bay, Pitt Island			
Stratigraphic column number		–	–	–	–
Sample running number		CH05-10.3B	CH05-10.3C	CH05-10.5	CH05-10.6
	Total bioclast %	73	75	60	77
	Bryozoans	A	VC	C	VC
	Bivalves	M	C	M	M
	Echinoderms	S	S	S	M
C	Benthic foraminifera	R	R	R	S
a	Planktic foraminifera	R	M	S	S
l	Gastropods	R			R
c	Calcareous algae				
i	Barnacles	R		S	R
c	Spicules & spines				
l	**Other**				
a	Brachiopods			R	
s	Serpulids				M
t	Ostracods				
s	Modal size 1 (mm)	0.23	0.30	0.30	0.50
	Modal size 2 (mm)	1.88	4.25	5.00	3.30
	Shape/abrasion	A	A	A	A
	Sorting	P	P	P	P
	Intraclast %	0	0	0	2
	Siliciclastic grain %	2	5	20	1
	Quartz	R	S	S	R
S	Feldspar	R		R	
i	VRFs	S	R	M	
l	SRFs	S		M	R
i	Micas				
c	Pyrite grains	R	R	S	R
i	Pyrite infills	R	R	S	R
c	Glauconite pellets	R		S	R
l	Glauconite infills	S		S	R
a	**Other**				
s	Phosphate	S	S	S	S
t	Limonite staining				
s	Modal size 1 (mm)	0.25	0.80	0.10	0.13
	Modal size 2 (mm)	1.53		2.20	0.93
	Shape/abrasion	SR	SR	SR	SR-R
	Sorting	P	P	P	P
	Interparticle material %	10	17	15	10
	Spar cement %	1	2	5	1
	Micrite %	9	15	10	9
Unoccluded pore space %		15	2	5	12

Table B15: Component data for the Onoua Limestone, north-east of the Bluff Homestead, Pitt Island.

Onoua Limestone		Bluff Farm NE, Pitt Island			
Stratigraphic column number		14	14	14	14
Sample running number		CH05-11.1	CH05-11.2	CH05-11.3	CH05-11.5
	Total bioclast %	70	70	73	68
	Bryozoans	A	A	A	VC
	Bivalves	VC	C	VC	C
	Echinoderms	S	R	S	S
C	Benthic foraminifera	R	R	R	
a	Planktic foraminifera	M	M	S	S
l	Gastropods				
c	Calcareous algae				
i	Barnacles	R	S	R	M
c	Spicules & spines		R		
l	**Other**				
a	Brachiopods	S		R	S
s	Serpulids				
t	Ostracods	R		R	
s	Modal size 1 (mm)	0.30	0.45	0.13	0.30
	Modal size 2 (mm)	1.00	4.25	4.50	4.88
	Shape/abrasion	VA	VA	VA	VA
	Sorting	PM	P	P	P
	Intraclast %	0	0	2	10
	Siliciclastic grain %	5	5	5	20
	Quartz	S	R	S	M
S	Feldspar		R		
i	VRFs		S		M
l	SRFs				M
i	Micas				
c	Pyrite grains	S	M	R	R
i	Pyrite infills	S	S	S	R
c	Glauconite pellets	S		R	S
l	Glauconite infills				M
a	**Other**				
s	Phosphate	S	S	M	M
t	Limonite staining		S	M	C
s	Modal size 1 (mm)	0.05	0.63	0.10	0.10
	Modal size 2 (mm)	0.30		1.38	2.00
	Shape/abrasion	SR-SA	SR-SA	SR-SA	SR-R
	Sorting	P	PM	P	P
	Interparticle material %	25	17	20	12
	Spar cement %	2	2	4	7
	Micrite %	23	15	16	5
Unoccluded pore space %		2	5	2	2

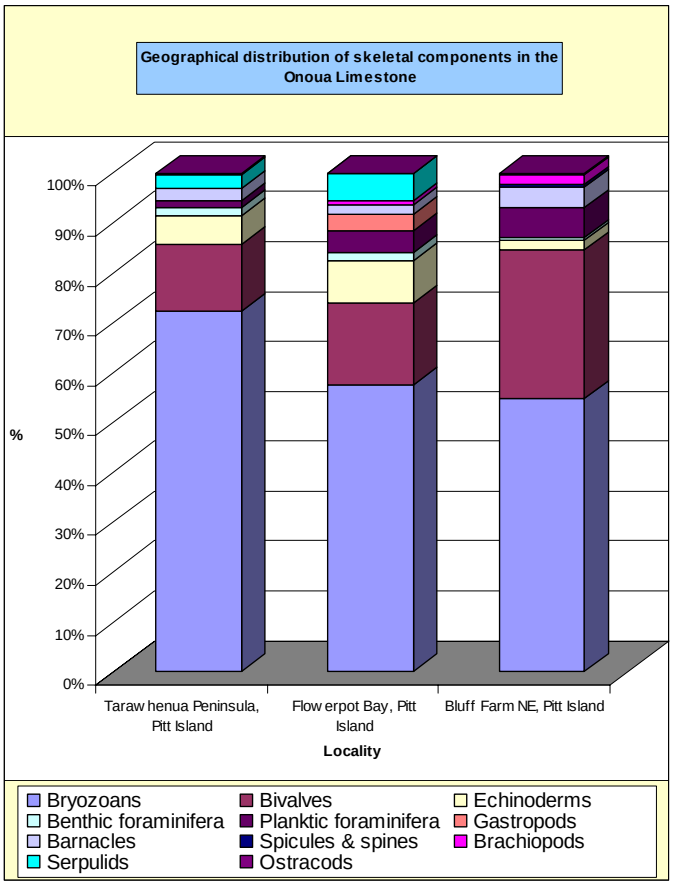

Figure B68: Geographical distribution in skeletal components of the Onoua Limestone on the Chatham Islands.

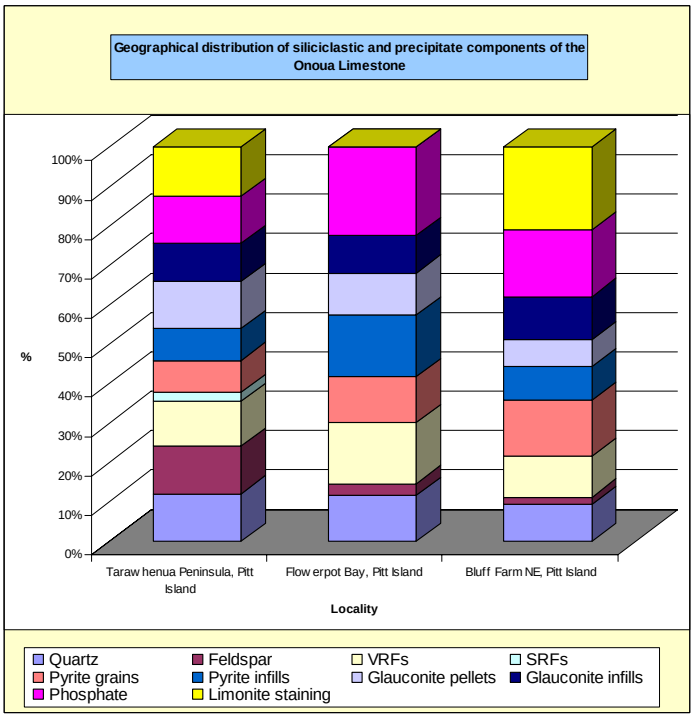

Figure B69: Geographical distribution of siliciclastic and precipitate components in the Onoua Limestone, Chatham Islands.

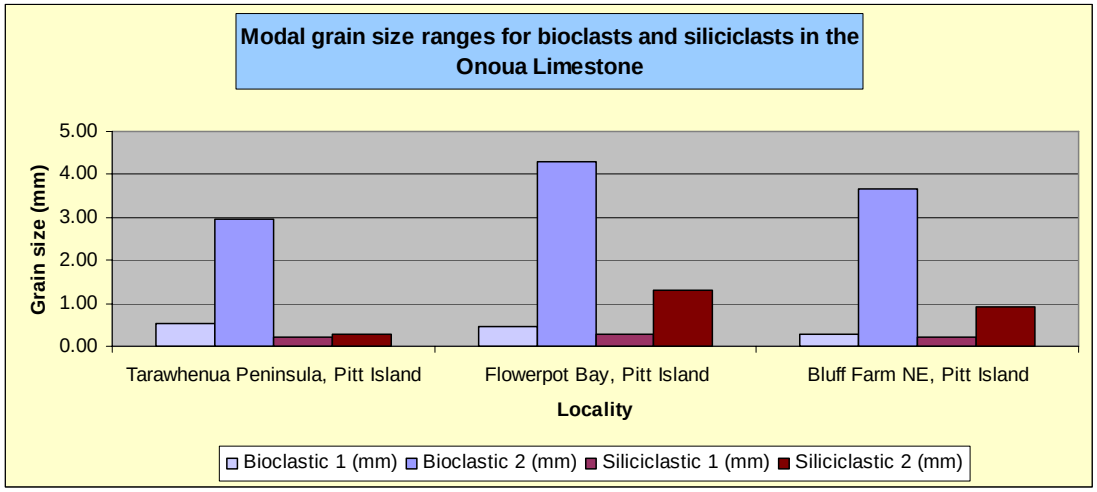

Figure B70: Geographical distribution of modal skeletal and siliciclastic/precipitate grain sizes in the Onoua Limestone, Chatham Islands.

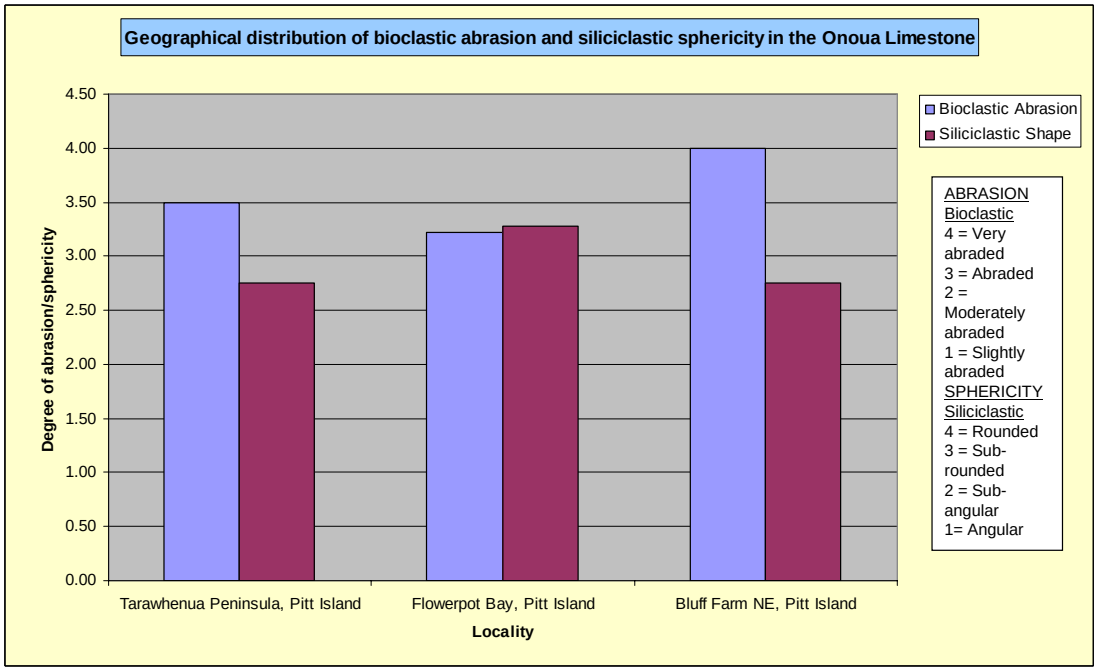

Figure B71: Geographical distribution of bioclastic abrasion and siliciclastic/precipitate grain sphericity in the Onoua Limestone, Chatham Islands.

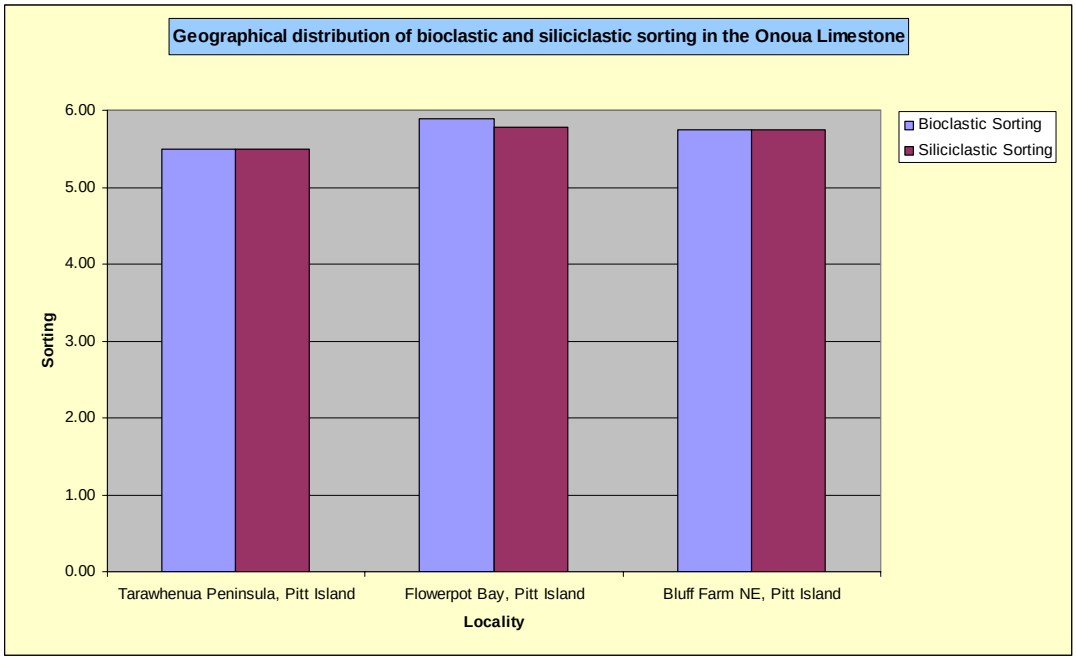

Figure B72: Geographical distribution of bioclast and siliciclastic/precipitate grain sorting in the Onoua Limestone, Chatham Islands.

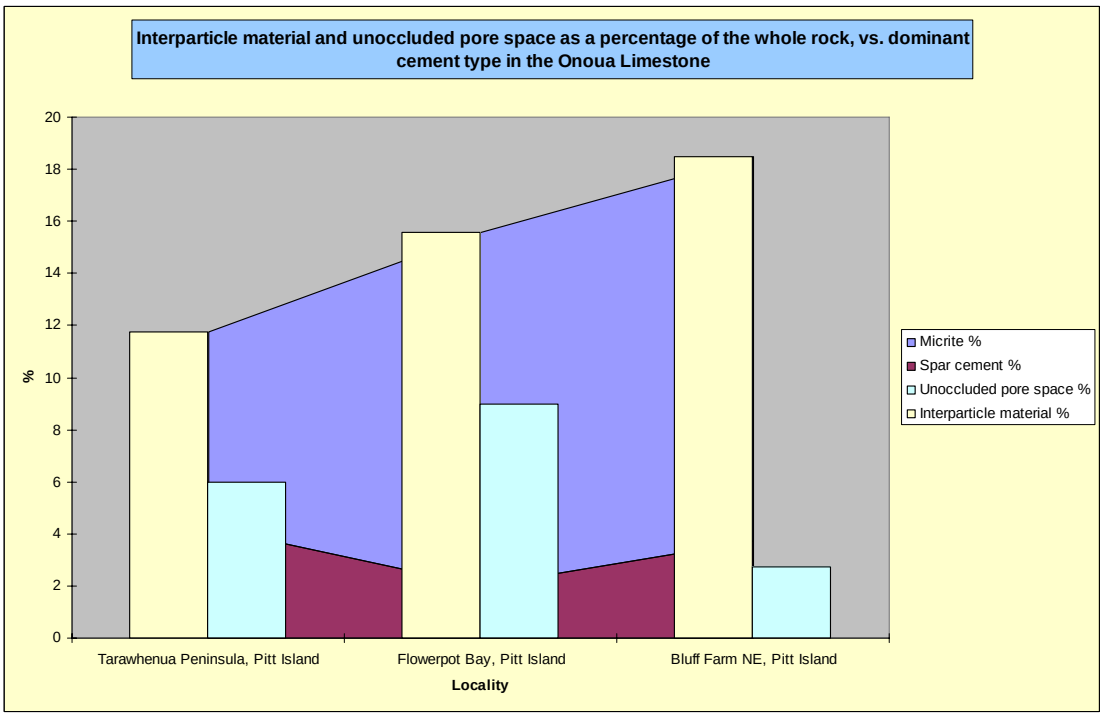

Figure B73: Geographical distribution of interparticle material and unoccluded pore space (foreground), and the amount of micrite and spar (background) present in the Onoua Limestone, Chatham Islands.

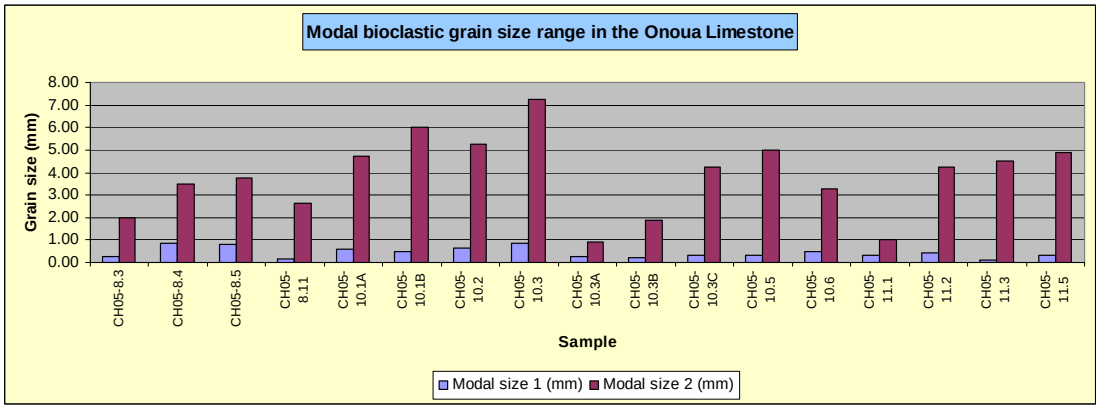

Figure B74: Modal bioclast grain sizes in the Onoua Limestone, Chatham Islands.

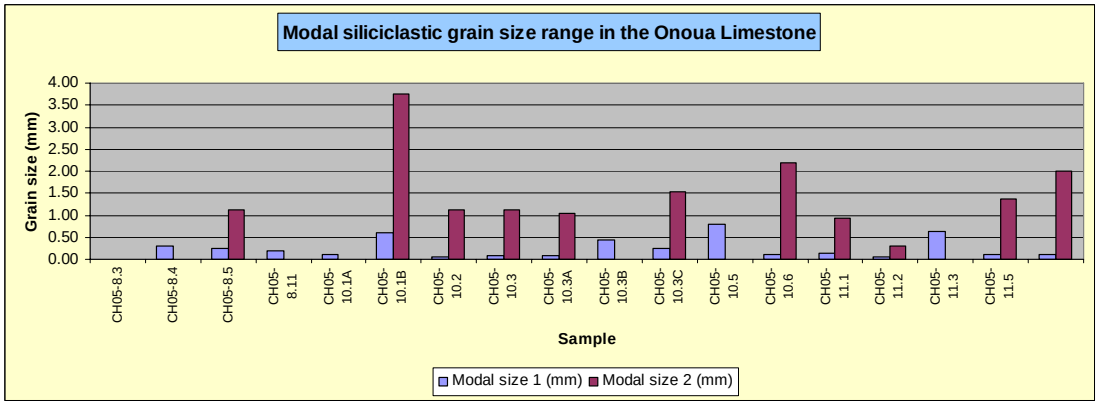

Figure B75: Modal siliciclastic grain sizes in the Onoua Limestone, Chatham Islands.

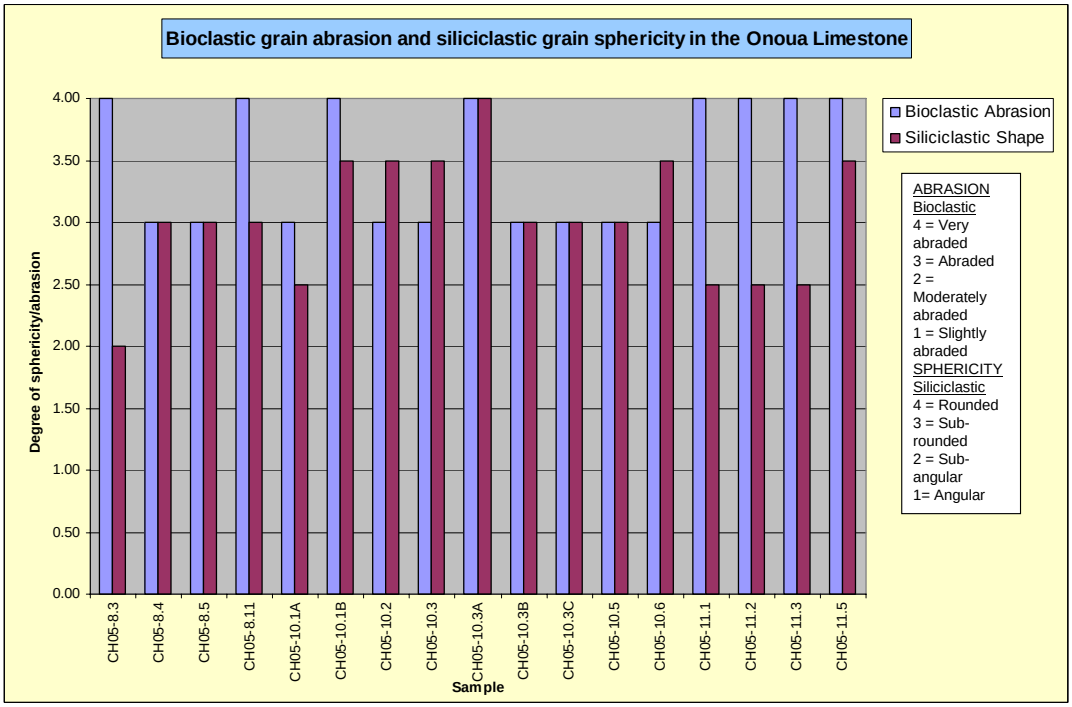

Figure B76: Bioclast abrasion and siliciclastic/precipitate sphericity in the Onoua Limestone, Chatham Islands.

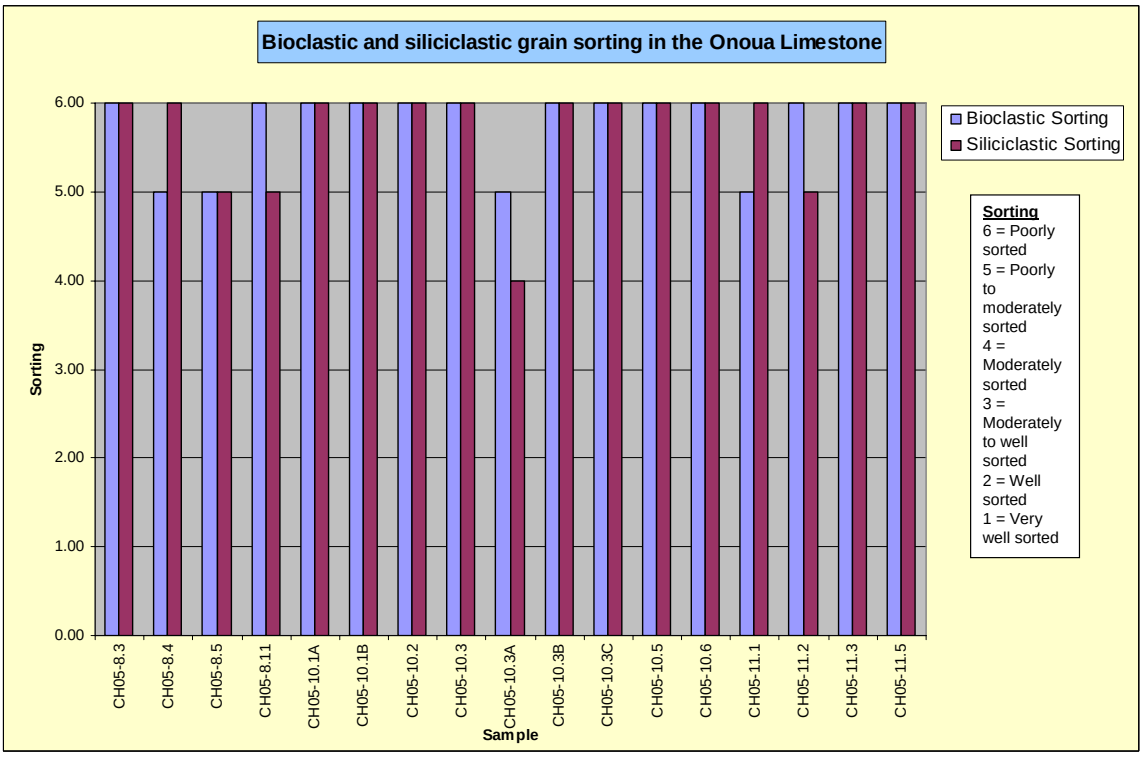

Figure B77: Bioclast and siliciclastic/precipitate grain sorting in the Onoua Limestone, Chatham Islands.

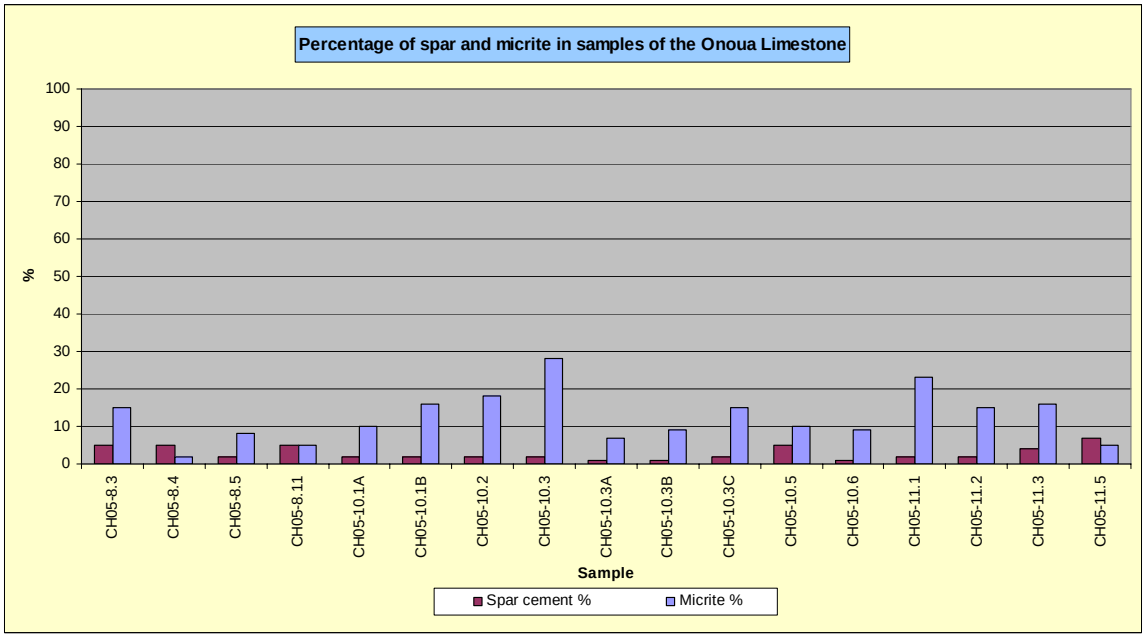

Figure B78: Percentage of spar versus micrite in samples of the Onoua Limestone, Chatham Islands.

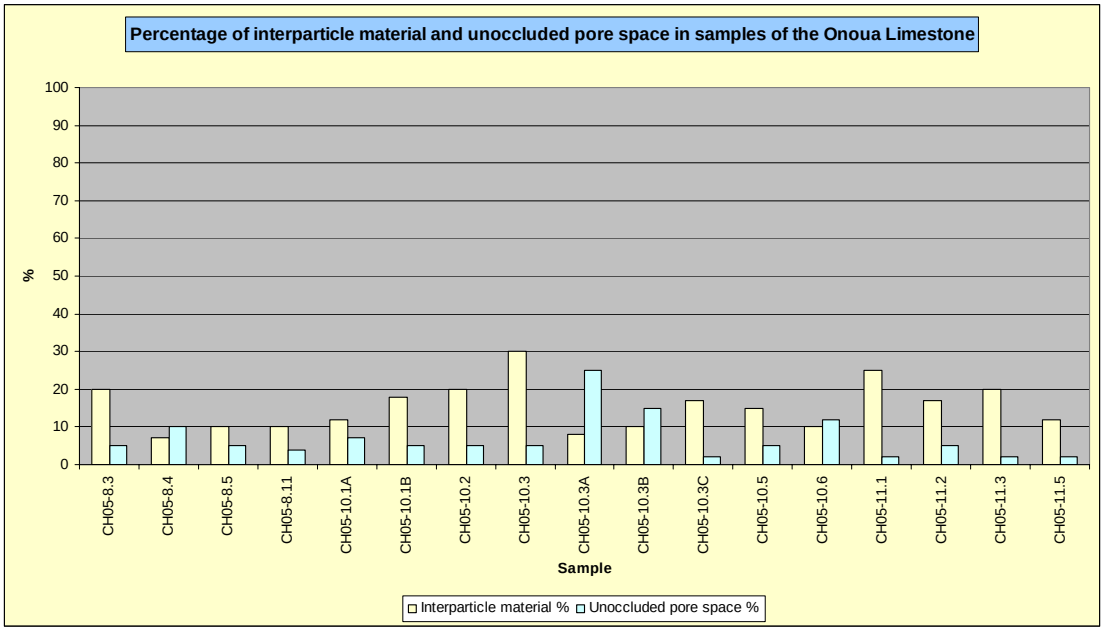

Figure B79: Percentage of interparticle material versus unoccluded pore space in samples of the Onoua Limestone, Chatham Islands.

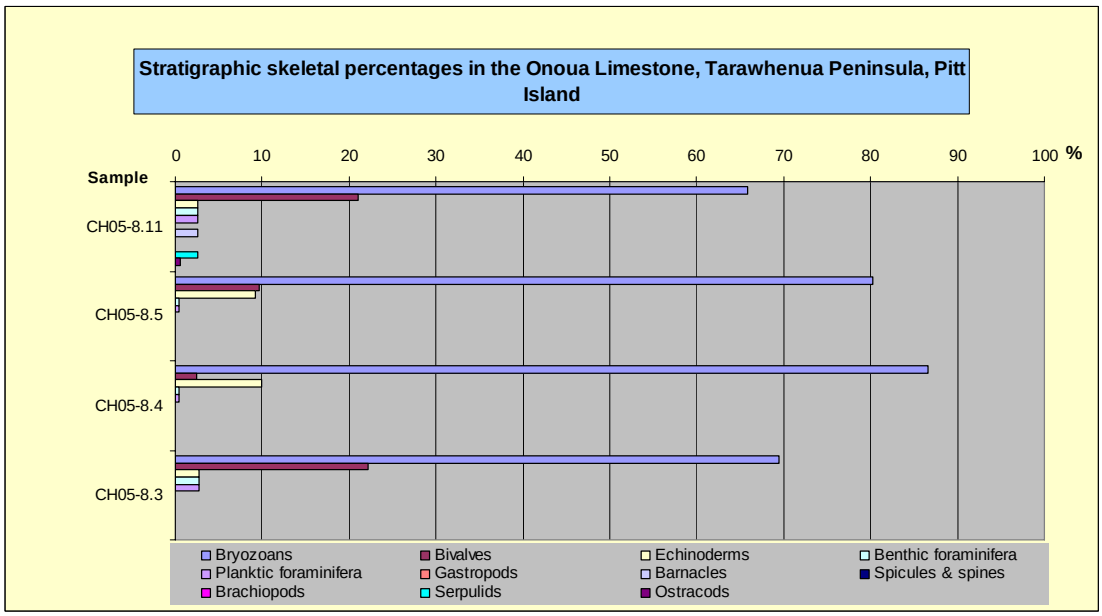

Figure B80: Stratigraphic skeletal percentages (up column) in the Onoua Limestone on the Tarawhenua Peninsula, Pitt Island.

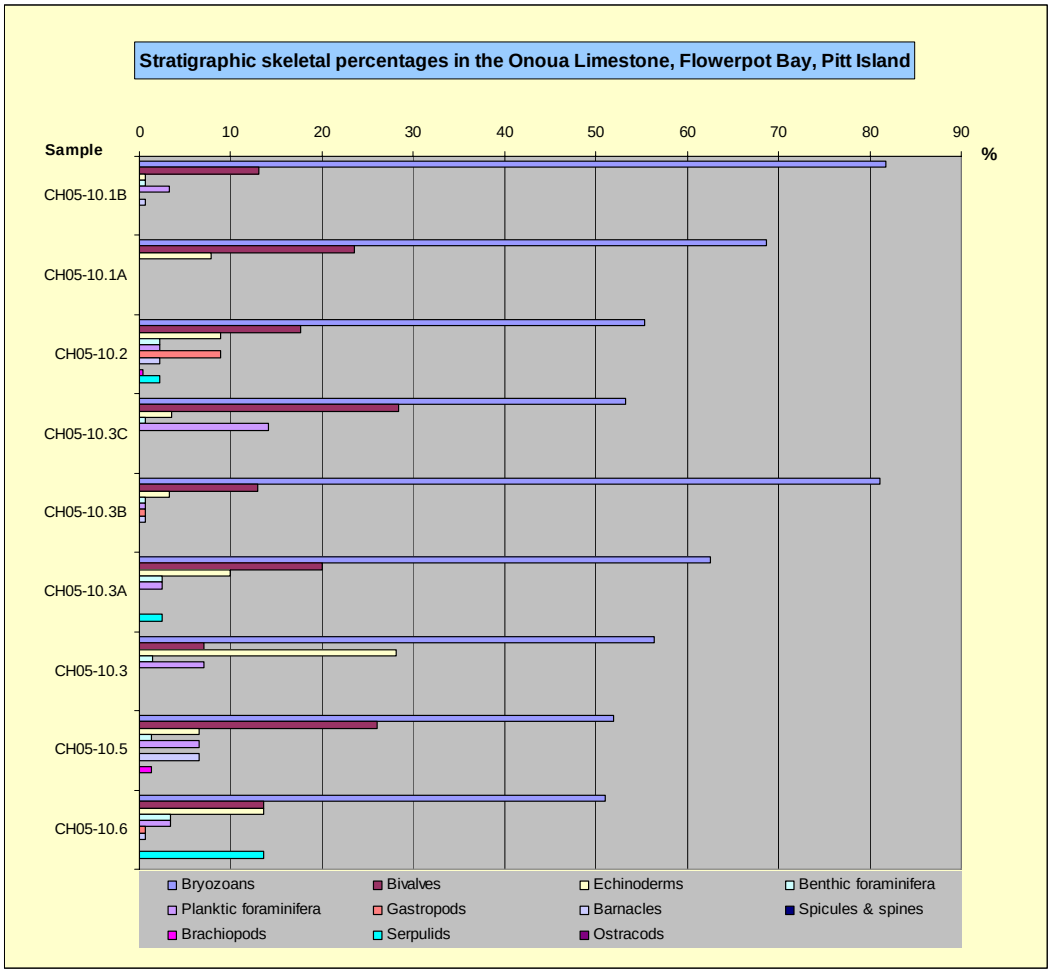

Figure B81: Stratigraphic skeletal percentages (up column) in the Onoua Limestone on the Flowerpot Bay, Pitt Island.

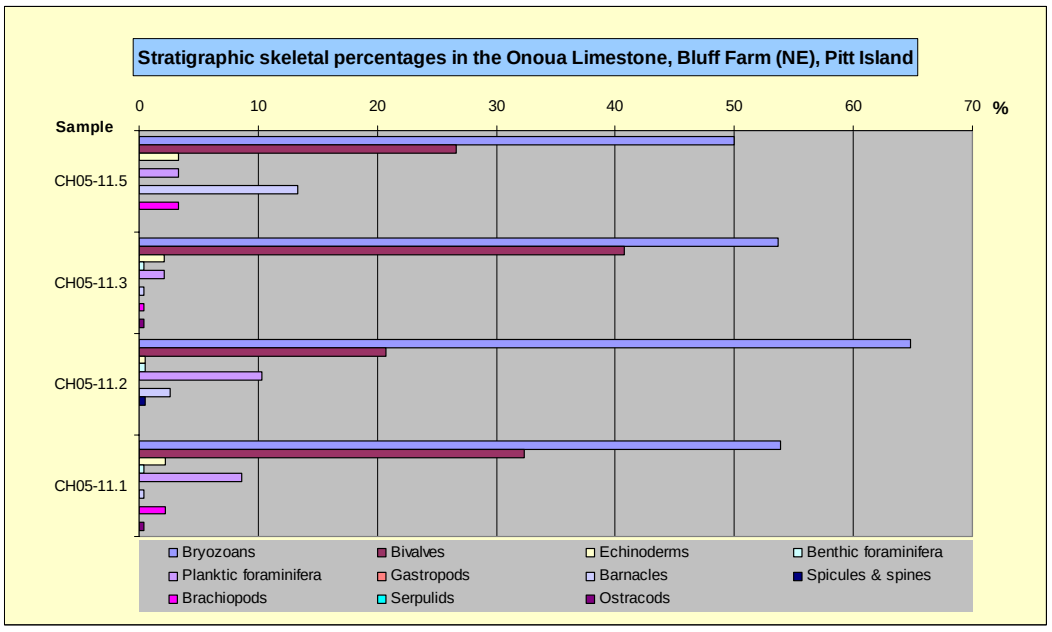

Figure B82: Stratigraphic skeletal percentages (up column) in the Onoua Limestone on the north-east of the Bluff Homestead, Pitt Island.

Other limestone occurrences

Tumaio Limestone

Table B16: Component data for the Tumaio limestone, north-western Manganui Beach, Chatham Island.

Tumaio Limestone		North western end of Manganui Beach, northern Chatham Island						GNS Sample
Stratigraphic column number		1	1	1	1	1	1	1
Sample running number		CH05-18A	CH05-18B1	CH05-18B2	CH05-18B3	CH05-18C1	CH05-18C2	E85 - GS12459
	Total bioclast %	10	30	20	10	74	66	65
	Bryozoans	R	S	M	VC	A	VC	VC
C	Bivalves		M	M	C	C	VC	A
a	Echinoderms	M	M	C	M	C	M	C
l	Benthic foraminifera		R			S	R	R
c	Planktic foraminifera		R	R	S	S	R	R
i	Gastropods		R				R	
c	Calcareous algae							
l	Barnacles					R	S	
a	Spicules & spines							
s	**Other**							
t	Brachiopods		S		R	S	R	
s	Collophane material	S	R		R	R	R	
	Modal size 1 (mm)	1.18	0.93	0.50	0.37	0.25	0.33	1.25
	Modal size 2 (mm)				1.00	2.38	0.78	
	Shape/abrasion	VA	VA	VA	VA	VA	VA	A
	Sorting	P	PM	P	P	P	P	PM
	Intraclast %	0	2	2	0	5	2	0
	Siliciclastic grain %	33	33	3	3	10	30	20
	Quartz	C	A	S	C	S	M	M
S	Feldspar					R	R	
i	VRFs	R			VC			
l	SRFs							
i	Micas							
c	Pyrite grains	S	R	R	R	R	R	
i	Pyrite infills	S	R	S				R
c	Glauconite pellets	M	C	M	M	C	VC	M
l	Glauconite infills		M		S	M	C	R
a	**Other**							
s	Phosphate	M	R	R	M	R	M	
t	Chert						S	
s	Limonite staining	M	M	M	M		S	R
	Modal size 1 (mm)	0.08	0.13	0.23	0.08	0.08	0.15	0.63
	Modal size 2 (mm)	2.50	2.38			0.50	1.13	
	Shape/abrasion	SR-R	SR-R	R	SR	SR-R	SR-R	SR
	Sorting	P	P	P	MP	P	P	PM
	Interparticle material %	66	30	77	85	6	32	10
	Spar cement %	1	3	1	2	4	2	2
	Micrite %	20	19	30	43	2	30	8
	Silica %	45	18	45	40	0	0	0
Unoccluded pore space %		1	1	1	1	10	2	4

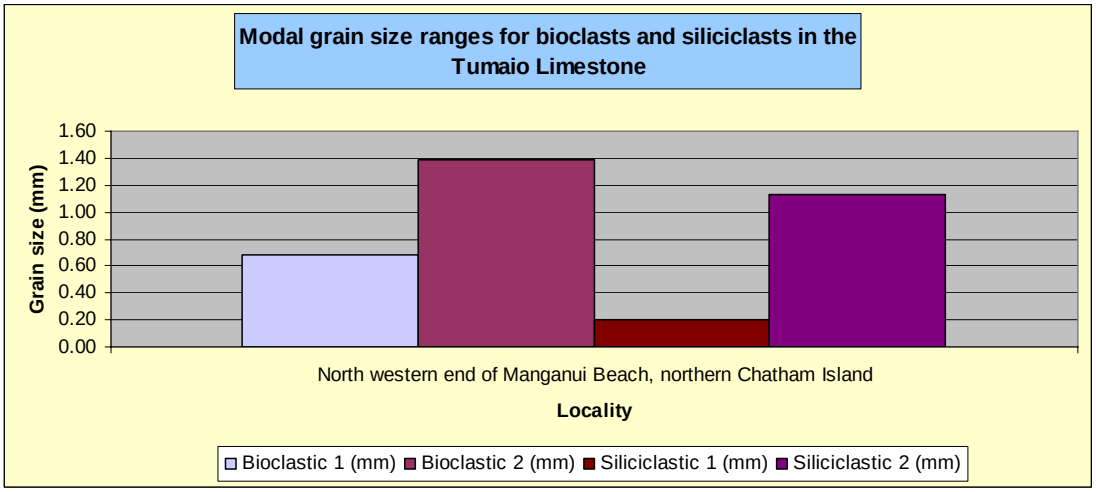

Figure B83: Modal skeletal and siliciclastic/precipitate grain sizes in the Tumaio Limestone, Chatham Islands.

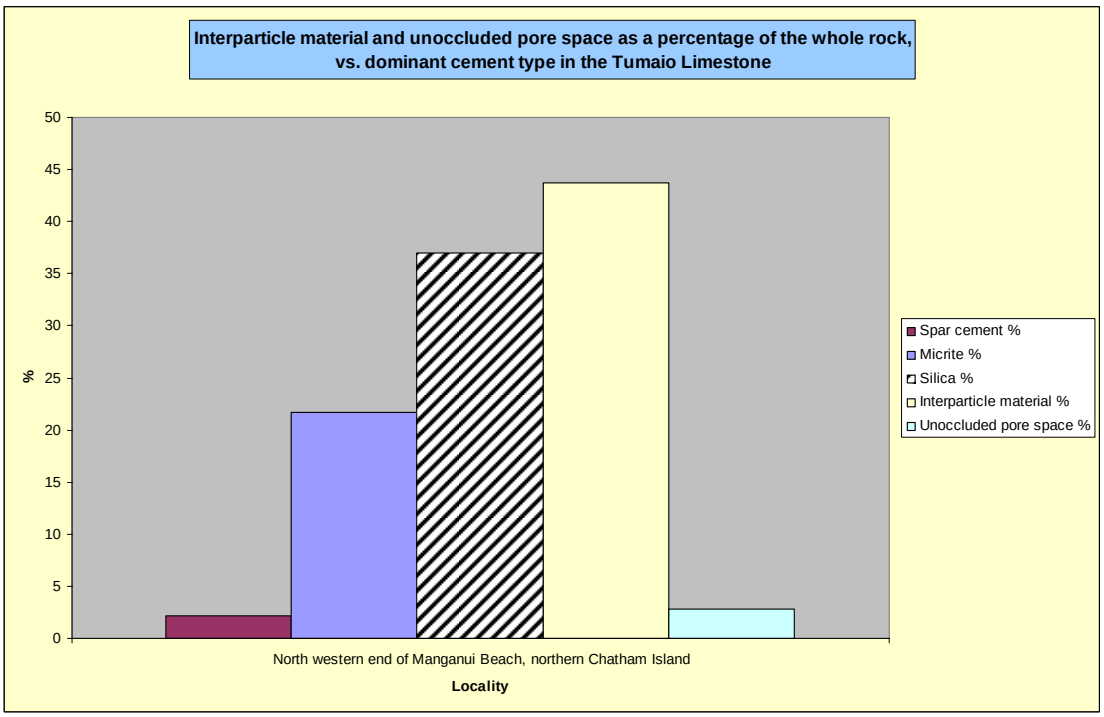

Figure B84: Percentages of interparticle material and unoccluded pore space, and the amount of silica, micrite and spar present in the Tumaio Limestone, Chatham Islands.

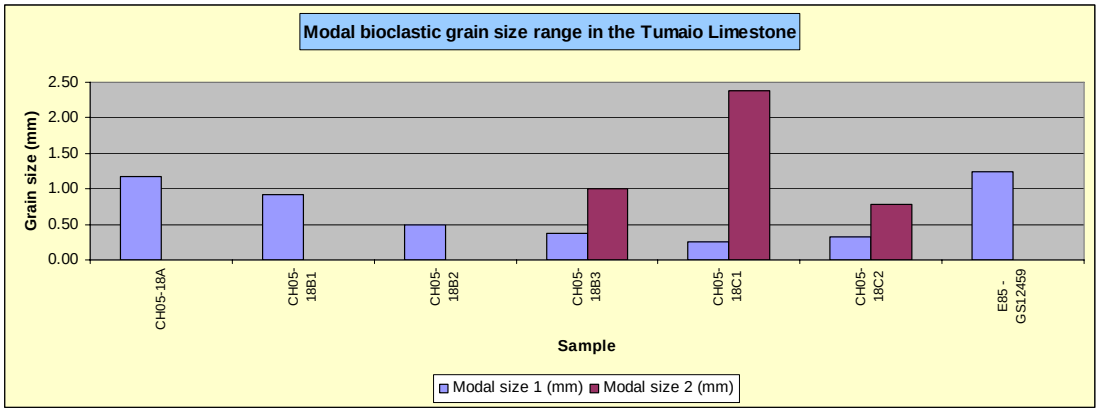

Figure B85: Modal bioclast grain sizes in the Tumaio Limestone, Chatham Islands.

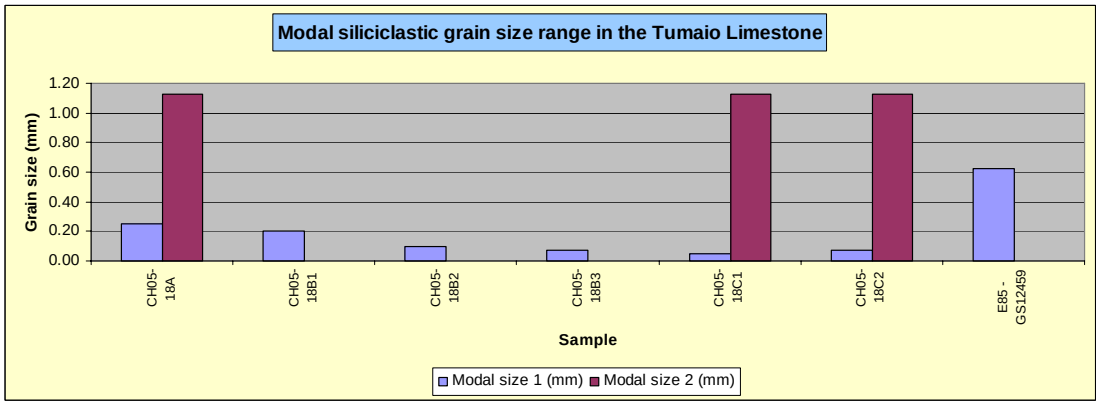

Figure B86: Modal siliciclastic grain sizes in the Tumaio Limestone, Chatham Islands.

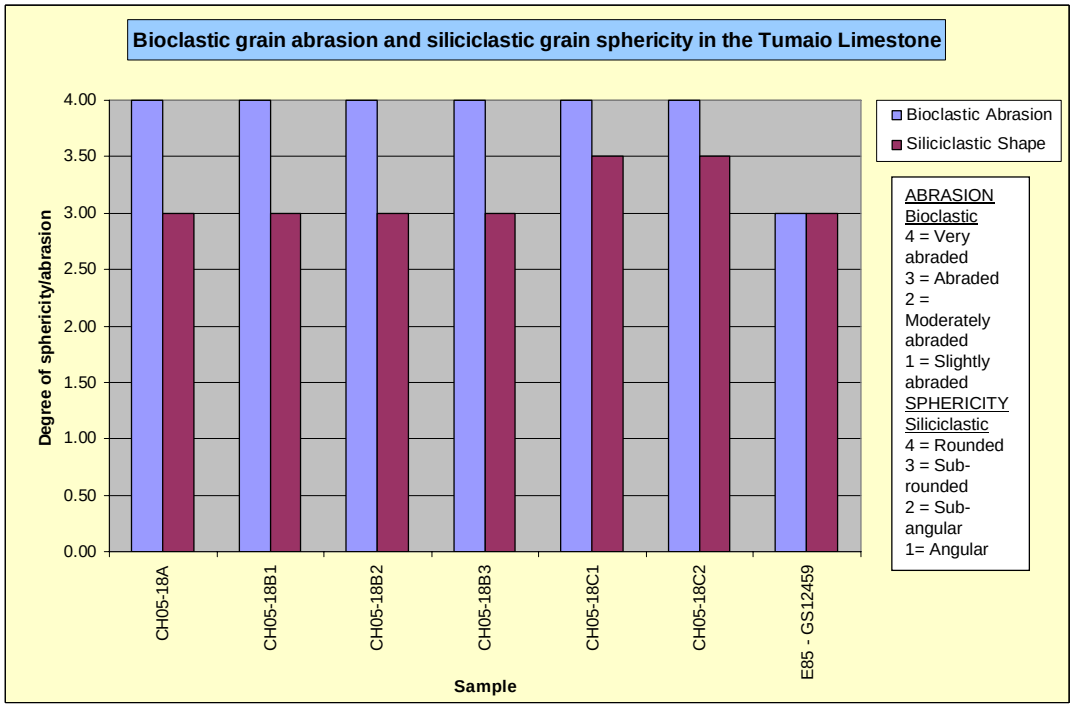

Figure B87: Bioclast abrasion and siliciclastic/precipitate sphericity in the Tumaio Limestone, Chatham Islands.

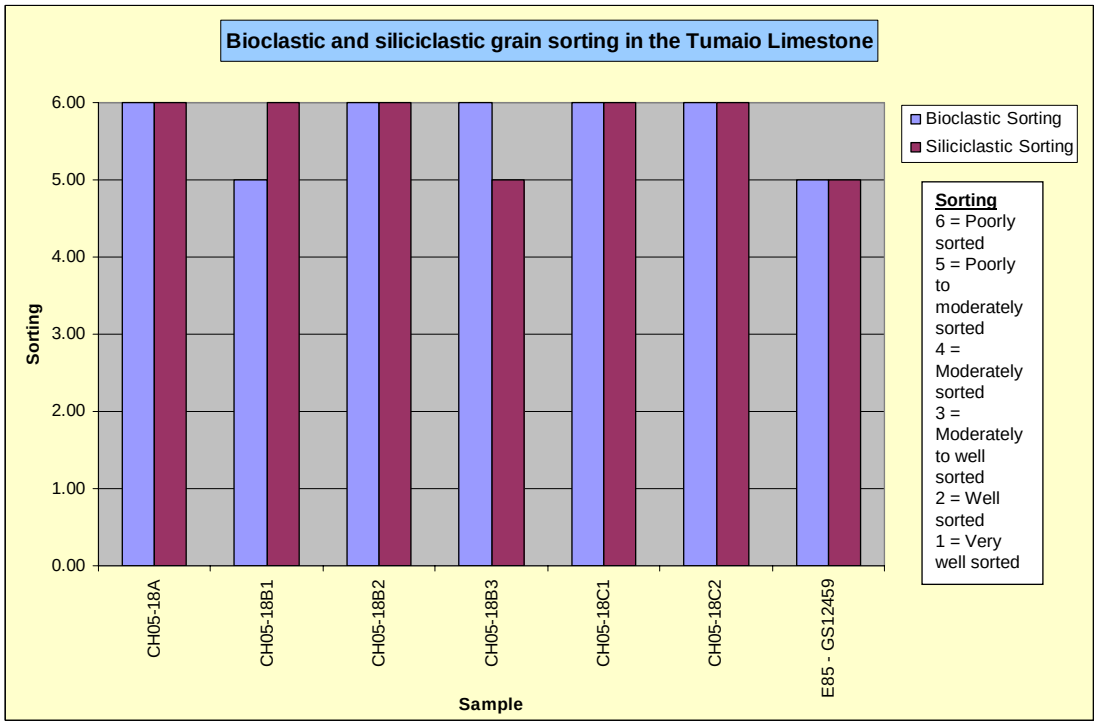

Figure B88: Bioclast and siliciclastic/precipitate grain sorting in the Tumaio Limestone, Chatham Islands.

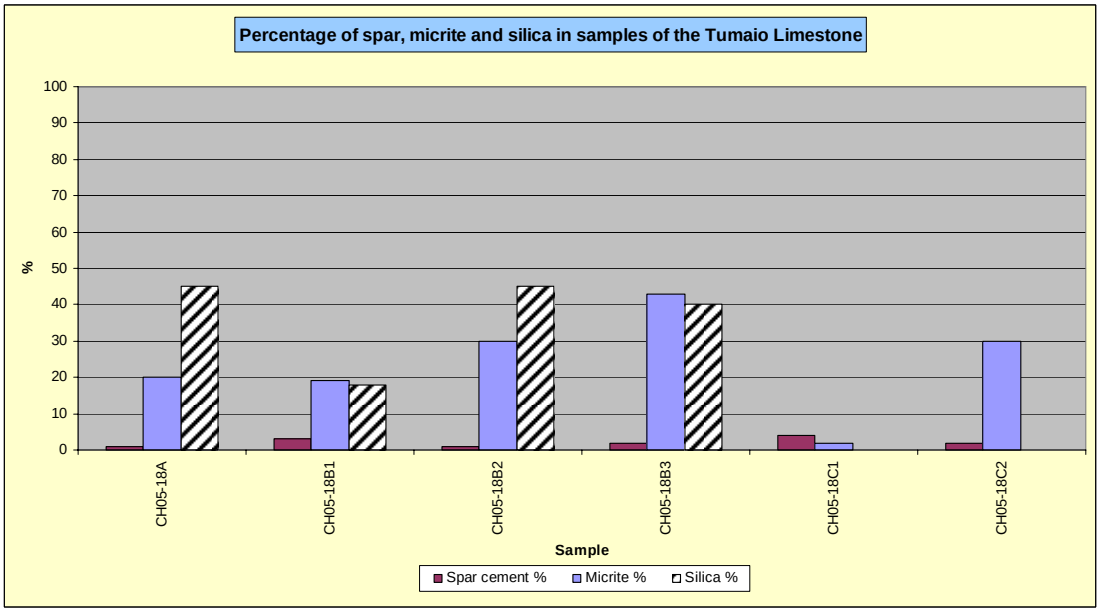

Figure B89: Percentage of spar versus micrite and silica in samples of the Tumaio Limestone, Chatham Islands.

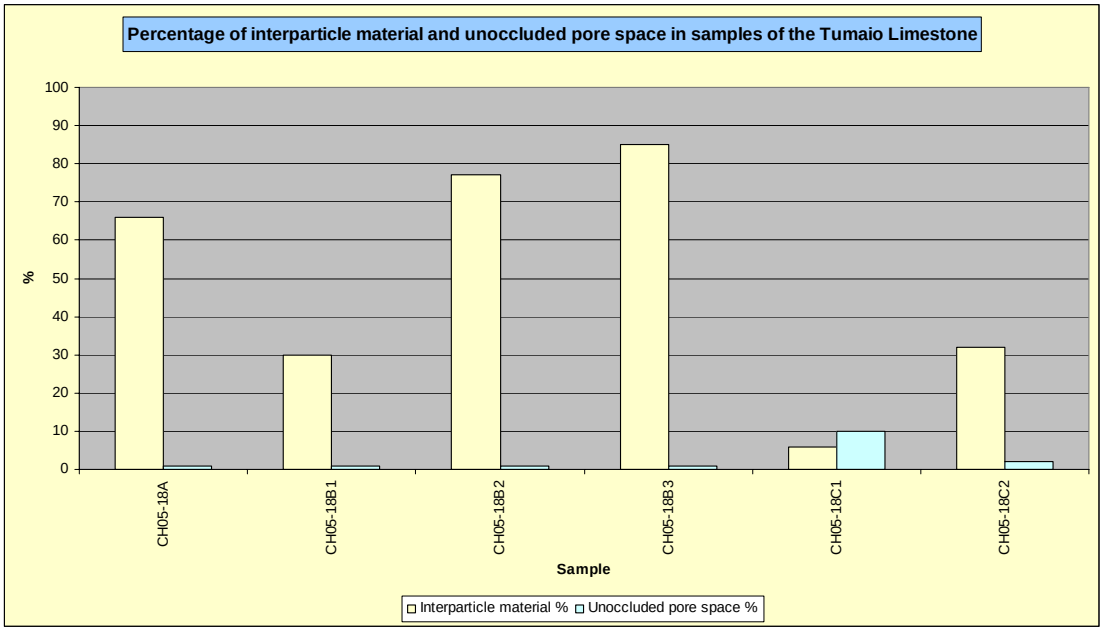

Figure B90: Percentage of interparticle material versus unoccluded pore space in samples of the Tumaio Limestone, Chatham Islands.

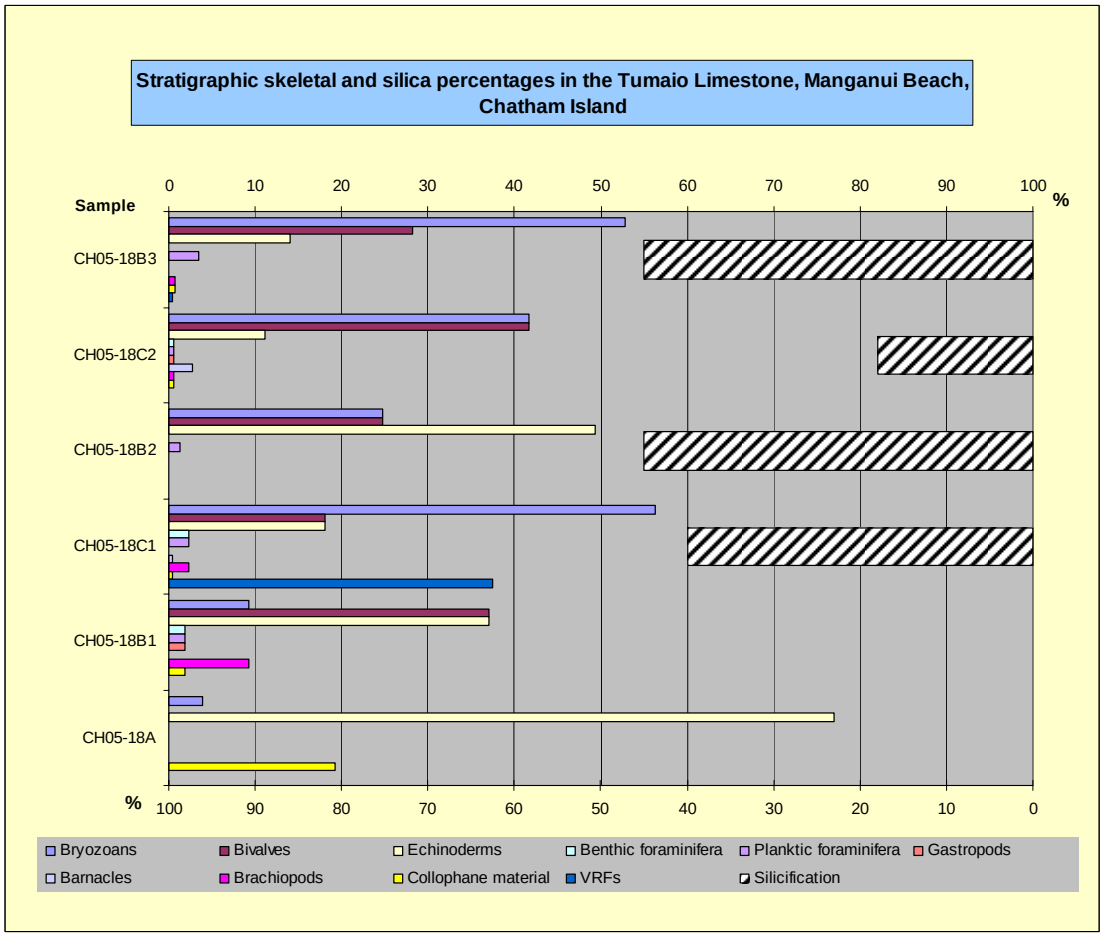

Figure B91: Stratigraphic skeletal and silica percentages (up column) in the Tumaio Limestone, north-eastern of Manganui Beach, northern Chatham Island.

***Victoriella* Limestone**

Table B17: Component data for the *Victoriella* Limestone, Wharekauri and North Road junction, northern Chatham Island.

***Victoriella* Limestone**		Wharekauri/North Road intersection, Chatham Island	
Stratigraphic column number		2	2
Sample running number		CH05-30A (1)	CH05-30A (2)
	Total bioclast %	75	80
	Bryozoans	VC	A
C	Bivalves	M	R
a	Echinoderms	C	S
l	Benthic foraminifera	S	S
c	Planktic foraminifera	R	R
i	Gastropods		
c	Calcareous algae		
l	Barnacles		
a	Spicules & spines		
s	**Other**		
t	Brachiopods		S
s	Serpulids	R	R
	Modal size 1 (mm)	0.63	0.88
	Modal size 2 (mm)	2	
	Shape/abrasion	A	VA
	Sorting	P	P
	Intraclast %	2	0
	Siliciclastic grain %	10	5
	Quartz		
S	Feldspar		
i	VRFs	M	
l	SRFs		
i	Micas		
c	Pyrite grains	S	
i	Pyrite infills		
c	Glauconite pellets	S	
l	Glauconite infills		
a	**Other**		
s	Hornblende	R	
t	Limonite staining	S	M
s	Modal size 1 (mm)	0.10	0.13
	Modal size 2 (mm)	2.50	
	Shape/abrasion	SR-R	SR
	Sorting	P	P
	Interparticle material %	15	15
	Spar cement %	5	2
	Micrite %	10	7
	Silica %	0	5
Unoccluded pore space %		2	2

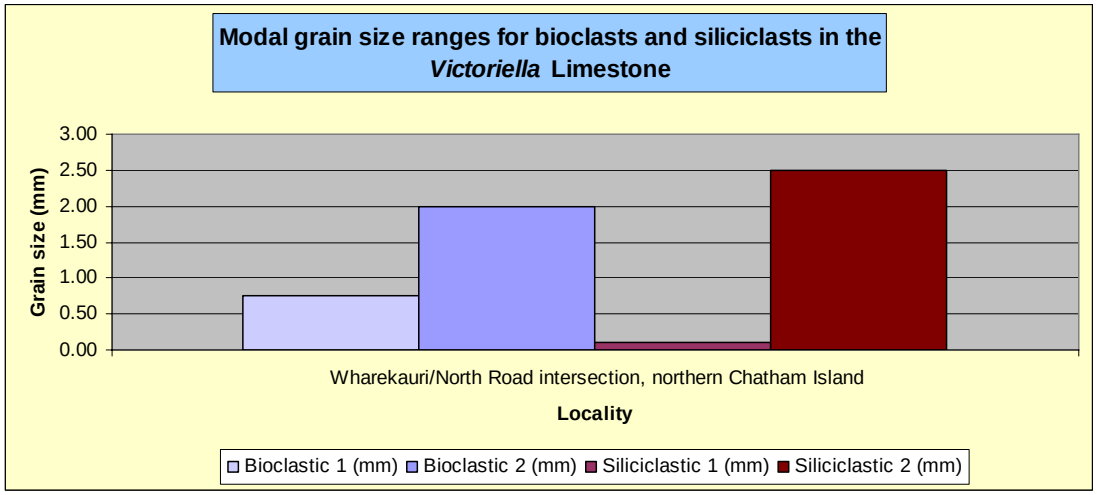

Figure B92: Modal skeletal and siliciclastic/precipitate grain sizes in the *Victoriella* Limestone, Chatham Islands.

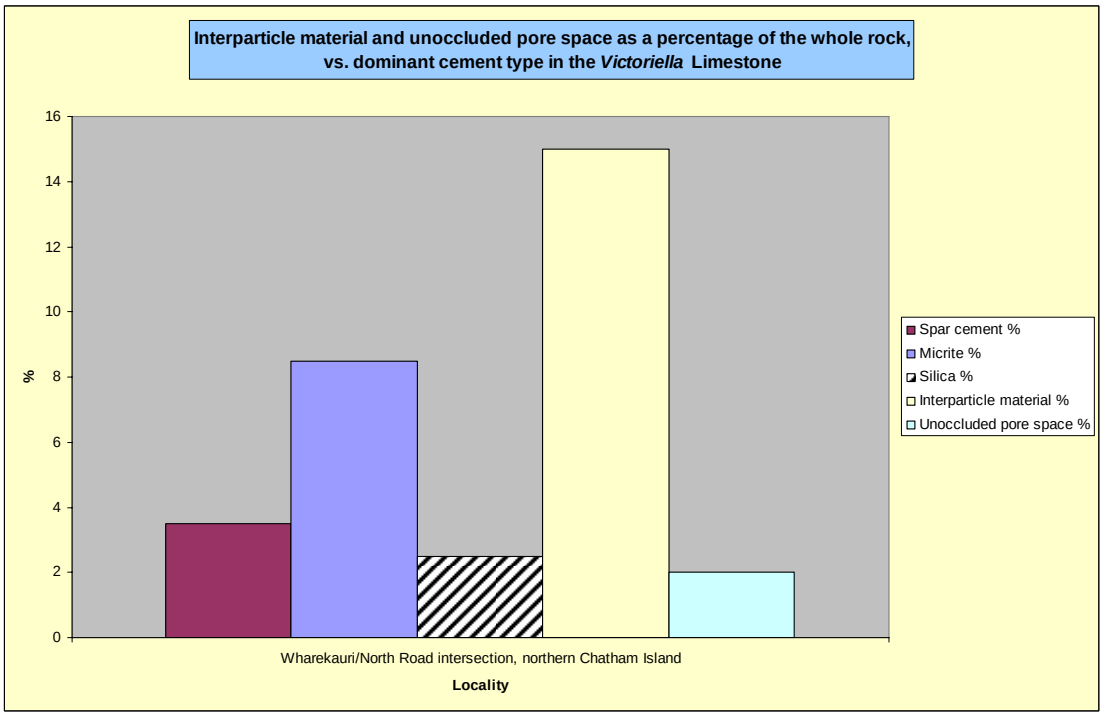

Figure B93: Percentages of interparticle material and unoccluded pore space, and the amount of silica, micrite and spar present in the *Victoriella* Limestone, Chatham Islands.

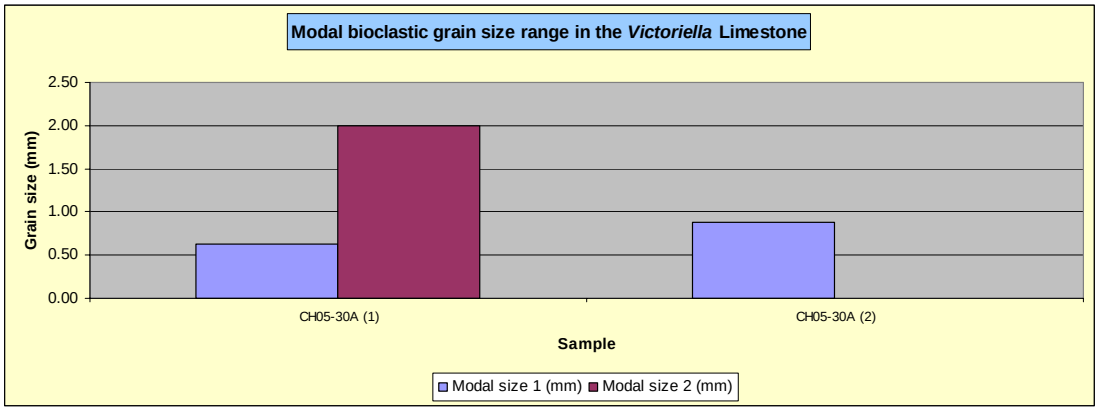

Figure B94: Modal bioclast grain sizes in the *Victoriella* Limestone, Chatham Islands.

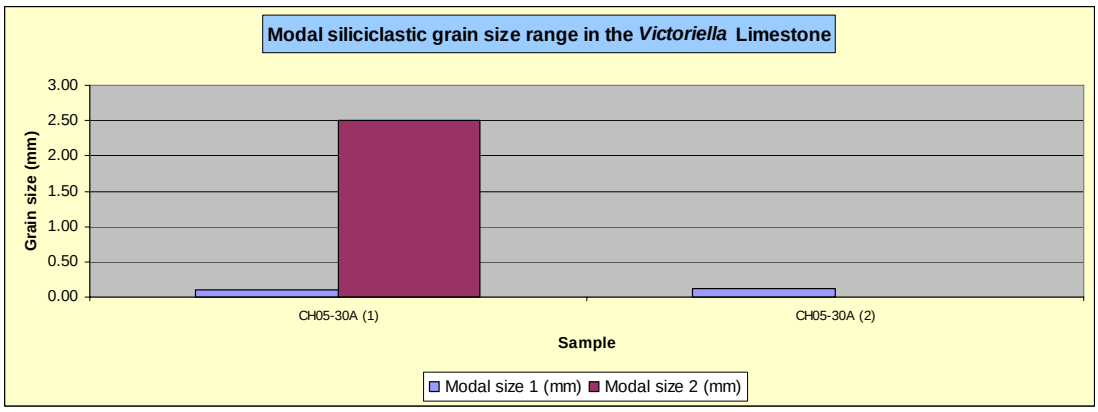

Figure B95: Modal siliciclastic grain sizes in the *Victoriella* Limestone, Chatham Islands.

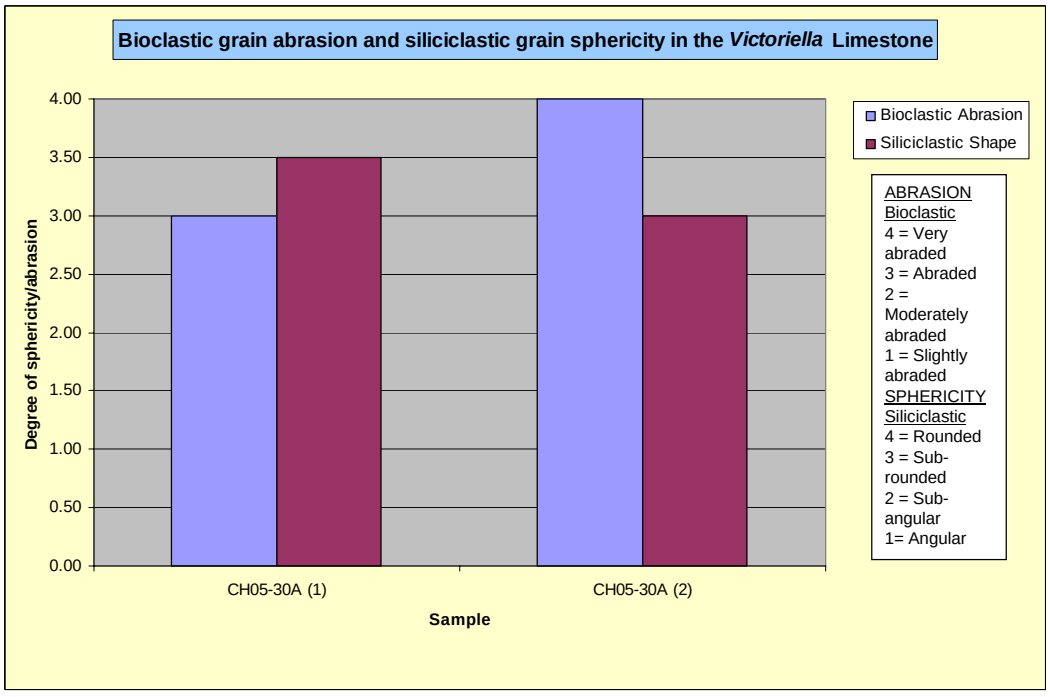

Figure B96: Bioclast abrasion and siliciclastic/precipitate sphericity in the *Victoriella* Limestone, Chatham Islands.

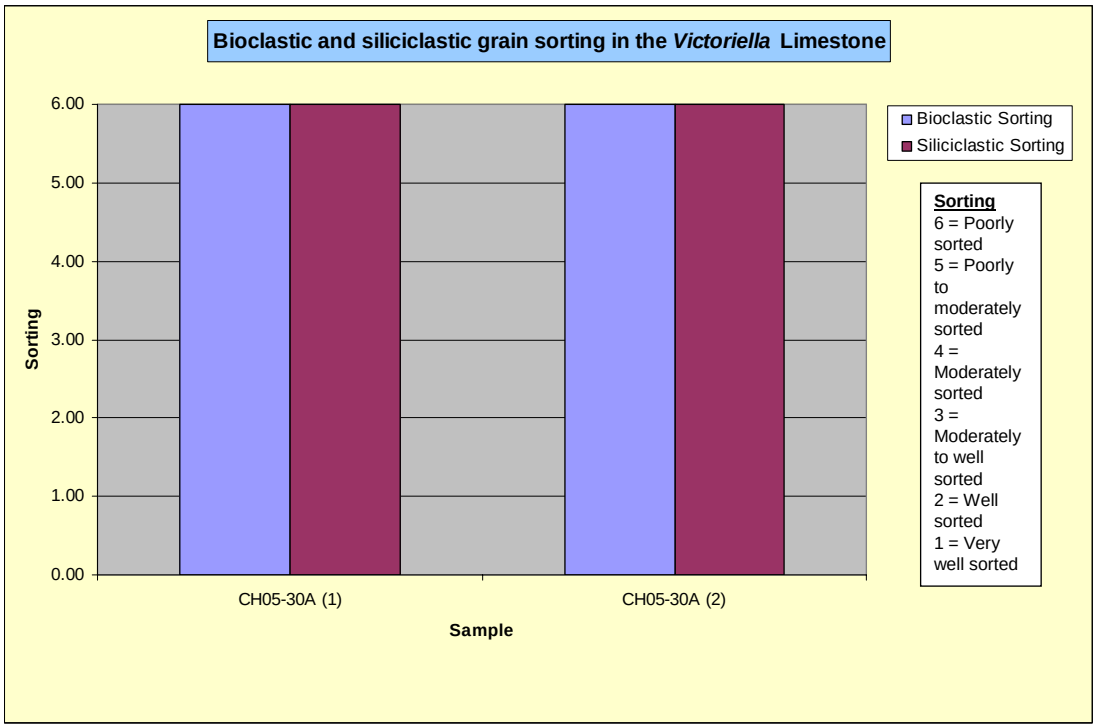

Figure B97: Bioclast and siliciclastic/precipitate grain sorting in the *Victoriella* Limestone, Chatham Islands.

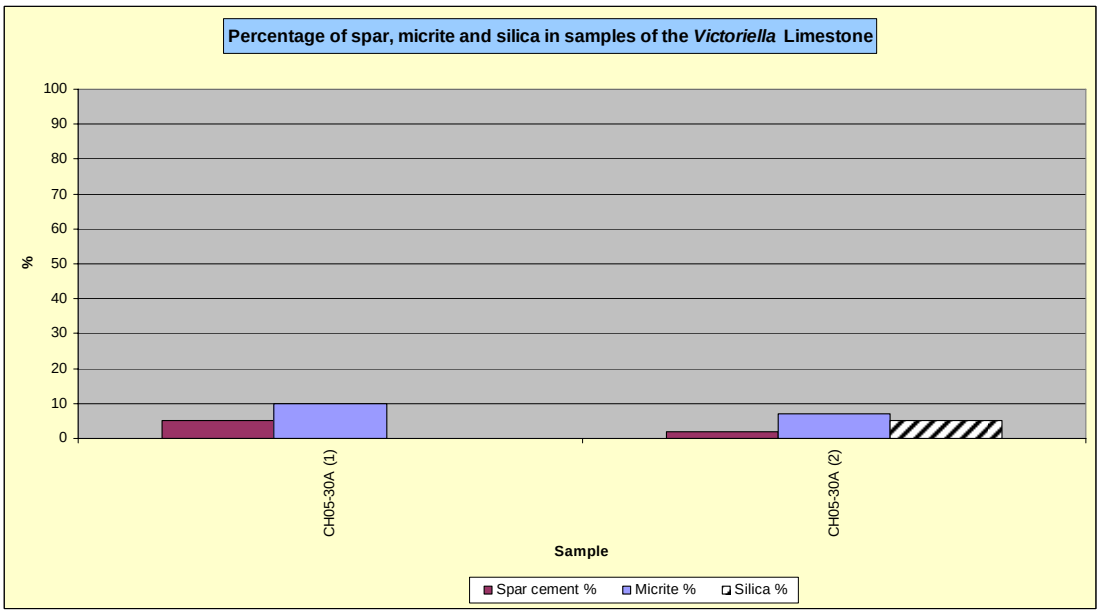

Figure B98: Percentage of spar versus micrite and silica in samples of the *Victoriella* Limestone, Chatham Islands.

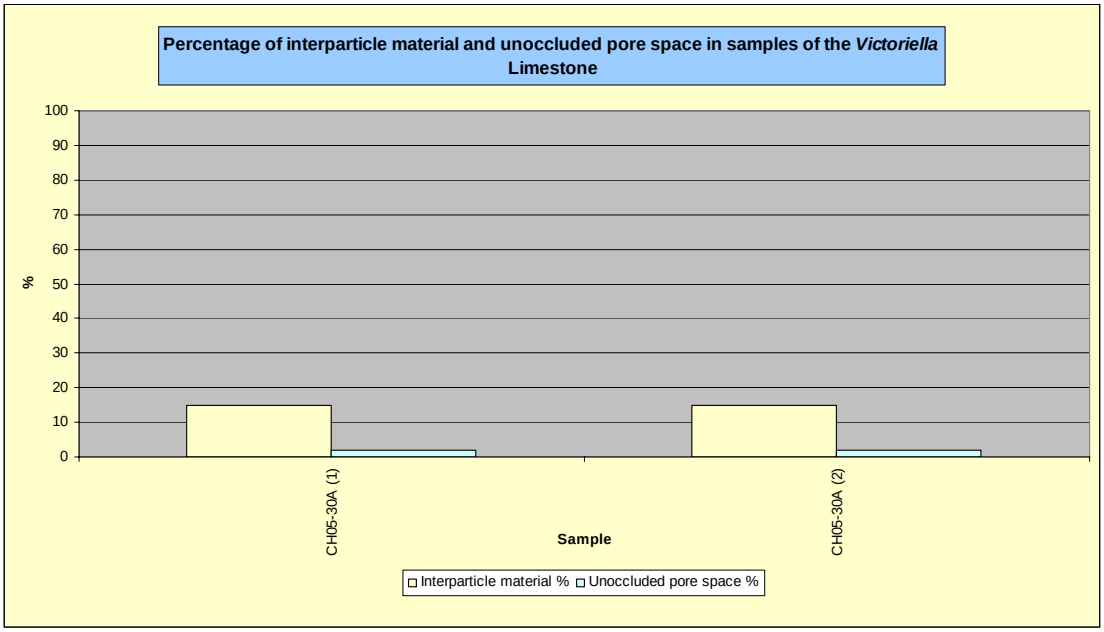

Figure B99: Percentage of interparticle material versus unoccluded pore space in samples of the *Victoriella* Limestone, Chatham Islands.

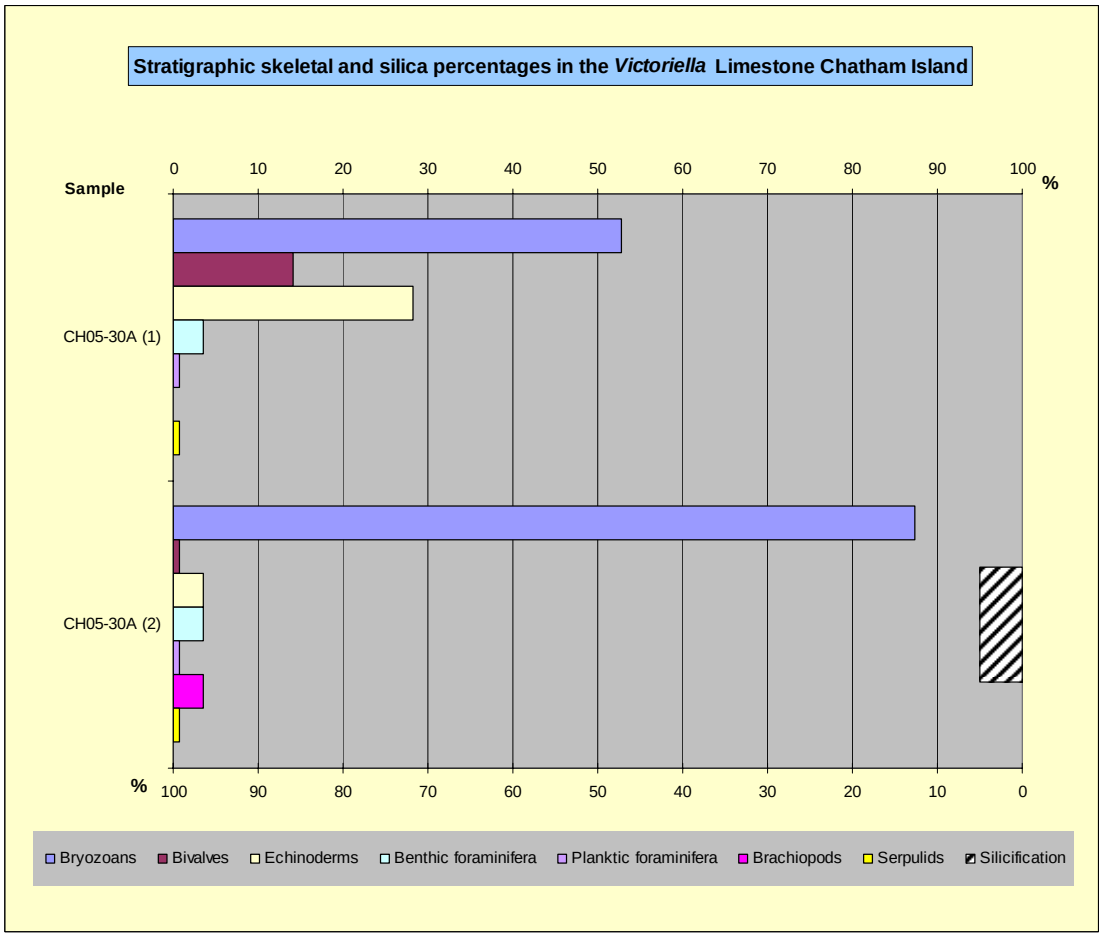

Figure B100: Stratigraphic skeletal and silica percentages (up column) in the *Victoriella* Limestone on the Wharekauri and North Road junction, northern Chatham Island.

Altonian limestone

Table B18: Component data for the Altonian limestone, Chatham Island.

Altonian limestone		Moutapu Point, Chatham Island
Stratigraphic column number		–
Sample running number		M363 - GS12998
	Total bioclast %	65
	Bryozoans	M
C	Bivalves	M
a	Echinoderms	S
l	Benthic foraminifera	S
c	Planktic foraminifera	VC
i	Gastropods	
c	Calcareous algae	
l	Barnacles	
a	Spicules & spines	
s	**Other**	
t	Brachiopods	S
s	Stromatolitic algae	M
	Modal size 1 (mm)	0.10
	Modal size 2 (mm)	2
	Shape/abrasion	MA
	Sorting	P
	Intraclast %	10
	Siliciclastic grain %	20
	Quartz	S
S	Feldspar	
i	VRFs	M
l	SRFs	S
i	Micas	
c	Pyrite grains	M
i	Pyrite infills	M
c	Glauconite pellets	M
l	Glauconite infills	R
a	**Other**	
s	Hornblende	
t	Phosphate	S
s	Limonite staining	M
	Modal size 1 (mm)	0.13
	Modal size 2 (mm)	2.25
	Shape/abrasion	SR-SA
	Sorting	P
	Interparticle material %	15
	Spar cement %	10
	Micrite %	2
Unoccluded pore space %		2

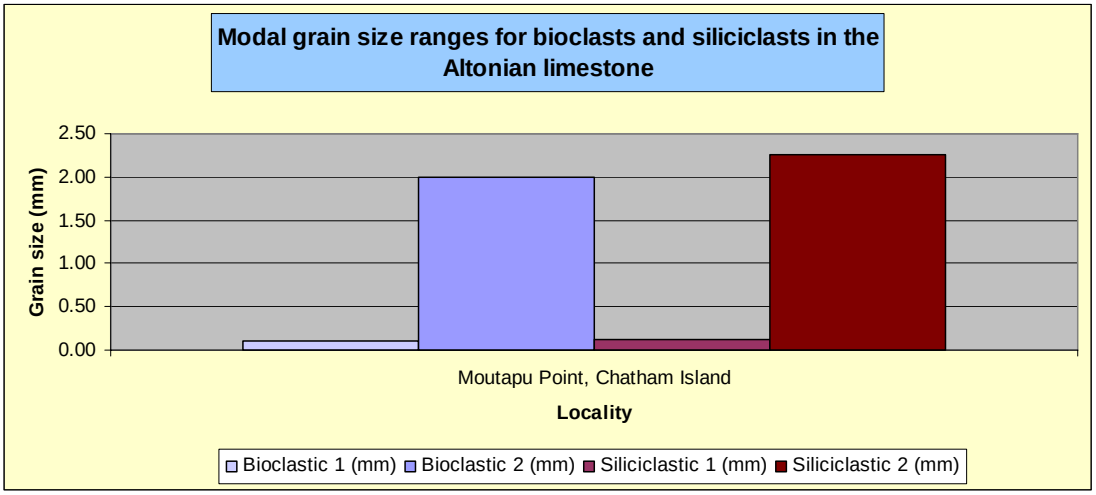

Figure B101: Modal skeletal and siliciclastic/precipitate grain sizes in the Altonian limestone, Chatham Islands.

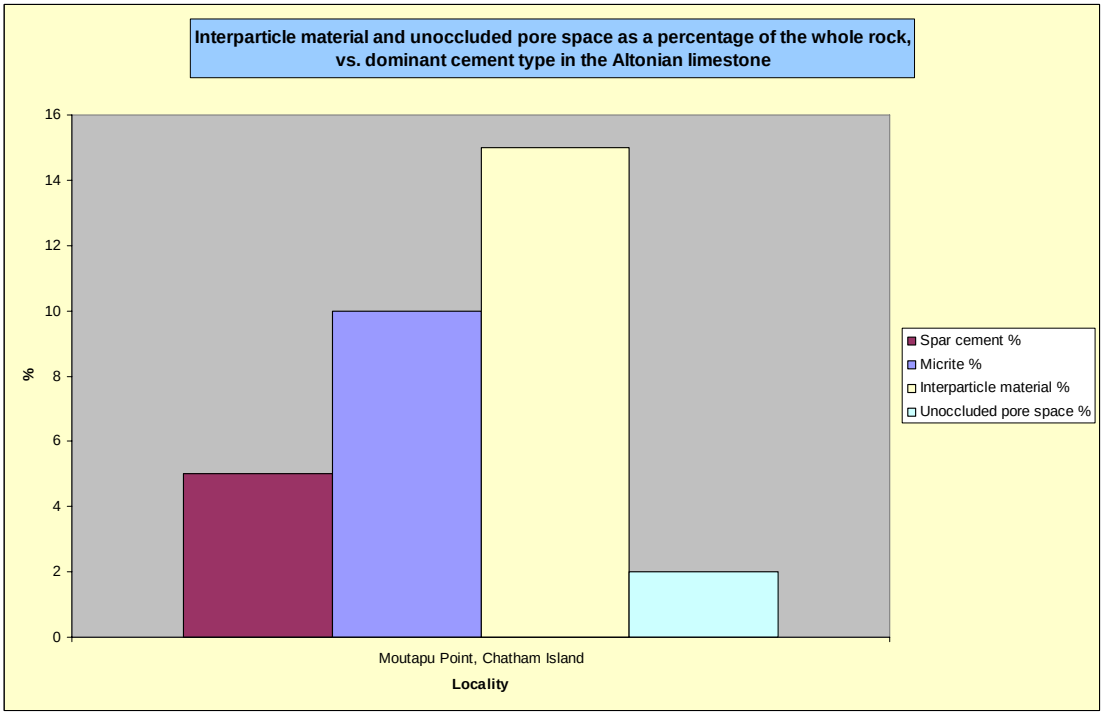

Figure B102: Geographical distribution of interparticle material and unoccluded pore space, and the amount of micrite and spar present in the Altonian limestone, Chatham Islands.

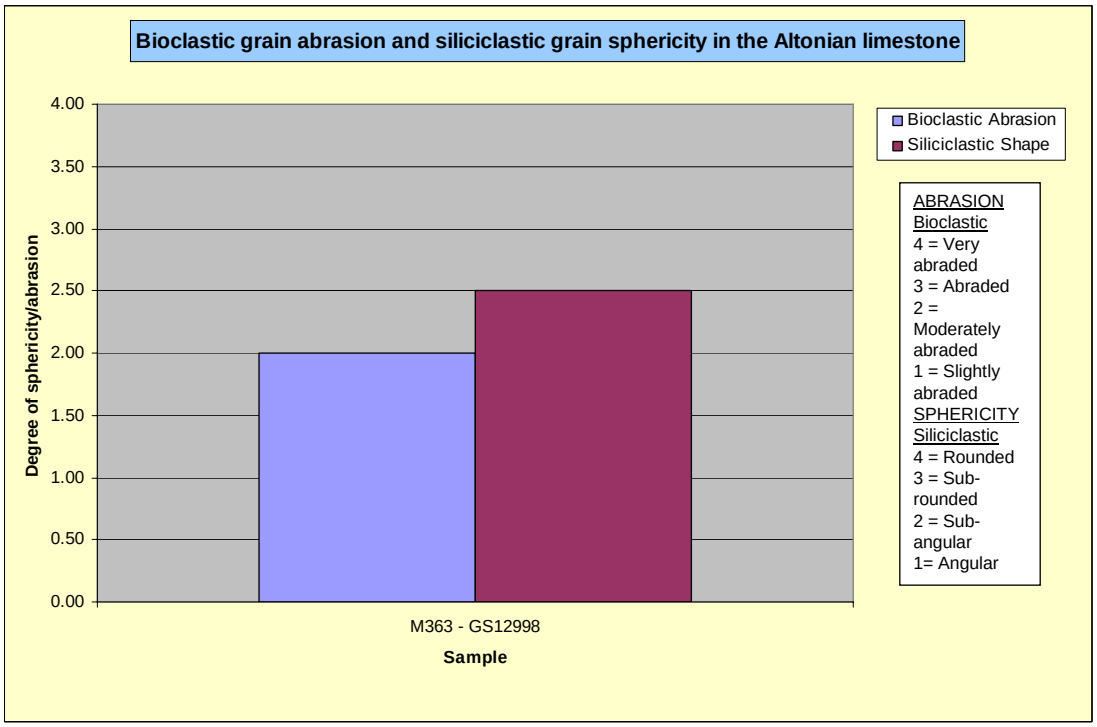

Figure B103: Bioclast abrasion and siliciclastic/precipitate sphericity in the Altonian limestone, Chatham Islands.

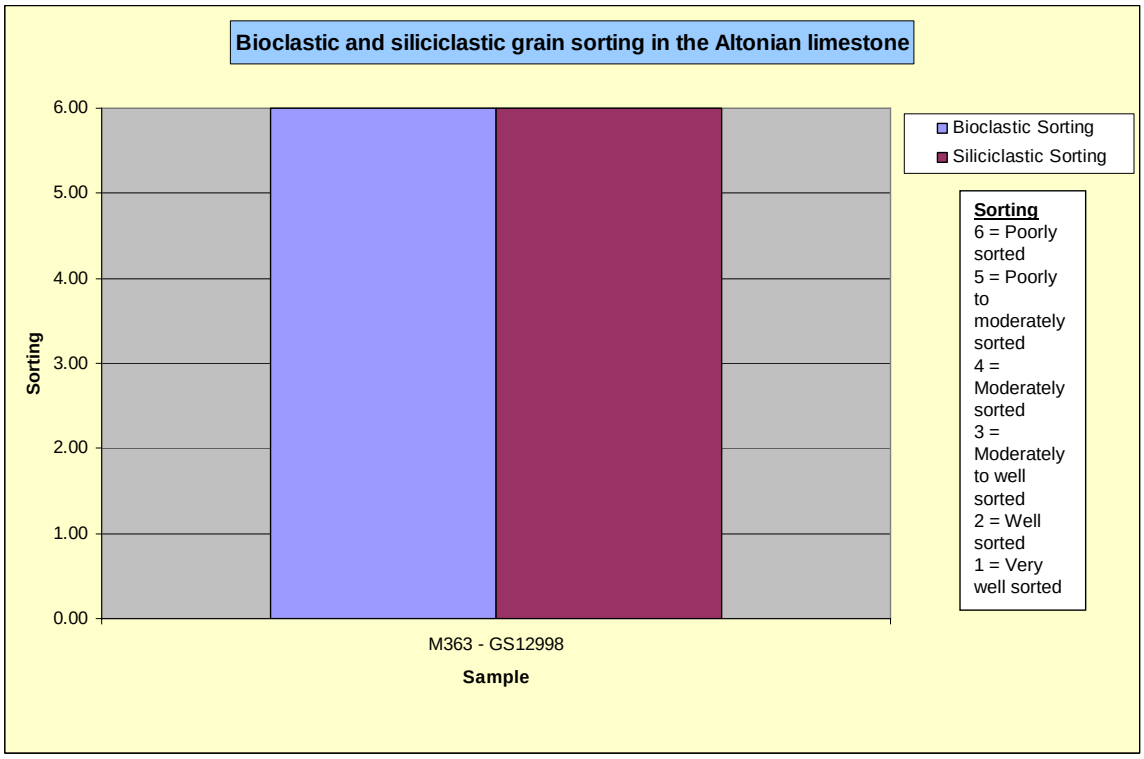

Figure B104: Bioclast and siliciclastic/precipitate grain sorting in the Altonian limestone, Chatham Islands.

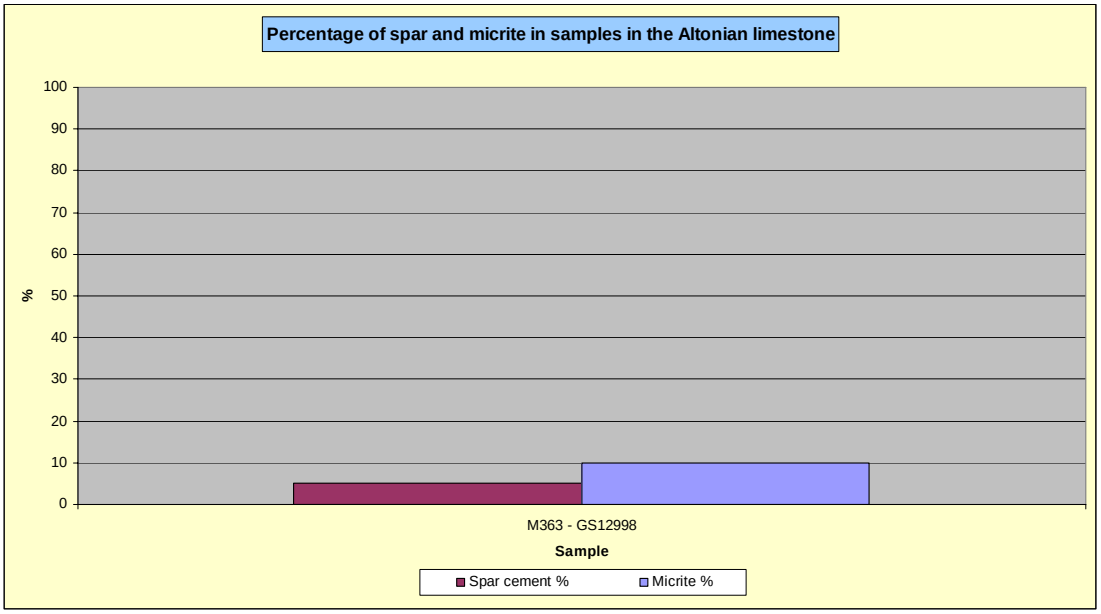

Figure B105: Percentage of spar versus micrite in samples of the Altonian limestone, Chatham Islands.

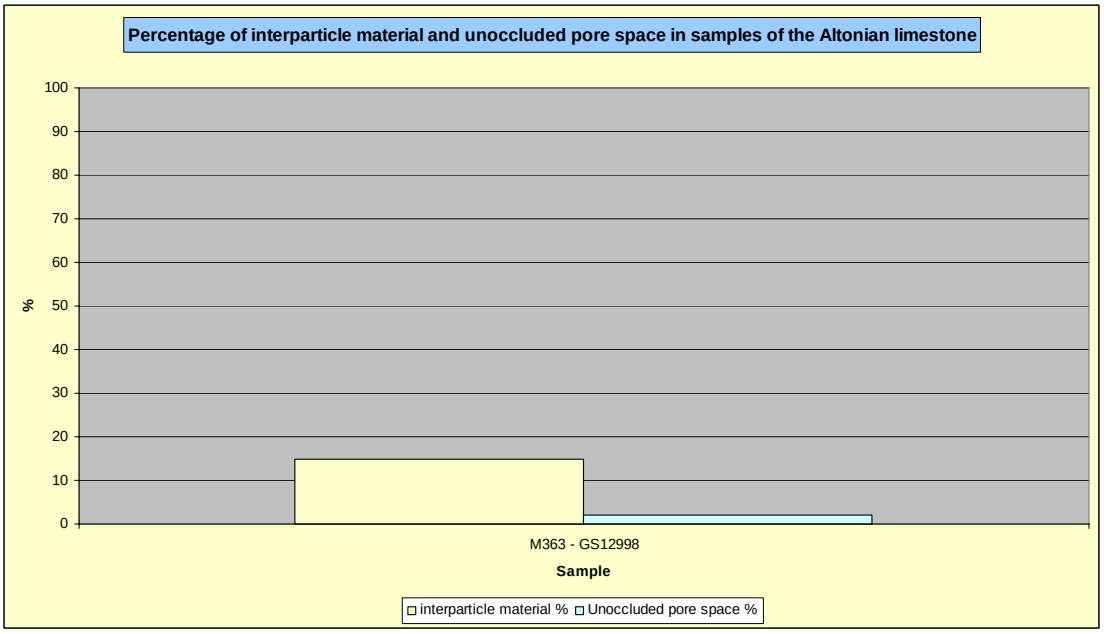

Figure B106: Percentage of interparticle material versus unoccluded pore space in samples of the Altonian limestone, Chatham Islands.

Waipipian limestone

Table B19: Component data for the Waipipian limestone, Chatham Island.

Waipipian limestone		Tioriori, Chatham Island
Stratigraphic column number		–
Sample running number		P-Q407 - GS14155
	Total bioclast %	80
	Bryozoans	A
C	Bivalves	C
a	Echinoderms	M
l	Benthic foraminifera	
c	Planktic foraminifera	R
i	Gastropods	
c	Calcareous algae	
l	Barnacles	R
a	Spicules & spines	
s	Modal size 1 (mm)	0.75
t	Modal size 2 (mm)	2
s	Shape/abrasion	VA
	Sorting	P
	Intraclast %	2
	Siliciclastic grain %	5
	Quartz	R
S	Feldspar	R
i	VRFs	R
l	SRFs	
i	Micas	
c	Pyrite grains	S
i	Pyrite infills	S
c	Glauconite pellets	R
l	Glauconite infills	R
a	**Other**	
s	Phosphate	S
t	Limonite staining	S
s	Modal size 1 (mm)	0.10
	Modal size 2 (mm)	
	Shape/abrasion	SR
	Sorting	PM
	Interparticle material %	15
	Spar cement %	2
	Micrite %	10
Unoccluded pore space %		2

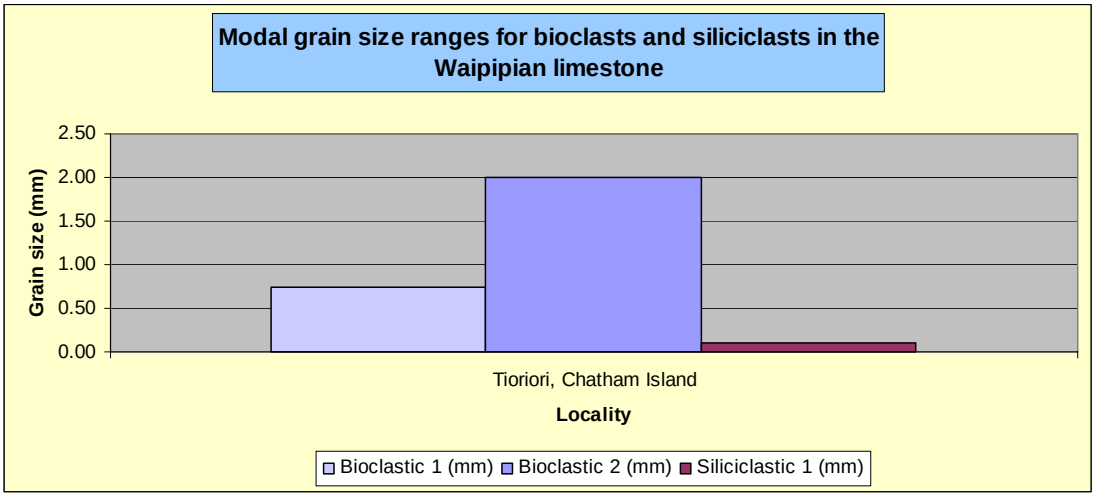

Figure B107: Modal skeletal and siliciclastic/precipitate grain sizes in the Waipipian limestone, Chatham Islands.

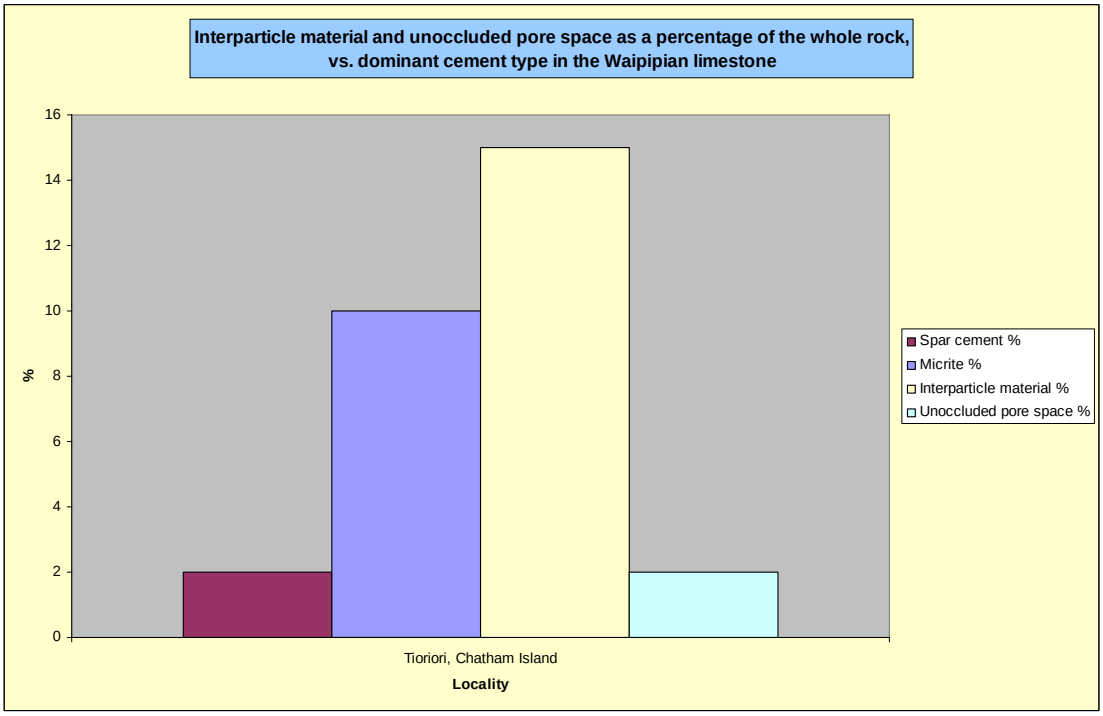

Figure B108: Percentage of interparticle material and unoccluded pore space, and the amount of micrite and spar present in the Waipipian limestone, Chatham Islands.

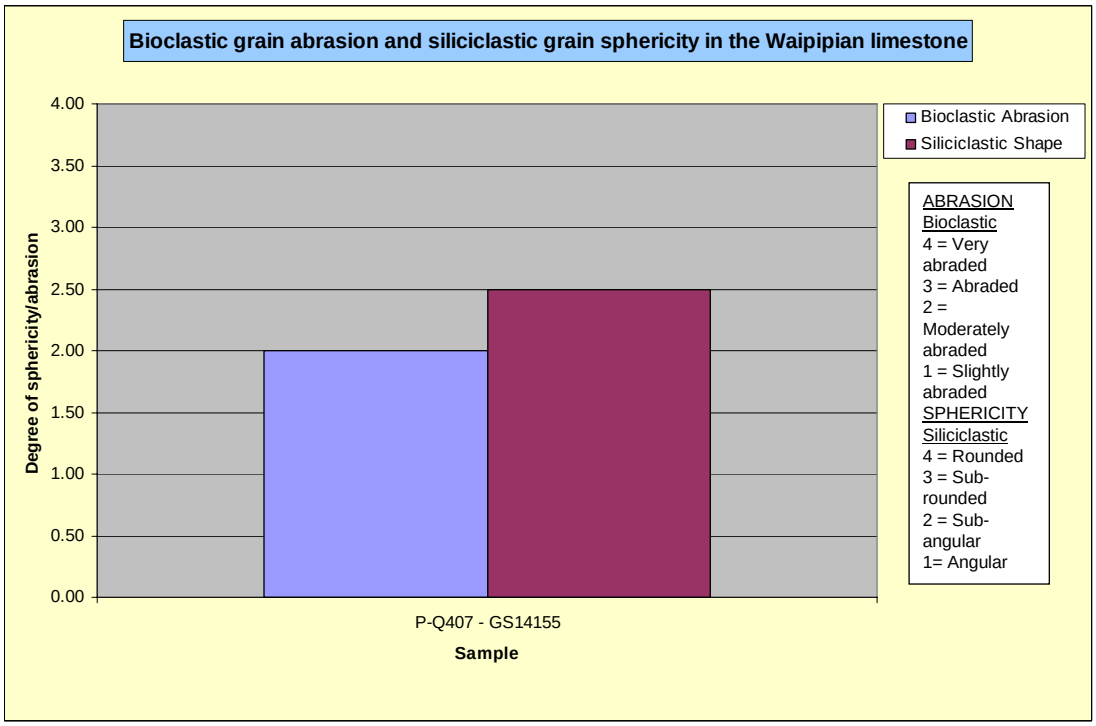

Figure B109: Bioclast abrasion and siliciclastic/precipitate sphericity in the Waipipian limestone, Chatham Islands.

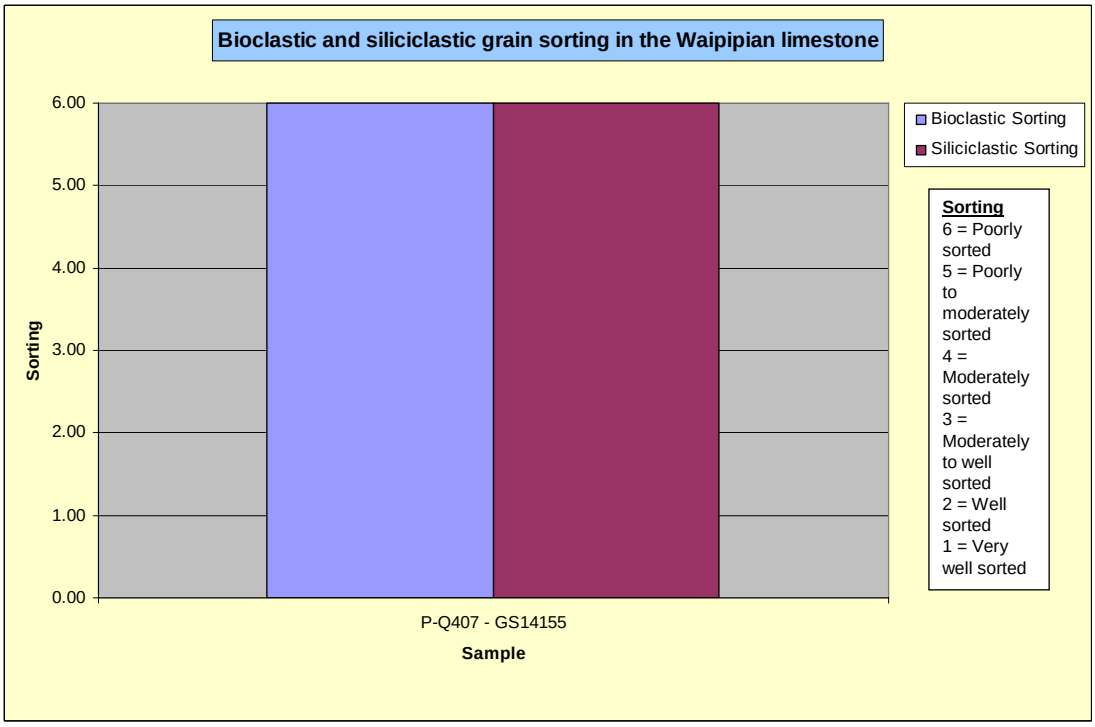

Figure B110: Bioclast and siliciclastic/precipitate grain sorting in the Waipipian limestone, Chatham Islands.

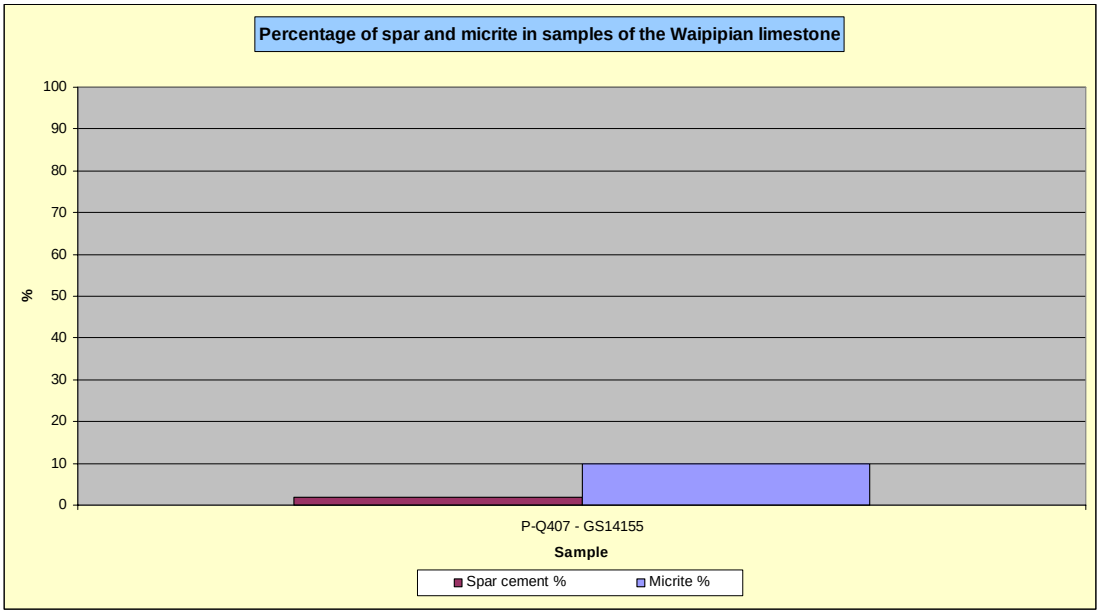

Figure B111: Percentage of spar versus micrite in samples of the Waipipian limestone, Chatham Islands.

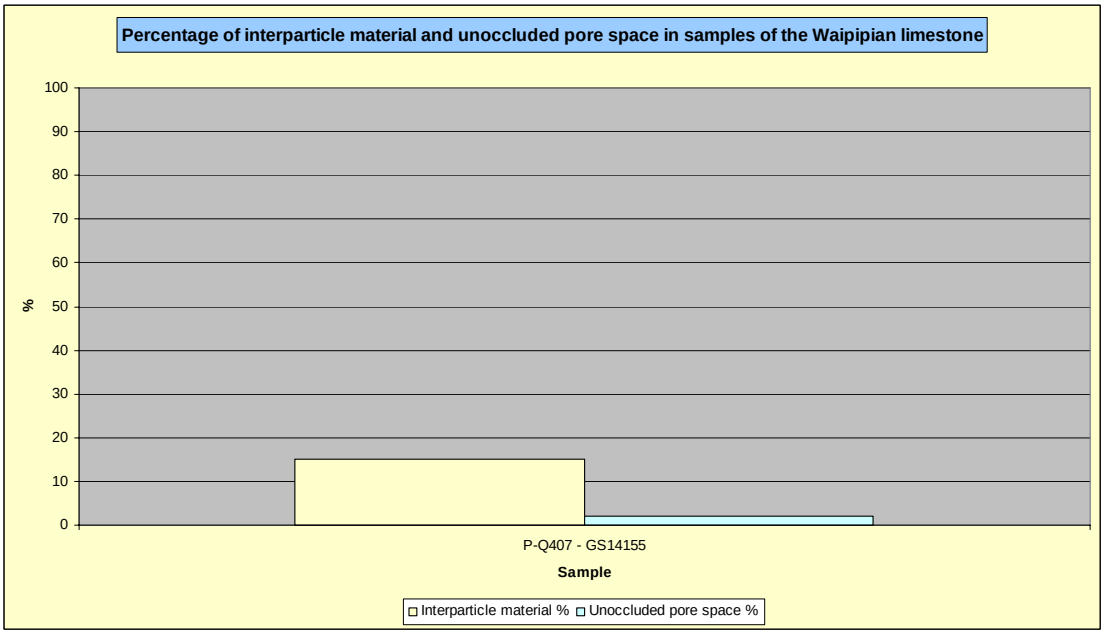

Figure B112: Percentage of interparticle material versus unoccluded pore space in samples of the Waipipian limestone, Chatham Islands.

Cape L'Eveque limestone

Table B20: Component data for the Cape L'Eveque limestone, southern Chatham Island.

Cape L'Eveque limestone		Snake Gully, Chatham Island
Stratigraphic column number		10
Sample running number		CH06-TH02D
	Total bioclast %	70
	Bryozoans	C
C	Bivalves	A
a	Echinoderms	S
l	Benthic foraminifera	S
c	Planktic foraminifera	R
i	Gastropods	
c	Calcareous algae	C
l	Barnacles	
a	Spicules & spines	
s	Modal size 1 (mm)	0.80
t	Modal size 2 (mm)	
s	Shape/abrasion	SA
	Sorting	MW
	Intraclast %	0
	Siliciclastic grain %	20
	Quartz	
S	Feldspar	
i	IRFs	C
l	SRFs	
i	Micas	
c	Pyrite grains	R
i	Pyrite infills	
c	Glauconite pellets	R
l	Glauconite infills	
a	**Other**	
s	Hornblende	R
t	Modal size 1 (mm)	0.35
s	Modal size 2 (mm)	10.00
	Shape/abrasion	SR
	Sorting	P
	Interparticle material %	7
	Spar cement %	2
	Micrite %	5
Unoccluded pore space %		2

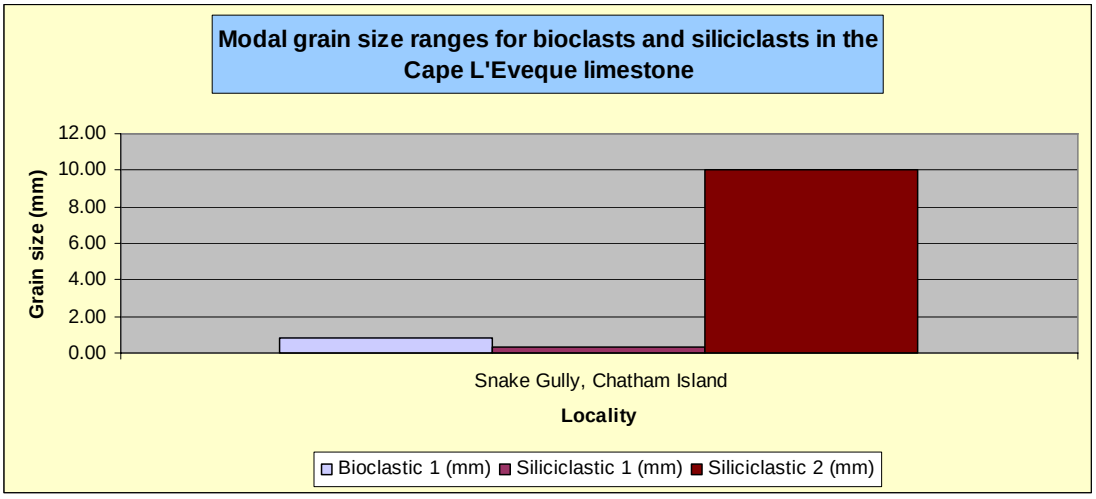

Figure B113: Modal skeletal and siliciclastic/precipitate grain sizes in the Cape L'Eveque limestone, Chatham Islands.

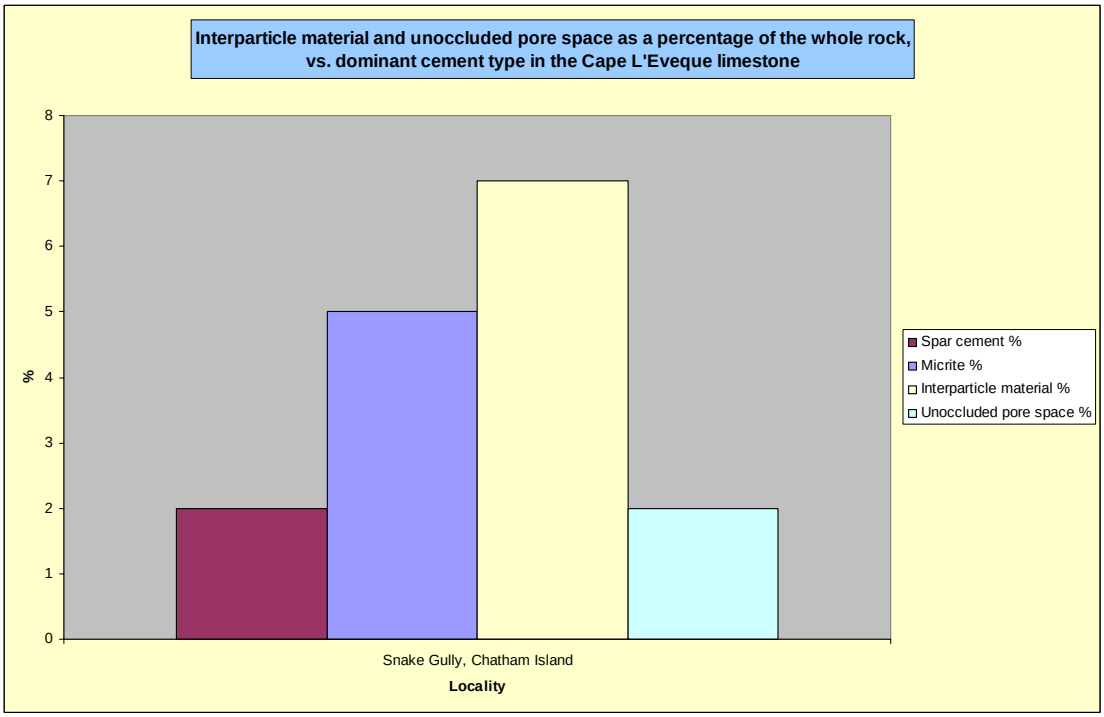

Figure B114: Percentage of interparticle material and unoccluded pore space, and the amount of micrite and spar present in the Cape L'Eveque limestone, Chatham Islands.

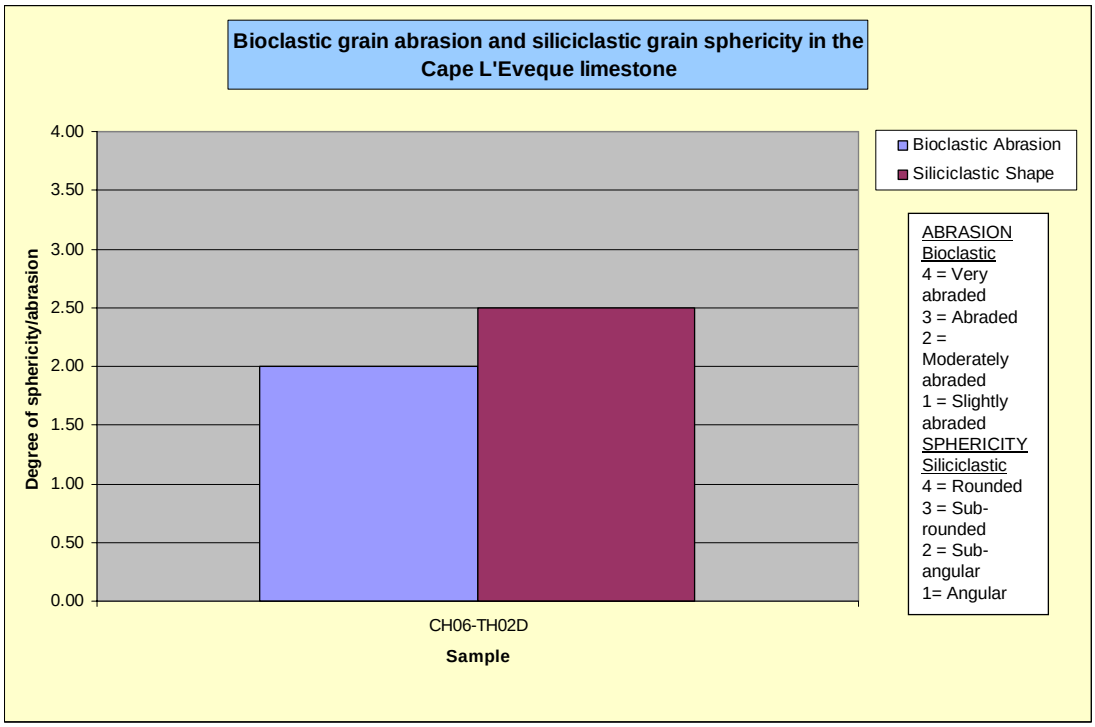

Figure B115: Bioclast abrasion and siliciclastic/precipitate sphericity in the Cape L'Eveque limestone, Chatham Islands.

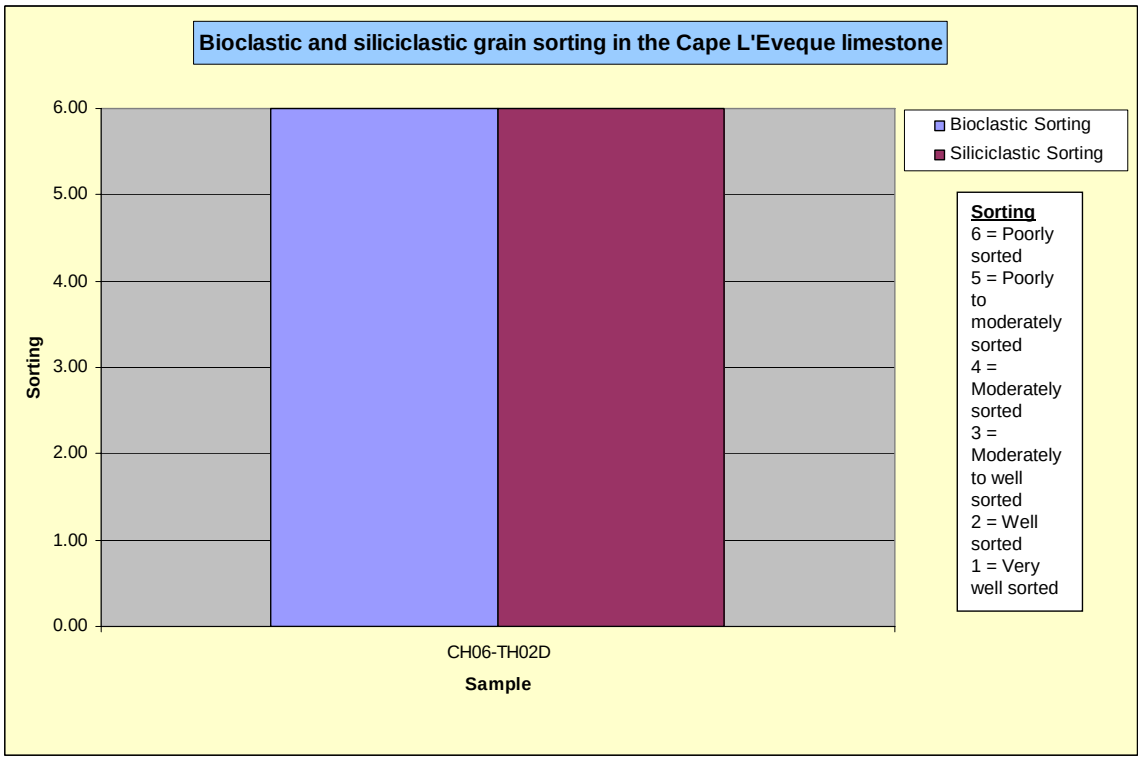

Figure B116: Bioclast and siliciclastic/precipitate grain sorting in the Cape L'Eveque limestone, Chatham Islands.

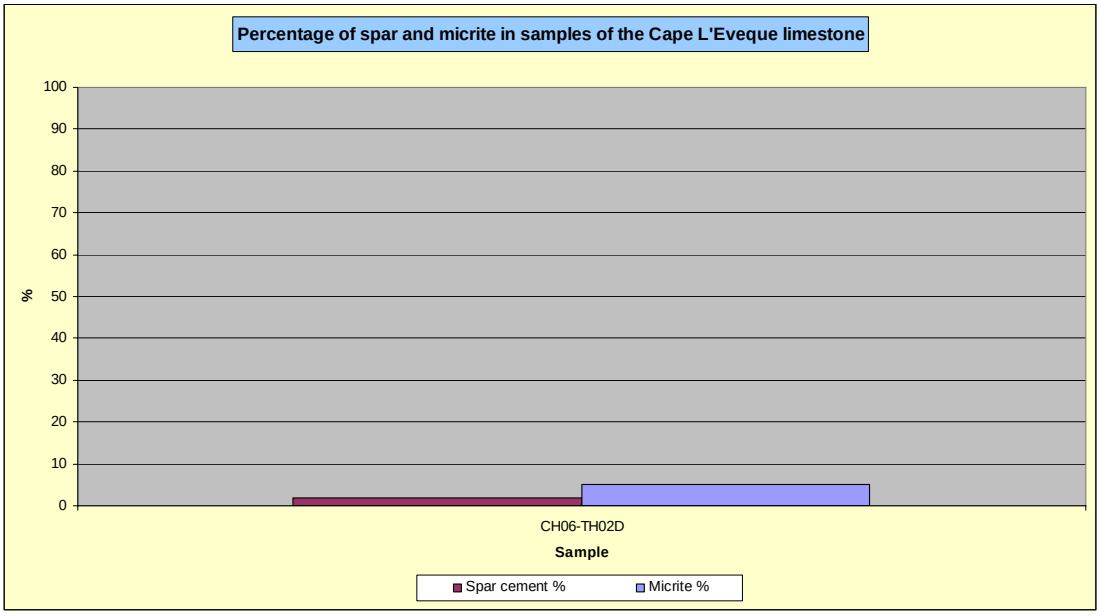

Figure B117: Percentage of spar versus micrite in samples of the Cape L'Eveque limestone, Chatham Islands.

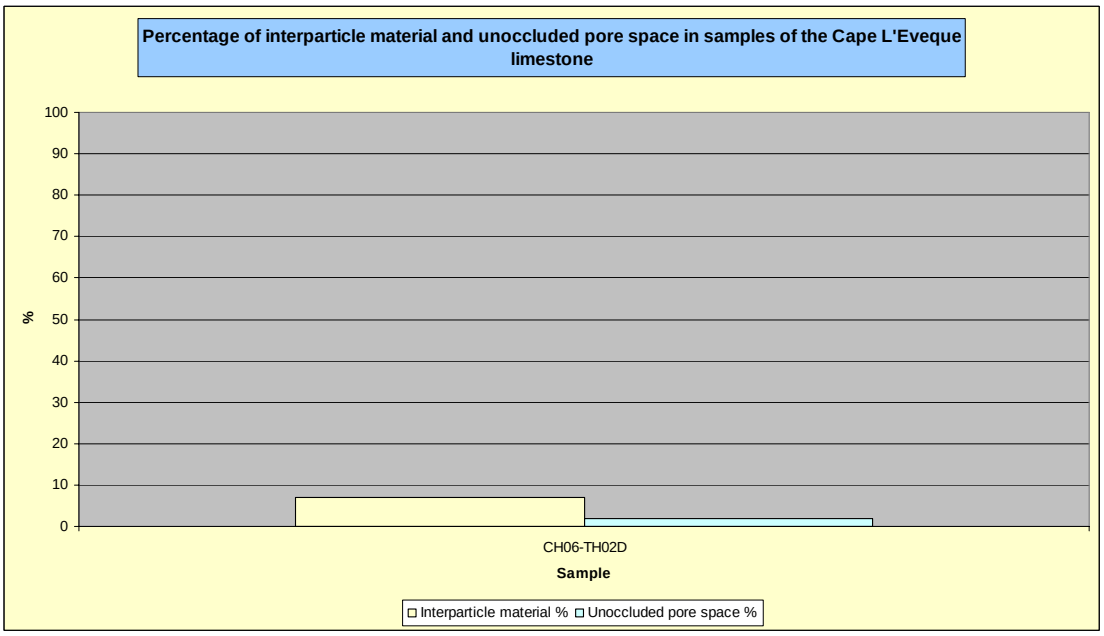

Figure B118: Percentage of interparticle material versus unoccluded pore space in samples of the Cape L'Eveque limestone, Chatham Islands.

APPENDIX C

Sedimentary Dykes Petrographic Data

Chatham Island dyke occurrence petrographic data

Red Bluff dyke occurrences

North Red Bluff locality

Table C1: Component data for dyke occurrences *A* and *B* at the *north Red Bluff* locality, Chatham Island.

Red Bluff Dykes		North Red Bluff dykes			
Dyke reference		A	A	B	B
Sample running number		CH06-RB02A	CH06-RB02A	CH06-RB02B	CH06-RB02B
Phase/pulse number		1	3	Lst fill	Volc fill
	Total bioclast %	75	50	60	2
	Bryozoans	VC	M	VC	R
C	Bivalves	S	R	S	R
a	Echinoderms	M		R	R
l	Benthic foraminifera	C	S	S	
c	Planktic foraminifera		R	R	
i	Gastropods				
c	Calcareous algae				
l	Barnacles				
a	Spicules & spines				
s	**Other**				
t	Brachiopods				
s	Serpulids	R			
	Modal size 1 (mm)	1.00	0.75	0.08	1.75
	Modal size 2 (mm)		1.72	3	
	Shape/abrasion	A	VA	A	VA
	Sorting	PM	P	P	M
	Lithoclast %	2	20	0	10
	Intraclast %	0	0	0	0
	Siliciclastic grain %	2	8	20	52
	Quartz			R	M
S	Feldspar				
i	VRFs	S	C	C	A
l	SRFs				
i	Micas				
c	Pyrite grains			R	S
i	Pyrite infills	R		S	M
c	Glauconite pellets			R	
l	Glauconite infills				
a	**Other**				
s	Phosphate				
t	Chert	R			
s	Hornblende	R		R	
	Limonite staining				
	Modal size 1 (mm)	0.13	0.60	0.10	0.13
	Modal size 2 (mm)			2.25	1.00
	Shape/abrasion	SR	R	SR	SR
	Sorting	PM	P	P	MW
	Interparticle material %	22	35	20	45
	Spar cement %	12	5	2	2
	Micrite %	10	30	18	43
Unoccluded pore space %		1	1	1	1

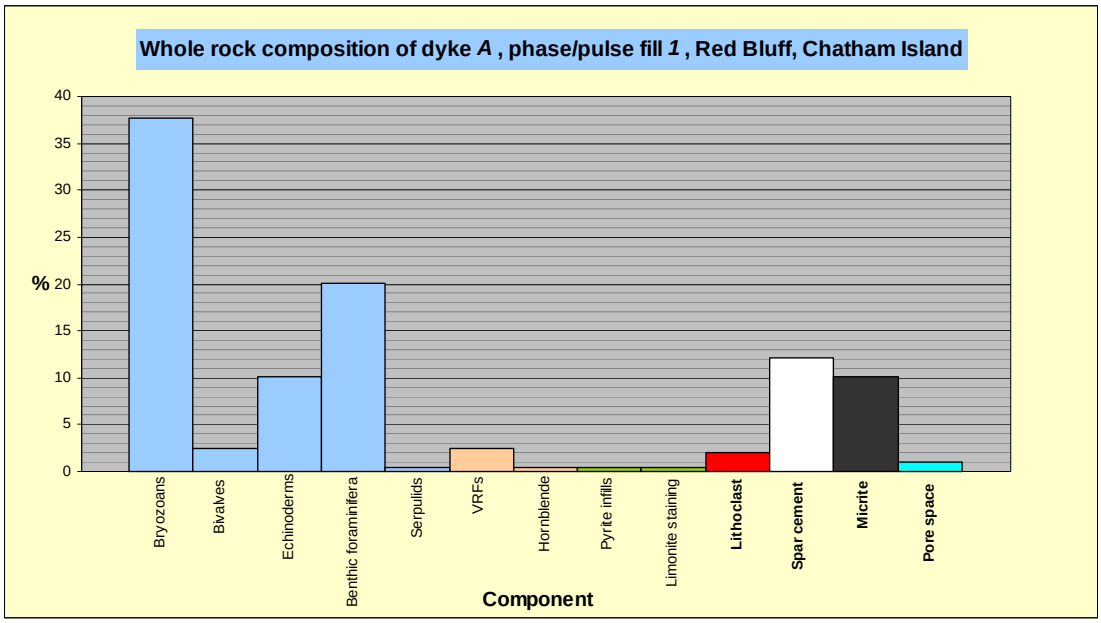

Figure C1: Component percentage of dyke *A*, fill phase *1*, *north Red Bluff* locality, Chatham Islands.

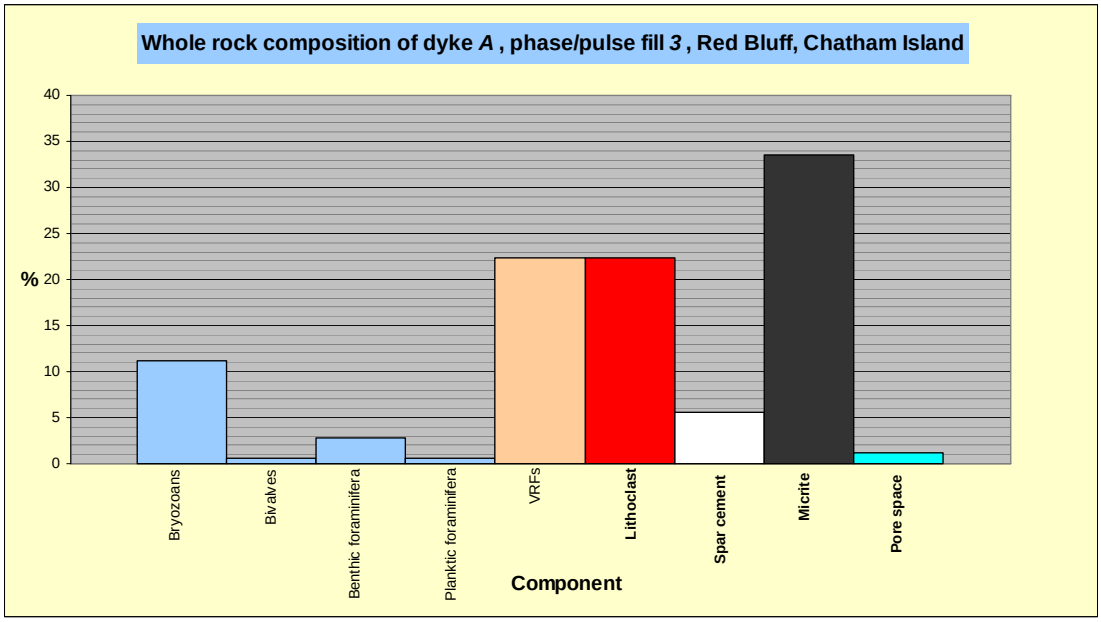

Figure C2: Component percentage of dyke *A*, fill phase *3*, *north Red Bluff* locality, Chatham Islands.

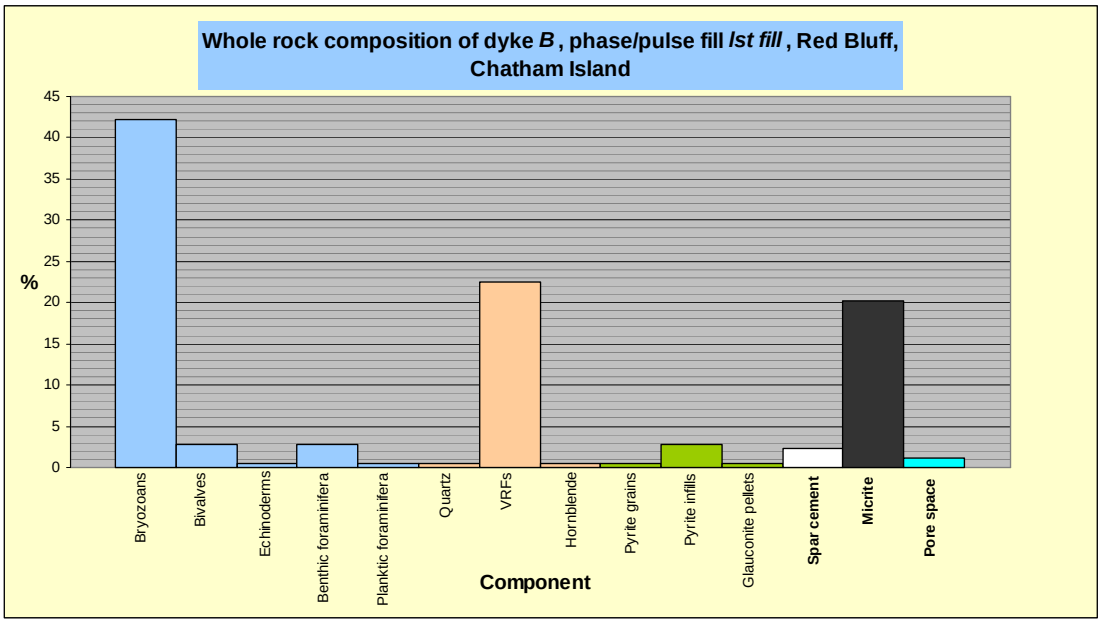

Figure C3: Component percentage of dyke *B*, fill phase *lst fill* (abbreviation for 'limestone fill'), *north Red Bluff* locality, Chatham Islands.

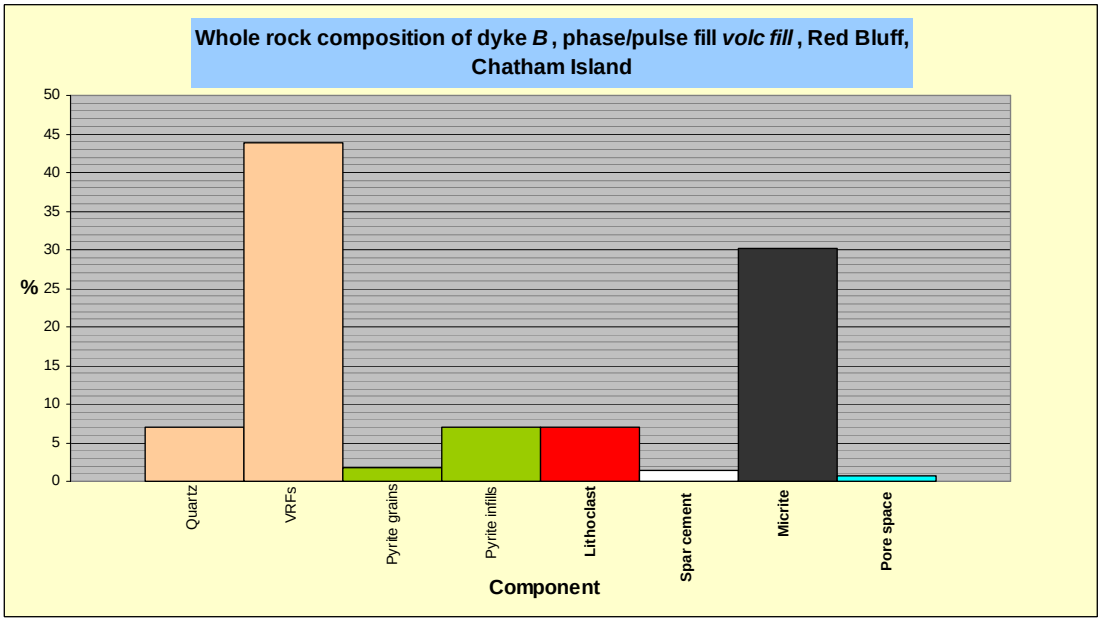

Figure C4: Component percentage of dyke *B*, fill phase *volc fill* (abbreviation for 'volcaniclastic fill'), *north Red Bluff* locality, Chatham Islands.

Table C2: Component data for dyke occurrences *H* at the *north Red Bluff* locality, Chatham Island.

Red Bluff Dykes		North Red Bluff dykes			
Dyke reference		H	H	H	H
Sample running number		CH06-RB02H	CH06-RB02H	CH06-RB02H	CH06-RB02H
Phase/pulse number		1	2	3	4
	Total bioclast %	80	75	80	10
	Bryozoans	VC	A	VC	M
C	Bivalves	M	S	S	R
a	Echinoderms	C	S	C	
l	Benthic foraminifera	C		C	M
c	Planktic foraminifera	S		S	R
i	Gastropods				
c	Calcareous algae				
l	Barnacles				
a	Spicules & spines				
s	**Other**				
t	Brachiopods				
s	Serpulids				
	Modal size 1 (mm)	0.50	1.38	0.18	1.38
	Modal size 2 (mm)			2.25	
	Shape/abrasion	A	A	A	A
	Sorting	PM	M	P	PM
	Lithoclast %	0	0	2	5
	Intraclast %	0	0	0	5
	Siliciclastic grain %	5	5	10	1
	Quartz				
S	Feldspar				
i	VRFs	M	M	M	R
l	SRFs				
i	Micas				
c	Pyrite grains			S	
i	Pyrite infills	S	S	S	S
c	Glauconite pellets	R			
l	Glauconite infills				
a	**Other**				
s	Phosphate				
t	Chert				
s	Hornblende				
	Limonite staining				
	Modal size 1 (mm)	0.23	0.75	0.13	0.25
	Modal size 2 (mm)			1.50	
	Shape/abrasion	SR	SR	SA-SR	SR
	Sorting	M	M	P	PM
	Interparticle material %	20	20	10	90
	Spar cement %	15	5	5	5
	Micrite %	5	15	5	75
Unoccluded pore space %		1	1	1	1

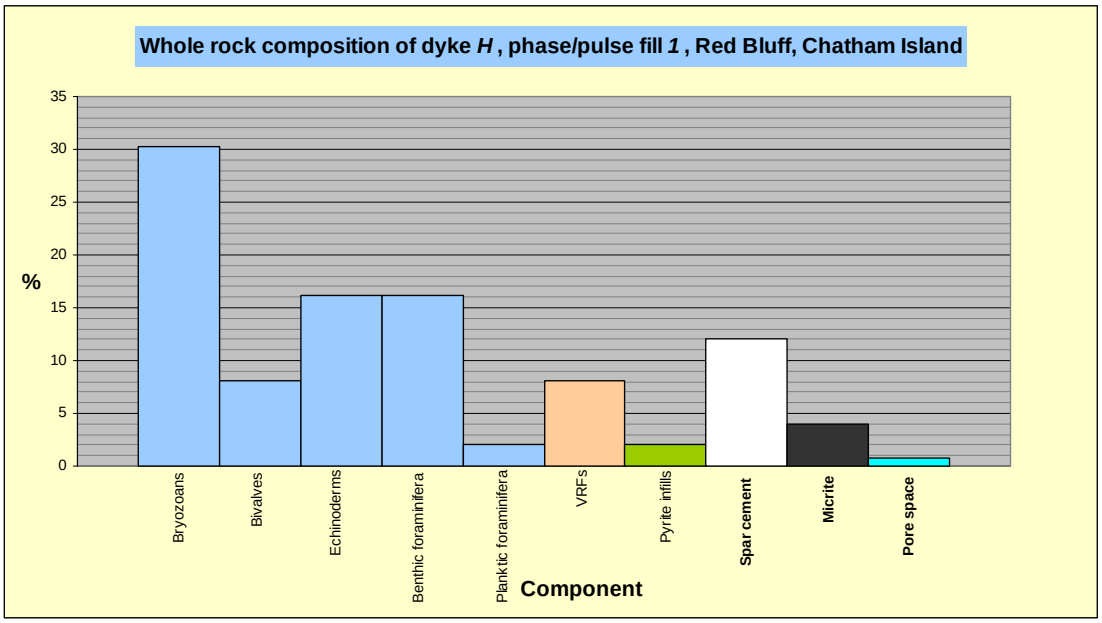

Figure C5: Component percentage of dyke *H*, fill phase *1*, *north Red Bluff* locality, Chatham Islands.

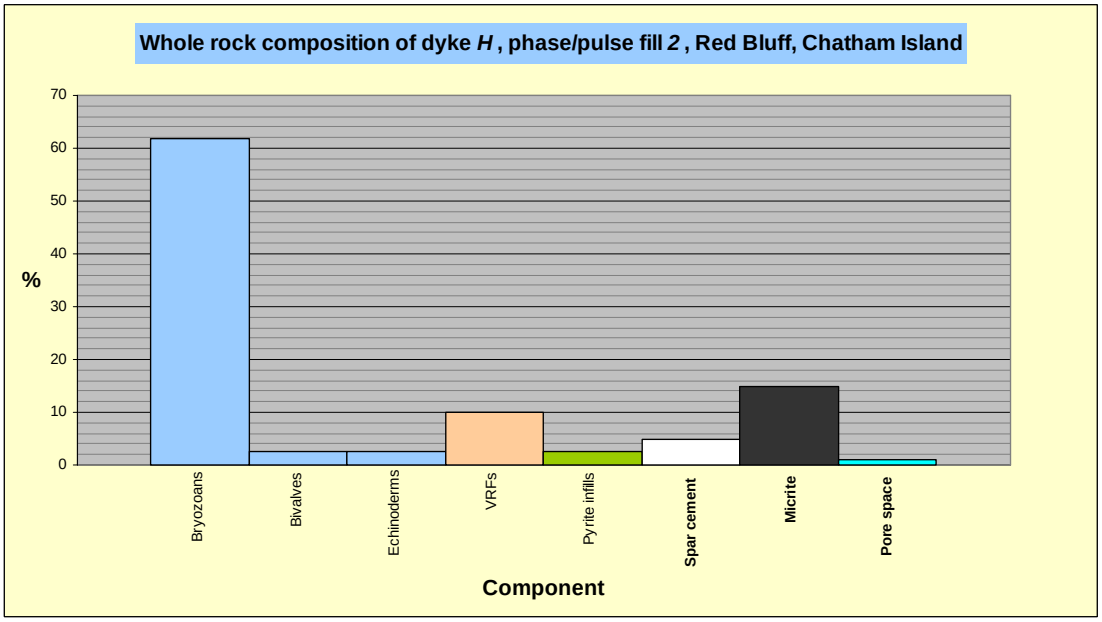

Figure C6: Component percentage of dyke *H*, fill phase *2*, *north Red Bluff* locality, Chatham Islands.

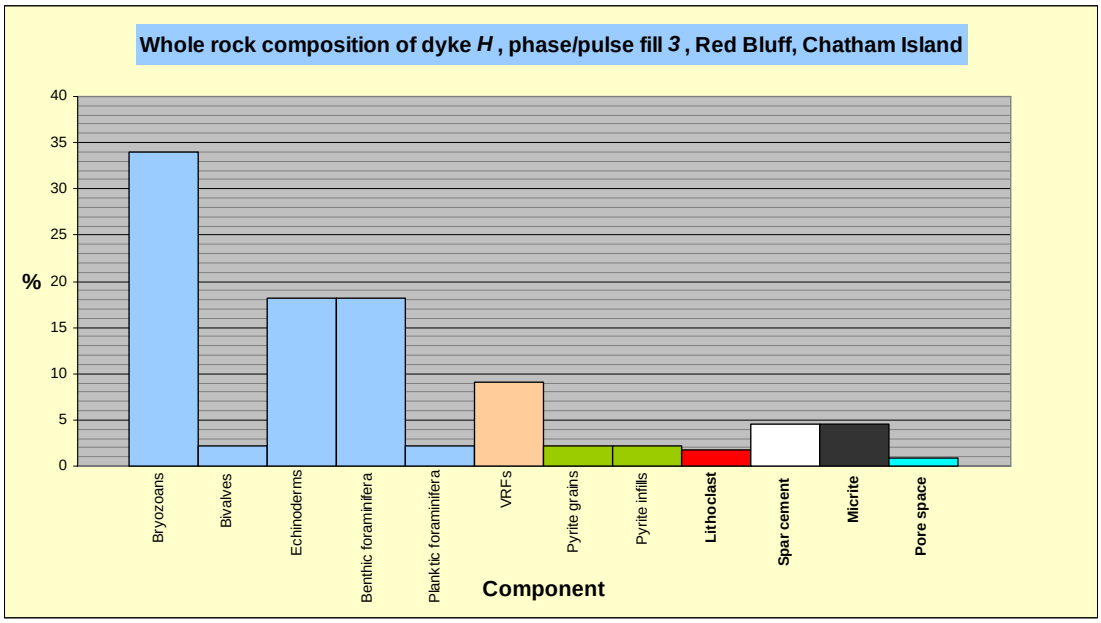

Figure C7: Component percentage of dyke *H*, fill phase *3*, *north Red Bluff* locality, Chatham Islands.

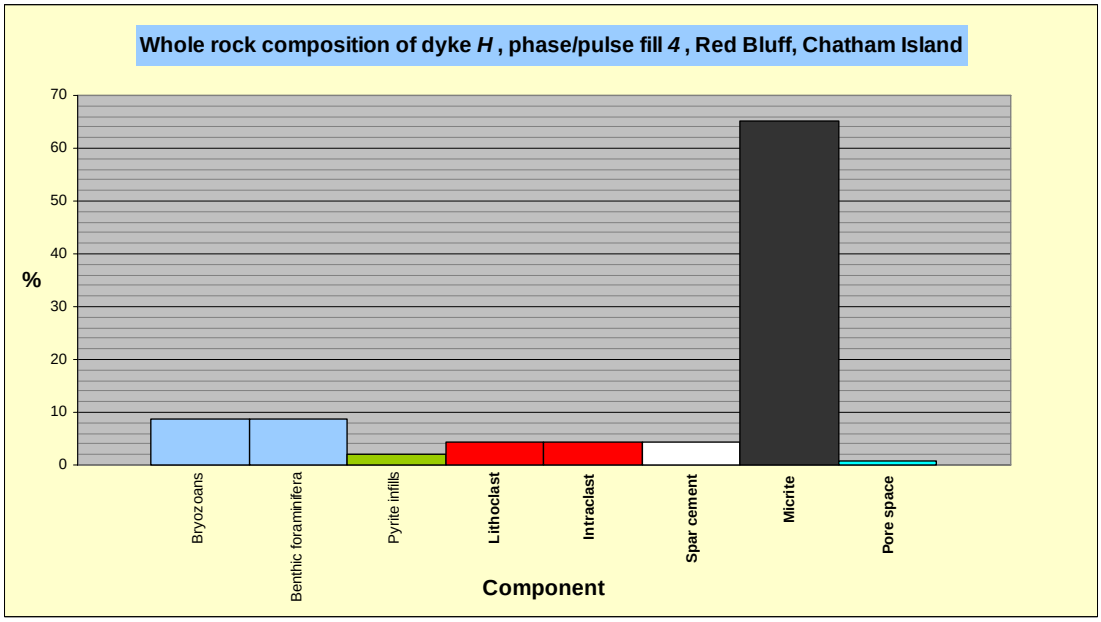

Figure C8: Component percentage of dyke *H*, fill phase *4*, *north Red Bluff* locality, Chatham Islands.

Table C3: Component data for dyke occurrences *I* at the *north Red Bluff* locality, Chatham Island.

Red Bluff Dykes		North Red Bluff dykes					
Dyke reference		I	I	I	I	I	I
Sample running number		CH06-RB02I	CH06-RB02I	CH06-RB02I	CH06-RB02I	CH06-RB02I	CH06-RB02I
Phase/pulse number		5	6 micrite	7	Micrite fill	8	9
	Total bioclast %	35	0	55	0	65	70
	Bryozoans	C		C		A	A
C	Bivalves	S		R		C	R
a	Echinoderms	R		R		R	R
l	Benthic foraminifera			R		VC	VC
c	Planktic foraminifera					R	R
i	Gastropods						
c	Calcareous algae						
l	Barnacles						
a	Spicules & spines						
s	**Other**						
t	Brachiopods						
s	Serpulids						
	Modal size 1 (mm)	0.88		0.70		1.63	0.75
	Modal size 2 (mm)						2
	Shape/abrasion	A		A		A	A
	Sorting	PM		PM		PM	P
	Lithoclast %	0	0	0	0	0	10
	Intraclast %	0	0	0	0	0	0
	Siliciclastic grain %	40	0.5	10	0.5	15	7
	Quartz						
S	Feldspar						
i	VRFs	A		C		M	M
l	SRFs						
i	Micas						
c	Pyrite grains						
i	Pyrite infills	S	R	S	R	S	S
c	Glauconite pellets						
l	Glauconite infills						
a	**Other**						
s	Phosphate						
t	Chert						
s	Hornblende						R
	Limonite staining						
	Modal size 1 (mm)	0.88	0.88	0.58	0.88	0.13	0.20
	Modal size 2 (mm)					2.13	1.38
	Shape/abrasion	SA-SR	SR	SA-SR	SR	SR	SA-SR
	Sorting	PM	PM	PM	PM	P	P
	Interparticle material %	25	99	35	99	20	20
	Spar cement %	23	5	20	5	5	5
	Micrite %	2	94	15	94	15	15
Unoccluded pore space %		1	0	2	0	1	1

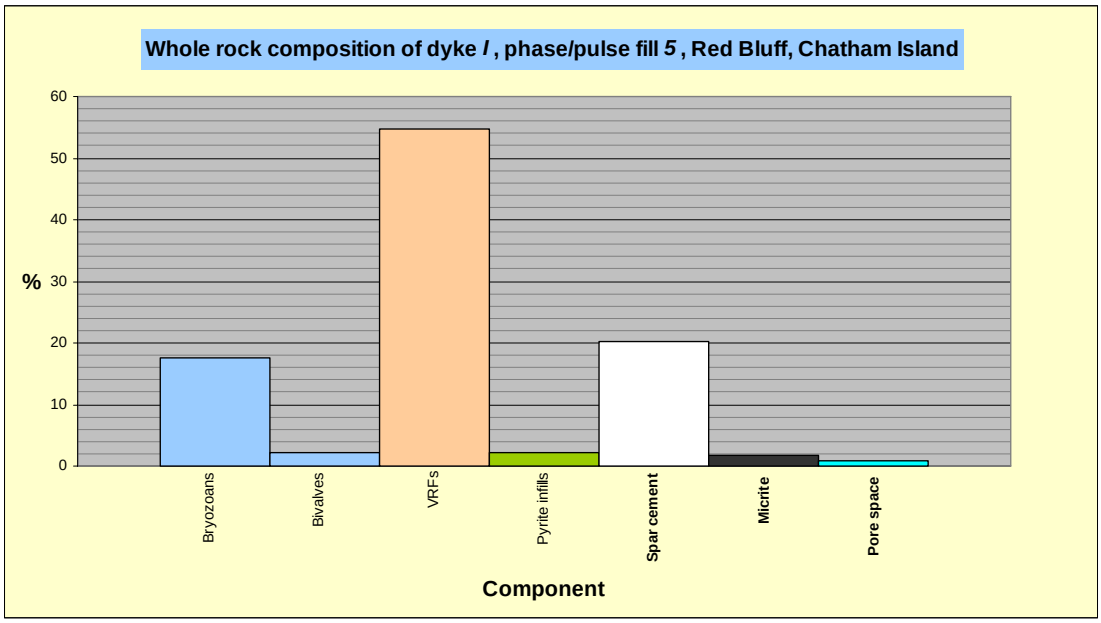

Figure C9: Component percentage of dyke *I*, fill phase *5*, *north Red Bluff* locality, Chatham Islands.

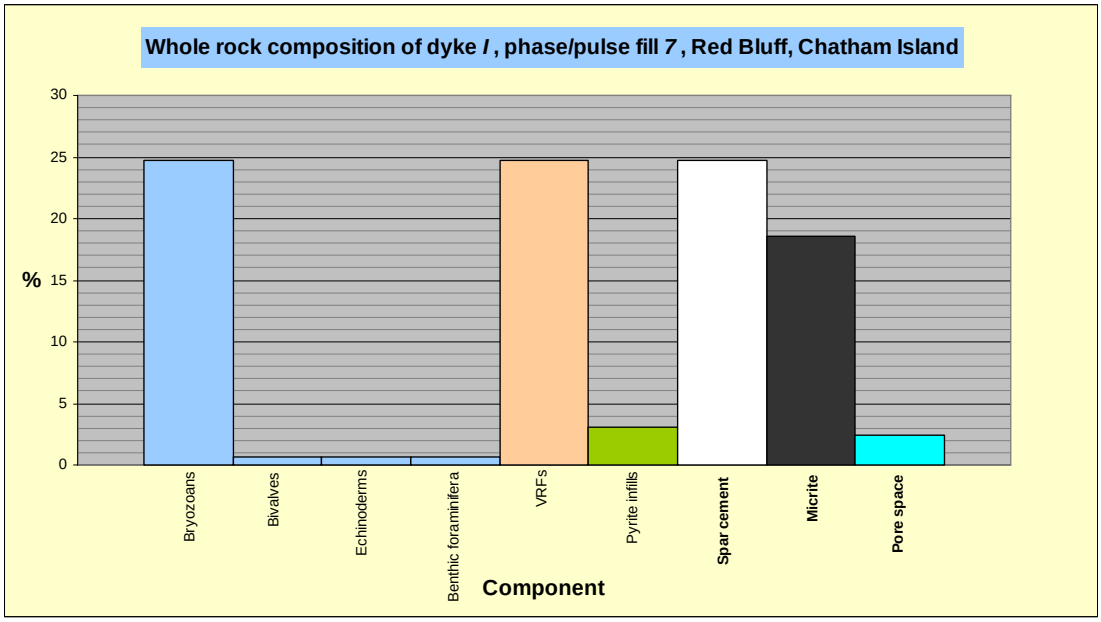

Figure C10: Component percentage of dyke *I*, fill phase *7*, *north Red Bluff* locality, Chatham Islands.

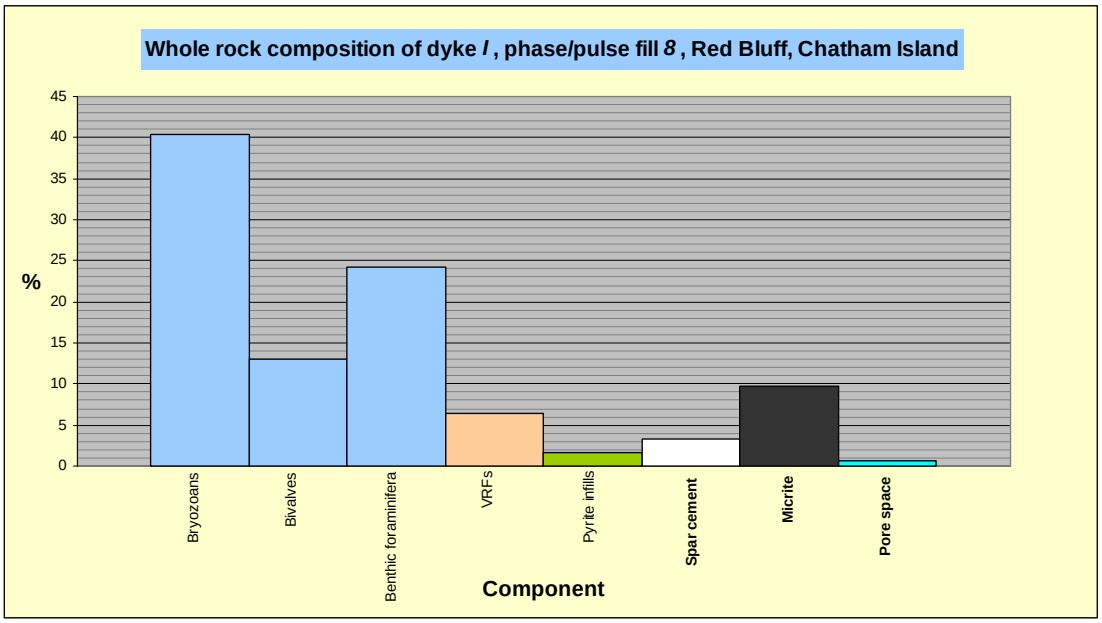

Figure C11: Component percentage of dyke *I*, fill phase *8*, *north Red Bluff* locality, Chatham Islands.

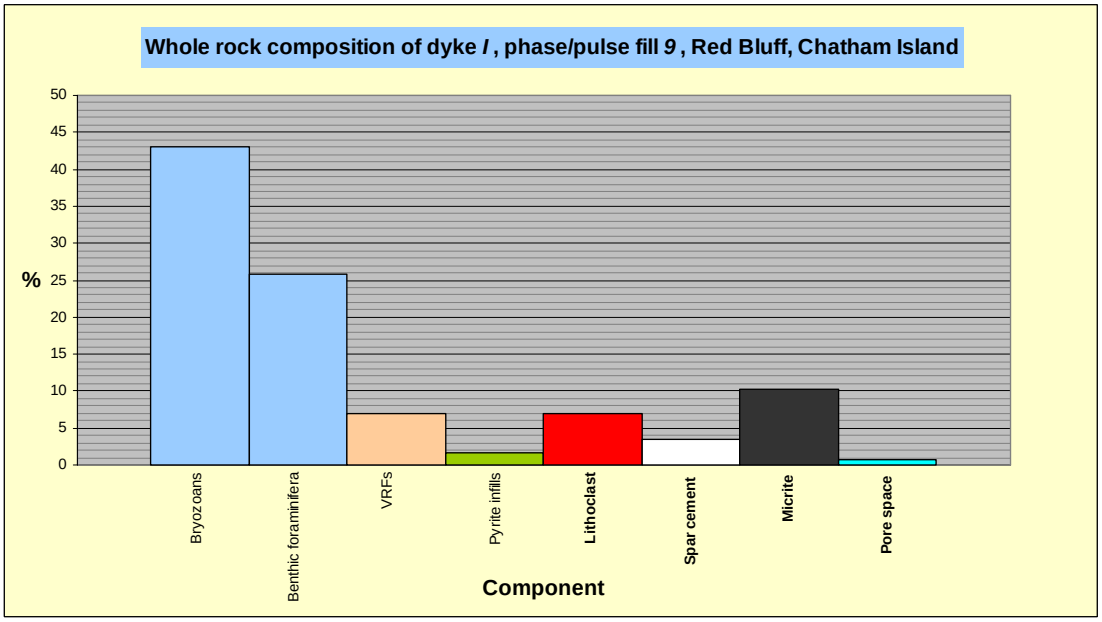

Figure C12: Component percentage of dyke *I*, fill phase *9*, *north Red Bluff* locality, Chatham Islands.

Table C4: Component data for dyke occurrences *N* and *P* at the *north Red Bluff* locality, Chatham Island.

Red Bluff Dykes		North Red Bluff dykes	
Dyke reference		N	P
Sample running number		CH05-28L	CH05-28K
Phase/pulse number		–	–
	Total bioclast %	5	60
	Bryozoans		A
C	Bivalves		
a	Echinoderms		R
l	Benthic foraminifera		
c	Planktic foraminifera	S	
i	Gastropods		R
c	Calcareous algae		
l	Barnacles		
a	Spicules & spines		
s	**Other**		
t	Brachiopods		
s	Serpulids		R
	Modal size 1 (mm)	0.02	0.37
	Modal size 2 (mm)		3.25
	Shape/abrasion	A	A
	Sorting	MW	P
	Lithoclast %	10	0.5
	Intraclast %	0	0
	Siliciclastic grain %	1	1
	Quartz		
S	Feldspar		
i	VRFs		
l	SRFs		
i	Micas		
c	Pyrite grains	R	R
i	Pyrite infills	R	
c	Glauconite pellets		
l	Glauconite infills		
a	**Other**		
s	Phosphate		
t	Chert		
s	Hornblende		
	Limonite staining	R	R
	Modal size 1 (mm)	0.02	0.05
	Modal size 2 (mm)		
	Shape/abrasion	SR	SR
	Sorting	MW	PM
	Interparticle material %	95	40
	Spar cement %	2	10
	Micrite %	95	30
Unoccluded pore space %		0	1

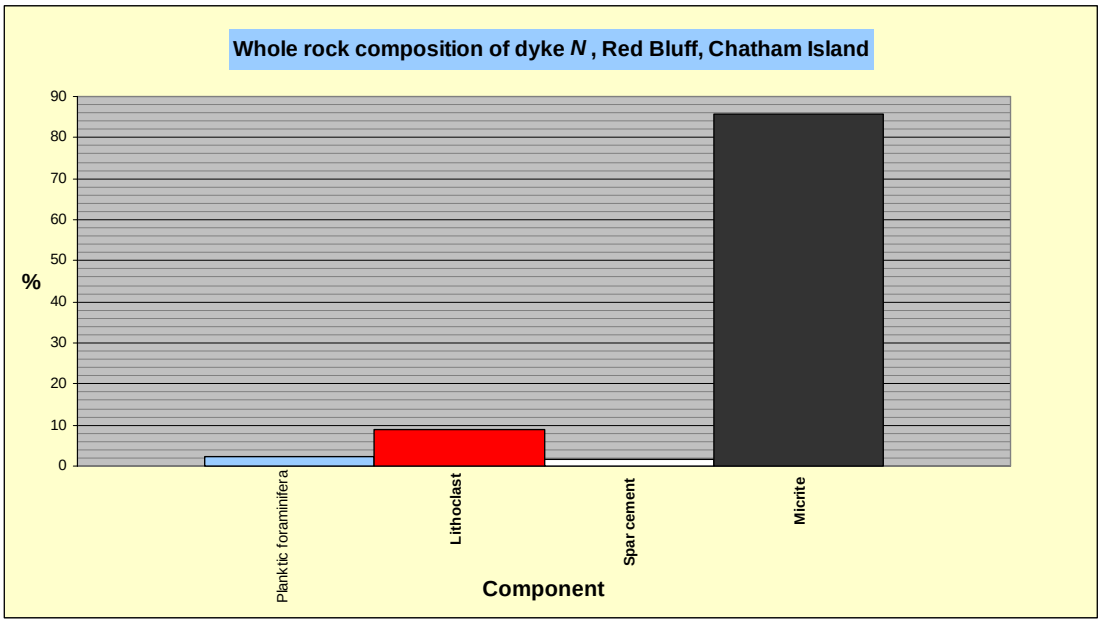

Figure C13: Component percentage of dyke *N*, *north Red Bluff* locality, Chatham Islands.

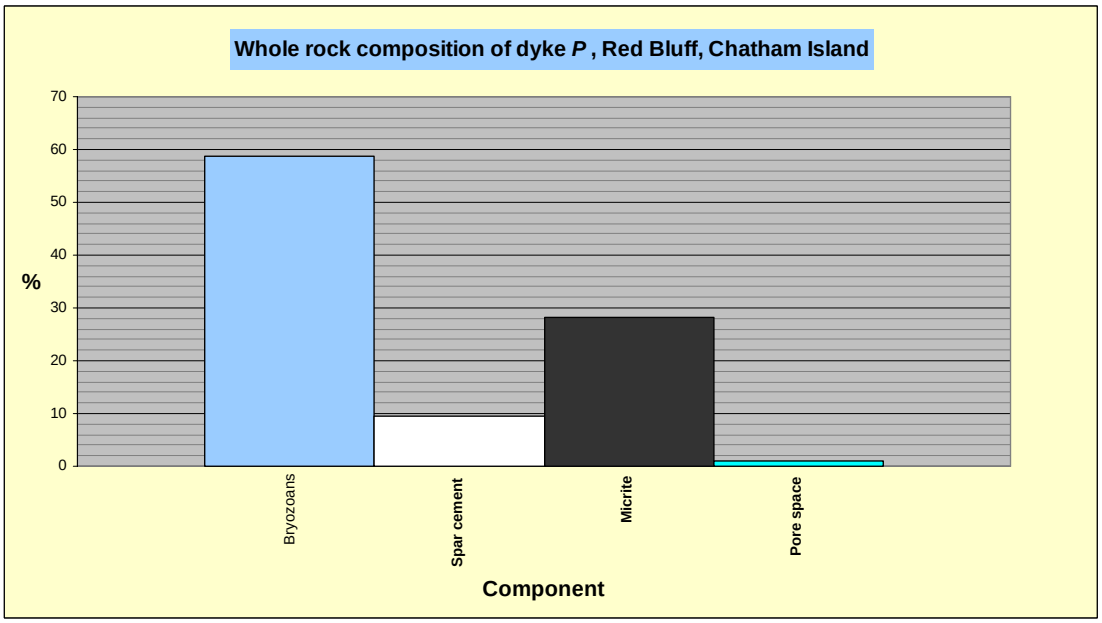

Figure C14: Component percentage of dyke *P*, *north Red Bluff* locality, Chatham Islands.

Table C5: Component data for dyke occurrences *M* ('main dyke') at the *north Red Bluff* locality, Chatham Island (continue over page).

Red Bluff Dykes		North Red Bluff dykes					
Dyke reference		M	M	M	M	M	M
Sample running number		CH06-RB02M	CH06-RB02M	CH05-28J	CH05-28C	CH05-28E	CH05-28B
Phase/pulse number		1	2	–	–	–	–
	Total bioclast %	80	60	65	80	75	75
	Bryozoans	S	A	VA	A	A	A
C	Bivalves	C	S	S	S		S
a	Echinoderms	C	R	S	S	S	M
l	Benthic foraminifera	M		S	S	M	M
c	Planktic foraminifera	A		R	S	R	M
i	Gastropods						S
c	Calcareous algae						
l	Barnacles				R		
a	Spicules & spines				R		
s	**Other**						
t	Brachiopods						
s	Serpulids						
	Modal size 1 (mm)	0.13	0.50	0.50	0.07	0.50	0.15
	Modal size 2 (mm)	1.375	3.25	2	3	3.75	2
	Shape/abrasion	MA	A	A	A	A	A
	Sorting	PM	P	P	P	P	P
	Lithoclast %	0	0	0	0	0	0
	Intraclast %	0	0	0	0	0	0
	Siliciclastic grain %	10	1	2	2	5	2
	Quartz	M					
S	Feldspar						
i	VRFs	S		R		M	
l	SRFs						
i	Micas						
c	Pyrite grains	R					R
i	Pyrite infills	S	R	R		R	S
c	Glauconite pellets	C	R	R	R	R	S
l	Glauconite infills			R	R	R	M
a	**Other**						
s	Phosphate			R	R	R	S
t	Chert						
s	Hornblende						
	Limonite staining			S	R		S
	Modal size 1 (mm)	0.15	0.03	0.07	0.15	0.13	0.10
	Modal size 2 (mm)						
	Shape/abrasion	SR	SR	SR	SA-SR	SR	SR
	Sorting	M	MW	PM	PM	PM	PM
	Interparticle material %	10	40	30	15	20	25
	Spar cement %	6	7	10	5	10	8
	Micrite %	4	33	20	10	10	17
Unoccluded pore space %		1	1	1	5	2	2

Red Bluff Dykes		North Red Bluff dykes					
Dyke reference		M	M	M	M	M	M
Sample running number		CH05-28A	CH05-28A	CH05-28D	CH05-28M	CH05-28M	CH05-28M
Phase/pulse number		1	2	–	1 float	2 float	3 float
	Total bioclast %	50	60	80	65	10	80
	Bryozoans	C	VC	VA	A	S	A
C	Bivalves	M	S	S	S		S
a	Echinoderms	S		M	S		S
l	Benthic foraminifera	R	S	S			S
c	Planktic foraminifera	S		S		R	S
i	Gastropods		S				
c	Calcareous algae						
l	Barnacles						
a	Spicules & spines						
s	**Other**						
t	Brachiopods		S	R			
s	Serpulids			R	S		R
	Modal size 1 (mm)	0.15	0.60	0.30	0.25	0.12	0.25
	Modal size 2 (mm)	2		2	3	1	2
	Shape/abrasion	A	A	A	A	A	A
	Sorting	P	PM	P	P	P	P
	Lithoclast %	0	0	0	2.5	10	0.5
	Intraclast %	0	0	0	0	0	0
	Siliciclastic grain %	1	1	2	1	2	2
	Quartz						
S	Feldspar						
i	VRFs						
l	SRFs						
i	Micas						
c	Pyrite grains	R			R		R
i	Pyrite infills	R		R	R	S	R
c	Glauconite pellets	R		R	R		R
l	Glauconite infills	R	R		R		R
a	**Other**						
s	Phosphate		R	R	R		R
t	Chert						
s	Hornblende						
	Limonite staining	S	R		R	S	S
	Modal size 1 (mm)	0.10	0.05	0.07	0.05	0.02	0.05
	Modal size 2 (mm)						
	Shape/abrasion	SR	SR	SR	SR	R	SR
	Sorting	M	M	PM	PM	M	M
	Interparticle material %	50	40	20	35	90	20
	Spar cement %	15	30	7	15	5	8
	Micrite %	35	10	13	20	85	12
Unoccluded pore space %		2	1	2	1	1	1

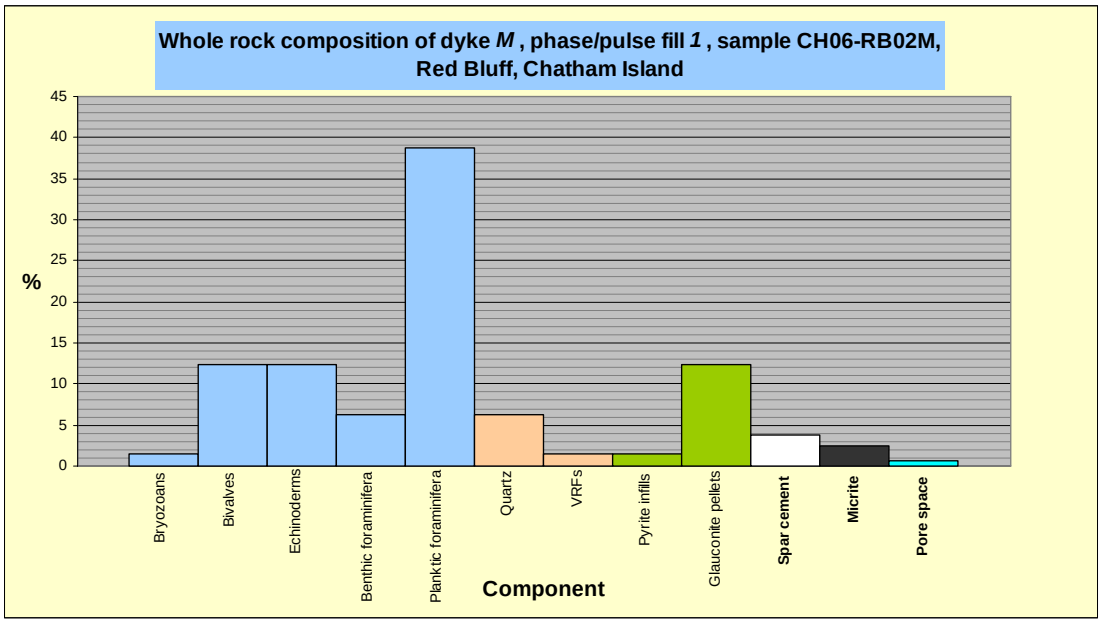

Figure C15: Component percentage of dyke *M*, fill phase *1*, *north Red Bluff* locality, Chatham Islands.

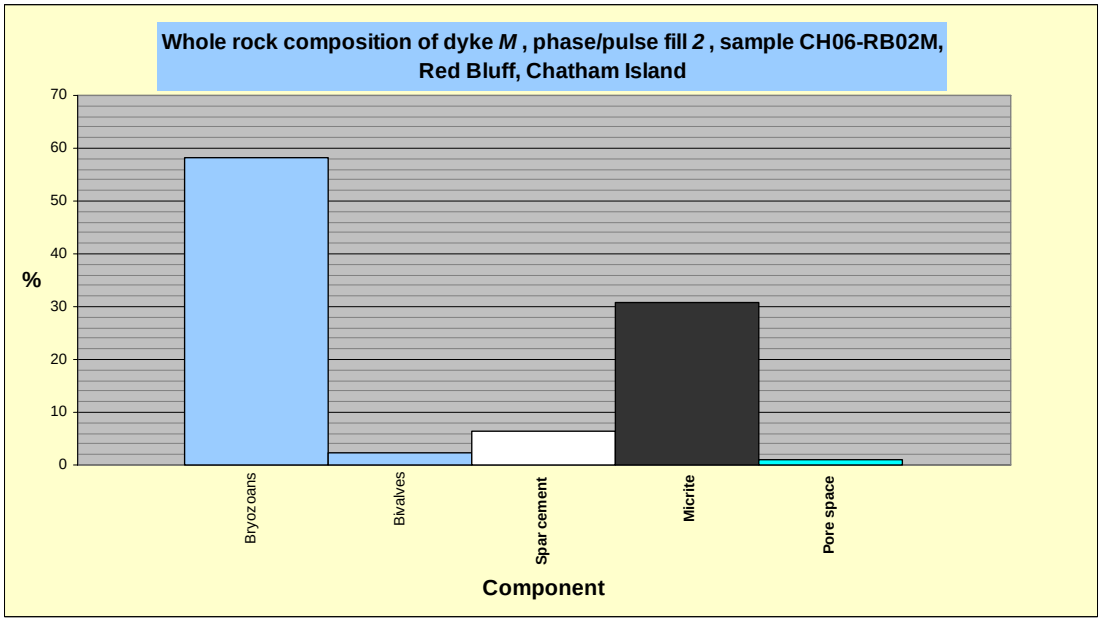

Figure C16: Component percentage of dyke *M*, fill phase *2*, *north Red Bluff* locality, Chatham Islands.

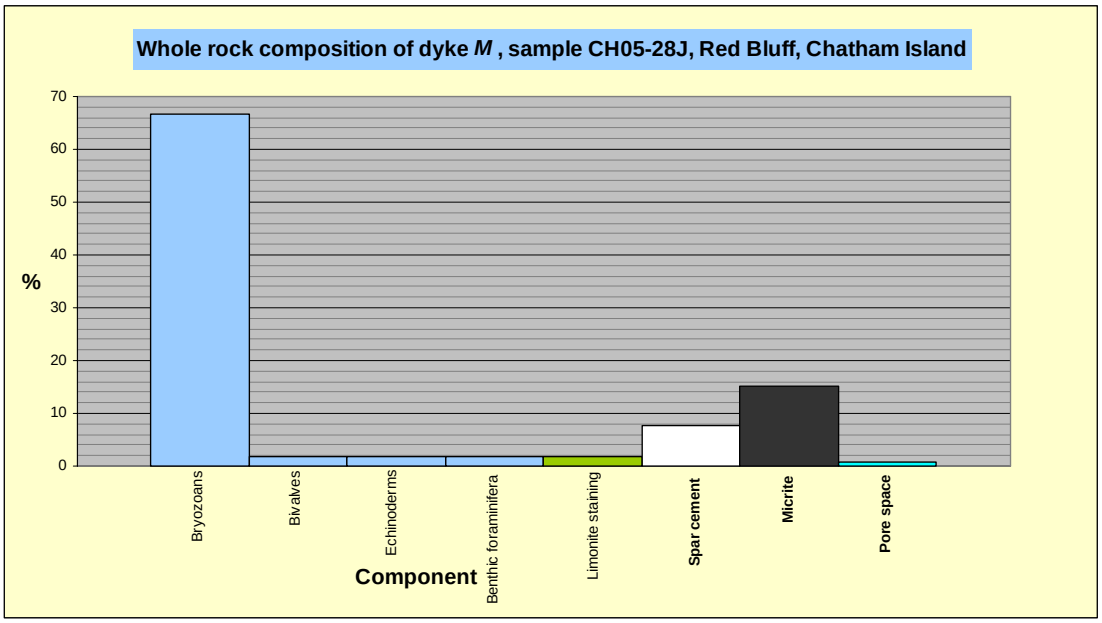

Figure C17: Component percentage of dyke *M*, sample CH05-28J, *north Red Bluff* locality, Chatham Islands.

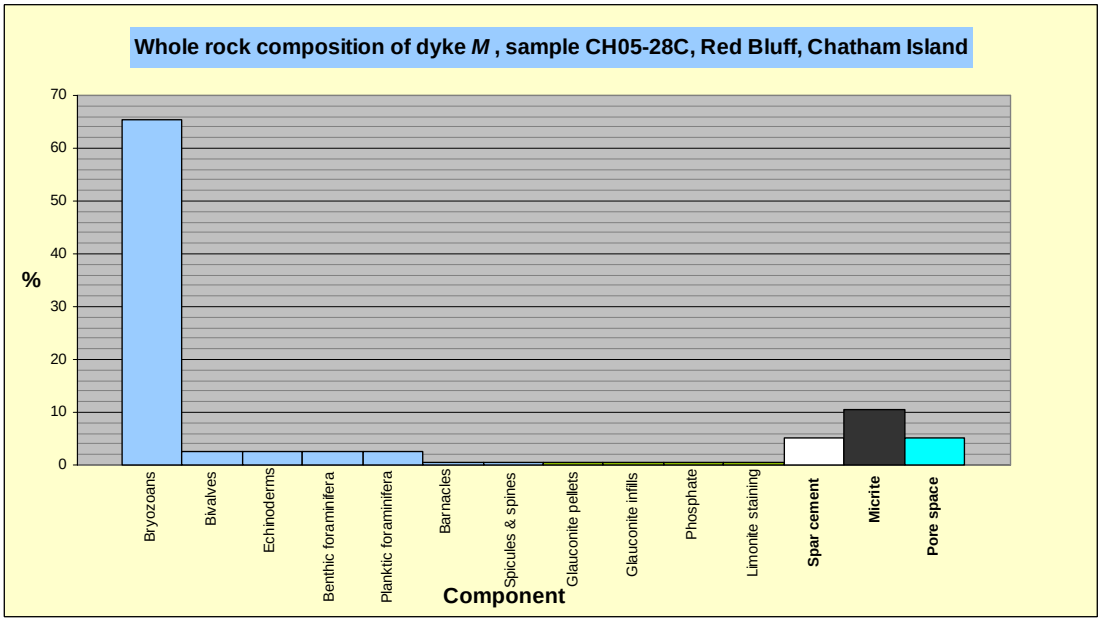

Figure C18: Component percentage of dyke *M*, sample CH05-28C, *north Red Bluff* locality, Chatham Islands.

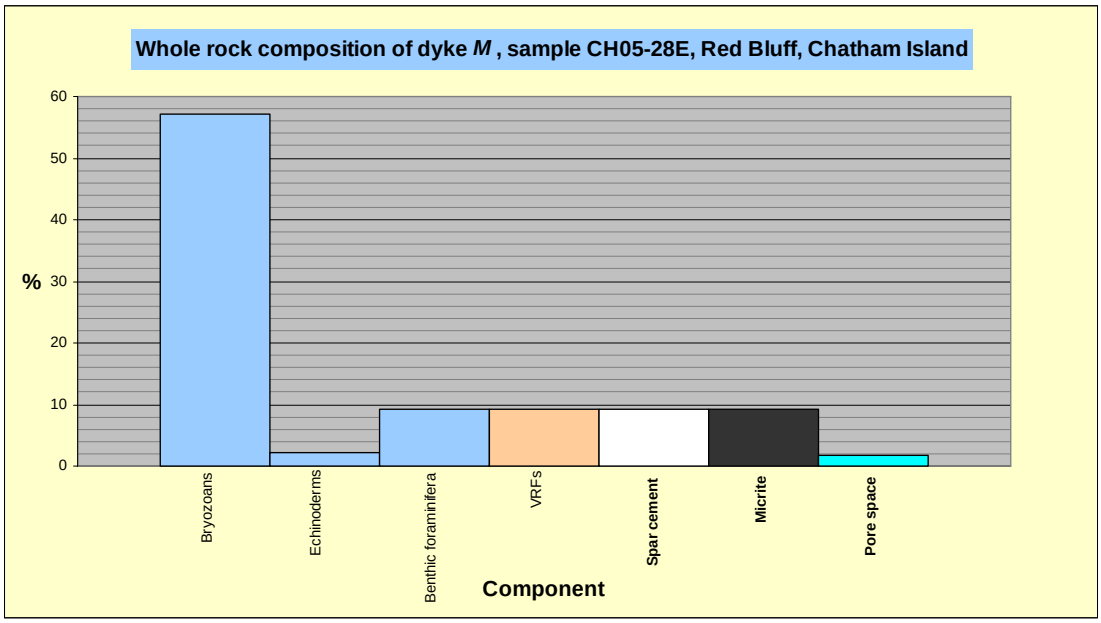

Figure C19: Component percentage of dyke *M*, sample CH05-28E, *north Red Bluff* locality, Chatham Islands.

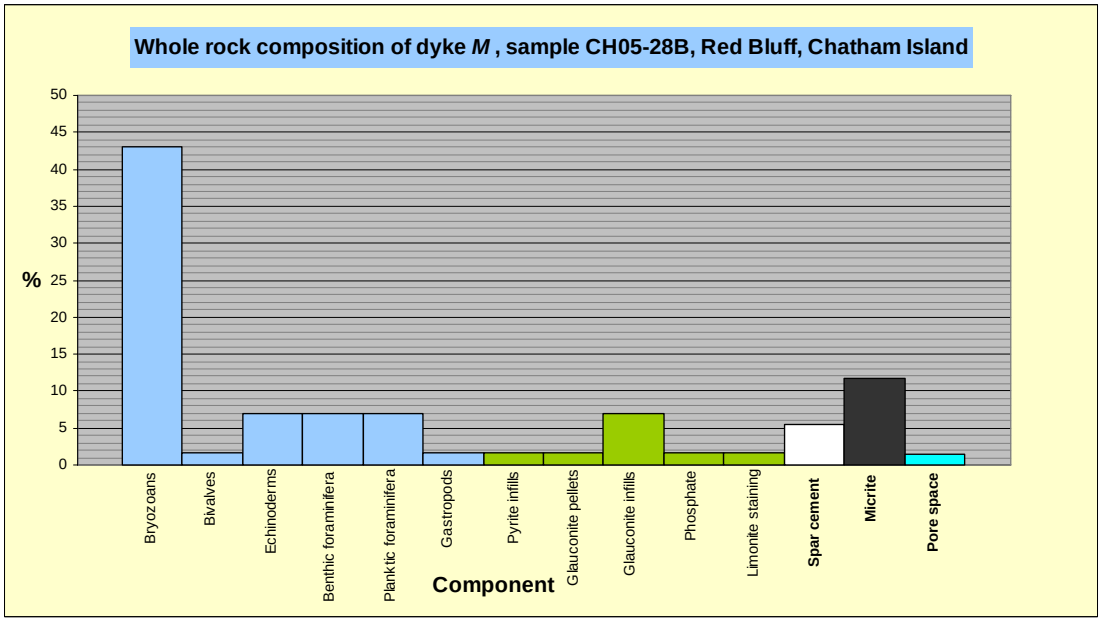

Figure C20: Component percentage of dyke *M*, sample CH05-28B, *north Red Bluff* locality, Chatham Islands.

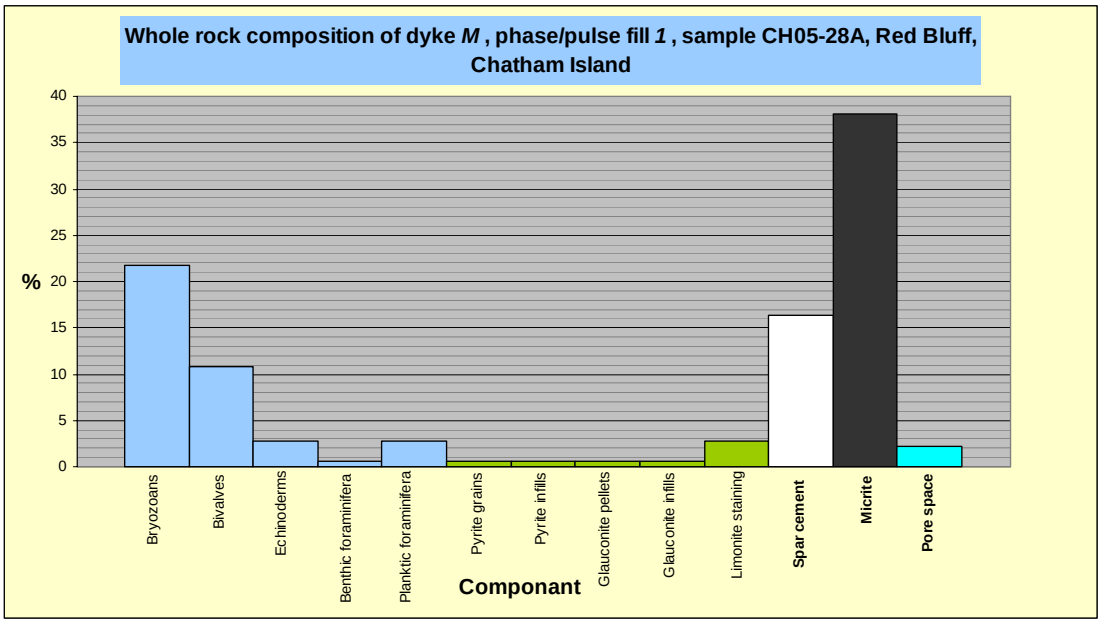

Figure C21: Component percentages of dyke *M*, phase fill *1*, *north Red Bluff* locality, Chatham Islands.

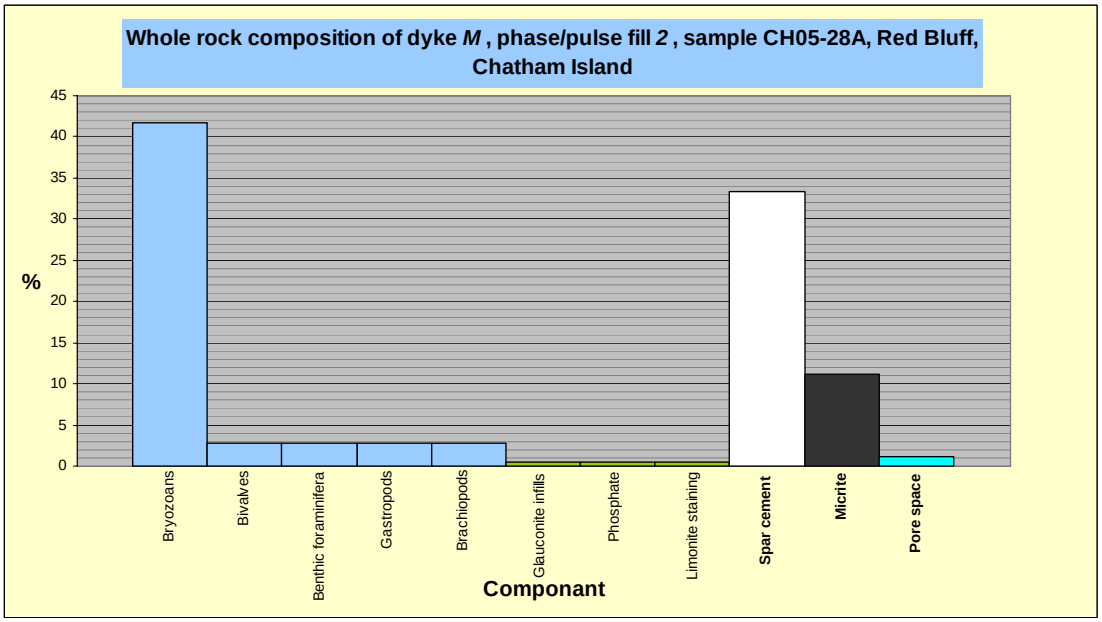

Figure C22: Component percentages of dyke *M*, phase fill *2*, *north Red Bluff* locality, Chatham Islands.

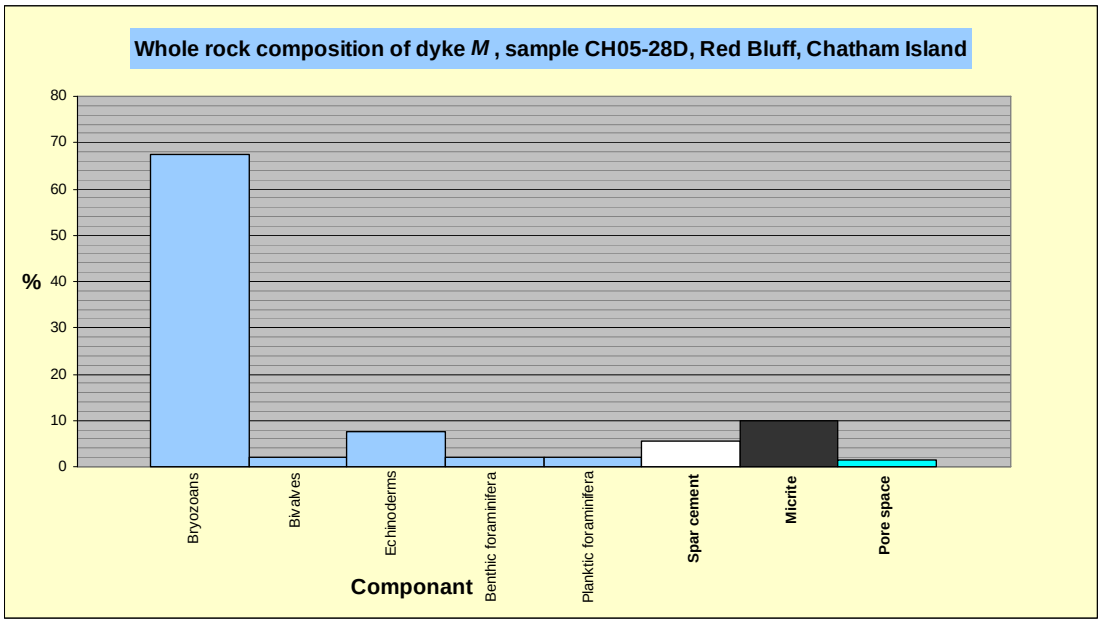

Figure C23: Component percentage of dyke *M*, sample CH05-28D, *north Red Bluff* locality, Chatham Islands.

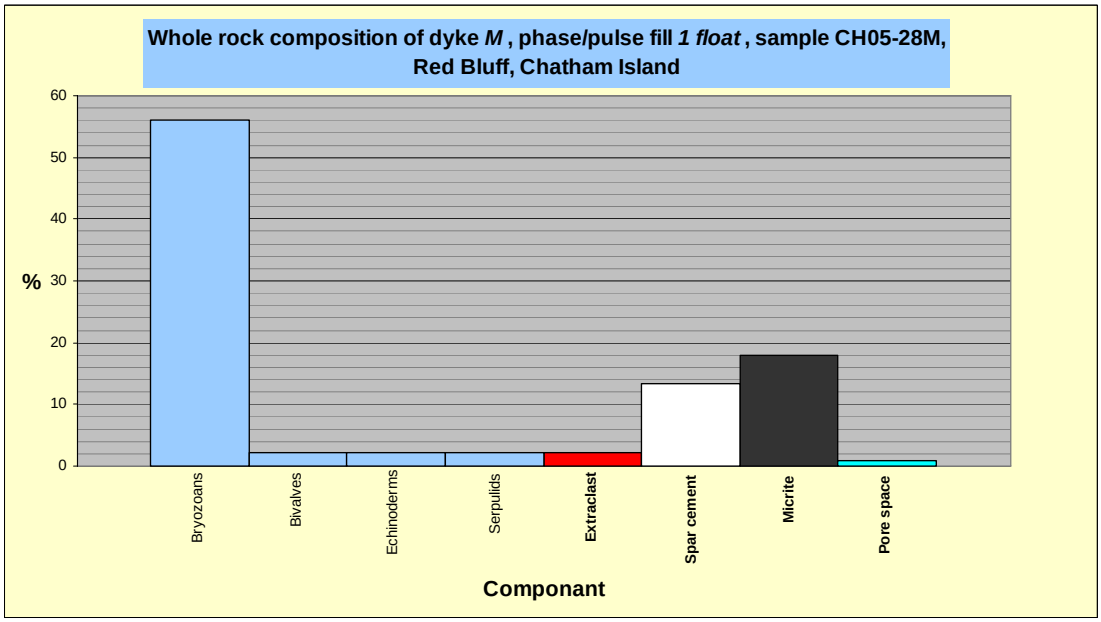

Figure C24: Component percentages of dyke *M*, phase fill *1 float*, *north Red Bluff* locality, Chatham Islands.

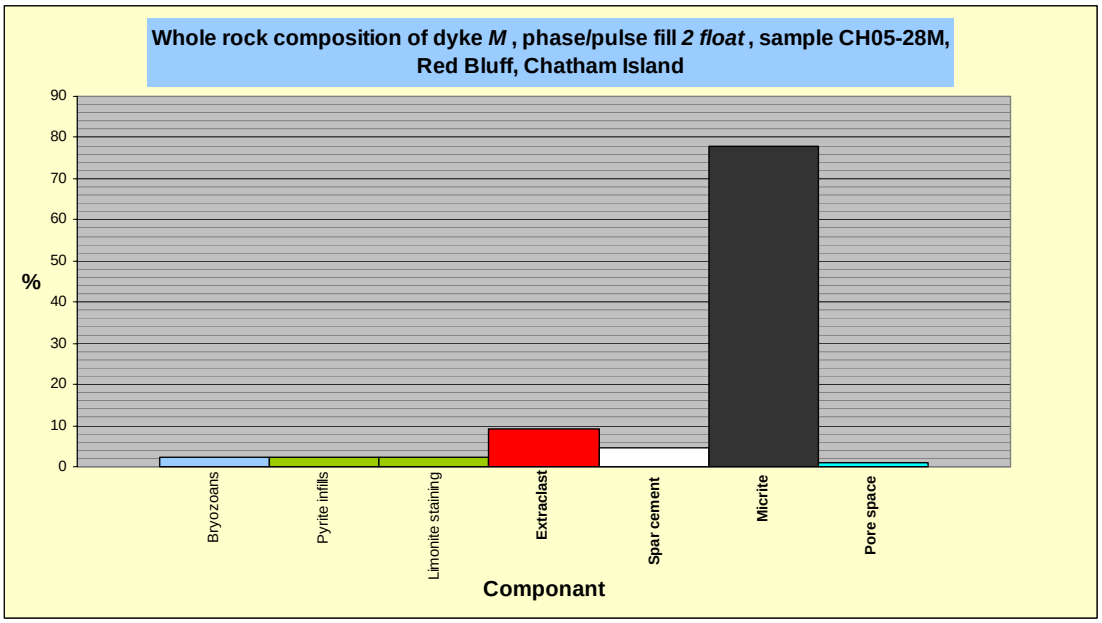

Figure C25: Component percentages of dyke *M*, phase fill *2 float*, *north Red Bluff* locality, Chatham Islands.

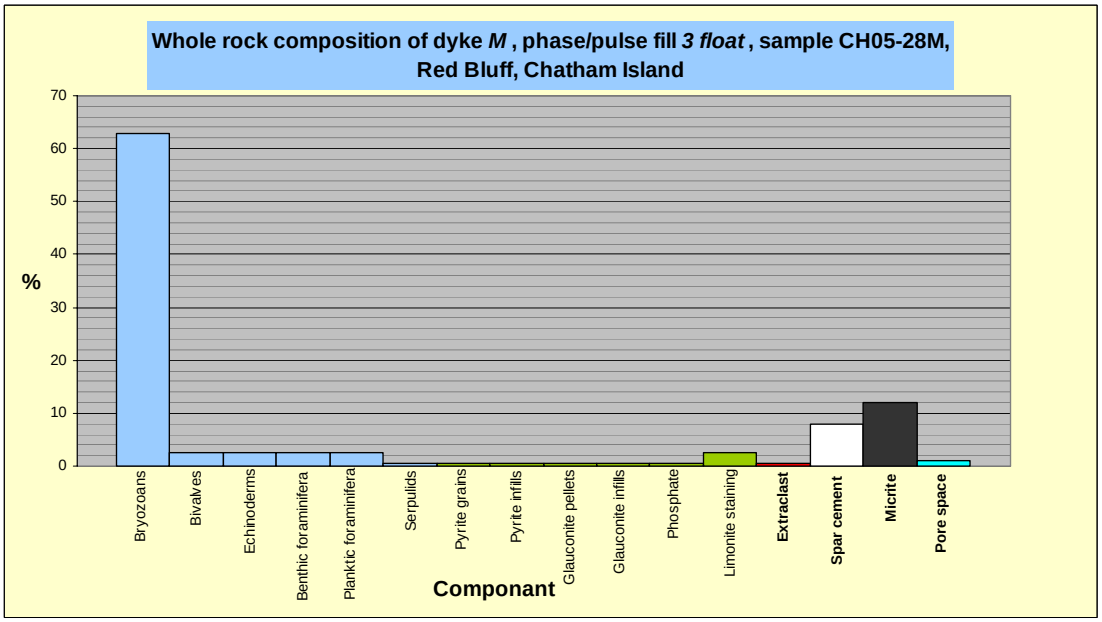

Figure C26: Component percentages of dyke *M*, phase fill *3 float*, *north Red Bluff* locality, Chatham Islands.

Table C6: Component data for dyke occurrences *R* (complex) at the *north Red Bluff* locality, Chatham Island.

Red Bluff Dykes		North Red Bluff dykes	
Dyke reference		R	R
Sample running number		CH05-28G	CH05-28H
Phase/pulse number		Centre	Edge
	Total bioclast %	65	0
	Bryozoans	A	
C	Bivalves	M	
a	Echinoderms	M	
l	Benthic foraminifera		
c	Planktic foraminifera		
i	Gastropods		
c	Calcareous algae		
l	Barnacles		
a	Spicules & spines		
s	**Other**		
t	Brachiopods		
s	Serpulids		
	Modal size 1 (mm)	0.70	
	Modal size 2 (mm)	2	
	Shape/abrasion	A	
	Sorting	P	
	Lithoclast %	0	0
	Intraclast %	0	0
	Siliciclastic grain %	2	0
	Quartz		
S	Feldspar		
i	VRFs		
l	SRFs		
i	Micas		
c	Pyrite grains		
i	Pyrite infills	R	
c	Glauconite pellets	R	
l	Glauconite infills		
a	**Other**		
s	Phosphate	R	
t	Chert		
s	Hornblende		
	Limonite staining	R	
	Modal size 1 (mm)	0.07	
	Modal size 2 (mm)		
	Shape/abrasion	SA-SR	
	Sorting	PM	
	Interparticle material %	35	100
	Spar cement %	30	0
	Micrite %	5	100
Unoccluded pore space %		0	0

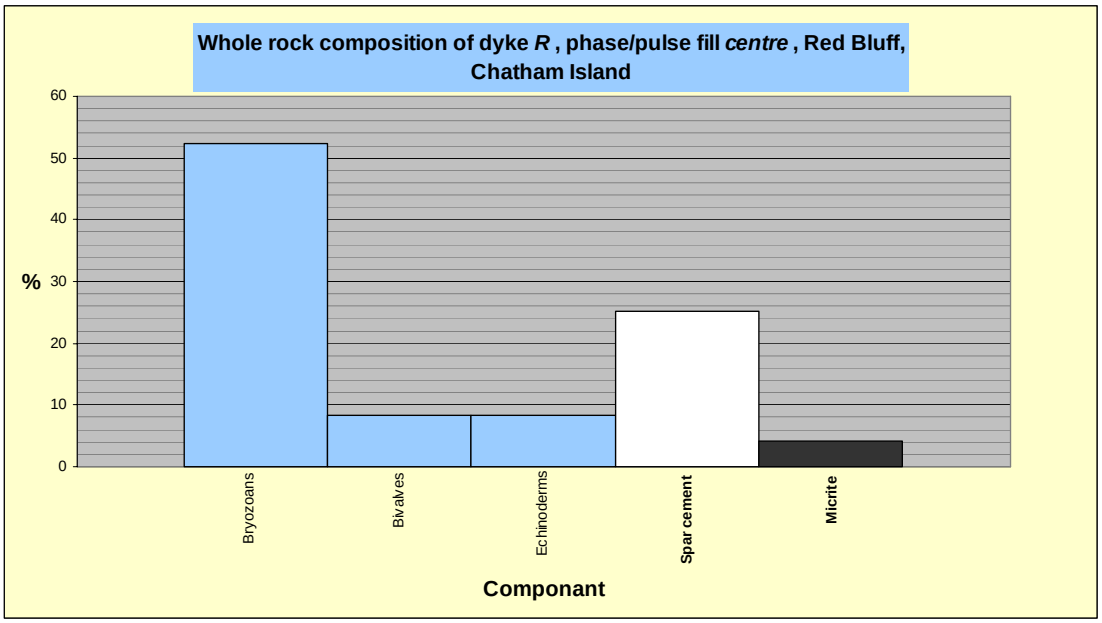

Figure C27: Component percentages of dyke *R* (complex), phase fill *centre*, *north Red Bluff* locality, Chatham Islands.

Big bluff locality

Table C7: Component data for dyke occurrences *T* and *U*, at the *big bluff* locality, Red Bluff, Chatham Island.

Red Bluff Dykes		Big bluff				
Dyke reference		T	U	U	U	U
Sample running number		CH06-RB02T	CH06-RB02U2	CH06-RB02U3	CH06-RB02U4	CH06-RB02U5
Phase/pulse number		–	–	–	–	–
	Total bioclast %	75	50	85	0	90
	Bryozoans	A	A	M		M
C	Bivalves	C	S			S
a	Echinoderms		C	S		S
l	Benthic foraminifera	M	R	M		S
c	Planktic foraminifera	S		VA		VA
i	Gastropods					
c	Calcareous algae					
l	Barnacles					
a	Spicules & spines					
s	**Other**					
t	Brachiopods					
s	Serpulids					
	Modal size 1 (mm)	0.25	0.75	0.13		0.13
	Modal size 2 (mm)	2.5	2			1
	Shape/abrasion	A	A	MA		MA
	Sorting	P	P	MW		MW
	Lithoclast %	0	37.5	0	0	0
	Intraclast %	10	0	0	0	0
	Siliciclastic grain %	1	2	1	2	1
	Quartz					
S	Feldspar					
i	VRFs	S	R	S		
l	SRFs					
i	Micas					
c	Pyrite grains	R				
i	Pyrite infills	R	S		S	
c	Glauconite pellets	R		R		R
l	Glauconite infills					
a	**Other**					
s	Phosphate		R			
t	Chert					
s	Hornblende					
	Limonite staining					
	Modal size 1 (mm)	0.38	0.08	0.05	0.05	0.03
	Modal size 2 (mm)					
	Shape/abrasion	SR	SR	SR	SR	SR
	Sorting	PM	PM	MW	P	W
	Interparticle material %	24	30	15	98	10
	Spar cement %	12	20	8	0	5
	Micrite %	12	10	8	98	5
Unoccluded pore space %		1	1	1	0	1

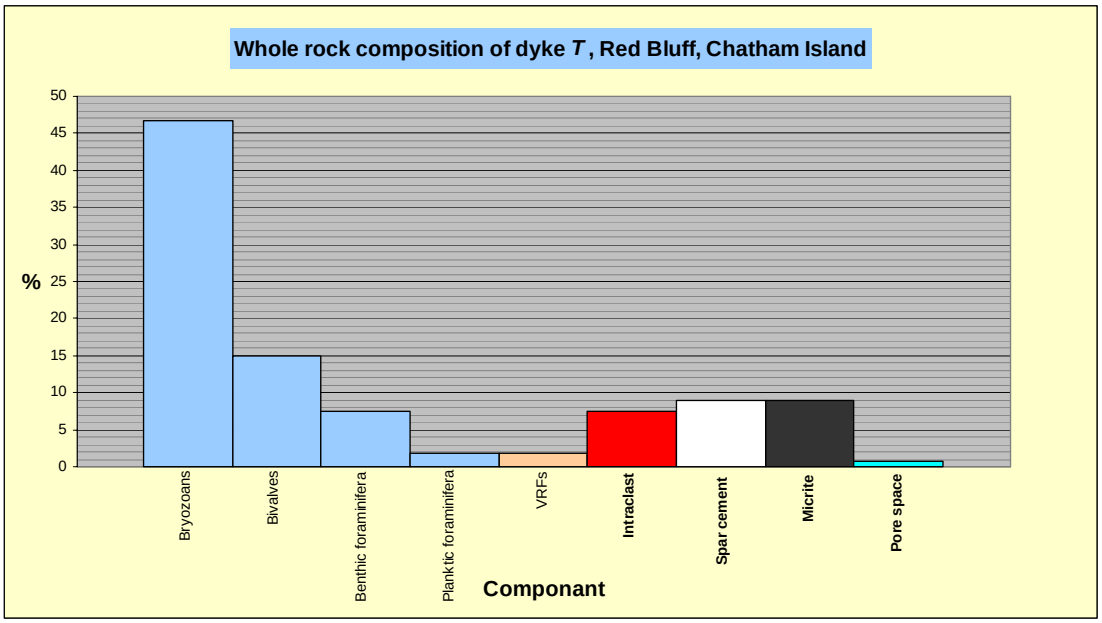

Figure C28: Component percentages of dyke *T*, *big bluff* locality, Red Bluff, Chatham Islands.

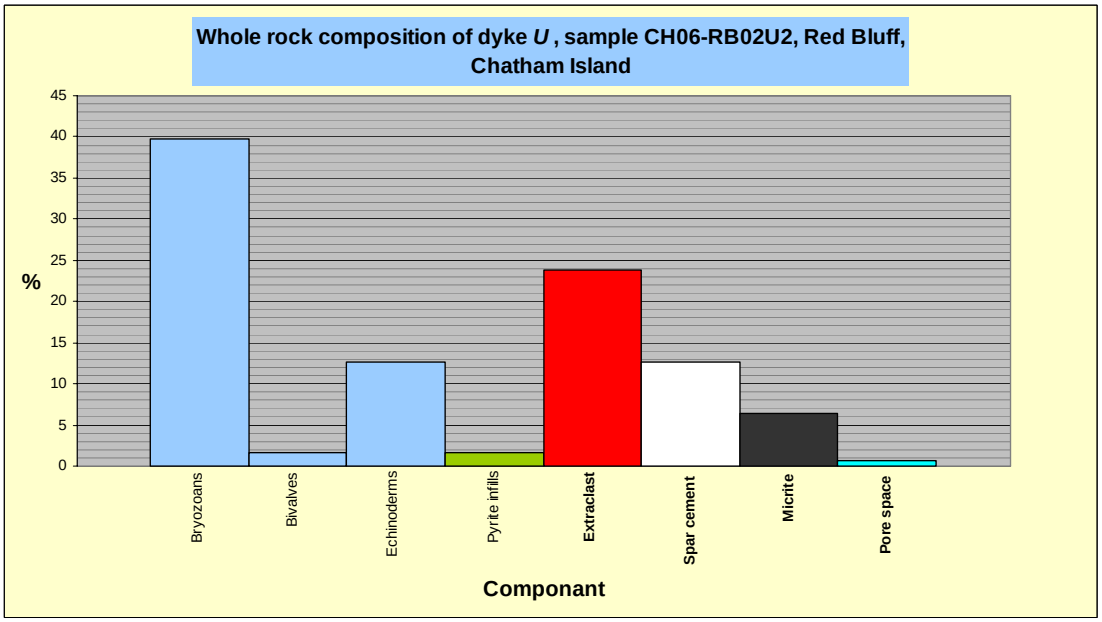

Figure C29: Component percentages of dyke *U*, sample CH06-RB02U2, *big bluff* locality, Red Bluff, Chatham Islands.

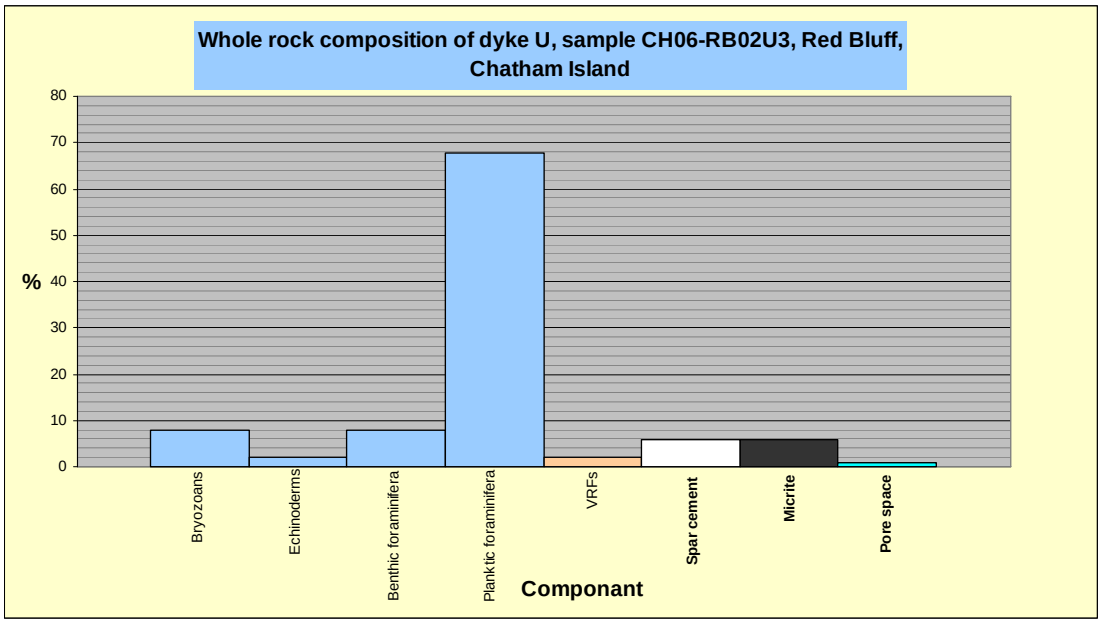

Figure C30: Component percentages of dyke *U*, sample CH06-RB02U3, *big bluff* locality, Red Bluff, Chatham Islands.

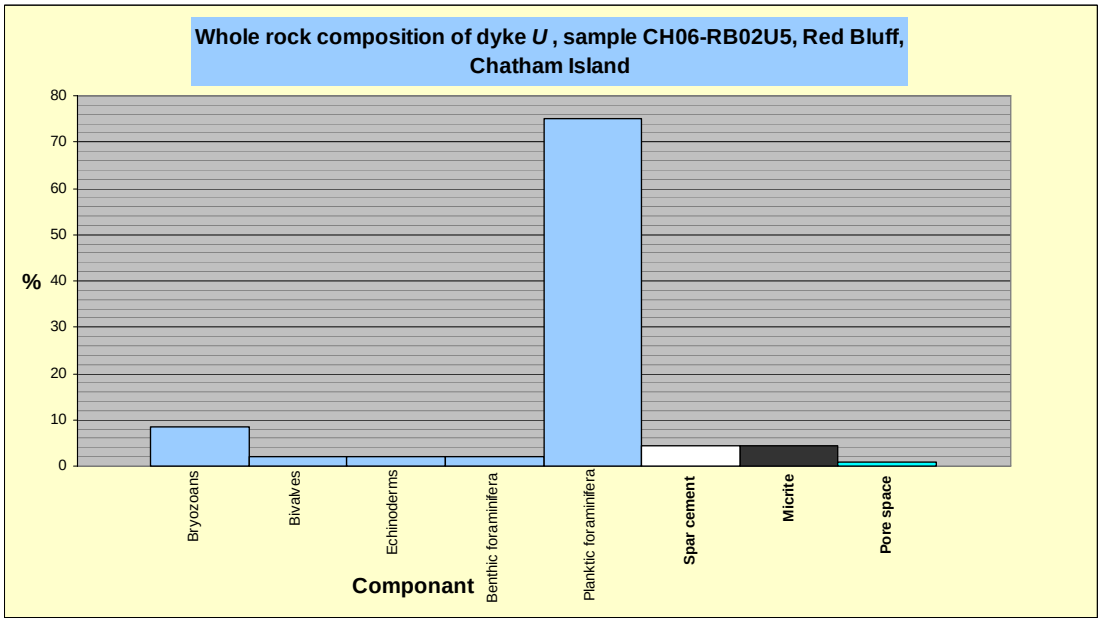

Figure C31: Component percentages of dyke *U*, sample CH06-RB02U5, *big bluff* locality, Red Bluff, Chatham Islands.

Below the twin masts locality (CH05-27)

Table C8: Component data for dyke occurrences at the *below the twin masts* locality (CH05-27), Red Bluff, Chatham Island (continued over page).

Red Bluff Dykes		Below the twin masts					
Dyke reference		—	—	—	—	—	—
Sample running number		CH05-27A	CH05-27A	CH05-27A	CH05-27B	CH05-27B	CH05-27B
Phase/pulse number		P1	P2	P3	P2	P3	P4
	Total bioclast %	29	14	5	27	7	20
	Bryozoans	VC	C		VC		C
C	Bivalves	M	S		M		R
a	Echinoderms	S	M		S		
l	Benthic foraminifera	S	S		S	S	S
c	Planktic foraminifera	S	C	M	S	M	M
i	Gastropods	S	S		R	R	
c	Calcareous algae						
l	Barnacles						
a	Spicules & spines						
s	**Other**						
t	Brachiopods	S	R			R	
s	Serpulids						
	Modal size 1 (mm)	1.18	1.18	0.08	0.25	0.18	0.38
	Modal size 2 (mm)		1		2.5		2.125
	Shape/abrasion	A	A	VA	VA	A	A
	Sorting	PM	P	P	P	P	P
	Lithoclast %	25	45	0	30	0	5
	Intraclast %	0	0	0	0	0	0
	Siliciclastic grain %	1	6	5	3	3	2
	Quartz	R	R		R	R	R
S	Feldspar					R	
i	VRFs	R	S	S	S		
l	SRFs						
i	Micas						
c	Pyrite grains		R	S	S	S	R
i	Pyrite infills	S	R	S	S	S	R
c	Glauconite pellets	R	S		S	S	S
l	Glauconite infills			S		S	
a	**Other**						
s	Phosphate	S	S	S	S	S	R
t	Chert						
s	Hornblende						
	Limonite staining						
	Modal size 1 (mm)	0.10	0.18	0.08	0.13	0.05	0.08
	Modal size 2 (mm)						
	Shape/abrasion	SR	SR	SR	SR	SR	SR
	Sorting	M	P	P	PM	P	PM
	Interparticle material %	45	40	90	40	90	75
	Spar cement %	30	20	2	30	2	5
	Micrite %	15	20	88	10	88	70
Unoccluded pore space %		1	1	0	1	0	1

Red Bluff Dykes		Below the twin masts				
Dyke reference		—	—	—	—	—
Sample running number		CH05-27C	CH05-27C	CH05-27C	CH05-27C	CH05-27P
Phase/pulse number		P2	P3	P4	–	Calcite
	Total bioclast %	50	10	10	0	0
	Bryozoans	VC		C		
C	Bivalves	S	R	R		
a	Echinoderms	C				
l	Benthic foraminifera	C	R	R		
c	Planktic foraminifera	M	M	M		
i	Gastropods	S				
c	Calcareous algae					
l	Barnacles					
a	Spicules & spines					
s	**Other**					
t	Brachiopods					
s	Serpulids					
	Modal size 1 (mm)	0.48	0.03	0.08		
	Modal size 2 (mm)	2.25		1		
	Shape/abrasion	VA	VA	A		
	Sorting	P	PM	P		
	Lithoclast %	0	5	20	0	0
	Intraclast %	0	0	0	0	0
	Siliciclastic grain %	1	2	2	2	0
	Quartz	S	R	R		
S	Feldspar		R			
i	VRFs	R				
l	SRFs					
i	Micas					
c	Pyrite grains	R	S	R	R	
i	Pyrite infills	R	S	R	R	
c	Glauconite pellets	R	R	R		
l	Glauconite infills			R		
a	**Other**					
s	Phosphate	R	R	R		
t	Chert					
s	Hornblende					
	Limonite staining					
	Modal size 1 (mm)	0.13	0.05	0.13	0.05	
	Modal size 2 (mm)					
	Shape/abrasion	SR	SR	SR	SR	
	Sorting	PM	P	P	PM	
	Interparticle material %	50	90	90	98	100
	Spar cement %	25	3	2	2	100
	Micrite %	25	87	88	96	0
Unoccluded pore space %		0	0	0	0	0

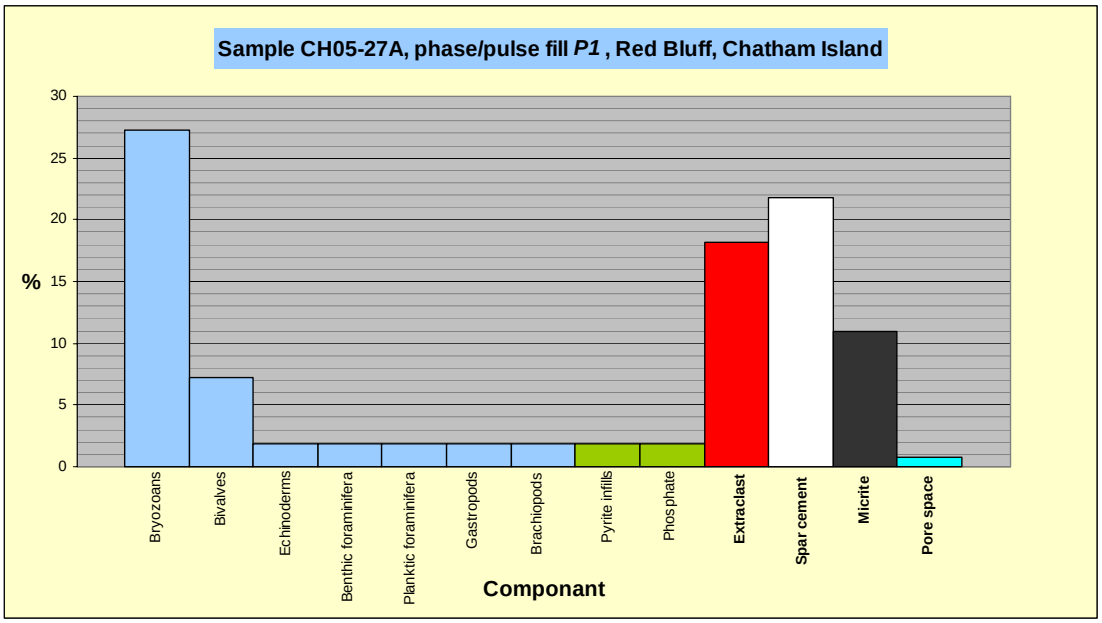

Figure C32: Component percentages of dyke sample CH05-27A, phase fill *P1*, *below the twin masts* locality, Red Bluff, Chatham Islands.

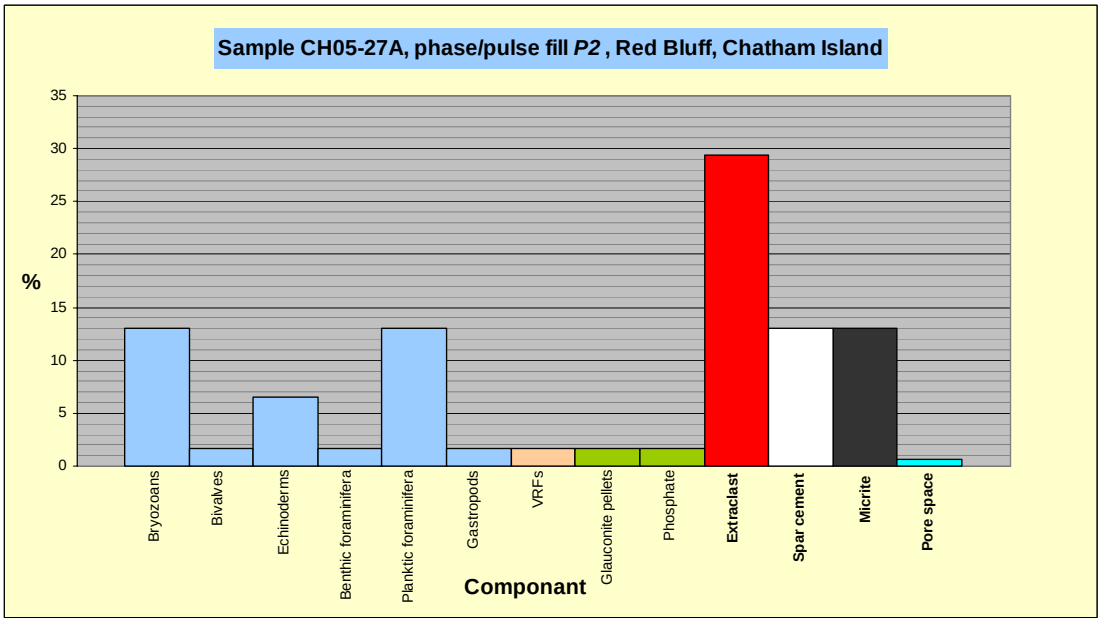

Figure C33: Component percentages of dyke sample CH05-27A, phase fill *P2*, *below the twin masts* locality, Red Bluff, Chatham Islands.

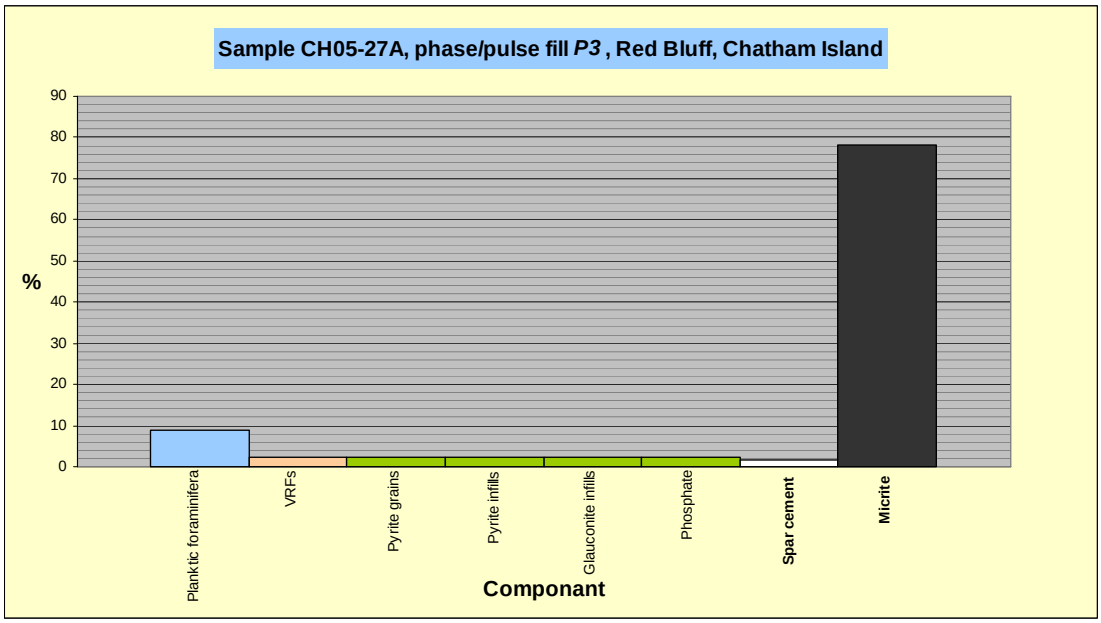

Figure C34: Component percentages of dyke sample CH05-27A, phase fill *P3*, *below the twin masts* locality, Red Bluff, Chatham Islands.

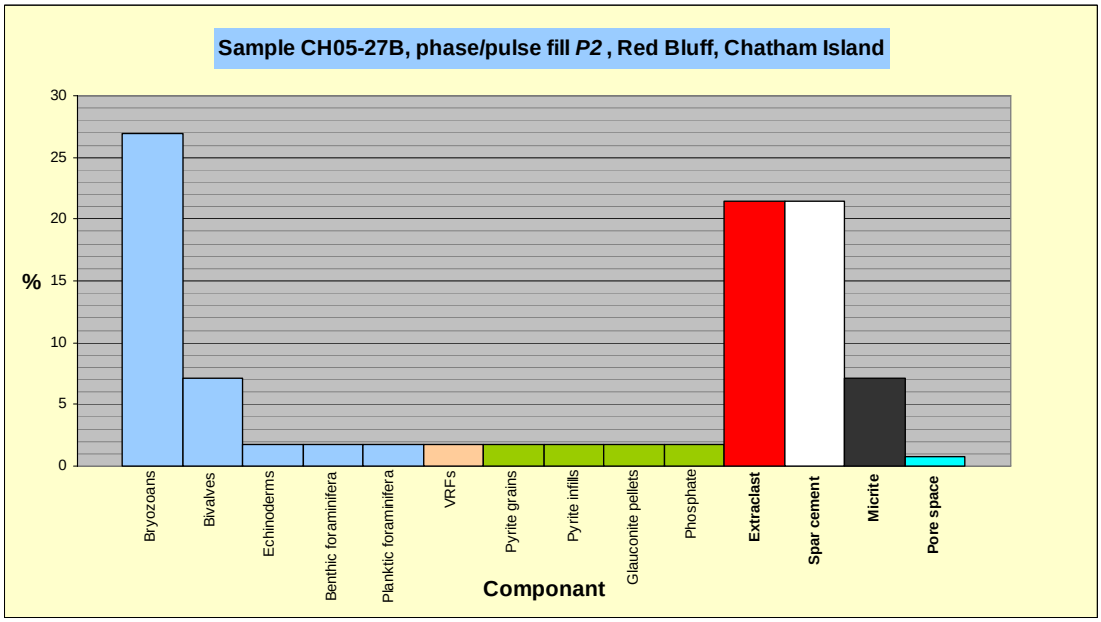

Figure C35: Component percentages of dyke sample CH05-27B, phase fill *P2*, *below the twin masts* locality, Red Bluff, Chatham Islands.

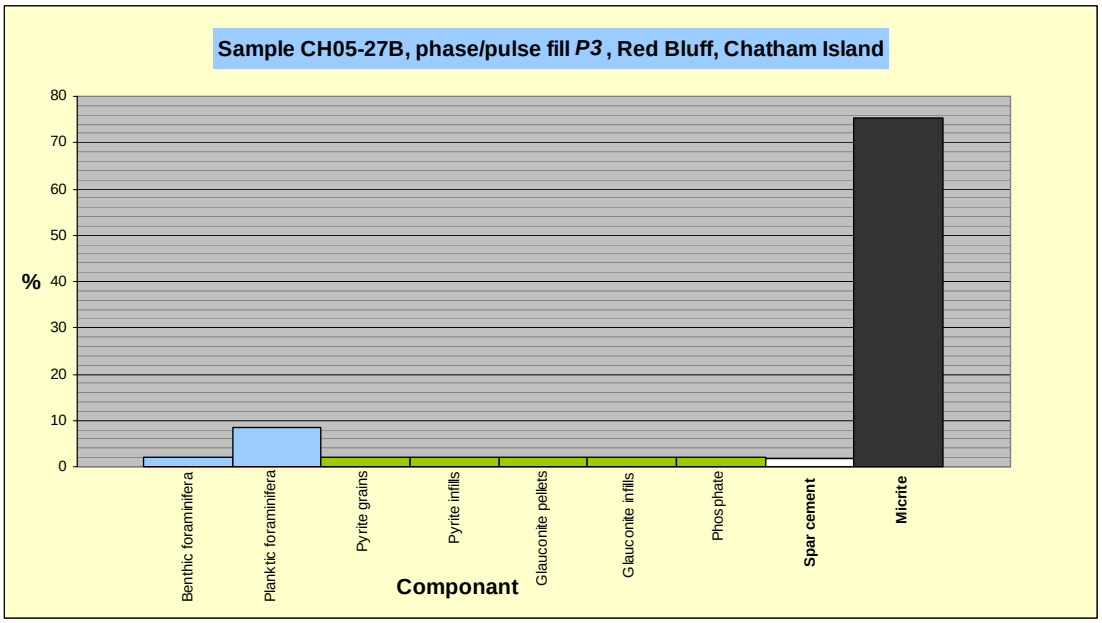

Figure C36: Component percentages of dyke sample CH05-27B, phase fill *P3*, *below the twin masts* locality, Red Bluff, Chatham Islands.

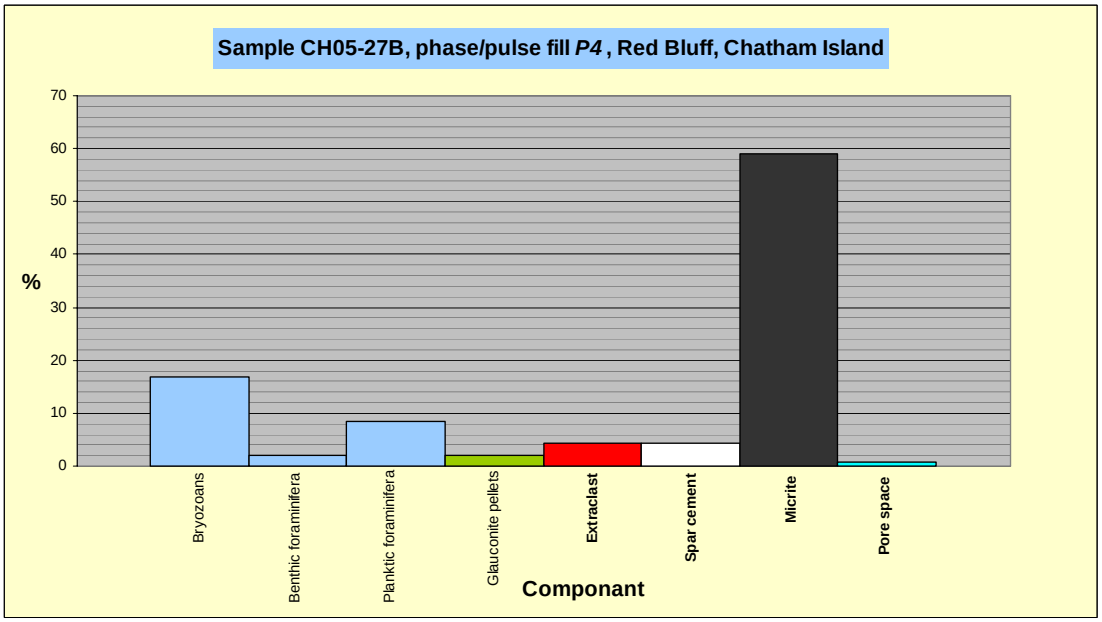

Figure C37: Component percentages of dyke sample CH05-27B, phase fill *P4*, *below the twin masts* locality, Red Bluff, Chatham Islands.

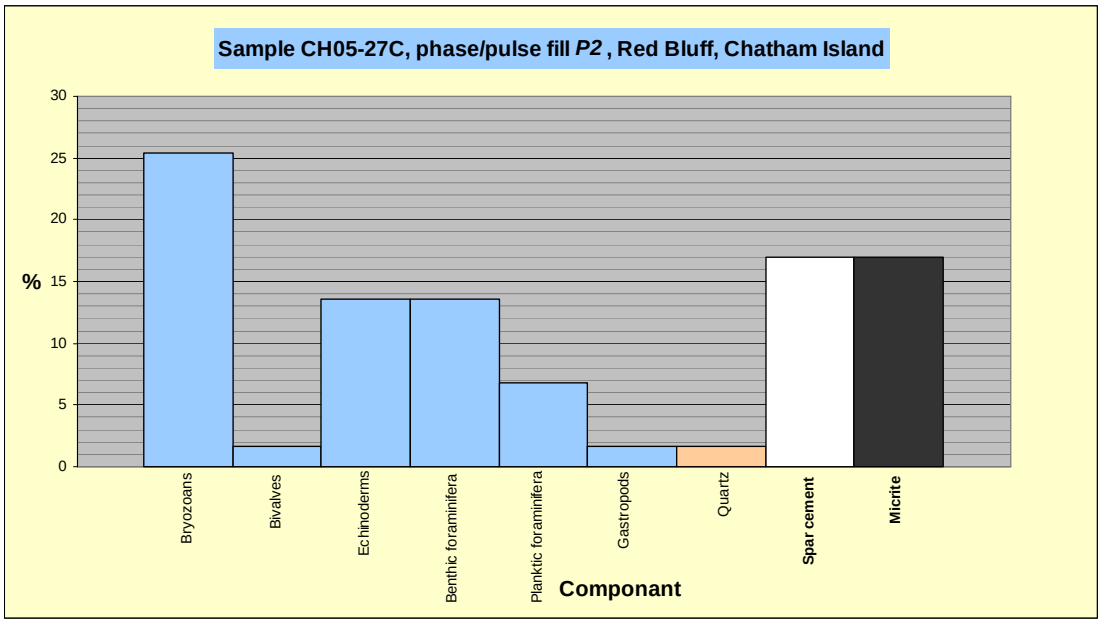

Figure C38: Component percentages of dyke sample CH05-27C, phase fill *P2*, *below the twin masts* locality, Red Bluff, Chatham Islands.

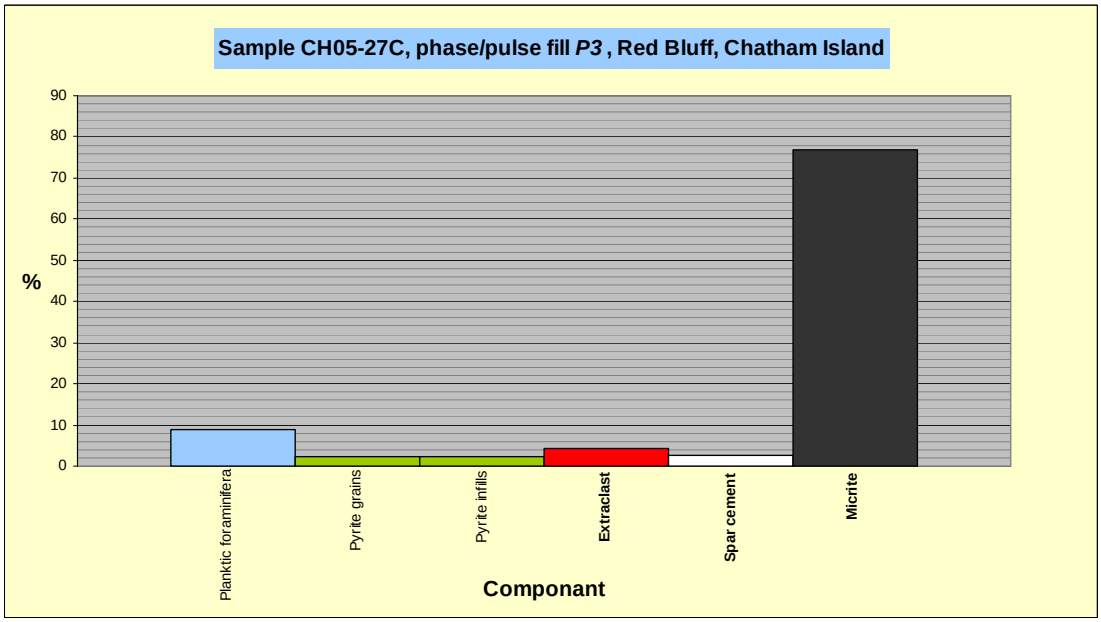

Figure C39: Component percentages of dyke sample CH05-27C, phase fill *P3*, *below the twin masts* locality, Red Bluff, Chatham Islands.

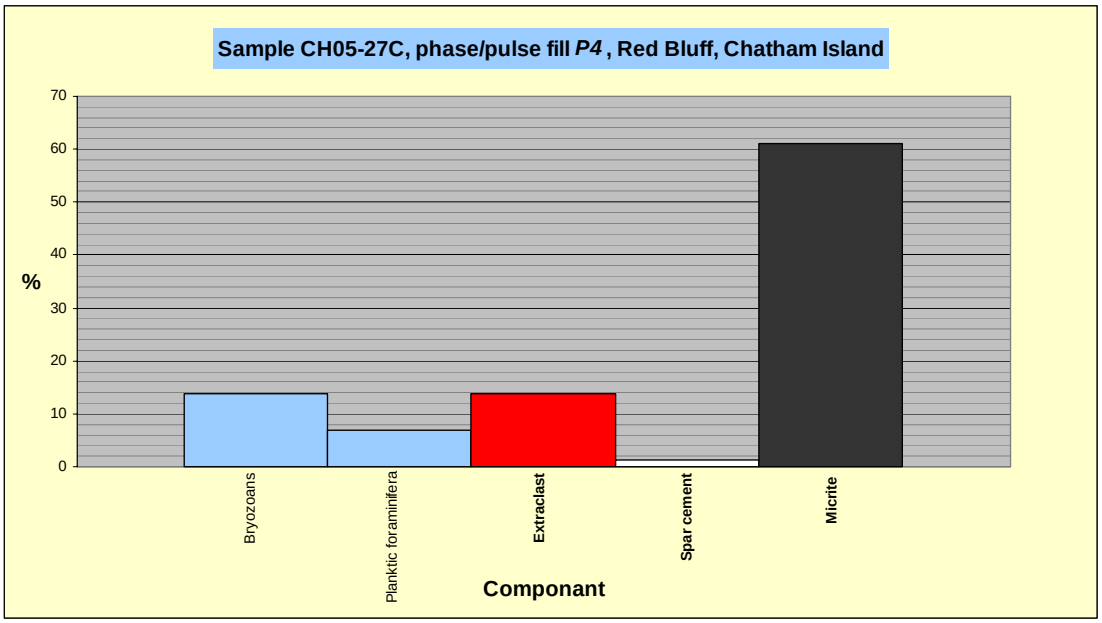

Figure C40: Component percentages of dyke sample CH05-27C, phase fill *P4*, *below the twin masts* locality, Red Bluff, Chatham Islands.

APPENDIX D

Chatham Islands Limestone

Paleontological Data

Chatham Island main limestone paleontological data

(from Campbell et al., 1993)

Main limestone occurrences

Haumurian limestone

Table D1: Foraminifera and calcareous nannoplankton from the unnamed Haumurian limestone, Pitt Island. Identifications by C.P. Strong and A.R. Edwards (from Strong and Edwards 1979).

Foraminifera	**Pitt Is.**	**Chatham Is.**
Allomorphina cretacea Reuss	?	x
Anomalina sp.	x	
Bolivina cf. incrassata Reuss	x	
Bolivinoides draco dorreeni Finlay	x	
Bolivinopsis spectabilis (Grzybowski)	x	
Charltonina acutimarginata Finlay	x	
Chilostomella sp.	x	
Colomia sp.	x	
Dentalina spp.	x	
Florilus tanumius (Finlay)	x	
Frondicularia bulla Belford	x	
Gaudryina healyi Finlay	x	
Gavelinella cf. stephensoni (Cushman)	x	
Gyroidinoides sp.	x	
Lagena cf. sulcata (Walker & Jacob)	x	
L. vulgaris Williamson	x	
Nodosaria cf. velascoensis Cushman		x
Nuttallides cf. tholus Finlay	x	
Patellina piripaua Finlay	x	
Pullenia cretacea Cushman	x	x
P. jarvisi Cushman	x	
Globigerinelloides volutus (White)	x	x
Hedbergella cf. monmouthensis Olsson	x	
Hedbergella sp.	x	
Heterohelix globulosa (Ehrenberg)	x	x
Rugoglobigerina rugosa (Plummer)		x
Calcareous nannoplankton		
Arkhangelskiella cymbiformis Veshina	x	
Eiffellithus cf. turriseiffeli (Deflandre)	x	
Kamptnerius cf. magnificus Deflandre	x	
Nephrolithus frequens Gorka	x	

Tumaio Limestone

Table D2: Tumaio Limestone macrofossils from, Takapu Creek, Chatham Island. Identifications by P.A. Maxwell, D.F. Squires and D.E. Lee.

Coelenterata (ident. D.F. Squires)
Madrepora granulata (Tenison-Woods)
Brachiopoda (ident. D.E. Lee)
Probolarina chathamensis Lee
Terebratulina suessi (Hutton)
Campages chathamensis Allan
Terebratella finlayi Allan
Mollusca (ident. J. Marwick, P.A. Maxwell)
Bivalvia
Serripecten tiorioriensis Marwick
Eburneopecten imperfectus (Marwick)
Pycnodonte (Notostrea) tarda (Hutton)
Crenostrea cannoni (Marwick)
Teredinidae gen. et sp. Indet.
Gastropoda
Cirsotrema (Tioria) youngi Marwick
Echinodermata (ident. P.A. Maxwell)
Apatopygus sp.
Eucidaris ?sp.
Eucidaris strobilata Fell
Temnopleuroidea

Table D3: Tumaio Limestone foraminifera, southwest of Takapu Creek, Chatham Island. Identifications by N. de B. Hornibrook.

Foraminifera	
Acarinina mackannai (White)	*Guttulina* sp.
Alabamina cf. *creta* (Finlay)	*Gyroidinoides* spp.
Alabamina cf. *tenuimarginata* (Chapman, Parr & Collins)	*Hastigerina* sp.
Alabamina tenuimarginata (Chapman, Parr & Collins)	*Heronallenia* sp.
Anomalina aotea Finlay	*Kolesnikovella* sp.
Anomalina visenda Finlay	Lagenidae, various taxa
Anomalinoides orbiculus (Stache)	*Lenticulina* cf. *pseudomamilligera* (Plummer)
Aragonia aragonensis Nuttall	*Lenticulina* spp.
Aragonia cf. *zelandica* Finlay	*Melonis maorica* (Stache)
Astacolus spp.	*Mississippina* sp.
Baggatella d. inconspicua Howe	*Nodosarella* sp.
Bolivinopsis compta Finlay	*Nodosaria callosa* Stache
Bulimina d. pupula Stache	*Nodosaria filiformis* d'Orbigny
Bulimina subbortonica Finlay	*Nodosaria longiscata* d'Orbigny
Chiloguembelina waiparaensis Jenkins	*Nodosaria* spp.
Cibicides cf. *pronovozelandicus* Srinivasan	*Oridorsalis umbonatus* (Reuss)
Cibicides pseudoconvexus Parr	*Osangularia lens* Brotzen
Cibicides spp.	*Osangularia* sp.
Coleites gagei Hornibrook	*Parvicarinina coronata* (Heron-Allen & Harland)
Dentalina spp.	*Patellina corrugata* Williamson
Discorbis cf. *vesicularis* (Lamarck)	*Pleurostomella* sp.
Discorbis sp.	*Pseudonodosaria* spp.
Dorothia bulletta Carsey	*Pullenia* spp.
Elphidium cf. *hampdenensis* Finlay	*Rectuvigerina?* Sp.
Elphidium sp.	*Rosalina* sp.
Gaudryina cf. *whangaia* Finlay	*Semirosalina deflata* Hornibrook
Gaudryina cf. *reliqua* Finlay	*Siphonina* sp.
Globigerina triloculinoides Plummer	*Stilostomella basicarinata* Hornibrook
Globigerina higginsi (Bolli)	*Stilostomella* spp.

(Table D3 continued)

Globorotalia australiformis Jenkins	*Tappanina* cf. *glaessneri* (Finlay)
Globorotalia cf. *aequa* Cushman & Renz	*Tappanina glaessneri* (Finlay)
Globorotalia cf. *broedermanni* Cushman & Bermudez	*Trifarina* sp.
Globorotalia ehrenbergi Bolli	*Truncorotaloides* ct. *collactea* (Finlay)
Globorotalia pseudomenardii (Parker, Jones & Brady)	*Vaginulina* spp.
Globorotalia pusilla laevigata Bolli	*Vulvulina espinosa* Finlay
Globorotalia reissi Loeblich & Tappan	*Vulvulineria* sp.
Guembelitria sp.	*Zeauvigerina parri* Finlay

Matanginui Limestone

Table D4: Matanginui Limestone macrofossils, Chatham Island. Identifications by P.A. Maxwell, D.E. Lee, J.*S.* Buckeridge and L W. Keyes.

	Chatham Island				**Pitt Island**		
Brachiopoda (ident. D. E. Lee)	**Waitaha Ck.**	**S of Waipapa Ck.**	**Lake Marakapia**	**Red Bluff**	**Rocky Side**	**Tupuangi Stream**	**Flower-pot Bay**
Lingula waikatoensis Penseler	x						
Discinisca sp.	x						
Crania sp.	x						
Thecidellina cf. *hedleyi* Thomson	x	x					
Tegulorhynchia squamosa (Hutton)	x	x			x	x	
Probolarina chathamensis Lee		x		x			
Terebratulina suessi (Hutton)		x			x	x	
Terebratulina n. sp.	x						
Liothyrella cf. *concentrica* Hutton	x					x	
Liothyrella sp.		x		x			
Argyrotheca n. sp.	x	x					
Terebratella? n. sp.				x			
Mollusca (ident. P. A. Maxwell) **Bivalvia**							
Arca? sp.					x		
Chlamys n. sp. aff. *chathamensis* (Hutton)		x		?	x		
Serripecten cf. *tiorioriensis* Marwick	x			x	x		
Eburneopecten cf. *imperfectus* (Marwick)					x		
Spondylus n. sp.	x	x		x	x		x
Acesta (Acesta) sp.				x	x		
A. (Plicacesta) n. sp.	x	x					
Pycnodonte (Notostrea) tarda (Hutton)	x			x	x, cf.		
Crenostrea sp.	x						

(Table D4 continued)

	Waitaha Ck.	S of Waipapa Ck.	Lake Marakapia	Red Bluff	Rocky Side	Tupuangi Stream	Flower-pot Bay
Ostreidae? gen. et sp. indet.		x		x			x
Cardiidae gen. et sp. indet.		x			x		
Teredinidae gen. et sp. indet.							
Gastropoda							
Pleurotomariidae gen. et sp. indet.					x		
Trochidae? gen. et sp. indet.							x
Volutidae gen. et sp. indet.					x		
Cirripedia (ident. J. S. Buckeridge)							
Smilium calanticoideum Buckeridge		x					
Verruca (Verruca) tasmanica chatheca Buckeridge	x	x					
Eolasma maxwelli Buckeridge		x					
Pachylasma veteranum Buckeridge					x		
Echinodermata (ident. P. A. Maxwell)							
Eucidaris strobilata Fell	x	x	x	x	x		
Giraliaster tertiarius (Gregory)				x			
Echinolampas? sp.				x			
Apatopygus sp.	x			x	x		
Crinoidea		x					
Pisces (ident. L W. Keyes)							
Notorynchus primigenius (Agassiz)		x					
Carcharodon auriculatus (Blainville)		x					
Striatolamia macrota (Agassiz)		x		x	x		
Lamna obliqua (Agassiz)		x					

Table D5: Matanginui Limestone foraminifera, Chatham Island. Identifications by N. de B. Hornibrook.

	Chatham Island					**Pitt island**	
Foraminifera	**Matanginui Ck.**	**Waipapa Ck.**	**Blind Jims Ck.**	**Moreroa**	**Waimahana Ck.**	**Tara. Pen.**	**Rocky Side**
Acarinina mackannai (White)		x	x		x	x	x
Alabamina ct. creta (Finlay)							x
Alabamina tenuimarginata (Chapman, Parr & Collins)	x	x	x				
Angulogerina sp. (minute, costate)	x	x	x	x			x
Anomalina aotea Finlay	x	x			x		
Anomalinoides orbiculus (Stache)	x				x		
Astacolus sp.				x			
Asterigerina sp. (small, depressed with raised dorsal sutures)	x						
Asterigerina sp. (very flattened)							x
Asterigerina sp.		x	x				
Asterigerinella? sp.				x			
Asterocyclina speighti (Chapman)		x	x			x	x
Astrononion impressum Hornibrook	x						
Baggatella cf. *inconspicua* Howe	x	x	x				
Bolivinopsis cf. *compta* Finlay							x
Bolivinopsis cubensis (Cushman and Bermudez)					x		
Bulimina bortonica Finlay				x	x		
Bulimina cf. *pupula* Stache		x					
Bulimina subbortonica Finlay	x	x	x				x
Bulimina truncanella Finlay	x						
Cancris sp.	x						
Carpenteria sp.	?	?	?	?	?	?	?
Chiloguembelina cf. *ototara* (Finlay)				x	x		
Chiloguembelina crinata (Glaessner)		x	x				
Chiloguembelina cubensis (palmer)				x			
Chiloguembelina waiparaensis Jenkins		x					
Cibicides cf. *parki* Finlay (small var.)	x		x				
Cibicides cf. *carinatus* (Terquem)							x
Cibicides cf. *umbonifer* Parr			x			x	x
Cibicides hampdenensis Hornibrook	x				x		
Cibicides parki Finlay					x		
Cibicides pseudoconvexus Parr	x	x		x			
Cibicides sp. (coarsely punctate)		x					
Coleites sp.				x		x	x
Dentalinoides sp.				x			
Discocyclina sp. (several worn specimens)				x			
Discorbinella sp.			x				
Discorbis cf. *vesicularis* (Lamarck)			x				x
Discorbis sp.				x		x	
Dorothia agrestis Finlay					x		
Dorothia bulletta Carsey	x					x	
Dorothia cf. *minima* (Karrer)				x			
Ellipsoglandulina subconica (Kreuzberg)	x				x		
Elphidium saginatum Finlay					x		
Eponides lornensis Finlay				x			

(Table D5 continued)

	Matanginui Ck.	Waipapa Ck.	Blind Jims Ck.	Moreroa	Waimahana Ck.	Tara. Pen.	Rocky Side
Fursenkoina sp.		x					
Gaudryina cf. *reliqua* Finlay	x	x					
Gaudryina cf. *whangaia* Finlay		x					
Gaudryina sp. A						x	x
Gaudryina sp. B (rugose)							x
Gaudryina sp. C (conical)							x
Globanomalina wilcoxensis (Cushman & Ponton)	x	x	x			x	x
Globigerapsis index (Finlay)				x			
Globigerina angiporoides minima Jenkins				x			
Globigerina linaperta Finlay				x	x		
Globigerina triloculinoides Plummer		x	x			x	x
Globorotalia australiformis Jenkins	x	x	x			x	x
Globorotalia cf. *aequa* Cushman & Renz (hispid)	x				x		
Globorotalia cf. *cerroazulensis* (Cole)				x			
Globorotalia crater Finlay	x						
Globorotalia pusilla laevigala Bolli		x					
Globorotalia reissi Loeblich & Tappan		x					
Globorotalia rex Martin							x
Guembelitria cf. *triseriata* (Terquem)	x		x				
Guembelitria triseriata samwelli Jenkins					x		
Gyroidina sp.						x	x
Hanzawaia sp.	x						
Hastigerina sp.		x	x				
Karreriella sp.	?	?	?	?	?	?	?
Karreria fallax Rzehak				x			x
Lagenidae, various taxa		x	x				
Lenticulina sp.	x			x		x	x
Lingulina sp.				x			
Marginulina subbullata Hantken							x
Marssonella sp.						x	x
Melonis maorica (Stache)	x	x	x	x	x	x	x
Mississippina concentrica (parker & Jones)		x					
Mississippina sp.	x				x	x	x
Nodosarella subnodosa Guppy					x		
Nodosaria spp.	x						x
Notorotalia ? sp.	x						
Notorotalia cf. *uttleyi* Hornibrook					x		
Osangularia cf. *lens* Brotzen	x	x					
Pararotalia sp.				x			
Parvicarinina coronata (Heron-Allen & Earland)			x				
Patellina cf. *piripaua* Finlay							x
Planodiscorbis sp.			x				
Pleurostomella sp.	x	x					
Polymorphinidae				x			x
Pseudoglobоquadrina primitiva (Finlay)	x			x	x		

(Table D5 continued)

	Matanginui Ck.	Waipapa Ck.	Blind Jims Ck.	Moreroa	Waimahana Ck.	Tara. Pen.	Rocky Side
Pseudohastigerina micra (Cole)				x	x		
Pullenia sp.	x						
Rosalina sp.			x	x			
Siphotextularia cf. *cordis* Hornibrook		x					
Siphotextularia cordis Hornibrook				x			
Stilostomella spp.	x						
Tappanina cf. *glaessneri* (Finlay)			x				
Textularia cuspis Finlay				x			
Textularia ototara Hornibrook				x			
Textularia sp.				x	x		
Trifarina sp.							x
Truncorotaloides collactea (Finlay)	x			x	x		
Vaginulina sp. (costate)				x			
Vaginulinopsis cf. *marshalli* (Finlay)							x
Verneuilina sp.		x					x
Virguloides sp.	x	x					x
Vulvulina espinosa Finlay	x						
Wadella cf. *globiformis* (Chapman)				x			
Zeauvigerina aff. *parri* Finlay			x				
Zeauvigerina parri Finlay	x			x	x		
Zeauvigerina zelandica Finlay			x	x	x		

Te One Limestone

Table D6: Te One Limestone macrofossils, Chatham Island. Identifications by P.A. Maxwell, D.E. Lee, J.S. Buckeridge. I.W. Keyes and R.F. Jenkins.

	Cattle Point	Moreroa	South of Motuhou	South of Ohuru	Big Bush	South of Kaiparakau
Brachiopoda (ident. D. E. Lee)						
Lingula waikatoensis Penseler			x			
Neocrania chathamensis (Allan)			x			
Thecidellina hedleyi Thomson			x			
Probolarina chathamensis Lee			x			
Terebratulina suessi (Hutton)			x			
Terebratulina sp.	x			x	x	x
Liothyrella cf. *kakanuiesis* (Hutton)			x			
Liothyrella sp.				x		
Terebratella finlayi Allan			x			
Terebratella sp.					x	x
Mollusca (ident. P. A. Maxwell) **Bivalvia**						
Chlamys sp.	x		x	x	x	x
Serripecten n. sp.			x			
Duplipecten parki (Marwick)		x				
Limea n. sp.			x			
Ostreidae gen. et. sp. Indet.		x	x	x		
Venericardia (s. 1.) sp.				x		
Cephalopoda						
Aturia sp.				x		

(Table D6 continued)

	Cattle Point	Moreroa	South of Motuhou	South of Ohuru	Big Bush	South of Kaiparakau
Cirripedia (ident. J. S. Buckeridge)						
Calantica (Scillaelepas) cf. studeri (Wehner)				x		
Pachylasma distortum Buckeridge				x		
Chionelasmus darwini (Pilsbry)					x	
Chordata						
Pisces (ident. I. W. Keyes)						
Heterodontus sp.						x
Carcharias acutissima (Agassiz)						x
Striatolamia macrota (Agassiz)					x	x
Odontaspis incurva (Davis)					x	
Pristiophorus lanceolatus (Davis)						x
Ikamauius ensifer (Davis)						x
Aves (ident. R. F. Jenkins)						
Palaeeudyptes cf. *antarcticus* Huxley			x			

Table D7: Te One Limestone foraminifera, Chatham Island. Identifications by N. de B. Hornibrook.

	Cattle Pt.	W. of Titirangi	Moreroa	Kaiparakau Pt.	Ohuru	Big Bush	Moutapu Pt.
Alabamina tenuimarginata C.P.& C.	x	x	x	x		x	
Angulogerina cf. *ototara* Hornibrook	x	x	x				
Angulogerina d. *costornata* Hornibrook						x	
Angulogerina sp.						X	
Anomalina visenda Finlay					x		
Arenodosaria antipoda (Stache)	x	x					x
Astrononion impressum Hornibrook		x		x		x	
Bolivina pontis Finlay		x				cf.	
Bolivinopsis cubensis (Cushman & Bermundez)		x					
Bulimina cf. *bortonica* Finlay		R?					
Bulimina truncanella Finlay			x				
Chiloguembelina ototara (Finlay)		x	x	x	x	x	
Cibicides hampdenensis Hornibrook				x			
Cibicides maculatus (Stache)		x					
Cibicides parki Finlay						?	
Cibicides pronovozelandicus Srinivasan	x	x					x
Cibicides pseudoconvexus Parr	x	x	x	x		x	x
Coleites cf. *abuillotensis* Cushman & Bermundez		x	x			x	
Coleites gagei Hornibrook	x	x	?		x	x	

(Table D7 continued)

	Cattle Pt.	W. of Titirangi	Moreroa	Kaiparakau Pt.	Ohuru	Big Bush	Moutapu Pt.
Coleites n. sp.		X	x				
Dentalina spp.		X		x			
Dentalinoides sp.		X					
Dorothia minima (Karrer)							x
Ellipsoglandulina sp.	X						
Elphidium sp.	X						
Eponides lornensis Finlay		x	x	x	x	x	x
Frondicularia sp.		X					
Gaudryina reussi Stache		x					
Globanomalina wilcoxensis (Cole)				R			
Globigerapsis index (Finlay)	x	x	x	x	x	x	
Globigerina ampliapertura Bolli			x			x	
Globigerina angiporoides Hornibrook		x	x			x	
Globigerina brevis Jenkins							x
Globigerina linaperta Finlay	x		x	x	x	x	
Globocassidulina subglobosa (Brady)			x			x	
Globorotalia aculeate Jenkins	x			x		x	
Globorotalia australiformis Jenkins				R			
Globorotalia cf. *nana* Bolli						x	
Globorotalia cf. *aequa* Cushman & Renz (hispid)		x	x			x	x
Globorotalia increbescens Bandy				x			
Globorotalia insolita Jenkins		x	x			x	
Globorotalia opima Bolli				x			
Globorotaloides suteri Bolli		x	x			x	
Globorotaloides turgidus (Finlay)		x	x	x			
Guembelitria sp.				R			
Guttulina sp.				x		x	x
Gyroidinoides sp.	x	x	x	x		x	
Hantkenina alabamensis Cushman		x					
Heronallenia sp.		x	x			x	
Hoeglundina sp.		?					
Karreriella novozealandica Cushman	x						
Kolesnikovella sp.	x	x	x				
Lenticulina sp.	x	x			x	x	x
Marginulinopsis allani Finlay							x
Melonis maorica (Stache)	x	x	x	x	x	x	x
Mississippina cf. *concentrica* (Parker & Jones)		x				x	

(Table D7 continued)

	Cattle Pt.	W. of Titirangi	Moreroa	Kaiparakau Pt.	Ohuru	Big Bush	Moutapu Pt.
Nodosarella subnodosa Guppy		x					
Nodosaria spp.	x						
Notorotalia sp.	x	x					
Notorotalia uttleyi Hornibrook						x cf.	
Oolina sp.					x		
Oridorsalis umbonatus (Reuss)			x				
Parvicarinata coronata (Heron-Allen & Earland)			x			x	
Planulinoides sp.		x					
Pleurostomella sp.			x	x			
Polymorphinidae	x	x	x	x	x	x	x
Pseudogloboquadrina primitiva (Finlay)	x	X	x	x	x	x	x
Pseudohastigerina micra (Cole)	x	x	x	x	x	x	
Pseudohastigerina sp. (minute)			x				
Pullenia bulloides (d'Orbigny)		x				x	
Pullenia sp.	x		x	x	x	x	
Rectuvigerina prisca (Finlay)	x	x	x		x	x	
Rosalina sp.			x	x		x	
Siphotextularia cordis Hornibrook		x	x				
Siphotextularia lornensis Hornibrook				x			
Sphaeroidina variabilis Reuss			x			x	
Stilostomella spp.		x	x			x	x
Textularia cuspis Finlay	x			x			
Textularia ototara Hornibrook			x			x	x
Textularia fistulosa Brady						x	
Trifarina parva Hornibrook	x	x	x			x	
Truncorotaloides collactea (Finlay)	x	R?	x			x	
Uvigerina sp. (of Burnside Marl)		x					
Vaginulina sp.			x				
Vaginulinopsis hochstetteri (Stache)	x	x					
Vaginulinopsis sp. (smooth)					x		
Vaginulinopsis sp. (costate)					x	x	
Virguloides sp.				x			
Wadella globiformis (Chapman)	x	x	x	x		x	x
Zeauvigerina zelandica Finlay	x	x	x	x		x	x
R = reworked							

***Victoriella* Limestone**

Table D8: Victoriella Limestone foraminifera, from a tributary of Waitaha Creek, Chatham Island. Identifications by N. de B. Hornibrook.

Bolivina reticulata Hantken
Carpenteria sp.
Catapsydrax unicavus Bolli
Chiloguembelina cf. *cubensis* (palmer)
Chiloguembelina sp.
Cibicides pronovozelandicus Srinivasan
Dentalina sp.
Dentalinopsis sp.
Eponides repandus (Fichtel & Moll)
Globigerina angiporoides Hornibrook (scarce)
Globigerina euapertura Jenkins (abundant)
Globigerina labiacrassata Jenkins
Globigerina linaperta Finlay
Globorotaloides testarugosus Jenkins
Guttulina sp.
Hanzawaia turgida (Finlay)
Hofkerina semiornata (Howchin)
Lenticulina spp.
Lingulina cf. *avellanoides* (Kreuzberg)
Pleurostomella sp.
Polymorphina cf. *waitakiensis* Hornibrook
Rectuvigerina cf. *clifdenensis* Hornibrook
Saracenaria sp.
Sigmomorphina cf. *pernaeformis* (Stache)
Sphaeroidina bulloides d'Orbigny
Vaginulina sp.
Victoriella conoidea (Rutten)
Wadella globiformis (Chapman)

Taoroa Limestone

Table D9: Taoroa Limestone foraminifera, Manganui, Chatham Island Identifications by N. de B. Hornibrook.

Amphicoryne sealaris (Batsch)
Angulogerina costornata Hornibrook
Bolivina reticulata Hantken
Bulimina miolaevis Finlay
Chiloguembelina cubensis Palmer (costate)
Cibicides novozelandicus (Karrer)
Cibicides perforatus (Karrer)
Cibicides temperatus Vella
Eponides broekhianus (Karrer)
Eponides repandus (Fichtel & Moll)
Gaudryina reussi Stache
Globigerina ciperoensis ciperoensis Bolli
Globigerina eamsi Blow
Globigerina euapertura Jenkins (abundant)
Globigerina woodi woodi Jenkins
Globocassidulina subglobosa (Brady)
Globoquadrina dehiscens (Chapman, Parr & Collins) (inflated form)
Globorotaloides suteri Bolli
Guttulina spp.
Gyroidinoides allani (Finlay)
Hanzawaia turgida (Finlay)
Heronallenia sp.
Karreria fallax Rzehak
Karreriella chilostoma (Reuss)
Kolesnikovella australis (Heron-Allen & Earland)
Lenticulina spp.
Melonis maorica (Stache)
Nodosarella sp.
Notorotalia cf. *stachei* Finlay
Operculina sp.
Orthomorphina sp.
Rectuvigerina rerensis (Finlay)
Stilostomella aequalis (Karrer)
Streptochilus pristinus Bronnimann
Vaginulinopsis recta (Karrer)
Victoriella conoidea (Rutten)

Altonian limestone

Table D10: Altonian limestone macrofossils, Moutapu Point, Chatham Island. Identifications by P. A. Maxwell, D. E. Lee, J. S. Buckeridge, I. W. Keyes, and R. E. Fordyce.

Porifea
Coelenterata (ident. LW. Keyes and P.A. Maxwell)
Alcyonarian corals
Balanophyllia (Balanophyllia) alta Tenison-Woods
Brachiopoda (ident. D.E. Lee and P.A. Maxwell)
Liothyrella? n.sp.
Campages n.sp.?
Terebratella n.sp. A?
Terebratella n.sp. B?
Tegulorhynchia sp.
Gastropoda
Volutidae gen. et sp. indet.
Bivalvia
Chlamys sp.
Ostreidae ? gen. et sp. indent.
Bivalvia indent.
Echinodermata
Annelida
Serpulidae gen. et sp. Indent.
Cirripedia (ident. J.S. Buckeridge)
Smilium chathecum Buckeridge
Chondrichthyes (indent. L. W. Keyes)
Isurus hastalis (Agassiz)
Pristiophorus lanceolatus (Davis)
Mammalia (indent. R.E. Fordyce)
Delphinidae gen. et sp. indent.

Table D11: Unnamed Altonian limestone foraminifera, Moutapu Point, Chatham Island. Identifications by G.H. Scott and H.E.G. Morgans.

Amphicoryne sealaris (Batsch)
Bolivina reticulata Hantken
Bolivina sp.
Cassidulina arata Finlay
Cibicides cf. *molestus* Hornibrook
Cibicides novozelandicus (Karrer)
Euuvigerina sp.
Fohsella peripheroronda (Blow & Banner)
Globigerina ciperoensis ciperoensis Bolli
Globigerina woodi woodi Jenkins
Globigerinoides trilobus trilobus (Reuss)
Globocassidulina subglobosa (Brady)
Globorotalia miozea Finlay
Globorotalia zealandica Hornibrook
Gyroidinoides sp.
Gyroidinoides zelandicus (Finlay)
Hanzawaia turgida (Finlay)
Melonis maorica (Stache)
Oridorsalis tenera Brady
Rectuvigerina aff. *vesca* (Finlay)
Rectuvigerina sp. (very finely striate)
Sphaeroidinellopsis cf. *disjuncta* (Finlay)

Motarata Limestone

Table D12: Motarata Limestone foraminifera, Chatham Island.
Identifications by N. de B. Hornibrook.

	Moutapu Pt.	Whareama
Alabamina tenuimarginata (Chapman, Parr & Collins)		x
Amphicoryne hirsuta (d'Orbigny)	x	x
Anomalina sp.		x
Bigenerina pliocenica Finlay	x	
Bolivina affiliata Finlay	x	x
Bulimina aculeata d'Orbigny	x	
Cibicides deliquatus Finlay	x	x
Cibicides sp.	x	
Discorbis balcombensis (Chapman, Parr & Collins)	x	x
Dyocibicides biserialis Cushman & Valentine	x	x
Ehrenbergina cf. *marwicki* Finlay	x	x
Florilus sp.	x	
Gaudryina convexa Karrer		x
Globigerina bulloides d'Orbigny	x	x
Globigerina woodi Jenkins group	x	
Globigerina nepenthes Todd		x
Globigerina sp. (3 chambers)		x
Globigerinoides conglobatus (Brady)		x
Globigerinoides trilobus (Reuss)		x
Globorotalia crassaformis (Galloway & Wissler) (unkeeled, sinistral)	x	x
Globorotalia humerosa Takayanagi & Saito cf.		x
Globorotalia pliozea Hornibrook		x
Globorotalia puncticulata (Deshayes)	x	x
Lenticulina calcar Defrance		x
Lenticulina sp.	x	
Marginulina sp.		x
Martinottiella communis d'Orbigny		x
Melonis d. *simplex* (Karrer)		x
Mississippina concentrica (parker & Jones)		x
Notorotalia sp. (reticulate)		x
Notorotalia sp. (smooth)	x	x
Orbulina universa d'Orbigny	x	x
Plectofrondicularia pellucida Finlay	x	
Pullenia sp.		x
Rectuvigerina pohana (Finlay)		x
Rosalina sp.		x
Siphouvigerina sp.	x	
Textularia fistulosa Brady		x
Textularia saggitula Defrance	x	
Uvigerina sp. (costate)	x	x

Onoua Limestone

Table D13: Onoua Limestone macrofossils, Pitt Island. Identifications by A.G. Ben, D.E. Lee and J.S. Buckeridge. 'T' indicates type locality of the species listed.

	Tarawhenua Peninsula	Flowerpot Bay
Brachiopoda (ident. D.E. Lee)		
Liothyrella pittensis Allan	x	x
Terebratella cf. *sanguinea* (Leach)	x	x
Neothyris thomsoni Allan	x	x
Terebratulina n.sp.?		x
Thecidellina n.sp.?		x
Mollusca (ident. A.G. Beu)		
Glycymeris (Glycymeris) hunti (Marwick)	x	
Chlamys n.sp. aff. *seymouri* Marwick	x	x
Kaparachlamys hectori (Hutton)		x
Lima zealandica Sowerby		x
Ctenoides n.sp.		x
Maoricolpus solomoni (Marwick)	x	
Cirsotrema propelyratum (Marwick)		T
Polychaeta		
Tubes	x	
Echinoidea		
Spatangoida, frag.	x	
Cidaroida, plates	x	
Cirripedia (ident. J.S. Buckeridge)		
Pachylasma distortum Buckeridge		x
Austromegabalanus (Notomegabalanus) miodecorus Buckeridge	x	
Fosterella chathamensis Buckeridge	x	x

Table D14: Onoua Limestone foraminifera, Pitt Island. Identifications by N. de B. Hornibrook.

	Tarawhenua Peninsula	**Flowerpot Bay**	**N. of Bluff Homestead**
Alabamina tenuimarginata (C.P.& C.)	x		
Amphicoryne hirsuta (d'Orbigny)	x		x
Amphicoryne scalaris (Batsch)	x		
Astrononion novozealandicum Cushman			x
Bigenerina pliocenica Finlay			x
Bulimina aculeata d'Orbigny			x
Cassidulina laevigata d'Orbigny	x		x
Cibicides cf. *deliquatus* Finlay	x		x
Cibicides perforatus (Karrer)			x
Discorbis opercularis (d'Orbigny)			x
Dyocibicides biserialis Cushman & Valentine	x		x
Ehrenbergina cf. *marwicki* Finlay	x		x
Elphidium sp.			x
Eponides repandus (Fichtel & Moll)	x		x
Gaudryina convexa Karrer	x		x
Globigerina bulloides d'Orbigny	x	x	x
Globigerina woodi Jenkins group		x	x
Globigerina eamsi Blow	x	x	
Globigerina sp. (3 chambers)			
Globigerinella aequilateralis (Brady)	x		x
Globigerinoides sacculifer (Brady)			
Globigerinoides trilobus (Reuss)	x		
Globocassidulina subglobosa (Brady)			x
Globorotalia cf. *puncticuloides* Hornibrook	x	x	x
Globorotalia crassaconica Hornibrook	S		
Globorotalia crassaformis (Galloway & Wissler) (unkeeled)	S	S	S/D
Globorotalia humerosa Takayanagi & Saito	x	x	x
Globorotalia inflata (d'Orbigny)	x	x	x
Globorotalia pliozea Hornibrook	x		
Globorotalia puncticulata (Deshayes)	x	x	x
Gyroidinoides cf. *zelandica* Finlay	x		
Karreria fallax Rzehak	x		x
Lagena yokoyamae Millett	x		x
Lenticulina sp.			x
Melonis d. *simplex* (Karrer)	x		x
Mississippina concentrica (parker & Jones)			
Notorotalia cf. *macinnesi* Kennett	x		x
Notorotalia cf. *spinosa* (Chapman)			
Orbulina universa d'Orbigny	x	x	x
Patellina corrugata Williamson			x
Patellinella inconspicua (Brady)	x		x
Pseudonodosaria sp.	x		
Pseudopolymorphina sp.	x		x
Pullenia cf. *salisburyi* Stewart (6 chambers)	x		x
Saracenaria sp.			x
Sigmoidella sp.	x		
Siphotextularia dawesi Kennett			
Textularia d. *vertebralis* Cushman	x		x
Textularia fistulosa Brady	x		x
Uvigerina sp. (costate)	x	x	x

D = predominantly dextral
S = predominantly sinistral

Waipipian limestone

Table D15: Waipipian limestone macrofossils, borehole CHA59 southeast of Motuariki Hill, northern Chatham Island. Identifications by A.G. Bell.

Bivalvia
Kaparachlamys hectori (Hutton), several fragments
Sectipecten sp., 1 fragment
Chlamys n. sp. aff. *seymouri* Marwick, 1 valve + fragment
Purpurocardia sp., incomplete moulds
Dosinia sp., incomplete moulds
Tawera sp. (not *T. marthae* Marwick), mould
Caryocorbula aff. *zelandica* (Quoy and Gaimard), mould
Gastropoda
Calliostoma? sp., incomplete mould
Maoricolpus solomoni Marwick, incomplete mould

Legend

- Tuffaceous deposit
- Fine bedded tuff
- Sandy tuff
- Lapillistone
- Tuffaceous conglomerate and claystone
- Tuffaceous conglomerate
- Tuffaceous breccia
- Basaltic lava flow
- Limestone
- Cross-bedded limestone
- Vaguely cross-bedded limestone
- Sandy limestone
- Limestone conglomerate
- Shell bed
- Quartzose sand
- Conglomerate
- Gravel lag
- Peat
- Schist
- Glauconitic
- Phosphatic
- Silicified or chert horizon
- Calcareous rubbly layer
- Karst surface
- Irregular or burrowed surface
- Burrowing/bioturbation
- Serpulids/worm tubes
- Unconformity
- Massive
- Cross-bedded
- Volcanic detritus
- Uncertain stratigraphy
- Fragmented shell material
- Foraminifera
- Planktic foraminifera
- Bryozoans
- Bryozoans - rigid sheet
- Bryozoans - rigid dendroid
- Echinoderms
- Bivalves
- Pectinids
- *Serripecten*
- Oysters
- Brachiopods
- Gastropods
- Barnacles

Time Scale

Inter. Age	NZ Series	NZ Stage
Pleist.	Wanganui	Haweran (Wq)
		Castlecliffian (Wc)
		Nukumaruan (Wn)
Pliocene		Mangapanian (Wm)
		Waipipian (Wp)
	Tara-naki	Opoitian (Wo)
		Kapitean (Tk)
Miocene		Tongaporutuan (Tt)
	Sth. Lnd.	Waiauan (Sw)
		Lillburnian (Sl)
	Pare-ora	Clifdenian (Sc)
		Altonian (Pl)
		Otaian (Po)
Oligo-cene	Landon	Waitakian (Lw)
		Duntroonian (Ld)
		Whaingaroan (Lwh)
Eocene	Arnold	Runangan (Ar)
		Kaiatan (Ak)
		Bortonian (Ab)
	Dannevirke	Porangan (Dp)
		Heretaungan (Dh)
		Mangaorapan (Dm)
Paleo-cene		Waipawan (Dw)
		Teurian (Dt)
Upper Cretaceous	Mata	Haumurian (Mh)
		Piripauan (Mp)
	Rauku-mara	Teratan (Rt)
		Mangaotanean (Rm)
		Arowhanan (Ra)
Lower Cretaceous	Clarence	Ngaterian (Cn)
		Motuan (Cm)
		Urutawan (Cu)
?Tai-hati		Korangan (Uk)
		??

Stratigraphic columns constructed from characteristics observed in field work conducted in 2005 and 2006 by Jeremy Titjen for partial fulfilment of MSc degree in Earth & Ocean Sciences at the University of Waikato, with information also sourced from columns in Campbell *et al.* (1993). Grid references given are from NZMS 260 1:50,000 maps of the Chatham Islands, Sheet 1 (CH1) and Sheet 2 (CH2).

Enclosure 1

Stratigraphic Columns

Jeremy Q. Titjen

2007

MSc Thesis

Tertiary limestones and sedimentary dykes on Chatham Islands, southwest Pacific Ocean, New Zealand

Department of Earth & Ocean Sciences

The University of Waikato

1 Tumaio Beach (CH1/380786)

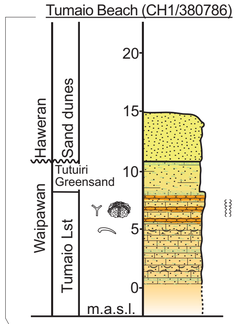

Sand dunes

Dark green, soft non-calcareous medium greensand

Hard nodular horizons, *Thalassinoides* burrowing

Soft, bryozoan-echinoid packstone, glauconitic

Gritty

Thin *Pycnodonte (Notostrea) tarda* shellbeds

2 Waitaha Creek (CH1/454787)

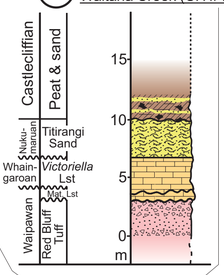

Peat and sand

Medium yellow-brown loose sand with rich bivalve shellbeds and peat stringers

Medium orange-brown to pale yellow soft massive grainstone

Hard pale grey-white pebbly limestone

Hard medium dark green-grey tuff

3 Maunganui (CH1/283760)

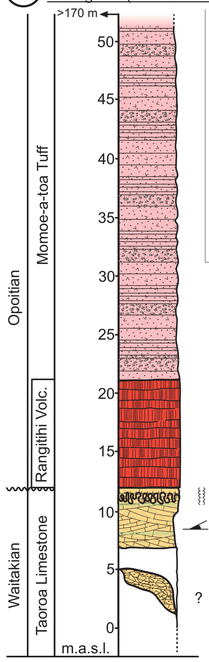

Well bedded coarse limburgitic tuff and lapillistone

Limburgitic basalt flows, some pillows exposed at base

Upper burrowed, bioclastic grainstone with lithoclast inclusions, glauconitic

Bryozoan-echinoid, fine grained packstone with fine grained matrix and low angle cross-bedding

White, microbioclastic, extremely fine grained, brecciated limestone, block flow?, stratigraphic relationship unclear

4 Waipapa Creek - Blind Jim's Creek (CH1/451755 - CH1/454745)

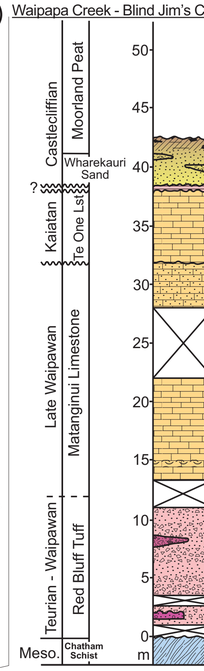

Peat and sand

Thin weathered tuff

Soft yellow bryozoan grainstone

Soft, white bryozoan-echinoid packstone

Soft, pale yellow-grey bryozoan-foraminiferal packstone with *Asterocyclina*

Brick red tuff and breccia

Pale green conglomeratic tuff and claystone

Schist

5 Moutapu Point (CH1/520698)

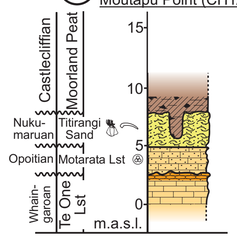

Peat, silt and soil

Thick shell bed, quartzose sand matrix, with rounded (5 cm) lithoclasts

Pale yellow, massive fine microbioclastic, planktic foram grainstone

Hard, Fe-PO_4 conglomerate surface, common stromatolitic mats

6 Moreroa (CH1/481653)

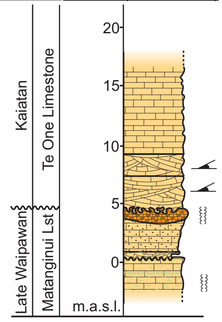

Soft, massive, pale yellow to orange-brown, bryozoan grainstone

Soft bryozoan grainstone, low angle planar cross-bedding

Soft bryozoan packstone

Thalassinoides, burrowed, hard, bryozoan rudstone-grainstone

Cross-bedding above disconformity

Soft, highly burrowed, glauconitic, bryozoan packstone

7 Big Bush Quarry (CH1/472629)

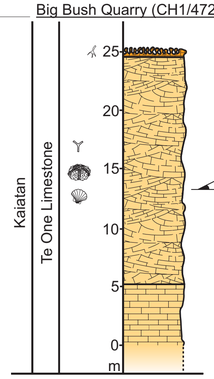

Uppermost calcrete horizon, root structures, preserved Fe-Mn stromatolitic mats, bryozoans with micritic matrix

Friable, cross-bedded (1-6 m sets), bryozoan-echinoderm grainstone and rudstone, rare pectinids

Lower quarry section poorly exposed, primary structures concealed by limestone extraction processes

8 Ohuru Point (CH1/497618 - CH1/495619)

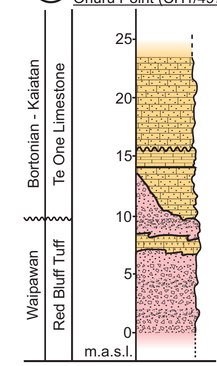

Soft, reddish brown, coarse echinoid-bryozoan grainstone

Prominent disconformity

Hard, pale yellow-brown echinoid-bryozoan-barnacle grainstone

Yellow to red-brown, calcareous medium lapillistone and coarse tuff with bands of tuffaceous limestone

9 Whareama (CH1/512558)

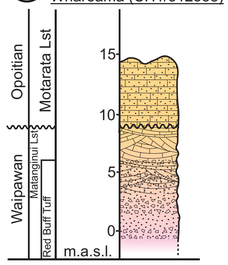

Soft, massive, fine grained, planktic foram rich with rare pectinids and discontinuous brachiopod horizon

Basal phosphatic pebble horizon

Case hardened, highly burrowed, coarse bryozoan grainstone, cross-bedding (2 m sets)

Massive, red-brown, coarse calcareous tuff

10 East of Cape L'Eveque, Snake Gully (CH2/418362)

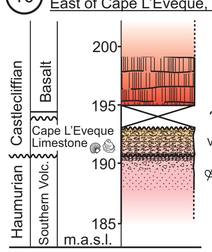

Columnar jointed, basaltic lava flows

Volcaniclastic limestone with large rounded volcanic clasts, conspicuous pectinid and oyster fragments

Inferred unconformity

Non-calcareous tuff, ?glauconitic, sparse shell material

11 Rocky Side (CH2/688225 - CH2/689224)

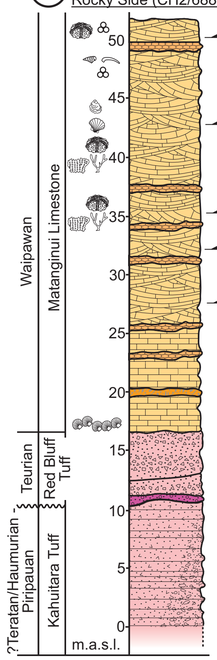

Upper case hardened surface over soft, cross-bedded rudstone grading into a grainstone, echinoid spines, *Celleporia* and *Asterocyclina*

Molluscan moulds of large bivalves and gastropods

Large oyster and pectinid shells

Rigid branching bryozoan dominated rudstone-packstone

Poorly cemented, bryozoan-echinoderm grainstone with low angle cross-bedding in upper sections, cyclic rubbly fossiliferous horizons present thoughout

Lower eroded surface with volcaniclastics

Abundant pectinids

Massive, red-brown tuff and breccia

Basal conglomerate

Well-bedded pale yellow-brown fine volcanic sandstones and grits

12 Tarawhenua Peninsula (CH2/679233)

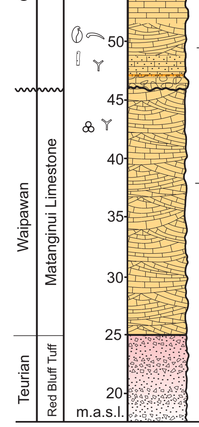

Massive, grey-brown basaltic and hornblende crystal coarse tuff and lapillistone

Brachiopods, serpulids, echinoderms (infaunal), pectinids and celleporid bryozoans

Serripecten shell bed 10 cm thick over 1 m extent

Massive with little obvious structure, fine grained bryozoan sand

Cross-bedded, granular rudstone with brachiopods, serpulids and bivalves

Basal shell gravel, burrowing, fine grained bryozoan sand

Hard, white bryozoan grainstone, *Asterocyclina*, *Scolicia* burrows

Red-brown coarse tuff and lapillistone

13 West of Flowerpot Bay (CH2/703232)

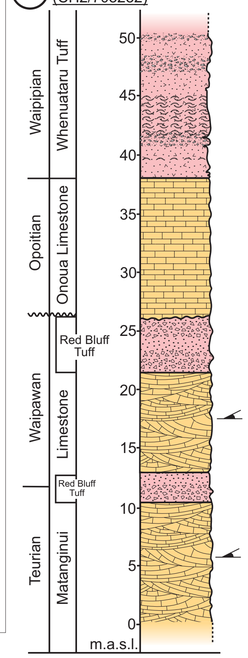

Red-brown, cross-bedded coarse tuff and lapillistone

Soft, massive, pale yellow-white bryozoan grainstone

Hard pale grey-brown tuff and volcanic sandstone

Hard, white foraminiferal packstone

Hard grey-brown tuff

Hard white foraminiferal packstone

14 North of the Bluff (CH2/714236 - CH2/715235)

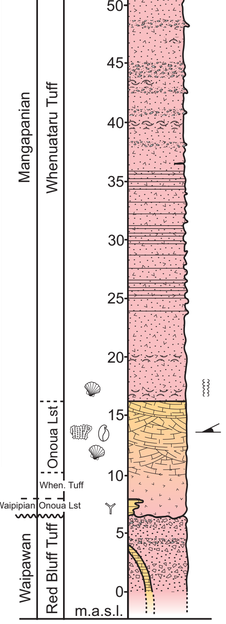

Lenses of hard, white cross-bedded bryozoan grainstone

Brown-grey well-bedded calcareous tuff and lapillistone

White, massive, vaguely cross-bedded (low angle) bryozoan grainstone with scattered brachiopods and pectinids

Pale yellow-green brown calcareous tuff and lapillistone

Lenses of massive, bryozoan rudstone

Vertical limestone dykes (8 cm wide) of mainly Onoua Limestone but also Matanginui Limestone

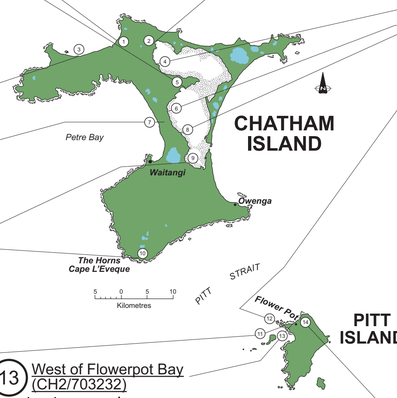

NORTH

SOUTH

Chatham Island

Pitt Strait

Pitt Island

Maunganui 3

>170 m

Opoitian (Early Pliocene)

Waitakian (Early Miocene)

Rangitihi Volc.

Momoe-a-toa Tuff

Taoroa Limestone

m.a.s.l.

Tumaio Beach 1

Waipawan (Early Eocene)

Holocene

Sand dunes

Tutuiri Greensand

Tumaio Lst

Waitaha Creek 2

Castlecliffian

Peat & sand

Titirangi Sand

Mukio-manuan

Whain-garoan

Victoriella Lst

Mid Lst

Waipawan

Red Bluff Tuff

m

Waipapa Creek - Blind Jim's Creek 4

Moutapu Point 5

Moreroa 6

Big Bush Quarry 7

Ohuru Point 8

Whareama 9

Te One Limestone

Matanginui Limestone

Red Bluff Tuff

Chatham Schist (pre-middle Cretaceous)

East of Cape L'Eveque, Snake Gully 10

Castlecliffian

Basalt

Cape L'Eveque Limestone

Haumurian

Southern Volc.

Tarawhenua Peninsula 12

Whenuataru Tuff

Onoua Limestone

West of Flowerpot Bay 13

North of the Bluff 14

Rocky Side 11

?Teratan/Haumurian - Piripauan (Late Cretaceous)

Kahuitara Tuff

Legend

- Quaternary Peat and Sands
- 1 Titirangi Sand (Late Pliocene)
- Whenuataru Tuff (Early-Late Pliocene)
- Onoua Limestone (Late Pliocene)
- 2 Motarata Limestone (Pliocene)
- Te One Limestone (Late Eocene-Early Oligocene)
- Matanginui Limestone (Early-Middle Eocene)
- Red Bluff Tuff (Late Paleocene-Early Eocene)

Stratigraphic columns constructed from characteristics observed in field work conducted in 2005 and 2006 by Jeremy Titjen for partial fulfilment of MSc degree in Earth & Ocean Sciences at the University of Waikato, with information also sourced from columns in Campbell *et al.* (1993). Grid references given are from NZMS 260 1:50,000 maps of the Chatham Islands, Sheet 1 (CH1) and Sheet 2 (CH2).

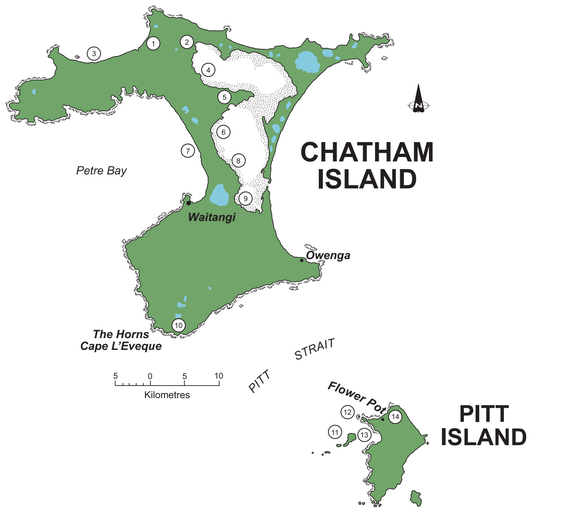

Enclosure 2

Stratigraphic Correlation

Jeremy Q. Titjen 2007

MSc Thesis

Tertiary limestones and sedimentary dykes on Chatham Islands, southwest Pacific Ocean, New Zealand

Department of Earth & Ocean Sciences

The University of Waikato